
Reviews in Computational Chemistry

Volume 14

Reviews in Computational Chemistry

Volume 14

Edited by

Kenny B. Lipkowitz and Donald B. Boyd



WILEY-VCH

NEW YORK • CHICHESTER • WEINHEIM • BRISBANE • SINGAPORE • TORONTO

Kenny B. Lipkowitz
Department of Chemistry
Indiana University—Purdue University
at Indianapolis
402 North Blackford Street
Indianapolis, Indiana 46202-3274,
U.S.A.
lipkowitz@chem.iupui.edu

Donald B. Boyd
Department of Chemistry
Indiana University—Purdue University
at Indianapolis
402 North Blackford Street
Indianapolis, Indiana 46202-3274,
U.S.A.
boyd@chem.iupui.edu

The authors, editors, and John Wiley and Sons, Inc., its subsidiaries, or distributors assume no liability and make no guarantees or warranties, express or implied, for the accuracy of the contents of this book, or the use of information, methods, or products described in this book. In no event shall the authors, editors, and John Wiley and Sons, Inc., its subsidiaries, or distributors be liable for any damages or expenses, including consequential damages and expenses, resulting from the use of the information, methods, or products described in this work.

This book is printed on acid-free paper. ☺

Copyright © 2000 by Wiley-VCH, Inc. All rights reserved.

Published simultaneously in Canada.

No part of this publication may be reproduced, stored in a retrieval system or transmitted in any form or by any means, electronic, mechanical, photocopying, recording, scanning or otherwise, except as permitted under Sections 107 or 108 of the 1976 United States Copyright Act, without either the prior written permission of the Publisher, or authorization through payment of the appropriate per-copy fee to the Copyright Clearance Center, 222 Rosewood Drive, Danvers, MA 01923, (978) 750-8400, fax (978) 750-4744. Requests to the Publisher for permission should be addressed to the Permissions Department, John Wiley & Sons, Inc., 605 Third Avenue, New York, NY 10158-0012, (212) 850-6011, fax (212) 850-6008, e-mail: permreq@wiley.com.

For ordering and customer service, call 1-800-CALL-WILEY.

ISBN 0-471-35495-3
ISSN 1069-3599

Preface

About five years ago, Michael Guillen of Harvard wrote a book entitled *Five Equations That Changed the World: The Power and Poetry of Mathematics*.^{*} He pointed out that Gottfried Wilhelm Leibniz, the German mathematician who independently invented calculus (besides Isaac Newton), published the first article on that discovery in 1684. Guillen writes, “The article did not elicit immediate response because very few people in the world could comprehend it. The author [Leibniz], with characteristic arrogance, had not tried very hard to explain his discovery [calculus], presumably because he wanted to remind people of how much smarter he was than they.” An attitude like that is inappropriate for our book series.

The present volume of *Reviews in Computational Chemistry*, our fourteenth, provides a cornucopia of unique tutorials and reviews on pertinent topics in computational chemistry. As with other volumes in this series, we asked our authors to aim their chapters to be part tutorial so that both a novice molecular modeler and a knowledgeable expert could benefit from them. Other books and journals publish traditional reviews that allow the authors to impress their peers by showing how much they know. In contrast, our chapters are intended to impress newcomers to a topic by clearly and thoroughly getting them “up to speed” on what might be very complex subject matter. We discourage our authors as much as possible from skipping mathematical steps in the manipulation of equations and from using the overworked expression “it can easily be shown that. . . .”

To theoretical and computational chemists, the world may seem to revolve around the Schrödinger equation, potential energy force field equations, or perhaps some quantitative structure-activity relationship equations for predicting biological activity. These various equations have been the basis of the livelihood of many a computational chemist. Interestingly, author Guillen apparently did not deem these equations to have risen to the level of having

^{*}M. Guillen, *Five Equations That Changed the World: The Power and Poetry of Mathematics*, Hyperion, New York, 1995. The five equations Guillen includes are Newton’s law of gravity, Bernoulli’s law of hydrodynamic pressure, Faraday’s law of electromagnetic induction, Clausius’s second law of thermodynamics, and Einstein’s theory of special relativity.

“changed the world.” Most of us have heard of “Dirac’s dictum.” British theoretician Paul Adrien Maurice Dirac (1902–1984) boldly wrote from the lofty perch of a physicist: “The underlying physical laws necessary for the mathematical theory of a large part of physics and the whole of chemistry are thus completely known, and the difficulty is only that the application of these laws leads to equations much too complicated to be soluble.”[†] Perhaps an equitable assessment of the importance of famous equations in science would be that the Schrödinger equation and other equations familiar to computational chemists may not have *changed* the world, but they have changed people’s view of the nanoworld of atoms and molecules. In any case, some humility and a sense of perspective in the grand scheme of things never hurt.

Chapter 1 deals with atomic charges, a topic computational chemists often encounter whether they work in the quantum chemistry or in molecular simulations. Molecules “perceive” each other by their electrostatic field and by their steric shape. It was considered quite an innovation when partial atomic charges, such as those used in evaluating Coulombic interactions, were derived by fitting the point charges to approximate the quantum mechanic electrostatic field of a molecule. The thought was that these charges would be better suited for studying the interaction of two or more molecules, such as the docking of a ligand in a receptor or the mutual approach of two reactants. However, after the initial euphoria about the innovation, chemists came to learn that the electrostatically fitted charges are sensitive to how they are computed: they depend on the sampling of points used in the fitting process, not just on the molecular orbital method and the conformation of the molecule used. Professors Michelle Miller Franci and Lisa Emily Chirlan have made major contributions to this subject. Chapter 1 describes the current status of the methods for obtaining these charges and looks at possible solutions.

In Volume 5 of this series, R. J. Bartlett and J. F. Stanton authored a popular tutorial on applications of post-Hartree–Fock methods. Here in Chapter 2, Dr. T. Daniel Crawford and Professor Henry F. Schaefer III explore coupled cluster theory in great depth. Despite the depth, the treatment is brilliantly clear. Beginning with fundamental concepts of cluster expansion of the wavefunction, the authors provide the formal theory and the derivation of the coupled cluster equations. This is followed by thorough explanations of diagrammatic representations, the connection to many-bodied perturbation theory, and computer implementation of the method. Directions for future developments are laid out.

Zeolites are microporous aluminosilicates that have interesting molecular sieve properties and contain microenvironments giving rise to a wide range of interesting chemical reactions. Because of the economic importance of these materials, scientists have been carrying out computational studies on both the

[†]P. A. M. Dirac, *Proc. R. Soc. (London)*, A123, 714 (1929). Quantum Mechanics of Many-Electron Systems.

structural and dynamical features of these systems along with the reactions taking place within their cavities. In Chapter 3, Professor Bastiaan van de Graaf and his coauthors, Drs. Swie Lan Njo and Konstantin S. Smirnov, provide a detailed treatment of quantum and potential-based methods needed for such calculations. Easy-to-follow explanations of self-consistent field, density functional, and semiempirical methods, as well as summation of long-range interactions, energy minimization methods, molecular dynamics, Monte Carlo simulation, and Car–Parrinello techniques are presented. The methods are illustrated with selected examples of aperture fluctuations, cation dynamics, isomorphic substitutions, and chemical reactivity.

Intermolecular potential functions stand center stage in the theater of molecular simulations. In Chapter 4, Professor Sarah L. Price points out that at one time very simple potential energy functions were deemed acceptable for use. The emphasis was on simplicity because of the limitations of computers, but, with the advances in hardware, one can now use more realistic and reliable potential functions. This chapter focuses on the lessons that can be learned from the current intermolecular potentials of small organic molecules. Definitions and limitations of intermolecular potential theory are presented along with explanations of the various contributions to the intermolecular pair potential. Methods used for deriving potentials are assessed. Systematic construction of potentials with distributed multipoles and distributed polarizabilities is explained. To help the reader, computer coding of anisotropic potentials and the issue of transferability of potential functions for organic molecules round out this tutorial. This chapter is particularly relevant because it foreshadows what the future of molecular modeling of organic and biological systems will look like.

Nonequilibrium molecular dynamics (NEMD) is covered in Chapter 5 by Drs. Christopher J. Mundy, Sundaram Balasubramanian, Ken Bagchi, Mark E. Tuckerman, Glenn J. Martyna, and Michael L. Klein. NEMD provides a framework for performing simulations in the way that an experiment is done in the laboratory, where the system is not at equilibrium. Because so few scientists seem to be aware of the methods and where and how they should be implemented, the authors provide a complete introduction to the topic, derive all the equations, and explain what is required to carry out such simulations successfully. Beginning from molecular dynamics and equilibrium statistical mechanics, the authors move to NEMD and linear response theory. After developing the formal methodology, the authors then explain the tools needed to numerically integrate the equations of motion. To illustrate why the methods are needed and how they are used, the authors provide several applications of shear flow. Many real systems that scientists want to model are not at equilibrium, so NEMD is necessary, and this chapter provides the tutorial for undertaking such calculations.

After the “meat and potatoes” of the first five chapters, the short essay of Chapter 6 chronicles the beginnings of the highly successful biennial Gordon

Research Conferences on Computational Chemistry. The editors write about the conference series they founded in the mid-1980s. An important part of the essay are the group photographs taken at the meetings. The pictorial record shows many of the major proponents of computational chemistry, as well as younger scientists who are contributing to the field. It is interesting to observe that not all of us had as much gray hair as we do now. Also in the essay are reproductions of the programs from the first two Gordon Research Conferences on Computational Chemistry. The titles of the presentations give a glimpse of what the vanguard areas of research were in 1986 and 1988.

This volume also features an appendix with a compilation of published molecular mechanics parameters. At the request of many of our readers, Professor Kenny B. Lipkowitz and his student Mehran Jalaie undertook a major update and expansion of the force field parameters collected in Volume 6 of this series. All too frequently, programs employing an empirical force field will be stumped in trying to treat a structure with an unusual combination of atoms types because no parameters are available in the program. The bibliography in the Appendix will help users of molecular mechanics and molecular dynamics programs track down supplemental parameters required for their calculations.

Information about *Reviews in Computational Chemistry* is available on the World Wide Web at <http://chem.iupui.edu/rcc/rcc.html>. Our web site includes the author and subject indexes of all volumes as a free online service. Color graphics and other material as adjuncts to the chapters are also available. A brief tutorial about the web can be found in Volume 11's appendix. That appendix and the one in Volume 7 provide links to suppliers of software and other resources of interest to practicing computational chemists.

Some of the unsung heroes in helping produce these volumes have included Barbara Chernow, Kathy Jackson, and anonymous copy editors and compositors. These contractors have worked behind the scenes handling many of the production details for John Wiley & Sons, which is the renowned marketing organization in the publishing business. We also thank Mrs. Joanne Hequembourg Boyd for editorial assistance. We are grateful to our authors for their excellent chapters. We hope that these books will have enduring value to our readers and authors in their learning, teaching, and research.

Donald B. Boyd and Kenny B. Lipkowitz
Indianapolis
January 1999

Contents

1.	The Pluses and Minuses of Mapping Atomic Charges to Electrostatic Potentials <i>Michelle Miller Franc and Lisa Emily Chirlian</i>	1
	Introduction	1
	Where Are the Electrons?	2
	Finding an Atom-Based Index	2
	Why Choose the Molecular Electrostatic Potential?	3
	Fitting the Charges	4
	Larger Molecules Provide Challenges	7
	Wobbly Charges: The Problem of “Conformational Instability”	8
	A Sampling of Point Distribution Schemes	8
	Variation with Conformation: How Much Is Too Much?	13
	Getting to the Root of the Problem	16
	A Closer Look at the Linear Least Squares Problem	17
	Linear Least-Squares Fit to the Molecular Electrostatic Potential	22
	Conclusions and Recommendations	28
	References	29
2.	An Introduction to Coupled Cluster Theory for Computational Chemists <i>T. Daniel Crawford and Henry F. Schaefer III</i>	33
	Introduction	33
	Fundamental Concepts	35
	Cluster Expansion of the Wavefunction	35
	Cluster Functions and the Exponential Ansatz	38
	Wavefunction Separability and Size Consistency of the Energy	42
	Formal Coupled Cluster Theory	45
	Truncation of the Exponential Ansatz	46
	The Hausdorff Expansion	47
	A Variational Coupled Cluster Theory?	49
	An Eigenvalue Approach to Coupled Cluster Theory	51

Derivation of the Coupled Cluster Equations	54
Normal-Ordered Second-Quantized Operators	55
Wick's Theorem for the Evaluation of Matrix Elements	56
The Fermi Vacuum and the Particle–Hole Formalism	60
The Normal-Ordered Electronic Hamiltonian	61
Simplification of the Coupled Cluster Hamiltonian	63
The CCSD Energy Equation	67
The CCSD Amplitude Equations	70
An Introduction to Coupled Cluster Diagrams	77
Diagrammatic Representation of the CCSD Energy Equation	82
Diagrammatic Representation of the CCSD Amplitude Equations	88
Size Extensivity of the Coupled Cluster Energy	95
Connection to Many-Body Perturbation Theory	98
Perturbational Decomposition of the Cluster Operators	99
Perturbation Theory Energies from the Coupled Cluster Hamiltonian	100
The (T) Correction	103
Computer Implementation of Coupled Cluster Theory	107
Factorization of the Coupled Cluster Equations	109
Matrix-Based Storage of Integrals and Amplitudes	110
Spatial Symmetry Simplifications	110
Spin Factorization of the Coupled Cluster Equations	112
Atomic-Orbital-Basis Algorithms	114
Current Research and Future Directions	115
Coupled Cluster Theory for Open-Shell Molecules	116
Spin-Restricted Triple-Excitation Corrections	117
Brueckner Orbitals in Coupled Cluster Theory	119
Future Research Prospects	122
Acknowledgments	124
References	125
 3. Introduction to Zeolite Modeling	
<i>Bastiaan van de Graaf, Swie Lan Njo, and Konstantin S. Smirnov</i>	137
Introduction	137
Approaches to Zeolite Modeling	140
Computational Approaches	140
Scope of Zeolite Modeling	142
Models	150
Quantum Mechanical Models	151
Potential Models for Framework Modeling	155
Hybrid Models	164

Methods	165
Structure and Periodicity	165
Summation of Long-Range Interactions	166
Energy Minimization	171
Method of Molecular Dynamics	174
Monte Carlo Methods	185
Car-Parrinello Approach	187
Some Selected Applications	189
Framework Dynamics	189
Zeolite/Template Interactions: Tetrabutylammonium and Tetrapropylammonium in MEL and MFI Structures	197
Isomorphic Substitution	200
Chemical Reactivity	206
Future Developments	213
Acknowledgments	214
References	214
4. Toward More Accurate Model Intermolecular Potentials for Organic Molecules	225
<i>Sarah L. Price</i>	
Introduction	225
Definitions and Limitations of Intermolecular Potential Theory	227
Coordinate Systems	228
Molecule-Centered Expansions Versus Atom–Atom Models	232
The Pairwise Additive Approximation	234
Contributions to the Intermolecular Pair Potential	235
Long-Range Contributions to the Intermolecular Energy	236
Contributions to the Intermolecular Potential from Molecular Overlap	240
Methods of Deriving Model Intermolecular Potentials	241
Empirical Model Potentials for Organic Molecules	241
Ab Initio Potential Energy Surfaces	246
Lessons from Intermolecular Perturbation Theory Calculations on Organic Molecules	249
Systematic Potentials	255
Electrostatic Contribution: Distributed Multipoles	255
Induction and Dispersion Contributions: Distributed Polarizabilities	263
Short-Range Terms	264
Damping Terms	266
Examples of Systematic Potentials	266

Model Potentials for Organic Molecules Constructed from Ab Initio Charge Distributions and Empirical Fitting	269
Computer Coding of Anisotropic Potentials	270
Transferability of Potentials for Organic Molecules	272
Transferability of Atom–Atom Nonbonded Parameters Between Molecules	273
Transferability Between Conformations	275
Future Model Potentials	280
Acknowledgments	280
References	281
 5. Nonequilibrium Molecular Dynamics	
<i>Christopher J. Mundy, Sundaram Balasubramanian, Ken Bagchi, Mark E. Tuckerman, Glenn J. Martyna, and Michael L. Klein</i>	291
Introduction	291
Why Nonequilibrium Molecular Dynamics?	291
Homogeneous Versus Inhomogeneous Methods	293
Molecular Dynamics and Equilibrium Statistical Mechanics	296
Microscopic Motion and Macroscopic Observables	296
Relation to Microcanonical Ensemble	302
Non-Hamiltonian Dynamics	304
Dynamical Generation of the <i>NVT</i> Ensemble	310
Dynamical Generation of the <i>NPT</i> Ensemble	317
Nonequilibrium Molecular Dynamics and Linear Response	323
Generalized Equations of Motion	323
Linear Response Theory	324
The SLLOD Equations of Motion	330
Other Types of Flow: GSLLOD Equations of Motion	336
Numerical Implementation of SLLOD Dynamics	339
Numerically Integrating the SLLOD Equations	339
Boundary Conditions	355
Applications of Shear Flow	361
Viscosity	361
Hydrodynamic Boundary Conditions	364
Profile-Unbiased Thermostat and String Phases	372
Small-Field Methods	379
Crack Propagation	384
Conclusions and Future Prospects	388
Appendix 1: Time Evolution of the Jacobian	389
Appendix 2: Geometric Derivation of the Generalized Liouville Equation	390
References	392

6. History of the Gordon Research Conferences on Computational Chemistry <i>Donald B. Boyd and Kenny B. Lipkowitz</i>	399
Introduction	399
Laying the Groundwork for a Gordon Research Conference on Computational Chemistry	401
The First Gordon Research Conference on Computational Chemistry	403
The Second Gordon Research Conference on Computational Chemistry	406
Recent Developments	407
Pictorial History	409
Acknowledgments	424
Appendix 1: 1986 Program	424
Appendix 2: 1988 Program	431
References	439
 Appendix: Published Force Field Parameters for Molecular Mechanics, Molecular Dynamics, and Monte Carlo Simulations <i>Mehran Jalaie and Kenny B. Lipkowitz</i>	441
Introduction	441
Sources of Force Field Parameters	444
Cited Literature	469
References	486
 Author Index	487
 Subject Index	513

Contributors

Ken Bagchi, Center for Molecular Modeling, Department of Chemistry, University of Pennsylvania, Philadelphia, Pennsylvania 19104–6323, U.S.A.
(Electronic mail: bagchi@cmm.chem.upenn.edu)

Sundaram Balasubramanian, Chemistry and Physics of Materials Unit, Jawaharlal Nehru Center for Advanced Scientific Research, Jakkur P. O., Bangalore 560 064, India (Electronic mail: bala@jncasr.ac.in)

Lisa Emily Chirlian, Bryn Mawr College, 101 North Merion Avenue, Bryn Mawr, Pennsylvania, 19010, U.S.A. (Electronic mail: lchirlia@brynmawr.edu)

T. Daniel Crawford, Institute for Theoretical Chemistry, Departments of Chemistry and Biochemistry, The University of Texas, Austin, Texas, 78712–1167, U.S.A. (Electronic mail: crawdad@jfs1.cm.utexas.edu)

Michelle Miller Franci, Bryn Mawr College, 101 North Merion Avenue, Bryn Mawr, Pennsylvania, 19010, U.S.A. (Electronic mail: mfranci@brynmawr.edu)

Mehran Jalaie, Department of Chemistry, Indiana University–Purdue University at Indianapolis, Indianapolis, Indiana 46202, U.S.A. (Electronic mail: jalaie@chem.iupui.edu)

Michael L. Klein, Center for Molecular Modeling, Department of Chemistry, University of Pennsylvania, Philadelphia, Pennsylvania 19104–6323, U.S.A.
(Electronic mail: klein@cmm.chem.upenn.edu)

Kenneth B. Lipkowitz, Department of Chemistry, Indiana University–Purdue University at Indianapolis, Indianapolis, Indiana, 46202-3274, U.S.A.
(Electronic mail: lipkowitz@chem.iupui.edu)

Glenn J. Martyna, Department of Chemistry, Indiana University, Bloomington, Indiana 47405, U.S.A. (Electronic mail: gmartyna@indiana.edu)

Christopher J. Mundy, Max-Planck-Institut für Festkörperforschung, Heisenbergstrasse 1, D-70569 Stuttgart, Germany (Electronic mail: mundy@prr.mpi-stuttgart.mpg.de)

Swie Lan Njo, Laboratory of Organic Chemistry and Catalysis, Department of Applied Sciences, Delft University of Technology, Julianalaan 136, 2628 BL Delft, The Netherlands (Electronic mail: l.njo@stm.tudelft.nl)

Sarah L. Price, Centre for Theoretical and Computational Chemistry, Department of Chemistry, University College London, 20 Gordon Street, London WC1H 0AJ, United Kingdom (Electronic mail: s.l.price@ucl.ac.uk)

Henry F. Schaefer III, Center for Computational Quantum Chemistry, Department of Chemistry, The University of Georgia, Athens, Georgia 30602–2525, U.S.A. (Electronic mail: hfsiii@arches.uga.edu)

Konstantin S. Smirnov, Laboratoire de Spectrochimie Infrarouge et Raman du CNRS, Batiment C5, Université des Sciences et Technologies de Lille, 59655 Villeneuve d'Ascq Cedex, France (Electronic mail: smirnov@simulix.univ-lille1.fr)

Mark E. Tuckerman, Department of Chemistry and Courant Institute of Mathematical Sciences, New York University, New York, New York 10003, U.S.A. (Electronic mail: tuck@tosca.chem.nyu.edu)

Bastiaan van de Graaf, Laboratory of Organic Chemistry and Catalysis, Department of Applied Sciences, Delft University of Technology, Julianalaan 136, 2628 BL Delft, The Netherlands (Electronic mail: b.vandegraaf@stm.tudelft.nl)

Contributors to Previous Volumes*

Volume 1

David Feller and Ernest R. Davidson, Basis Sets for Ab Initio Molecular Orbital Calculations and Intermolecular Interactions.

James J. P. Stewart,[†] Semiempirical Molecular Orbital Methods.

Clifford E. Dykstra,[‡] **Joseph D. Augspurger**, **Bernard Kirtman**, and **David J. Malik**, Properties of Molecules by Direct Calculation.

Ernest L. Plummer, The Application of Quantitative Design Strategies in Pesticide Design.

Peter C. Jurs, Chemometrics and Multivariate Analysis in Analytical Chemistry.

Yvonne C. Martin, **Mark G. Bures**, and **Peter Willett**, Searching Databases of Three-Dimensional Structures.

Paul G. Mezey, Molecular Surfaces.

Terry P. Lybrand,[¶] Computer Simulation of Biomolecular Systems Using Molecular Dynamics and Free Energy Perturbation Methods.

Donald B. Boyd, Aspects of Molecular Modeling.

*When no author of a chapter can be reached at the addresses shown in the original volume, the current affiliation of the senior or corresponding author is given here as a convenience to our readers.

[†]Current address: 15210 Paddington Circle, Colorado Springs, CO 80921 (Electronic mail: jstewart@fai.com).

[‡]Current address: Indiana University-Purdue University at Indianapolis, Indianapolis, IN 46202 (Electronic mail: dykstra@chem.iupui.edu).

[¶]Current address: University of Washington, Seattle, WA 98195 (Electronic mail: lybrand@proteus.bioeng.washington.edu).

Donald B. Boyd, Successes of Computer-Assisted Molecular Design.

Ernest R. Davidson, Perspectives on Ab Initio Calculations.

Volume 2

Andrew R. Leach,* A Survey of Methods for Searching the Conformational Space of Small and Medium-Sized Molecules.

John M. Troyer and Fred E. Cohen, Simplified Models for Understanding and Predicting Protein Structure.

J. Phillip Bowen and Norman L. Allinger, Molecular Mechanics: The Art and Science of Parameterization.

Uri Dinur and Arnold T. Hagler, New Approaches to Empirical Force Fields.

Steve Scheiner, Calculating the Properties of Hydrogen Bonds by Ab Initio Methods.

Donald E. Williams, Net Atomic Charge and Multipole Models for the Ab Initio Molecular Electric Potential.

Peter Politzer and Jane S. Murray, Molecular Electrostatic Potentials and Chemical Reactivity.

Michael C. Zerner, Semiempirical Molecular Orbital Methods.

Lowell H. Hall and Lemont B. Kier, The Molecular Connectivity Chi Indexes and Kappa Shape Indexes in Structure-Property Modeling.

I. B. Bersuker[†] and A. S. Dimoglo, The Electron-Topological Approach to the QSAR Problem.

Donald B. Boyd, The Computational Chemistry Literature.

*Current address: Glaxo Wellcome, Greenford, Middlesex, UB6 0HE, U.K. (Electronic mail: arl22958@ggr.co.uk).

[†]Current address: College of Pharmacy, The University of Texas, Austin, TX 78712 (Electronic mail: bersuker@eeyore.cm.utexas.edu).

Volume 3

Tamar Schlick, Optimization Methods in Computational Chemistry.

Harold A. Scheraga, Predicting Three-Dimensional Structures of Oligopeptides.

Andrew E. Torda and **Wilfred F. van Gunsteren**, Molecular Modeling Using NMR Data.

David F. V. Lewis, Computer-Assisted Methods in the Evaluation of Chemical Toxicity.

Volume 4

Jerzy Cioslowski, Ab Initio Calculations on Large Molecules: Methodology and Applications.

Michael L. McKee and **Michael Page**, Computing Reaction Pathways on Molecular Potential Energy Surfaces.

Robert M. Whitnell and **Kent R. Wilson**, Computational Molecular Dynamics of Chemical Reactions in Solution.

Roger L. DeKock, **Jeffry D. Madura**, **Frank Rioux**, and **Joseph Casanova**, Computational Chemistry in the Undergraduate Curriculum.

Volume 5

John D. Bolcer and **Robert B. Hermann**, The Development of Computational Chemistry in the United States.

Rodney J. Bartlett and **John F. Stanton**, Applications of Post-Hartree-Fock Methods: A Tutorial.

Steven M. Bachrach, Population Analysis and Electron Densities from Quantum Mechanics.

Jeffry D. Madura, **Malcolm E. Davis**, **Michael K. Gilson**, **Rebecca C. Wade**, **Brock A. Luty**, and **J. Andrew McCammon**, Biological Applications of Electrostatic Calculations and Brownian Dynamics Simulations.

K. V. Damodaran and Kenneth M. Merz Jr., Computer Simulation of Lipid Systems.

Jeffrey M. Blaney and J. Scott Dixon, Distance Geometry in Molecular Modeling.

Lisa M. Balbes, S. Wayne Mascarella, and Donald B. Boyd, A Perspective of Modern Methods in Computer-Aided Drug Design.

Volume 6

Christopher J. Cramer and Donald G. Truhlar, Continuum Solvation Models: Classical and Quantum Mechanical Implementations.

Clark R. Landis, Daniel M. Root, and Thomas Cleveland, Molecular Mechanics Force Fields for Modeling Inorganic and Organometallic Compounds.

Vassilios Galiatsatos, Computational Methods for Modeling Polymers: An Introduction.

Rick A. Kendall, Robert J. Harrison, Rik J. Littlefield, and Martyn F. Guest, High Performance Computing in Computational Chemistry: Methods and Machines.

Donald B. Boyd, Molecular Modeling Software in Use: Publication Trends.

Eiji Ōsawa and Kenny B. Lipkowitz, Appendix: Published Force Field Parameters.

Volume 7

Geoffrey M. Downs and Peter Willett, Similarity Searching in Databases of Chemical Structures.

Andrew C. Good and Jonathan S. Mason, Three-Dimensional Structure Database Searches.

Jiali Gao, Methods and Applications of Combined Quantum Mechanical and Molecular Mechanical Potentials.

Libero J. Bartolotti and Ken Flurhick, An Introduction to Density Functional Theory.

Alain St-Amant, Density Functional Methods in Biomolecular Modeling.

Danya Yang and Arvi Rauk, The A Priori Calculation of Vibrational Circular Dichroism Intensities.

Donald B. Boyd, Appendix: Compendium of Software for Molecular Modeling.

Volume 8

Zdeněk Slanina, Shyi-Long Lee, and Chin-hui Yu, Computations in Treating Fullerenes and Carbon Aggregates.

Gernot Frenking, Iris Antes, Marlis Böhme, Stefan Dapprich, Andreas W. Ehlers, Volker Jonas, Arndt Neuhaus, Michael Otto, Ralf Stegmann, Achim Veldkamp, and Sergei F. Vyboishchikov, Pseudopotential Calculations of Transition Metal Compounds: Scope and Limitations.

Thomas R. Cundari, Michael T. Benson, M. Leigh Lutz, and Shaun O. Sommerer, Effective Core Potential Approaches to the Chemistry of the Heavier Elements.

Jan Almlöf and Odd Gropen,* Relativistic Effects in Chemistry.

Donald B. Chesnut, The Ab Initio Computation of Nuclear Magnetic Resonance Chemical Shielding.

Volume 9

James R. Damewood, Jr., Peptide Mimetic Design with the Aid of Computational Chemistry.

T. P. Straatsma, Free Energy by Molecular Simulation.

Robert J. Woods, The Application of Molecular Modeling Techniques to the Determination of Oligosaccharide Solution Conformations.

Ingrid Pettersson and Tommy Liljefors, Molecular Mechanics Calculated Conformational Energies of Organic Molecules: A Comparison of Force Fields.

Gustavo A. Arteca, Molecular Shape Descriptors.

*Address: Institute of Mathematical and Physical Sciences, University of Tromsø, N-9037 Tromsø, Norway (Electronic mail: oddg@chem.uit.no).

Volume 10

Richard Judson,* Genetic Algorithms and Their Use in Chemistry.

Eric C. Martin, David C. Spellmeyer, Roger E. Critchlow, Jr., and Jeffrey M. Blaney, Does Combinatorial Chemistry Obviate Computer-Aided Drug Design?

Robert Q. Topper, Visualizing Molecular Phase Space: Nonstatistical Effects in Reaction Dynamics.

Raima Larter and Kenneth Showalter, Computational Studies in Nonlinear Dynamics.

Stephen J. Smith and Brian T. Sutcliffe, The Development of Computational Chemistry in the United Kingdom.

Volume 11

Mark A. Murcko, Recent Advances in Ligand Design Methods.

David E. Clark, Christopher W. Murray, and Jin Li, Current Issues in De Novo Molecular Design.

Tudor I. Oprea and Chris L. Waller, Theoretical and Practical Aspects of Three-Dimensional Quantitative Structure–Activity Relationships.

Giovanni Greco, Ettore Novellino, and Yvonne Connolly Martin, Approaches to Three-Dimensional Quantitative Structure–Activity Relationships.

Pierre-Alain Carrupt, Bernard Testa, and Patrick Gaillard, Computational Approaches to Lipophilicity: Methods and Applications.

Ganesan Ravishanker, Pascal Auffinger, David R. Langley, Bhyravabhotla Jayaram, Matthew A. Young, and David L. Beveridge, Treatment of Counterions in Computer Simulations of DNA.

Donald B. Boyd, Appendix: Compendium of Software and Internet Tools for Computational Chemistry.

*Current address: CuraGen Corporation, 322 East Main Street, Branford, CT 06405 (Electronic mail: rjudson@curagen.com).

Volume 12

Hagai Meirovitch, Calculation of the Free Energy and the Entropy of Macromolecular Systems by Computer Simulation.

Ramzi Kutteh and **T. P. Straatsma**, Molecular Dynamics with General Holonomic Constraints and Application to Internal Coordinate Constraints.

John C. Shelley and **Daniel R. Bérard**, Computer Simulation of Water Physisorption at Metal–Water Interfaces.

Donald W. Brenner, **Olga A. Shenderova**, and **Denis A. Areshkin**, Quantum-Based Analytic Interatomic Forces and Materials Simulation.

Henry A. Kurtz and **Douglas S. Dудис**, Quantum Mechanical Methods for Predicting Nonlinear Optical Properties.

Chung F. Wong, **Tom Thacher**, and **Herschel Rabitz**, Sensitivity Analysis in Biomolecular Simulation.

Paul Verwer and **Frank J. J. Leusen**, Computer Simulation to Predict Possible Crystal Polymorphs.

Jean-Louis Rivail and **Bernard Maigret**, Computational Chemistry in France: A Historical Survey.

Volume 13

Thomas Bally and **Weston Thatcher Borden**, Calculations on Open-Shell Molecules: A Beginner’s Guide.

Neil R. Kestner and **Jaime E. Combariza**, Basis Set Superposition Errors: Theory and Practice.

James B. Anderson, Quantum Monte Carlo: Atoms, Molecules, Clusters, Liquids, and Solids.

Anders Wallqvist and **Raymond D. Mountain**, Molecular Models of Water: Derivation and Description.

James M. Briggs and **Jan Antosiewicz**, Simulation of pH-Dependent Properties of Proteins Using Mesoscopic Models.

Harold E. Helson, Structure Diagram Generation.

CHAPTER 1

The Pluses and Minuses of Mapping Atomic Charges to Electrostatic Potentials

Michelle Miller Francl and Lisa Emily Chirlian

*Bryn Mawr College, 101 North Merion Avenue, Bryn Mawr,
Pennsylvania, 19010*

INTRODUCTION

This chapter describes methods for extracting atomic charges from molecular wavefunctions. Many methods have been proposed to accomplish this, ranging from algorithms so simple that they are taught to first year chemistry students to ones so complex that they require substantial computational effort. No single model has achieved dominance, and none is appropriate to every situation. Of special interest are the methods based on fitting atomic charges to the molecular electrostatic potential (MEP). These methods are appealing since, unlike many charge models, they are based on a quantum mechanical observable. Charges derived from such methods are used widely, and the numerical methods used to derive them seem quite straightforward. Although there are many positive attributes of charges based on electrostatic potentials, there are a few negative aspects as well, most notable being that such charges seem to be peculiarly sensitive to apparently small changes in the molecular structure or in the sampling of the electrostatic potential. In fact these sensitivities are often artifacts of the fitting procedure. We examine these problems in this chapter,

Reviews in Computational Chemistry, Volume 14
Kenny B. Lipkowitz and Donald B. Boyd, Editors
Wiley-VCH, John Wiley and Sons, Inc., New York, © 2000

paying particular attention to the reliability of the numerical methods being used in the fit. Recommendations for improving the reliability of these charges are made.

WHERE ARE THE ELECTRONS?

Finding an Atom-Based Index

Continuing advances in computational power make calculations of molecular wavefunctions possible for larger and larger systems. The square of the wavefunction—the molecular electron density distribution—contains a wealth of information about properties. Unfortunately, extracting information directly that extends chemical intuition and understanding from these complex functions is generally difficult. Molecular orbital theory, by definition, spreads the electron density among many of the atoms in the molecule, thus blurring the distinctions between atoms. However, chemists, from their earliest training, treat molecules as a collection of discrete units—atoms. It is understandable then that chemists are often more comfortable assigning electrons to individual atoms so they can use their intuitive notions regarding the differences in charge between atoms in a molecule, despite knowing that boundaries between atoms do not exist in the overall charge distribution. Whereas molecular orbital theory yields a generally realistic theoretical representation of a molecule, some loss of insight is possible.

Methods are sought that allow us to regain some atomic perspective on the information provided by the electron density by recasting the overall charge distribution into atom-centered point charges. Reducing the information this way can be helpful in elucidating the reactivities of individual molecular sites as well as the overall molecular reactivity. In addition, the point atomic charges are often used to model the electrostatic component of the energy in molecular mechanics force fields, which are used to study a vast array of chemical questions.¹

The concept of atomic charge is problematic.² Unlike other properties such as dipole moments, individual charges on atoms in molecules may not be measured experimentally or determined as a quantum mechanical observable. Methods or protocols must be developed that apportion the charge to atoms in some logical and consistent manner. The concept of population analysis, proposed by Mulliken³ over 40 years ago, was the first attempt to define an atomic charge using a computed wavefunction. One major concern with this method involved the equal partitioning of the shared atomic density between two atoms with differing electronegativities. Despite this, Mulliken populations continue to be used and are routinely available in the major computational chemistry software packages such as Gaussian⁴ and Spartan.⁵

Cramer, Truhlar and their students have grouped the general methods currently being used to calculate atomic charges into four broad classes, based on the methods used to partition the electron density.⁶ One class of methods uses experimental data (class I),⁷ another directly partitions the wavefunction (class II), for example, Mulliken charges and Bader population analyses.⁸ One way to try to ensure that the resulting charges have some physical meaning is to use a quantum mechanically defined quantity as an integral part of the charge division scheme. Class III methods fit charges to some physical quantity that itself is calculated from the wavefunction. A fourth class of methods uses charges determined by one of the first three classes of methods and then attempts to improve the overall quality of the charges by fitting them to other physical observables.⁶

Because atomic charge is not a quantum mechanical observable, we must use some indirect method to calculate these values. Moreover, since we lack experimental results to guide us, other methods of validating our assignments must be devised. Accurate reproduction of some observable, whether experimentally measured (dipole moment) or determined directly from the wavefunction (electrostatic potential, molecular moments, etc.), increases our confidence in the reliability of the assigned charges.

Why Choose the Molecular Electrostatic Potential?

We focus here on class III charges fit to the molecular electrostatic potential (MEP), a widely used assessment of molecular reactivity.⁹ The MEP is a quantum mechanical observable that can be conveniently calculated from the total electron density, using either an ab initio or semiempirical wavefunction or results from density functional theory. The MEP can be written as a sum of monopole potentials centered at the atomic positions, thus enabling the contribution of each atom to be identified from the whole. MEP's appeal as a basis for charge fitting is increased by the fact that this molecular property can be extracted from crystallographic data.⁷ Atom-centered point charges that reproduce the MEP thus have a direct connection to a rigorously defined molecular property. This chapter provides a brief history of the development of methods to fit charges to electrostatic potentials and then proceeds to analyze the numerical issues that arise in attempts to implement the fitting algorithm.

The molecular electrostatic potential at a point in space \mathbf{r} can be calculated from the charge distribution using¹⁰

$$V(\mathbf{r}) = \sum_{\text{nuclei}} \frac{Z_A}{|\mathbf{r} - \mathbf{R}_A|} - \int \frac{\rho(\mathbf{r}')}{|\mathbf{r} - \mathbf{r}'|} d\mathbf{r}' \quad [1]$$

This can be written in the linear-combination-of-atomic-orbitals molecular orbital (LCAO-MO) formalism as follows

$$V(\mathbf{r}) = \sum_{\text{A}}^{\text{nuclei}} \frac{Z_{\text{A}}}{|\mathbf{r} - \mathbf{R}_{\text{A}}|} - \sum_{\mu, \nu} P_{\mu, \nu} \int \frac{\phi_{\mu}(\mathbf{r}) \phi_{\nu}(\mathbf{r}')}{|\mathbf{r} - \mathbf{r}'|} d\mathbf{r}' \quad [2]$$

where Z_{A} is the nuclear charge on atom A centered at \mathbf{R}_{A} , $P_{\mu, \nu}$ is the density matrix element connecting basis functions μ and ν , and $\phi_{\mu}(\mathbf{r})$ and $\phi_{\nu}(\mathbf{r})$ are basis functions.

Fitting the Charges

Kollman¹¹ suggested that the electron density could be partitioned into a set of monopole charges based on the electrostatic potential. At the same time, Momany showed that a set of monopole charges could be fit to the electrostatic potential.¹² Atom-centered point charges that best fit the overall MEP were determined by iterative minimization of the following function:

$$\gamma(q_1, q_2, \dots, q_n) = \sum_{i=1}^m [V(\mathbf{r}_i) - E_i(q_1, q_2, \dots, q_n)]^2 \quad [3]$$

where m is equal to the number of points in space where the MEP is calculated from the wavefunction, V_i is the value of the MEP at each point, and E_i is the electrostatic potential generated by the point charges calculated over the n atoms in the molecule by Eq. [4].

$$E_i(q_1, q_2, \dots, q_n) = \sum_{j=1}^n \frac{q_j}{|\mathbf{r}_i - \mathbf{r}_j|} \quad [4]$$

The constraint of reproducing the overall charge on the species is placed on the assignment of the point charges.

The electrostatic potential for a simple molecule, acetamide, is shown as an example. By convention, negatively charged contours correspond to regions of space in which a probe with a unit positive charge would be attracted to the molecule, and positive contours reflect repulsive regions for that positive charge. The oxygen is expected to have a negative charge because the electrostatic potential in its vicinity would be negative toward the probe; the opposite is true for the carbon (Figure 1). Atomic charges fit to the electrostatic potential should reflect these expectations. When point charges centered on the atoms are fit to this electrostatic potential, these expectations are realized. The oxygen has a charge of $-0.66 e$, and the carbon's charge is $+1.02 e$, where e is the absolute value of the charge on an electron. These results are also consonant with our intuitive notions about the polarity of the carbonyl bond.

The complete charge set is listed in Table 1, and the electrostatic potential generated from these monopoles is shown in Figure 2. A qualitative comparison

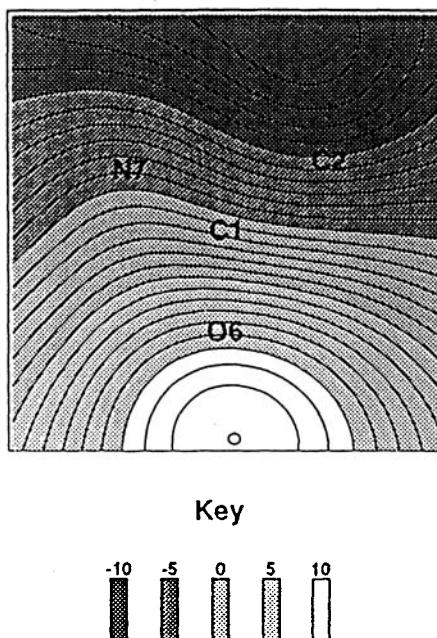


Figure 1 Contour map of the *negative* of the molecular electrostatic potential for acetamide at the HF/3–21G(*) level calculated from the full molecular wavefunction. Shading indicates approximate value of the potential in the region. Thus, the MEP near the oxygen is negative, and the MEP near the amide hydrogens (not shown) is positive. The basis set has polarization functions only on second-row atoms.

of Figures 1 and 2 shows no substantive differences, demonstrating that, in principle, point charges that reproduce the MEP of the entire molecule may be assigned to each atomic center. Figure 3 plots the difference between the MEP and the potential from the set of monopoles, giving a quantitative demonstration of the similarity. The magnitudes of the errors in this plot are typical of those seen for other molecules. As the root-mean-square (rms) deviation of the

Table 1 Net Atomic Charges for Heavy Atoms and Amide Hydrogens in Acetamide at the HF/3–21G(*) Level Calculated with the CHELP Model

Atom	Charges
C1	1.02
C2	-0.69
O6	-0.66
N7	-1.12
H8	0.45
H9	0.47

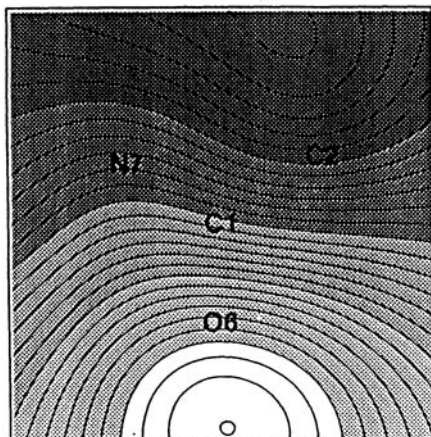
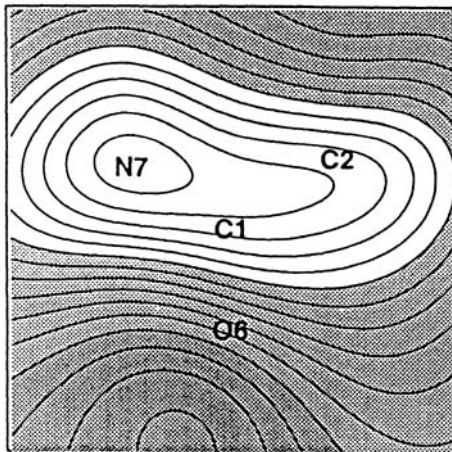


Figure 2 Contour map of the negative of the molecular electrostatic potential for acetamide at the HF/3–21G(*) level calculated using the monopole approximation and the CHELP charges. Scale same as in Figure 1.



Key



Figure 3 Contour map of the difference between the molecular electrostatic potential from the full wavefunction and that from the monopole approximation using the CHELP charges. Shading indicates approximate value of the potential in the region. Note scale change from Figures 1 and 2.

fit to the MEP improves, the magnitudes of the differences between the calculated MEP and the MEP predicted from the charges will obviously drop.

Cox and Williams¹³ showed that the problem of obtaining charges could be solved using a least squares fitting procedure, rather than an iterative method, whereas Chirlian and Franci¹⁴ introduced the use of Lagrange multipliers into the fitting scheme. The latter approach allowed the straightforward imposition of additional constraints, such as reproducing the dipole moment. The program CHELP (CHELP rhymes with “help” and stands for CHarges from Electrostatic Potentials) and methods derived from it (CHELP-SVD¹⁵ and CHELPG¹⁶) use this approach. The minimum of the function $y(q_1, q_2, \dots, q_n)$ is obtained by finding the stationary points of the function z :

$$z(q_1, q_2, \dots, q_n) = y(q_1, q_2, \dots, q_n) - \sum_{i=1}^k \lambda_i g_i(q_1, q_2, \dots, q_n) \quad [5]$$

where g_i are the set of k constraints imposed on the fit, for example,

$$g_i(q_1, q_2, \dots, q_n) = \left(\sum_{i=1}^n q_i \right) - q_{\text{tot}} = 0 \quad [6]$$

and λ_i are the associated Lagrangian multipliers. A set of $n + k$ equations in $n + k$ unknowns is generated by solving for $\partial z / \partial \lambda = 0$ and $\partial z / \partial q_i = 0$. The CHELP program uses ab initio wavefunctions, but Merz and Kollman have extended this methodology to extract charges from semiempirical calculations.¹⁷

Larger Molecules Provide Challenges

Charge assignment becomes more complicated as molecular size increases. Because the electrostatic potential is essentially a measure of the charge distribution on the surface of the molecule, it does not make physical sense to assign charges to atoms buried beneath the “molecular surface.”¹⁸ In addition, problems with the linear least-squares method used to assign the charges arise as the number of atoms increases. An inspection of the method described above seems to indicate that as long as the MEP is calculated at a number of points greater than the number of atoms, a unique set of monopoles will be generated. Because the MEP is generally sampled at hundreds or even thousands of points, the problem seems to be overdetermined. However, further investigation showed this to be untrue, especially for larger, more conformationally flexible molecules. Although point selection was first blamed for these inconsistencies, a more careful analysis demonstrated that such difficulties stem from intrinsic numerical problems with the methodology used. Specifically, the problem can be *underdetermined*. Because of the nature of the MEP, underdetermination will be

particularly acute in large molecules, and it can be further exacerbated by poor choices in the numerical approach taken to solve the least-squares equations.

WOBBLY CHARGES: THE PROBLEM OF “CONFORMATIONAL INSTABILITY”

As “routine” rather than demonstration applications of class III charges began to appear in the literature, it became apparent that, as with all models for atomic charges, there were problems with the methodology. For example, some atomic charges varied with molecular conformation in ways that were not as smooth as expected. A more troubling note was sounded when charges from the CHELP model were found to be dependent on the orientation in space of the molecule relative to the grid of points selected for the fitting of the electrostatic potential. Equally disturbing was the observation that atoms equivalent by symmetry were not always assigned equivalent charges. These difficulties were attributed to deficiencies in the distribution of points, and various schemes were proposed to produce a “better” sample. Whereas such machinations did lead to charges less susceptible to variation due to conformational changes, there were indications that the choice of point distribution was not entirely the source of the “instabilities.” Eventually these hints led to a careful reconsideration of the numerical methods underlying the fitting schemes.

The following is not intended as a comprehensive review of applications of class III charges, or even of schemes to improve such charges. Instead we focus on two subsets of papers: those that illustrate the effects of altering the sampling algorithm and those that attempt a statistical analysis of the conformational stability. The key questions to consider are: To what extent does the sampling matter? and Are variations in charge with conformation real, or are they artifacts of the overall fitting procedure? We show that much of the conformational variation is not a result of poor sampling technique, but rather of a naive numerical approach.

A Sampling of Point Distribution Schemes

Random Point Distribution

Woods et al.¹⁹ determined class III charges for two monosaccharides, β -D-fructopyranose and 6-thio- β -D-fructopyranose and two amino acids, N-acetyl-L-alanyl amide and N-acetyl-L-serinyl amide using a modified version of the CHELP algorithm. In the course of their work, they observed that CHELP assigned different charges when the electrostatic potential was computed from a wavefunction calculated using Gaussian 82²⁰ and when

GAMESS²¹ was used for obtaining the wavefunction. The authors traced the problem to the different default orientations of the molecule relative to the Cartesian axes used by the two programs. Because the point selection depended only upon the molecular orientation in space, a new scheme was devised to locate the points that would be independent of the orientation of the molecule.

The scheme proposed by Woods et al.¹⁹ selects points at random within a shell surrounding the van der Waals surface of each atom; points falling within the van der Waals radius of any other atom are discarded. A mirror of each of these points, produced by taking the negative of each of the coordinates, is added to the working set, which typically contains 1000–2000 points per atom. This selection scheme was incorporated into their PDQC (potential derived quantities charge) code, which used an algorithm similar to that of CHELP to fit charges. The fits were typically constrained to reproduce the molecular charge and dipole moment.

The effects of increasing the density and number of points in the sample set can be seen in Figure 4. As the number of points increases, the variation in the assigned PDQC charges, particularly on carbon, is substantially reduced. Note that even at very high densities, the charges do not necessarily converge; the carbon value in particular continues to exhibit large oscillations.

Table 2 compares PDQC charges based on a fit to roughly 12,000 data points per molecule to CHELP charges fit to a data set of about 250 points for two different orientations of methanol. The charges fit to the two different orientations of methanol in principle should be identical, however, neither CHELP nor PDQC assigns an identical set to both orientations. The variation as a function of orientation is generally substantially lower for the PDQC charges as compared to the CHELP assignments: for example, in methanol the mean absolute deviation between orientations is 0.012 e for PDQC, whereas it more than doubles, to 0.026 e , for CHELP. Even the lower value, however, is within the realm of what most practitioners would consider to be chemically significant, $\pm 0.01 e$, and therefore undesirable.

Note also that neither CHELP nor PDQC assigns identical charges to the two hydrogens that are equivalent by symmetry. The differences are small, on the order of 0.001 e , but nonnegligible. This effect, which had been noted previously in fitting multipoles to potentials,²² was treated by aligning the major symmetry axis of the molecule with one of the Cartesian axes, a measure that obscures, but does not fix, the problem.

In all cases, the variability for the PDQC charges in Table 2 is highest for the central carbon atom. As Woods et al.¹⁹ note, the exposure of the van der Waals surface of the methanol carbon atom is quite limited. As a result, the electrostatic potential will be more sparsely sampled in this region and perhaps therefore will not be as well described by the final parameters. Classical electrostatics is likely playing a role here as well. Classically, all the charge on a charged object is found on the surface of the object. Because class III charge

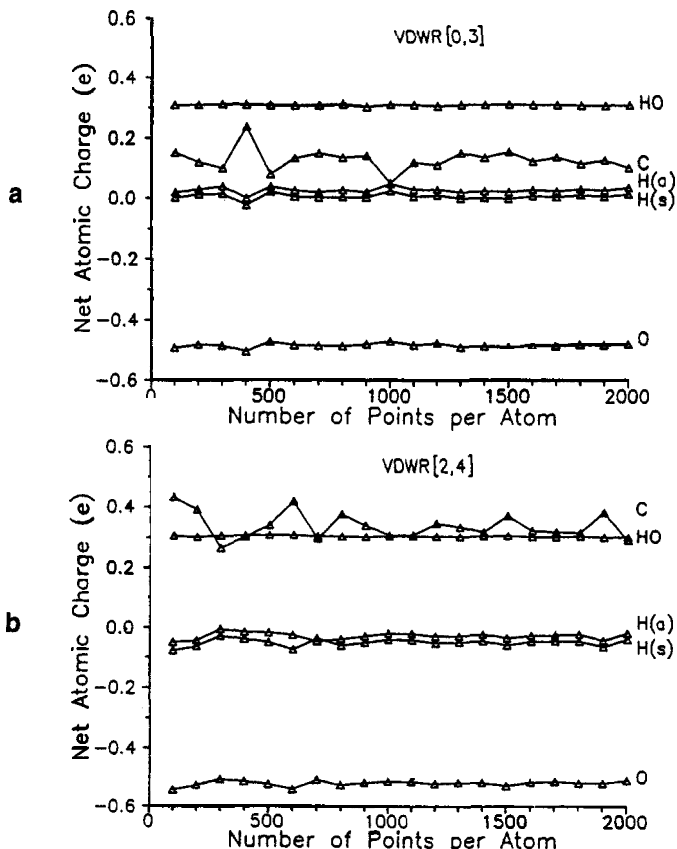


Figure 4 Dependence of net atomic charges on the number of points per atom. Data shown are for methanol. Hydrogens are labeled as follows: HO, hydroxyl hydrogen; H(a), methyl hydrogen anti to hydroxyl group; H(s), methyl hydrogen syn to hydroxyl group. (a) All points are located between the van der Waals surface and a surface drawn 3 Å from the van der Waals surface. (b) All points are located between a surface 2 Å from the van der Waals surface and a surface drawn 4 Å from the van der Waals surface. [From Figure 1 of Ref. 18 (Copyright © 1990 John Wiley & Sons. Reprinted by permission of John Wiley & Sons, Inc.).]

models are viewing the molecule *from the outside* as a collection of point charges distributed in space, it is not unreasonable that the charge should “migrate” to the surface of the molecule. In other words, these models will be biased toward assigning charges to exposed atoms, and we will see later that this is a general phenomenon in such charge models irrespective of sampling bias.

Woods et al. concluded that to prevent or reduce the dependence of the assigned charged on orientation, the electrostatic potential should be sampled

Table 2 Net Atomic Charges for CH₃OH at the HF/6–31G** Level Calculated Using PDQC and CHELP Models for Different Spatial Orientations^{a,b}

Atom	PDQC		CHELP	
	Standard	Rotated	Standard	Rotated
C	0.182	0.148	0.236	0.302
O	-0.657	-0.652	-0.652	-0.689
H (O)	0.415	0.416	0.407	0.419
H (anti)	0.061	0.070	0.042	0.036
H (syn)	0.000	0.008	-0.017	-0.034
H' (syn)	-0.001	0.010	-0.017	-0.035

^aData from Ref. 19.^bStandard orientation is the default orientation from GAMESS; in the rotated orientation the molecule has been rotated 10° about each of the three axes.

at a large number of points (1500–2500 per atom). They also presumed that the random point choice improved the symmetry of the charges, although this is difficult to assess from the data presented in their paper.¹⁹ It is critical to note that even though the electrostatic potential is being sampled with a very large numbers of points, the derived charges are sensitive to the orientation and do not always reflect the symmetry of the molecule. Thus, the density of sampling is not the only source of variability in these charges.

Grid Sampling

Breneman and Wiberg¹⁶ used class III charges to examine the changes in charge distribution in formamide as a function of the conformation. The authors noted that the charges from CHELP did not vary smoothly as the conformation was varied about the carbon–nitrogen bond. In accord with the work described in the preceding discussion, they recognized the sensitivity of CHELP charges toward reorientation of the molecule. Once again the difficulties were attributed to the choice of sampling algorithm for the electrostatic potential. Breneman and Wiberg then produced a modified version of CHELP, CHELPG, which uses a regular cubic grid and an increased density of sample points.

When sampling densities comparable to those of CHELP are used, CHELPG charges are less sensitive to changes in orientation, suggesting that the use of a uniform grid offers some advantage over a grid that maps onto the van der Waals surface of the molecule. For example, the standard deviation of the mean charge on nitrogen in formamide for seven different orientations is 0.0177 *e* for CHELP versus only 0.0089 *e* for CHELPG.¹⁶ Differences between the average charges assigned by the two different models are statistically significant.

Again with CHELPG, increasing both the density and number of points sampled appears to reduce the variation in charge with changing orientation. It is difficult to make direct comparisons between CHELP and CHELPG from

that paper¹⁶ because the former calculation used roughly half the number of fitting points as the latter, and each used a different sampling algorithm. For example, when the number of points is doubled in CHELPG, the density of sampled points roughly doubles because CHELPG places additional points between existing points. In contrast, increasing the number of points in CHELP, where points are sampled on a series of surfaces or “shells” around the molecule, the additional points are selected on shells that lie farther from the molecular center. Reducing the spacing between these shells compensates to some extent for this change in the sampling region relative to CHELPG, but the increase in point density is not smooth. Increasing the number of points in CHELP by a factor of 10 generally, though not always, results in less variation in charge as a function of orientation. The standard deviation on the nitrogen charge for seven different orientations of formamide is 0.0177 e when a sparse sample is used, compared to 0.0066 e when the electrostatic potential is more densely sampled. The effect on charge sensitivity of increasing the sampling density in CHELPG is more consistent, increasing the point density by a factor of 20 leads to a reduction in the standard deviation of the charges for a set of molecular orientations of about 20%.

Figure 5 shows the variation in CHELP and CHELPG charges as a function of conformation about the carbon–nitrogen bond in formamide. The

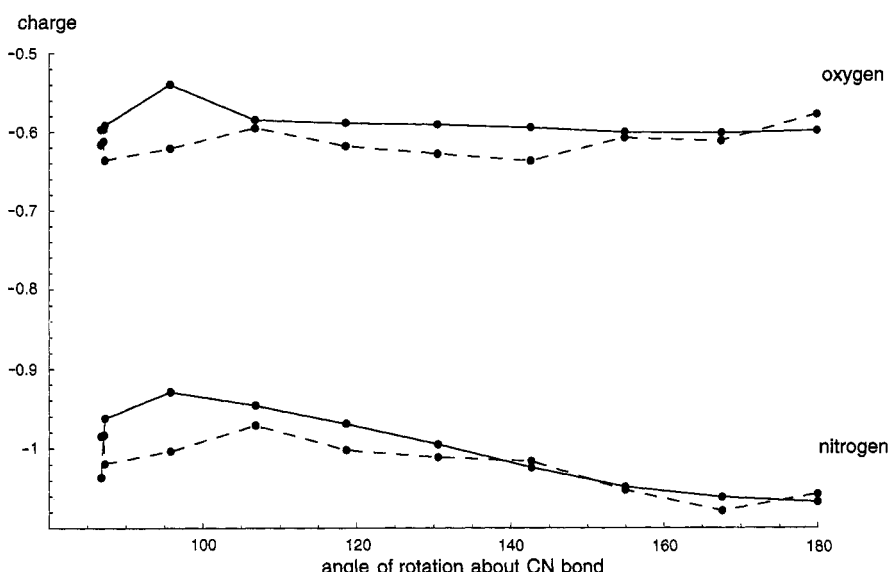


Figure 5 Comparison of CHELP (dashed line) and CHELPG (solid line) nitrogen and oxygen charges for various conformers of formamide. (Data from Ref. 16.)

CHELPG charges vary somewhat more smoothly with dihedral angle than do the CHELP charges, but both show similar trends.

It is clear from the work of both Woods et al. and Breneman and Wiberg that fitting to a large number of points reduces, though does not completely eliminate, the sensitivity of these charges to changes in orientation. It is important to note that the problem with symmetry remains, however. For example, the charges assigned to the symmetry equivalent amino protons in the syn transition state by CHELPG differ, on average, by 0.0002 e . This does not represent any improvement over CHELP (with a sparse sampling algorithm), where the average deviation is only half that, 0.0001 e . Yet another indication of the unstable nature of the assigned charges is that the charge values for the standard orientation of the syn transition state reported in the two different sections of the Breneman paper also differ on average by nearly 0.001 e . Though not significant with respect to the conclusions drawn in this paper, the discrepancy underscores the realization that the source of difficulty with these methods does not lie in the density and distribution of sampling points for the electrostatic potential alone.

Variation with Conformation: How Much Is Too Much?

In the best of all molecular modeling worlds, one could hope that the atomic charges, of whatever type, for one conformation of a molecule could be used to model the entire conformational space. Barring such good fortune, one instead might wish that the variation in charge with conformation would be systematic and predictable. The ramifications of the conformationally dependent atomic charges, in particular with respect to force field construction, has been examined by various groups over the last decade.^{23–28}

It is clear in many instances that charges do depend on conformation to such an extent that a single set cannot do justice to the entire conformational space. For example, Jorgensen and Gao noted that two different sets of charges must be used if the optimized potential for liquid simulation (OPLS) is to adequately reflect the hydration free energy of N-methylacetamide.²³ In a subsequent study of this system using class III charges, Cieplak and Kollman²⁴ came to a similar conclusion. Williams²⁵ showed that using a composite set of charges to describe the electrostatic potentials of various conformations of alanyl dipeptide results in a 7.4% relative rms error, which is two to four times the error found when the charges for the individual conformations were used. A study of the head group in glycerylphosphorylcholine (GPC) by Stouch and Williams²⁶ revealed that some charges varied between conformations by as much as 1.3 e (see Figure 6). Urban and Famini,²⁷ using CHELPG, also demonstrated a high degree of variation in charge for a series of six dopamine conformations.

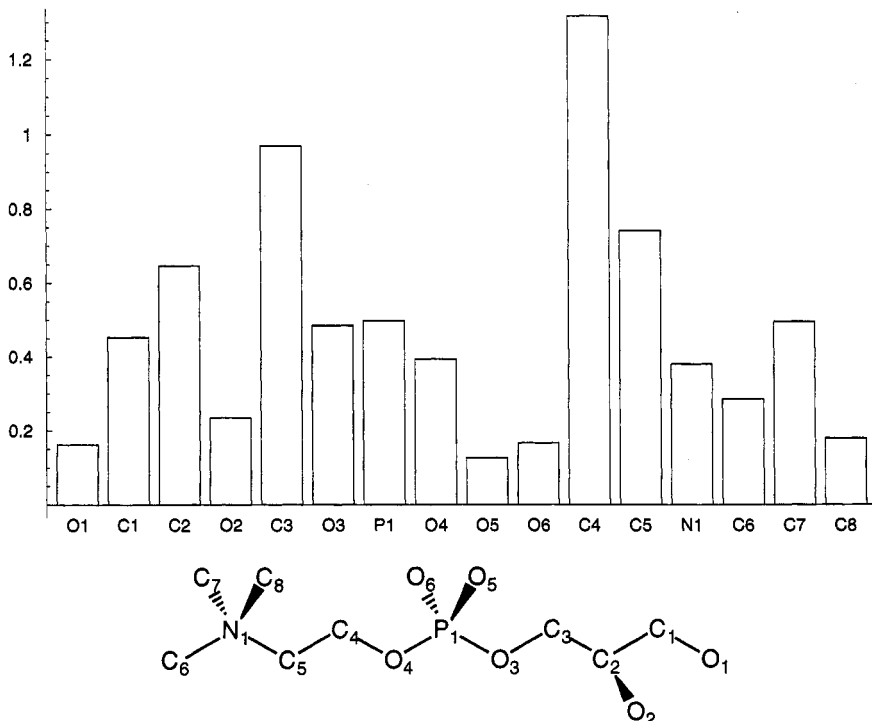


Figure 6 Magnitude of the range of class III charges in glycerylphosphorylcholine. In the accompanying atom numbering scheme, hydrogens have been omitted for clarity. (Data from Ref. 26.)

From these studies, it is not so evident that the charge variability is a function of the conformation alone. Common chemical sense suggests that for most conformational variations, corresponding changes in the atomic charge should not be on the order of a full unit unless some substantial change in the electronic wavefunction has taken place (e.g., rotation around a double bond or partial double bond); yet such changes are routinely observed. Since charge is not a quantum mechanical observable, and assuming chemical intuition is always consistent with quantum mechanics, it could be argued that chemical intuition does not apply. Because these swings in charge are generally not accompanied by similarly substantive changes in the molecular electrostatic potential, which is an observable, the swings raise the issue that these variations are artifacts of the monopole parameterization of the electrostatic potential.

As an example of the disconnect between swings in charge and values of the electrostatic potential, a comparison of the molecular electrostatic potential for two different conformations of glycerylphosphorylcholine²⁶ in the vicinity of C5 (see Figure 6 for numbering scheme) shows that although the charges for

C5 for the two conformers are -0.082 e and -0.539 e , respectively, the electrostatic potential maps are qualitatively indistinguishable. Charges on neighboring atoms N1 and C4 also vary substantially, -0.106 e to $+0.173\text{ e}$ and $+0.444\text{ e}$ to -0.068 e , respectively.

Statistical Correlations

Since atomic charge is not a quantum mechanical observable, error in charges cannot be assessed by simply comparing calculated values to experiment. Alternative means for defining the error must be sought. The error in class III charges had typically been based on the error in the reproduction of various measurable global properties, such as the dipole moment or molecular electrostatic potential. Error in individual charges were generally estimated using the range of values assigned for various conformations or for symmetry-equivalent atoms. Using the latter concept, Stouch and Williams²⁶ offered an estimate for the *minimum* error in a charge value of about 10% for the large molecules they consider. In a similar fashion, one can get estimates ranging from 0.1% (using data from Breneman and Wiberg's study¹⁶) to 3% (based on Woods et al.¹⁹) for smaller molecules.

Recognizing that variations in class III atomic charges with conformation were not solely a function of either basis set selection or the choice of sampling algorithm, Stouch and Williams assessed the fitting procedure itself.²⁸ In their earlier study of glycerylphosphorylcholine,²⁶ the authors had noted that the charges, particularly on neighboring atoms, were highly correlated with each other. They used a principal components analysis of the least-squares variance-covariance matrices to quantitatively assess the correlation. Whereas naively it would seem that the fitting problem posed here is overdetermined (the size of the data set far exceeds the number of parameters to be fit), Stouch and Williams showed that fewer than 15 of the 36 possible atomic point charges were required to reproduce the electrostatic potential data in glycerylphosphorylcholine. Hence the *effective* dimensionality of the problem is much smaller than its apparent dimensionality. When the size of the problem is reduced, for example, by constraining all the carbon atoms to a charge of 0.2 e , the variability of the remaining charges also decreases (see Figure 7). It should be noted that reducing the dimensionality this way from 36 to 28 did not substantially affect the quality of the fit to the electrostatic potential; the rms deviation for the full fit is 1.4% compared to 2% for the reduced problem. Stouch and Williams offered various schemes for reducing the effective dimensionality of the problem, including fixing the atomic charges for a subset of the molecule to specific values, e.g., chemically "intuitive" values or simply to zero.

Although sampling bias and density do affect the quality of atomic charges fit to MEP, they are not the only factors that must be considered. In the work of Woods et al. and that of Wiberg and Breneman, there are hints of more fundamental numerical problems. Indeed, Stouch and Williams show unequivocally that numerical problems contribute to the sensitivity of the charges to

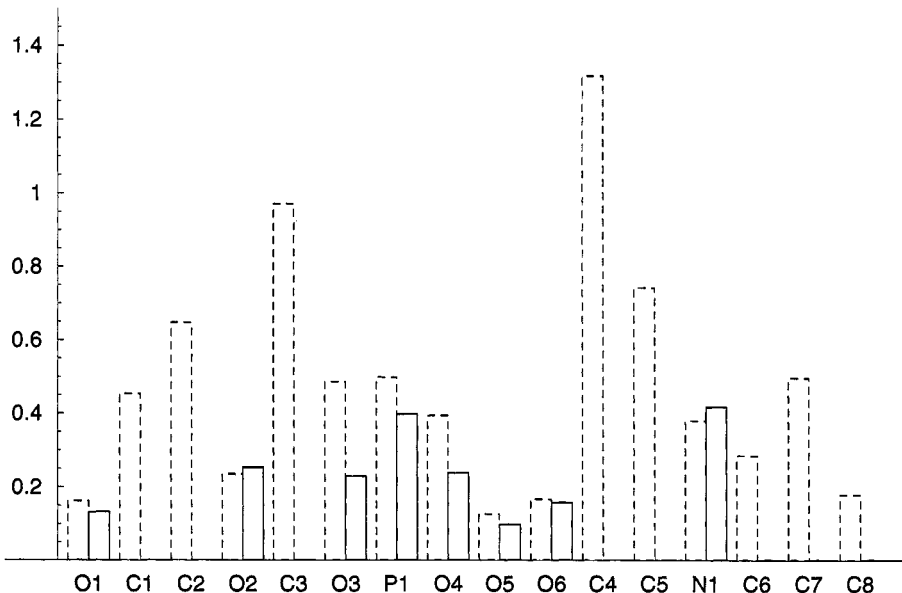


Figure 7 Range of class III charges in glycerylphosphorylcholine. Dashed bars are for a fit to the full set of atoms, and solid bars are for a fit when all carbon atoms have been set to a fixed value of 0.2 e . For atom numbering scheme, see Figure 6. (Data from Ref. 28.)

conformational changes. Before examining this point in more detail, a closer look at the numerical methods being used is in order.

GETTING TO THE ROOT OF THE PROBLEM

Given a system of N linear equations in n unknowns, one generally assumes that as long as N exceeds n , an approximation to the solution set may be found by searching for a set of n parameters that lead to the least error in the N equations. The method of linear least squares (LLS)²⁹ is commonly employed in these situations and will, in most cases, generate a solution. It is critical to be aware that the existence of a solution does not imply anything about either the quality or the uniqueness of the solution. In particular, there is no guarantee that all n parameters can be determined.

As the speck in another's eye is usually much easier to find than the plank in one's own, consider the following somewhat prosaic example from engineering. Suppose the height range through which a suspension bridge will oscillate is postulated in the following model:

$$\text{flex} = (P_1 \times \text{length}) + (P_2 \times \text{width}) + (P_3 \times \text{windspeed}) \\ + (P_4 \times \text{wavelength of maximum absorbance of paint color}) \quad [7]$$

A series of $N > 4$ measurements are made, and suppose a solution for \mathbf{P} is found using a linear least-square fit, $\mathbf{P} = \{1.527, 3.264, 10.578, 0.492\}$. The results suggest that wind speed is the most critical factor because its coefficient is largest, whereas bridge color is least important, as indicated by its small coefficient. The question that comes immediately to mind is, Does it matter at all what color the bridge is? This is, in essence, the same question that surfaced in the work of Stouch and Williams: For glycerylphosphorylcholine, does it matter what the charge on carbon is? The answer, as we shall see, is that even though chemists may *care* what the charge is, it may not “matter” to the fit. That is, the charge may not be determinable by a linear least-squares fit to the electrostatic potential.

In the following section, we give a brief mathematical overview of the LLS problem, considering in particular situations in which not all the parameters can be adequately determined. Far more detail is available in the numerical methods literature, and the interested reader is urged to consult it.²⁹

A Closer Look at the Linear Least Squares Problem

Rank Deficiency

The LLS problem can be conveniently formulated as follows:

$$\begin{pmatrix} A_{11} & \cdots & \\ \vdots & & \\ & \ddots & \\ & & A_{mn} \end{pmatrix}_{m \times n} \begin{pmatrix} x_1 \\ \vdots \\ x_n \end{pmatrix}_{n \times 1} \approx \begin{pmatrix} b_1 \\ \vdots \\ b_m \end{pmatrix}_{m \times 1} \quad \text{or } \mathbf{Ax} \approx \mathbf{b} \quad [8]$$

The list of parameters \mathbf{x} is found by minimizing the Euclidean norm $\|\mathbf{Ax} - \mathbf{b}\|_2$. Finding \mathbf{x} is straightforward; assessing its validity less so. Consider the case of an LLS matrix \mathbf{A} that is rank deficient. In other words, the dimension of the space spanned by the row and column vectors is less than n . The principal consequence of a rank-deficient LLS \mathbf{A} matrix is the reduction in the number of parameters that may be used to describe the data vector \mathbf{b} .

Rank deficiency in LLS can be difficult to catch and problematic to deal with once detected. Signatures of rank deficiency include sensitivity of solutions to changes in the numerical accuracy of the data vector, to changes in the computing device, or to small alterations in the data set. The rank deficiency can be a result of poor data such that some columns of \mathbf{A} are linearly related to one another or can result from other factors, such as noise.

Singular Value Decomposition

The singular value decomposition (SVD) of the LLS matrix \mathbf{A} can be used to both detect and remedy rank deficiency. The SVD writes the matrix \mathbf{A} as

$$\mathbf{A} = \mathbf{U}\mathbf{S}\mathbf{V}^T \quad [9]$$

where \mathbf{U} and \mathbf{V} are orthogonal matrices, for example,

$$\sum_i U_{ki} U_{in} = \delta_{kn} \quad [10]$$

\mathbf{S} is a diagonal matrix with elements $\{s_1, s_2, \dots, s_n\}$, and the superscript T indicates transpose of the matrix. The diagonal elements of \mathbf{S} , or singular values, are positive and nonincreasing. For example, consider the matrix \mathbf{A}

$$\begin{pmatrix} 3 & 4 & 1 \\ 7 & 4.0011 & -3 \\ 2 & 5 & 3 \\ -1 & 4 & 5 \end{pmatrix}$$

which can be decomposed as follows:

$$\begin{pmatrix} -0.4732 & 0.0441 & 0.6462 \\ -0.6540 & -0.617526 & -0.4369 \\ -0.5125 & 0.3445 & 0.2802 \\ -0.2925 & 0.7057 & -0.5995 \end{pmatrix} \begin{pmatrix} 10.75 & 0 & 0 \\ 0 & 8.03 & 0 \\ 0 & 0 & 0.0002775 \end{pmatrix} \begin{pmatrix} -0.6262 & -0.7669 & -0.1406 \\ -0.5239 & 0.2803 & 0.8043 \\ 0.5774 & -0.5773 & 0.5773 \end{pmatrix}$$

Whereas there are many ways to orthogonally decompose \mathbf{A} , the SVD is particularly suited to assessing the sensitivity of the solutions vector, \mathbf{x} , toward changes in the data set. Consider a slight perturbation of the original LLS problem

$$(\mathbf{A} + \varepsilon)\mathbf{y} \cong (\mathbf{b} + \varepsilon) \quad [11]$$

Take the perturbation, ε , to be positive and less than the smallest singular value of \mathbf{A} , s_n . How different is the solution to the perturbed problem, \mathbf{y} , from the original solution \mathbf{x} ? Taking the distance between the two solutions to be $\|\mathbf{y} - \mathbf{x}\|_2$, or the Euclidean length of the vector difference $\mathbf{y} - \mathbf{x}$

$$\|\mathbf{y} - \mathbf{x}\|_2 = \sqrt{(\mathbf{y} - \mathbf{x}) \cdot (\mathbf{y} - \mathbf{x})} = \sqrt{\sum_i (y_i - x_i)^2}$$

It can be shown³⁰ that $\|\mathbf{y} - \mathbf{x}\|_2$ is limited as follows

$$\|\mathbf{y} - \mathbf{x}\|_2 \geq \frac{\varepsilon}{s_n} \|\mathbf{x}\|_2 \frac{|\mathbf{U}_n^T \mathbf{b}|}{\|\mathbf{b}\|_2} \quad [12]$$

where U_n^T are column vectors of U^T . Note that changes to the data set on the order of ε lead to changes in the solution vector on the order of ε/s_k for the k th data value. Obviously when the diagonal matrix element s_n is very small, the solution to the perturbed problem can be quite different from that of the original. The singular values can be used to further quantify the sensitivity of the solution vector to small changes in the data set. Let us define the condition number, κ as

$$\kappa(A) = \|A\| \|A^{-1}\| \quad [13]$$

where A^{-1} is the Moore–Penrose inverse or pseudoinverse.³¹ If we base κ on the Euclidean norm, it can be expressed in terms of the singular values

$$\kappa_2(A) = \|A\|_2 \|A^{-1}\|_2 \quad [14]$$

$$= \frac{s_1}{s_n} \quad [15]$$

Here s_1 is the largest singular value. The error in the solution vector is κ times the error in the data. A so-called well-conditioned data set has $\kappa = 1$, indicating all the singular values are of similar magnitude. Although it is difficult to give universal guidelines for deciding whether any given LLS matrix is well conditioned, an arbitrary starting point would be to consider a matrix to be well conditioned if κ were less than 1000.

Once an LLS matrix has been identified as poorly conditioned, what are the implications, and what can be done to improve the conditioning if that appears to be desirable? The solution to a least-squares problem obtained from a poorly conditioned LLS matrix is, in a word, unreliable. Some components of the solution may be artifacts, and not part of a realistic description of the problem at hand. Reducing the rank of the matrix generally improves its conditioning, and hence the reliability of the solution. However, arriving at an estimate for the actual rank of A and deciding how to reduce the data set such that A becomes full rank are nontrivial problems.

Reducing the Rank

The sensitivity of the solution vector, the charges, can be curtailed by reducing the rank of the problem. Deciding which subset of parameters should be retained is not trivial. Consider the following LLS problem:

$$\begin{pmatrix} 3 & 4 & 1 \\ 7 & 4 & -3 \\ 2 & 5 & 3 \\ -1 & 4 & 5 \end{pmatrix} \begin{pmatrix} x_1 \\ x_2 \\ x_3 \end{pmatrix} = \begin{pmatrix} 1 \\ 1 \\ 1 \\ 1 \end{pmatrix}$$

A least-squares solution yields $\mathbf{x} = \{0.00815, 0.1545, 0.0730\}$, where the rms deviation of the predicted values from the measured values (the residual 2-norm) is 0.1966. Computing the singular values to check the stability of the solution, we find $\mathbf{s} = \{10.75, 8.030, 0.0\}$. The condition number of the matrix as it stands is ∞ (i.e., $10.75/0.0$). Shrinking the matrix by one column (appropriately chosen) will reduce the condition number to $10.75/8.030$, quite close to 1. Thus, while the apparent rank of the LLS matrix is 3, a better estimate of the rank is only 2. Which of the three parameters should be ignored? One line of reasoning might lead us to ignore the smallest value, essentially removing the third column of data. Another choice would be to delete the middle parameter because it differs the most from the other two. Neither of these lines of reasoning guarantees that the new fit will be any less sensitive. Such a trial-and-error approach, like that used by Stouch and Williams,²⁸ is most convenient for extremely small problems. A more methodical approach is appropriate to larger systems.

Many numerical algorithms exist for selecting subsets. One such algorithm, developed by Golub, Klema, and Stewart,³² is designed to preserve, as much as possible, the residual norm. In other words, the reproduction of the true electrostatic potential by the monopole potential should remain unaffected by the change in problem. We feel this scheme is more likely than some of the others to give good dipole moments and good reproduction of the molecular electrostatic potential. One can also consider intuitive methods for reducing the rank, including selecting those atoms important to the investigator, selecting only heavy atoms, ignoring buried atoms, or, as Stouch and Williams suggest,²⁸ eliminating atoms with highly variable charges.

The new subset is selected by first computing the SVD of the least squares matrix \mathbf{A} . A rank estimate, \tilde{r} , is obtained by first determining the condition number of the matrix from the singular values and then deciding upon the number of parameters that must be eliminated to reduce κ to an acceptable value. The QR scheme with column pivoting is then applied to \mathbf{V}^T

$$\mathbf{Q}^T \mathbf{V}^T \mathbf{P} = \begin{pmatrix} \mathbf{R}_1 & 0 \\ 0 & \mathbf{R}_2 \end{pmatrix} \quad \text{where } \mathbf{R}_1 \in \Re^{\tilde{r} \times \tilde{r}} \text{ (i.e., is an } \tilde{r} \times \tilde{r} \text{ matrix with real elements) and } \mathbf{R}_2 \in \Re^{(N-\tilde{r}) \times (N-\tilde{r})} \quad [16]$$

to generate a diagonal permutation matrix \mathbf{P} , which can be used to reorder the data in \mathbf{A} such that the first \tilde{r} parameters in \mathbf{A} correspond to the “best” subset, which will be refit to the data in \mathbf{A} .

$$\mathbf{A}\mathbf{P} = \begin{pmatrix} \mathbf{B}_1 & 0 \\ 0 & \mathbf{B}_2 \end{pmatrix} \quad \text{where } \mathbf{B}_1 \in \Re^{m \times \tilde{r}} \text{ and } \mathbf{B}_2 \in \Re^{m \times (N-\tilde{r})} \quad [17]$$

\mathbf{B}_1 now contains the data needed to fit a new, smaller, set of charges that will still satisfy the original least squares conditions, but should be more stable. The new set of charges $\{q\}$ can be obtained by minimizing

$$\|\mathbf{B}_1^{m \times \tilde{r}} \mathbf{q}^{\tilde{r}} - \hat{\mathbf{V}}^m\| \quad [18]$$

subject to the constraints of the original problem.

Applying this algorithm to our sample problem is revealing. The permutation matrix is found to be

$$\mathbf{P} = \begin{pmatrix} 0 & 1 & 0 \\ 1 & 0 & 0 \\ 0 & 0 & 1 \end{pmatrix}$$

Extracting the first \tilde{r} columns of \mathbf{A} using \mathbf{P} , we write

$$\mathbf{AP} = \begin{pmatrix} 3 & 4 & 1 \\ 7 & 4 & -3 \\ 2 & 5 & 3 \\ -1 & 4 & 5 \end{pmatrix} \begin{pmatrix} 1 & 0 & 0 \\ 0 & 0 & 1 \\ 0 & 1 & 0 \end{pmatrix} = \left(\begin{array}{cc|c} 3 & 1 & 4 \\ 7 & -3 & 4 \\ 2 & 3 & 5 \\ -1 & 5 & 4 \end{array} \right)$$

Now the reduced problem becomes

$$\begin{pmatrix} 3 & 1 \\ 7 & -3 \\ 2 & 3 \\ -1 & 5 \end{pmatrix} \begin{pmatrix} x_1 \\ x_3 \end{pmatrix} \cong \begin{pmatrix} 1 \\ 1 \\ 1 \\ 1 \end{pmatrix}$$

which has the solution $\mathbf{x} = \{0.2360, 0.2275\}$ with a residual norm of 0.1966. Note that the second parameter, the largest of the three, was discarded and that the solution for the other two parameters is quite different from the original.

The key, for our purposes, is that the second, limited solution is more stable than the original. The second problem is less sensitive to changes in the data used. When one data point is eliminated, the solution vector to the rank reduced problem differs, on average, by 5% from the fit obtained using all the data. In contrast, the variability is higher for the original problem, ranging from 5 to 15%. Interestingly, the sensitivity to data choice is highest for the third parameter, not the second. Solutions for the second parameter differ by about 5% from the full solution, whereas the variation is roughly 15% for the third parameter. Eliminating the parameters with the highest variability will not necessarily improve the stability of the fit!

Applying Golub's algorithm²⁹ to the specific case of fitting atomic charges to the electrostatic potential, we find that while the set of charges must generally be reduced, the manner in which charges are selected is not critical. If there are n atoms and the rank of the LLS matrix is determined to be \tilde{r} , the algorithm generally selects the first $(n - \tilde{r})$ atoms to use in the fit, as long as the atoms are distributed evenly in space. Selecting all the atoms on one side of the molecule, not surprisingly, leads to a degradation in the residual norm. In fact, any $(n - \tilde{r})$ well-distributed atomic sites would probably do as well. Such a set would not

necessarily have a chemical meaning, though sets including points to represent lone pairs have been constructed. Thus the investigator is free to select a subset of atoms that suit the problem at hand as long as the dimension of the set is roughly the rank estimate obtained from the SVD and the atoms are distributed evenly across the molecule.

Linear Least-Squares Fit to the Molecular Electrostatic Potential

Rank deficiency should be an obvious consideration for class III atomic charges. The sensitivity of the fit to small changes in the data sample (e.g., changes in molecular orientation, conformation, or sampling algorithm) is highly suggestive of a rank-deficient problem. The consequence of a rank-deficient LLS matrix in this problem is the inability to determine atomic charges for all nuclear centers on a molecule. Table 3 shows the rank of the CHELP LLS matrix for a number of molecules. The rank estimates were obtained using an SVD of the CHELP LLS matrix. The rank of the matrix was taken to be the number of singular values for which the ratio s_k/s_1 does not exceed 10^{-4} (recall that s_1 is the largest singular value); that is, LLS matrices with condition numbers greater than 10^4 were considered poorly conditioned. This corresponds to a “noise” level in the molecular electrostatic potential on the order of 10^{-7} hartree. The results clearly show that, particularly for larger molecules, the matrices are generally ill conditioned. For example, the rank estimate suggest that only 25 of 36 charges can be obtained by a fit to the electrostatic potential in glycerylphosphorylcholine. Stouch and Williams,²⁸ as discussed above, noted a significant decrease in the sensitivity of the solution vector when the carbon charges were disregarded, reducing the number of charges extracted from 36 to 28.

The problem of rank deficiency is particularly acute for larger molecules, as one might expect considering classical electrostatic models. Classically, all

Table 3 SVD Rank Estimates for CHELP LLS^a

Molecule	Full Rank ^b	SVD Rank Estimate
Formamide	6	5
Acetamide	9	8
Dimethylphosphate	13	10
Phenol	13	10
L-Cysteine	14	11
tert-Butoxide	14	11
Neopentane	17	13
Alanine dipeptide	23	16
Glycerylphosphorylcholine	36	25

^aFits are to HF/3-21G(*) electrostatic potential calculated at 1000 points in a shell between 1.0 and 3.0 times the van der Waals surface of the molecule. The rank estimate is taken as the number of singular values for which the ratio s_k to s_1 does not exceed 10^{-4} .

^bNumber of atoms.

the charge on an object is located on the surface of the object. The electrostatic potential calculated outside the molecular van der Waals surface will tend to reflect this proclivity. To a first approximation, the percentage of assignable charges should fall off as $r^{-1/3}$. This $r^{-1/3}$ dependence assumes that the molecules are spheres, where the volume of the sphere is proportional to the total number of atoms, and the number of exterior charges is proportional to the surface area of the molecular sphere. This curve, where the constants of proportionality were determined by best fit to the data plotted, is shown superimposed on the data in Figure 8 and describes well the decrease in the percentage of assignable charges.

Contrary to popular wisdom, more is not necessarily better. It is interesting to note (Table 4) that increasing the sampling density does not always result in an increase in the rank of the LLS problem. When the density of points is increased from a sparse sample (100 points), the rank may increase slightly, but further increases do not lead to increases in the rank. In fact, in many instances the rank actually decreases as the sample size gets much beyond 1000 points.

As Woods et al.¹⁹ noted, the quality of the fit can be improved by including points within the van der Waals envelope of the molecule. As the data in Figure 9 indicate, when points at roughly one half the van der Waals radius are included, the rank increases significantly. The price paid for this, however, is a decline in the ability of the overall fit to reproduce the electrostatic potential,

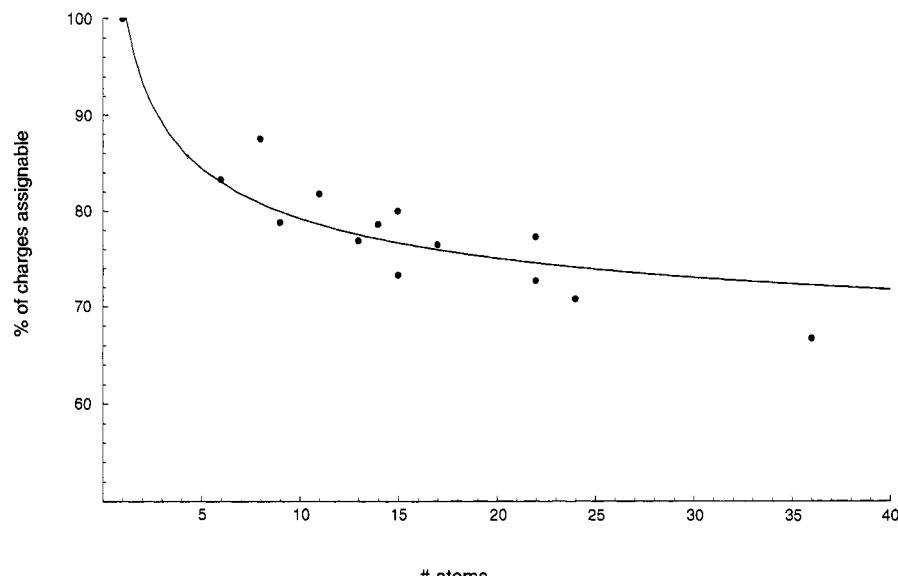


Figure 8 Percentage of charges that can be assigned as a function of the total number of atoms in the molecule. Data from CHELP linear least-squares (LLS) fits at the HF/3-21G(*) level using a sample of 1000 points.

Table 4 SVD Rank Estimates for CHELP LLS as a Function of Sample Size^a

Molecule	Sample Size		
	100	1000	10,000
Acetamide	7	7	6
Dimethylphosphate	10	10	9
Phenol	10	10	9
L-Cysteine	10	11	10
tert-Butoxide	10	11	10
Neopentane	12	12	12
Alanine dipeptide (7 α)	16	16	16
Glycerylphosphorylcholine	21	24	23

^aFits are to HF/3–21G(*) electrostatic potential calculated in a shell between 1.0 and 3.0 times the van der Waals surface of the molecule. The rank estimate is taken as the number of singular values for which the ratio s_k to s_1 does not exceed 10^{-4} .

because the monopole approximation at the root of the class III model is invalid close to the nuclei. One must then determine whether the cure is worse than the disease!

Kollman and coworkers³³ take an alternative tack to reducing the effective size of the problem. Rather than eliminating atoms from the fit, essentially reducing the value of their charge to zero, the authors' RESP method produced a problem of lower rank by imposing symmetry constraints when available. The RESP approach also incorporates a hyperbolic penalty function into the fit.

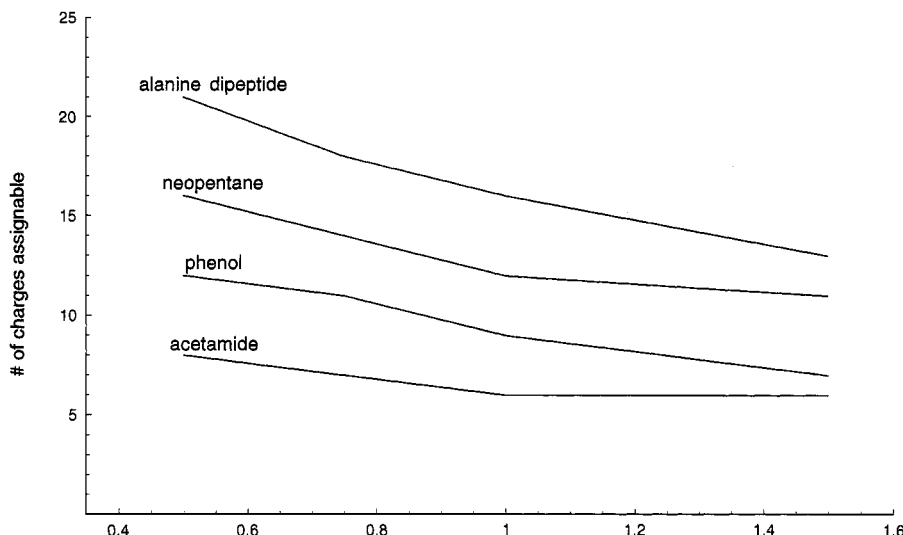


Figure 9 Rank estimates for LLS fits for alanine dipeptide, neopentane, phenol, and acetamide as a function of the size of the sampling envelope. Data from CHELP LLS fits at the HF/3–21G(*) level using a sample of 1000 points.

Smaller Is Better—Most of the Time

One of the recognized failures of CHELP and related methods has been that it can assign very different charges to atoms that are equivalent by symmetry. Common wisdom attributes this to a low density of points and/or the asymmetry of the points sampled for the fit. It is not necessarily due to either factor, but can be a result of attempts to fit more charges than one has adequate data to assign. Consider the symmetry equivalent carbon atoms C₆ and C₇ in dimethylphosphate (Figure 10). CHELP charges differ by almost 0.2 e. The difference in the CHELP charges on the two oxygens equivalent by symmetry (O₃ and O₅) is smaller, but still significant, -0.75 e compared to -0.70 e. On the other hand, CHELP assigns nearly equal charges to the two nonequivalent oxygens (O₁ and O₄)! When a reduced set of seven charges (O₁, P₂, O₃, O₄, O₅, C₆, C₇) is used in place of the full set of 13, the fit yields identical or nearly identical charges ($\Delta q = 0.01$ e) on both the C₆/C₇ and O₃/O₅ pairs, while assigning distinctly different charges to the nonequivalent set of O₁/O₄. The ability of the fit to reproduce the electrostatic potential is unaffected; the rms deviation for the reduced set is 1.78 kcal/mol, compared to 1.61 for the full fit.

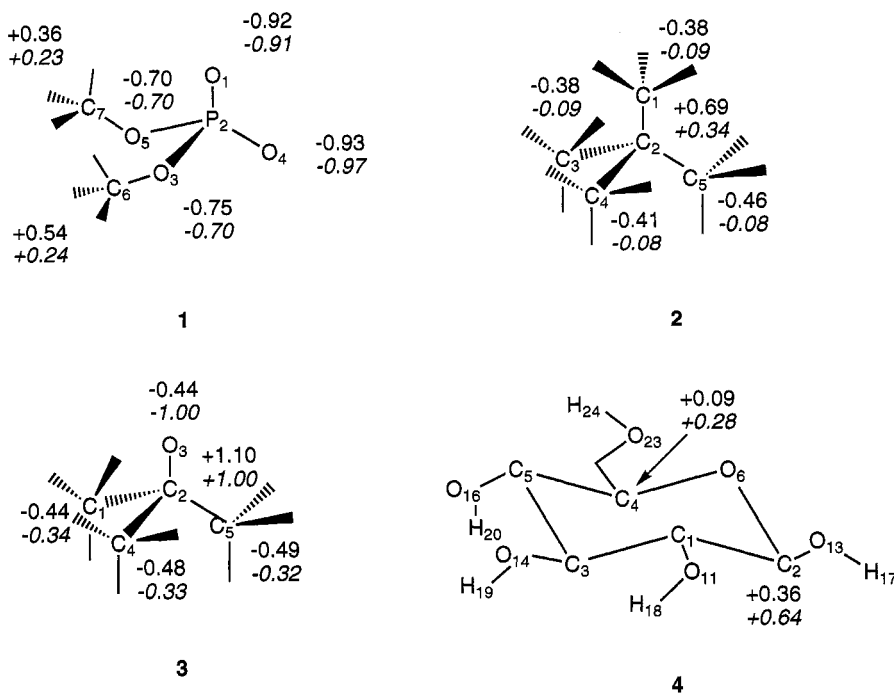


Figure 10 Comparison of selected atomic charges from HF/3-21G(*) CHELP and CHELP-SVD fits for dimethylphosphate (1), neopentane (2), tert-butoxide (3), and glucose (4). Data from CHELP-SVD are in italics.

A similar improvement in the symmetry of the charges is seen both with *tert*-butoxide and neopentane (Figure 10). The CHELP charges on the three carbon atoms of *tert*-butoxide that are equivalent by symmetry (C_1 , C_4 , and C_5) differ by roughly 0.05 e . The SVD suggests the set of parameters should be limited to 11 of the 14 atoms. The charges from a reduced version of the problem (fits to only C_1 , C_2 , O_3 , C_4 , C_5) differ by less than 0.01 e . A more dramatic improvement is seen in neopentane where the charges on the four equivalent carbon atoms (C_1 , C_3 , C_4 , and C_5) differ by as much as 0.08 e when all atoms are used, whereas a fit to a reduced set (C_1 , C_2 , C_3 , C_4 , C_5) yields differences of only 0.01 e .

Charges from reduced sets are often more chemically appealing. Note that in glucose the SVD rank estimate suggests fitting a maximum of 16 of the total 24 atoms. Reducing the size of the parameter set apparently improves the description of buried atoms. The charges on C_2 and C_4 are assigned in the full fit to be 0.36 e and 0.09 e , respectively (Figure 10). Although the trend is certainly what one might expect from simple electronegativity arguments (C_2 more positive than C_4), the nearly neutral character of C_4 is unanticipated. Charges fit to the smaller set still display the trend (0.64 e vs. 0.28 e), but the more electron-deficient nature of C_2 is now revealed.

There are, however, perils in reducing the problem. Care must be taken not to reduce the subset too far. For example, if one selects a subset of eight atoms (O_1 , C_2 , C_3 , C_4 , C_5 , C_6 , C_7 , and H_{13}) as an appropriate set for phenol, the resulting charges do not meet intuitive expectations. C_6 , for example, is not predicted to be δ^+ , but instead bears a significant negative charge! The rms deviation of the predicted electrostatic potential from the actual values points up the poor quality of the overreduced fit: it is nearly 5 kcal/mol . Charges from fits with high rms deviations ($\geq 5\text{ kcal/mol}$), no matter what the model, should be suspect. Since the SVD suggests that up to 10 charges can be fit, adding two

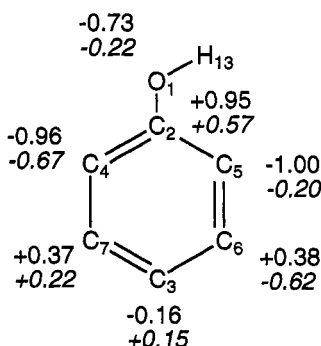


Figure 11 Comparison of selected atomic charges from two different HF/3-21G(*) CHELP-SVD fits for phenol. Data from a fit for which the set of charges was overreduced are in italics.

more atoms to the subset should (and does) alleviate the problem, as the data in Figure 11 show. The intuitively predicted pattern of alternating charges now appears, and the charges properly reflect the near- C_{2v} symmetry of the molecule.

The Method Matters

Sigfridsson and Ryde³⁴ have recently shown that the method chosen for solving the least-squares problem as well as the method used to impose the constraints influence the rank deficiency. Those authors point out that the LLS solution for CHELP and CHELPG is found by starting with $\mathbf{Aq} = \mathbf{f}$, where \mathbf{q} is the vector of charges and \mathbf{f} is the data to be fit. Then left multiplying leads to

$$\mathbf{A}^T \mathbf{A} \mathbf{q} = \mathbf{A}^T \mathbf{f} \quad [19]$$

and

$$\mathbf{q} = (\mathbf{A}^T \mathbf{A})^{-1} \mathbf{A}^T \mathbf{f} \quad [20]$$

which is solved by forming the inverse of the square matrix ($\mathbf{A}^T \mathbf{A}$). Hinsen and Roux³⁵ note that such a procedure can exacerbate the rank deficiency. When a pseudoinverse solution is used, that is,

$$\mathbf{q} = \mathbf{A}^{-1} \mathbf{f} \quad [21]$$

the condition number is effectively reduced to the square root of the previous value.

The choice of treatment for the constraints is also critical. Using Lagrange multipliers, as in the CHELP, CHELPG, RESP, and Merz–Kollman methods, enlarges the \mathbf{A} matrix, thereby also increasing the potential for rank deficiency. Sigfridsson and Ryde's CHELP-BOW results suggest that using a restraint method that *reduces* the \mathbf{A} matrix should lead to better conditioned matrices. For example, using the algorithm suggested by Hinsen and Roux,³⁵ they find condition numbers (κ , the ratio of largest to smallest singular value) for small molecules such as formamide and methyl acetate to be less than 100. The \mathbf{A} matrices for larger molecules are not as well conditioned as those of smaller systems. However, even for a model myoglobin with 84 atoms, κ is on the order of 10^4 . For comparison, the corresponding matrix from a modified version of CHELP for lactose (40 atoms) has a condition number in excess of 10^6 . CHELP condition numbers for smaller molecules are on the order of 10^4 .

An alternative to the method of Lagrange multipliers for imposing the necessary constraints is sketched below. It derives a lower dimensional *unconstrained* problem from the original constrained problem by using an orthogonal basis for the null space of the constraint matrix.³⁶ This method is well suited to the potentially rank-deficient problem at hand, where steps may be taken to

stabilize the solution by limiting the length of the solution vector. Constructing the new problem in this way also allows us to use the SVD to check the stability of the \mathbf{A} matrix.

To minimize $\|\mathbf{Ax} - \mathbf{b}\|_2$ subject to the constraints $\mathbf{Cx} = \mathbf{d}$ in this way, one can find a matrix \mathbf{K} such that \mathbf{KC} is of lower triangular form. Next form

$$\begin{bmatrix} \mathbf{C} \\ \mathbf{A} \end{bmatrix} \mathbf{K} = \begin{bmatrix} \tilde{\mathbf{C}}_1 & \mathbf{0} \\ \tilde{\mathbf{E}}_1 & \tilde{\mathbf{E}}_2 \end{bmatrix} \quad [22]$$

Then solve the modified constraint equations for \mathbf{y}_1

$$\tilde{\mathbf{C}}_1 \mathbf{y}_1 = \mathbf{d} \quad [23]$$

From this, one can construct a data vector $\tilde{\mathbf{b}}$ in the new basis

$$\tilde{\mathbf{b}} = \mathbf{b} - \tilde{\mathbf{E}}_1 \mathbf{y}_1 \quad [24]$$

and finally find a solution \mathbf{y}_2 to

$$\tilde{\mathbf{E}}_2 \mathbf{y}_2 \approx \tilde{\mathbf{b}} \quad [25]$$

by minimizing $\|\tilde{\mathbf{B}}_2 \mathbf{y}_2 - \tilde{\mathbf{b}}\|_2$ in the usual way. Note that the LLS is being applied to a smaller problem than would have been expressed if the constraints had been included explicitly. To find the solution in the original basis, back-transform using \mathbf{K} :

$$\mathbf{x} = \mathbf{K} \begin{bmatrix} \mathbf{y}_1 \\ \mathbf{y}_2 \end{bmatrix} \quad [26]$$

Using this method leads to a substantial improvement in the condition number.³⁷ For example, the CHELP fit using the original algorithm based on Lagrange multipliers to the electrostatic potential of butanol has an rms deviation of 0.79 kcal/mol, but a condition number of 53,000. When the method of Hanson and Lawson is applied in conjunction with a pseudoinverse solution, we find, as do Sigfridsson and Ryde,³⁴ that the conditioning of the matrix is substantially improved. The new condition number is only 40, and the fit is of equal quality.

CONCLUSIONS AND RECOMMENDATIONS

The fitting of atomic charges to molecular electrostatic potentials, while appearing to be a straightforward overdetermined linear least square problem,

should not be approached naively. Although the density and location of points sampled for the electrostatic potential are important factors, it is clear that the potential for rank deficiency must be considered. Merely increasing the density of points sampled rarely will reduce the sensitivity of the solution. In particular, users should be aware that methods that rely on solving the normal equations to obtain the solution to the LLS problem as well as methods that use Lagrange multipliers to impose the necessary constraints are particularly susceptible to rank deficiency. Such methods include the original version of CHELP, CHELPG, and the Merz-Kollman semiempirical charges. Though RESP charges use Lagrange multipliers to impose the constraints, the introduction of a penalty function into the fit may make these charges more reliable than charges extracted from an unweighted fit. Results derived from such methods should be examined closely.

Methods (e.g., CHELP-BOW) that favor selecting sample points close to or within the van der Waals volume of the molecule are preferable. We further recommend, particularly when one is working with large systems, that the LLS equations be solved by means of pseudoinverse solutions and that constraints be imposed via the reduction of the problem rather than via Lagrange multipliers.

REFERENCES

1. J. P. Bowen and N. L. Allinger, in *Reviews in Computational Chemistry*, K. B. Lipkowitz and D. B. Boyd, Eds., VCH Publishers, New York, 1991, Vol. 2, pp. 81–97. Molecular Mechanics: The Art and Science of Parameterization. I. Pettersson and T. Liljefors, *Reviews in Computational Chemistry*, K. B. Lipkowitz and D. B. Boyd, Eds., VCH Publishers, New York: 1996, Vol. 9, pp. 167–189. Molecular Mechanics Calculated Conformational Energies of Organic Molecules: A Comparison of Force Fields.
2. S. M. Bachrach, in *Reviews in Computational Chemistry*, K. B. Lipkowitz and D. B. Boyd, Eds., VCH Publishers, New York, 1994, Vol. 5, pp. 171–227. Population Analysis and Electron Densities from Quantum Mechanics.
3. R. S. Mulliken, *J. Chem. Phys.*, **23**, 1833 (1955). Electronic Population Analysis on LCAO-MO Molecular Wavefunctions. I.
4. M. J. Frisch, G. W. Trucks, H. B. Schlegel, P. M. W. Gill, B. G. Johnson, M. A. Robb, J. R. Cheeseman, T. Keith, G. A. Petersson, J. A. Montgomery, K. Raghavachari, M. A. Al-Laham, V. G. Zakrzewski, J. V. Ortiz, J. B. Foresman, J. Cioslowski, B. B. Stefanov, A. Nanayakkara, M. Challacombe, C. Y. Peng, P. Y. Ayala, W. Chen, M. W. Wong, J. L. Andres, E. S. Replogle, R. Gomperts, R. L. Martin, D. J. Fox, J. S. Binkley, D. J. DeFrees, J. Baker, J. P. Stewart, M. Head-Gordon, C. Gonzalez, and J. A. Pople, Gaussian, Inc., Carnegie Office Park, Building 6, Suite 230, Carnegie, PA 15106.
5. Spartan, Wavefunction, Inc., 18401 Von Karman Ave., Suite 370, Irvine, CA 92612.
6. C. C. Chambers, G. D. Hawkins, C. J. Cramer, and D. G. Truhlar, *J. Phys. Chem.*, **100**, 16385 (1996). Models for Aqueous Solvation Based on Class IV Atomic Charges and First Solvation Shell Effects.
7. One such algorithm uses data from X-ray diffraction experiments to compute a molecular electrostatic potential to which charges are fit. See: Z. Su, *J. Comput. Chem.* **14**, 1036 (1993). New Method for the Derivation of Net Atomic Charges from the Electrostatic Potential.

8. R. F. W. Bader, *Chem. Rev.*, **91**, 893 (1991). A Quantum Theory of Molecular Structure and Its Applications. R. F. W. Bader, P. L. A. Popelier, and T. A. Keith, *Angew. Chem., Intl. Ed. Engl.*, **33**, 620 (1994). Theoretical Definition of a Functional Group and the Molecular Orbital Paradigm.
9. P. Politzer and J. S. Murray, in *Reviews in Computational Chemistry*, K. B. Lipkowitz and D. B. Boyd, Eds., VCH Publishers, New York, 1991, Vol. 2, pp. 273–312. Molecular Electrostatic Potentials and Chemical Reactivity. D. E. Williams, in *Reviews in Computational Chemistry*, K. B. Lipkowitz and D. B. Boyd, Eds., VCH Publishers, New York, 1991, Vol. 2, pp. 219–271. Net Atomic Charge and Multipole Models for the Ab Initio Molecular Electric Potential.
10. E. Scrocco and J. Tomasi, *Top. Curr. Chem.*, **42**, 95 (1973). The Electrostatic Molecular Potential as a Tool for the Interpretation of Molecular Properties.
11. P. A. Kollman, *J. Am. Chem. Soc.* **100**, 2974 (1978). A Method of Describing the Charge Distribution in Simple Molecules.
12. F. A. Momany, *J. Phys. Chem.*, **82**, 592 (1978). Determination of Partial Atomic Charges from Ab Initio Molecular Electrostatic Potentials. Application to Formamide, Methanol, and Formic Acid.
13. S. R. Cox and D. E. Williams, *J. Comput. Chem.*, **2**, 304 (1981). Representation of the Molecular Electrostatic Potential by a Net Atomic Charge Model.
14. L. E. Chirlian and M. M. Franci, *J. Comput. Chem.*, **8**, 894 (1987). Atomic Charges Derived from Electrostatic Potentials: A Detailed Study.
15. C. Carey, L. E. Chirlian, D. Gange, and M. M. Franci, *J. Comput. Chem.*, **17**, 167 (1996). Charges Fit to Electrostatic Potentials. II. Can Atomic Charges Be Unambiguously Fit to Electrostatic Potentials?
16. C. M. Breneman and K. B. Wiberg, *J. Comput. Chem.*, **11**, 361 (1990). Determining Atom-Centered Monopoles from Molecular Electrostatic Potentials. The Need for High Sampling Density in Formamide Conformational Analysis.
17. B. H. Besler, K. M. Merz, and P. A. Kollman, *J. Comput. Chem.*, **11**, 431 (1990). Atomic Charges Derived from Semiempirical Methods.
18. P. G. Mezey, in *Reviews in Computational Chemistry*, K. B. Lipkowitz and D. B. Boyd, Eds., VCH Publishers, New York, 1990, Vol. 1, pp. 265–294. Molecular Surfaces.
19. R. J. Woods, M. Khalil, W. Pell, S. H. Moffat, and V. H. Smith Jr., *J. Comput. Chem.*, **11**, 297 (1990). Derivation of Net Atomic Charges from Molecular Electrostatic Potentials.
20. J. S. Binkley, M. J. Frisch, R. Krishnan, D. J. DeFrees, H. B. Schlegel, R. A. Whiteside, E. M. Fluder, R. Seeger, and J. A. Pople, Gaussian 82, Carnegie Mellon University, 1982.
21. M. W. Schmidt, J. A. Boatz, K. K. Baldwin, S. Koseki, M. S. Gordon, S. T. Elbert, and B. Lam, *QCPE Bull.*, **7**, 115 (1987). GAMESS.
22. D. E. Williams, *J. Comput. Chem.*, **9**, 745 (1981). Representation of the Molecular Electrostatic Potential by Atomic Multipole and Bond Dipole Models.
23. W. L. Jorgensen and J. Gao, *J. Am. Chem. Soc.*, **110**, 4212 (1988). Cis-trans Energy Difference for the Peptide Bond in the Gas Phase and in Aqueous Solution.
24. P. Cieplak and P. A. Kollman, *J. Comput. Chem.*, **12**, 1232 (1991). On the Use of Electrostatic Potential Derived Charges in Molecular Mechanics Force Fields: Relative Solvation Free Energy of *cis*- and *trans*-*N*-Methylacetamide.
25. D. E. Williams, *Biopolymers*, **29**, 1367 (1990). Alanyl Dipeptide Potential-Derived Net Atomic Charges and Bond Dipoles, and Their Variation with Molecular Conformation.
26. T. R. Stouch and D. E. Williams, *J. Comput. Chem.*, **13**, 622 (1992). Conformational Dependence of Electrostatic Potential Derived Charges of a Lipid Headgroup: Glycerylphosphorylcholine.
27. J. J. Urban and G. R. Farnini, *J. Comput. Chem.*, **14**, 353 (1993). Conformational Dependence of the Electrostatic Potential-Derived Charges of Dopamine: Ramifications in Molecular Force Field Calculations in the Gas Phase and in Aqueous Solution.

-
28. T. R. Stouch and D. E. Williams, *J. Comput. Chem.*, **14**, 858 (1993). Conformational Dependence of Electrostatic Potential-Derived Charges: Studies of the Fitting Procedure.
 29. See, e.g.: (a) G. H. Golub and C. F. van Loan, *Matrix Computations*, 3rd ed., Johns Hopkins University Press, Baltimore, 1996. (b) C. L. Lawson and R. J. Hanson, *Solving Least Squares Problems*, Prentice-Hall, Englewood Cliffs, NJ, 1974. (c) W. H. Press, B. P. Flannery, S. A. Teukolsky, and W. T. Vetterling, *Numerical Recipes*, Cambridge University Press, Cambridge, 1986.
 30. See Ref. 29(a), p. 80.
 31. From a pragmatic point of view, the pseudoinverse is merely a definition of the inverse for matrices that are not square. More technically, they should satisfy the Moore–Penrose conditions (where B is the original matrix and B^+ is the pseudoinverse): $AA^+A = A$, $A^+A A^+ = A^+$, and $(A^+A)^T = A^+A$. See also Ref. 29(b), pp. 36–38, and R. Penrose, *Proc. Cambridge Philos. Soc.*, **51**, 406 (1955). A Generalized Inverse for Matrices.
 32. See Ref. 29(a), pp. 590–591.
 33. C. I. Bayly, P. Cieplak, W. D. Cornell, and P. A. Kollman, *J. Phys. Chem.*, **97**, 10269 (1993). A Well-Behaved Electrostatic Potential Based Method Using Charge Restraints for Deriving Atomic Charges: The RESP Model.
 34. E. Sigfridsson and U. Ryde, *J. Comput. Chem.*, **19**, 377 (1998). Comparison of Methods for Deriving Atomic Charges from the Electrostatic Potential and Moments.
 35. K. Hinsen and B. Roux, *J. Comput. Chem.*, **18**, 368 (1997). A Potential Function for Computer Simulation Studies of Proton Transfer in Acetylacetone.
 36. R. J. Hanson and C. L. Lawson, *Math. Comp.*, **23**, 787 (1969). Extensions and Applications of the Householder Algorithm for Solving Linear Least Squares Problems.
 37. M. M. Franci, unpublished work, 1998.

CHAPTER 2

An Introduction to Coupled Cluster Theory for Computational Chemists

T. Daniel Crawford* and Henry F. Schaefer III

*Center for Computational Quantum Chemistry, Department of Chemistry, The University of Georgia, Athens, Georgia 30602-2525, (present address): *Institute for Theoretical Chemistry, Departments of Chemistry and Biochemistry, The University of Texas, Austin, Texas, 78712-1167*

INTRODUCTION

Since its introduction into quantum chemistry in the late 1960s by Čížek and Paldus,^{1–3} coupled cluster theory has emerged as perhaps the most reliable, yet computationally affordable method for the approximate solution of the electronic Schrödinger equation and the prediction of molecular properties. The purpose of this chapter is to provide computational chemists who seek a deeper knowledge of coupled cluster theory with the background necessary to understand the extensive literature on this important ab initio technique.

In spite of the method's present utility and popularity, the quantum chemical community was slow to accept coupled cluster theory, perhaps because the earliest researchers in the field used elegant but unfamiliar mathematical tools such as Feynman-like diagrams and second quantization to derive working equations. Nearly 10 years after the essential contributions of Paldus and Čížek, Hurley presented a re-derivation of the coupled cluster doubles (CCD) equa-

Reviews in Computational Chemistry, Volume 14
Kenny B. Lipkowitz and Donald B. Boyd, Editors
Wiley-VCH, John Wiley and Sons, Inc., New York, © 2000

tions⁴ in terms which were more familiar to quantum chemists. Soon thereafter Monkhorst⁵ developed a general coupled cluster response theory for calculating molecular properties. By the end of the 1970s, computer implementations of the theory for realistic systems began to appear as the groups of Pople⁶ and Bartlett⁷ each developed and tested spin-orbital CCD programs. A few years later, Purvis and Bartlett derived the coupled cluster singles and doubles (CCSD) equations and implemented them in a practical computer program.⁸ Since that pioneering achievement, the popularity of coupled cluster methods has blossomed, and tremendous efforts have been made in the construction of highly efficient CCSD energy codes,^{8–14} inclusion of higher excitations in the coupled cluster wavefunction,^{15–34} spin-adaptation of open-shell methods,^{35–42} as well as development of analytic first^{43–54} and second^{55–59} energy derivatives, and methods to treat excited states.^{60–74}

In the following section, we will use the cluster function approach developed by Sinanoğlu⁷⁵ to justify the well-known exponential form of the coupled cluster wavefunction. This task requires use of the mathematical technique known as second quantization (also called “occupation-number” formalism), and we introduce important concepts as they are needed. We then construct the operator equations of coupled cluster theory and address issues such as the Hausdorff expansion, variational approaches, and an eigenvalue perspective on the coupled cluster problem. In the third section, we develop a set of algebraic and diagrammatic tools needed to derive programmable equations for the CCSD method, and, using these tools, we discuss the property of the energy known as size extensivity. Next, we examine the relationship between the coupled cluster equations and those of finite-order many-body perturbation theory, leading to an explanation of the popular (T) correction implemented in many quantum chemical program packages. We then discuss some of the issues associated with an efficient computer implementation of coupled-cluster-like equations, such as matrix formulations, intermediate factorization, spin and spatial symmetry simplifications, and atomic-orbital-based algorithms. Finally, we describe some of the latest developments in the theory, including the implementation of open-shell Brueckner methods, an area of coupled cluster theory which in recent years has proven to be valuable for a number of difficult open-shell symmetry-breaking problems.

We would like to stress that this chapter is a review of coupled cluster *theory*. It is not primarily intended to provide an analysis of the numerical performance of the coupled cluster model, and we direct readers in search of such information to several recent publications.^{76–79} Instead, we offer a detailed explanation of the most important aspects of coupled cluster theory at a level appropriate for the general computational chemistry community. Although many of the topics described here have been discussed by other authors,^{77,78,80,81} this chapter is unique in that it attempts to provide a concise, practical introduction to the mathematical techniques of coupled cluster theory (both algebraic and diagrammatic), as well as a discussion of the efficient

implementation of the method on high performance computers, in a manner accessible to newcomers to the field.

FUNDAMENTAL CONCEPTS

In this section we examine some of the critical ideas that contribute to most wavefunction-based models of electron correlation, including coupled cluster, configuration interaction, and many-body perturbation theory. We begin with the concept of the cluster function which may be used to include the effects of electron correlation in the wavefunction. Using a formalism in which the cluster functions are constructed by cluster operators acting on a reference determinant, we justify the use of the “exponential ansatz” of coupled cluster theory.⁸⁰

Cluster Expansion of the Wavefunction

Consider a model system of four electrons moving in an arbitrary electrostatic field generated by the nuclei in a molecule. For our purposes, it is not necessary to specify the number of these nuclei, their types, or positions; only the general form of the electronic wavefunction is of interest. It is convenient to describe the motions of each electron separately by assigning them to one-electron functions, $\phi_i(\mathbf{x}_1)$, where \mathbf{x}_1 is a vector of the coordinates (including spin) of electron 1. In addition, electrons are fermions, so the electronic wavefunction must be antisymmetric with respect to interchange of the coordinates of any pair of electrons. A traditional and very useful starting point for such a four-electron wavefunction is the so-called Slater determinant

$$\Phi_0 = \frac{1}{\sqrt{4!}} \begin{vmatrix} \phi_i(\mathbf{x}_1) & \phi_j(\mathbf{x}_1) & \phi_k(\mathbf{x}_1) & \phi_l(\mathbf{x}_1) \\ \phi_i(\mathbf{x}_2) & \phi_j(\mathbf{x}_2) & \phi_k(\mathbf{x}_2) & \phi_l(\mathbf{x}_2) \\ \phi_i(\mathbf{x}_3) & \phi_j(\mathbf{x}_3) & \phi_k(\mathbf{x}_3) & \phi_l(\mathbf{x}_3) \\ \phi_i(\mathbf{x}_4) & \phi_j(\mathbf{x}_4) & \phi_k(\mathbf{x}_4) & \phi_l(\mathbf{x}_4) \end{vmatrix} \quad [1]$$

where the $1/\sqrt{4!}$ is a normalization constant. Expansion of this determinant reveals a linear combination of products of the four functions, ϕ_i , ϕ_j , ϕ_k , and ϕ_l , with the electronic coordinates \mathbf{x}_n distributed among them in all possible ways. Since permutation of any two rows in the determinant—which is equivalent to interchanging the coordinates of any two electrons—changes the sign of Φ_0 , the antisymmetry principle is maintained.

The component functions ϕ_i may be chosen in a variety of ways. For example, if the nuclear field were only a single beryllium nucleus, the one-electron spatial functions could be constructed to mimic the atomic 1s and 2s orbitals. For a molecular system, the functions can be constructed as a linear combination of atomic orbitals (AOs) in which each one-electron function

represents a molecular orbital (MO) whose AO coefficients are optimized via the Hartree–Fock self-consistent field (SCF) procedure.⁸² A convenient shorthand notation for this wavefunction consists of a Dirac-notation ket containing only the diagonal elements of the matrix above,

$$\Phi_0 = |\phi_i(\mathbf{x}_1)\phi_j(\mathbf{x}_2)\phi_k(\mathbf{x}_3)\phi_l(\mathbf{x}_4)\rangle \quad [2]$$

where the normalization factor is included implicitly. As discussed in detail elsewhere in *Reviews in Computational Chemistry*,⁷⁷ the single-determinant wavefunction fails to account for the instantaneous Coulombic interactions that keep the electrons of opposite spin apart.⁸²

How can we improve this so-called independent-particle approximation such that the motions of the electrons are correlated? Often the set of *occupied* orbitals (i.e., those functions that compose the Slater determinant above) is chosen from a larger set of one-electron functions. These “extra” functions are frequently referred to as *virtual* orbitals and may, for example, arise as a by-product of the SCF procedure.^a Within the space described by the full set of orbitals, any function of N variables may be written in terms of N -tuple products of the ϕ_p . For example, a function of two variables may be constructed by using all possible binary products of the set of one-electron functions:

$$f(\mathbf{x}_1, \mathbf{x}_2) = \sum_{p>q} c_{pq} \phi_p(\mathbf{x}_1)\phi_q(\mathbf{x}_2) \quad [3]$$

where the double-summation runs over the entire set of one-electron functions and the notation $p > q$ indicates that only unique pairs of functions are included. Instead of correlating the motions of a specific pair of electrons, however, we may use a modified form of this expansion to correlate the motions of any two electrons within a selected pair of occupied orbitals—say functions i and j —using a two-particle *cluster* function,

$$f_{ij}(\mathbf{x}_m, \mathbf{x}_n) = \sum_{a>b} t_{ij}^{ab} \phi_a(\mathbf{x}_m)\phi_b(\mathbf{x}_n) \quad [4]$$

where the t_{ij}^{ab} are the cluster coefficients whose specific values are determined via the electronic Schrödinger equation (see the next section on Formal Coupled Cluster Theory). Inserting this into Φ_0 leads to the somewhat-improved electronic wavefunction

$$\Psi = |[\phi_i(\mathbf{x}_1)\phi_j(\mathbf{x}_2) + f_{ij}(\mathbf{x}_1, \mathbf{x}_2)]\phi_k(\mathbf{x}_3)\phi_l(\mathbf{x}_4)\rangle \quad [5]$$

^aWe will denote those functions that are part of the occupied space with the subscripts i, j, k, \dots , those within the virtual space with a, b, c, \dots , and arbitrary functions that may lie in either space with p, q, r, \dots .

where the Dirac shorthand implies a correctly antisymmetrized wavefunction including normalization factors as in Eq. [2]. Inclusion of the cluster function, f_{ij} , in the wavefunction produces a linear combination of Slater determinants involving replacement of occupied orbitals ϕ_i and ϕ_j by virtual orbitals ϕ_a and ϕ_b , such that

$$\Psi = \Phi_0 + \sum_{a>b} t_{ij}^{ab} |\phi_a(\mathbf{x}_1)\phi_b(\mathbf{x}_2)\phi_k(\mathbf{x}_3)\phi_l(\mathbf{x}_4)\rangle \quad [6]$$

In addition, the determinantal form of the individual terms in this expansion implies antisymmetrization of the cluster coefficients, such that $t_{ij}^{ab} = -t_{ji}^{ab} = -t_{ij}^{ba} = t_{ji}^{ba}$.

It should be carefully noted here that the cluster function, $f_{ij}(\mathbf{x}_1, \mathbf{x}_2)$, is intended to correlate the motions of *any* pair of electrons placed in orbitals i and j , and not just the motions of electrons 1 and 2. Since the Slater determinant produces a linear combination of orbital products, including terms such as

$$[\phi_i(\mathbf{x}_1)\phi_j(\mathbf{x}_2) + f_{ij}(\mathbf{x}_1, \mathbf{x}_2)]\phi_k(\mathbf{x}_3)\phi_l(\mathbf{x}_4) \quad [7]$$

and

$$[\phi_i(\mathbf{x}_3)\phi_j(\mathbf{x}_4) + f_{ij}(\mathbf{x}_3, \mathbf{x}_4)]\phi_k(\mathbf{x}_1)\phi_l(\mathbf{x}_2) \quad [8]$$

which differ only in their distribution of electronic coordinates, the cluster function correlates the motion of *every* pair of electrons found in orbitals ϕ_i and ϕ_j .

Depending on the chemical system of interest, however, it might be more prudent to correlate the motions of electrons in orbitals k and l rather than orbitals i and j . For example, ϕ_i and ϕ_j might correspond to molecular core orbitals, while ϕ_k and ϕ_l might correspond to the atomic or molecular valence orbitals. Electron correlation can be particularly important in the latter set of functions because the valence orbitals are often directly involved in the formation of chemical bonds. In this case, the wavefunction would be written as

$$\Psi = |[\phi_i(\mathbf{x}_1)\phi_j(\mathbf{x}_2)[\phi_k(\mathbf{x}_3)\phi_l(\mathbf{x}_4) + f_{kl}(\mathbf{x}_3, \mathbf{x}_4)]]\rangle \quad [9]$$

On the other hand, a more intelligent approach might be to correlate all possible pairwise combinations of orbitals in this four-electron system, that is,

$$\begin{aligned} \Psi = & |\phi_i\phi_j\phi_k\phi_l\rangle + |f_{ij}\phi_k\phi_l\rangle - |f_{ik}\phi_j\phi_l\rangle + |f_{il}\phi_j\phi_k\rangle + |\phi_i f_{jk}\phi_l\rangle \\ & - |\phi_i f_{jl}\phi_k\rangle + |\phi_i\phi_j f_{kl}\rangle + |f_{ij}f_{kl}\rangle - |f_{ik}f_{jl}\rangle + |f_{il}f_{jk}\rangle \end{aligned} \quad [10]$$

where the electronic coordinates are now implicit in the notation, and the signs on individual terms arise from the permutations in the orbital ordering needed to define the appropriate cluster functions. However, there is no need to limit this approach to orbital pairs only. Following Harris et al.,⁸⁰ we introduce three-orbital cluster functions and include these in our new wavefunction to give

$$\begin{aligned}\Psi = & |\phi_i\phi_j\phi_k\phi_l\rangle + |f_{ij}\phi_k\phi_l\rangle - |f_{ik}\phi_j\phi_l\rangle + |f_{il}\phi_j\phi_k\rangle + |\phi_i f_{jk}\phi_l\rangle \\ & - |\phi_i f_{jl}\phi_k\rangle + |\phi_i\phi_j f_{kl}\rangle + |f_{ij}f_{kl}\rangle - |f_{ik}f_{jl}\rangle + |f_{il}f_{jk}\rangle \\ & + |f_{ijk}\phi_l\rangle - |f_{ijl}\phi_k\rangle + |f_{ikl}\phi_j\rangle + |\phi_i f_{jkl}\rangle\end{aligned}\quad [11]$$

If one continues this process to include all cluster functions for up to N orbitals (four in the case discussed here), as well as single-orbital “cluster” functions that account for adjustment of the one-electron basis as other cluster functions are added, we could obtain the exact wavefunction within the space spanned by the $\{\Phi_p\}$. On the other hand, we might assume that clusters larger than pairs are less important to an adequate description of the system—an assumption supported by the fact that the electronic Hamiltonian contains operators describing pairwise electronic interactions at most.⁷⁵ We therefore write a four-electron wavefunction that includes all clusters of only one and two orbitals as^{80,83}

$$\begin{aligned}\Psi = & |\phi_i\phi_j\phi_k\phi_l\rangle + |f_i\phi_j\phi_k\phi_l\rangle + |\phi_i f_j\phi_k\phi_l\rangle + |\phi_i\phi_j f_k\phi_l\rangle + |\phi_i\phi_j\phi_k f_l\rangle \\ & + |f_i f_j\phi_k\phi_l\rangle + |f_i\phi_j f_k\phi_l\rangle + |f_i\phi_j\phi_k f_l\rangle + |\phi_i f_j f_k\phi_l\rangle + |\phi_i f_j\phi_k f_l\rangle \\ & + |\phi_i\phi_j f_k f_l\rangle + |f_i f_j f_k\phi_l\rangle + |f_i f_j\phi_k f_l\rangle + |f_i\phi_j f_k f_l\rangle + |\phi_i f_j f_k f_l\rangle \\ & + |f_{ij}\phi_k\phi_l\rangle - |f_{ik}\phi_j\phi_l\rangle + |f_{il}\phi_j\phi_k\rangle + |\phi_i f_{jk}\phi_l\rangle - |\phi_i f_{jl}\phi_k\rangle \\ & + |\phi_i\phi_j f_{kl}\rangle + |f_{ij}f_{kl}\rangle - |f_{ik}f_{jl}\rangle + |f_{il}f_{jk}\rangle + |f_{ij}f_{jk}f_l\rangle \\ & + |f_{ij}f_k\phi_l\rangle + |f_{ij}\phi_k f_l\rangle + |f_{ij}f_j f_l\rangle - |f_{ik}f_j\phi_l\rangle - |f_{ik}\phi_j f_l\rangle - |f_{ik}f_j f_l\rangle \\ & + |f_{il}f_j\phi_k\rangle + |f_{il}\phi_j f_k\rangle + |f_{il}f_j f_k\rangle + |f_{ij}f_{jk}\phi_l\rangle + |\phi_i f_{jk}f_l\rangle + |f_i f_{jk}f_l\rangle \\ & - |f_i f_{jl}\phi_k\rangle - |\phi_i f_{jl}f_k\rangle - |f_i f_{jl}f_k\rangle + |f_i\phi_j f_{kl}\rangle + |\phi_i f_j f_{kl}\rangle + |f_i f_j f_{kl}\rangle\end{aligned}\quad [12]$$

Cluster Functions and the Exponential Ansatz

The complicated notation of Eq. [12] can be drastically reduced by using a simple analytic form for the cluster functions. Note again that each determinant involving a cluster function is actually a linear combination of determinants each of which differs from the reference, Φ_0 , by a specific number of orbitals. For example, the 27th term on the right-hand side of in Eq. [12] expands to become

$$|f_{ij}\phi_k f_l\rangle = \sum_{a>b} \sum_c t_{ij}^{ab} t_l^c |\phi_a \phi_b \phi_k \phi_c\rangle \quad [13]$$

where we have inserted the definition of the two-electron cluster function in Eq. [4] and its one-electron counterpart to indicate the pairwise correlation of electrons in orbitals ϕ_i and ϕ_j as well as the “correlation” of electrons in orbital ϕ_l . Note that each determinant in the summation above differs from the reference by exactly three orbitals; orbitals ϕ_i , ϕ_j , and ϕ_l are replaced by orbitals ϕ_a , ϕ_b , and ϕ_c , respectively. Hence, each term can be written as the result of some substitution operator (or products of such operators) acting on Φ_0 . This task is perhaps most easily accomplished using the mathematical technique known as second quantization.^{80,82,84}

We will define a *creation* operator by its action on a Slater determinant:

$$a_p^\dagger |\phi_q \cdots \phi_s\rangle = |\phi_p \phi_q \cdots \phi_s\rangle \quad [14]$$

where we have added one more column (orbital) and one more row (electron) to form the new determinant on the right-hand side. We may define an *annihilation* operator in a similar manner to obtain

$$a_p |\phi_p \phi_q \cdots \phi_s\rangle = |\phi_q \cdots \phi_s\rangle \quad [15]$$

where we have removed the first column (orbital) and the first row (electron) from the original function.^b A given Slater determinant may be written as a chain of creation operators acting on the true vacuum (a state containing no electrons or orbitals), that is;

$$a_p^\dagger a_q^\dagger \cdots a_s^\dagger |0\rangle = |\phi_p \phi_q \cdots \phi_s\rangle \quad [16]$$

Note also that an annihilation operator acting on the vacuum state gives a zero result,

$$a_p |0\rangle = 0 \quad [17]$$

Pairwise permutations of the operators introduce changes in the sign of the resulting determinant, for example,

^bThe annihilation operator a_p is simply the Hermitian conjugate of the creation operator a_p^\dagger . An equivalent perspective on Eq. [14], therefore, is the annihilation operator a_p acting to the left on the bra state, $\langle \Phi_0 |$, to give

$$\langle \phi_q \cdots \phi_s | a_p = \langle \phi_p \phi_q \cdots \phi_s | = (\langle \phi_p \phi_q \cdots \phi_s |)^\dagger = (a_p^\dagger | \phi_q \cdots \phi_s \rangle)^\dagger$$

$$a_q^\dagger a_p^\dagger | \rangle = |\phi_q \phi_p \rangle = - |\phi_p \phi_q \rangle = - a_p^\dagger a_q^\dagger | \rangle \quad [18]$$

Therefore, the *anticommutation* relation for a pair of creation operators is simply

$$a_p^\dagger a_q^\dagger + a_q^\dagger a_p^\dagger = 0 \quad [19]$$

The analogous relation for a pair of annihilation operators is

$$a_p a_q + a_q a_p = 0 \quad [20]$$

Therefore, if we change the ordering of a pair of annihilation or creation operators, we must also change the sign of the resulting expression. Finally, it may be shown that the anticommutation relation for the “mixed” product is

$$a_p^\dagger a_q + a_q^\dagger a_p^\dagger = \delta_{pq} \quad [21]$$

where δ_{pq} is the conventional Kronecker delta, which equals 1 if $p = q$ and 0 if $p \neq q$.

Using these so-called second-quantized operators, we may define the single-orbital cluster operator

$$\hat{t}_i \equiv \sum_a t_i^a a_a^\dagger a_i \quad [22]$$

where the operator a_i deletes the orbital ϕ_i from the determinant on which the operator acts, whereas a_a^\dagger introduces the orbital ϕ_a in its place. (The \wedge is used to indicate a second-quantized operator.) Similarly, a two-orbital cluster operator that substitutes orbital ϕ_a for ϕ_i and ϕ_b for ϕ_j is given by

$$\hat{t}_{ij} \equiv \sum_{a>b} t_{ij}^{ab} a_a^\dagger a_b^\dagger a_j a_i \quad [23]$$

(Again note that the order of replacement is important for the sign of the resulting determinant.) Hence, the 27th term on the right-hand side of Eq. [12] shown explicitly in Eq. [13] may be written simply as

$$|f_{ij}\phi_k f_l\rangle = \hat{t}_{ij} \hat{t}_l |\Phi_0\rangle \quad [24]$$

The creation operators in Eqs. [22] and [23] are restricted to act only on the virtual orbitals, and the annihilation operators may act only on the occupied orbitals. Therefore, by Eq. [21], the creation–annihilation operator pairs exactly anticommute:

$$a_a^\dagger a_i + a_i a_a^\dagger = \delta_{ia} = 0 \quad [25]$$

since the occupied orbital ϕ_i and the virtual orbital ϕ_a cannot be the same. Therefore, by the equation above as well as the anticommutation relations given in Eqs. [19] and [20], *all* the creation and annihilation operators in \hat{t}_i and \hat{t}_{ij} anticommute. Given the additional fact that the cluster operators always contain even numbers of second-quantized operators, the \hat{t}_i and \hat{t}_{ij} operators will exactly commute.^c

Equations [22] and [23] may be used to rewrite the long one- and two-orbital cluster wavefunction in Eq. [12] above as

$$\Psi = \left(1 + \sum_i \hat{t}_i + \frac{1}{2} \sum_{ij} \hat{t}_i \hat{t}_j + \frac{1}{6} \sum_{ijk} \hat{t}_i \hat{t}_j \hat{t}_k + \frac{1}{2} \sum_{ij} \hat{t}_{ij} + \frac{1}{8} \sum_{ijkl} \hat{t}_{ij} \hat{t}_{kl} \right. \\ \left. + \frac{1}{24} \sum_{ijkl} \hat{t}_i \hat{t}_j \hat{t}_k \hat{t}_l + \frac{1}{2} \sum_{ijk} \hat{t}_{ij} \hat{t}_k + \frac{1}{4} \sum_{ijkl} \hat{t}_{ij} \hat{t}_k \hat{t}_l \right) \Phi_0 \quad [26]$$

We may simplify this expression even further by defining the total one- and two-orbital cluster operators

$$\hat{T}_1 \equiv \sum_i \hat{t}_i = \sum_{ia} t_i^a a_a^\dagger a_i \quad [27]$$

and

$$\hat{T}_2 \equiv \frac{1}{2} \sum_{ij} \hat{t}_{ij} = \frac{1}{4} \sum_{ijab} t_{ij}^{ab} a_a^\dagger a_b^\dagger a_j a_i \quad [28]$$

respectively.^d More generally, an n -orbital cluster operator may be defined as

$$\hat{T}_n = \left(\frac{1}{n!} \right)^2 \sum_{ij\dots ab\dots}^n t_{ij\dots ab\dots}^{ab\dots} a_a^\dagger a_b^\dagger \dots a_j a_i \quad [29]$$

^cNote that commutation of cluster operators holds only when the occupied and virtual orbital spaces are disjoint, as is the case in spin-orbital or spin-restricted closed-shell theories. For spin-restricted open-shell approaches, where singly occupied orbitals contribute terms to both the occupied and virtual orbital subspaces, the commutation relations of cluster operators are significantly more complicated. See Ref. 36 for a discussion of this issue.

^dThe factors of $1/2$ and $1/4$ are included here to correct for the “double counting” resulting from the now unrestricted summations over i , j , a , and b .

This reduces the wavefunction expression to

$$\Psi = \left(1 + \hat{T}_1 + \frac{1}{2!} \hat{T}_1^2 + \frac{1}{3!} \hat{T}_1^3 + \hat{T}_2 + \frac{1}{2!} \hat{T}_2^2 + \frac{1}{4!} \hat{T}_1^4 + \hat{T}_2 \hat{T}_1 + \frac{1}{2!} \hat{T}_2 \hat{T}_1^2 \right) \Phi_0 \quad [30]$$

Higher order terms (e.g., \hat{T}_2^3) do not appear, of course, because our example system contains only four electrons. If we remember that \hat{T}_1 and \hat{T}_2 commute, then *all* the terms from the equation above match those from the power series expansion of an exponential function! Thus, the general expression for Eq. [30] is

$$\Psi = e^{\hat{T}_1 + \hat{T}_2} \Phi_0 \equiv e^{\hat{T}} \Phi_0 \quad [31]$$

which is a rather convenient reduction from the original Eq. [12].

The “exponential ansatz” given in Eq. [31] is one of the central equations of coupled cluster theory. The exponentiated cluster operator, \hat{T} , when applied to the reference determinant, produces a new wavefunction containing cluster functions, each of which correlates the motion of electrons within specific orbitals. If \hat{T} includes contributions from all possible orbital groupings for the N -electron system (that is, $\hat{T}_1, \hat{T}_2, \dots, \hat{T}_N$), then the exact wavefunction within the given one-electron basis may be obtained from the reference function. The cluster operators, \hat{T}_n , are frequently referred to as *excitation* operators, since the determinants they produce from Φ_0 resemble excited states in Hartree–Fock theory. Truncation of the cluster operator at specific substitution/excitation levels leads to a hierarchy of coupled cluster techniques (e.g., $\hat{T} \equiv \hat{T}_1 + \hat{T}_2 \rightarrow \text{CCSD}$; $\hat{T} \equiv \hat{T}_1 + \hat{T}_2 + \hat{T}_3 \rightarrow \text{CCSDT}$, etc., where “S,” “D,” and “T,” indicate that single, double, and triple excitations, respectively, are included in the wavefunction expansion).

Wavefunction Separability and Size Consistency of the Energy

It is perhaps useful to compare the exponential ansatz of Eq. [31] with the analogous expansions of other wavefunctions. In the configuration interaction (CI) approach,^{85,86} for example, a linear excitation operator is used instead of an exponential,

$$\Psi_{\text{CI}} = (1 + \hat{C}) \Phi_0 \quad [32]$$

where \hat{C} is a linear combination of cluster-like operators defined similarly to \hat{T} , namely,

$$\begin{aligned}\hat{C} &= \hat{C}_1 + \hat{C}_2 + \dots \\ &= \sum_{ia} c_i^a a_a^\dagger a_i + \frac{1}{4} \sum_{ijab} c_{ij}^{ab} a_a^\dagger a_b^\dagger a_j a_i + \dots\end{aligned}\quad [33]$$

Truncation of \hat{C} at the single- and double-excitation level (CISD) leads to a wavefunction with exactly the same number of amplitudes (c_i^a and c_{ij}^{ab}) as that needed for the CCSD wavefunction (t_i^a and t_{ij}^{ab}). However, the latter implicitly includes higher excitation levels (triples and quadruples) by the inclusion of \hat{T} products in the power series expansion of $e^{\hat{T}}$. Such products are commonly referred to in the literature as *disconnected* wavefunction contributions.^e Both the CI and CC methods will produce exact wavefunctions if one does not truncate \hat{C} (full CI) or \hat{T} (full CC). In fact, in the limit of exact linear and exponential wavefunction expansions, a relationship between the CI and CC amplitudes may be developed⁵ that reveals the factorization of each level of CI excitation into connected and disconnected components, for example,

$$\hat{C}_2 = \hat{T}_2 + \frac{1}{2} \hat{T}_1^2 \quad [34]$$

The two different forms of the excitation operator in CI and CC theory have significant consequences for both the energy and wavefunction as the number of electrons is increased or as the (molecular) system is separated into fragments.

Consider the structure of the coupled cluster and configuration interaction wavefunctions for a generic system involving two infinitely separated (and therefore noninteracting) components X and Y. If the molecular orbitals used to define the cluster functions \hat{T} and \hat{C} are localized on each of the two fragments—a choice that will not affect the energy associated with either the reference determinant, Φ_0 , or the correlated wavefunction, Ψ_{CI} or Ψ_{CC} —then the cluster operators may be separated into components involving intrafragment excitations only, that is,

$$\hat{T} = \hat{T}_X + \hat{T}_Y \quad \text{and} \quad \hat{C} = \hat{C}_X + \hat{C}_Y \quad [35]$$

For example, the amplitudes t_{ij}^{ab} or c_{ij}^{ab} , in which orbitals ϕ_i and ϕ_a are localized on fragment X and orbitals ϕ_j and ϕ_b are localized on fragment Y, will be zero. Thus, the total coupled cluster exponential operator may be written as a product of independent coupled cluster operators for each fragment, namely,⁸⁷

$$\Psi_{\text{CC}} = e^{\hat{T}} \Phi_0 = e^{\hat{T}_X + \hat{T}_Y} \Phi_0 = e^{\hat{T}_X} e^{\hat{T}_Y} \Phi_0 \quad [36]$$

Since the reference determinant, Φ_0 , is factorizable into determinants isolated on each fragment (in the localized orbital description), the total coupled cluster

^eThis terminology should not be confused with so-called *disconnected* diagrammatic contributions, which are discussed later in the chapter.

wavefunction may be written as a product of coupled cluster wavefunctions for each of the separated fragments.^f As a result, the sum of the coupled cluster energies computed for each fragment separately is the same as that computed for the “supermolecule” in which the fragments are included together in the calculation,

$$E_{\text{CC}} = E_{\text{CC}}^{\text{X}} + E_{\text{CC}}^{\text{Y}} \quad [37]$$

This property of the coupled cluster energy is commonly known as “size consistency.”⁸⁹

For the configuration interaction wavefunction, however, multiplicative separability is not possible:

$$\Psi_{\text{CI}} = (1 + \hat{C})\Phi_0 = (1 + \hat{C}_{\text{X}} + \hat{C}_{\text{Y}})\Phi_0 \quad [38]$$

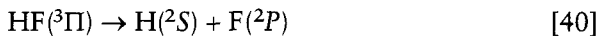
As a result, the CI energy is not size consistent, and the sum of the energies of the separated fragments differs from the CI energy of the supermolecule,

$$E_{\text{CI}} \neq E_{\text{CI}}^{\text{X}} + E_{\text{CI}}^{\text{Y}} \quad [39]$$

In the event that the CI cluster operator, \hat{C} , is not truncated, however, it is possible to write the resulting full CI wavefunction as a product of wavefunctions for each separated fragment, since the linear operator may be transformed into an exponential using a generalized form of Eq. [34].

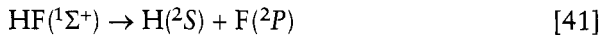
Consider the classic example of an ensemble of hydrogen molecules. Both the CCSD and CISD wavefunctions are exact (within the given one-electron basis set) for a single H_2 molecule, since there are only two electrons to be correlated. Because of the lack of multiplicative separability of the wavefunction, however, errors are introduced in the CI energy in the case of two (or more) noninteracting H_2 units. The size-consistent CCSD method, on the other hand, produces the correct total energy, regardless of the number of noninteracting H_2 monomers in the system, since the total coupled cluster wavefunction may be written as a product of separated wavefunctions, each of which is exact for the given hydrogen molecule.

Some caution should be exercised in the application of the size consistency concept to open-shell fragments, however. As Taylor has pointed out,⁸¹ a given method may be size consistent for some systems but not for others. For example, the spin-restricted Hartree–Fock (RHF) approach is size consistent for the dissociation of the hydrogen fluoride in its ${}^3\Pi$ excited state into atoms,



^fIt should be noted that the localized orbital requirement is used here strictly for ease of analysis, and the property of multiplicative separability of the coupled cluster wavefunction does not strictly depend on this computational requirement, as discussed in Ref. 88.

since the single determinant wavefunction can correctly describe the high-spin electronic states in both the supermolecule and the separated fragments. The RHF method is not size consistent, however, when it describes the dissociation of the ground state of HF into these same atomic states,



This size inconsistency occurs because the two open-shell electrons on the atoms must be singlet-coupled to produce the correct dissociation limit, and a supermolecule, two-determinant approach is therefore required. This difficulty also applies to coupled cluster or perturbation-based wavefunctions that use the RHF determinant as a reference; these methods cannot be size consistent for a given molecular system unless the reference wavefunction is size consistent.

A more general property of the coupled cluster energy that is related to size consistency is “size extensivity.” This is a strictly mathematical characteristic of the wavefunction which relates to scaling of the computed energy with respect to the number of correlated electrons and the resulting energy dependence of the wavefunction amplitude equations. Size extensivity is not dependent on the system under study, and it applies to all regions of the potential energy surface—not just to the fragmentation limit. We will return to this topic later in the chapter after we have discussed the algebraic and diagrammatic techniques needed to derive working coupled cluster equations.

FORMAL COUPLED CLUSTER THEORY

The exponential ansatz described above is essential to coupled cluster theory, but we do not yet have a recipe for determining the so-called cluster amplitudes (t_i^a , t_{ij}^{ab} , etc.) that parameterize the power series expansion implicit in Eq. [31]. Naturally, the starting point for this analysis is the electronic Schrödinger equation,

$$\hat{H}|\Psi\rangle = E|\Psi\rangle \quad [42]$$

where the coupled cluster wavefunction, $\Psi_{\text{CC}} \equiv e^{\hat{T}}\Phi_0$, is used to approximate the exact solution, Ψ ,

$$\hat{H}e^{\hat{T}}|\Phi_0\rangle = E e^{\hat{T}}|\Phi_0\rangle \quad [43]$$

Using a “projective” technique, one may left-multiply this equation by the reference, Φ_0 , to obtain an expression for the energy,

$$\langle\Phi_0|\hat{H}e^{\hat{T}}|\Phi_0\rangle = E\langle\Phi_0|e^{\hat{T}}|\Phi_0\rangle = E \quad [44]$$

where intermediate normalization, $\langle \Phi_0 | \Psi_{CC} \rangle = 1$, is assumed. Additionally, one may obtain expressions for the cluster amplitudes by left-projecting the Schrödinger equation by the excited determinants produced by the action of the cluster operator, \hat{T} , on the reference,

$$\langle \Phi_{ij\cdots}^{ab\cdots} | \hat{H} e^{\hat{T}} | \Phi_0 \rangle = E \langle \Phi_{ij\cdots}^{ab\cdots} | e^{\hat{T}} | \Phi_0 \rangle \quad [45]$$

where $|\Phi_{ij\cdots}^{ab\cdots}\rangle$ represents an excited determinant in which orbitals ϕ_i , ϕ_j , etc. have been replaced with orbitals ϕ_a , ϕ_b , etc.^g Projection by the determinant $|\Phi_{ij}^{ab}\rangle$, for example, will produce an equation for the specific amplitude t_{ij}^{ab} (coupled to other amplitudes). These equations are nonlinear (owing to the presence of $e^{\hat{T}}$) and energy dependent. Furthermore, they are formally exact; if the cluster operator, \hat{T} , is not truncated, the exact wavefunction within the space spanned by the set of orthogonal one-electron functions, ϕ_p , may be obtained.

Truncation of the Exponential Ansatz

Recall that the exponentiated operator may be expanded in a power series as

$$e^{\hat{T}} = 1 + \hat{T} + \frac{\hat{T}^2}{2!} + \frac{\hat{T}^3}{3!} + \dots \quad [46]$$

Inserting this into the energy expression Eq. [44] we obtain

$$\langle \Phi_0 | \hat{H} \left(1 + \hat{T} + \frac{\hat{T}^2}{2!} + \frac{\hat{T}^3}{3!} + \dots \right) | \Phi_0 \rangle = E \quad [47]$$

which becomes, after distributing terms,

$$\langle \Phi_0 | \hat{H} | \Phi_0 \rangle + \langle \Phi_0 | \hat{H} \hat{T} | \Phi_0 \rangle + \left\langle \Phi_0 | \hat{H} \frac{\hat{T}^2}{2!} | \Phi_0 \right\rangle + \left\langle \Phi_0 | \hat{H} \frac{\hat{T}^3}{3!} | \Phi_0 \right\rangle + \dots = E \quad [48]$$

Note that \hat{H} is at most a two-particle operator and that \hat{T} is at least a one-particle excitation operator. Then, assuming that the reference wavefunction is a single determinant constructed from a set of one-electron functions, Slater's rules⁸² state that matrix elements of the Hamiltonian between determinants that differ by more than two orbitals are zero. Thus, the fourth term on the left-hand side of Eq. [48] contains, at the least, threefold excitations, and, as a result, that matrix element (and *all* higher order elements) necessarily vanish. The energy equation then simplifies to

^gIn second-quantization terminology, $|\Phi_{ij\cdots}^{ab\cdots}\rangle = a_a^\dagger a_b^\dagger \cdots a_i a_j |\Phi_0\rangle$.

$$\langle \Phi_0 | \hat{H} | \Phi_0 \rangle + \langle \Phi_0 | \hat{H} \hat{T} | \Phi_0 \rangle + \left\langle \Phi_0 | \hat{H} \frac{\hat{T}^2}{2!} | \Phi_0 \right\rangle = E \quad [49]$$

This is the natural truncation of the coupled cluster energy equation; an analogous phenomenon occurs for the amplitude equation (Eq. [45]). This truncation depends *only* on the form of \hat{H} and not on that of \hat{T} or on the number of electrons. Equation [49] is correct even if \hat{T} is truncated to a particular excitation level.

The Hausdorff Expansion

Although the energy and amplitude expressions (Eqs. [44] and [45], respectively) are useful for gaining a formal understanding of the coupled cluster method, they are not amenable to practical computer implementation.⁹⁰ One must first rewrite these expressions in terms of the one- and two-electron integrals arising from the electronic Hamiltonian as well as the cluster amplitudes, which, apart from the energy itself, are the only unknown quantities. To that end, it is convenient to exercise mathematical foresight and multiply the Schrödinger equation (Eq. [43]) by the inverse of the exponential operator, $e^{\hat{T}}$. Upon subsequent left-projection by the reference, Φ_0 , and the excited determinants, $\Phi_{ij\dots}^{ab\dots}$, one obtains modified energy and amplitude equations,

$$\langle \Phi_0 | e^{-\hat{T}} \hat{H} e^{\hat{T}} | \Phi_0 \rangle = E \quad [50]$$

and

$$\langle \Phi_{ij\dots}^{ab\dots} | e^{-\hat{T}} \hat{H} e^{\hat{T}} | \Phi_0 \rangle = 0 \quad [51]$$

respectively, which involve the similarity-transformed Hamiltonian, $e^{-\hat{T}} \hat{H} e^{\hat{T}}$. Equations [50] and [51] define the conventional coupled cluster method. It may be shown that these expressions are equivalent to Eqs. [44] and [45],^{5,80} but with two advantages. First, the amplitude equations (Eq. [51]) are now decoupled from the energy equation (Eq. [50]). Second, a simplification via the so-called Campbell–Baker–Hausdorff formula⁹¹ of $e^{-\hat{T}} \hat{H} e^{\hat{T}}$ leads to a linear combination of nested commutators of \hat{H} with the cluster operator, \hat{T} , namely,

$$\begin{aligned} e^{-\hat{T}} \hat{H} e^{\hat{T}} &= \hat{H} + [\hat{H}, \hat{T}] + \frac{1}{2!} [[\hat{H}, \hat{T}], \hat{T}] + \frac{1}{3!} [[[[\hat{H}, \hat{T}], \hat{T}], \hat{T}]] \\ &\quad + \frac{1}{4!} [[[[[\hat{H}, \hat{T}], \hat{T}], \hat{T}], \hat{T}]] + \dots \end{aligned} \quad [52]$$

This expression is usually referred to simply as the Hausdorff expansion, and although it may not immediately appear to be a simplification of the coupled

cluster equations, the infinite series truncates naturally in a manner somewhat analogous to that described earlier for the operator, $\hat{H}e^T$.

As shown explicitly in Refs. 80, 84, and 92, the creation and annihilation operators described earlier may be used to represent dynamical operators such as the electronic Hamiltonian:

$$\hat{H} = \sum_{pq} h_{pq} a_p^\dagger a_q + \frac{1}{4} \sum_{pqrs} \langle pq||rs\rangle a_p^\dagger a_q^\dagger a_s a_r \quad [53]$$

In this expression, $h_{pq} \equiv \langle \phi_p | \hat{h} | \phi_q \rangle$ represents a matrix element of the one-electron component of the Hamiltonian, \hat{h} , while $\langle pq||rs\rangle \equiv \langle \phi_p \phi_q | \phi_r \phi_s \rangle - \langle \phi_p \phi_q | \phi_s \phi_r \rangle$ is its antisymmetrized two-electron counterpart. Equation [53] contains *general* annihilation and creation operators (e.g., a_p^\dagger or a_q) that may act on orbitals in either occupied or virtual subspaces. The cluster operators, \hat{T}_n , on the other hand, contain operators that are restricted to act in only one of these spaces (e.g., a_b^\dagger , which may act only on the virtual orbitals). As pointed out earlier, the cluster operators therefore commute with one another, but not with the Hamiltonian, \hat{H} . For example, consider the commutator of the pair of general second-quantized operators from the one-electron component of the Hamiltonian in Eq. [53] with the single-excitation pair found in the cluster operator, \hat{T}_1 :

$$[a_p^\dagger a_q, a_a^\dagger a_i] = a_p^\dagger a_q a_a^\dagger a_i - a_a^\dagger a_i a_p^\dagger a_q \quad [54]$$

The anticommutation relations of annihilation and creation operators given in Eqs. [19], [20], and [21] may be applied to the two terms on the right-hand side of this expression to give

$$[a_p^\dagger a_q, a_a^\dagger a_i] = a_p^\dagger \delta_{qa} a_i - a_a^\dagger \delta_{ip} a_q \quad [55]$$

The Kronecker delta functions, δ_{qa} and δ_{ip} , resulting from Eq. [21], cannot be simplified to 1 or 0 because the indices p and q may refer to either occupied or virtual orbitals. The important point here, however, is that the commutator has reduced the number of general-index second-quantized operators by one. Therefore, each nested commutator from the Hausdorff expansion of \hat{H} and \hat{T} serves to *eliminate* one of the electronic Hamiltonian's general-index annihilation or creation operators in favor of a simple delta function. Since \hat{H} contains at most *four* such operators (in its two-electron component), all creation or annihilation operators arising from \hat{H} will be eliminated beginning with the quadruply nested commutator in the Hausdorff expansion. All higher order terms will contain commutators of only the cluster operators, \hat{T} , and are therefore zero. Hence, Eq. [52] truncates itself naturally after the first five terms on the right-hand side.⁸⁰ This convenient property results entirely from the two-electron property of the Hamiltonian and from the fact that the cluster opera-

tors commute; it is not dependent on the number of electrons in the system, the level of substitution included in \hat{T} , or any consideration of the types of determinant upon which the operators act.

Using the truncated Hausdorff expansion, we may obtain analytic expressions for the commutators in Eq. [52] and insert these into the coupled cluster energy and amplitude equations (Eqs. [50] and [51], respectively). However, this is only the first step in obtaining expressions that may be efficiently implemented on the computer. We must next choose a truncation of \hat{T} and then derive expressions containing only one- and two-electron integrals and cluster amplitudes. This is a formidable task to which we will return in later sections.

A Variational Coupled Cluster Theory?

The “projective” techniques described above for solving the coupled cluster equations represent a particularly convenient way of obtaining the amplitudes that define the coupled cluster wavefunction, $e^{\hat{T}}\Phi_0$. However, the asymmetric energy formula shown in Eq. [50] does not conform to any variational conditions in which the energy is determined from an expectation value equation. As a result, the computed energy will not be an upper bound to the exact energy in the event that the cluster operator, \hat{T} , is truncated. But the exponential ansatz does not *require* that we solve the coupled cluster equations in this manner. We could, instead, construct a variational solution by requiring that the amplitudes minimize the expression^{1,2}

$$E_{\text{exact}} \leq E = \frac{\langle \Phi_0 | (e^{\hat{T}})^\dagger \hat{H} e^{\hat{T}} | \Phi_0 \rangle}{\langle \Phi_0 | (e^{\hat{T}})^\dagger e^{\hat{T}} | \Phi_0 \rangle} = \frac{\langle \Psi | \hat{H} | \Psi \rangle}{\langle \Psi | \Psi \rangle} \quad [56]$$

Unfortunately, this equation is considerably more complex than the projective energy expression given in Eq. [50], since there is no natural truncation of its power series expansion,

$$\langle \Phi_0 | (e^{\hat{T}})^\dagger \hat{H} e^{\hat{T}} | \Phi_0 \rangle = \langle \Phi_0 | (1 + \hat{T}^\dagger + \frac{1}{2}(\hat{T}^\dagger)^2 + \dots) \hat{H} (1 + \hat{T} + \frac{1}{2}(\hat{T})^2 + \dots) | \Phi_0 \rangle \quad [57]$$

For example, in the term $\langle \Phi_0 | \hat{T}^\dagger \hat{H} \hat{T} | \Phi_0 \rangle$, which is included in Eq. [57], as \hat{T} creates an excited determinant from $|\Phi_0\rangle$ on the right, \hat{T}^\dagger creates an excited determinant from $\langle\Phi_0|$ on the left. Thus, the Hamiltonian matrix elements will not vanish at some high excitation level, and the series will not terminate before the N -electron limit. Truncation of this expression for large numbers of terms appears to be arbitrary at best.

The ostensible impracticality of a variational coupled cluster theory raises an important question regarding the physical reality of the coupled cluster energy as computed using projective, asymmetric techniques. Quantum mechanics dictates that physical observables (such as the energy) are expectation

values of Hermitian operators. The coupled cluster energy expression contains the operator $e^{-\hat{T}}\hat{H}e^{\hat{T}}$, which is not Hermitian, regardless of the truncation of \hat{T} :^b

$$(e^{-\hat{T}}\hat{H}e^{\hat{T}})^\dagger = (e^{\hat{T}})^\dagger \hat{H}(e^{-\hat{T}})^\dagger = e^{\hat{T}^\dagger}\hat{H}e^{-\hat{T}^\dagger} \neq e^{-\hat{T}}\hat{H}e^{\hat{T}} \quad [58]$$

However, if \hat{T} is not truncated, the similarity transformed operator has an energy eigenvalue spectrum that is *identical* to the original Hermitian operator, \hat{H} , thus justifying its formal use in quantum mechanical models. Practically speaking, the coupled cluster energy tends to closely approximate the expectation value result even when \hat{T} is truncated. Furthermore, one might speculate that some measure of the difference between the expectation value and asymmetric energies—perhaps as measured by the asymmetry of the coupled cluster reduced density⁶⁵—might prove to be a useful diagnostic of the reliability of results obtained from the coupled cluster method for specific systems. This issue has been recently discussed by Kutzelnigg.⁹³

Variational coupled cluster methods that make use of Eq. [57] have been studied by several researchers. The unitary coupled cluster (UCC) approach in which the cluster operator \hat{T} is replaced by $\hat{T} - \hat{T}^\dagger$ (where \hat{T}^\dagger indicates a de-excitation operator that is the Hermitian adjoint of \hat{T}) was pursued by Hoffmann and Simons.^{94,95} The infinite series in this case is not truncated arbitrarily, but instead by identifying which terms are needed to complete the series through a particular order of perturbation theory. Bartlett and Noga have constructed an alternative theory, termed the expectation value coupled cluster (XCC) method,⁹⁶ in which the usual definition of \hat{T} is retained and Eq. [57] is used, but again the series truncation is based on perturbation theory arguments. Finally, we note the extended coupled cluster method (ECCM) of Arponen and Bishop,^{97,98} which uses a modified energy functional including an additional exponentiated de-excitation operator analogous to $e^{\hat{T}^\dagger}$. These as well as other variational and semivariational approaches to the cluster expansion have been reviewed by Bartlett et al.⁹⁹ and by Szalay et al.¹⁰⁰

^bThe inequality with the final term in this expression relies on the fact that the Hermitian adjoint of an excitation (cluster) operator, \hat{T} , is a de-excitation operator, as can be seen from the properties of its component annihilation and creation operators. For example, we note that

$$\hat{T}_1 = \sum_{ia} t_i^a a_a^\dagger a_i \neq \hat{T}_1^\dagger = \sum_{ia} (t_i^a)^* a_i^\dagger a_a$$

On the other hand, the inverse of the exponentiated excitation operator, $e^{-\hat{T}}$, is also an excitation operator, as can be seen from its power series expansion,

$$e^{-\hat{T}} = 1 - \hat{T} + \frac{1}{2!} \hat{T}^2 - \frac{1}{3!} \hat{T}^3 + \dots$$

An Eigenvalue Approach to Coupled Cluster Theory

Up to this point, our discussion has focused on the expansion of the wavefunction using the exponential ansatz given in Eq. [31]. When the cluster operator, \hat{T} , is truncated, the resulting CC wavefunction may be viewed as an approximate eigenfunction of the exact electronic Hamiltonian. However, another equally valid perspective focuses instead on construction of the *exact* eigenvectors of an *approximate* Hamiltonian. In configuration interaction theory, for example, one conventionally represents the electronic Hamiltonian within a determinantal basis consisting of the reference (Φ_0), single excitations (Φ_i^a), double excitations (Φ_{ij}^{ab}), and so on. In the CISD approximation, the Hamiltonian is represented schematically as

$$\hat{H}_{\text{CISD}} = \begin{pmatrix} E_{\text{SCF}} & 0 & \hat{H}_{0D} \\ 0 & \hat{H}_{SS} & \hat{H}_{SD} \\ \hat{H}_{D0} & \hat{H}_{DS} & \hat{H}_{DD} \end{pmatrix} \quad [59]$$

where \hat{H}_{SD} , for example, represents the block of Hamiltonian matrix elements between singly and doubly excited determinants and $E_{\text{SCF}} = \langle \Phi_0 | \hat{H} | \Phi_0 \rangle$. We assume here that Brillouin's theorem⁸² holds for the reference determinant, and therefore the matrix elements involving Φ_0 and singly excited determinants are zero. The CISD energy is the lowest eigenvalue of this Hermitian matrix, and the CISD wavefunction is the corresponding eigenvector, that is,

$$\hat{H}_{\text{CISD}} |\Psi_{\text{CISD}}\rangle = E_{\text{CISD}} |\Psi_{\text{CISD}}\rangle \quad [60]$$

The coupled cluster “Schrödinger equation,” which leads to the energy and amplitude expressions given in Eqs. [50] and [51], may be written as

$$e^{-\hat{T}} \hat{H} e^{\hat{T}} |\Phi_0\rangle = E |\Phi_0\rangle \quad [61]$$

Like Eq. [60], this equation represents an eigenvalue problem¹⁰¹ in which the similarity-transformed Hamiltonian, $\bar{H} \equiv e^{-\hat{T}} \hat{H} e^{\hat{T}}$, is used in place of the bare electronic Hamiltonian, \hat{H} . The ground state eigenvector of \bar{H} is simply $|\Phi_0\rangle$ with eigenvalue E . However, \bar{H} is not Hermitian, unlike the CI Hamiltonian, and its matrix representation is therefore nonsymmetric. In the CCSD approximation, for example,

$$\bar{H}_{\text{CCSD}} = \begin{pmatrix} E_{\text{CCSD}} & \bar{H}_{0S} & \bar{H}_{0D} \\ 0 & \bar{H}_{SS} & \bar{H}_{SD} \\ 0 & \bar{H}_{DS} & \bar{H}_{DD} \end{pmatrix} \quad [62]$$

where the CCSD energy is given by $\langle \Phi_0 | \bar{H} | \Phi_0 \rangle$, by Eq. [50] and $\bar{H}_{DS} \neq \bar{H}_{SD}$. The blocks of matrix elements $\langle \Phi_i^a | \bar{H} | \Phi_0 \rangle$ and $\langle \Phi_{ij}^{ab} | \bar{H} | \Phi_0 \rangle$ are both zero because the \hat{T} amplitudes that parameterize the similarity transformation of \bar{H} into \bar{H} satisfy the equations

$$0 = \langle \Phi_i^a | \bar{H} | \Phi_0 \rangle \quad [63]$$

and

$$0 = \langle \Phi_{ij}^{ab} | \bar{H} | \Phi_0 \rangle \quad [64]$$

which are simply specific cases of Eq. [51]. Furthermore, unlike the CI case, \bar{H}_{0S} is nonzero in spite of Brillouin's theorem because \bar{H} includes contributions from products of the bare Hamiltonian with the cluster operators, \hat{T} .

As a result of the asymmetry of \bar{H} , the right-hand eigenvalue problem given in Eq. [61] is different from the left-hand eigenvalue problem,

$$\langle \mathcal{L} | \bar{H} = \langle \mathcal{L} | E \quad [65]$$

The computed energy, E , however, is the same for both equations. In Eq. [65], the left eigenvector, $\langle \mathcal{L} |$, may be written in terms of a cluster operator, $\hat{\mathcal{L}}$, acting on the reference from the right, namely,

$$\langle \mathcal{L} | \equiv \langle \Phi_0 | \hat{\mathcal{L}} \quad [66]$$

The operator $\hat{\mathcal{L}}$ may be defined in analogy to the cluster operator, \hat{T} , as a sum of cluster operators,

$$\hat{\mathcal{L}} = 1 + \hat{\mathcal{L}}_1 + \hat{\mathcal{L}}_2 + \dots \quad [67]$$

The leading term of 1, which does not appear in \hat{T} (cf. Eq. [29]), is required in order that the left- and right-hand eigenvectors have unit overlap with one another. Unlike the cluster operators, \hat{T}_n , the operators $\hat{\mathcal{L}}_n$ act to the left on $\langle \Phi_0 |$. Therefore, it is convenient to define them as *de-excitation* operators (or, equivalently, as bra-state excitation operators),

$$\hat{\mathcal{L}}_n = \left(\frac{1}{n!} \right)^2 \sum_{ij\dots ab\dots}^n l_{ab\dots}^{ij\dots} a_i^\dagger a_j^\dagger \dots a_b a_a \quad [68]$$

The task of determining the left-hand ground state eigenvector of \bar{H} is thus reduced to determining the amplitudes $l_{ab\dots}^{ij\dots}$. The ground state coupled cluster energy may then be written as

$$E = \langle \Phi_0 | \hat{\mathcal{L}} \bar{H} | \Phi_0 \rangle \quad [69]$$

where the left and right wavefunctions are assumed to be normalized according to $\langle \Phi_0 | \hat{\mathcal{L}} | \Phi_0 \rangle = 1$. Equation [69] which is more general than Eq. [50], provides a particularly useful starting point for the derivation of coupled cluster analytic energy derivatives; the left-hand eigenvector, $\langle \Phi_0 | \hat{\mathcal{L}}$, is related to the $\hat{\Lambda}$ operator that arises as a result of the response of the cluster amplitudes to an external perturbation parameter.⁴⁹

The concept of the coupled cluster method as an eigenvalue problem may be easily generalized to include excited states (in this case, states that are not the lowest in energy within a given symmetry). We may write the more general right-hand problem as

$$\bar{H} \hat{\mathcal{R}}(m) | \Phi_0 \rangle = E_m \hat{\mathcal{R}}(m) | \Phi_0 \rangle \quad [70]$$

where

$$\hat{\mathcal{R}}(m) = \hat{\mathcal{R}}_0(m) + \hat{\mathcal{R}}_1(m) + \hat{\mathcal{R}}_2(m) + \dots \quad [71]$$

represents a cluster operator expansion for the m th excited state with energy E_m . For the ground state, $\hat{\mathcal{R}}(0) = 1$, as described above. Similarly, the left-hand eigenvalue problem becomes

$$\langle \Phi_0 | \hat{\mathcal{L}}(m) \bar{H} = \langle \Phi_0 | \hat{\mathcal{L}}(m) E_m \quad [72]$$

“Biorthonormality” of the left-hand and right-hand eigenvectors may be enforced such that

$$\langle \Phi_0 | \hat{\mathcal{L}}(m) \hat{\mathcal{R}}(n) | \Phi_0 \rangle = \delta_{mn} \quad [73]$$

which leads to the generalized coupled cluster energy expression

$$E_m = \langle \Phi_0 | \hat{\mathcal{L}}(m) \bar{H} \hat{\mathcal{R}}(m) | \Phi_0 \rangle \quad [74]$$

Note that the biorthonormality of the left- and right-hand states does not imply orthonormality of the left- or right-hand states among themselves, for example,

$$\langle \Phi_0 | \hat{\mathcal{R}}^\dagger(m) \hat{\mathcal{R}}(n) | \Phi_0 \rangle \neq \delta_{mn} \quad [75]$$

The eigenvalue perspective described above does not offer any computational convenience for the ground state problem because one must still use Eq. [51] to determine the cluster amplitudes that define the similarity transformation of the electronic Hamiltonian, \hat{H} , into the CC Hamiltonian, \bar{H} . However,

this perspective does provide a rather simple CI-like approach for determining excited state wavefunctions. Equation-of-motion coupled cluster theory (EOM-CC),^{5,60–63,65} the name of which is based on early formulations involving response operators, has seen a considerable rise in popularity in recent years. The EOM-CCSD method,^{65,73} for example, is defined as the diagonalization of the CCSD effective Hamiltonian, \bar{H}_{CCSD} (where the cluster amplitudes are taken from the corresponding CCSD ground state energy calculation) in the space of all singly and doubly excited determinants. It should be noted, however, that truncation of the cluster operator, \hat{T} , in the definition of \bar{H} does not introduce errors into the EOM-CC energy because the exact energy would still be obtained if the diagonalization basis were complete.

Much effort has been devoted recently to the development of a variety of excited state coupled cluster techniques that are related to EOM-CC. For example, the linear response coupled cluster (LR-CC) approach⁷³ originally described by Monkhorst⁵ and implemented by several groups^{69,70,102–105} can be used to obtain identical results to those given by conventional EOM-CC. In addition, the symmetry-adapted cluster (SAC-CI) method devised independently by Nakatsuji^{106–108} in the late 1970s may be viewed as an approximation to EOM-CC and LR-CC. A relationship between EOM-CC and Fock-space multireference coupled cluster theory (FS-MRCC)^{64,109–112} has been exploited in the construction of methods for describing classes of doublet electronic states that are accessible via either electron attachment (EOMEA-CC)^{88,113} or ionization (EOMIP-CC)^{67,109–111} from a given reference. Finally, we note the work by Nooijen and Bartlett on the similarity-transformed equation-of-motion coupled cluster (STEOM-CC) method,^{74,114} in which the effective Hamiltonian described above is further transformed using a reduced cluster operator, \hat{S} , which serves to decouple singly excited determinants from doubly and triply excited determinants in \bar{H} .

DERIVATION OF THE COUPLED CLUSTER EQUATIONS

It is the need to remove the “unlinked clusters” and the introduction of Feynman diagrams which make MBPT [and CC theory] appear unfamiliar to quantum chemists.¹¹⁵

—K. F. Freed

In this section we construct working equations for the coupled cluster singles and doubles (CCSD) method. Beginning from the approximation $\hat{T} \equiv \hat{T}_1 + \hat{T}_2$, we use algebraic and diagrammatic techniques to obtain programmable

equations for the cluster amplitudes, t_i^a and t_{ij}^{ab} , in terms of the one- and two-electron integrals of the electronic Hamiltonian. As a first step we must introduce a few important tools of second quantization such as normal ordering and Wick's theorem to make the mathematical analysis much less complicated. The approach described here may easily be extended to higher order cluster approximations (e.g., CCSDT and CCSDTQ, where the latter includes quadruple excitations), as well as to many-body perturbation theory expressions.

As indicated by Karl Freed in the quotation above, the general quantum chemistry community has been slow to accept diagrammatic analyses of many-body perturbation theory and coupled cluster methods, and, until recently, these techniques have been used by relatively few researchers in the field. One of the goals of this review is to explain in straightforward terms one diagrammatic approach commonly used for the construction of coupled cluster equations. While attempting to be somewhat rigorous in the algebraic derivation of the coupled cluster equations, we present the corresponding diagrams with only minimal justification. For readers with a strong mathematical background who are interested in more detail, an extensive analysis of a similar diagrammatic technique may be found in a text by Harris, Monkhorst, and Freeman.⁸⁰

Normal-Ordered Second-Quantized Operators

As stated in Merzbacher's text on quantum mechanics⁹¹ (Chapter 21, Section 4), a normal-ordered string of second-quantization operators is one in which we find "all annihilation operators standing to the right of all creation operators." Normal ordering of such strings provides a bookkeeping system by which the nonzero matrix elements of second-quantized operators may be more easily identified. As an example, consider an arbitrary string of annihilation and creation operators, $\hat{A} = a_p a_q^\dagger a_r a_s^\dagger$. By application of the anticommutation relations given in Eqs. [19], [20], and [21], we may move the two annihilation operators to the right and therefore write the string in an equivalent form as

$$\begin{aligned}\hat{A} &= a_p a_q^\dagger a_r a_s^\dagger \\ &= \delta_{pq} a_r a_s^\dagger - a_q^\dagger a_p a_r a_s^\dagger \\ &= \delta_{pq} \delta_{rs} - \delta_{pq} a_s^\dagger a_r - \delta_{rs} a_q^\dagger a_p + a_q^\dagger a_p a_s^\dagger a_r \\ &= \delta_{pq} \delta_{rs} - \delta_{pq} a_s^\dagger a_r - \delta_{rs} a_q^\dagger a_p + \delta_{ps} a_q^\dagger a_r - a_q^\dagger a_s^\dagger a_p a_r\end{aligned}\quad [76]$$

Three of the five terms in the final rearrangement contain operator strings of reduced length, and the first term contains only Kronecker delta functions. Note also that all the operator strings on the right-hand side of the final equality are normal-ordered by Merzbacher's definition. If we now evaluate the quan-

tum mechanical expectation value of this operator in the true vacuum state,ⁱ | ⟩, we obtain

$$\begin{aligned}\langle \hat{A} \rangle &= \langle |\delta_{pq}\delta_{rs}| \rangle - \langle |\delta_{pq}a_s^\dagger a_r| \rangle - \langle |\delta_{rs}a_q^\dagger a_p| \rangle + \langle |\delta_{ps}a_q^\dagger a_r| \rangle - \langle |a_q^\dagger a_s^\dagger a_p a_r| \rangle \\ &= \delta_{pq}\delta_{rs}\end{aligned}\quad [77]$$

where we assume that the vacuum state is normalized. Hence, the only term of \hat{A} in Eq. [76] that produces a nonzero result is the one containing no second-quantized operators; all other terms involve application of an annihilation operator to | ⟩ on the right.

If, on the other hand, we wish to evaluate a matrix element of \hat{A} involving determinants other than | ⟩ on the left and right, normal ordering simplifies this analysis as well. For example, consider the matrix element of \hat{A} between the single-particle states $\langle \phi_t |$ and $| \phi_u \rangle$:

$$\langle \phi_t | \hat{A} | \phi_u \rangle = \langle | a_t \hat{A} a_u^\dagger | \rangle \quad [78]$$

Since the left- and right-hand states may be written simply as single annihilation and creation operators acting on the vacuum, the desired matrix element of \hat{A} may be rewritten as the vacuum expectation value of a new operator, $\hat{B} \equiv a_t \hat{A} a_u^\dagger$. Therefore, we need only rewrite \hat{B} in normal order and select only the terms that contain no annihilation or creation operators, as we did in Eq. [77]. After much algebraic manipulation, which we shall omit here, it can be shown that

$$\langle \phi_t | \hat{A} | \phi_u \rangle = \langle | \hat{B} | \rangle = \delta_{tu}\delta_{pq}\delta_{rs} + \delta_{tq}\delta_{ps}\delta_{ru} - \delta_{tq}\delta_{pu}\delta_{rs} - \delta_{ts}\delta_{pq}\delta_{ru} \quad [79]$$

By rearranging a given string of annihilation and creation operators into a normal-ordered form, matrix elements of such operators between determinantal wavefunctions may be evaluated in a relatively algorithmic manner. However, such an approach based on the direct application of the anticommutation relations can be quite tedious even for relatively short operator strings, and many opportunities for error may arise.

Wick's Theorem for the Evaluation of Matrix Elements

Using the anticommutation relations of Eqs. [19], [20], and [21], an arbitrary string of annihilation and creation operators can be written as a linear combination of normal-ordered strings (most of which contain reduced num-

ⁱThe vacuum, | ⟩, is a state containing no electrons.

bers of operators) multiplied by Kronecker delta functions. These reduced terms may be viewed as arising from so-called contractions between operator pairs. A *contraction* between two arbitrary annihilation/creation operators, A and B , is defined as

$$\overline{AB} \equiv AB - \{AB\}_v \quad [80]$$

where the notation $\{AB\}_v$ indicates the normal-ordered form of the pair (the subscript v for vacuum will be explained shortly). The contraction between the operators is simply the original ordering of the pair minus the normal-ordered pair. For example, if both operators are annihilation or creation operators, the contraction is zero because such pairs are already normal-ordered:

$$\overline{a_p^{\dagger}a_q} = a_p^{\dagger}a_q - \{a_p^{\dagger}a_q\}_v = a_p^{\dagger}a_q - a_p^{\dagger}a_q = 0 \quad [81]$$

and

$$\overline{a_p^{\dagger}a_q^{\dagger}} = a_p^{\dagger}a_q^{\dagger} - \{a_p^{\dagger}a_q^{\dagger}\}_v = a_p^{\dagger}a_q^{\dagger} - a_p^{\dagger}a_q^{\dagger} = 0 \quad [82]$$

In addition, a third combination in which A is a creation operator and B is an annihilation operator is also zero, since the string is again already normal-ordered:

$$\overline{a_p^{\dagger}a_q} = a_p^{\dagger}a_q - \{a_p^{\dagger}a_q\}_v = a_p^{\dagger}a_q - a_p^{\dagger}a_q = 0 \quad [83]$$

The final combination, in which A is an annihilation operator and B is a creation operator, is not zero, however, owing to the anticommutation relations in Eq. [21].^j Thus we write

$$\overline{a_p^{\dagger}a_q^{\dagger}} = a_p^{\dagger}a_q^{\dagger} - \{a_p^{\dagger}a_q^{\dagger}\}_v = a_p^{\dagger}a_q^{\dagger} + a_q^{\dagger}a_p^{\dagger} = \delta_{pq} \quad [84]$$

Note that we must maintain the correct sign when the operators in the braces, $\{ \ }_v$, are reordered.

Wick's theorem¹¹⁶ provides a recipe by which an arbitrary string of annihilation and creation operators, $ABC \cdots XYZ$, may be written as a linear combination of normal-ordered strings. Schematically, Wick's theorem is

^jNote that the use of the braces, $\{ \ }_v$, around a string implies that the operators contained therein, except for any pair being contracted, exactly anticommute. Hence, a general term such as $\{ABC \cdots XYZ\}_v$ may be written *exactly* as $-\{BAC \cdots XYZ\}_v$, without concern for the anticommutation relations.

$$\begin{aligned}
 ABC \cdots XYZ &= \{ABC \cdots XYZ\}_v \\
 &\quad + \sum_{singles} \{\overline{AB} \cdots XYZ\}_v \\
 &\quad + \sum_{doubles} \{\overline{\overline{ABC}} \cdots XYZ\}_v \\
 &\quad + \dots
 \end{aligned} \tag{85}$$

where the limits (“singles,” “doubles,” etc.) refer to the number of pairwise contractions included in the summation. The notation $\{ \}_v$ has again been used to indicate the normal-ordered form of the given string. If we apply this theorem to the operator from the last section, \hat{A} , we obtain

$$\hat{A} = \{a_p a_q^\dagger a_r a_s^\dagger\}_v + \{\overline{a_p} a_q^\dagger a_r a_s^\dagger\}_v + \{\overline{a_p} \overline{a_q}^\dagger a_r a_s^\dagger\}_v + \{a_p a_q^\dagger \overline{a_r} a_s^\dagger\}_v + \{\overline{a_p} \overline{a_q}^\dagger \overline{a_r} a_s^\dagger\}_v \tag{86}$$

where only the nonzero contractions have been included (cf. Eqs. [81]–[84]). The evaluation of the pairwise contractions may introduce sign changes because the string of operators must be permuted to bring the pair together before the contraction may be evaluated. If the number of permutations is odd, the sign is negative; if the number is even, the sign is positive. For example, a contraction of the form

$$\{\overline{\overline{ABCD}}\}_v = \{\overline{AB} \overline{CD}\}_v \tag{87}$$

would have a positive sign because two permutations are necessary to bring operators A and D into adjacency; but a contraction of the form

$$\{\overline{AB} \overline{CD}\}_v = - \{\overline{AC} \overline{BD}\}_v \tag{88}$$

would have a negative sign, since only one permutation is necessary to bring operators A and C together. Thus, the contraction introduces the sign $(-1)^P$, where P is the number of permutations required to bring the operators into adjacency. Evaluating the contractions above for \hat{A} gives

$$\begin{aligned}
 \hat{A} &= \{a_p a_q^\dagger a_r a_s^\dagger\}_v + \delta_{pq} \{a_r a_s^\dagger\}_v + \delta_{ps} \{a_q^\dagger a_r\}_v + \delta_{rs} \{a_p a_q^\dagger\}_v + \delta_{pq} \delta_{rs} \\
 &= a_q^\dagger a_s^\dagger a_p a_r - \delta_{pq} a_s^\dagger a_r + \delta_{ps} a_q^\dagger a_r - \delta_{rs} a_q^\dagger a_p + \delta_{pq} \delta_{rs}
 \end{aligned} \tag{89}$$

This result is identical to that obtained using the anticommutation relations and given in Eq. [76].

How does Wick’s theorem help us in evaluating matrix elements of second-quantized operators? Recall that any matrix element of an operator may be written as a vacuum expectation value by simply writing its left- and right-hand determinants as operator strings acting on the vacuum state, $| \rangle$. The

composite string of annihilation and creation operators may then be rewritten using Wick's theorem as an expansion of normal-ordered strings. *However, the only terms that need to be retained in this expansion are those that are "fully contracted."* All other terms will give a zero result, by construction. For example, for the operator \hat{B} from the last section, Wick's theorem gives the following fully contracted terms:

$$\{\overbrace{a_t a_p a_q^+ a_r a_s^+ a_u^+}\}_{\text{v}} + \{\overbrace{a_t a_p a_q^+ a_r a_s^+ a_u^+}\}_{\text{v}} + \{\overbrace{a_t a_p a_q^+ a_r a_s^+ a_u^+}\}_{\text{v}} + \{\overbrace{a_t a_p a_q^+ a_r a_s^+ a_u^+}\}_{\text{v}} \quad [90]$$

which, when the contractions are evaluated, will give exactly the result given in Eq. [79]. The large number of contractions in Eq. [90] also suggests a useful rule of thumb for determining the sign of a fully contracted term: if the number of crossings in the contraction lines is odd, the sign on the term is negative; if the number of crossings is even, the sign is positive. For example, the sign on the second term in Eq. [90] is positive, since there are two crossings, whereas the sign on the third term is negative, since there is only one crossing.^k

A somewhat more general version of Wick's theorem may be developed which involves products of operator strings, some or all of which may be normal-ordered.¹¹⁷ The original form of Wick's theorem is only slightly modified in that the contractions need be evaluated only between normal-ordered strings and not within them. For example, for a product of two normal-ordered strings, the generalized Wick's theorem says that

$$\begin{aligned} \{ABC \dots\}_{\text{v}} \{XYZ \dots\}_{\text{v}} &= \{ABC \dots XYZ \dots\}_{\text{v}} + \sum_{\text{singles}} \{\overbrace{ABC \dots XYZ \dots}\}_{\text{v}} \\ &\quad + \sum_{\text{doubles}} \{\overbrace{ABC \dots XYZ \dots}\}_{\text{v}} + \dots \end{aligned} \quad [91]$$

This equation easily extends to products of several strings.

Another approach to the problem of matrix element evaluation and operator algebra is presented in the text by Harris, Monkhorst, and Freeman,⁸⁰ who describe the so-called contraction theorem. While Wick's theorem serves as a convenient approach to the conversion of a general string of construction operators (or products of strings) into sums of reduced normal-ordered strings, the contraction theorem avoids all use of normal ordering and deals strictly with commutators and anticommutators of general strings. This latter approach will give identical results to the application of Wick's theorem and has a few subtle differences, including an altered sign rule. Note also that one rarely (if ever) finds a proof of Wick's theorem in the modern literature, but Harris, Monkhorst, and Freeman give an explicit proof of their contraction theorem.

^kThis sign rule applies only to fully contracted terms and assumes that one places all the contraction lines above the expression.

The Fermi Vacuum and the Particle–Hole Formalism

In many-electron theories such as configuration interaction or coupled cluster theory, it is more convenient to deal with the n -electron reference determinant, $|\Phi_0\rangle$, rather than the true vacuum state, $| \rangle$. In the evaluation of matrix elements using Wick's theorem as described above, even the use of normal-ordered strings would be tremendously tedious if one had to include the complete set of operators required to generate $|\Phi_0\rangle$ from the true vacuum (i.e., $|\Phi_0\rangle = a_1^\dagger a_2^\dagger a_3^\dagger \cdots | \rangle$).

We will therefore alter the definition of normal ordering from one given relative to the true vacuum to one given relative to the reference state $|\Phi_0\rangle$ (which is sometimes called the “Fermi vacuum”). The one-electron states occupied in $|\Phi_0\rangle$ are referred to as *hole states*, and those unoccupied in $|\Phi_0\rangle$ are referred to as *particle states*. This perhaps nonintuitive nomenclature is based upon the determinant produced when annihilation–creation operator strings act on the Fermi vacuum. That is, a “hole” is created when an originally occupied state is acted upon by an annihilation operator such as a_i , whereas a “particle” is created when an originally unoccupied state is acted upon by a creation operator such as a_i^\dagger . Therefore, we will refer to operators that create or destroy holes and particles as *quasiparticle* (or just *q-particle*) construction operators. That is, *q*-annihilation operators are those that annihilate holes and particles (e.g., a_i^\dagger and a_i), and *q*-creation operators are those that create holes and particles (e.g., a_i and a_i^\dagger).¹ Therefore, a string of second-quantized operators is normal-ordered relative to the Fermi vacuum if all *q*-annihilation operators lie to the right of all *q*-creation operators. We will use $\{ \}$ to denote such normal-ordered strings (note the lack of the subscript v, which we implicitly used earlier to indicate normal ordering relative to the true vacuum).

This new definition of normal ordering changes our analysis of the Wick's theorem contractions only slightly. Whereas before, the only nonzero pairwise contraction required the annihilation operator to be to the left of the creation operator (cf. Eq. [84]), now the only nonzero contractions place the *q*-particle operator to the left of the *q*-particle creation operator. There are only two ways this can occur, namely,

$$\overline{a_i^\dagger a_j} = a_i^\dagger a_j - \{a_i^\dagger a_j\} = a_i^\dagger a_j + a_j a_i^\dagger = \delta_{ij} \quad [92]$$

and

$$\overline{a_a a_b^\dagger} = a_a a_b^\dagger - \{a_a a_b^\dagger\} = a_a a_b^\dagger + a_b^\dagger a_a = \delta_{ab} \quad [93]$$

¹Note that this *q*-particle definition of annihilation and creation simply reverses the roles of second-quantized operators acting in the occupied (hole) space, but leaves those acting in the unoccupied (particle) space untouched.

The analogous contractions that place the q -particle annihilation operator to the right of the q -particle creation operators are zero:

$$\overline{a_a^\dagger a_b} = \overline{a_i^\dagger a_j} = 0 \quad [94]$$

All other combinations necessarily involve mixed hole and particle indices for which the Kronecker delta functions will give zero.

The Normal-Ordered Electronic Hamiltonian

The second-quantized form of the electronic Hamiltonian^{80,84,92}

$$\hat{H} = \sum_{pq} \langle p|\hat{h}|q\rangle a_p^\dagger a_q + \frac{1}{4} \sum_{pqrs} \langle pq||rs\rangle a_p^\dagger a_q^\dagger a_s a_r \quad [95]$$

may be cast into normal-ordered form using Wick's theorem. We may begin by rewriting the pair of operators in the one-electron part of the Hamiltonian as

$$a_p^\dagger a_q = \{a_p^\dagger a_q\} + \{\overline{a_p^\dagger a_q}\} \quad [96]$$

The contraction rules we examined earlier (cf. Eqs. [92] and [93]) state that since the creation operator is on the left, the contraction is zero unless a_p^\dagger and a_q both act in the hole space and give δ_{pq} . This simplifies the one-electron part of the equation to

$$\sum_{pq} \langle p|\hat{h}|q\rangle \{a_p^\dagger a_q\} + \sum_i \langle i|h|i\rangle \quad [97]$$

Now we rewrite the string of annihilation and creation operators from the two-electron part of \hat{H} as

$$\begin{aligned} a_p^\dagger a_q^\dagger a_s a_r &= \{a_p^\dagger a_q^\dagger a_s a_r\} + \{\overline{a_p^\dagger a_q^\dagger a_s a_r}\} + \{a_p^\dagger \overline{a_q^\dagger a_s a_r}\} + \{\overline{a_p^\dagger a_q^\dagger a_s a_r}\} \\ &\quad + \{a_p^\dagger \overline{a_q^\dagger a_s a_r}\} + \{\overline{a_p^\dagger a_q^\dagger a_s a_r}\} + \{\overline{a_p^\dagger a_q^\dagger a_s a_r}\} \end{aligned} \quad [98]$$

Again, all these contractions are zero unless the leftmost operator of the contraction acts in the hole space. This leads to the simplified form

$$\begin{aligned} a_p^\dagger a_q^\dagger a_s a_r &= \{a_p^\dagger a_q^\dagger a_s a_r\} - \delta_{p \in i} \delta_{ps} \{a_q^\dagger a_r\} + \delta_{q \in i} \delta_{qs} \{a_p^\dagger a_r\} + \delta_{p \in i} \delta_{pr} \{a_q^\dagger a_s\} \\ &\quad - \delta_{q \in i} \delta_{qr} \{a_p^\dagger a_s\} - \delta_{p \in i} \delta_{ps} \delta_{q \in i} \delta_{qr} + \delta_{p \in i} \delta_{pr} \delta_{q \in j} \delta_{qs} \end{aligned} \quad [99]$$

where the notation $p \in i$ means that p must be contained in the set of occupied orbitals and the Kronecker delta indicates that p must be equal to i . Note that the signs on each of the terms are derived from the contraction rules discussed earlier. Inserting this expression back into the equation for the two-electron part of the Hamiltonian, we obtain

$$\begin{aligned} & \frac{1}{4} \sum_{pqrs} \langle pq||rs \rangle \{a_p^\dagger a_q^\dagger a_s a_r\} - \frac{1}{4} \sum_{qri} \langle iq||ri \rangle \{a_q^\dagger a_r\} + \frac{1}{4} \sum_{pri} \langle pi||ri \rangle \{a_p^\dagger a_r\} \\ & + \frac{1}{4} \sum_{qsi} \langle iq||is \rangle \{a_q^\dagger a_s\} - \frac{1}{4} \sum_{psi} \langle pi||is \rangle \{a_p^\dagger a_s\} - \frac{1}{4} \sum_{ij} \langle ij||ji \rangle + \frac{1}{4} \sum_{ij} \langle ij||ij \rangle \end{aligned} \quad [100]$$

Remembering that for antisymmetrized two-electron integrals in Dirac's notation, $\langle pq||rs \rangle = -\langle pq||sr \rangle = -\langle qp||rs \rangle = \langle qp||sr \rangle$, we may re-index sums and combine terms where appropriate to obtain

$$\frac{1}{4} \sum_{pqrs} \langle pq||rs \rangle \{a_p^\dagger a_q^\dagger a_s a_r\} + \sum_{pri} \langle pi||ri \rangle \{a_p^\dagger a_r\} + \frac{1}{2} \sum_{ij} \langle ij||ij \rangle \quad [101]$$

The complete Hamiltonian is therefore

$$\begin{aligned} \hat{H} = & \sum_{pq} \langle p|b|q \rangle \{a_p^\dagger a_q\} + \sum_{pri} \langle pi||ri \rangle \{a_p^\dagger a_r\} + \frac{1}{4} \sum_{pqrs} \langle pq||rs \rangle \{a_p^\dagger a_q^\dagger a_s a_r\} \\ & + \sum_i \langle i|b|i \rangle + \frac{1}{2} \sum_{ij} \langle ij||ij \rangle \end{aligned} \quad [102]$$

Note that the first and second terms on the right-hand side of this equation are simply the spin-orbital Fock operator (in normal-ordered form), and the last two terms are the Hartree–Fock energy (i.e., the Fermi vacuum expectation value of the Hamiltonian). Thus, we may write

$$\hat{H} = \sum_{pq} f_{pq} \{a_p^\dagger a_q\} + \frac{1}{4} \sum_{pqrs} \langle pq||rs \rangle \{a_p^\dagger a_q^\dagger a_s a_r\} + \langle \Phi_0 | \hat{H} | \Phi_0 \rangle \quad [103]$$

or

$$\hat{H} = \hat{F}_N + \hat{V}_N + \langle \Phi_0 | \hat{H} | \Phi_0 \rangle \quad [104]$$

where the subscript N indicates normal ordering of all the component operator strings. Therefore, the normal-ordered Hamiltonian is simply

$$\hat{H}_N \equiv \hat{F}_N + \hat{V}_N = \hat{H} - \langle \Phi_0 | \hat{H} | \Phi_0 \rangle \quad [105]$$

This result is easily generalized: the normal-ordered form of an operator is simply the operator itself minus its reference expectation value. For the Hamiltonian example, above, the normal-ordered Hamiltonian is just the Hamiltonian minus the SCF energy (i.e., \hat{H}_N may be considered to be a *correlation* operator). Owing to its considerable convenience for coupled cluster and many-body perturbation theory analyses, this conventional form of \hat{H} given in Eq. [105] is adopted for the remainder of this chapter.

Simplification of the Coupled Cluster Hamiltonian

The concepts of normal ordering and Wick's theorem provide the mathematical tools needed to derive programmable coupled cluster equations from the more formal expressions given in Eqs. [50] and [51]. If we truncate the cluster operator such that $\hat{T} \equiv \hat{T}_1 + \hat{T}_2$ and insert it into the similarity-transformed normal-ordered Hamiltonian, $\bar{H} \equiv e^{-\hat{T}} \hat{H}_N e^{\hat{T}}$, we obtain

$$\begin{aligned}\bar{H} = & \hat{H}_N + [\hat{H}_N, \hat{T}_1] + [\hat{H}_N, \hat{T}_2] + \frac{1}{2}[[\hat{H}_N, \hat{T}_1], \hat{T}_1] \\ & + \frac{1}{2}[[\hat{H}_N, \hat{T}_2], \hat{T}_2] + [[\hat{H}_N, \hat{T}_1], \hat{T}_2] + \dots\end{aligned}\quad [106]$$

where the Hausdorff expansion above terminates naturally at quadruply nested commutators as described earlier.⁷⁹ Our task in constructing the CCSD equations is to obtain second-quantized expressions for each term of \bar{H} above, insert these into Eqs. [50] and [51], and finally evaluate the resulting matrix elements.

The first commutator of Eq. [106] expands to give

$$[\hat{H}_N, \hat{T}_1] = [\hat{F}_N, \hat{T}_1] + [\hat{V}_N, \hat{T}_1] = \hat{F}_N \hat{T}_1 - \hat{T}_1 \hat{F}_N + \hat{V}_N \hat{T}_1 - \hat{T}_1 \hat{V}_N \quad [107]$$

using the definition of \hat{H}_N given in Eq. [105]. The second-quantized definition of \hat{T}_1 is simply

$$\hat{T}_1 = \sum_{ia} t_i^a \{a_a^\dagger a_i\} \quad [108]$$

where the braces indicate that the operator string is already normal-ordered (i.e., this is the only nonzero term resulting from application of Wick's theorem

⁷⁹Since the cluster operators commute, we have

$$[[\hat{H}_N, \hat{T}_1], \hat{T}_2] = \frac{1}{2}[[\hat{H}_N, \hat{T}_1], \hat{T}_2] + \frac{1}{2}[[\hat{H}_N, \hat{T}_2], \hat{T}_1]$$

Therefore, a factor of $1/2$ does not appear in front of this term in the expansion above.

to Eq. [27]). Given the second-quantized form of \hat{F}_N from the preceding section, the first term of the commutator may be written as

$$\hat{F}_N \hat{T}_1 = \sum_{pq} \sum_{ia} f_{pq} t_i^a \{a_p^\dagger a_q\} \{a_a^\dagger a_i\} \quad [109]$$

The generalized form of Wick's theorem (see Eq. [91]) says that this product of normal-ordered operator strings may be written using only contractions between the two strings. That is,

$$\begin{aligned} \{a_p^\dagger a_q\} \{a_a^\dagger a_i\} &= \{a_p^\dagger a_q a_a^\dagger a_i\} + \{\overline{a_p^\dagger a_q} \overline{a_a^\dagger a_i}\} + \{a_p^\dagger \overline{a_q} a_a^\dagger a_i\} + \{\overline{a_p^\dagger a_q} \overline{a_a^\dagger a_i}\} \\ &= \{a_p^\dagger a_q a_a^\dagger a_i\} + \delta_{pi} \{a_q a_a^\dagger\} + \delta_{qa} \{a_p^\dagger a_i\} + \delta_{pi} \delta_{qa} \end{aligned} \quad [110]$$

For the second term of the expanded commutator, $\hat{T}_1 \hat{F}_N$, where the operator strings from \hat{F}_N and \hat{T}_1 are simply reversed in order, Wick's theorem gives only one term, namely,

$$\{a_a^\dagger a_i\} \{a_p^\dagger a_q\} = \{a_a^\dagger a_i a_p^\dagger a_q\} = \{a_p^\dagger a_q a_a^\dagger a_i\} \quad [111]$$

All other contractions, which involve a_a^\dagger and a_i on the left, are zero by Eq. [94]. The final equality in this expression arises from the fact that, by construction, all operators within the braces anticommute. Therefore, using Eqs. [110] and [111], we may write

$$\begin{aligned} \hat{F}_N \hat{T}_1 - \hat{T}_1 \hat{F}_N &= \sum_{pq} \sum_{ia} f_{pq} t_i^a (\delta_{pi} \{a_q a_a^\dagger\} + \delta_{qa} \{a_p^\dagger a_i\} + \delta_{pi} \delta_{qa}) \\ &= \sum_{qia} f_{iq} t_i^a \{a_q a_a^\dagger\} + \sum_{pia} f_{pa} t_i^a \{a_p^\dagger a_i\} + \sum_{ia} f_{ia} t_i^a \end{aligned} \quad [112]$$

This example illustrates how the commutator allows only those terms involving contractions between the operators to survive; the “uncontracted” terms are eliminated. Note that the final term on the right-hand side involves components of the Fock operator in the occupied-virtual block; if Brillouin's theorem⁸² holds for the set of molecular orbitals used to construct Φ_0 , then this term is zero.

Now consider the first doubly nested commutator from Eq. [106]. The term involving the Fock operator expands to give

$$\frac{1}{2} [[\hat{F}_N, \hat{T}_1], \hat{T}_1] = \frac{1}{2} \hat{F}_N \hat{T}_1^2 - \hat{T}_1 \hat{F}_N \hat{T}_1 + \frac{1}{2} \hat{T}_1^2 \hat{F}_N \quad [113]$$

Applying Wick's theorem to the operator strings in the first term on the right-hand side of this equation gives

$$\begin{aligned} \frac{1}{2}\hat{F}_N\hat{T}_1^2 = & \frac{1}{2}\sum_{pq}\sum_{ia}\sum_{jb}f_{pq}t_i^at_j^b(\{a_p^\dagger a_q a_a^\dagger a_i a_b^\dagger a_j\} + \{\overline{a_p^\dagger a_q a_a^\dagger a_i} \overline{a_b^\dagger a_j}\} + \{\overline{a_p^\dagger a_q a_a^\dagger a_i} \overline{a_b^\dagger a_j}\}) \\ & + \{a_p^\dagger a_q \overline{a_a^\dagger a_i} a_b^\dagger a_j\} + \{a_p^\dagger a_q \overline{a_a^\dagger a_i} \overline{a_b^\dagger a_j}\} + \{a_p^\dagger a_q \overline{a_a^\dagger a_i} a_b^\dagger a_j\} \\ & + \{a_p^\dagger a_q \overline{a_a^\dagger a_i} a_b^\dagger a_j\} + \{a_p^\dagger a_q \overline{a_a^\dagger a_i} \overline{a_b^\dagger a_j}\} + \{a_p^\dagger a_q \overline{a_a^\dagger a_i} a_b^\dagger a_j\}) \end{aligned} \quad [114]$$

Evaluating the contractions leads to

$$\begin{aligned} \frac{1}{2}\hat{F}_N\hat{T}_1^2 = & \frac{1}{2}\sum_{aibj}t_i^at_j^b\left(\sum_{pq}f_{pq}\{a_p^\dagger a_q a_a^\dagger a_i a_b^\dagger a_j\} + \sum_qf_{iq}\{a_q a_a^\dagger a_b^\dagger a_j\}\right. \\ & + \sum_qf_{iq}\{a_q a_a^\dagger a_i a_b^\dagger\} + \sum_pf_{pa}\{a_p^\dagger a_i a_b^\dagger a_j\} \\ & + \sum_pf_{pb}\{a_p^\dagger a_a^\dagger a_i a_j\} + f_{ia}\{a_b^\dagger a_j\} + f_{ja}\{a_i a_b^\dagger\} \\ & \left.- f_{ib}\{a_a^\dagger a_j\} + f_{jb}\{a_a^\dagger a_i\}\right) \end{aligned} \quad [115]$$

This expression may be simplified significantly by recognizing that because of the summation outside the parentheses, i , j , a , and b are dummy indices and may be exchanged. For example, the second and third terms on the right-hand side are identical:

$$\sum_{aibj}t_i^at_j^b\left(\sum_qf_{iq}\{a_q a_a^\dagger a_b^\dagger a_j\} + \sum_qf_{jq}\{a_q a_a^\dagger a_i a_b^\dagger\}\right) \quad [116]$$

$$= \sum_{aibj}\sum_q(f_{jq}t_i^at_j^b\{a_q a_a^\dagger a_i a_b^\dagger\} + f_{iq}t_i^at_j^b\{a_q a_a^\dagger a_i a_b^\dagger\}) \quad [117]$$

The first step in this analysis results from simply swapping index i with j and index a with b . Similarly, one may show equivalence of terms four and five, six and nine, and seven and eight (with appropriate sign changes). The final, simplified expression is thus

$$\begin{aligned} \frac{1}{2}\hat{F}_N\hat{T}_1^2 = & \frac{1}{2}\sum_{aibj}t_i^at_j^b\left(\sum_{pq}f_{pq}\{a_p^\dagger a_q a_a^\dagger a_i a_b^\dagger a_j\} + 2\sum_qf_{iq}\{a_q a_a^\dagger a_i a_b^\dagger\}\right. \\ & \left.+ 2\sum_pf_{pb}\{a_p^\dagger a_a^\dagger a_i a_j\} + 2f_{ib}\{a_a^\dagger a_i\} + 2f_{ja}\{a_i a_b^\dagger\}\right) \end{aligned} \quad [118]$$

A similar analysis for the remaining two terms of the doubly nested commutator gives

$$\begin{aligned} \hat{T}_1 \hat{F}_N \hat{T}_1 &= \sum_{aibj} t_i^a t_j^b \left(\sum_{pq} f_{pq} \{a_a^\dagger a_i a_p^\dagger a_q a_b^\dagger a_j\} + \sum_q f_{jq} \{a_a^\dagger a_i a_q a_b^\dagger\} \right. \\ &\quad \left. + \sum_p f_{pb} \{a_a^\dagger a_i a_p^\dagger a_j\} + f_{jb} \{a_a^\dagger a_i\} \right) \end{aligned} \quad [119]$$

and

$$\frac{1}{2} \hat{T}_1^2 \hat{F}_N = \frac{1}{2} \sum_{aibj} \sum_{pq} f_{pq} t_i^a t_j^b \{a_a^\dagger a_i a_b^\dagger a_j a_p^\dagger a_q\} \quad [120]$$

Inserting these expressions into Eq. [113] and canceling terms gives the rather simple result

$$\frac{1}{2} [[\hat{F}_N, \hat{T}_1], \hat{T}_1] = \sum_{aibj} f_{ja} t_i^a t_j^b \{a_i a_b^\dagger\} \quad [121]$$

The two examples given so far, $[\hat{F}_N, \hat{T}_1]$ and $\frac{1}{2} [[\hat{F}_N, \hat{T}_1], \hat{T}_1]$, allow us to make an important generalization when Wick's theorem is applied to the commutators in Eq. [106]:

The only nonzero terms in the Hausdorff expansion are those in which the Hamiltonian, \hat{H}_N , has at least one contraction with every cluster operator, \hat{T}_n , on its right.

That is, the Hamiltonian must share at least one index with every cluster operator component in the final expression. We may therefore rewrite Eq. [106] in a simpler form:

$$\begin{aligned} \bar{H} &= (\hat{H}_N + \hat{H}_N \hat{T}_1 + \hat{H}_N \hat{T}_2 + \frac{1}{2} \hat{H}_N \hat{T}_1^2 + \frac{1}{2} \hat{H}_N \hat{T}_2^2 + \hat{H}_N \hat{T}_1 \hat{T}_2 \\ &\quad + \frac{1}{6} \hat{H}_N \hat{T}_1^3 + \frac{1}{2} \hat{H}_N \hat{T}_1^2 \hat{T}_2 + \frac{1}{2} \hat{H}_N \hat{T}_1 \hat{T}_2^2 + \frac{1}{6} \hat{H}_N \hat{T}_2^3 \\ &\quad + \frac{1}{24} \hat{H}_N \hat{T}_1^4 + \frac{1}{6} \hat{H}_N \hat{T}_1^3 \hat{T}_2 + \frac{1}{4} \hat{H}_N \hat{T}_1^2 \hat{T}_2^2 + \frac{1}{6} \hat{H}_N \hat{T}_1 \hat{T}_2^3 + \frac{1}{24} \hat{H}_N \hat{T}_2^4)_c \end{aligned} \quad [122]$$

where we have now written every term in the CCSD Hausdorff expansion explicitly and the subscript c indicates that only those terms in which the Hamiltonian is connected (in the Wick's theorem sense) to every cluster operator on its right should be included in the algebraic interpretation of the operator.

This is often referred to as the “connected cluster” form of the similarity-transformed Hamiltonian.² This expression makes the truncation of the Hausdorff expansion even clearer; since the Hamiltonian contains at most four annihilation and creation operators (in \hat{V}_N), \hat{H}_N can connect to at most four cluster operators at once. Therefore, the Hausdorff expansion must truncate at the quartic terms.

The CCSD Energy Equation

Using the connected cluster form of \bar{H} defined above, as well as the techniques of Wick’s theorem and normal ordering, we may derive a programmable form of the energy expression in the CCSD approximation. In accord with Eq. [50] and the normal-ordered Hamiltonian, the energy is given by

$$E_{\text{CCSD}} - E_0 = \langle \Phi_0 | \bar{H} | \Phi_0 \rangle \quad [123]$$

where the CCSD effective Hamiltonian of Eq. [122] is inserted for \bar{H} and E_0 is the SCF energy, $\langle \Phi_0 | \hat{H} | \Phi_0 \rangle$. The leading term in this expression is the reference expectation value of the normal-ordered Hamiltonian, which is zero by construction:

$$\langle \Phi_0 | \hat{H}_N | \Phi_0 \rangle = 0 \quad [124]$$

For all other terms, we may use the advantage of normal-ordering of the operators to determine all the fully contracted terms of the operator product. For example, for the second term on the right-hand side of Eq. [122], insertion of the definition of the normal-ordered Hamiltonian gives

$$(\hat{H}_N \hat{T}_1)_c = (\hat{F}_N \hat{T}_1)_c + (\hat{V}_N \hat{T}_1)_c \quad [125]$$

where the subscript c has the same meaning as in Eq. [122]. We have already evaluated the first component of this pair, and the result is given in Eq. [112], which contains only one fully contracted term, that is,

$$\langle \Phi_0 | (\hat{F}_N \hat{T}_1)_c | \Phi_0 \rangle = \sum_{ia} f_{ia} t_i^a \quad [126]$$

The two-electron component, on the other hand, contributes nothing to the energy expression because no fully contracted terms can be generated from it:

$$\begin{aligned}
(\hat{V}_N \hat{T}_1)_c &= \frac{1}{4} \sum_{pqrs} \sum_{ia} \langle pq || rs \rangle t_i^a \{a_p^\dagger a_q^\dagger a_s a_r\} \{a_a^\dagger a_i\} \\
&= \frac{1}{4} \sum_{pqrs} \sum_{ia} \langle pq || rs \rangle t_i^a (\{a_p^\dagger a_q^\dagger a_s a_r a_a^\dagger a_i\} + \{a_p^\dagger a_q^\dagger a_s a_r a_a^\dagger a_i\} \\
&\quad + \{a_p^\dagger a_q^\dagger \overline{a_s a_r a_a^\dagger a_i}\} + \{a_p^\dagger a_q^\dagger \overline{a_s a_r a_a^\dagger a_i}\} + \{a_p^\dagger a_q^\dagger \overline{a_s a_r a_a^\dagger a_i}\} \\
&\quad + \{a_p^\dagger a_q^\dagger \overline{a_s a_r a_a^\dagger a_i}\} + \{a_p^\dagger a_q^\dagger \overline{a_s a_r a_a^\dagger a_i}\} + \{a_p^\dagger a_q^\dagger \overline{a_s a_r a_a^\dagger a_i}\} \\
&\quad + \{a_p^\dagger a_q^\dagger \overline{a_s a_r a_a^\dagger a_i}\})
\end{aligned} \tag{127}$$

Therefore, the energy contribution from the linear \hat{T}_1 operator is

$$E_{CCSD} \leftarrow \langle \Phi_0 | (\hat{H}_N \hat{T}_1)_c | \Phi_0 \rangle = \sum_{ia} f_{ia} t_i^a \tag{128}$$

(The left arrow indicates that this is only one of several terms contributing to the energy on the left-hand side.) However, this term will be zero if Brillouin's theorem holds for the molecular orbitals in which the Fock matrix is represented.⁸²

Next consider the contribution to the energy from the linear \hat{T}_2 term in Eq. [123],

$$\langle \Phi_0 | (\hat{H}_N \hat{T}_2)_c | \Phi_0 \rangle = \langle \Phi_0 | \left[(\hat{F}_N \hat{T}_2)_c + (\hat{V}_N \hat{T}_2)_c \right] | \Phi_0 \rangle \tag{129}$$

The normal-ordered form of \hat{T}_2 may be derived from Eq. [28] to obtain

$$\hat{T}_2 = \frac{1}{4} \sum_{aibj} t_{ij}^{ab} \{a_a^\dagger a_b^\dagger a_j a_i\} \tag{130}$$

The reference expectation value of the first term on the right-hand side of Eq. [129] is zero because it cannot produce any fully contracted components:

$$\begin{aligned}
(\hat{F}_N \hat{T}_2)_c &= \frac{1}{4} \sum_{pq} \sum_{aibj} f_{pq} t_{ij}^{ab} \{a_p^\dagger a_q\} \{a_a^\dagger a_b^\dagger a_j a_i\} \\
&= \frac{1}{4} \sum_{pq} \sum_{aibj} f_{pq} t_{ij}^{ab} (\{a_p^\dagger a_q a_a^\dagger a_b^\dagger a_j a_i\} + \{a_p^\dagger a_q a_a^\dagger a_b^\dagger a_j a_i\} \\
&\quad + \{a_p^\dagger a_q \overline{a_a^\dagger a_b^\dagger a_j a_i}\} + \{a_p^\dagger a_q \overline{a_a^\dagger a_b^\dagger a_j a_i}\} + \{a_p^\dagger a_q \overline{a_a^\dagger a_b^\dagger a_j a_i}\} \\
&\quad + \{a_p^\dagger a_q \overline{a_a^\dagger a_b^\dagger a_j a_i}\} + \{a_p^\dagger a_q \overline{a_a^\dagger a_b^\dagger a_j a_i}\} + \{a_p^\dagger a_q \overline{a_a^\dagger a_b^\dagger a_j a_i}\} \\
&\quad + \{a_p^\dagger a_q \overline{a_a^\dagger a_b^\dagger a_j a_i}\})
\end{aligned} \tag{131}$$

The two-electron component, however, produces four equivalent fully contracted terms, and therefore contributes to the coupled cluster energy:

$$\begin{aligned}
 \langle \Phi_0 | (\hat{V}_N \hat{T}_2)_c | \Phi_0 \rangle &= \frac{1}{16} \sum_{pqrs} \sum_{aibj} \langle pq || rs \rangle t_{ij}^{ab} \langle \Phi_0 | \{a_p^\dagger a_q^\dagger a_s a_r\} \{a_a^\dagger a_b^\dagger a_j a_i\} | \Phi_0 \rangle \\
 &= \frac{1}{16} \sum_{pqrs} \sum_{aibj} \langle pq || rs \rangle t_{ij}^{ab} \left(\{a_p^\dagger a_q^\dagger a_s a_r a_a^\dagger a_b^\dagger a_j a_i\} + \{a_p^\dagger a_q^\dagger a_s a_r a_a^\dagger a_b^\dagger a_j a_i\} \right. \\
 &\quad \left. + \{a_p^\dagger a_q^\dagger a_s a_r a_a^\dagger a_b^\dagger a_j a_i\} + \{a_p^\dagger a_q^\dagger a_s a_r a_a^\dagger a_b^\dagger a_j a_i\} \right) \\
 &= \frac{1}{16} \sum_{pqrs} \sum_{aibj} \langle pq || rs \rangle t_{ij}^{ab} (\delta_{pi} \delta_{qj} \delta_{ra} \delta_{sb} + \delta_{pj} \delta_{qi} \delta_{rb} \delta_{sa} - \delta_{pj} \delta_{qi} \delta_{ra} \delta_{sb} - \delta_{pi} \delta_{qj} \delta_{rb} \delta_{sa}) \\
 &= \frac{1}{4} \sum_{aibj} \langle ij || ab \rangle t_{ij}^{ab}
 \end{aligned} \tag{132}$$

The factor of $\frac{1}{16}$ appearing in the first three equalities arises simply from the product of the factors of $\frac{1}{4}$ that appear in the definitions of \hat{V}_N (Eq. [104]) and \hat{T}_2 (Eq. [130]), and the final factor of $\frac{1}{4}$ results from the collection of the last four terms together.

Next we consider the first quadratic term from Eq. [123], which involves two \hat{T}_1 cluster operators. The reference expectation value of the one-electron component, $\frac{1}{2}(\hat{F}_N \hat{T}_1^2)_c$, is zero because the single construction operator pair in the Fock operator cannot produce fully contracted terms with the two construction operator pairs in \hat{T}_1^2 . The two-electron component, on the other hand, does produce fully contracted terms, namely,

$$\begin{aligned}
 \frac{1}{2} \langle \Phi_0 | (\hat{V}_N \hat{T}_1^2)_c | \Phi_0 \rangle &= \frac{1}{8} \sum_{pqrs} \sum_{ai} \sum_{bj} \langle pq || rs \rangle t_i^a t_j^b \langle \Phi_0 | \{a_p^\dagger a_q^\dagger a_s a_r\} \{a_a^\dagger a_i\} \{a_b^\dagger a_j\} | \Phi_0 \rangle \\
 &= \frac{1}{8} \sum_{pqrs} \sum_{aibj} \langle pq || rs \rangle t_i^a t_j^b \left(\{a_p^\dagger a_q^\dagger a_s a_r a_a^\dagger a_i a_b^\dagger a_j\} + \{a_p^\dagger a_q^\dagger a_s a_r a_a^\dagger a_i a_b^\dagger a_j\} \right. \\
 &\quad \left. + \{a_p^\dagger a_q^\dagger a_s a_r a_a^\dagger a_b^\dagger a_i a_j\} + \{a_p^\dagger a_q^\dagger a_s a_r a_a^\dagger a_i a_b^\dagger a_j\} \right) \\
 &= \frac{1}{8} \sum_{pqrs} \sum_{aibj} \langle pq || rs \rangle t_i^a t_j^b (-\delta_{pj} \delta_{qi} \delta_{ra} \delta_{sb} + \delta_{pj} \delta_{qi} \delta_{rb} \delta_{sa} + \delta_{pi} \delta_{qj} \delta_{ra} \delta_{sb} - \delta_{pi} \delta_{qj} \delta_{rb} \delta_{sa}) \\
 &= \frac{1}{2} \sum_{aibj} \langle ij || ab \rangle t_i^a t_j^b
 \end{aligned} \tag{133}$$

The factor of $\frac{1}{8}$ appearing in the first three equalities arises from product of the factor of $\frac{1}{2}$ from the Hausdorff expansion and the $\frac{1}{4}$ from the definition of \hat{V}_N (Eq. [104]).

In all the remaining terms in the energy expression in Eq. [123], the cluster operators contribute more construction operator pairs than the Hamiltonian

components. For example, the “mixed” term, $(\hat{H}_N \hat{T}_1 \hat{T}_2)_{\epsilon}$, involves three pairs from the cluster operators (one from \hat{T}_1 and two from \hat{T}_2) but only two from the two-electron component of the Hamiltonian. Therefore, none of these terms can produce fully contracted products, and their reference expectation values are zero. The absence of these “higher order” components might also be rationalized in terms of Slater’s rules: since the Hamiltonian is a two-electron operator, the $\hat{T}_1 \hat{T}_2$ product produces on the right a triply excited determinant that cannot couple to the reference Φ_0 through the Hamiltonian. However, as we will see in the next section, this interpretation is inadequate because it fails to explain why certain terms are missing from the amplitude equations for higher excitations (e.g., the CCSDT \hat{T}_3 amplitude equation).

We have now derived all the contributions to the CCSD energy. Summing Eqs. [126], [132], and [133], we obtain the final expression

$$E_{\text{CCSD}} - E_0 = \sum_{ia} f_{ia} t_i^a + \frac{1}{4} \sum_{aibj} \langle ij || ab \rangle t_{ij}^{ab} + \frac{1}{2} \sum_{aibj} \langle ij || ab \rangle t_i^a t_j^b \quad [134]$$

This equation is not restricted to the CCSD approximation, however. Since higher excitation cluster operators such as \hat{T}_3 and \hat{T}_4 cannot produce fully contracted terms with the Hamiltonian, their contribution to the coupled cluster energy expression is zero. Therefore, Eq. [134] also holds for more complicated methods such as CCSDT and CCSDTQ. Higher excitation cluster operators can contribute to the energy indirectly, however, through the equations used to determine the amplitudes, t_i^a and t_{ij}^{ab} , which are needed in the energy equation above.

The CCSD Amplitude Equations

As discussed earlier, the cluster amplitudes that parameterize the coupled cluster wavefunction may be determined from the “projective” Schrödinger equation given in Eq. [51]. In the CCSD approximation, the single-excitation amplitudes, t_i^a , may be determined from

$$0 = \langle \Phi_i^a | \bar{H} | \Phi_0 \rangle \quad [135]$$

and the double-excitation amplitudes, t_{ij}^{ab} , from

$$0 = \langle \Phi_{ij}^{ab} | \bar{H} | \Phi_0 \rangle \quad [136]$$

where \bar{H} is given by Eq. [122]. For reasons we describe in detail later in the section entitled Computer Implementation of Coupled Cluster Theory, Eq. [135] is commonly referred to as the \hat{T}_1 amplitude equation and Eq. [136] as the \hat{T}_2 amplitude equation. Rather than dealing with all 15 terms arising from the insertion of Eq. [122] into Eqs. [135] and [136], we will focus on only a few representative examples.

The construction of the coupled cluster amplitude equations is somewhat more complicated than the energy equation in that the latter requires only reference expectation values of the second-quantized operators. For the amplitude equations, we now require matrix elements between the reference, Φ_0 , on the right and specific excited determinants on the left. We must therefore convert these into reference expectation value expressions by writing the excited determinants as excitation operator strings acting on Φ_0 . For example, a doubly excited bra determinant may be written as

$$\langle \Phi_{ij}^{ab} | = \langle \Phi | \{a_i^\dagger a_j^\dagger a_b a_a\} \quad [137]$$

The final matrix element therefore requires that we obtain all fully contracted Wick's theorem terms from the product of the operator string above and the elements of \bar{H} .

The leading term of \bar{H} in Eq. [122] is simply the electronic Hamiltonian itself. For its contribution to the \hat{T}_1 amplitude equation, we must therefore evaluate matrix elements of \hat{H}_N between singly excited determinants and Φ_0 ,

$$\begin{aligned} \langle \Phi_i^a | (\hat{F}_N + \hat{V}_N) | \Phi_0 \rangle &= \sum_{pq} f_{pq} \langle \Phi_0 | \{a_i^\dagger a_a\} \{a_p^\dagger a_q\} | \Phi_0 \rangle \\ &\quad + \frac{1}{4} \sum_{pqrs} \langle pq || rs \rangle \langle \Phi_0 | \{a_i^\dagger a_a\} \{a_p^\dagger a_q^\dagger a_s a_r\} | \Phi_0 \rangle \end{aligned} \quad [138]$$

The two-electron component of this equation cannot produce full contractions and is therefore zero. The one-electron term, however, simplifies to a single Fock matrix element:

$$\begin{aligned} \langle \Phi_i^a | \hat{F}_N | \Phi_0 \rangle &= \sum_{pq} f_{pq} \langle \Phi_0 | \{a_i^\dagger a_a\} \{a_p^\dagger a_q\} | \Phi_0 \rangle \\ &= \sum_{pq} f_{pq} \overline{\{a_i^\dagger a_a\}} \overline{\{a_p^\dagger a_q\}} \\ &= \sum_{pq} f_{pq} \delta_{iq} \delta_{ap} \\ &= f_{ai} \end{aligned} \quad [139]$$

For the contribution of \hat{H}_N to the \hat{T}_2 amplitude equation, on the other hand, we must evaluate the matrix elements of the normal-ordered Hamiltonian between doubly excited determinants and Φ_0 , namely,

$$\begin{aligned} \langle \Phi_{ij}^{ab} | (\hat{F}_N + \hat{V}_N) | \Phi_0 \rangle &= \sum_{pq} f_{pq} \langle \Phi_0 | \{a_i^\dagger a_j^\dagger a_b a_a\} \{a_p^\dagger a_q\} | \Phi_0 \rangle \\ &\quad + \frac{1}{4} \sum_{pqrs} \langle pq || rs \rangle \langle \Phi_0 | \{a_i^\dagger a_j^\dagger a_b a_a\} \{a_p^\dagger a_q^\dagger a_s a_r\} | \Phi_0 \rangle \end{aligned} \quad [140]$$

In this case, it is the one-electron component that cannot produce full contractions, whereas the two-electron component contributes only a single integral:

$$\begin{aligned}
 \langle \Phi_{ij}^{ab} | \hat{V}_N | \Phi_0 \rangle &= \frac{1}{4} \sum_{pqrs} \langle pq || rs \rangle \langle \Phi_0 | \{a_i^\dagger a_j^\dagger a_b a_a\} \{a_p^\dagger a_q^\dagger a_s a_r\} | \Phi_0 \rangle \\
 &= \frac{1}{4} \sum_{pqrs} \langle pq || rs \rangle \left(\{a_i^\dagger a_j^\dagger a_b a_a \overbrace{a_p^\dagger a_q^\dagger a_s a_r} + \{a_i^\dagger a_j^\dagger a_b a_a \overbrace{a_p^\dagger a_q^\dagger a_s a_r} \right. \\
 &\quad \left. + \{a_i^\dagger a_j^\dagger a_b a_a \overbrace{a_p^\dagger a_q^\dagger a_s a_r} + \{a_i^\dagger a_j^\dagger a_b a_a \overbrace{a_p^\dagger a_q^\dagger a_s a_r} \right) \\
 &= \frac{1}{4} \sum_{pqrs} \langle pq || rs \rangle (\delta_{pa} \delta_{qb} \delta_{ri} \delta_{sj} - \delta_{pb} \delta_{qa} \delta_{ri} \delta_{sj} - \delta_{pa} \delta_{qb} \delta_{rj} \delta_{si} + \delta_{pb} \delta_{qa} \delta_{rj} \delta_{si}) \\
 &= \langle ab || ij \rangle
 \end{aligned} \tag{141}$$

The second term of Eq. [122], which is linear in \hat{T}_1 , provides a more interesting example than \hat{H}_N alone. Its contribution to the \hat{T}_1 amplitude equation involves the matrix elements

$$\begin{aligned}
 \langle \Phi_i^a | ([\hat{F}_N + \hat{V}_N] \hat{T}_1)_c | \Phi_0 \rangle &= \sum_{pq} \sum_{jb} f_{pq} t_j^b \langle \Phi_0 | \{a_i^\dagger a_a\} (\{a_p^\dagger a_q^\dagger\} \{a_b^\dagger a_j\})_c | \Phi_0 \rangle \\
 &\quad + \frac{1}{4} \sum_{pqrs} \sum_{jb} \langle pq || rs \rangle t_j^b \langle \Phi_0 | \{a_i^\dagger a_a\} (\{a_p^\dagger a_q^\dagger a_s a_r\} \{a_b^\dagger a_j\})_c | \Phi_0 \rangle
 \end{aligned} \tag{142}$$

where the subscript c reminds us that we must retain at least one contraction between the Hamiltonian fragment and the cluster operator on its right. For the two-electron term, Wick's theorem gives

$$\begin{aligned}
 \langle \Phi_i^a | (\hat{V}_N \hat{T}_1)_c | \Phi_0 \rangle &= \frac{1}{4} \sum_{pqrs} \sum_{jb} \langle pq || rs \rangle t_j^b \langle \Phi_0 | \{a_i^\dagger a_a\} (\{a_p^\dagger a_q^\dagger a_s a_r\} \{a_b^\dagger a_j\})_c | \Phi_0 \rangle \\
 &= \frac{1}{4} \sum_{pqrs} \sum_{jb} \langle pq || rs \rangle t_j^b \left(\{a_i^\dagger a_a \overbrace{a_p^\dagger a_q^\dagger a_s a_r} a_b a_j\} + \{a_i^\dagger a_a \overbrace{a_p^\dagger a_q^\dagger a_s a_r} a_b a_j^\dagger\} \right. \\
 &\quad \left. + \{a_i^\dagger a_a \overbrace{a_p^\dagger a_q^\dagger a_s a_r} a_b^\dagger a_j\} + \{a_i^\dagger a_a \overbrace{a_p^\dagger a_q^\dagger a_s a_r} a_b a_j^\dagger\} \right) \\
 &= \frac{1}{4} \sum_{pqrs} \sum_{jb} \langle pq || rs \rangle t_j^b (-\delta_{pa} \delta_{qj} \delta_{rb} \delta_{si} + \delta_{pj} \delta_{qa} \delta_{rb} \delta_{si} + \delta_{pa} \delta_{qj} \delta_{ri} \delta_{sb} - \delta_{pj} \delta_{qa} \delta_{ri} \delta_{sb}) \\
 &= \sum_{bj} \langle ja || bi \rangle t_j^b
 \end{aligned} \tag{143}$$

The contribution of $(\hat{H}_N \hat{T}_1)_c$ to the \hat{T}_2 equation involves the matrix elements

$$\begin{aligned} \langle \Phi_{ij}^{ab} | (\hat{F}_N + \hat{V}_N) \hat{T}_1 \rangle_c |\Phi_0\rangle &= \sum_{pq} \sum_{kc} f_{pq} t_k^c \langle \Phi_0 | \{a_i^\dagger a_j^\dagger a_b a_a\} (\{a_p^\dagger a_q^\dagger\} \{a_c^\dagger a_k^\dagger\})_c |\Phi_0\rangle \\ &\quad + \frac{1}{4} \sum_{pqrs} \sum_{kc} \langle pq || rs \rangle t_k^c \langle \Phi_0 | \{a_i^\dagger a_j^\dagger a_b a_a\} (\{a_p^\dagger a_q^\dagger a_s a_r\} \{a_c^\dagger a_k^\dagger\})_c |\Phi_0\rangle \end{aligned} \quad [144]$$

In this case, the two-electron term simplifies to four contributions after some rather complicated manipulation:

$$\begin{aligned} \langle \Phi_{ij}^{ab} | (\hat{V}_N \hat{T}_1)_c |\Phi_0\rangle &= \frac{1}{4} \sum_{pqrs} \sum_{kc} \langle pq || rs \rangle t_k^c \langle \Phi_0 | \{a_i^\dagger a_j^\dagger a_b a_a\} (\{a_p^\dagger a_q^\dagger a_s a_r\} \{a_c^\dagger a_k^\dagger\})_c |\Phi_0\rangle \\ &= \frac{1}{4} \sum_{pqrs} \sum_{kc} \langle pq || rs \rangle t_k^c \left(\{a_i^\dagger a_j^\dagger a_b a_a a_p^\dagger a_q^\dagger a_s a_r a_c^\dagger a_k\} + \{a_i^\dagger a_j^\dagger a_b a_a a_p^\dagger a_q^\dagger a_s a_r a_c^\dagger a_k\} \right. \\ &\quad + \{a_i^\dagger a_j^\dagger a_b a_a a_p^\dagger a_q^\dagger a_s a_r a_c^\dagger a_k\} + \{a_i^\dagger a_j^\dagger a_b a_a a_p^\dagger a_q^\dagger a_s a_r a_c^\dagger a_k\} \\ &\quad + \{a_i^\dagger a_j^\dagger a_b a_a a_p^\dagger a_q^\dagger a_s a_r a_c^\dagger a_k\} + \{a_i^\dagger a_j^\dagger a_b a_a a_p^\dagger a_q^\dagger a_s a_r a_c^\dagger a_k\} \\ &\quad + \{a_i^\dagger a_j^\dagger a_b a_a a_p^\dagger a_q^\dagger a_s a_r a_c^\dagger a_k\} + \{a_i^\dagger a_j^\dagger a_b a_a a_p^\dagger a_q^\dagger a_s a_r a_c^\dagger a_k\} \\ &\quad + \{a_i^\dagger a_j^\dagger a_b a_a a_p^\dagger a_q^\dagger a_s a_r a_c^\dagger a_k\} + \{a_i^\dagger a_j^\dagger a_b a_a a_p^\dagger a_q^\dagger a_s a_r a_c^\dagger a_k\} \\ &\quad + \{a_i^\dagger a_j^\dagger a_b a_a a_p^\dagger a_q^\dagger a_s a_r a_c^\dagger a_k\} + \{a_i^\dagger a_j^\dagger a_b a_a a_p^\dagger a_q^\dagger a_s a_r a_c^\dagger a_k\} \\ &\quad + \{a_i^\dagger a_j^\dagger a_b a_a a_p^\dagger a_q^\dagger a_s a_r a_c^\dagger a_k\} + \{a_i^\dagger a_j^\dagger a_b a_a a_p^\dagger a_q^\dagger a_s a_r a_c^\dagger a_k\} \\ &\quad + \{a_i^\dagger a_j^\dagger a_b a_a a_p^\dagger a_q^\dagger a_s a_r a_c^\dagger a_k\} + \{a_i^\dagger a_j^\dagger a_b a_a a_p^\dagger a_q^\dagger a_s a_r a_c^\dagger a_k\} \\ &\quad + \{a_i^\dagger a_j^\dagger a_b a_a a_p^\dagger a_q^\dagger a_s a_r a_c^\dagger a_k\} + \{a_i^\dagger a_j^\dagger a_b a_a a_p^\dagger a_q^\dagger a_s a_r a_c^\dagger a_k\} \\ &\quad + \{a_i^\dagger a_j^\dagger a_b a_a a_p^\dagger a_q^\dagger a_s a_r a_c^\dagger a_k\} + \{a_i^\dagger a_j^\dagger a_b a_a a_p^\dagger a_q^\dagger a_s a_r a_c^\dagger a_k\} \Big) \\ &= \frac{1}{4} \sum_{pqrs} \sum_{kc} \langle pq || rs \rangle t_k^c \times (\delta_{pa} \delta_{qb} \delta_{rc} \delta_{si} \delta_{ik} - \delta_{pb} \delta_{qa} \delta_{rc} \delta_{sj} \delta_{ik} - \delta_{pa} \delta_{qb} \delta_{rc} \delta_{si} \delta_{jk} \\ &\quad + \delta_{pb} \delta_{qa} \delta_{rc} \delta_{si} \delta_{jk} - \delta_{pa} \delta_{qb} \delta_{ri} \delta_{sc} \delta_{ik} + \delta_{pb} \delta_{qa} \delta_{ri} \delta_{sc} \delta_{ik} + \delta_{pa} \delta_{qb} \delta_{ri} \delta_{sc} \delta_{jk} \\ &\quad - \delta_{pb} \delta_{qa} \delta_{ri} \delta_{sc} \delta_{jk} - \delta_{pa} \delta_{qk} \delta_{ri} \delta_{sj} \delta_{bc} + \delta_{pb} \delta_{qk} \delta_{ri} \delta_{sj} \delta_{ac} - \delta_{pb} \delta_{qk} \delta_{rj} \delta_{si} \delta_{ac} \\ &\quad + \delta_{pa} \delta_{qk} \delta_{rj} \delta_{si} \delta_{bc} + \delta_{pk} \delta_{qa} \delta_{ri} \delta_{sj} \delta_{bc} - \delta_{pk} \delta_{qb} \delta_{ri} \delta_{sj} \delta_{ac} - \delta_{pk} \delta_{qa} \delta_{rj} \delta_{si} \delta_{bc} \\ &\quad + \delta_{pk} \delta_{qb} \delta_{rj} \delta_{si} \delta_{ac}) \\ &= \sum_c (\langle ab || cj \rangle t_i^c - \langle ab || ci \rangle t_j^c) + \sum_k (\langle ij || bk \rangle t_k^a - \langle ij || ak \rangle t_k^b) \end{aligned} \quad [145]$$

As our third example, we consider the contribution of the one-electron component of the fourth term of Eq. [122] to the \hat{T}_1 amplitude equation. The matrix element of interest in this case is

$$\frac{1}{2} \langle \Phi_i^\alpha | (\hat{F}_N \hat{T}_1^2)_c | \Phi_0 \rangle = \frac{1}{2} \sum_{pq} \sum_{jb} \sum_{kc} f_{pq} t_j^b t_k^c \langle \Phi_0 | \{a_i^\dagger a_a\} \{a_p^\dagger a_q\} \{a_b^\dagger a_j\} \{a_c^\dagger a_k\})_c | \Phi_0 \rangle$$

[146]

When applied to the operator strings in this expression, Wick's theorem gives only two nonzero contractions, in spite of the relatively large number of construction operators:

$$\begin{aligned} \langle \Phi_0 | \{a_i^\dagger a_a\} \{a_p^\dagger a_q\} \{a_b^\dagger a_j\} \{a_c^\dagger a_k\})_c | \Phi_0 \rangle &= \overbrace{\{a_i^\dagger a_a a_p^\dagger a_q a_b^\dagger a_j a_c^\dagger a_k\}} + \overbrace{\{a_i^\dagger a_a a_p^\dagger a_q a_b^\dagger a_j a_c^\dagger a_k\}} \\ &= -\delta_{pk} \delta_{qb} \delta_{ij} \delta_{ac} - \delta_{pj} \delta_{qc} \delta_{ik} \delta_{ac} \end{aligned}$$

[147]

When the Kronecker delta strings are inserted back into the matrix element expression, we obtain

$$\frac{1}{2} \langle \Phi_i^\alpha | (\hat{F}_N \hat{T}_1^2)_c | \Phi_0 \rangle = - \sum_{kc} f_{kc} t_i^c t_k^\alpha$$

[148]

Additional contractions such as

$$\overbrace{\{a_i^\dagger a_a a_p^\dagger a_q a_b^\dagger a_j a_c^\dagger a_k\}} \quad \text{and} \quad \overbrace{\{a_i^\dagger a_a a_p^\dagger a_q a_b^\dagger a_j a_c^\dagger a_k\}}$$

[149]

are not included even though they are nonzero because, as our earlier analysis of the commutators of the Hausdorff expansion indicated, the Hamiltonian fragment must be connected at least once to every cluster operator on the right. Similar analyses apply to other contributions such as $(\hat{V}_N \hat{T}_2^2)_c$, $(\hat{V}_N \hat{T}_1 \hat{T}_2)_c$, and so on.

This last point also has interesting consequences for the higher excitation amplitude equations such as that for \hat{T}_3 . For example, one term that arises in the general Hausdorff expansion is $\frac{1}{5!} (\hat{V}_N \hat{T}_1^5)_c$. This term does not contribute to the \hat{T}_3 amplitude equation

$$0 = \frac{1}{5!} \langle \Phi_{ijk}^{abc} | (\hat{V}_N \hat{T}_1^5)_c | \Phi_0 \rangle$$

[150]

From a configuration interaction perspective, such a matrix element of the Hamiltonian between the quintuply excited determinant generated by the oper-

ator \hat{T}_1^5 on the right and the triply excited determinant on the left is nonzero according to Slater's rules. However, because the two-electron fragment of the Hamiltonian cannot connect to more than four cluster operators on its right, such a matrix element cannot contribute to the amplitude equation by the connected cluster properties of the Hausdorff expansion. Similarly, the $(\hat{F}_N \hat{T}_2)_c$ contribution to \hat{T}_3 is also zero because any connection between \hat{F}_N and \hat{T}_2 does not leave enough construction operator pairs to completely connect to the triply excited determinant on the left.

The final example of this section is the contribution of the $\frac{1}{2}(\hat{V}_N \hat{T}_1^2 \hat{T}_2)_c$ term of Eq. [122] to the \hat{T}_2 amplitude equation. The matrix elements of interest in this case involve only the two-electron component of \hat{H}_N , because the one-electron component cannot connect to more than two cluster operators:

$$\begin{aligned} \frac{1}{2} \langle \Phi_{ij}^{ab} | (\hat{V}_N \hat{T}_1^2 \hat{T}_2)_c | \Phi_0 \rangle = & \frac{1}{32} \sum_{pqrs} \sum_{kc} \sum_{ld} \sum_{mnef} \langle pq || rs \rangle t_k^c t_l^d t_{mn}^{ef} \\ & \times \langle \Phi_0 | \{a_i^\dagger a_j^\dagger a_b a_a\} \{a_p^\dagger a_q^\dagger a_s a_r\} \{a_c^\dagger a_k\} \{a_d^\dagger a_l\} \{a_e^\dagger a_f^\dagger a_n a_m\} \}_c | \Phi_0 \rangle \end{aligned} \quad [151]$$

The factor of $\frac{1}{32}$ appearing here arises as the product of the factor of $\frac{1}{2}$ from the Hausdorff expansion and the two factors of $\frac{1}{4}$ from the definitions of \hat{V}_N (Eq. [104]) and \hat{T}_2 (Eq. [130]). To derive from this matrix element an expression involving only two-electron integrals and cluster amplitudes, we must apply Wick's theorem to the string of 16 annihilation and creation operators above. Although this might be a useful exercise for those readers who wish to test their own stamina and patience, we will avoid it here. We note that this task is tedious at best and recognize that Wick's theorem has not eliminated all the opportunities for error when one is dealing with complicated second-quantized equations.

Once all the contributions of Eq. [122] to Eqs. [135] and [136] have been determined in the manner described above, they are summed to give the amplitude equations. For \hat{T}_1 , the resulting equation is

$$\begin{aligned} 0 = & f_{ai} + \sum_c f_{ac} t_i^c - \sum_k f_{ki} t_k^a + \sum_{kc} \langle ka || ci \rangle t_k^c + \sum_{kc} f_{kc} t_{ik}^{ac} + \frac{1}{2} \sum_{kcd} \langle ka || cd \rangle t_{ki}^{cd} \\ & - \frac{1}{2} \sum_{klc} \langle kl || ci \rangle t_{kl}^{ca} - \sum_{kc} f_{kc} t_i^c t_k^a - \sum_{klc} \langle kl || ci \rangle t_k^c t_l^a - \sum_{kcd} \langle ka || cd \rangle t_k^c t_i^d \\ & - \sum_{klcd} \langle kl || cd \rangle t_k^c t_i^d t_l^a + \sum_{klcd} \langle kl || cd \rangle t_k^c t_l^d - \frac{1}{2} \sum_{klcd} \langle kl || cd \rangle t_{ki}^{cd} t_l^a - \frac{1}{2} \sum_{klcd} \langle kl || cd \rangle t_{kl}^{cad} t_i^d \end{aligned} \quad [152]$$

whereas for \hat{T}_2 , the resulting equation is

$$\begin{aligned}
0 = & \langle ab||ij\rangle + \sum_c (f_{bc} t_{ij}^{ac} - f_{ac} t_{ij}^{bc}) - \sum_k (f_{ki} t_{ik}^{ab} - f_{ki} t_{jk}^{ab}) + \frac{1}{2} \sum_{kl} \langle kl||ij\rangle t_{kl}^{ab} \\
& + \frac{1}{2} \sum_{cd} \langle ab||cd\rangle t_{ij}^{cd} + P(ij)P(ab) \sum_{kc} \langle kb||cj\rangle t_{ik}^{ac} + P(ij) \sum_c \langle ab||cj\rangle t_i^c \\
& - P(ab) \sum_k \langle kb||ij\rangle t_k^a + \frac{1}{2} P(ij)P(ab) \sum_{klcd} \langle kl||cd\rangle t_{ik}^{act} t_{lj}^{db} + \frac{1}{4} \sum_{klcd} \langle kl||cd\rangle t_{ij}^{ecd} t_{kl}^{ab} \\
& - P(ab) \frac{1}{2} \sum_{klcd} \langle kl||cd\rangle t_{ij}^{act} t_{kl}^{bd} - P(ij) \frac{1}{2} \sum_{klcd} \langle kl||cd\rangle t_{ik}^{ab} t_{jl}^{cd} + P(ab) \frac{1}{2} \sum_{kl} \langle kl||ij\rangle t_k^a t_l^b \\
& + P(ij) \frac{1}{2} \sum_{cd} \langle ab||cd\rangle t_i^c t_j^d - P(ij)P(ab) \sum_{kc} \langle kb||ic\rangle t_k^a t_j^c + P(ab) \sum_{kc} f_{kc} t_k^c t_{ij}^{bc} \\
& + P(ij) \sum_{kc} f_{kc} t_i^c t_{jk}^{ab} - P(ij) \sum_{klc} \langle kl||ci\rangle t_k^c t_{ij}^{ab} + P(ab) \sum_{kcd} \langle ka||cd\rangle t_k^c t_{ij}^{db} \\
& + P(ij)P(ab) \sum_{kcd} \langle ak||dc\rangle t_i^d t_{jk}^{bc} + P(ij)P(ab) \sum_{klc} \langle kl||ic\rangle t_l^a t_{jk}^{bc} \\
& + P(ij) \frac{1}{2} \sum_{klc} \langle kl||cj\rangle t_i^c t_{kl}^{ab} - P(ab) \frac{1}{2} \sum_{kcd} \langle kb||cd\rangle t_k^a t_{ij}^{cd} \\
& - P(ij)P(ab) \frac{1}{2} \sum_{kcd} \langle kb||cd\rangle t_i^c t_k^a t_j^d + P(ij)P(ab) \frac{1}{2} \sum_{klc} \langle kl||cj\rangle t_i^c t_k^a t_l^b \\
& - P(ij) \sum_{klcd} \langle kl||cd\rangle t_k^c t_i^d t_{lj}^{ab} - P(ab) \sum_{klcd} \langle kl||cd\rangle t_k^c t_l^a t_{ij}^{db} + P(ij) \frac{1}{4} \sum_{klcd} \langle kl||cd\rangle t_i^c t_j^d t_{kl}^{ab} \\
& + P(ab) \frac{1}{4} \sum_{klcd} \langle kl||cd\rangle t_k^a t_l^b t_{ij}^{cd} + P(ij)P(ab) \sum_{klcd} \langle kl||cd\rangle t_i^c t_l^b t_{kj}^{ad} \\
& + P(ij)P(ab) \frac{1}{4} \sum_{klcd} \langle kl||cd\rangle t_i^c t_k^a t_j^d t_l^b
\end{aligned} \tag{153}$$

The notation $P(pq)$ indicates a permutation operator whose action on a given function is defined by

$$P(pq)f(p, q) = f(p, q) - f(q, p) \tag{154}$$

For example, from the \hat{T}_2 equation above, one of the terms becomes

$$P(ij) \sum_{kc} f_{kc} t_i^c t_{jk}^{ab} = \sum_{kc} (f_{kc} t_i^c t_{jk}^{ab} - f_{kc} t_j^c t_{ik}^{ab}) \tag{155}$$

Relative to direct application of the anticommutation relations for annihilation and creation operators, Wick's theorem helps to dramatically reduce the tedium involved in deriving the rather complicated amplitude equations above. However, as illustrated by Eq. [151], Wick's theorem still does not go far enough. Even if the cluster operator is truncated to include only double excitations, the resulting algebra provides many opportunities for error. When even

higher excitations are desired, the number of algebraic manipulations required by Wick's theorem becomes rapidly insurmountable. A number of computer algorithms for the derivation of coupled-cluster-related equations have been described in the literature,^{33,36,118} but these have thus far been difficult to apply in a general fashion. Diagrammatic techniques offer a more practical approach to the construction of complicated coupled cluster equations. They provide a simple bookkeeping system for the numerous terms generated by Wick's theorem (most of which are redundant) and allow us to identify in advance which terms will not contribute to the wavefunction and/or the energy. In the next section we will outline one diagrammatic approach that is particularly convenient for deriving a variety of coupled-cluster-like equations, including ground state energies, energy derivatives, and EOM-CC equations.

An Introduction to Coupled Cluster Diagrams

In this section, we present a simple diagrammatic formalism popularized by Kucharski and Bartlett²⁰ by which one may construct the coupled cluster energy and amplitude equations far more quickly than by direct application of Wick's theorem.^o We begin by describing some of the general features of the diagrams, including their relationship to the particle–hole formalism and how they may be used to represent normal-ordered dynamical operators. Next we describe how the operator diagrams may be connected together to form operator products in a manner analogous to Wick's theorem. We then construct the diagrammatic form of the CCSD energy and amplitude equations, and, as each new diagram is presented, we provide rules for its algebraic interpretation. The diagrams described here may be used to represent either wavefunctions, operators, or matrix elements, depending on the context of the mathematical analysis. However, the set of rules we present for interpreting the diagrams algebraically apply only to the matrix element representation, because that is the most appropriate context for the coupled cluster energy and amplitude equations.^o

We make use of the particle–hole formalism in diagrammatic analyses by drawing upward- and downward-directed lines that identify those orbitals which differ from those in the reference determinant, Φ_0 , as shown in Figure 1.

^oMany varieties of diagrams have used throughout the chemical physics literature for many years (e.g., see Refs. 1, 2, 80, 117, and 119). The diagrammatic formalism we have chosen here has been frequently used in work by the Bartlett group among others¹²⁰ and is particularly straightforward for “conventional” coupled cluster and many-body perturbation theories.

^oThe algebraic rules for interpreting the diagrams as operators or wavefunctions differ only slightly from the matrix element approach discussed here. We recommend Refs. 80 and 88 for additional information.

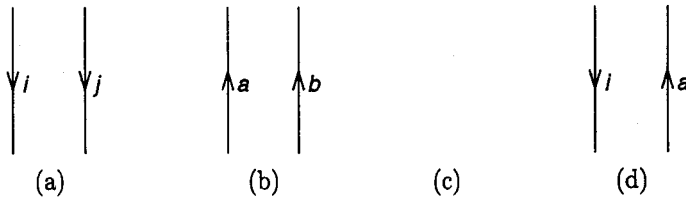


Figure 1 Some basic components of coupled cluster diagrams: (a) hole lines; (b) particle lines; (c) the reference wavefunction, Φ_0 , represented by empty space; and (d) a single-determinant wavefunction, Φ^1 which differs from the reference by a single excitation.

Downward-directed lines represent hole states (orbitals occupied in the reference) and upward directed lines represent particle states (orbitals unoccupied in the reference). Hence, one may interpret Figure 1(d) as a single-determinant wavefunction that differs from the reference by a single excitation from orbital ϕ_i to orbital ϕ_a . Furthermore, this convention implies that the reference wavefunction itself is represented by empty space, as indicated in Figure 1(c).

Diagrams representing dynamical operators (such as the one- and two-electron components of the normal-ordered Hamiltonian, \hat{H}_N) are depicted by horizontal “interaction lines,” with vertical-directed lines like those in Figure 1 representing the annihilation and creation operator strings. We will choose different interaction lines to represent different types of operator, e.g., a dashed line to indicate components of the electronic Hamiltonian, a solid line for cluster operators, \hat{T}_1 , \hat{T}_2 , etc. The directed lines emanate from “vertices” on the interaction line; each vertex represents the action of the operator on individual electrons. Thus, one-electron diagrams have one vertex, two-electron diagrams have two vertices, and so on. Attached to each vertex are two directed lines, one incoming and one outgoing, which are associated with the annihilation and creation operators of the operator’s normal-ordered string. Since one-electron operators contain two second-quantized components (see, e.g., Eq. [53]), their diagrammatic representations contain two directed lines. Similarly, diagrams representing two-electron operators contain four directed lines, three-electron operators contain six directed lines, and so on. The upward and downward directions of these lines are dependent on the orbital subspaces in which the second-quantized operators act: q -creation operators lie above the interaction line, whereas q -annihilation lines lie below the interaction line.^p

For example, we denote the one-electron component of the Hamiltonian, \hat{F}_N , by a dashed interaction line capped by an “X.” This operator may be

^pFor an explanation of q -creation and q -annihilation operators, see the earlier discussion of the particle-hole formalism in the section on The Fermi Vacuum and Particle-Hole Formalism.

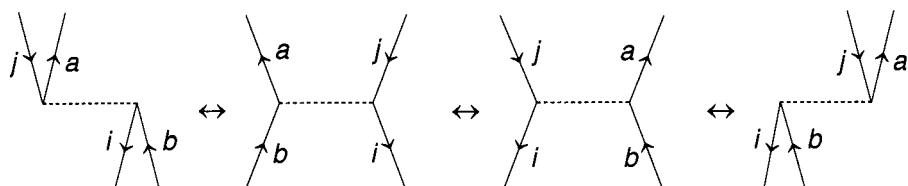
$$\hat{F}_N = \sum_{ab} f_{ab} \{a_a^\dagger a_b\} + \sum_{ij} f_{ij} \{a_i^\dagger a_j\} + \sum_{ia} f_{ia} \{a_i^\dagger a_a\} + \sum_{ia} f_{ai} \{a_a^\dagger a_i\}$$

$$= \begin{array}{c} \text{Diagram 1: } \text{Two vertical lines meeting at a dashed horizontal line labeled 'X'.} \\ 0 \end{array} + \begin{array}{c} \text{Diagram 2: } \text{Two vertical lines meeting at a dashed horizontal line labeled 'X'.} \\ 0 \end{array} + \begin{array}{c} \text{Diagram 3: } \text{Two vertical lines meeting at a dashed horizontal line labeled 'X'.} \\ -1 \end{array} + \begin{array}{c} \text{Diagram 4: } \text{Two vertical lines meeting at a dashed horizontal line labeled 'X'.} \\ +1 \end{array}$$

Figure 2 Diagrammatic representation of each fragment of the one-particle component of the Hamiltonian operator \hat{F}_N . The excitation level of each diagram is indicated beneath it. The interaction line is indicated by the dashed horizontal line capped by the "X".

written in four fragments as shown in Figure 2. The first fragment, which involves only operators in the particle (unoccupied) space, has one q -creation line above the interaction line corresponding to the a_a^\dagger component of its operator string, and one q -annihilation line below the interaction line corresponding to the a_b component. Similarly, the second fragment in the figure, which involves only operators in the hole (occupied) space, has one q -creation line above the interaction line corresponding to the a_i^\dagger component of the operator string, and one q -annihilation line below the interaction line corresponding to the a_j component. The third \hat{F}_N fragment contains only q -annihilation lines below the interaction line since the operator string consists of a_i^\dagger and a_a components only. Finally, the fourth fragment contains only q -creation lines above the interaction line representing the a_a^\dagger and a_i^\dagger components of the operator string.

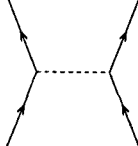
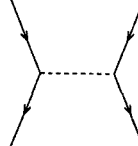
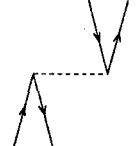
The two-electron fragment of the Hamiltonian may be partitioned in a similar manner as shown in Figure 3, with a dashed horizontal interaction line and with implicit antisymmetry with respect to permutation of the lines leaving or entering the left and right vertices. For example, in the third diagram, corresponding to a sum over the operator components, $\langle i a || b j \rangle \{a_i^\dagger a_a^\dagger a_j a_b\}$, the diagram as shown may be written in four equivalent ways (differing only by a sign), each formed by permuting either the two outgoing lines or the two incoming lines from the left and right vertices:



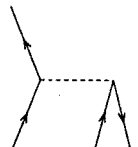
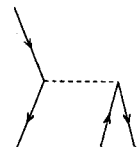
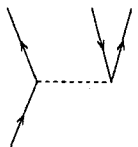
$$\hat{V}_N = \frac{1}{4} \sum_{abcd} \langle ab||cd \rangle \{a_a^\dagger a_b^\dagger a_d a_c\} + \frac{1}{4} \sum_{ijkl} \langle ij||kl \rangle \{a_i^\dagger a_j^\dagger a_l a_k\} + \sum_{iabj} \langle ia||bj \rangle \{a_i^\dagger a_a^\dagger a_j a_b\}$$

$$+ \frac{1}{2} \sum_{aibc} \langle ai||bc \rangle \{a_a^\dagger a_i^\dagger a_c a_b\} + \frac{1}{2} \sum_{ijka} \langle ij||ka \rangle \{a_i^\dagger a_j^\dagger a_a a_k\} + \frac{1}{2} \sum_{abci} \langle ab||ci \rangle \{a_a^\dagger a_b^\dagger a_i a_c\}$$

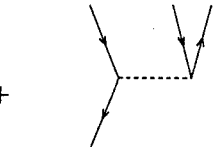
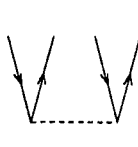
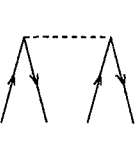
$$+ \frac{1}{2} \sum_{iajk} \langle ia||jk \rangle \{a_i^\dagger a_a^\dagger a_k a_j\} + \frac{1}{4} \sum_{abij} \langle ab||ij \rangle \{a_a^\dagger a_b^\dagger a_j a_i\} + \frac{1}{4} \sum_{ijab} \langle ij||ab \rangle \{a_i^\dagger a_j^\dagger a_b a_a\}$$

=  +  + 

0 0 0

+  +  + 

-1 -1 +1

+  +  + 

+1 +2 -2

Figure 3 Diagrammatic representation of each fragment of the two-particle component of the Hamiltonian operator \hat{V}_N . The excitation level of each diagram is indicated beneath it. The interaction line is indicated by the dashed horizontal line.

Diagrammatic representations of the cluster operators, \hat{T} , are shown in Figure 4, with solid horizontal interaction lines. Since the cluster operators contain only q -creation strings (and thereby generate excited determinants from the reference wavefunction), they contain no lines below the horizontal bar. Furthermore, these representations are also fully antisymmetric in that exchange of any pair of outgoing or incoming lines introduces a change in the

$$\hat{T}_1 = \sum_{ia} t_i^a \{a_a^\dagger a_i\} = \begin{array}{c} \diagdown \\ \diagup \end{array} +1$$

$$\hat{T}_2 = \frac{1}{4} \sum_{ijab} t_{ij}^{ab} \{a_a^\dagger a_b^\dagger a_j a_i\} = \begin{array}{c} \diagdown \quad \diagup \\ \diagup \quad \diagdown \end{array} +2$$

$$\hat{T}_3 = \frac{1}{36} \sum_{ijkabc} t_{ijk}^{abc} \{a_a^\dagger a_b^\dagger a_c^\dagger a_k a_j a_i\} = \begin{array}{c} \diagdown \quad \diagup \quad \diagdown \\ \diagup \quad \diagdown \quad \diagup \end{array} +3$$

Figure 4 Diagrammatic representation of the \hat{T}_1 , \hat{T}_2 , and \hat{T}_3 excitation operators. The excitation level of each diagram is indicated to its right. The interaction line is indicated by a solid horizontal bar.

sign of the diagram. We will discuss this point in greater detail later when we introduce rules for interpreting the diagrams algebraically.

Other than the operator representation above, we will interpret the diagrams in this chapter from bottom to top as matrix elements of operators (or operator products) between determinants. For the coupled cluster energy and amplitude equations shown in Eqs. [50] and [51], the pertinent matrix elements always contain the reference determinant, Φ_0 , on the right and either Φ_0 or excited determinants such as Φ_i^{ab} on the left. Diagrams are particularly convenient for constructing such matrix elements because they provide a straightforward method for evaluating the types of determinants to which individual operator fragments in Figures 2–4 may be applied or what determinants they produce. As an example, consider the fourth \hat{F}_N fragment in Figure 2, which contains no lines below and two lines above the horizontal operator line. Since the reference wavefunction, Φ_0 , is represented by empty space, and a singly excited determinant, Φ_i^a , by a pair of directed lines such as those in Figure 1(d), we may interpret the diagram from bottom to top to obtain the matrix element

$$\langle \Phi_i^a | \hat{F}_N | \Phi_0 \rangle = i \begin{array}{c} \diagdown \\ \diagup \end{array} a \quad [156]$$

A similar analysis may be applied to the two-electron operator in the third diagram in Figure 3, which contains particle–hole pairs of lines both above and

below the interaction line. Each of these pairs may be interpreted as singly excited determinants to obtain the general matrix element

$$\langle \Phi_i^a | \hat{V}_N | \Phi_j^b \rangle = \begin{array}{c} i \swarrow \searrow a \\ \cdots \cdots \cdots \\ j \swarrow \searrow b \end{array} [157]$$

The cluster operator diagrams are particularly simple to interpret as matrix elements; the diagrams always involve the reference determinant on the right (because they contain no lines below the interaction line) and an excited determinant on the left, for example,

$$\langle \Phi_{ij}^{ab} | \hat{T}_2 | \Phi_0 \rangle = \begin{array}{c} i \swarrow \searrow a \quad j \swarrow \searrow b \\ \cdots \cdots \cdots \end{array} [158]$$

We also make use of a simple bookkeeping system²⁰ that indicates the “excitation level” produced by a particular operator fragment. This value is determined by subtracting the number of q -annihilation lines from the number of q -creation lines and dividing the result by 2. For example, the first and second one-electron Hamiltonian fragments shown in Figure 2 are assigned an excitation level of +1, since both the wavefunction to which they are applied (at the bottom of the diagram) and the wavefunction they produce (at the top of the diagram) differ from the reference by a single orbital; no net excitation is produced. The fourth one-electron fragment, however, has an excitation level of +1 since it effectively produces a single excitation from the reference wavefunction. Two-electron Hamiltonian fragments have excitation levels ranging from +2 to -2, as indicated in Figure 3, and the \hat{T} operators have the obvious excitation levels indicated in Figure 4.

Diagrammatic Representation of the CCSD Energy Equation

As discussed in detail earlier, products of normal-ordered operators can be simplified algebraically using Wick’s theorem by evaluating pairs of contractions between the component annihilation and creation operators. Many of these contractions produce mathematically redundant terms that can be combined after complicated manipulation to eventually produce a much simpler expression. Diagrams provide a straightforward scheme by which these redundancies may be eliminated.

As an example, consider the CCSD energy equation derived earlier in Eq. [134] using Wick’s theorem. Each term of the general expression

$$E_{\text{CCSD}} - E_0 = \langle \Phi_0 | \hat{H}_N + \left(\hat{H}_N \hat{T}_1 + \hat{H}_N \hat{T}_2 + \frac{1}{2} \hat{H}_N \hat{T}_1^2 + \dots \right)_c | \Phi_0 \rangle \quad [159]$$

is a matrix element of a component of $e^{-\hat{T}} \hat{H}_N e^{\hat{T}}$ involving the reference determinant, Φ_0 , on both the right and left. Since Φ_0 is depicted diagrammatically by empty space, the diagrams associated with the energy equation must contain no directed lines that extend above or below the first (lowest) or last (highest) operator interaction lines; that is, the energy diagrams can contain no “external” lines. Clearly none of the diagrams representing fragments of \hat{H}_N shown in Figures 2 and 3 satisfy this criterion, and they therefore do not contribute to the CCSD energy. This is the expected result because all these diagrams represent normal-ordered operators whose reference expectation value is zero, by construction.

Next we consider the term from Eq. [159] that is linear in \hat{T}_1

$$E_{\text{CCSD}} \leftarrow \langle \Phi_0 | (\hat{H}_N \hat{T}_1)_c | \Phi_0 \rangle \quad [160]$$

which we examined earlier to obtain Eq. [126]. (The left arrow indicates that this is only one of several terms that contribute to the energy on the left-hand side.) The rightmost operator in this matrix element is \hat{T}_1 , so its interaction line must lie at the bottom of the final diagram. Making use of the excitation levels associated with the operator diagrams described above, we note that the \hat{T}_1 diagram produces an excitation level of +1 from the reference determinant. Since the matrix element of interest must contain Φ_0 on the left, the total excitation level of the final diagram must be 0. Therefore, we require the Hamiltonian diagrams that have an excitation level of -1 and contain the reference determinant at the top of the diagram. Of the \hat{F}_N and \hat{V}_N diagrams given above, only the third diagram of Figure 2 meets these criteria. We may then connect the \hat{T}_1 diagram with this \hat{F}_N fragment to obtain

$$\langle \Phi_0 | (\hat{F}_N \hat{T}_1)_c | \Phi_0 \rangle = \text{Diagram} \quad [161]$$

Note that to avoid external lines, both lines from the \hat{T}_1 diagram must connect to each line from the \hat{F}_N fragment. The diagram may be interpreted algebraically using the following rules:

- Label all directed lines with appropriate indices. By the convention we have used so far, hole lines would be labeled with i, j, k, l, \dots and particle lines with a, b, c, d, \dots . Therefore, for the diagram above we label the

hole line with i and the particle line with a to obtain



- Each operator interaction line contributes an integral or amplitude to the matrix element expression. Fock matrix elements are constructed from the diagram by the rule $\langle \text{out} | \hat{T} | \text{in} \rangle$, where **out** indicates the index of the outgoing directed line and **in** indicates the index of the incoming directed line at the interaction line's vertex. \hat{T} operators contribute amplitudes to the expression, constructed using the hole and particle indices in their left-to-right order in the diagram. In this case, the Fock matrix element is f_{ia} and the amplitude is t_i^a .
- Summations are included over all “internal” indices—that is, all indices associated with lines that begin and end at operator interaction lines and do not extend to infinity above or below the diagram like the external lines described above. Thus, the present diagram requires a summation over indices i and a .
- The sign of the diagram is determined based on the formula $(-1)^{h+l}$, where h is the number of hole lines in the diagram and l is the number of “loops.” A loop is a route along a series of directed lines that either returns to its beginning or begins at one external line and ends at another. In this case, we have only one hole line (i) and one loop, so the sign on the diagram is positive.

According to these rules, the final algebraic interpretation of the diagram above is therefore



$$= \sum_{ia} f_{ia} t_i^a \quad [162]$$

which is identical to Eq. [126] obtained earlier using Wick’s theorem.

Now consider the next term of Eq. [159] which is linear in \hat{T}_2 ,

$$E_{\text{CCSD}} \leftarrow \langle \Phi_0 | (\hat{H}_N \hat{T}_2)_c | \Phi_0 \rangle \quad [163]$$

which we examined earlier in Eq. [132]. Again the cluster operator must lie at the bottom of the final diagram because it is the rightmost operator in the matrix element. Since \hat{T}_2 produces an excitation level of +2 (see Figure 4), we require Hamiltonian diagrams that have an excitation level of -2 (to obtain a total excitation level of 0) and contain the reference wavefunction above the Hamiltonian interaction line. The only \hat{H}_N diagram that meets these criteria is

the last diagram of Figure 3,  , which contains four q -annihilation lines.

Connecting this diagram with that of \hat{T}_2 such that there are no external lines gives

$$\langle \Phi_0 | (\hat{V}_N \hat{T}_2)_c | \Phi_0 \rangle = \text{Diagram} [164]$$

To construct the algebraic interpretation of this diagram, we first assign labels

to the hole and particle lines as before, to obtain By the rules

described above, there are four internal lines and thus four summation indices. In addition, there are two loops in this diagram (one involving the i and a lines and the other involving the j and b lines) and two hole lines, giving an overall + sign. For the remainder of the algebraic expression, we require two rules in addition to those described above:

- The \hat{V}_N fragment contributes the two-electron integral, $\langle ij || ab \rangle$, which is constructed by the rule `left-out, right-out||left-in, right-in`, where **left-out** and **right-out** indicate the left and right outgoing lines from the \hat{V}_N diagram vertex, respectively, and **left-in** and **right-in** indicate the left and right incoming lines, respectively. The contribution of the \hat{T}_2 operator to the expression is obtained by taking the hole and particle indices from the \hat{T}_2 vertex in their left-to-right ordering in the diagram. For this diagram, \hat{V}_N contributes the integral $\langle ij || ab \rangle$ and \hat{T}_2 contributes the amplitude t_{ij}^{ab} .
- This diagram contains two pairs of “equivalent” lines—that is, lines beginning at the same operator interaction line and ending at the same interaction line. For each such pair, a prefactor of $\frac{1}{2}$ is multiplied onto the algebraic expression.⁹

The final algebraic interpretation of this diagram is therefore

$$\text{Diagram} = \frac{1}{4} \sum_{ijab} \langle ij || ab \rangle t_{ij}^{ab} [165]$$

We could have used a connectivity for the \hat{V}_N and \hat{T}_2 diagram fragments somewhat different from the one shown above. For example, we could also have chosen instead to build this diagram as

$$\langle \Phi_0 | (\hat{V}_N \hat{T}_2)_c | \Phi_0 \rangle = \text{Diagram} [166]$$

⁹It is possible for groups of three or more lines to be identified as equivalent, though this can happen only in many-body perturbation theory, expectation value coupled cluster theory, or unitary coupled cluster theory. For such diagrams, a prefactor of $\frac{1}{n!}$, where n is the number of electron lines, must be included.

However, recall that the \hat{V}_N and \hat{T}_2 operator diagrams from Figures 3 and 4 are antisymmetric with respect to permutation of either the pair of outgoing lines or the pair of incoming lines at the two vertices. Hence, we have the relations,

[167]

Therefore, the two energy diagrams are equivalent, because the two hole lines and the two particle lines from the \hat{T}_2 diagram both connect to the same \hat{V}_N diagram fragment:

[168]

The equivalence of the two diagrams can also be seen through their algebraic interpretations, which we obtain by applying the same rules given above to the new diagram from Eq. [166]. Again, we label the hole and particle lines using

the indices i, j, a , and b , to obtain . In this case, the algebraic

analysis is identical to that given for the diagram of Eq. [164], with two exceptions: (1) the two-electron integral contributed by the \hat{V}_N fragment is $\langle ij||ba \rangle$ rather than $\langle ij||ab \rangle$ because its two incoming particle lines have been reversed; and (2) although there are still two hole lines, there is now only one loop, which involves all four directed lines, giving rise to a negative sign for the diagram. Hence, the algebraic interpretation of the diagram is

[169]

where we have used the antisymmetry of the Dirac notation two-electron integrals to make the equivalence of the two diagrams clearer.

Next consider the component of Eq. [159] which is quadratic in \hat{T}_1 ,

$$E_{\text{CCSD}} \leftarrow \frac{1}{2} \langle \Phi_0 | (\hat{H}_N \hat{T}_1^2)_c | \Phi_0 \rangle \quad [170]$$

Since the two cluster operators act on the reference determinant to produce a total excitation level of +2, we require the same Hamiltonian –2 diagram fragment used in Eq. [164]. Also, because the cluster operators act before the Hamiltonian operator in the matrix element, they are placed at the bottom of the diagram. Furthermore, because the \hat{T}_1 operators commute, their vertical

ordering in the diagram is not important. The complete diagram is formed by connecting the \hat{V}_N vertex to both of the \hat{T}_1 diagrams to give

$$\frac{1}{2} \langle \Phi_0 | (\hat{V}_N \hat{T}_1^2)_c | \Phi_0 \rangle = \text{Diagram} [171]$$

For this diagram, the algebraic analysis is quite similar to that used to obtain Eq. [165]. There are two hole lines, and two particle lines, all of which are summation indices. Since there are two loops, the total sign on the diagram is positive. The two-electron integral provided by the \hat{V}_N fragment is again $\langle ij || ab \rangle$, but there are now two \hat{T}_1 amplitude fragments, one contributing t_i^a and the other t_j^b . Note also that the two pairs of hole lines and particle lines are no longer equivalent as they were in Eq. [165]. We require only one additional rule to evaluate this diagram:

Unlike the diagram in Eq. [165], this diagram contains a pair of “equivalent” vertices; since both \hat{T}_1 fragments are connected to the same \hat{V}_N interaction line in exactly the same manner (each by a hole line and a particle line), a prefactor of $\frac{1}{2}$ is multiplied into the final expression. Generally speaking, if there are n equivalent vertices in the diagram, they contribute a prefactor of $1/n!$ to the final expression.

Thus, the final algebraic expression for this diagram is

$$\text{Diagram} = \frac{1}{2} \sum_{ijab} \langle ij || ab \rangle t_i^a t_j^b [172]$$

The diagrammatic analysis also makes it clearer that no higher order contributions to the Hausdorff expansion in Eq. [159] can contribute to the coupled cluster energy. All remaining terms contain cluster operator products that produce excitation levels higher than +2. However, there are no Hamiltonian operator diagrams that can decrease this excitation level by more than -2. Therefore, there can be no higher-order contributions to the coupled cluster energy equation, which must have a total excitation level of 0.

Summing diagrammatic Eqs. [162], [165], and [172], we obtain the final energy equation

$$E_{CCSD} - E_0 = \text{Diagram} + \text{Diagram} + \text{Diagram} [173]$$

$$= \sum_{ia} f_{ia} t_i^a + \frac{1}{4} \sum_{ijab} \langle ij || ab \rangle t_{ij}^{ab} + \frac{1}{2} \sum_{ijab} \langle ij || ab \rangle t_i^a t_j^b$$

which is identical to that derived earlier using Wick’s theorem.

Diagrammatic Representation of the CCSD Amplitude Equations

The same diagrammatic concepts used to derive the CCSD energy equation (Eq. [173]) may also be applied to the CCSD \hat{T}_1 and \hat{T}_2 amplitude equations, with a few additional rules. Here we consider the contribution of each term of \bar{H} given in Eq. [122] to the amplitude equations in the same order as we did using Wick's theorem before. The resulting matrix elements always contain the reference determinant, Φ_0 , on the right and an excited determinant on the left (e.g., Φ_i^a for the \hat{T}_1 equation and Φ_{ij}^{ab} for the \hat{T}_2 equation). The corresponding diagrams always have the same general structure: no q -annihilation lines below the diagram and a certain number of q -creation lines extending above. For example, diagrams contributing to the \hat{T}_1 amplitude equation contain exactly two q -creation lines above (and therefore a total excitation level of +1), and diagrams contributing to the \hat{T}_2 amplitude equation contain four q -creation lines above (and a total excitation level of +2).

The leading term of \bar{H} is just the electronic Hamiltonian itself. For its contribution to the \hat{T}_1 amplitude equation, we must evaluate the matrix elements, $\langle \Phi_i^a | (\hat{F}_N + \hat{V}_N) | \Phi_0 \rangle$, as before. Since these elements contain the reference determinant on the right and a singly excited determinant on the left, we require those +1 Hamiltonian diagrams that contain no lines below the interaction line and a single pair of lines above it. The only diagram from Figures 2 and 3 that meets this criterion is the fourth fragment of the one-electron operator, \hat{F}_N . Hence, there is no contribution from \hat{V}_N in this case, and the matrix element is represented diagrammatically as

$$\langle \Phi_i^a | \hat{F}_N | \Phi_0 \rangle = \begin{array}{c} \diagdown \quad \diagup \\ i \quad a \\ \diagdown \quad \diagup \\ \dots \quad X \end{array} \quad [174]$$

The algebraic interpretation of this diagram is straightforward: (1) we label the two lines using indices i and a to maintain consistency with the singly excited determinant, Φ_i^a , used in the matrix element itself; (2) there are no internal lines and therefore no summation indices; (3) the \hat{F}_N fragment contributes the Fock matrix element, f_{ai} ; and (4) there is only one loop (which starts at one external line and ends at another) and one hole line, giving a positive sign. Thus, the final expression is simply

$$\begin{array}{c} \diagdown \quad \diagup \\ i \quad a \\ \diagdown \quad \diagup \\ \dots \quad X \end{array} = f_{ai} \quad [175]$$

which we derived earlier in Eq. [139] using Wick's theorem.

For the contribution of \hat{H}_N to the \hat{T}_2 amplitude equation, we must evaluate the matrix element, $\langle \Phi_{ij}^{ab} | (\hat{F}_N + \hat{T}_N) | \Phi_0 \rangle$, which contains the reference deter-

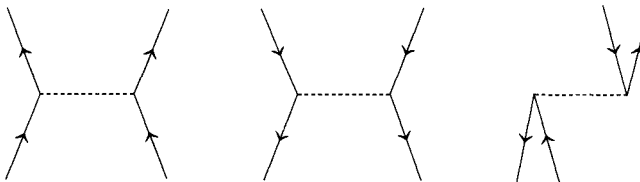
minant on the right and a doubly excited determinant on the left. Therefore, we require the \hat{H}_N diagrams that produce a +2 excitation and have no q -annihilation lines. Only the eighth diagram of Figure 3,  , meets this criterion.

Its algebraic interpretation is carried out as follows: (1) we label the lines (in order) as i , a , j , and b , for consistency with the doubly excited determinant in the matrix element; (2) there are no internal lines and therefore no summation indices; (3) the two-electron integral contributed by the \hat{V}_N interaction line is $\langle ab||ij\rangle$; and (4) there are two hole lines and two loops, giving a positive sign. Therefore, this matrix element may be written as

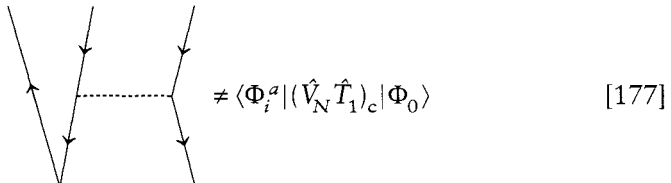
$$\langle \Phi_{ij}^{ab} | \hat{V}_N | \Phi_0 \rangle = i \begin{array}{c} \diagdown \\ \diagup \end{array} a \quad j \begin{array}{c} \diagup \\ \diagdown \end{array} b = \langle ab || ij \rangle \quad [176]$$

which is the same as that derived earlier in Eq. [141].

The contribution of the second term of Eq. [122] to the \hat{T}_1 amplitude equation is only slightly more complicated. This term involves the matrix element, $\langle \Phi_i^a | (\hat{F}_N + \hat{V}_N) \hat{T}_1 |_c | \Phi_0 \rangle$, and, as before, we will consider only the contribution of \hat{V}_N . The \hat{T}_1 operator, which acts first and is therefore placed at the bottom of the diagram, produces a +1 excitation from the reference on the right. Since the singly excited determinant on the left-hand side of the matrix element indicates an overall +1 excitation level, we require the three diagram fragments of \hat{V}_N that have an overall excitation level of 0:



However, the first two of these fragments can connect to the \hat{T}_1 diagram in only one index—via either a single hole line or particle line—thus leaving an additional line extending below the \hat{T}_1 interaction line in the final diagram, for example,



Because such diagrams cannot represent matrix elements that have the reference wavefunction on the right, only the third diagram above can contribute to

the \hat{T}_1 amplitude equation. Connecting this \hat{V}_N fragment to the \hat{T}_1 diagram gives

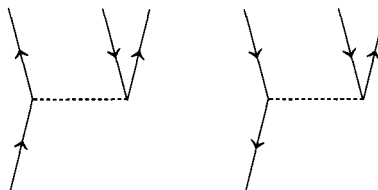
$$\langle \Phi_i^a | (\hat{V}_N \hat{T}_1)_c | \Phi_0 \rangle = \text{Diagram} [178]$$

The algebraic interpretation of this diagram proceeds exactly as before: (1) we label the external lines using i and a for consistency with the singly excited determinant in the matrix element, and the internal lines are labeled with the summation indices j and b ; (2) the appropriate two-electron integral contributed by the \hat{V}_N component is $\langle ja||bi\rangle$, and the \hat{T}_1 amplitude is t_j^b ; and (3) there are two loops and two hole lines, giving the diagram a positive sign. The final expression for this diagram is therefore

$$\text{Diagram} = \sum_{jb} \langle ja||bi\rangle t_j^b [179]$$

which is identical to the result in Eq. [143].

The contribution of $(\hat{V}_N \hat{T}_1)_c$ to the \hat{T}_2 amplitude equation involves the matrix element $\langle \Phi_{ij}^{ab} | (\hat{V}_N \hat{T}_1)_c | \Phi_0 \rangle$. In this case, we require an overall excitation level of +2 as dictated by the doubly excited determinant on the left. Since the \hat{T}_1 operator produces a +1 excitation from Φ_0 , we require the sixth and seventh diagrams of \hat{V}_N in Figure 3, which produce a +1 excitation:



These may be connected to the \hat{T}_1 amplitude diagram from below to give two terms

$$\langle \Phi_{ij}^{ab} | (\hat{V}_N \hat{T}_1)_c | \Phi_0 \rangle = \text{Diagram} + \text{Diagram} [180]$$

These two diagrams may be interpreted using the rules described above: (1) we assign indices i , j , a , and b (from left to right) to the external lines for consistency with the doubly excited determinant in the matrix element; (2) there is only one internal (summation) line in each diagram to which we assign the indices c in the left diagram and k in the right diagram; (3) in the left diagram, there are two loops and two hole lines giving a positive sign, and in the right diagram there are two loops and three hole lines giving a negative sign; (4) the two-electron integral in the left diagram is $\langle ab||cj\rangle$ and in the right diagram is $\langle kb||ij\rangle$; (5) the \hat{T}_1 amplitude in the left diagram is t_i^c and in the right diagram is t_k^i ; and (6) there are neither equivalent lines nor equivalent vertices, so no additional factors of $1/2$ appear in the final expression.

Before the algebraic interpretation is complete, however, we require one additional rule:

Each pair of unique, external hole or particle lines introduces a permutation function, $P(pq)$ (as defined earlier in Eq. [154]), to ensure antisymmetry of the final expression.

Note again that the four external q -creation lines of the \hat{T}_2 amplitude diagrams correspond to the wavefunction lines of a doubly excited determinant; in the diagrams above, the i , j , a , and b external lines correspond to the excitation orbitals of the determinant, Φ_{ij}^{ab} . Since this determinant is antisymmetric with respect to permutation of either the i and j indices or the a and b indices, this antisymmetry must be maintained in the final algebraic expression. Pairs of external lines that originate from the same operator interaction line (such as the two particle lines in the leftmost diagram of Eq. [180]) are not unique, and the expression is already antisymmetric with respect to permutation of such pairs. Pairs of external lines that do not originate on the same operator interaction line (such as the hole lines of the leftmost diagram) are unique, and a permutation operator must be included in the algebraic interpretation to ensure proper antisymmetry. For example, in the left-hand diagram above, there are two external particle lines and two external hole lines. The diagram is already antisymmetric to permutation of the two particle lines because they both connect to the \hat{V}_N diagram fragment. The hole lines, on the other hand, connect to different vertices—one to \hat{T}_1 and the other to \hat{V}_N . Therefore, the diagram is not antisymmetric to permutation of these lines, and we must include the operator $P(ij)$ in the algebraic expression corresponding to this diagram:

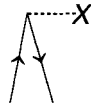
$$= P(ij) \sum_c \langle ab || cj \rangle t_i^c \quad [181]$$

Similarly, the external particle lines in the rightmost diagram must be permuted in its algebraic expression:

$$= -P(ab) \sum_k \langle kb || ij \rangle t_k^a \quad [182]$$

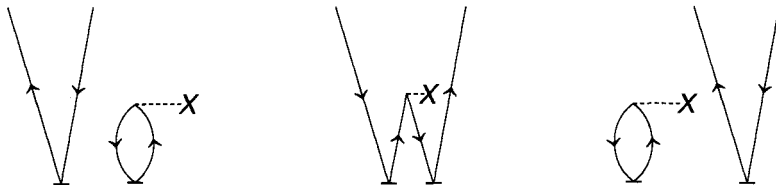
When the permutation operators are expanded, these expressions are identical to those given in Eq. [145] derived earlier using Wick's theorem and some complicated algebra.

The next example is the contribution of $(\hat{F}_N \hat{T}_1^2)_c$ to the \hat{T}_1 amplitude equation, which requires the matrix element $\langle \Phi_i^a | (\hat{F}_N \hat{T}_1^2)_c | \Phi_0 \rangle$. To obtain an overall excitation level of +1, as dictated by the singly excited determinant on the left and the reference on the right, we must use the -1 diagram fragment of



, since the two \hat{T}_1 operators produce an excitation level of +2. There

are three ways to connect this \hat{F}_N diagram fragment to the cluster operator diagrams to produce a matrix element with the appropriate determinants above and below the diagrams:



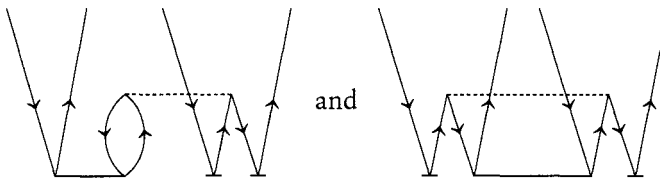
The first and third diagrams above are equivalent and correspond to the contractions indicated in Eq. [149]. These violate the “connected cluster” form of $e^{-\hat{T}} \hat{H}_N e^{\hat{T}} \equiv (\hat{H}_N e^{\hat{T}})_c$ discussed earlier, which requires that the Hamiltonian fragment share at least one index with every cluster operator on its right. The second diagram is therefore the only acceptable contribution from this matrix element to the \hat{T}_1 amplitude equation. Its algebraic interpretation proceeds as usual: (1) the external lines are labeled i and a to match the singly excited determinant, Φ_i^a in the matrix element; (2) the internal (summation) lines are labeled by the dummy indices k and c ; (3) the Fock operator contributes the element f_{kc} , and the \hat{T}_1 operators contribute the amplitudes t_k^c and t_k^a ; (4) there are two hole lines and only one loop, giving an overall negative sign to the diagram; and (5) there are no equivalent, internal lines, nor are the two \hat{T}_1 fragments equivalent since they do not connect to the \hat{F}_N diagram fragment in

the same way (one connects via a hole line and the other via a particle line). The final expression is therefore

$$\frac{1}{2} \langle \Phi_i^a | (\hat{F}_N \hat{T}_1^2)_c | \Phi_0 \rangle = \begin{array}{c} \text{Diagram showing two V-shaped lines meeting at a central point labeled } X. \end{array} = - \sum_{kc} f_{kc} t_i^c t_k^a \quad [183]$$

which is the same as the result given in Eq. [148].

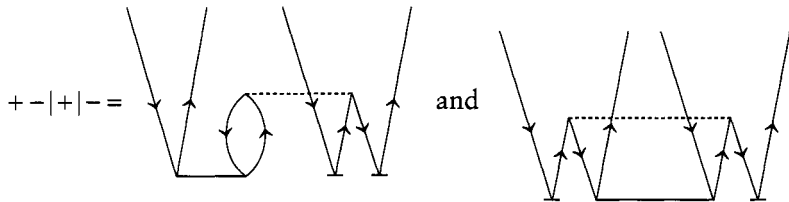
As a final example, consider the contribution of the $\frac{1}{2}(\hat{V}_N \hat{T}_1^2 \hat{T}_2)_c$ operator to the \hat{T}_2 equation. As discussed earlier, the corresponding matrix element, which involves a doubly excited determinant on the left and the reference determinant on the right, requires considerable effort if analyzed using Wick's theorem. Diagrammatically, however, this analysis is much simpler. The only difficulty arises in the construction of only uniquely connected diagrams. For example, one might construct the two seemingly different diagrams:



Careful inspection, however, reveals that the diagrams are equivalent because one can be produced from the other by permutation of the hole or particle lines on the \hat{T}_2 fragment. (This equivalence can also be proven algebraically, and the reader is encouraged to carry this analysis out independently.)

One can ensure that only unique diagrams are produced by using a straightforward procedure developed by Kucharski and Bartlett.²⁰ In this approach, one first assigns + symbols to particle lines and - symbols to hole lines lying below the interaction line of the Hamiltonian fragment or above the interaction line for the cluster operators. Unique connectivities of the operator diagrams are produced by combining these signs in all unique ways. In the present example, the two \hat{T}_1 operators each contribute one + sign and one - sign, the \hat{T}_2 operator contributes two + signs and two - signs, and the -2 excitation level fragment of \hat{V}_N contributes two + signs and two - signs. Since in this case every directed line from the Hamiltonian fragment must connect to lines from the cluster operators, we must match the + and - signs from \hat{V}_N to the same signs on the cluster operators. For example, we might choose one + and one - from the \hat{T}_2 operator, leaving one + for one of the \hat{T}_1 fragments and one - for the remaining \hat{T}_1 . We will denote this "sign sequence" as + - | + | -, where the first pair of signs belong to the \hat{T}_2 operator, and the remaining signs (sepa-

rated by the vertical bars) belong to the \hat{T}_1 operator fragments. The corresponding diagram would be



where the connectivity dictated by the sign sequence is maintained in the diagram. The sign sequence helps to reveal the equivalence of the two diagrams; the \hat{T}_2 operator in each diagram connects to the \hat{V}_N fragment by a particle-hole pair of lines, while the \hat{T}_1 operators connect by either a particle or a hole line. Note that this sequence is equivalent to the sequence $+ - | - | +$ because the \hat{T}_1 operators commute. For this matrix element, there are only five unique sign sequences, including the one given above: (1) $+ - | + | -$, (2) $+ + | - | -$, (3) $- - | + | +$, (4) $- | + | + -$, and (5) $+ | - | + -$. These five Kucharski-Bartlett sign sequences give rise to the diagrams (in order)

$$\frac{1}{2} \langle \Phi_{ij}^{ab} | (\hat{V}_N \hat{T}_1^2 \hat{T}_2)_c | \Phi_0 \rangle =$$

[184]

The algebraic interpretation of each of these diagrams, using the rules described earlier, is easily shown to be (in the same order as the diagrams above)

$$\begin{aligned} \frac{1}{2}\langle\Phi_{ij}^{ab}|\hat{V}_N\hat{T}_1^2\hat{T}_2\rangle_c|\Phi_0\rangle &= -P(ij)P(ab)\sum_{klcd}\langle kl||cd\rangle t_{ik}^{ac}t_j^dt_l^b \\ &\quad + \frac{1}{4}P(ab)\sum_{klcd}\langle kl||cd\rangle t_{ij}^{cd}t_k^at_l^b + \frac{1}{4}P(ij)\sum_{klcd}\langle kl||cd\rangle t_{kl}^{ab}t_i^ct_l^d \\ &\quad - P(ij)\sum_{klcd}\langle kl||cd\rangle t_{ik}^{ab}t_j^ct_l^d - P(ab)\sum_{klcd}\langle kl||cd\rangle t_{ij}^{ac}t_k^bt_l^d \end{aligned} \quad [185]$$

The permutation operators appear in order to maintain the antisymmetry of the algebraic expressions, as explained earlier. Note that the factors of $\frac{1}{4}$ appearing in the second and third terms result from both a pair of equivalent lines and a pair of equivalent vertices in each of the corresponding diagrams.

Size Extensivity of the Coupled Cluster Energy

Earlier in the chapter we discussed the property of the coupled cluster energy known as size consistency, which implies that the energy of two noninteracting fragments computed separately is the same as that computed for both fragments simultaneously. A related property is known as size extensivity, which is applied to methods whose energy scales linearly with N (the number of electrons), just as the exact energy scales. Whereas size consistency applies only to noninteracting molecular fragments, size extensivity is a more general mathematical concept that applies to any point on the potential energy surface. The term was popularized in electronic structure theory by Bartlett⁸⁷ and is based on analogous extensive thermodynamic properties. In this section, we show that the exponential ansatz of coupled cluster theory guarantees size extensivity, but the truncated CI approach does not.

Consider the structure of the CI Schrödinger equation (assuming intermediate normalization as well as normal-ordered \hat{H}_N and \hat{C} operators), beginning from the linear ansatz of Eq. [32]:

$$\hat{H}_N(1 + \hat{C}_1 + \hat{C}_2 + \dots)|\Phi_0\rangle = (E_{\text{CI}} - E_0)(1 + \hat{C}_1 + \hat{C}_2 + \dots)|\Phi_0\rangle \quad [186]$$

Left-projection of this equation by the reference determinant, Φ_0 , leads to the energy equation,

$$E_{\text{CI}} - E_0 = \langle\Phi_0|(\hat{H}_N(\hat{C}_1 + \hat{C}_2))|\Phi_0\rangle \quad [187]$$

where truncation of the CI expansion is a natural consequence of Slater's rules. By application of Wick's theorem (or the corresponding diagrams, of course), this equation may be written in algebraic form as

$$E_{\text{CI}} - E_0 = \sum_{ia}f_{ia}c_i^a + \frac{1}{4}\sum_{ijab}\langle ij||ab\rangle c_{ij}^{ab} \quad [188]$$

If canonical Hartree–Fock orbitals are chosen, the first term is zero by Bril-louin’s theorem.

How do the individual terms on the right-hand side of Eq. [188] scale as more electrons are added to the system? If we assume a localized orbital basis (which does not limit the validity of this analysis), then, for a given occupied orbital, ϕ_i , the two-electron integral, $\langle ij||ab\rangle$, for example, will be zero unless the orbitals, ϕ_j , ϕ_a , and ϕ_b , are in reasonably close proximity to ϕ_i , owing to the relatively short range of the interelectronic potential. Assuming that the number of orbitals that fulfill this proximity requirement for (i.e., are “local” to) ϕ_i is finite, then all the individual two-electron integrals, $\langle ij||ab\rangle$, associated with ϕ_i are *independent* of the number of electrons in the system. That is, as more electrons (and therefore more occupied and virtual orbitals) enter the calculation, the set of individual two-electron integrals associated with orbital ϕ_i remains unaffected. Assuming that the CI coefficients, c_{ij}^{ab} , in the second term of Eq. [188] have the same independence—an assumption we will examine momentarily—then the i -independent summation,

$$Z_i \equiv \sum_{jab} \langle ij||ab\rangle c_{ij}^{ab} \quad [189]$$

will be unaffected as the size of the system increases. Since there are N electrons, the final summation over occupied orbital index i produces N independent Z_i contributions,

$$E_{\text{CI}} \leftarrow \sum_i Z_i \quad [190]$$

(The left arrow indicates that the term on the right-hand side is one of several terms that contribute to E_{CI} .) Therefore the second term of Eq. [188] scales *linearly* with the number of electrons if and only if the CI coefficients, c_{ij}^{ab} , are independent of N . A similar argument holds for the first term on the right-hand side of the equation as well.

The CI coefficient equations are obtained by left-projection of Eq. [186] by excited determinants. For example, the \hat{C}_1 equation from full CI is

$$\langle \Phi_i^a | \hat{H}_N (1 + \hat{C}_1 + \hat{C}_2 + \hat{C}_3) | \Phi_0 \rangle = (E_{\text{CI}} - E_0) \langle \Phi_i^a | \hat{C}_1 | \Phi_0 \rangle = E_{\text{CI}} \xi_i^a \quad [191]$$

which is energy dependent, unlike the corresponding coupled cluster amplitude equation. Every term on the left-hand side of this equation involves either bare Hamiltonian matrix elements, which are independent of N , or contractions of such matrix elements with CI coefficients, whose N -scaling is not yet known. The term on the right-hand side, which contains the CI energy, on the other hand, does depend on the system size—as N increases, E_{CI} increases (with some undetermined order). This nonunit scaling implies that if size extensivity is to be

maintained, terms on the left-hand side of Eq. [191] must scale similarly with N in order to cancel out the “errors” introduced by the presence of E_{CI} . If all excitation operators are included in the CI ansatz, this compensation is included in the corresponding coefficient equations. For example, we see that in Eq. [191], \hat{C}_3 can contribute to \hat{C}_1 by Slater’s rules. The \hat{C}_3 equation itself is

$$\langle \Phi_{ijk}^{abc} | \hat{H}_N (\hat{C}_1 + \hat{C}_2 + \hat{C}_3 + \hat{C}_4 + \hat{C}_5) | \Phi_0 \rangle = (E_{\text{CI}} - E_0) c_{ijk}^{abc} \quad [192]$$

which includes contributions from up to \hat{C}_5 . The first term on the left-hand side involving \hat{C}_1 may be written as

$$c_{ijk}^{abc} \leftarrow \langle jk||bc \rangle = c_i^a \langle jk||bc \rangle \quad [193]$$

where the thick bar in the diagram distinguishes the \hat{C}_1 operator from the corresponding \hat{T}_1 operator. Since the orbitals on the \hat{C}_1 component are completely independent of those of the two-electron integral (i.e., the diagram is “disconnected”), this term will produce nonzero \hat{C}_3 components involving orbitals that are spatially distant as the size of the system is increased. That is, for a given orbital, ϕ_i , the number of nonzero coefficients, c_{ijk}^{abc} , involving the orbitals ϕ_j , ϕ_k , etc., increases as more electrons (orbitals) are added to the system. Therefore, the term from Eq. [191] involving \hat{C}_3 , which may be written as

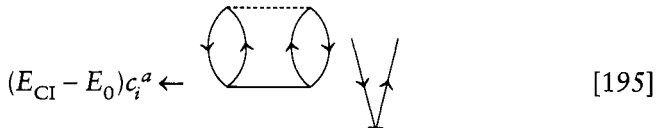
$$c_i^a \leftarrow \frac{1}{4} \sum_{jkbc} c_{ijk}^{abc} \langle jk||bc \rangle \quad [194]$$

scales approximately linearly as N increases. This term would therefore contribute to the “compensating errors” described above to ensure appropriate linear scaling of the CI energy with respect to the number of electrons. Similarly, the N -scaling of the \hat{C}_3 equation itself is corrected by such disconnected terms arising from higher excitation levels such as \hat{C}_4 and \hat{C}_5 . Therefore, if the CI equations are truncated at a particular excitation level, the higher excitation terms needed to cancel the incorrect N -scaling of the energy-dependent term in each coefficient equation will be lost, and the errors in the truncated CI energy relative to the exact (full CI) energy will be compounded as the size of the system increases. The well-known Davidson correction for the CISD energy is designed to account for the size extensivity error of this method.^{121,122}

The coupled cluster energy, on the other hand, does not suffer from this lack of size extensivity for two reasons: (1) the amplitude equations in Eq. [50] are independent of the coupled cluster energy; and (2) the Hausdorff expansion of the similarity-transformed Hamiltonian in Eq. [106], for example, guarantees that the only nonzero terms are those in which the Hamiltonian is con-

nected to all the cluster operators on its right, regardless of the truncation of \hat{T} . Hence, no diagrams such as that in Eq. [193] appear in the coupled cluster amplitude equations. As a result, the \hat{T} amplitudes are independent of the system size, and the coupled cluster energy computed via Eq. [123] scales linearly with the number of electrons.

A size extensive method is frequently defined esoterically as one whose energy and amplitude/coefficient equations contain no “unlinked” diagrams, such as



in which the two diagram components cannot be connected to each other even by application of other interaction lines.⁷ Although such terms are indeed absent in the coupled cluster equations (as well as those of many-body perturbation theory), the disconnected amplitude components, such as those in Eq. [193] (which also contribute to the improper N -dependence of the amplitudes), must be excluded to ensure correct scaling of the energy.

CONNECTION TO MANY-BODY PERTURBATION THEORY

In this section we examine the fundamental relationship between many-body perturbation theory (MBPT) and coupled cluster theory. As originally pointed out by Bartlett,^{87,123} this connection allows one to construct finite-order perturbation theory energies and wavefunctions via “iterations” of the coupled cluster equations. The essential aspects of MBPT have been discussed in Volume 5 of *Reviews in Computational Chemistry*,⁷⁷ as well as in numerous other texts.^{80,82,124,125} We therefore only summarize the main points of MBPT and focus on its intimate link to coupled cluster theory, as well as how MBPT can be used to construct energy corrections for higher order cluster operators such as the popular (T) correction for connected triple excitations.

⁷The “disconnected” diagram of Eq. [193] is not unlinked because the inclusion of an additional \hat{V}_N fragment can connect its two components—Harris et al. (Ref. 80) have recommended that such terms be called “linkable.” With terms such as “disconnected,” “connected,” “linked,” and “unlinked” used to describe diagrams, it is not surprising that these techniques caused much confusion in the past.

Perturbational Decomposition of the Cluster Operators

Two essential concepts underlie the construction of MBPT from basic Rayleigh–Schrödinger perturbation theory:^{77,82}

The zeroth-order component of the electronic Hamiltonian is taken to be the Fock operator such that the perturbation operator (sometimes called the fluctuation potential) is then the remaining two-electron operator, \hat{V}_N :

$$\hat{H}_N = \hat{H}^{(0)} + \hat{H}^{(1)} = \hat{F}_N + \hat{V}_N \quad [196]$$

This partitioning, when applied in conjunction with the set of canonical Hartree–Fock orbitals (in which \hat{F}_N is diagonal), corresponds to the Møller–Plesset variant of many-body perturbation theory.¹²⁶ A Hartree–Fock determinant, which is an eigenfunction of \hat{F}_N , is therefore the natural choice for the zeroth-order wavefunction.^s

Each perturbed wavefunction, $\Psi^{(n)}$, is expanded in a CI-like fashion as a linear combination of excited determinants,

$$\Psi^{(n)} = \sum_{ia} a_i^{a(n)} \Phi_i^a + \frac{1}{4} \sum_{ijab} a_{ij}^{ab(n)} \Phi_{ij}^{ab} + \dots \quad [197]$$

As discussed in detail in Refs. 77 and 82, for example, this expansion is not N -fold (where N is the number of electrons in the system) for the lower perturbational orders, but truncates to include only modest excitation levels. For example, the first-order wavefunction, which may be used to compute both the second- and third-order energies, contains contributions from doubly excited determinants only, whereas the second-order wavefunction, which contributes to the fourth- and fifth-order perturbed energies, contains contributions from singly, doubly, triply, and quadruply excited determinants. Furthermore, the sum of the zeroth- and first order energies is equal to the SCF energy. This determinantal expansion of the perturbed wavefunctions suggests that we may also decompose the cluster operators, \hat{T}_n , by orders of perturbation theory:

$$\hat{T}_n = \hat{T}_n^{(1)} + \hat{T}_n^{(2)} + \hat{T}_n^{(3)} + \dots \quad [198]$$

Depending on the choice of molecular orbital basis, the earliest terms for certain excitation levels are naturally zero. For example, in Møller–Plesset theory, only

^sThe choice of \hat{F}_N as the zeroth-order Hamiltonian requires the use of either a spin-restricted (closed-shell) Hartree–Fock (RHF) or spin-unrestricted Hartree–Fock (UHF) determinant as the zeroth-order (reference) wavefunction. Since spin-restricted open-shell Hartree–Fock (ROHF) reference functions are not eigenfunctions of the spin-orbital \hat{F}_N , other partitions are required (Refs. 127–134).

\hat{T}_2 contains a nonzero first-order component; contributions to \hat{T}_1 , \hat{T}_3 , and \hat{T}_4 first appear in second order because the corresponding second-order wavefunction contains single, double, triple, and quadruple excitations.

Perturbation Theory Energies from the Coupled Cluster Hamiltonian

The partitioning of the electronic Hamiltonian and the corresponding breakdown of the cluster operators leads to an expansion of the coupled cluster effective Hamiltonian, \bar{H} , in orders of perturbation theory through the Hausdorff expansion given in Eq. [122]:

$$\bar{H} = \bar{H}^{(0)} + \bar{H}^{(1)} + \bar{H}^{(2)} + \dots \quad [199]$$

Since the zeroth-order component of \bar{H} consists of just the Fock operator in Møller–Plesset theory, the first-order components of \bar{H} may be written as

$$\bar{H}^{(1)} = \hat{V}_N + (\hat{F}_N \hat{T}_2^{(1)})_c \quad [200]$$

and the second-order term as

$$\bar{H}^{(2)} = (\hat{F}_N \hat{T}_1^{(2)} + \hat{V}_N \hat{T}_2^{(1)} + \frac{1}{2} \hat{F}_N (\hat{T}_2^{(1)})^2)_c \quad [201]$$

Each of these expressions is constructed by simply assigning the appropriate perturbational orders to each operator in Eq. [122] and retaining only the terms that correspond to the desired order, n . Using $\bar{H}^{(n)}$ as an approximate Hamiltonian, one may construct n th-order Schrödinger equations of the form

$$\bar{H}^{(n)} |\Phi_0\rangle = E^{(n)} |\Phi_0\rangle \quad [202]$$

One computes the energy in the n th order of MBPT via a zeroth-order expectation value, namely,

$$E^{(n)} = \langle \Phi_0 | \bar{H}^{(n)} | \Phi_0 \rangle \quad [203]$$

obtained by left-projection of Eq. [202] by Φ_0 . For example, the second-order energy (often referred to as the MP2 energy) may be computed from

$$E^{(2)} = \langle \Phi_0 | (\hat{F}_N \hat{T}_1^{(2)})_c | \Phi_0 \rangle + \langle \Phi_0 | (\hat{V}_N \hat{T}_2^{(1)})_c | \Phi_0 \rangle + \frac{1}{2} \langle \Phi_0 | (\hat{F}_N (\hat{T}_2^{(1)})^2)_c | \Phi_0 \rangle \quad [204]$$

which may be evaluated as usual using Wick's theorem or the diagrammatic techniques described earlier in the chapter. We denote the cluster operators of a

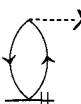
particular order diagrammatically by adding hash marks to the corresponding interaction line. For example, the first-order \hat{T}_2 operator may be written as

$$\hat{T}_2^{(1)} = \begin{array}{c} \diagdown \quad \diagup \\ \diagdown \quad \diagup \\ + \end{array} \quad [205]$$

and the second-order \hat{T}_1 operator as

$$\hat{T}_1^{(2)} = \begin{array}{c} \diagdown \quad \diagup \\ \diagdown \quad \diagup \\ + \end{array} \quad [206]$$

The first term on the right-hand side of Eq. [204] involving $\hat{T}_1^{(2)}$ must be zero in

MBPT because the corresponding diagram, , involves the f_{ia} elements

of the spin-orbital Fock matrix, which are necessarily zero in the basis of canonical Hartree–Fock orbitals. Furthermore, the third term on the right-hand side of the equation cannot contribute to the energy because \hat{F}_N cannot cancel the +4 excitation level produced by the cluster operators. Therefore, Eq. [204] may be written as

$$E^{(2)} = \begin{array}{c} \text{---} \\ \diagdown \quad \diagup \\ \diagdown \quad \diagup \\ + \end{array} = \frac{1}{4} \sum_{ijab} \langle ij || ab \rangle t_{ij}^{ab(1)} \quad [207]$$

The first-order \hat{T}_2 amplitudes, which are required for Eq. [207], may be determined by left-projecting the first-order variant of Eq. [202] involving $\bar{H}^{(1)}$ by a doubly excited determinant, Φ_{ij}^{ab} , as we did earlier in the construction of the coupled cluster amplitude equations,

$$0 = \langle \Phi_{ij}^{ab} | \bar{H}^{(1)} | \Phi_0 \rangle = \langle \Phi_{ij}^{ab} | \hat{V}_N | \Phi_0 \rangle + \langle \Phi_{ij}^{ab} | (\hat{F}_N \hat{T}_2^{(1)})_c | \Phi_0 \rangle \quad [208]$$

Evaluating this expression diagrammatically, we obtain

$$\begin{aligned} 0 &= \begin{array}{c} \diagdown \quad \diagup \\ \diagdown \quad \diagup \\ + \end{array} + \begin{array}{c} \diagdown \quad \diagup \\ \diagdown \quad \diagup \\ + \end{array} \text{---} X + \begin{array}{c} \diagdown \quad \diagup \\ \diagdown \quad \diagup \\ + \end{array} \text{---} X \\ &= \langle ab || ij \rangle + \sum_c (f_{bc} t_{ij}^{ac(1)} - f_{ac} t_{ij}^{bc(1)}) - \sum_k (f_{kj} t_{ik}^{ab(1)} - f_{ki} t_{jk}^{ab(1)}) \end{aligned} \quad [209]$$

Again assuming canonical Hartree–Fock orbitals, the terms containing Fock matrix elements are reduced to include the diagonal elements only:

$$(f_{ii} + f_{jj} - f_{aa} - f_{bb})t_{ij}^{ab(1)} = \langle ab || ij \rangle \quad [210]$$

Thus, the diagrammatic equation could be rewritten more simply as

$$D_2 \begin{array}{c} \diagdown \\ \diagup \end{array} \begin{array}{c} \diagup \\ \diagdown \end{array} = \begin{array}{c} \diagdown \\ \diagup \end{array} \begin{array}{c} \diagup \\ \diagdown \end{array} \quad [211]$$

where $D_2 \equiv D_{ij}^{ab} \equiv f_{ii} + f_{jj} - f_{aa} - f_{bb}$ denotes the separation of the orbital energies (the diagonal Fock matrix elements) from the terms involving the Fock operator. This equation may be rearranged further by another slight modification of our current diagrammatic notation:

$$t_{ij}^{ab(1)} = \begin{array}{c} \diagdown \\ \diagup \end{array} \begin{array}{c} \diagup \\ \diagdown \end{array} = \begin{array}{c} \diagdown \\ \diagup \end{array} \begin{array}{c} \diagup \\ \diagdown \end{array} = \frac{\langle ab || ij \rangle}{D_{ij}^{ab}} \quad [212]$$

The extra horizontal bar across the lines emanating from the \hat{V}_N fragment denotes division by the D_{ij}^{ab} “energy denominator” from the foregoing algebraic expression. This new diagrammatic feature may be used to indicate other such denominators, including those from the $\hat{T}_1^{(n)}$ and $\hat{T}_3^{(n)}$ equations, as we will see later in the chapter. Inserting Eq. [212] into Eq. [207], we may write the final MBPT(2) energy expression as

$$E^{(2)} = \begin{array}{c} \diagdown \\ \diagup \end{array} \begin{array}{c} \diagup \\ \diagdown \end{array} = \frac{1}{4} \sum_{ijab} \frac{\langle ij || ab \rangle \langle ab || ij \rangle}{D_{ij}^{ab}} \quad [213]$$

This expression is identical to that derived directly from perturbation theory in Refs. 77 and 82.

As the preceding analysis clearly shows, the MBPT(2) energy may be determined by approximating the CCSD energy using only those components which contribute to $\bar{H}^{(2)}$. The CCSD energy is therefore “complete” through at least the second order of MBPT. One can carry this discussion further to construct the MBPT(3) energy as well. However, beginning with fourth order, the CCSD fails to include all the necessary terms. This result makes sense, of course, because of the excitation level included in each perturbed wavefunction. The MBPT(2) and MBPT(3) energies require only doubly excited determinants, which are included explicitly in the CCSD approximation; but the MBPT(4) energy includes contributions from singly, doubly, triply, and quadruply excited determinants. It may be shown^{6,87,135,136} that the MBPT(4) quadruple-exci-

tation contributions may be factored exactly into products of double excitations, but no such factorization is possible for the corresponding triples. As a result, the CCSD energy lacks only triple excitation contributions to be complete through fourth order.

Recognition of this relationship between coupled cluster theory and MBPT has inspired research efforts to construct perturbation-based corrections to the CCSD energy to account for higher excitation contributions. Undoubtedly, the most successful and popular of these is the (T) correction first described for closed-shell molecular systems by Raghavachari et al.²⁴ In the next section, we will describe the structure of this correction using diagrammatic techniques.

The (T) Correction

Numerous studies over the last 15 years have confirmed the importance of triple and higher excitations for the accurate prediction of many molecular properties.^{15–17,24,25,27,51,137,138} Unfortunately, the full CCSDT approach,^{22,23,26} in which triple excitations are included explicitly via the $\hat{T} \equiv \hat{T}_1 + \hat{T}_2 + \hat{T}_3$ cluster operator, is far too computationally expensive for general application to most systems of chemical interest.

As pointed out in the preceding section, the CCSD energy contains contributions identical to those of the MBPT(2) and MBPT(3) energy, but lacks triple-excitation contributions necessary for MBPT(4). Thus, a natural approach to the “triples problem” is to correct the CCSD energy for the missing MBPT(4) terms,¹⁸ using the CCSDT similarity-transformed Hamiltonian,

$$\bar{H}_{\text{CCSDT}} = e^{-\hat{T}_1 - \hat{T}_2 - \hat{T}_3} \hat{H}_N e^{\hat{T}_1 + \hat{T}_2 + \hat{T}_3} \quad [214]$$

for the perturbational decomposition. The fourth-order energy depends on this effective Hamiltonian as

$$E^{(4)} = \langle \Phi_0 | \bar{H}^{(4)} | \Phi_0 \rangle = \langle \Phi_0 | (\hat{V}_N \hat{T}_2^{(3)})_c | \Phi_0 \rangle = \begin{array}{c} \text{Diagram of two circles connected by a horizontal line with three vertical bars below it} \end{array} = \frac{1}{4} \sum_{ijab} \langle ij || ab \rangle t_{ij}^{ab(3)} \quad [215]$$

(Note that we have omitted numerous $\bar{H}^{(4)}$ components, which cannot contribute to the energy expression.) The third-order \hat{T}_2 component of this equation is determined via

$$\begin{aligned} 0 &= \langle \Phi_{ij}^{ab} | \bar{H}^{(3)} | \Phi_0 \rangle \\ &= \langle \Phi_{ij}^{ab} | (\hat{F}_N \hat{T}_2^{(3)} + \hat{V}_N \hat{T}_1^{(2)} + \hat{V}_N \hat{T}_2^{(2)} + \hat{V}_N \hat{T}_3^{(2)} + \frac{1}{2} \hat{V}_N (\hat{T}_2^{(1)})^2)_c | \Phi_0 \rangle \end{aligned} \quad [216]$$

Note the appearance of the \hat{T}_3 operator through the use of \bar{H}_{CCSDT} . Since we wish to construct a correction to the CCSD energy, which already contains the contributions from the \hat{T}_1 and \hat{T}_2 terms, we need to construct only the $(\hat{V}_N \hat{T}_3^{(2)})_c$ component of Eq. [216], which may be represented diagrammatically as

$$\hat{T}_2^{(3)} = \begin{array}{c} \text{Diagram 1: } \text{Two vertical lines with arrows pointing down, meeting at a V-shape with a horizontal bar below it.} \\ \leftarrow \end{array} + \begin{array}{c} \text{Diagram 2: } \text{Two vertical lines with arrows pointing down, meeting at a V-shape with a horizontal bar below it. A dashed horizontal line connects the top of the V to a circle with a clockwise arrow.} \\ \text{Diagram 3: } \text{Two vertical lines with arrows pointing down, meeting at a V-shape with a horizontal bar below it. A dashed horizontal line connects the top of the V to a circle with a clockwise arrow.} \end{array} [217]$$

where we have indicated the two-electron denominator D_2 using the horizontal bar notation described earlier. The $\hat{T}_3^{(2)}$ amplitudes needed for this equation may be determined from the corresponding second-order amplitude equation:

$$0 = \langle \Phi_{ijk}^{abc} | (\hat{V}_N \hat{T}_2^{(1)} + \hat{F}_N \hat{T}_3^{(2)})_c | \Phi_0 \rangle [218]$$

which we may write using the denominator notation from the preceding section as

$$D_3 \begin{array}{c} \text{Diagram 1: } \text{Three vertical lines with arrows pointing down, meeting at a V-shape with a horizontal bar below it.} \end{array} = \begin{array}{c} \text{Diagram 1: } \text{Three vertical lines with arrows pointing down, meeting at a V-shape with a horizontal bar below it. A dashed horizontal line connects the top of the V to a circle with a clockwise arrow.} \\ + \end{array} \begin{array}{c} \text{Diagram 2: } \text{Three vertical lines with arrows pointing down, meeting at a V-shape with a horizontal bar below it. A dashed horizontal line connects the top of the V to a circle with a clockwise arrow.} \end{array} [219]$$

This equation may be interpreted algebraically as

$$\begin{aligned} D_{ijk}^{abc} t_{ijk}^{abc(2)} &= P(k|ij)P(a|bc) \sum_d \langle bc || dk \rangle t_{ij}^{ad(1)} \\ &\quad - P(i|jk)P(c|ab) \sum_l \langle lc || jk \rangle t_{il}^{ab(1)} \end{aligned} [220]$$

where the $P(p|qr)$ permutation operators perform antisymmetric permutations of index p with indices q and r , in analogy to the two-index $P(pq)$ operator defined earlier in the chapter. The first-order \hat{T}_2 amplitudes here are computed using Eq. [212]. These $\hat{T}_3^{(2)}$ amplitudes may then be inserted into Eq. [217] to compute the $\hat{T}_2^{(3)}$ amplitudes, which may then be used in Eq. [215] to compute

the triple-excitation contribution to the fourth-order energy, $E_{\text{T}}^{(4)}$.^t The corrected CCSD energy,

$$E_{\text{CCSD+T(4)}} = E_{\text{CCSD}} + E_{\text{T}}^{(4)} \quad [221]$$

was referred to as CCSD+T(4) by Urban et al.¹⁸ because $E_{\text{T}}^{(4)}$ is the true fourth-order triples energy when Eq. [220] is used to compute $\hat{T}_3^{(2)}$. If, on the other hand, we choose to use the *converged* CCSD \hat{T}_2 amplitudes rather than first-order \hat{T}_2 in Eq. [220]—that is, amplitudes that solve Eq. [153]—we obtain a different correction, which Urban et al. denoted CCSD+T(CCSD) (although more recently this method has been called CCSD[T]):

$$E_{\text{CCSD+T(CCSD)}} = E_{\text{CCSD}} + E_{\text{T}}^{[4]} \quad [222]$$

where the superscript [4] indicates that the usual fourth-order triples energy formula is evaluated using CCSD \hat{T}_2 amplitudes. It has been shown^{24,140} that the CCSD+T(CCSD)/CCSD[T] approach has a tendency to overestimate triple-excitation effects, which for some systems leads to qualitatively incorrect predictions of molecular properties.²⁴

A few years after the work by Urban et al., Pople and coworkers¹⁷ developed a triples correction for the QCISD (quadratic configuration interaction—a method commonly viewed as an approximation to CCSD) energy. In their work,¹⁷ they noted that to properly balance the contribution of single and double excitations to the triples correction, an additional term beyond $E_{\text{T}}^{[4]}$ must be included. In 1989 a similar analysis was developed by Raghavachari et al., who determined that a fifth-order energy contribution involving single excitations, denoted $E_{\text{ST}}^{[5]}$, should be included in the CCSD correction, as well.²⁴ This component may be derived based on the second-order \hat{T}_3 contribution to the third-order \hat{T}_1 operator, which subsequently contributes to fourth-order \hat{T}_2 . Although the diagrammatic techniques described above are particularly convenient for deriving $E_{\text{ST}}^{[5]}$, we will avoid this task here, and simply present the final equation

$$E_{\text{ST}}^{[5]} = \frac{1}{4} \sum_{ijkabc} \langle jk \| bc \rangle t_i^a t_{ijk}^{abc} \quad [223]$$

^tIt should be noted that the “procedure” outlined here for computing $E_{\text{T}}^{(4)}$ is certainly not the most efficient approach. As discussed more than two decades ago (Refs. 136, 139), the expression for $E_{\text{T}}^{(4)}$ may be cast into the form

$$E_{\text{T}}^{(4)} = \frac{1}{36} \sum_{ijkabc} t_{ijk}^{abc(2)} D_{ijk}^{abc} t_{ijk}^{abc(2)}$$

where D_{ijk}^{abc} is the three-electron counterpart of D_{ij}^{ab} . Instead of storing individual triple-excitation amplitudes, however, each contribution to the summation above is computed separately using equations involving only two-electron integrals and energy denominators.

where the triple-excitation amplitudes are determined using a modified form of Eq. [220] that includes converged \hat{T}_2 amplitudes

$$D_{ijk}^{abc} t_{ijk}^{abc} = P(i/jk)P(a/bc) \left[\sum_d \langle bc \parallel di \rangle t_{jk}^{ad} - \sum_l \langle la \parallel jk \rangle t_{il}^{bc} \right] \quad [224]$$

Hence, the total CCSD(T) energy may be succinctly written as

$$E_{\text{CCSD(T)}} = E_{\text{CCSD}} + E_{\text{T}}^{[4]} + E_{\text{ST}}^{[5]} \quad [225]$$

We again note that large-scale computer implementations of the (T) method do not actually use Eq. [224] to compute and subsequently store the \hat{T}_3 amplitudes. Instead, a much more efficient algorithm is employed in which the contributions to $E_{\text{T}}^{[4]}$ and $E_{\text{ST}}^{[5]}$ are computed for each unique combination of i , j , and k indices,^{141,142} thus avoiding the $\mathcal{O}(N^6)$ storage requirement associated with solving Eq. [224] explicitly. We also note that Deegan and Knowles constructed an augmented triples correction, denoted CCSD+T, which includes additional fifth-order terms missing in CCSD.³⁰

What is the motivation for the inclusion of this particular fifth-order term over other such terms in the (T) correction? There have been influential numerical studies that serve to rationalize the success of the (T) correction from a purely empirical standpoint,^{24,25,143,144} but here we are more interested in a physical motivation. Pople and coworkers¹⁷ referred to $E_{\text{ST}}^{[5]}$ as necessary to “balance” single and double excitation contributions. A more complete fifth-order analysis than that presented here^{20,24,143,144} would show that CCSD alone already includes fifth-order double-triple interaction terms. Hence, we may consider this apparent mismatch to be the explanation for the inadequacy of CCSD [and especially CCSD+T(CCSD)] in certain difficult cases, such as the asymmetric stretching frequency of O₃.²⁴ However, the physical interpretation behind a balancing of single and double excitation contributions is unclear. For Møller–Plesset perturbation theory, single excitations do not contribute until the second-order wavefunction, and double excitations provide the earliest correction of the zeroth-order state. This suggests, then, that double excitations should be more important in the perturbational analysis than single excitations and that no such balancing of the two is important. On the other hand, we recognize that the delayed appearance of single excitations in the perturbed wavefunctions is an artifact of Brillouin’s theorem.⁸² That is, it is strictly because of the form of the arbitrarily chosen molecular orbitals that single excitations do not appear in first order. If we make our perturbational analysis more general, such that single excitations appear alongside double excitations in the wavefunction expansion, then the $E_{\text{ST}}^{[5]}$ energy term shifts to fourth order rather than fifth order. From this perspective, then, single and double excitations should perhaps be treated alike, and the perturbational order has less to do with the selection of corrections terms than the excitation types themselves. This

shifting of perturbational orders is seen, for example, in certain types of open-shell perturbation theory.¹³⁴ Extension of the (T) correction to open-shell systems based on a spin-restricted reference wavefunction presents numerous difficulties,³¹ and recent work in this area has produced a number of interesting techniques.^{27,29,33,51}

Recently, it has been shown³² that equation-of-motion coupled cluster theory (EOM-CC)^{5,60–63,65} provides a unique perspective on the CCSD(T) method. Instead of taking the Hartree-Fock determinant as the zeroth-order wavefunction and subsequently decomposing the CCSD and CCSDT equations in terms of the many-body perturbation expansion, as we have done above, the CCSD wavefunction is taken as zeroth-order and the energy viewed as the lowest eigenvalue of an effective Hamiltonian with associated left and right eigenvectors. By substituting converged CCSD cluster amplitudes in place of the left eigenvector in the lowest order energy correction, the usual (T) energy expression is obtained. In such an analysis, both single and double contributions arrive in the same order (third) of this “perturbation theory,” and no arguments based on balancing the two are necessary. This unique perspective on the (T) correction has also led to the construction of a new “asymmetric” triples correction, denoted a-CCSD(T),^{34,145} which utilizes the left eigenvector for the ground state CCSD eigenvalue problem.

COMPUTER IMPLEMENTATION OF COUPLED CLUSTER THEORY

In this section we discuss many of the issues involved in writing an efficient computer program for solving the coupled cluster amplitude and energy equations derived earlier in the chapter. Since the original implementations of the CCD^{6,7} and CCSD⁸ methods, streamlining the complicated coupled cluster equations has been the subject of intense research. Here we focus on five main ideas used in practical CCSD programs: (1) factorization of the amplitude equations [Eqs. (152) and (153)] into terms that are at most linear in the cluster amplitudes, \hat{T}_1 and \hat{T}_2 ; (2) matrix-based storage and manipulation of the amplitudes and integrals; (3) spatial symmetry simplifications; (4) inclusion of spin factorization in calculations for both closed- and open-shell molecules; and (5) atomic-orbital-based algorithms for the reduction of disk storage requirements.

It is perhaps not immediately clear how one may go about solving the \hat{T}_1 and \hat{T}_2 amplitude equations given in Eqs. [152] and [153] for the individual amplitudes, t_i^a and t_{ij}^{ab} . A simple rearrangement of the equations, however, provides a more palatable form of these expressions that leads to a simple iterative approach for determining the coupled cluster wavefunction amplitudes. For example, the first few terms of Eq. [152] may be written as

$$0 = f_{ai} + f_{aa}t_i^a - f_{ii}t_i^a + \sum_c (1 - \delta_{ca})f_{ac}t_i^c - \sum_k (1 - \delta_{ik})f_{ik}t_k^a + \dots \quad [226]$$

where the diagonal components of the second and third terms on the right-hand side of Eq. [152] have been separated from the summation. Defining

$$D_i^a \equiv f_{ii} - f_{aa} \quad [227]$$

we may rewrite the amplitude equation as

$$D_i^a t_i^a = f_{ai} + \sum_c (1 - \delta_{ca})f_{ac}t_i^c - \sum_k (1 - \delta_{ik})f_{ik}t_k^a + \dots \quad [228]$$

Similarly, if we define

$$D_{ij}^{ab} \equiv f_{ii} + f_{jj} - f_{aa} - f_{bb} \quad [229]$$

the \hat{T}_2 amplitude equation may be rewritten as

$$D_{ij}^{ab} t_{ij}^{ab} = \langle ab || ij \rangle + P(ab) \sum_c (1 - \delta_{bc})f_{bc}t_{ij}^{ac} - P(ij) \sum_k (1 - \delta_{kj})f_{kj}t_{ik}^{ab} + \dots \quad [230]$$

To determine the values of the amplitudes, one must solve this set of coupled nonlinear equations iteratively. A simple starting approximation for t_i^a and t_{ij}^{ab} on the left-hand sides of the equations may be obtained by setting all the amplitudes on the right-hand side to zero. Hence, for the \hat{T}_1 amplitudes we have

$$t_i^a = f_{ai}/D_i^a \quad [231]$$

and for the \hat{T}_2 amplitudes,

$$t_{ij}^{ab} = \langle ab || ij \rangle / D_{ij}^{ab} \quad [232]$$

This initial guess may then be inserted on the right-hand sides of the equations and subsequently used to obtain new amplitudes. The process is continued until self-consistency is reached. For the special case in which canonical Hartree-Fock molecular orbitals are used, the Fock matrix is diagonal and the \hat{T}_2 amplitude approximation above is exactly the same as the first-order perturbed wavefunction parameters derived from Møller-Plesset theory (cf. Eq. [212]). In that case, the D_i^a and D_{ij}^{ab} arrays contain the usual molecular orbital energies, and the initial guess for the \hat{T}_1 amplitudes vanishes.

Factorization of the Coupled Cluster Equations

The form of Eqs. [152] and [153] is perhaps misleading in that many of the terms appear to be computationally more expensive than is necessary. For example, Eq. [153] contains the following term which is quadratic in the \hat{T}_2 amplitudes:

$$D_{ij}^{ab} t_{ij}^{ab} \leftarrow \frac{1}{4} \sum_{klcd} \langle kl || cd \rangle t_{ij}^{cd} t_{kl}^{ab} \quad [233]$$

where the left arrow indicates that we are examining only one of several terms which contribute to the expression on the left-hand side. This term scales as $\mathcal{O}(h^4 p^4)$, where h denotes the number of occupied orbitals and p denotes the number of unoccupied orbitals. However, this expression may be factored into a product of two terms, for example,

$$\frac{1}{4} \sum_{klcd} \langle kl || cd \rangle t_{ij}^{cd} t_{kl}^{ab} = \frac{1}{2} \sum_{kl} t_{kl}^{ab} \frac{1}{2} \sum_{cd} \langle kl || cd \rangle t_{ij}^{cd} \equiv \frac{1}{2} \sum_{kl} t_{kl}^{ab} X_{ij}^{kl} \quad [234]$$

where the X intermediate is defined as

$$X_{ij}^{kl} \equiv \frac{1}{2} \sum_{cd} \langle kl || cd \rangle t_{ij}^{cd} \quad [235]$$

Now the original term may be evaluated in two steps: (1) construction and storage of X ; and (2) contraction of the X array with the t_{kl}^{ab} amplitudes. Each of these steps scales as $\mathcal{O}(h^4 p^2)$ —a significant reduction from the original $\mathcal{O}(h^4 p^4)$.

Every term in the coupled cluster amplitude equations that is nonlinear in \hat{T} may be factored into linear components. As a result, each step of the iterative solution of the CCSD equations scales at worst as ca. $\mathcal{O}(N^6)$ (where N is the number of molecular orbitals). The full CCSDT method in which all \hat{T}_3 -containing terms are included requires an iterative $\mathcal{O}(N^8)$ algorithm, whereas the CCSD(T) method, which is designed to approximate CCSDT, requires a non-iterative $\mathcal{O}(N^7)$ algorithm. The inclusion of all \hat{T}_4 clusters in the CCSDTQ method scales as $\mathcal{O}(N^{10})$.

The most efficient scheme for factorization of the amplitude equations as described above is not obvious, however, and over the past 20 years numerous researchers have developed sets of intermediates to streamline their own coupled cluster programs.^{6–8,11–13,21,22,146,147} Many of these factorizations have been based on careful inspection of the amplitude equations.^{6–8,11–13} Scuseria, Janssen, and Schaefer, for example, developed a set of intermediates based on their reformulation of the CCSD amplitude and energy equations¹³ in a unitary group formalism designed to offer special efficiency when the refer-

ence wavefunction, Φ_0 , is a spin-restricted closed-shell Hartree–Fock determinant. Closely related intermediates were utilized in certain open-shell theories developed by Scuseria²⁷ for the PSI program package¹⁴⁸ and by Knowles, Hampel, and Werner³⁷ for the MOLPRO package.¹⁴⁹

Diagrammatic techniques also provide a route to the construction of efficient coupled cluster intermediates.^{21,146,147} Kucharski and Bartlett,¹⁴⁷ for example, described a particularly clever approach by which one uses matrix elements of the similarity transformed Hamiltonian as the desired intermediates. Consider the matrix element of \bar{H} between the reference (on the left) and a singly excited determinant (on the right). Diagrammatically, this matrix element is resolved into two terms as

$$\begin{aligned} \langle \Phi_0 | \bar{H} | \Phi_i^a \rangle &= \text{Diagram A} + \text{Diagram B} \\ &= f_{ia} + \sum_{kc} \langle ik \| ac \rangle t_k^c \quad [236] \\ &\equiv \text{Diagram C} \end{aligned}$$

We have chosen the double bar with the “#” sign in the final diagram to simply denote the sum of the two diagrams corresponding to the matrix element. If we contract this diagram with a \hat{T}_2 operator fragment from below, we obtain two contributions to the \hat{T}_1 amplitude equations, namely,

$$\text{Diagram C} = \text{Diagram D} + \text{Diagram E} \quad [237]$$

The last two diagrams are equivalent to the fifth and twelfth terms from the \hat{T}_1 amplitude equation in Eq. [152]. These intermediates have the particular advantage that, if the final goal of the calculation is actually an analytic energy gradient or an EOM-CCSD-based approach, for example, one need not recompute the required matrix elements of \bar{H} . Intermediates derived in this manner have been utilized in the coupled cluster programs found in the ACES II¹⁵⁰ and PSI¹⁴⁸ ab initio program packages.

Matrix-Based Storage of Integrals and Amplitudes

Additional computational efficiency in the solution of the coupled cluster equations may be employed by formulating each of the terms as matrix–matrix or matrix–vector products,¹⁴ for which modern workstations and supercom-

puters are particularly adept.¹⁵¹ For example, the set of \hat{T}_2 amplitudes, t_{ij}^{cd} , could be stored as a matrix by defining compound row and column indices ij and cd , respectively, in terms of the individual orbital indices i , j , c , and d . Ignoring permutational symmetry, this storage scheme produces a “supermatrix” with b^2 rows and p^2 columns and whose elements may be labeled $T_2(ij, cd)$. Similarly, the set of two-electron integrals used in the construction of the X intermediate above could be stored as a matrix by defining a compound row index kl and a compound column index cd to give a supermatrix with elements $I(kl, cd)$. The contraction between these matrices given explicitly in Eq. [235] could then be written as a multiplication between the amplitude matrix \mathbf{T}_2 and the transpose of the integral matrix \mathbf{I} to produce the new matrix \mathbf{X} :

$$\mathbf{X} = \mathbf{T}_2 \mathbf{I}^+ \quad [238]$$

where the individual elements of \mathbf{X} may be denoted as $X(ij, kl)$. This type of notation is often used in the coupled cluster literature because it provides a much more compact presentation of the energy and amplitude equations than that given above, and it relates directly to a streamlined computer implementation.

Spatial Symmetry Simplifications

Spatial symmetry also provides a means for improving the efficiency of coupled cluster programs. As shown by the work of Čársky and coworkers,¹⁵² the solution of the coupled cluster equations may be greatly simplified by exploiting constraints on the cluster amplitudes imposed by the point group symmetry of the molecule of interest. In particular, given that the molecular orbital basis is based on symmetry-adapted functions (as is commonly done in ab initio programs such as PSI,¹⁴⁸ ACES II,¹⁵⁰ and MOLPRO¹⁴⁹), the cluster amplitudes (as well as one- and two-electron integrals) vanish unless the direct product of the irreducible representations (“irreps”) associated with each orbital component contains the totally symmetric irrep. For example, a given \hat{T}_2 amplitude, t_{ij}^{ab} , is zero unless

$$\Gamma_i \otimes \Gamma_j \otimes \Gamma_a \otimes \Gamma_b = A_1 \quad [239]$$

where A_1 is the totally symmetric irrep of the molecular point group. Since the direct product (\otimes) of any irrep with itself always contains A_1 , Eq. [239] implies that, for example,[“]

$$\Gamma_{ij} \equiv \Gamma_i \otimes \Gamma_j = \Gamma_a \otimes \Gamma_b \equiv \Gamma_{ab} \quad [240]$$

[“]Of course, other partitionings of the four indices i , j , a , and b are equally valid. For example, the following equality also holds based on Eq. [239]:

$$\Gamma_i = \Gamma_{jab} \equiv \Gamma_j \otimes \Gamma_a \otimes \Gamma_b.$$

If the molecular orbitals are organized such that all orbitals of a given irrep are grouped together, the matrix-based storage scheme described above takes on a particularly convenient form.¹⁴ Using the C_{2v} point group as an example, the T_2 matrix of Eq. [238] may be schematically written as

		cd			
		A_1	A_2	B_1	B_2
$T_2 = ij$	A_1	X	0	0	0
	A_2	0	X	0	0
	B_1	0	0	X	0
	B_2	0	0	0	X

where X implies a submatrix of nonzero values, and we have labeled the rows and columns of the supermatrix by the appropriate compound indices ij and cd . In addition, we have indicated the C_{2v} irrep labels for the given compound index. The B_2 label for the ij row index, for example, denotes the set of i and j index combinations with $\Gamma_{ij} \equiv \Gamma_i \otimes \Gamma_j = B_2$. If a given amplitude falls within the A_2 diagonal subblock, then the compound indices meet the criterion, $\Gamma_{ij} = \Gamma_{cd} = A_2$.

Clearly, one needs to store only the nonzero diagonal subblocks of the matrix above. Assuming that the same number of molecular orbitals belong within each irrep of the point group, this corresponds to memory/disk savings of the order of the group (4 in the case of the C_{2v} group). Furthermore, if this symmetry scheme were also used to store the X and I matrices of Eq. [238], then the matrix multiplication would be reduced to four independent products involving only the symmetry-restricted diagonal blocks—a computational savings of the square of the order of the point group (16 for C_{2v}). This matrix-based approach to symmetry simplification of the coupled cluster equations has been referred to as the “direct product decomposition” (DPD) technique¹⁴ and has been discussed in the literature for both energies¹⁴ and analytic gradients⁵⁰ for nondegenerate (Abelian) point groups. In their recent work on coupled cluster analytic second derivatives, Stanton and Gauss have extended their DPD approach for derivatives of cluster amplitudes, which are generally not totally symmetric quantities.^{57,58} Furthermore, work on the extension of symmetry methods to include non-Abelian point groups has also been reported.^{153–155}

Spin Factorization of the Coupled Cluster Equations

The coupled cluster and configuration interaction equations presented thus far in this chapter have implicitly used spin-dependent molecular orbitals for their definitions of determinants, integrals, and wavefunction amplitudes.

This spin-orbital formulation has the advantage that it may be used with any set of orbitals, including spin-restricted Hartree–Fock (RHF), spin-unrestricted Hartree–Fock (UHF), spin-restricted open-shell Hartree–Fock (ROHF), quasi-restricted Hartree–Fock (QRHF), and Brueckner orbitals. That is, by inclusion of all components of the spin-orbital Fock matrix, \hat{F}_N , the CCSD equations in Eqs. [134], [152], and [153], for example, are valid for any choice of orbitals.^v By assigning the conventional spin functions, α and β , to each occupied and virtual orbital, we may factor the coupled cluster energy and amplitude equations into their spin-dependent components. Owing to the spin-symmetry associated with the one- and two-electron integrals, most of these components will be zero following spin integration, and may be ignored in the computational implementation of the equations. For example, consider the linear \hat{T}_1 contribution to the CCSD energy given in Eq. [134],

$$E_{\text{CCSD}} \leftarrow \sum_{ia} f_{ia} t_i^a \quad [241]$$

The summation may be factored into a number of spin cases as

$$\begin{aligned} \sum_{ia} f_{ia} t_i^a &= \sum_{i_\alpha a_\alpha} f_{i_\alpha a_\alpha} t_{i_\alpha}^{a_\alpha} + \sum_{i_\beta a_\beta} f_{i_\beta a_\beta} t_{i_\beta}^{a_\beta} + \sum_{i_\alpha a_\beta} f_{i_\alpha a_\beta} t_{i_\alpha}^{a_\beta} + \sum_{i_\beta a_\alpha} f_{i_\beta a_\alpha} t_{i_\beta}^{a_\alpha} \\ &= \sum_{i_\alpha a_\alpha} f_{i_\alpha a_\alpha} t_{i_\alpha}^{a_\alpha} + \sum_{i_\beta a_\beta} f_{i_\beta a_\beta} t_{i_\beta}^{a_\beta} \end{aligned} \quad [242]$$

where the mixed spin terms vanish after spin integration of the Fock matrix integrals over the orthogonal spin functions α and β . Similarly, the \hat{T}_2 contribution to E_{CCSD} may be factored into three nonvanishing spin cases, namely,

$$\begin{aligned} \frac{1}{4} \sum_{ijab} \langle ij \| ab \rangle t_{ij}^{ab} &= \frac{1}{4} \sum_{i_\alpha j_\alpha a_\alpha b_\alpha} \langle i_\alpha j_\alpha \| a_\alpha b_\alpha \rangle t_{i_\alpha j_\alpha}^{a_\alpha b_\alpha} + \frac{1}{4} \sum_{i_\beta j_\beta a_\beta b_\beta} \langle i_\beta j_\beta \| a_\beta b_\beta \rangle t_{i_\beta j_\beta}^{a_\beta b_\beta} \\ &\quad + \sum_{i_\alpha j_\beta a_\alpha b_\beta} \langle i_\alpha j_\beta \| a_\alpha b_\beta \rangle t_{i_\alpha j_\beta}^{a_\alpha b_\beta} \end{aligned} \quad [243]$$

where we have used the permutational antisymmetry of the cluster amplitudes and the two-electron integrals to simplify the nonzero mixed spin cases into a single term. Similar factorization of the \hat{T}_1 and \hat{T}_2 amplitude equations is possible. To avoid wasted storage and computation of the many vanishing

^vAlthough a spin-orbital formulation is conceptually simple, desirable properties such as spin-adaptation may be lost when the electronic state of interest is open shell, for example. A rigorously spin-adapted theory must include spin-free definitions of the cluster operators, \hat{T} , and an appropriate (perhaps multideterminant) reference wavefunction (Refs. 39, 41, 42, 156–158). Such general coupled cluster derivations are beyond the scope of this chapter, though some of the issues associated with difficult open-shell problems are discussed in the next section.

amplitudes, the most computationally efficient implementation of the CCSD equations must take these factorizations into account.

Atomic-Orbital-Basis Algorithms

The iterative procedure for solving the amplitude equations described above requires storage of a number of quantities, including \hat{T}_1 and \hat{T}_2 amplitudes, as well as one- and two-electron integrals in the molecular orbital (MO) basis. Of these, the set of two-electron integrals involving four virtual orbitals (e.g., $\langle ab||cd\rangle$) requires the most disk space and quickly becomes the computational bottleneck as the size of the basis set is increased. One way of circumventing this problem is to avoid the transformation and storage of this integral class completely and to instead evaluate their contribution to the \hat{T}_2 amplitude equation (cf. Eq. [153]),

$$t_{ij}^{ab} \leftarrow \sum_{cd} t_{ij}^{cd} \langle ab||cd \rangle \quad [244]$$

using the two-electron integrals in the atomic-orbital (AO) [or, symmetry-orbital (SO)] basis. The advantage is that, unlike the MO basis functions, the AO functions are often strongly localized at the atomic centers and, as a result, only a fraction of the total number of associated two-electron integrals are nonzero for large basis sets. The outline of this AO-basis algorithm may become clearer if we rewrite Eq. [244] in terms of the untransformed integrals:

$$t_{ij}^{ab} \leftarrow \sum_{cd} t_{ij}^{cd} \sum_{\mu\nu\lambda\sigma} C_\mu^a C_\nu^b C_\lambda^c C_\sigma^d \langle \mu\nu||\lambda\sigma \rangle \quad [245]$$

where the indices μ , ν , λ , and σ are used to denote AO-basis functions, and, for convenience, we assume that the MO-basis transformation coefficients such as C_μ^a are real. Reordering the summations in this equation we obtain

$$t_{ij}^{ab} \leftarrow \sum_{\mu\nu} C_\mu^a C_\nu^b \sum_{\lambda\sigma} \langle \mu\nu||\lambda\sigma \rangle \sum_{cd} C_\lambda^c C_\sigma^d t_{ij}^{cd} \quad [246]$$

The last summation may be interpreted as the “back-transformation” of the two virtual indices on the \hat{T}_2 amplitude into the AO basis, that is,

$$t_{ij}^{\lambda\sigma} = \sum_{cd} C_\lambda^c C_\sigma^d t_{ij}^{cd} \quad [247]$$

If this set of “half-AO” amplitudes is computed and stored (using two standard $\mathcal{O}(N^5)$ steps¹⁵⁹), the amplitudes may be subsequently contracted with the AO-basis integrals to give

$$t_{ij}^{\mu\nu} = \sum_{\lambda\sigma} \langle \mu\nu || \lambda\sigma \rangle t_{ij}^{\lambda\sigma} \quad [248]$$

which requires an $\mathcal{O}(N^6)$ algorithm. The final summation is then evaluated to transform the final half-AO amplitudes back to the MO basis to obtain the complete contribution to \hat{T}_2 ,

$$t_{ij}^{ab} \leftarrow \sum_{\mu\nu} C_{\mu}^a C_{\nu}^b t_{ij}^{\mu\nu} \quad [249]$$

A similar procedure may be constructed for terms involving three virtual index integrals, $\langle ab || ci \rangle$.¹⁶⁰

AO-basis algorithms have been exploited for many years in the construction of correlated wavefunctions,¹⁶¹ particularly in MBPT(2).^{154,162} In coupled cluster theory, a number of approaches have recently been discussed in the literature. For example, Hampel, Peterson, and Werner¹⁶⁰ have reported an efficient implementation of the Brueckner-orbital-based CCD method that avoids the transformation and storage of the $\langle ab || cd \rangle$ integrals and computes the appropriate contributions as described above. Koch, Helgaker, Christiansen, and coworkers^{163,164} have carried the approach even further by avoiding storage of even the AO-basis two-electron integrals and computing limited distributions of these “on the fly” as they are needed. Their largest single-point CCSD energy calculations using this algorithm have involved more than 500 basis functions.¹⁶⁴ Rendell and Lee¹⁶⁵ have taken a somewhat different tack in CCSD(T) energy calculations by approximating the $\langle ab || ci \rangle$ and $\langle ab || cd \rangle$ integrals via a “resolution of the identity” technique. In their approach, a set of auxiliary functions is used to rewrite these four-center electron repulsion integrals as products of three-center integrals, which require significantly less storage space. Finally, we note that AO-basis techniques have proven to be vital to the recent work of Stanton and Gauss on analytic second derivatives for a number of correlated techniques, including SDQ-MBPT(4), CCSD, and CCSD(T).^{57,58}

CURRENT RESEARCH AND FUTURE DIRECTIONS

In this final section, we examine in detail a number of recent research efforts in coupled cluster theory. This review is far from exhaustive, and because of space considerations, we choose to focus primarily on two specific areas in which the present authors have made contributions. We will then discuss some of the most important theoretical and computational advances expected in the near future. We also recommend Refs. 78 and 79 for a discussion of other recent work.

Coupled Cluster Theory for Open-Shell Molecules

For the closed-shell electronic states of many small molecules, the task of determining molecular properties is generally well understood, and coupled cluster methods—particularly the CCSD(T) approach—in conjunction with large basis sets, have been found to give exceptionally accurate results relative to experiment for properties such as molecular geometries, harmonic vibrational frequencies, infrared intensities, and electric dipole moments.^{78,79,137,138,166} The potential energy surfaces of open-shell species,^w on the other hand, often present serious computational problems. In the most widely used open-shell CCSD(T) approaches,^{27,35,51} a calculation for a radical cation, for example, requires approximately *three times* the computational effort of its closed-shell counterpart, even if a spin-restricted open-shell Hartree–Fock (ROHF) determinant is chosen as the reference wavefunction. This difficulty is due to an unbalanced exchange interaction between open- and closed-shell electrons such that the Fock matrix, which appears in the spin-orbital coupled cluster expressions presented in Eqs. [152] and [153], contains *different* α and β components. As a result, the cluster operators may be factored into two different spin cases for \hat{T}_2 ($t_{i_\alpha j_\alpha}^{a_\alpha b_\alpha}$, $t_{i_\beta j_\beta}^{a_\beta b_\beta}$, and $t_{i_\alpha j_\beta}^{a_\alpha b_\beta}$).

Several researchers have recently devoted considerable effort to the derivation and efficient implementation of techniques based on spin-restricted reference determinants that reduce the computational discrepancy between closed- and open-shell systems.^{33,38,171–173} This emphasis on spin-restricted techniques has resulted in part from a bias toward reference wavefunctions that maintain the spin symmetry of the exact wavefunction (such as the ROHF determinant), but also because of the possible efficiency advantages of spin-restricted methods over unrestricted techniques. Thus, since the component molecular orbitals are constrained to have identical spatial parts for each spin function, it should be possible to construct the correlated wavefunction in a manner that takes advantage of this symmetry.

It should be noted, however, that the use of a spin-symmetry-adapted determinant such as the ROHF wavefunction as a reference in a coupled cluster calculation does produce a spin-pure energy,^x but does not imply that the correlated wavefunction itself is an eigenfunction of \hat{S}^2 as well.^{27,35} For the spin-orbital definition of \hat{T} described here, spin contamination can still enter into the coupled cluster wavefunction through the nonlinear contributions of cluster operators to the amplitude equations,³⁷ though the importance of this

^wWe emphasize that the present discussion focuses only on *high-spin* open-shell systems to which a single-determinant reference wavefunction is applicable. Coupled cluster techniques for low-spin cases, such as open-shell singlets, have been pursued in the literature for many years, however, and provide a fertile area of research (Refs. 158, 167–170).

^xThe ROHF-CCSD energy is indeed completely spin-projected, as discussed in Refs. 35, 27, and 37, but is still different from that computed using a spin-adapted coupled cluster wavefunction.

contamination has been questioned.¹⁷⁴ A great deal of effort has been devoted recently to the efficient construction of spin-adapted open-shell coupled cluster wavefunctions and/or correct spin expectation value equations.^{36–42,158}

Spin-Restricted Triple-Excitation Corrections

The (T) correction discussed earlier beginning with the presentation of Eq. [214] is derived via a perturbational decomposition of the coupled cluster energy and amplitude equations. This decomposition depends on a particular partitioning of the electronic Hamiltonian, \hat{H}_N , into a zeroth-order component and a fluctuation potential—that is, a particular definition of many-body perturbation theory. When based upon the canonical Hartree–Fock orbitals of an RHF or UHF reference determinant, this partitioning is simple, and $\hat{H}^{(0)}$ is taken to be the (diagonal) Fock matrix. For ROHF reference wavefunctions, however, the choice of partitioning is less obvious, and a variety of spin-restricted open-shell theories have been reported in the literature in recent years.^{127–134,175} For example, in the RMP¹²⁹ or ROHF-MBPT¹³⁰ method, the diagonal occupied and virtual blocks of the Fock operator are chosen as $\hat{H}^{(0)}$, and the off-diagonal occupied-virtual blocks are included in $\hat{H}^{(1)}$ along with \hat{V}_N . The resulting perturbed energy and wavefunction equations have much in common with the conventional ROHF-CCSD energy and amplitude equations, leading to a convenient form for the ROHF-CCSD(T) method.²⁹ One drawback of this approach, however, is that the off-diagonal f_{ij} and f_{ab} components of the Fock matrix (contained in the first and second diagrams in Figure 2) are nonzero. Thus, Eq. [224] presented earlier takes on a more general form,^{29,31}

$$\begin{aligned} D_{ijk}^{abc} t_{ijk}^{abc} = & P(i/jk)P(a/bc) \left[\sum_d \langle bc || di \rangle t_{jk}^{ad} - \sum_i \langle la || jk \rangle t_{il}^{bc} + t_i^a \langle bc || jk \rangle + f_{ia} t_{jk}^{bc} \right] \\ & - P(i/jk) \sum_l (1 - \delta_{il}) f_{il} t_{jkl}^{abc} + P(a/bc) \sum_d (1 - \delta_{ad}) f_{ad} t_{ijk}^{bcd} \end{aligned} \quad [250]$$

The presence of f_{il} and f_{ad} components requires an iterative solution of this equation—an approach that necessitates storage of the \hat{T}_3 amplitudes in each iteration! This scheme is unreasonable because the number of such amplitudes would rapidly become the computational bottleneck as the size of the molecular system increased. This problem may be circumvented, however, by utilizing the so-called semicanonical molecular orbital basis in which the occupied-occupied and virtual-virtual blocks of the Fock matrix are diagonal.^{29,129,130} In this basis, the two final terms in the \hat{T}_3 equation above vanish, and the conventional noniterative computational procedure described earlier in the chapter may be employed.

The use of semicanonical orbitals does have a drawback, however, in that one is necessarily forced to use a computational procedure comparable to that

of the UHF-CCSD(T) approach. Since the ROHF-based spin-orbital Fock matrix contains different α and β components, rotation to the semicanonical basis breaks the spin restriction on the molecular orbitals.⁷ Thus, the integrals used in Eq. [250] are broken into UHF-like $\alpha - \alpha$, $\beta - \beta$, and $\alpha - \beta$ spin cases with a requisite threefold increase in storage requirements.

This problem can be avoided, however, if an appropriate open-shell perturbation theory is defined such that the zeroth-order Hamiltonian is diagonal in the truly spin-restricted molecular orbital basis. The “Z-averaged” perturbation theory (ZAPT) defined by Lee and Jayatilaka¹³² fulfills this requirement. ZAPT takes advantage of the symmetric spin orbital basis. For each doubly occupied spatial orbital and each unoccupied spatial orbital, the usual α and β spin functions are used, but for the singly occupied orbitals, new spin functions,

$$\sigma^+ = \frac{1}{\sqrt{2}}(\alpha + \beta) \quad [251]$$

and

$$\sigma^- = \frac{1}{\sqrt{2}}(\alpha - \beta) \quad [252]$$

are assigned. By convention, σ^+ functions are associated with occupied spin orbitals, and σ^- functions with unoccupied spin orbitals. In this basis, the spin orbital Fock operator takes on the schematic form,

$$\hat{F}^{\text{ZAPT}} = \begin{matrix} d_\alpha & \left| \begin{array}{cccccc} \hat{F}_{L\alpha}^{M\alpha} & \hat{F}_{L\beta}^{M\alpha} & \hat{F}_{T\sigma^+}^{L\alpha} & 0 & 0 & \hat{F}_{L\alpha}^{D\beta} \\ \hat{F}_{L\beta}^{M\alpha} & \hat{F}_{L\alpha}^{M\alpha} & \hat{F}_{T\sigma^+}^{L\alpha} & 0 & \hat{F}_{L\alpha}^{D\beta} & 0 \\ \hat{F}_{T\sigma^+}^{L\alpha} & \hat{F}_{T\sigma^+}^{L\alpha} & \hat{F}_{T\sigma^+}^{U\sigma^+} & 0 & 0 & 0 \end{array} \right| \\ d_\beta & \\ s_{\sigma^+} & \\ \hat{F}^{\text{ZAPT}} = s_{\sigma^-} & \left| \begin{array}{cccccc} 0 & 0 & 0 & \hat{F}_{T\sigma^-}^{U\sigma^-} & \hat{F}_{T\sigma^-}^{D\alpha} & -\hat{F}_{T\sigma^-}^{D\alpha} \\ 0 & \hat{F}_{L\alpha}^{D\beta} & 0 & \hat{F}_{T\sigma^-}^{D\alpha} & \hat{F}_{D\alpha}^{E\alpha} & \hat{F}_{D\alpha}^{E\beta} \\ \hat{F}_{L\alpha}^{D\beta} & 0 & 0 & -\hat{F}_{T\sigma^-}^{D\alpha} & \hat{F}_{D\alpha}^{E\beta} & \hat{F}_{D\alpha}^{E\alpha} \end{array} \right| \\ v_\alpha & \\ v_\beta & \end{matrix} \quad [253]$$

where capital letters L and M denote doubly occupied spatial orbitals, T and U denote singly occupied spatial orbitals, and D and E denote unoccupied spatial orbitals. Using a standard definition of ROHF orbitals, the diagonal blocks of

⁷This diagonalization affects neither the ROHF determinant itself nor the ROHF or CCSD energies, owing to the well-known invariance of those methods with respect to certain classes of orbital rotations (Ref. 134).

this Fock matrix are themselves diagonal when the theory is applied to conventional high-spin, open-shell systems.^{132,134}

With the diagonal blocks of the Fock operator above taken as the ZAPT zeroth-order Hamiltonian, the various excitation operators of coupled cluster theory may be decomposed into perturbational orders, as described earlier in the chapter. The same \hat{T}_3 contributions used to define the conventional (T) correction can then be constructed to produce a ZAPT-based triples correction—denoted (zT).³³ This analysis is complicated by the fact that the theory requires one to distinguish the singly occupied orbitals from the doubly occupied and unoccupied orbitals. Hence, the particle–hole formalism used throughout this chapter must be generalized such that there are two types of hole (doubly occupied and singly occupied) and two types of particle (unoccupied and singly occupied). The tedious algebraic approach to the derivation of the (zT) correction was carried out in Ref. 33 by the construction of a symbolic manipulation program (designed for the Mathematica interface¹⁷⁶) for the application of Wick's theorem to second-quantized operator strings. This program is described in detail in Ref. 118. The related diagrammatic analysis involves essentially the same rules outlined earlier in the chapter with the complication that cluster operators and Hamiltonian fragments must be factored such that the diagrams differentiate between the two types of hole and particle lines. The rather complicated equations for the (zT) correction are presented in an Appendix in Ref. 33.

The performance of the (zT) correction is essentially identical to that of the conventional ROHF-CCSD(T) method. Application of both to a series of diatomic molecules in ground and excited states indicates insignificant differences between the two in the prediction of bond lengths, harmonic vibrational frequencies, anharmonic constants, and so on. Unfortunately, the complicated equations associated with the (zT) correction have thus far precluded its large scale implementation and, as a result, further systematic studies involving larger basis sets have not yet been carried out.

Brueckner Orbitals in Coupled Cluster Theory

In 1958, Nesbet extended Brueckner's theory for infinite nuclear matter¹⁷⁷ to nonuniform systems of atoms and molecules.¹⁷⁸ By consideration of the CISD problem in which the electronic Hamiltonian is diagonalized within the basis of the reference and all singly and doubly excited determinants, Nesbet explained that Brueckner theory allows one to construct a set of orthonormal molecular orbitals for which the correlated wavefunction coefficients for all singly excited determinants vanish. Unfortunately, the construction of the set of orbitals that fulfill this “Brueckner condition” can be determined only a posteriori from the single excitation coefficients computed in a given orbital basis. As a result, the practical implementation of Brueckner-orbital-based methods has

usually required the repeated construction of the correlated wavefunction (along with the associated integral transformation). Despite this drawback, Brueckner orbitals have found new life within coupled cluster theory in recent years.^{173,179–192} In 1981, Chiles and Dykstra¹⁷⁹ introduced the first molecular application of the Brueckner coupled cluster doubles (B-CCD) method, which they referred to as CCD($\hat{T}_1=0$). Some years later, Handy and coworkers^{182–184} also implemented B-CCD energies, along with a perturbational triple-excitation correction [known as B-CCD(T)] and analytic energy gradients. Since these important theoretical developments, perhaps the most significant work in this area has been reported by Hampel, Peterson, and Werner,¹⁶⁰ who explained that the special form of the B-CCD amplitude equations allows one to avoid the repeated transformation of certain classes of two-electron integrals. This advantage, when coupled to specially designed extrapolation schemes that converge the Brueckner orbitals and cluster amplitudes simultaneously, permits significant reduction in the computational expense of the method, such that B-CCD may cost no more than a conventional CCSD calculation.

Perhaps the greatest need for Brueckner-orbital-based methods arises in systems suffering from artificial symmetry-breaking orbital instabilities,^{140,193–196} where the approximate wavefunction fails to maintain the selected spin and/or spatial symmetry characteristics of the exact wavefunction. Such instabilities arise in SCF-like wavefunctions as a result of a competition between valence-bond-like solutions to the Hartree–Fock equations; these solutions typically allow for localization of an unpaired electron onto one of two or more symmetry-equivalent atoms in the molecule. In the ground $^2\Pi_g$ state of O_2^- , for example, a pair of symmetry-broken Hartree–Fock wavefunctions may be constructed with the unpaired electron localized onto one oxygen atom or the other. Though symmetry-broken wavefunctions have sometimes been exploited to produce providentially correct results in a few systems, they are often not beneficial or even acceptable,¹⁹⁷ and the question of whether to relax constraints in the presence of an instability was originally described by Löwdin as the “symmetry dilemma.”¹⁹⁸

The effects of symmetry-breaking orbital instabilities on properties computed using correlated wavefunctions built from a single-determinant reference has recently been investigated¹⁴⁰ for a number of finite-order MBPT and coupled cluster methods. Owing to a corresponding singularity in the molecular orbital Hessian,^{193,196,199–201} nearby orbital instabilities can produce sometimes dramatically distorted results for second-order properties such as harmonic vibrational frequencies and polarizabilities. However, one important conclusion of Ref. 140 is that the choice of reference wavefunction can significantly affect the location of this Hessian singularity on the potential energy surface, and, as a result, a properly selected set of molecular orbitals can often eliminate the symmetry-breaking problem by moving the instability out of the region of interest. In recent years, Brueckner orbitals have been utilized in conjunction with coupled cluster theory for precisely this purpose for a number

of “difficult” molecular systems,^{185,186,202–205} such as the nitrate radical,¹⁸⁶ the O₄⁺ ion,^{192,202} the hydrogen peroxide radical cation,^{203,204} and the C²A₂ excited state of NO₂.²⁰⁵

The implementation of B-CC methods for open-shell systems (where symmetry-breaking instabilities are the most likely to occur¹⁹⁵) is straightforward when either a UHF or an ROHF reference wavefunction is used as the initial guess for the Brueckner determinant. Unfortunately in the ROHF case, it is not possible to maintain spin restriction on the molecular orbitals because the single-excitation amplitudes, which may be used as the rotation parameters for the iterative construction of the Brueckner orbitals, are not symmetric in the spin indices owing to the uneven exchange interaction between the open- and closed-shell electrons discussed earlier. As a result, the repeated construction of the coupled cluster wavefunction requires the transformation and storage of roughly three times the number of two-electron integrals needed for the initial ROHF-CCSD calculation. This difficulty, which is directly comparable to the problem of semicanonical orbitals described in the last section, represents a significant obstacle for open-shell B-CCD implementations.

The symmetric spin-orbital basis, which was also used to construct the spin-restricted (zT) correction, also provides a route to a spin-restricted open-shell B-CC theory (RB-CC).¹⁷³ In this spin basis, the \hat{T}_1 amplitudes may be shown to have the symmetries

$$t_{I_\alpha}^{A_\beta} = t_{I_\beta}^{A_\alpha} \quad [254]$$

$$t_{I_\alpha}^{A_\alpha} = t_{I_\beta}^{A_\beta} \quad [255]$$

$$t_{I_\alpha}^{W_{\sigma^-}} = -t_{I_\beta}^{W_{\sigma^-}} \quad [256]$$

and

$$t_{W_\sigma^+}^{A_\alpha} = t_{W_\sigma^+}^{A_\beta} \quad [257]$$

where I , A , and W indicate doubly occupied, unoccupied, and singly occupied spatial orbitals, respectively. The “spin-flip” \hat{T}_1 amplitudes of the type $t_{I_\alpha}^{A_\beta}$ are generally nonzero in the symmetric spin-orbital basis, but it may be argued¹³² that these amplitudes should instead be classified as double excitations. The remaining three classes of \hat{T}_1 amplitudes may be used to carry out a series of first-order rotations among the orbital subspaces, namely,

$$\tilde{\phi}_I = \phi_I + t_{I_\alpha}^{A_\alpha} \phi_A + t_{I_\alpha}^{W_{\sigma^-}} \phi_W \quad [258]$$

$$\tilde{\phi}_W = \phi_W + t_{W\sigma^+}^{A_\alpha} \phi_A - t_{I_\alpha}^{W\sigma^-} \phi_I \quad [259]$$

At convergence, the orbitals will obey the Brueckner conditions

$$t_{I_\alpha}^{A_\alpha} = t_{W\sigma^+}^{A_\alpha} = t_{I_\alpha}^{W\sigma^-} = 0 \quad [260]$$

These equations provide the basis for the RB-CC method, since they do not imply any loss of spin restriction on the molecular orbitals as the rotation is applied. Furthermore, the RB-CC method may be trivially implemented within existing ROHF-CCSD programs by a simple “symmetrization” of the standard $(\alpha, \beta) \tilde{T}_1$ amplitudes into the new spin basis¹⁷³ prior to the rotation.

The performance of the RB-CCD method (which is analogous to the conventional unrestricted B-CCD method) has been tested on the nitrate radical, NO₃, and the \tilde{C}^2A_2 state of NO₂, both of which have presented difficulties for a variety of theoretical methods due in part to symmetry-breaking instabilities in the Hartree–Fock reference wavefunction. The RB-CCD method was found to provide results in excellent agreement with the B-CCD method, including the correct prediction of C_s symmetry for the equilibrium geometry of the \tilde{C} state of NO₂.^{205,206} Work is presently under way for extension of the RB-CCD method to include triples [i.e., a RB-CCD(T) method where the triples correction is defined similarly to the (zT) correction described above] and analytical energy gradients.

Future Research Prospects

Thanks in part to the computational advances described in the preceding section, coupled cluster theory has developed into arguably the most accurate and computationally affordable method of modern computational quantum chemistry. The results of coupled cluster calculations are commonly found in the chemical physics literature, and, when the accuracy of experimental results is questioned, the CCSD(T) method is often used to settle the debate. In spite of this success, coupled cluster theory is far from applicable to all problems of chemical interest. The majority of the current research efforts may be divided into four overlapping categories:

- **Large molecules and extended systems.** As noted near the beginning of the section on Factorization of Coupled Cluster Equations, the CCSD(T) method scales as $\mathcal{O}(N^7)$, where N is the number of basis functions. This implies that a factor of two increase in the size of the molecular system involves a ca. 128 increase in the CPU cost of the calculation. For example, a high accuracy CCSD(T) energy calculation for the amino acid alanine requires approximately 5 days on modern workstations; an equivalent calculation for the alanine dimer would require nearly *two years* to complete. In addition, the storage requirements of the CCSD(T) method scale roughly as $\mathcal{O}(N)^4$, leading to rapidly insurmountable disk space limitations as the size of the system increases. Our own

recent CCSD(T) calculations on isomers of [10]annulene (molecular formula C₁₀H₁₀) involving more than 300 basis functions and low symmetry may represent the current limit of “conventional” coupled cluster programs.²⁰⁷

One of the most promising approaches to overcoming the scaling problems of the coupled cluster method lies in the local correlation concept developed primarily by Sæbø and Pulay.^{208–212} This scheme relies on the use of a set of localized, nonorthogonal molecular orbitals to drastically reduce the number of nonnegligible parameters in the correlated wave function. Some effort in this direction has been reported by Hampel and Werner,²¹³ and it is likely that new implementations and extensions of the “local-CC” method will appear in the next few years. In addition, the storage bottleneck associated with large molecules has been examined by several researchers, leading to “integral direct”^{163,164} and “resolution of the identity” methods,¹⁶⁵ described earlier in the section on Atomic-Orbital-Basis Algorithms.

- **Excited electronic states.** One deficiency of the conventional coupled cluster methods is that they apply only to ground electronic states (or, more accurately, to the lowest energy states of a given spin and spatial symmetry). The equation-of-motion coupled cluster method^{5,60–63,65} and related methods such as SAC-CI^{106–108} and STEOM-CC^{74,114} have been devised such that higher lying electronic states may be studied. These methods have proven to provide reliable accuracy (on the order of 0.2 eV) in the prediction of electronic excitation spectra for states that are well described by promotion of a single electron from the ground state. Perhaps the most important work in excited state coupled cluster theory in the next several years will be the development of methods for treating “doubly excited” states and the improvement of the accuracy of EOM-CC to better than 0.1 eV through extension of existing methods for the efficient inclusion of triply excited determinants in the diagonalization space of \bar{H} .^{70,71,105,214–217}

- **Potential energy surfaces.** All coupled cluster methods depend implicitly upon a reference wavefunction (usually the single-configuration Hartree–Fock determinant). However, for cases in which this reference fails dramatically, even the CCSD(T) method cannot be expected to provide reliable results. Bond breaking provides an excellent example of this behavior; as a σ bond is separated, for instance, a single determinant fails to properly include both electronic configurations [$(\sigma)^2$ and $(\sigma^*)^2$] needed to describe the dissociation process with even qualitative accuracy. Since a complete potential energy surface is vital to research efforts in reaction dynamics, for instance, much effort has been devoted to the construction of multireference coupled cluster (MRCC) schemes based primarily on multiconfigurational SCF (MCSCF) reference wavefunctions.^{76,78,125,218–223} Of particular interest is the work by Piecuch, Adamowicz, and coworkers,^{218,219,223} in which a MRCCSD wavefunction, for example, is obtained via selected triple and quadruple excitations from a full CCSDTQ wavefunction constructed from a single electronic configuration. This approach is similar to that used earlier in multireference configuration

interaction methods.^{86,224} By retaining a single-determinant reference formalism, one avoids many of the difficulties of a “true” MCSCF-based approach, and automated techniques for the construction of higher excitation levels (i.e., beyond quadruples) are promising. In addition, multideterminantal coupled cluster methods such as the unitary group approach^{39,158,167,168} have been actively pursued in recent years^{41,42,169,170} for describing biradicals and other “low-spin” electronic states for which a single-determinant reference is inadequate.

- **High accuracy methods.** For properties such as dissociation and fragmentation energies, coupled cluster theory used in conjunction with large basis sets is often expected to provide “chemical accuracy,” that is, ± 1 kcal/mol. In recent years, many researchers have asked what would be required to obtain “spectroscopic accuracy,” that is, ± 1 cm⁻¹.^z It has been shown in numerous studies in the past decade^{226–231} that the convergence of the coupled cluster (as well as CI and perturbation theory) energies toward a “basis set limit” is much slower than that possible with Hartree–Fock. That is, for a given level of electron correlation (e.g., CCSD), one must use much more complete basis sets (perhaps including high levels of orbital angular momentum, *s*, *p*, *d*, *f*, etc.) relative to Hartree–Fock before additional improvements to the basis set make no significant contributions to the computed energy. The source of this problem is a well-known failure by correlated techniques such as coupled cluster when used with common Gaussian-type basis functions to describe the behavior of many-electron wavefunctions as electrons approach one another closely.²³² One technique for overcoming this difficulty is to include terms that explicitly involve the interelectronic distance, $1/r_{12}$, in the correlated wavefunction. When applied in coupled cluster theory, such an approach has the advantage that the conventional formalism and implementation remain largely intact, with a number of sophisticated modifications needed to account for the additional mathematical term(s). The recent work on the linear r_{12} -CCSD method by Klopper, Kutzelnigg, Noga, and coworkers²³² and on Gaussian geminals by Persson and Taylor²²⁹ is promising, and further impressive developments are likely to be reported in the next several years.

ACKNOWLEDGMENTS

Our understanding of coupled cluster theory as described in this chapter has been cultivated by conversations and collaborations with numerous colleagues over the past several years. In particular, we would like to acknowledge many fruitful interactions with Professor John F. Stanton of the University of Texas, Dr. Timothy J. Lee of NASA Ames Research Center, Professor Marcel

^zIt should be noted that the goal of true spectroscopic accuracy may be unattainable because of the implicit errors associated with the use of a Born–Oppenheimer, nonrelativistic Hamiltonian to describe molecular systems (Ref. 225).

Nooijen of Princeton University, and Professor Rodney J. Bartlett of the University of Florida. We thank Sullivan Beck of the University of Florida for the use of his diag program used to typeset the many diagrams in the chapter. We also thank Drs. Rollin A. King and Matthew L. Leininger of the University of Georgia and Dr. C. David Sherrill of the University of California at Berkeley for their critical reading of the manuscript. Finally, TDC wishes to express his sincere appreciation to Emily A. Crawford for her work in the development of the contract LaTeX package for typesetting complicated Wick's theorem expressions, and for her patience and support during the preparation of the manuscript.

REFERENCES

1. J. Čížek, *J. Chem. Phys.*, **45**, 4256 (1966). On the Correlation Problem in Atomic and Molecular Systems. Calculation of Wavefunction Components in Ursell-Type Expansion Using Quantum-Field Theoretical Methods.
2. J. Čížek, *Adv. Chem. Phys.*, **14**, 35 (1969). On the Use of the Cluster Expansion and the Technique of Diagrams in Calculations of Correlation Effects in Atoms and Molecules.
3. J. Čížek and J. Paldus, *Int. J. Quantum Chem.*, **5**, 359 (1971). Correlation Problems in Atomic and Molecular Systems. III. Rederivation of the Coupled-Pair Many-Electron Theory Using the Traditional Quantum Chemical Methods.
4. A. C. Hurley, *Electron Correlation in Small Molecules*, Academic Press, London, 1976.
5. H. J. Monkhorst, *Int. J. Quantum Chem. Symp.*, **11**, 421 (1977). Calculation of Properties with the Coupled-Cluster Method.
6. J. A. Pople, R. Krishnan, H. B. Schlegel, and J. S. Binkley, *Int. J. Quantum Chem. Symp.*, **14**, 545 (1978). Electron Correlation Theories and Their Application to the Study of Simple Reaction Potential Surfaces.
7. R. J. Bartlett and G. D. Purvis, *Int. J. Quantum Chem.*, **14**, 561 (1978). Many-Body Perturbation Theory, Coupled-Pair Many-Electron Theory, and the Importance of Quadruple Excitations for the Correlation Problem.
8. G. D. Purvis and R. J. Bartlett, *J. Chem. Phys.*, **76**, 1910 (1982). A Full Coupled-Cluster Singles and Doubles Model: The Inclusion of Disconnected Triples.
9. G. D. Purvis and R. J. Bartlett, *J. Chem. Phys.*, **75**, 1284 (1981). The Reduced Linear Equation Method in Coupled Cluster Theory.
10. G. E. Scuseria, T. J. Lee, and H. F. Schaefer, *Chem. Phys. Lett.*, **130**, 236 (1986). Accelerating the Convergence of the Coupled-Cluster Approach. The Use of the DIIS Method.
11. G. E. Scuseria, A. C. Scheiner, T. J. Lee, J. E. Rice, and H. F. Schaefer, *J. Chem. Phys.*, **86**, 2881 (1987). The Closed-Shell Coupled-Cluster Single and Double Excitation (CCSD) Model for the Description of Electron Correlation. A Comparison with Configuration Interaction (CISD) Results.
12. T. J. Lee and J. E. Rice, *Chem. Phys. Lett.*, **150**, 406 (1988). An Efficient Closed-Shell Singles and Doubles Coupled-Cluster Method.
13. G. E. Scuseria, C. L. Janssen, and H. F. Schaefer, *J. Chem. Phys.*, **89**, 7382 (1988). An Efficient Reformulation of the Closed-Shell Coupled-Cluster Single and Double Excitation (CCSD) Equations.
14. J. F. Stanton, J. Gauss, J. D. Watts, and R. J. Bartlett, *J. Chem. Phys.*, **94**, 4334 (1991). A Direct Product Decomposition Approach for Symmetry Exploitation in Many-Body Methods. I. Energy Calculations.
15. R. J. Bartlett, H. Sekino, and G. D. Purvis, *Chem. Phys. Lett.*, **98**, 66 (1983). Comparison of MBPT and Coupled-Cluster Methods with Full CI. Importance of Triplet Excitations and Infinite Summations.
16. Y. S. Lee, S. A. Kucharski, and R. J. Bartlett, *J. Chem. Phys.*, **81**, 5906 (1984). A Coupled-Cluster Approach with Triple Excitations.

17. J. A. Pople, M. Head-Gordon, and K. Raghavachari, *J. Chem. Phys.*, **87**, 5968 (1987). Quadratic Configuration Interaction. A General Technique for Determining Electron Correlation Energies.
18. M. Urban, J. Noga, S. J. Cole, and R. J. Bartlett, *J. Chem. Phys.*, **83**, 4041 (1985). Towards a Full CCSDT Model for Electron Correlation.
19. M. R. Hoffmann and H. F. Schaefer, *Adv. Quantum Chem.*, **18**, 207 (1986). A Full Coupled-Cluster Singles, Doubles, and Triples Model for the Description of Electron Correlation.
20. S. A. Kucharski and R. J. Bartlett, *Adv. Quantum Chem.*, **18**, 281 (1986). Fifth-Order Many-Body Perturbation Theory and Its Relationship to Various Coupled-Cluster Approaches.
21. J. Noga, R. J. Bartlett, and M. Urban, *Chem. Phys. Lett.*, **134**, 126 (1987). Towards a Full CCSDT Model for Electron Correlation. CCSDT-*n* Models.
22. J. Noga and R. J. Bartlett, *J. Chem. Phys.*, **86**, 7041 (1987); Erratum: **89**, 3401 (1988). The Full CCSDT Model for Molecular Electronic Structure.
23. G. E. Scuseria and H. F. Schaefer, *Chem. Phys. Lett.*, **152**, 382 (1988). A New Implementation of the Full CCSDT Model for Molecular Electronic Structure.
24. K. Raghavachari, G. W. Trucks, J. A. Pople, and M. Head-Gordon, *Chem. Phys. Lett.*, **157**, 479 (1989). A Fifth-Order Perturbation Comparison of Electron Correlation.
25. R. J. Bartlett, J. D. Watts, S. A. Kucharski, and J. Noga, *Chem. Phys. Lett.*, **165**, 513 (1990); Erratum: **167**, 609 (1990). Non-iterative Fifth-Order Triple and Quadruple Excitation Energy Corrections in Correlated Methods.
26. J. D. Watts and R. J. Bartlett, *J. Chem. Phys.*, **93**, 6104 (1990). The Coupled-Cluster Single, Double, and Triple Excitation Model for Open-Shell Single Reference Functions.
27. G. E. Scuseria, *Chem. Phys. Lett.*, **176**, 27 (1991). The Open-Shell Restricted Hartree–Fock Singles and Doubles Coupled-Cluster Method Including Triple Excitations CCSD(T): Application to C₃⁺.
28. S. A. Kucharski and R. J. Bartlett, *J. Chem. Phys.*, **97**, 4282 (1992). The Coupled-Cluster Single, Double, Triple, and Quadruple Excitation Method.
29. J. D. Watts, J. Gauss, and R. J. Bartlett, *J. Chem. Phys.*, **98**, 8718 (1993). Coupled-Cluster Methods with Noniterative Triple Excitations for Restricted Open-Shell Hartree–Fock and Other General Single Determinant Reference Functions. Energies and Analytical Gradients.
30. M. J. O. Deegan and P. J. Knowles, *Chem. Phys. Lett.*, **227**, 321 (1994). Perturbative Corrections to Account for Triple Excitations in Closed- and Open-Shell Coupled-Cluster Theories.
31. T. D. Crawford and H. F. Schaefer, *J. Chem. Phys.*, **104**, 6259 (1996). A Comparison of Two Approaches to Perturbational Triple Excitation Corrections to the Coupled-Cluster Singles and Doubles Method for High-Spin Open-Shell Systems.
32. J. F. Stanton, *Chem. Phys. Lett.*, **281**, 130 (1997). Why CCSD(T) Works: A Different Perspective.
33. T. D. Crawford, T. J. Lee, and H. F. Schaefer, *J. Chem. Phys.*, **107**, 7943 (1997). A New Spin-Restricted Triple Excitation Correction for Coupled Cluster Theory.
34. T. D. Crawford and J. F. Stanton, *Int. J. Quantum Chem. Symp.*, **70**, 601 (1998). Investigation of an Asymmetric Triple-Excitation Correction for Coupled Cluster Energies.
35. M. Rittby and R. J. Bartlett, *J. Phys. Chem.*, **92**, 3033 (1988). An Open-Shell Spin-Restricted Coupled-Cluster Method: Application to Ionization Potentials in N₂.
36. C. L. Janssen and H. F. Schaefer, *Theor. Chim. Acta*, **79**, 1 (1991). The Automated Solution of Second Quantization Equations with Applications to the Coupled-Cluster Approach.
37. P. J. Knowles, C. Hampel, and H.-J. Werner, *J. Chem. Phys.*, **99**, 5219 (1993). Coupled-Cluster Theory for High-Spin, Open-Shell Reference Wave Functions.
38. P. Neogrády, M. Urban, and I. Hubač, *J. Chem. Phys.*, **100**, 3706 (1994). Spin Adapted Restricted Hartree–Fock Reference Coupled-Cluster Theory for Open-Shell Systems.

39. X. Li and J. Paldus, *J. Chem. Phys.*, **101**, 8812 (1994). Automation of the Implementation of Spin-Adapted Open-Shell Coupled-Cluster Theories Relying on the Unitary Group Formalism.
40. X. Li and J. Paldus, *J. Chem. Phys.*, **102**, 2013 (1995). Spin-Adapted Open-Shell State-Selective Coupled-Cluster Approach and Doublet Stability of Its Hartree–Fock Reference.
41. M. Nooijen and R. J. Bartlett, *J. Chem. Phys.*, **104**, 2652 (1996). General Spin Adaptation of Open-Shell Coupled Cluster Theory.
42. P. G. Szalay and J. Gauss, *J. Chem. Phys.*, **107**, 9028 (1997). Spin-Restricted Open-Shell Coupled-Cluster Theory.
43. P. Jørgensen and J. Simons, *J. Chem. Phys.*, **79**, 334 (1983). Ab Initio Analytical Molecular Gradients and Hessians.
44. L. Adamowicz, W. D. Laidig, and R. J. Bartlett, *Int. J. Quantum Chem. Symp.*, **18**, 245 (1984). Analytical Gradients for the Coupled-Cluster Method.
45. G. Fitzgerald, R. Harrison, W. D. Laidig, and R. J. Bartlett, *Chem. Phys. Lett.*, **117**, 433 (1985). Analytical Gradient Evaluation in Coupled-Cluster Theory.
46. R. J. Bartlett, in *Geometrical Derivatives of Energy Surfaces and Molecular Properties*, P. Jørgensen and J. Simons, Eds., D. Reidel, Dordrecht, 1986, pp. 35–61. Analytical Evaluation of Gradients in Coupled-Cluster and Many-Body Perturbation Theory.
47. G. Fitzgerald, R. J. Harrison, and R. J. Bartlett, *J. Chem. Phys.*, **85**, 5143 (1986). Analytic Energy Gradients for General Coupled-Cluster Methods and Fourth-Order Many-Body Perturbation Theory.
48. A. C. Scheiner, G. E. Scuseria, J. E. Rice, T. J. Lee, and H. F. Schaefer, *J. Chem. Phys.*, **87**, 5361 (1987). Analytic Evaluation of Energy Gradients for the Single and Double Excitation Coupled Cluster (CCSD) Wave Function: Theory and Application.
49. E. A. Salter, G. W. Trucks, and R. J. Bartlett, *J. Chem. Phys.*, **90**, 1752 (1989). Analytic Energy Derivatives in Many-Body Methods. I. First Derivatives.
50. J. Gauss, J. F. Stanton, and R. J. Bartlett, *J. Chem. Phys.*, **95**, 2623 (1991). Coupled-Cluster Open-Shell Analytic Gradients: Implementation of the Direct Product Decomposition Approach in Energy Gradient Calculations.
51. J. Gauss, W. J. Lauderdale, J. F. Stanton, J. D. Watts, and R. J. Bartlett, *Chem. Phys. Lett.*, **182**, 207 (1991). Analytic Energy Gradients for Open-Shell Coupled-Cluster Singles and Doubles Calculations Using Restricted Open-Shell Hartree–Fock (ROHF) Reference Functions.
52. J. Gauss, J. F. Stanton, and R. J. Bartlett, *J. Chem. Phys.*, **95**, 2639 (1991). Analytic Evaluation of Energy Gradients at the Coupled-Cluster Singles and Doubles Level Using Quasi-Restricted Hartree–Fock Open-Shell Reference Functions.
53. G. E. Scuseria, *J. Chem. Phys.*, **94**, 442 (1991). Analytic Evaluation of Energy Gradients for the Singles and Doubles Coupled-Cluster Method Including Perturbative Triple Excitations: Theory and Applications to FOOF and Cr².
54. T. J. Lee and A. P. Rendell, *J. Chem. Phys.*, **94**, 6229 (1991). Analytic Gradients for Coupled-Cluster Energies That Include Noniterative Connected Triple Excitations: Application to *cis*- and *trans*-HONO.
55. E. A. Salter and R. J. Bartlett, *J. Chem. Phys.*, **90**, 1767 (1989). Analytic Energy Derivatives in Many-Body Theory. II. Second Derivatives.
56. H. Koch, H. J. Aa. Jensen, P. Jørgensen, T. Helgaker, G. E. Scuseria, and H. F. Schaefer, *J. Chem. Phys.*, **92**, 4924 (1990). Coupled-Cluster Energy Derivatives. Analytic Hessian for the Closed-Shell Coupled-Cluster Singles and Doubles Wave Functions: Theory and Applications.
57. J. F. Stanton and J. Gauss, in *Recent Advances in Coupled-Cluster Methods*, R. J. Bartlett, Ed., World Scientific Publishing, Singapore, 1997, pp. 49–79. Analytic Evaluation of Second Derivatives of the Energy: Computational Strategies for the CCSD and CCSD(T) Approximations.

58. J. Gauss and J. F. Stanton, *Chem. Phys. Lett.*, **276**, 70 (1997). Analytic CCSD(T) Second Derivatives.
59. P. G. Szalay, J. Gauss, and J. F. Stanton, *Theor. Chim. Acta*, **100**, 5 (1998). Analytic UHF-CCSD(T) Second Derivatives: Implementation and Application to the Calculation of the Vibration–Rotation Interaction Constants of NCO and NCS.
60. D. Mukherjee and P. K. Mukherjee, *Chem. Phys.*, **39**, 325 (1979). A Response–Function Approach to the Direct Calculation of the Transition-Energy in a Multiple-Cluster Expansion Formalism.
61. K. Emrich, *Nucl. Phys. A*, **351**, 379 (1981). An Extension of the Coupled Cluster Formalism to Excited States (I).
62. S. Ghosh and D. Mukherjee, *Proc. Indian Acad. Sci. (Chem. Sci.)*, **93**, 947 (1984). Use of Cluster Expansion Techniques in Quantum Chemistry. A Linear Response Model for Calculating Energy Differences.
63. H. Sekino and R. J. Bartlett, *Int. J. Quantum Chem. Symp.*, **18**, 255 (1984). A Linear Response, Coupled-Cluster Theory for Excitation Energy.
64. L. Meissner and R. J. Bartlett, *J. Chem. Phys.*, **94**, 6670 (1991). Transformation of the Hamiltonian in Excitation Energy Calculations: Comparison Between Fock-Space Multi-reference Coupled-Cluster and Equation-of-Motion Coupled-Cluster Methods.
65. J. F. Stanton and R. J. Bartlett, *J. Chem. Phys.*, **98**, 7029 (1993). The Equation of Motion Coupled-Cluster Method. A Systematic Biorthogonal Approach to Molecular Excitation Energies, Transition Probabilities, and Excited State Properties.
66. J. F. Stanton and J. Gauss, *J. Chem. Phys.*, **99**, 8840 (1993). Many-Body Methods for Excited State Potential Energy Surfaces. I. General Theory of Energy Gradients for the Equation-of-Motion Coupled-Cluster Method.
67. J. F. Stanton and J. Gauss, *J. Chem. Phys.*, **101**, 8938 (1994). Analytic Energy Derivatives for Ionized States Described by the Equation-of-Motion Coupled-Cluster Method.
68. J. F. Stanton, J. Gauss, N. Ishikawa, and M. Head-Gordon, *J. Chem. Phys.*, **103**, 4160 (1995). A Comparison of Single Reference Methods for Characterizing Stationary Points of Excited State Potential Energy Surfaces.
69. H. Koch and P. Jørgensen, *J. Chem. Phys.*, **93**, 3333 (1990). Coupled Cluster Response Functions.
70. H. Koch, O. Christiansen, P. Jørgensen, and J. Olsen, *Chem. Phys. Lett.*, **244**, 75 (1995). Excitation Energies of BH, CH₂, and Ne in Full Configuration Interaction and the Hierarchy CCS, CC2, CCSD, and CC3 of Coupled-Cluster Models.
71. J. D. Watts, S. R. Gwaltney, and R. J. Bartlett, *J. Chem. Phys.*, **105**, 6979 (1996). Coupled-Cluster Calculations of the Excitation Energies of Ethylene, Butadiene, and Cyclopentadiene.
72. O. Christiansen, H. Koch, A. Halkier, P. Jørgensen, T. Helgaker, and A. S. De Merás, *J. Chem. Phys.*, **105**, 6921 (1996). Large-Scale Calculations of Excitation Energies in Coupled-Cluster Theory: The Singlet Excited States of Benzene.
73. M. Head-Gordon and T. J. Lee, in *Recent Advances in Coupled-Cluster Methods*, R. J. Bartlett, Ed., World Scientific Publishing, Singapore, 1997, pp. 221–253. Single Reference Coupled Cluster and Perturbation Theories of Electronic Excitation Energies.
74. M. Nooijen and R. J. Bartlett, *J. Chem. Phys.*, **106**, 6441 (1997). A New Method for Excited States: Similarity Transformed Equation-of-Motion Coupled-Cluster Theory.
75. O. Sinanoğlu, *Adv. Chem. Phys.*, **6**, 315 (1964). Many-Electron Theory of Atoms, Molecules, and Their Interactions.
76. R. J. Bartlett, *J. Phys. Chem.*, **93**, 1697 (1989). Coupled-Cluster Approach to Molecular Structure and Spectra: A Step Toward Predictive Quantum Chemistry.
77. R. J. Bartlett and J. F. Stanton, in *Reviews in Computational Chemistry*, K. B. Lipkowitz and D. B. Boyd, Eds., VCH Publishers, New York, 1994, Vol. 5, pp. 65–169. Applications of Post-Hartree–Fock Methods: A Tutorial.

78. R. J. Bartlett, in *Modern Electronic Structure Theory*, Vol. 2 of *Advanced Series in Physical Chemistry*, D. R. Yarkony, Ed., World Scientific Publishing, Singapore, 1995, pp. 1047–1131. Coupled-Cluster Theory: An Overview of Recent Developments.
79. T. J. Lee and G. E. Scuseria, in *Quantum Mechanical Electronic Structure Calculations with Chemical Accuracy*, S. R. Langhoff, Ed., Kluwer Academic Publishers, Dordrecht, 1995, pp. 47–108. Achieving Chemical Accuracy with Coupled-Cluster Theory.
80. F. E. Harris, H. J. Monkhorst, and D. L. Freeman, *Algebraic and Diagrammatic Methods in Many-Fermion Theory*, Oxford University Press, New York, 1992.
81. P. R. Taylor, in *Lecture Notes in Quantum Chemistry: European Summer School II*, Vol. 64 of *Lecture Notes in Chemistry*, B. O. Roos, Ed., Springer-Verlag, Berlin, 1994, pp. 125–202. Coupled-Cluster Methods in Quantum Chemistry.
82. A. Szabo and N. S. Ostlund, *Modern Quantum Chemistry: Introduction to Advanced Electronic Structure Theory*, 1st ed., McGraw-Hill, New York, 1989.
83. W. Kutzelnigg, in *Methods of Electronic Structure Theory*, H. F. Schaefer, Ed., Plenum Press, New York, 1977, pp. 129–188. Pair-Correlation Theories.
84. P. Jørgensen and J. Simons, *Second Quantization-Based Methods in Quantum Chemistry*, Academic Press, New York, 1981.
85. I. Shavitt, in *Methods of Electronic Structure Theory*, H. F. Schaefer, Ed., Plenum Press, New York, 1977, pp. 189–275. The Method of Configuration Interaction.
86. C. D. Sherrill and H. F. Schaefer, *Adv. Quantum Chem.*, **34**, 143 (1999). The Configuration Interaction Method: Advances in Highly Correlated Approaches.
87. R. J. Bartlett, *Annu. Rev. Phys. Chem.*, **32**, 359 (1981). Many-Body Perturbation Theory and Coupled-Cluster Theory for Electron Correlation in Molecules.
88. M. Nooijen, Ph.D. Thesis, Vrije Universiteit Amsterdam, 1992. The Coupled Cluster Green's Function.
89. J. A. Pople, in *Energy, Structure, and Reactivity*, D. W. Smith and W. B. McRae, Eds., Wiley, New York, 1973, pp. 51–61. Theoretical Models for Chemistry.
90. R. J. Bartlett, C. E. Dykstra, and J. Paldus, in *Advanced Theories and Computational Approaches to the Electronic Structure of Molecules*, C. E. Dykstra, Ed., D. Reidel, Dordrecht, 1984, pp. 127–159. Coupled-Cluster Methods for Molecular Calculations.
91. E. Merzbacher, *Quantum Mechanics*, 2nd ed., Wiley, New York, 1970.
92. J. F. Stanton, unpublished notes, Austin, TX, 1996. Fundamentals of Second Quantization.
93. W. Kutzelnigg, *Mol. Phys.*, **94**, 65 (1998). Almost Variational Coupled Cluster Theory.
94. M. R. Hoffmann and J. Simons, *J. Chem. Phys.*, **88**, 993 (1988). A Unitary Coupled-Cluster Method: Theory and Applications.
95. M. R. Hoffmann and J. Simons, *Chem. Phys. Lett.*, **142**, 451 (1987). Analytical Energy Gradients for a Unitary Coupled-Cluster Theory.
96. R. J. Bartlett and J. Noga, *Chem. Phys. Lett.*, **150**, 29 (1988). The Expectation Value Coupled-Cluster Method and Analytical Energy Derivatives.
97. J. S. Arponen, *Ann. Phys.*, **151**, 311 (1983). Variational Principles and Linked-Cluster Exp S Expansions for Static and Dynamic Many-Body Problems.
98. R. F. Bishop and J. S. Arponen, *Int. J. Quantum Chem. Symp.*, **24**, 197 (1990). Correlations in Extended Systems: A Microscopic Multilocal Method for Describing Both Local and Global Properties.
99. R. J. Bartlett, S. A. Kucharski, J. Noga, J. D. Watts, and G. W. Trucks, in *Lecture Notes in Quantum Chemistry*, Vol. 52 of *Lecture Notes in Chemistry*, U. Kaldor, Ed., Springer-Verlag, Berlin, 1989, pp. 125–149. Some Consideration of Alternative Ansätze in Coupled-Cluster Theory.
100. P. G. Szalay, M. Nooijen, and R. J. Bartlett, *J. Chem. Phys.*, **103**, 281 (1995). Alternative Ansätze in Single Reference Coupled-Cluster Theory. III. A Critical Analysis of Different Methods.

101. J. F. Stanton, unpublished notes, Austin, TX, 1998. Coupled Cluster Theory for the Ambidextrous.
102. H. Koch, H. J. Aa. Jensen, P. Jørgensen, and T. Helgaker, *J. Chem. Phys.*, **93**, 3345 (1990). Excitation Energies from the Coupled Cluster Singles and Doubles Linear Response Function (CCSDLR). Applications to Be, CH⁺, CO, and H₂O.
103. R. J. Rico and M. Head-Gordon, *Chem. Phys. Lett.*, **213**, 224 (1993). Single-Reference Theories of Molecular Excited States with Single and Double Substitutions.
104. O. Christiansen, H. Koch, and P. Jørgensen, *Chem. Phys. Lett.*, **243**, 409 (1995). The Second-Order Approximate Coupled Cluster Singles and Doubles Model CC2.
105. O. Christiansen, H. Koch, and P. Jørgensen, *J. Chem. Phys.*, **103**, 7429 (1995). Response Functions in the CC3 Iterative Triple Excitation Model.
106. H. Nakatsuji and K. Hirao, *J. Chem. Phys.*, **68**, 2053 (1978). Cluster Expansion of the Wavefunction. Symmetry-Adapted-Cluster Expansion, Its Variational Determination, and Extension of Open-Shell Orbital Theory.
107. H. Nakatsuji, *Chem. Phys. Lett.*, **59**, 362 (1978). Cluster Expansion of the Wavefunctions. Excited States.
108. H. Nakatsuji, *Chem. Phys. Lett.*, **67**, 329 (1979). Cluster Expansion of the the Wavefunction. Electron Correlations in Ground and Excited States by SAC (Symmetry-Adapted-Cluster) and SAC CI Theories.
109. U. Kaldor, *Theor. Chim. Acta*, **80**, 427 (1991). The Fock Space Coupled Cluster Method: Theory and Application.
110. D. Mukhopadhyay, S. Mukhopadhyay, R. Chaudhuri, and D. Mukherjee, *Theor. Chim. Acta*, **80**, 441 (1991). Aspects of Separability in the Coupled Cluster Based Direct Method for Energy Differences.
111. C. M. L. Rittby and R. J. Bartlett, *Theor. Chim. Acta*, **80**, 469 (1991). Multireference Coupled Cluster Theory in Fock Space.
112. J. F. Stanton, R. J. Bartlett, and C. M. L. Rittby, *J. Chem. Phys.*, **97**, 5560 (1992). Fock Space Multireference Coupled-Cluster Theory for General Single Determinant Reference Functions.
113. M. Nooijen and R. J. Bartlett, *J. Chem. Phys.*, **102**, 3629 (1995). Equation-of-Motion Coupled-Cluster Method for Electron Attachment.
114. M. Nooijen and R. J. Bartlett, *J. Chem. Phys.*, **106**, 6449 (1997). Similarity Transformed Equation-of-Motion Coupled-Cluster Study of Ionized, Electron Attached, and Excited States of Free Base Porphyrin.
115. K. F. Freed, *Annu. Rev. Phys. Chem.*, **22**, 313 (1971). Many-Body Theories of the Electronic Structure of Atoms and Molecules.
116. G. C. Wick, *Phys. Rev.*, **80**, 268 (1950). The Evaluation of the Collision Matrix.
117. J. Paldus and J. Čížek, *Adv. Quantum Chem.*, **9**, 105 (1975). Time-Independent Diagrammatic Approach to Perturbation Theory of Fermion Systems.
118. T. D. Crawford, Ph.D. Thesis, University of Georgia, 1996. Many-Body Perturbation Theory and Perturbational Triple Excitation Corrections to the Coupled-Cluster Singles and Doubles Method for High-Spin Open-Shell Systems.
119. R. J. Bartlett and D. M. Silver, *Int. J. Quantum Chem. Symp.*, **9**, 183 (1975). Some Aspects of Diagrammatic Perturbation Theory.
120. R. J. Bartlett, unpublished notes, Gainesville, FL, 1994. Systematic Derivation of Coupled-Cluster Equations.
121. E. R. Davidson, in *The World of Quantum Chemistry*, R. Daudel and B. Pullman, Eds., D. Reidel, Dordrecht, 1974, pp. 17–30. Configuration Interaction Description of Electron Correlation.
122. S. R. Langhoff and E. R. Davidson, *Int. J. Quantum Chem.*, **8**, 61 (1974). Configuration Interaction Calculations on the Nitrogen Molecule.

123. R. J. Bartlett, I. Shavitt, and G. D. Purvis, *J. Chem. Phys.*, **71**, 281 (1979). The Quartic Force Field of H₂O Determined by Many-Body Methods That Include Quadruple Excitation Effects.
124. F. L. Pilar, *Elementary Quantum Chemistry*, 2nd ed., McGraw-Hill, New York, 1990.
125. M. Urban, I. Černušák, V. Kellö, and J. Noga, in *Electron Correlation in Atoms and Molecules*, Vol. 1 of *Methods in Computational Chemistry*, S. Wilson, Ed., Plenum Press, New York, 1987, pp. 117–250. Electron Correlation in Molecules.
126. C. Møller and M. S. Plesset, *Phys. Rev.*, **46**, 618 (1934). Note on an Approximation Treatment for Many-Electron Systems.
127. I. Hubač and P. Čársky, *Phys. Rev.*, **A22**, 2392 (1980). Correlation Energy of Open-Shell Systems. Application of the Many-Body Rayleigh–Schrödinger Perturbation Theory in the Restricted Roothaan–Hartree–Fock Formalism.
128. R. D. Amos, J. S. Andrews, N. C. Handy, and P. J. Knowles, *Chem. Phys. Lett.*, **185**, 256 (1991). Open-Shell Møller-Plesset Perturbation Theory.
129. P. J. Knowles, J. S. Andrews, R. D. Amos, N. C. Handy, and J. A. Pople, *Chem. Phys. Lett.*, **186**, 130 (1991). Restricted Møller-Plesset Theory for Open-Shell Molecules.
130. W. J. Lauderdale, J. F. Stanton, J. Gauss, J. D. Watts, and R. J. Bartlett, *Chem. Phys. Lett.*, **187**, 21 (1991). Many-Body Perturbation Theory with a Restricted Open-Shell Hartree–Fock Reference.
131. C. Murray and E. R. Davidson, *Chem. Phys. Lett.*, **187**, 451 (1991). Perturbation Theory for Open-Shell Systems.
132. T. J. Lee and D. Jayatilaka, *Chem. Phys. Lett.*, **201**, 1 (1993). An Open-Shell Restricted Hartree–Fock Perturbation Theory Based on Symmetric Spin Orbitals.
133. P. M. Kozlowski and E. R. Davidson, *Chem. Phys. Lett.*, **226**, 440 (1994). Construction of Open-Shell Perturbation Theory Invariant with Respect to Orbital Degeneracy.
134. T. D. Crawford, H. F. Schaefer, and T. J. Lee, *J. Chem. Phys.*, **105**, 1060 (1996). On the Energy Invariance of Open-Shell Perturbation Theory with Respect to Unitary Transformations of Molecular Orbitals.
135. R. Krishnan and J. A. Pople, *Int. J. Quantum Chem.*, **14**, 91 (1978). Approximate Fourth-Order Perturbation Theory of the Electron Correlation Energy.
136. R. Krishnan, M. J. Frisch, and J. A. Pople, *J. Chem. Phys.*, **72**, 4244 (1980). Contribution of Triple Substitutions to the Electron Correlation Energy in Fourth Order Perturbation Theory.
137. J. R. Thomas, B. J. DeLeeuw, G. Vacek, and H. F. Schaefer, *J. Chem. Phys.*, **98**, 1336 (1993). A Systematic Study of the Harmonic Vibrational Frequencies for Polyatomic Molecules: The Single, Double, and Perturbative Triple Excitation Coupled-Cluster [CCSD(T)] Method.
138. J. R. Thomas, B. J. DeLeeuw, G. Vacek, T. D. Crawford, Y. Yamaguchi, and H. F. Schaefer, *J. Chem. Phys.*, **99**, 403 (1993). The Balance Between Theoretical Method and Basis Set Quality: A Systematic Study of Equilibrium Geometries, Dipole Moments, Harmonic Vibrational Frequencies, and Infrared Intensities.
139. R. J. Bartlett and I. Shavitt, *Chem. Phys. Lett.*, **50**, 190 (1977). Comparison of High-Order Many-Body Perturbation Theory and Configuration Interaction for H₂O.
140. T. D. Crawford, J. F. Stanton, W. D. Allen, and H. F. Schaefer, *J. Chem. Phys.*, **107**, 10626 (1997). Hartree–Fock Orbital Instability Envelopes in Highly Correlated Single-Reference Wavefunctions.
141. T. J. Lee, A. P. Rendell, and P. R. Taylor, *J. Phys. Chem.*, **94**, 5463 (1990). Comparison of the Quadratic Configuration Interaction and Coupled-Cluster Approaches to Electron Correlation Including the Effect of Triple Excitations.
142. A. P. Rendell, T. J. Lee, and A. Komornicki, *Chem. Phys. Lett.*, **178**, 462 (1991). A Parallel Vectorized Implementation of Triple Excitations in CCSD(T): Application to the Binding Energies of the AlH₃, AlH₂F, AlHF₂, and AlF₃ Dimers.

143. K. Raghavachari, J. A. Pople, E. S. Replogle, and M. Head-Gordon, *J. Phys. Chem.*, **94**, 5579 (1990). Fifth-Order Möller-Plesset Perturbation Theory: Comparison of Existing Correlation Methods and Implementation of New Methods Correct to Fifth Order.
144. A. L. L. East, Ph.D. Thesis, Stanford University, 1994. Selected Theoretical Studies of Vibrational Anharmonicity and Thermochemistry.
145. S. A. Kucharski and R. J. Bartlett, *J. Chem. Phys.*, **108**, 5243 (1998). Noniterative Energy Corrections Through Fifth-Order to the Coupled Cluster Singles and Doubles Method.
146. V. Kvasnička, V. Lurinc, S. Biskupič, and M. Haring, *Adv. Chem. Phys.*, **52**, 181 (1983). Coupled-Cluster Approach in the Electronic-Structure Theory of Molecules.
147. S. A. Kucharski and R. J. Bartlett, *Theor. Chim. Acta*, **80**, 387 (1991). Recursive Intermediate Factorization and Complete Computational Linearization of the Coupled-Cluster Single, Double, Triples, and Quadruple Excitation Equations.
148. C. L. Janssen, E. T. Seidl, G. E. Scuseria, T. P. Hamilton, Y. Yamaguchi, R. B. Remington, Y. Xie, G. Vacek, C. D. Sherrill, T. D. Crawford, J. T. Fermann, W. D. Allen, B. R. Brooks, G. B. Fitzgerald, D. J. Fox, J. F. Gaw, N. C. Handy, W. D. Laidig, T. J. Lee, R. M. Pitzer, J. E. Rice, P. Saxe, A. C. Scheiner, and H. F. Schaefer, PSI 2.0.8, PSITECH, Inc., Watkinsville, GA 30677, 1995. E-mail: psi@ccqc.uga.edu. This program is available for a handling fee of \$100.
149. MOLPRO is a package of ab initio programs written by H.-J. Werner and P. J. Knowles with contributions from R. D. Amos, A. Berning, D. L. Cooper, M. J. O. Deegan, A. J. Dobbyn, F. Eckert, C. Hampel, T. Leininger, R. Lindh, A. W. Lloyd, W. Meyer, M. E. Mura, A. Nicklass, P. Palmieri, K. Peterson, R. Pitzer, P. Pulay, G. Rauhut, M. Schütz, H. Stoll, A. J. Stone, and T. Thorsteinsson. E-mail: molpro-support@tc.bham.ac.uk.
150. J. F. Stanton, J. Gauss, J. D. Watts, W. J. Lauderdale, and R. J. Bartlett, ACES II. The package also contains modified versions of the MOLECULE Gaussian integral program of J. Almlöf and P. R. Taylor, the ABACUS integral derivative program written by T. U. Helgaker, H. J. Aa. Jensen, P. Jørgensen and P. R. Taylor, and the PROPS property evaluation integral code of P. R. Taylor. E-mail: aces2@qpp.ufl.edu.
151. K. Dowd, *High Performance Computing: RISC Architectures, Optimization, and Benchmarks*, O'Reilly and Associates, Sebastopol, CA, 1993.
152. P. Čársky, L. J. Schaad, B. A. Hess, M. Urban, and J. Noga, *J. Chem. Phys.*, **87**, 411 (1987). Use of Molecular Symmetry in Coupled-Cluster Theory.
153. M. Häser, *J. Chem. Phys.*, **95**, 8259 (1991). Molecular Point-Group Symmetry in Electronic Structure Calculations.
154. F. Haase and R. Ahlrichs, *J. Comput. Chem.*, **14**, 907 (1993). Semidirect MP2 Gradient Evaluation on Workstation Computers—The MPGRAD Program.
155. M. Kollwitz, M. Häser, and J. Gauss, *J. Chem. Phys.*, **108**, 8295 (1998). Non-Abelian Point Group Symmetry in Direct Second-Order Many-Body Perturbation Theory Calculations of NMR Chemical Shifts.
156. R. Pauncz, *Spin Eigenfunctions: Construction and Use*, Plenum Press, New York, 1979.
157. R. Pauncz, *The Symmetric Group in Quantum Chemistry*, CRC Press, Boca Raton, FL, 1995.
158. X. Li and J. Paldus, *J. Chem. Phys.*, **103**, 6536 (1995). Unitary Group Based Open-Shell Coupled-Cluster Approach and Triplet and Open-Shell Singlet Stabilities of Hartree–Fock References.
159. S. Wilson, in *Electron Correlation in Atoms and Molecules*, Vol. 1 of *Methods in Computational Chemistry*, S. Wilson, Ed., Plenum Press, New York, 1987, pp. 251–309. Four-Index Transformations.
160. C. Hampel, K. A. Peterson, and H.-J. Werner, *Chem. Phys. Lett.*, **190**, 1 (1992). A Comparison of the Efficiency and Accuracy of the Quadratic Configuration Interaction (QCISD), Coupled-Cluster (CCSD), and Brueckner Coupled-Cluster (BCCD) Methods.
161. P. R. Taylor, *Int. J. Quantum Chem.*, **31**, 521 (1987). Integral Processing in Beyond-Hartree–Fock Calculations.

162. M. J. Frisch, M. Head-Gordon, and J. A. Pople, *Chem. Phys. Lett.*, **166**, 281 (1990). Semi-Direct Algorithms for the MP2 Energy and Gradient.
163. H. Koch, O. Christiansen, R. Kobayashi, P. Jørgensen, and T. Helgaker, *Chem. Phys. Lett.*, **228**, 233 (1994). A Direct Atomic Orbital Driven Implementation of the Coupled Cluster Singles and Doubles (CCSD) Model.
164. H. Koch, A. S. De Merás, T. Helgaker, and O. Christiansen, *J. Chem. Phys.*, **104**, 4157 (1996). The Integrals-Direct Coupled-Cluster Singles and Doubles Model.
165. A. P. Rendell and T. J. Lee, *J. Chem. Phys.*, **101**, 400 (1994). Coupled-Cluster Theory Employing Approximate Integrals: An Approach to Avoid the Input/Output and Storage Bottlenecks.
166. J. M. L. Martin, *J. Chem. Phys.*, **100**, 8186 (1994). On the Performance of Correlation Consistent Basis Sets for the Calculation of Total Atomization Energies, Geometries and Harmonic Frequencies.
167. J. Paldus, in *New Horizons of Quantum Chemistry: Proceedings of the Fourth International Congress of Quantum Chemistry*, P.-O. Löwdin and B. Pullman, Eds., D. Reidel, Dordrecht, 1983, pp. 31–60. Coupled Cluster Approaches to the Many-Electron Correlation Problem.
168. J. Paldus, in *Methods in Computational Molecular Physics*, S. Wilson and G. H. F. Diercksen, Eds., Plenum Press, New York, 1992, pp. 99–194. Coupled Cluster Theory.
169. A. Balkova and R. J. Bartlett, *Chem. Phys. Lett.*, **193**, 364 (1992). Coupled-Cluster Method for Open-Shell Singlets.
170. A. Balkova and R. J. Bartlett, *J. Chem. Phys.*, **99**, 7907 (1993). The 2-Determinant Coupled-Cluster Method for Electric Properties of Excited Electronic States: The Lowest 1B_1 and 3B_1 States of the Water Molecule.
171. D. Jayatilaka and T. J. Lee, *Chem. Phys. Lett.*, **199**, 211 (1992). The Form of Spin Orbitals for Open-Shell Restricted Hartree–Fock Reference Functions.
172. D. Jayatilaka and T. J. Lee, *J. Chem. Phys.*, **98**, 9734 (1993). Open-Shell Coupled-Cluster Theory.
173. T. D. Crawford, T. J. Lee, and H. F. Schaefer, *J. Chem. Phys.*, **107**, 9980 (1997). Spin-Restricted Brueckner Orbitals for Coupled-Cluster Wavefunctions.
174. J. F. Stanton, *J. Chem. Phys.*, **101**, 371 (1994). On the Extent of Spin Contamination in Open-Shell Coupled-Cluster Wave Functions.
175. T. J. Lee, A. P. Rendell, K. G. Dyall, and D. Jayatilaka, *J. Chem. Phys.*, **100**, 7400 (1994). Open-Shell Restricted Hartree–Fock Perturbation Theory: Some Considerations and Comparisons.
176. S. Wolfram, *Mathematica: A System for Doing Mathematics by Computer*, 2nd ed., Addison-Wesley, New York, 1991.
177. K. A. Brueckner, *Phys. Rev.*, **96**, 508 (1954). Nuclear Saturation and Two-Body Forces. II. Tensor Forces.
178. R. K. Nesbet, *Phys. Rev.*, **109**, 1632 (1958). Brueckner's Theory and the Method of Superposition of Configurations.
179. R. A. Chiles and C. E. Dykstra, *J. Chem. Phys.*, **74**, 4544 (1981). An Electron Pair Operator Approach to Coupled-Cluster Wave Functions. Application to He_2 , Be_2 , and Mg_2 and Comparison with CEPA Methods.
180. L. Z. Stolarczyk and H. J. Monkhorst, *Int. J. Quantum Chem. Symp.*, **18**, 267 (1984). Coupled-Cluster Method with Optimized Reference State.
181. G. E. Scuseria and H. F. Schaefer, *Chem. Phys. Lett.*, **142**, 354 (1987). The Optimization of Molecular Orbitals for Coupled Cluster Wavefunctions.
182. N. C. Handy, J. A. Pople, M. Head-Gordon, K. Raghavachari, and G. W. Trucks, *Chem. Phys. Lett.*, **164**, 185 (1989). Size-Consistent Brueckner Theory Limited to Double Substitutions.
183. R. Kobayashi, N. C. Handy, R. D. Amos, G. W. Trucks, M. J. Frisch, and J. A. Pople, *J. Chem. Phys.*, **95**, 6723 (1991). Gradient Theory Applied to the Brueckner Doubles Method.

184. R. Kobayashi, R. D. Amos, and N. C. Handy, *Chem. Phys. Lett.*, **184**, 195 (1991). The Analytic Gradient of the Perturbative Triple Excitations Correction to the Brueckner Doubles Method.
185. T. J. Lee, R. Kobayashi, N. C. Handy, and R. D. Amos, *J. Chem. Phys.*, **96**, 8931 (1992). Comparison of the Brueckner and Coupled-Cluster Approaches to Electron Correlation.
186. J. F. Stanton, J. Gauss, and R. J. Bartlett, *J. Chem. Phys.*, **97**, 5554 (1992). On the Choice of Orbitals for Symmetry Breaking Problems with Application to NO_3 .
187. R. Kobayashi, H. Koch, P. Jørgensen, and T. J. Lee, *Chem. Phys. Lett.*, **211**, 94 (1993). Comparison of Coupled-Cluster and Brueckner Coupled-Cluster Calculations of Molecular Properties.
188. V. A. Kozlov and V. I. Pupyshev, *Chem. Phys. Lett.*, **206**, 151 (1993). Self-Consistent Brueckner Theory for Molecular Orbitals.
189. R. Kobayashi, R. D. Amos, and N. C. Handy, *J. Chem. Phys.*, **100**, 1375 (1994). Large Basis Set Calculations Using Brueckner Theory.
190. J. D. Watts and R. J. Bartlett, *Int. J. Quantum Chem. Symp.*, **28**, 195 (1994). Coupled-Cluster Singles, Doubles, and Triples Calculations with Hartree–Fock and Brueckner Orbital Reference Determinants: A Comparative Study.
191. G. E. Scuseria, *Int. J. Quantum Chem.*, **55**, 165 (1995). On the Connections Between Brueckner-Coupled-Cluster, Density-Dependent Hartree–Fock, and Density Functional Theory.
192. C. D. Sherrill, A. I. Krylov, E. F. C. Byrd, and M. Head-Gordon, *J. Chem. Phys.*, **109**, 4171 (1998). Energies and Analytic Gradients for a Coupled-Cluster Doubles Model Using Variational Brueckner Orbitals. Application to Symmetry Breaking in O_4^+ .
193. J. Čížek and J. Paldus, *J. Chem. Phys.*, **47**, 3976 (1967). Stability Conditions for the Solutions of the Hartree–Fock Equations for Atomic and Molecular Systems. Application to the Pi-Electron Model of Cyclic Polyenes.
194. J. Paldus and J. Čížek, *Chem. Phys. Lett.*, **3**, 1 (1969). Stability Conditions for the Solutions of the Hartree–Fock Equations for the Simple Open-Shell Case.
195. E. R. Davidson and W. T. Borden, *J. Phys. Chem.*, **87**, 4783 (1983). Symmetry Breaking in Polyatomic Molecules: Real and Artifactual. See also: T. Bally and W. T. Borden, in *Reviews in Computational Chemistry*, K. B. Lipkowitz and D. B. Boyd, Eds., Wiley-VCH, New York, Vol. 13, pp. 1–97. Calculations on Open-Shell Molecules: A Beginner’s Guide.
196. W. D. Allen, D. A. Horner, R. L. DeKock, R. B. Remington, and H. F. Schaefer, *Chem. Phys.*, **133**, 11 (1989). The Lithium Superoxide Radical: Symmetry Breaking Phenomena and Potential Energy Surfaces.
197. O. Goscinski, *Int. J. Quantum Chem. Symp.*, **19**, 51 (1986). Are Localized Broken Symmetry Solutions Acceptable in Molecular Calculations?
198. P.-O. Löwdin, *Rev. Mod. Phys.*, **35**, 496 (1963). Discussion on the Hartree–Fock Approximation.
199. K. Deguchi, K. Nishikawa, and S. Aono, *J. Chem. Phys.*, **75**, 4165 (1981). Instabilities of the Hartree–Fock Solution and the Vibrational Mode in a Molecule.
200. Y. Yamaguchi, I. L. Alberts, J. D. Goddard, and H. F. Schaefer, *Chem. Phys.*, **147**, 309 (1990). Use of the Molecular Orbital Hessian for Self-Consistent-Field (SCF) Wavefunctions.
201. N. A. Burton, Y. Yamaguchi, I. L. Alberts, and H. F. Schaefer, *J. Chem. Phys.*, **95**, 7466 (1991). Interpretation of Excited State Hartree–Fock Analytic Derivative Anomalies for NO_2 and HCO_2 Using the Molecular Orbital Hessian.
202. L. A. Barnes and R. Lindh, *Chem. Phys. Lett.*, **223**, 207 (1994). Symmetry Breaking in O_4^+ : An Application of the Brueckner Coupled-Cluster Method.
203. Y. Xie, W. D. Allen, Y. Yamaguchi, and H. F. Schaefer, *J. Chem. Phys.*, **104**, 7615 (1996). Is the Oxywater Radical Cation More Stable Than Neutral Oxywater?
204. J. Hrušák and S. Iwata, *J. Chem. Phys.*, **106**, 4877 (1997). The Vibrational Spectrum of H_2O_2^+ Radical Cation: An Illustration of Symmetry Breaking.

205. T. D. Crawford, J. F. Stanton, P. G. Szalay, and H. F. Schaefer, *J. Chem. Phys.*, **107**, 2525 (1997). The \tilde{C}^2A_2 Excited State of NO_2 : Evidence for a C_s Equilibrium Structure and a Failure of Some Spin-Restricted Reference Wavefunctions.
206. K. Shibuya, C. Terauchi, M. Sugawara, K. Aoki, K. Tsuji, and S. Tsuchiya, *J. Mol. Struct.*, **413–414**, 501 (1997). Vibrational Level Structure of $\text{NO}_2 \tilde{C}^2A_2$ in the Energy Region of $16200\text{--}21000\text{ cm}^{-1}$: Evidence for the Breakdown of C_{2v} Symmetry.
207. R. A. King, T. D. Crawford, J. F. Stanton, and H. F. Schaefer, *J. Am. Chem. Soc.*, submitted, 1999. Conformations of [10]Annulene. More Bad News for Density-Functional Theory and Perturbation Theory.
208. P. Pulay, *Chem. Phys. Lett.*, **100**, 151 (1983). Localizability of Dynamic Electron Correlation.
209. S. Sæbø and P. Pulay, *Chem. Phys. Lett.*, **113**, 13 (1985). Local Configuration Interaction: An Efficient Approach for Larger Molecules.
210. P. Pulay and S. Sæbø, *Theor. Chim. Acta*, **69**, 357 (1986). Orbital-Invariant Formulation and Second-Order Gradient Evaluation in Møller-Plesset Perturbation Theory.
211. S. Sæbø and P. Pulay, *J. Chem. Phys.*, **86**, 914 (1987). Fourth-Order Møller-Plesset Perturbation Theory in the Local Correlation Treatment. I. Method.
212. S. Sæbø, W. Tong, and P. Pulay, *J. Chem. Phys.*, **98**, 2170 (1993). Efficient Elimination of Basis Set Superposition Errors by the Local Correlation Method: Accurate Ab Initio Studies of the Water Dimer.
213. C. Hampel and H.-J. Werner, *J. Chem. Phys.*, **104**, 6286 (1996). Local Treatment of Electron Correlation in Coupled Cluster Theory.
214. J. D. Watts and R. J. Bartlett, *J. Chem. Phys.*, **101**, 3073 (1994). The Inclusion of Connected Triples Excitations in the Equation-of-Motion Coupled-Cluster Methods.
215. J. D. Watts and R. J. Bartlett, *Chem. Phys. Lett.*, **233**, 81 (1995). Economical Triple Excitation Equation-of-Motion Coupled-Cluster Methods for Excitation-Energies.
216. J. D. Watts and R. J. Bartlett, *Chem. Phys. Lett.*, **258**, 581 (1996). Iterative and Noniterative Triple Excitation Corrections in Coupled-Cluster Methods for Excited Electronic States—The EOM-CCSDT-3 and EOM-CCSD(T) Methods.
217. O. Christiansen, H. Koch, and P. Jørgensen, *J. Chem. Phys.*, **105**, 1451 (1996). Perturbative Triple Excitation Corrections to Coupled Cluster Singles and Doubles Excitation Energies.
218. P. Piecuch, N. Oliphant, and L. Adamowicz, *J. Chem. Phys.*, **99**, 1875 (1993). A State-Selective Multireference Coupled-Cluster Theory Employing the Single-Reference Formalism.
219. P. Piecuch and L. Adamowicz, *J. Chem. Phys.*, **102**, 898 (1995). Breaking Bonds with the State-Selective Multireference Coupled-Cluster Methods Employing the Single-Reference Formalism.
220. A. Banerjee and J. Simons, *J. Chem. Phys.*, **76**, 4548 (1982). Applications of Multiconfigurational Coupled-Cluster Theory.
221. W. D. Laidig and R. J. Bartlett, *Chem. Phys. Lett.*, **104**, 424 (1984). A Multi-Reference Coupled-Cluster Method for Molecular Applications.
222. P. G. Szalay and R. J. Bartlett, *J. Chem. Phys.*, **103**, 3600 (1995). Approximately Extensive Modifications of the Multireference Configuration Interaction Method: A Theoretical and Practical Analysis.
223. K. B. Ghose, P. Piecuch, and L. Adamowicz, *J. Chem. Phys.*, **103**, 9331 (1995). Improved Computational Strategy for the State-Selective Coupled-Cluster Theory with Semi-Internal Triexcited Clusters: Potential Energy Surface of the HF Molecule.
224. J. T. Fermann, C. D. Sherrill, T. D. Crawford, and H. F. Schaefer, *J. Chem. Phys.*, **100**, 8132 (1994). Benchmark Studies of Electron Correlation in Six-Electron Systems.
225. N. C. Handy and A. M. Lee, *Chem. Phys. Lett.*, **252**, 425 (1996). The Adiabatic Approximation.

226. J. Almlöf and P. R. Taylor, *J. Chem. Phys.*, **86**, 4070 (1987). General Contraction of Gaussian Basis Sets. I. Atomic Natural Orbitals for First- and Second-Row Atoms.
227. J. Almlöf, T. Helgaker, and P. R. Taylor, *J. Phys. Chem.*, **92**, 3029 (1988). Gaussian Basis Sets for High-Quality Ab Initio Calculations.
228. T. H. Dunning, *J. Chem. Phys.*, **90**, 1007 (1989). Gaussian Basis Sets for Use in Correlated Molecular Calculations. I. The Atoms Boron Through Neon.
229. B. J. Persson and P. R. Taylor, *J. Chem. Phys.*, **105**, 5915 (1996). Accurate Quantum-Chemical Calculations: The Use of Gaussian-Type Geminal Functions in the Treatment of Electron Correlation.
230. J. M. L. Martin and P. R. Taylor, *J. Chem. Phys.*, **106**, 8620 (1997). Benchmark Quality Total Atomization Energies of Small Polyatomic Molecules.
231. T. Helgaker, W. Klopper, H. Koch, and J. Noga, *J. Chem. Phys.*, **106**, 9639 (1997). Basis-Set Convergence of Correlated Calculations on Water.
232. W. Klopper, Habilitationsschrift, Eidgenössischen Technischen Hochschule, Zürich, 1996. r_{12} -Dependent Wave Functions.

CHAPTER 3

Introduction to Zeolite Modeling

Bastiaan van de Graaf,* Swie Lan Njo,* and
Konstantin S. Smirnov†

**Laboratory for Organic Chemistry and Catalysis, Waterman Institute of Precision Chemical Technology, Faculty of Applied Sciences, Delft University of Technology, Julianalaan 136, 2628 BL Delft, The Netherlands, and †Laboratoire de Spectrochimie Infrarouge et Raman du CNRS, Bâtiment C5, Université des Sciences et Technologies de Lille, 59655 Villeneuve d'Ascq Cedex, France, (permanent address): Institute of Physics, St. Petersburg University, St. Petersburg 198904, Russia*

INTRODUCTION

Zeolites are microporous crystalline aluminosilicates built from corner-connected TO_4 ($\text{T} = \text{Si or Al}$) tetrahedra. Their micropores with uniform dimensions give rise to molecular sieve properties. Tetracoordinated aluminum atoms lead to ion-exchange properties and make internal acid sites possible. They are economically important as detergent builders, as adsorbents, and, because zeolites have high thermal stability, as catalysts in the petrochemical industry. They are also considered to have a high potential as catalysts in the synthesis of fine chemicals.

There is a large variety of zeolite framework topologies, and new framework topologies are still discovered regularly. These topologies are identified by

Reviews in Computational Chemistry, Volume 14
Kenny B. Lipkowitz and Donald B. Boyd, Editors
Wiley-VCH, John Wiley and Sons, Inc., New York, © 2000

three-letter acronyms assigned by the International Zeolite Association (IZA). A compilation of internationally recognized different topologies with their acronyms is available in the *Atlas of Zeolite Structure Types*.¹ Since zeolites can be modified by ion exchange, by isomorphic substitution (i.e., replacement of Si and Al by other elements in the framework), and by introduction of metal particles into the framework, there exist an almost uncountable number of zeolite materials.

Four of the more important framework topologies are shown in Figure 1. Zeolite NaA (LTA topology) is widely used as sequestering material for Ca^{2+} and Mg^{2+} ions in detergent formulations. In petrochemistry, both zeolite CaA

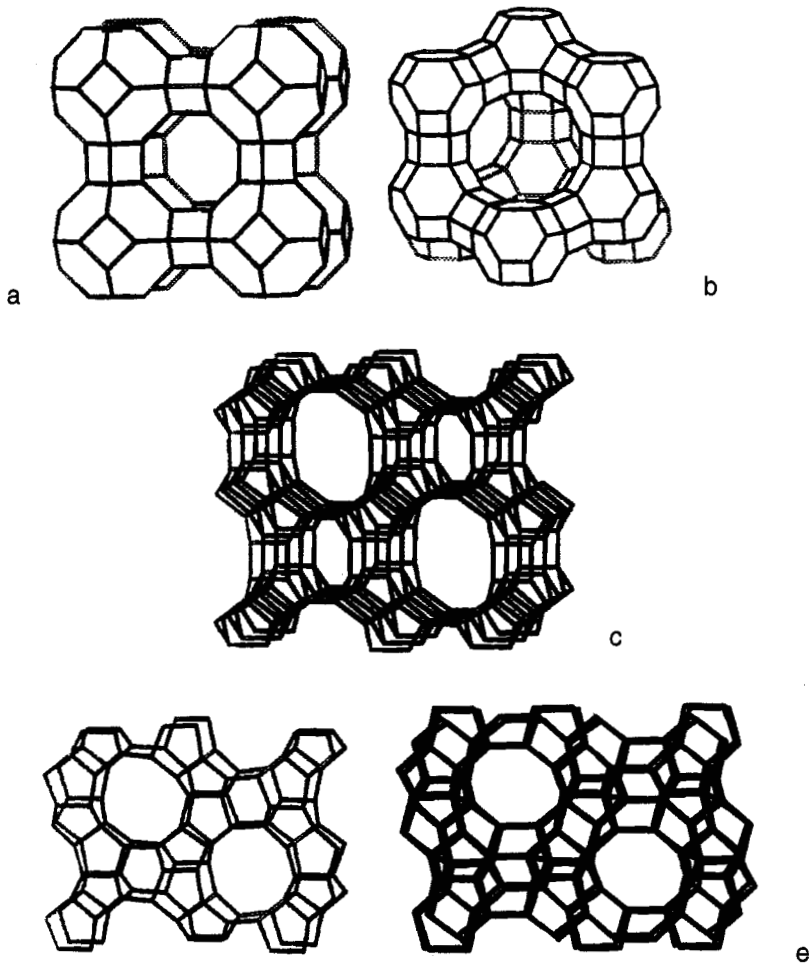


Figure 1 Topologies of five important zeolite frameworks: (a) LTA; (b) FAU; (c) MOR; (d) MFI along the b-axis; (e) MFI along the a-axis.

(LTA topology) and zeolite Pt-H-mordenite (MOR topology) are used in the total isomerization process (TIP): the former is used to separate linear paraffins from branched ones, whereas the latter is employed for the isomerization. The use of zeolites in petrochemistry is dominated by fluid catalyst cracking (FCC) of oil feedstocks. For this purpose, mostly zeolite USY (FAU topology) is used, sometimes together with ZSM-5 (MFI topology). Applications of zeolites as catalysts outside petrochemistry are still limited but growing. For example, titanium-containing MFI (zeolite TS-1) is commercially applied in oxidation reactions, as illustrated by the oxidation of phenol to catechol and hydroquinone.

The special properties of zeolites (Figure 2 illustrates the molecular sieve property for zeolite CaA), and the possibility to tailor zeolite materials to suit one's need, have created much interest in zeolite science. Accordingly, thousands of studies appear in the literature each year. Paralleling this is interest in zeolite modeling. About 1000 studies have been reported in the literature during the last decade, and the number of modeling studies is still growing fast. One of the reasons for the interest in theoretical methods is that, in spite of the advanced techniques and instrumentation available at the moment, many aspects of zeolite science are difficult or even impossible to study experimentally.

Zeolite modeling is quite a diverse field. A literature survey reveals studies using all available levels of theory and methodology. For example, simple force fields are used, but so are high level quantum mechanics, time-consuming molecular dynamics, and, of course, molecular graphics. This chapter introduces experimentalists and others to the variety of methods used in zeolite modeling, shows some of the "tricks of the trade," and provides a basis for understanding the scope and limitations of theoretical methods in this field of study. It is our firm belief that in the field of zeolite science, as in other sub-disciplines of science, experimental and theoretical methods can complement each other. Moreover, experimentalists can now relatively easily enter the field of modeling.

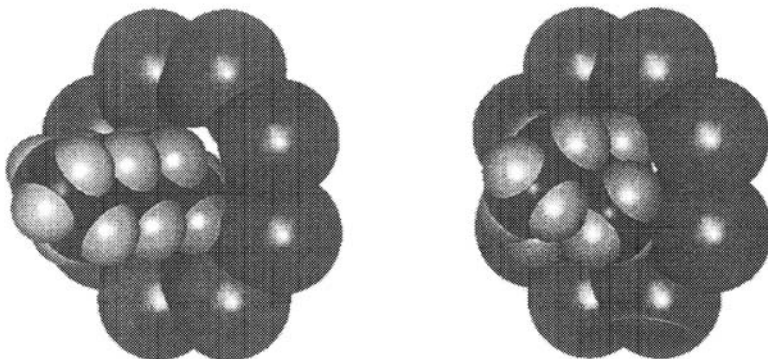


Figure 2 The sieve effect of zeolite CaA demonstrated for the separation of butane (left) and isobutane (right).

The next section reviews the state of zeolite modeling on the basis of a literature survey. However, this survey is not presented in all details because parts of the field of zeolite modeling have been reviewed recently,^{2–6} and it is our opinion that our readers are better served with a selection of reviews rather than with an endless list of references. The sections following the literature survey address models and methods, some selected applications, and further developments. An effort is made to keep mathematical formulas as simple as possible, with an emphasis on the physical meaning of the written equations.

APPROACHES TO ZEOLITE MODELING

During the last two decades, the number of molecular modeling studies on zeolites published annually has grown enormously. As a result of advances in both the development of computational methodologies and new computer architectures, modeling has become an important tool in zeolite research. It can provide useful insight into the structure and reactivity of zeolites and into the sorption of molecules in zeolites. This section gives a brief introduction to computational approaches, as well as a short overview on applications in zeolite research.

Computational Approaches

Many computational approaches have been applied in zeolite modeling. Each uses a different combination of the description of the system (model) and the technique (method) that may be suited for a particular problem (application) (see Figure 3). This section mentions briefly the frequently encountered models and methods in zeolite modeling, to provide a basic understanding. In the following sections, they are discussed in more detail.

Although there are many ways to describe a zeolite system, models are based either on classical mechanics, quantum mechanics, or a mixture of classical and quantum mechanics. Classical models employ parameterized interatomic potentials, so-called force fields, to describe the energies and forces acting in a system. Classical models have been shown^{7–9} to be able to describe accurately the structure and dynamics of zeolites, and they have also been employed to study aspects of adsorption in zeolites, including the interaction between adsorbates and the zeolite framework, adsorption sites, and diffusion of adsorbates. The forming and breaking of bonds, however, cannot be studied with classical models. In studies on zeolite-catalyzed chemical reactions, therefore, a quantum mechanical description is typically employed where the electronic structure of the atoms in the system is taken into account explicitly.¹⁰

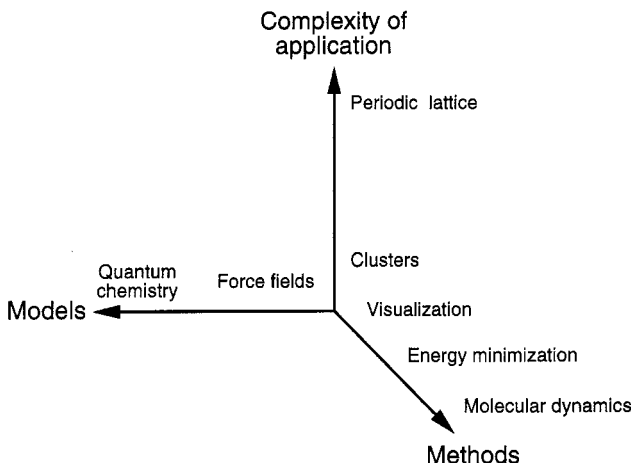


Figure 3 Approaches to zeolite modeling depicted in a three-dimensional graph.

Conventional methods based on quantum mechanical models use matrix diagonalization to find a self-consistent solution of the time-independent Schrödinger equation. Unfortunately, the cost of matrix diagonalization grows extremely rapidly with the number of atoms in the system. Consequently, methods based on quantum mechanical models tend to be computationally expensive. As a result, the zeolite framework is often treated as a cluster instead of as a periodical system. To overcome this obstacle, hybrid models have been put forward in which the problem is circumvented: the reaction center is described in a quantum mechanical way, whereas the surroundings are described in a classical way.¹¹

A wide range of classical techniques have been applied in zeolite modeling, the three most common being energy minimization, molecular dynamics, and Monte Carlo simulations.^{12–14} Computational approaches can utilize one of these main techniques, a combination of these techniques, or a variation on one or more of these techniques. In an energy minimization calculation, the energy of the system is minimized by optimizing the three-dimensional structure of the system until a state of minimum energy is reached. This type of calculation is used in modeling zeolite structures, studying adsorbate–zeolite framework interactions, and in predicting adsorption sites. Molecular dynamics (MD) is used to study the zeolite framework flexibility and transport properties of adsorbates in zeolites. The system is permitted to evolve in time by solving the classical equations of motion. After a certain number of steps, an equilibrium is reached in which the property of a system fluctuates around some average value. The simulation is then continued until sampling of microstates provides statistically meaningful results. Sometimes these sampling stages are very long, making molecular dynamics calculations impractical or even impossible. In such cases the Monte Carlo (MC) technique, in which step and time are

unrelated, may be of help. Most MC studies employ the Metropolis method. At the beginning of each MC step, random moves are made in the system, resulting in a trial configuration of the system. This trial configuration is accepted if its energy, E_{trial} , is lower than that of the previously accepted configuration, E_{accept} , or if $\exp[-\beta(E_{\text{trial}} - E_{\text{accept}})]$ with $\beta = 1/k_B T$, is higher than a random number between 0 and 1. If the trial configuration is rejected, the system returns to the previously accepted configuration and then the next step begins, and the whole process is repeated. The Monte Carlo method is often used to study distributions of adsorbates in zeolites and of atoms other than silicon (e.g., aluminum) in the zeolite framework.

Scope of Zeolite Modeling

This subsection gives a short overview of the general themes from the literature, showing how simulations can be of help in zeolite research.

Framework Structure and Dynamics

Zeolite structures can be determined with single crystal X-ray diffraction (XRD) methods. Often no crystals of sufficient size are available, and as a consequence, powder XRD techniques have to be used. One of the most crucial aspects in these techniques is creating a reasonable starting structure, a problem that molecular modeling can help to overcome. The unit cell parameters and possible space groups can be derived from the powder pattern. The framework density can be obtained from chemical analysis and sorption data. This information can then be used to calculate the number of tetrahedra per unit cell from which an initial structure can be built. Using force fields to describe the energy of the system, both energy minimization and simulating annealing methods¹⁵ can improve a reasonable starting structure. (A force field consists of a set of potential energy functions and an associated set of parameters chosen to model experimental data.) Simulated annealing is based on the use of the MD or MC methods. Thus, in an MC simulation, the probability that higher energy configurations are accepted is greater at high “temperature” than at low temperature. Large configurational jumps can be made, so more configurational space can be sampled without entrapment in a local energy minimum. In simulated annealing therefore, the system is first modeled at high temperature. When the configuration of the system no longer changes dramatically, the temperature is slowly decreased, and the system is gradually brought to an energy minimum. Other aspects of zeolite chemistry that have been studied employing energy minimization include polymorphism in zeolite BEA¹⁶ and the orthorhombic-to-monoclinic phase transition in silicalite.¹⁷

Molecular dynamics has been used to study dynamics of zeolite frameworks,³ particularly fluctuations in zeolite aperture dimensions, whereby the zeolite framework can breathe substantially depending on the topology. For example, some O—O distances across the window were found to vary by as

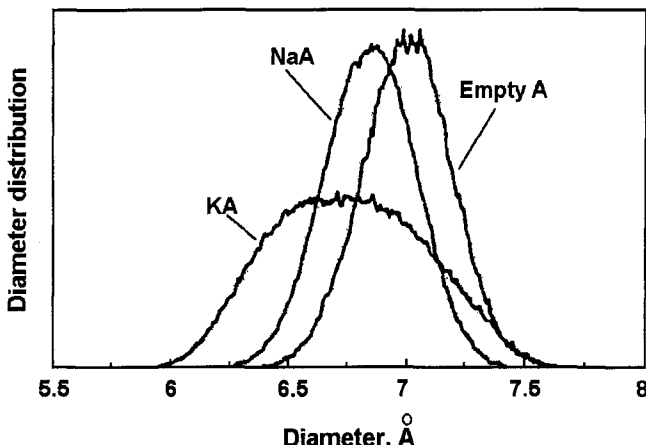


Figure 4 Window distribution function in zeolite A demonstrating the influence of two different cations. (From Ref. 19.)

much as 0.5 \AA .¹⁸ The zeolite aperture dimensions can also change considerably with ion exchange,¹⁹ as shown in Figure 4, or with isomorphous substitution.²⁰ This property may have considerable influence on the diffusion of adsorbates in zeolites. Molecular dynamics has also been applied in combination with data from experimental vibrational spectroscopy to derive more insight into the structure-spectra relationship for zeolites. For example, it has been shown that the band at 960 cm^{-1} in the infrared spectrum of TS-1 can be assigned to a localized Si–O vibration in Si–O–Ti bridges.²¹

Isomorphous Framework Substitution

The catalytic properties of zeolites can be influenced by rearranging the Si and Al atoms in the framework, modifying the Si/Al ratio, or by introducing other metal atoms into the framework (the latter is called isomorphous framework substitution). Knowledge of the location of the substitution site is desirable to better understand the catalytic behavior of substituted zeolites. This information is hard to obtain experimentally, so modeling studies have been devoted to isomorphous framework substitution. Some recent examples are given in Refs. 22–24.

ZSM-5 (Al-MFI) is used as a catalyst in petroleum refining, in the production of synthetic fuels, and in other petrochemical processes, whereas TS-1 (Ti-MFI) is applied as a catalyst in fine chemical processes.²⁵ The orthorhombic MFI structure exhibits 12 crystallographically unique tetrahedral sites. Calculations have been carried out on substitution preferences using classical as well as quantum models.^{21,26–30} In most studies 12 simulations were conducted, and in each run, one or more crystallographically equivalent sites of the subsequently crystallographically unique tetrahedral sites were substituted. Energy minimization and molecular dynamics techniques were employed to calculate

the energies of those substituted systems. In some studies, the unit cell parameters were used as preference criteria instead of the system energies. All investigations led to the same conclusion that there exists no clear substitution preference. Another study,³¹ to be discussed in some detail in the applications section, based on the MC method, led to the same result.

Framework Acidity

As mentioned in the Introduction, the zeolite structures are based on corner-sharing TO_4 tetrahedra, with T being a Si or Al atom, building a three-dimensional network. Brønsted acidity occurs if protons are present to compensate the negative charge of AlO_4^- tetrahedra. The protons are attached to the bridging oxygen species as shown in Figure 5. The acidity of zeolites is affected by framework structure, Si/Al ratio, and Al distribution and can be characterized experimentally by measuring the strength of the interaction between the protonated zeolite and a basic molecule. Numerous theoretical studies have been carried out to investigate one or more aspects of zeolite acidity, several examples of which follow.

Employing a classical model, Monte Carlo calculations were performed to investigate the Al distribution in zeolites.^{32–34} Si and Al atoms were randomly distributed over the tetrahedral sites, and in each step an attempt was made to interchange each Al with a nearby Si. Loewenstein's rule,³⁵ which forbids Al–O–Al bridging, was investigated, and results from the simulation indicate that the Al distribution in zeolite structures is generally in accordance with this rule.

Quantum mechanical approaches using a cluster approximation have been used extensively to determine proton affinities.^{36–38} The influence of the local composition on the structure and proton affinity of a zeolite was studied

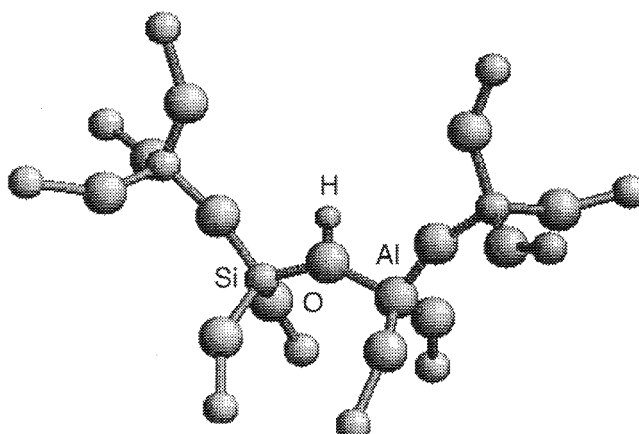


Figure 5 Zeolite cluster with proton located on the Si–O–Al bridge.

by energy minimization. Unfortunately, the cluster size influences the results, as does the extent of geometry optimization (i.e., whether the whole cluster or only the center of the cluster retains the resemblance of the cluster with a particular crystallographic site). These geometrical effects can be avoided in hybrid studies^{39,40} in which the acid site is described quantum mechanically and the surroundings with a force field, thereby accounting for long-range effects. The Car–Parrinello approach (discussed in a later section of that name) has also been applied to study proton affinities.⁴¹ The interaction of a base such as ammonia with zeolites, often used as an experimental probe, was modeled to obtain more insight into the acidic properties of zeolites.^{4,5,10}

Templates in Zeolites

In zeolite synthesis, organic molecules (e.g., tetraalkylammonium ions) are often used as structure directing agents. As the zeolite crystallizes, the organic molecules are trapped inside but can be removed via calcination to leave a micropore structure that derives its shape from the template. The exact relationship between zeolite and template is still under discussion, however. A better understanding of this templating phenomenon is of importance if one is to be able to synthesize particular zeolite frameworks by choosing the right templates. Determining the location and conformation of the organic molecules in the uncalcined materials is experimentally difficult, but molecular modeling can provide some insight concerning the host–guest interactions between zeolite and template (see Figure 6⁴²).

In all studies to date, these host–guest systems have been described classically. The framework was often kept fixed in the energy minimization, and initial configurations were obtained either by intuition or by the following two-step procedure: (1) a set of guest conformations is generated by means of a high temperature molecular dynamics run, and (2) a set of host–guest configurations is then created by docking the guest in a randomly selected conformation from the step (1) set at a random location in the host. An energy threshold is defined such that only energetically reasonable initial configurations are selected. This kind of calculation shows that templates can exhibit a favorable host–guest interaction energy, but it cannot explain why, for example, tetrabutylammonium (TBA) cations are in practice less effective templates in the synthesis of ZSM-5 than are tetrapropylammonium (TPA) cations, in spite of the more favorable host–guest interaction energy of TBA. Simulations in which more than one template are put into the zeolite framework show that template–template interactions also play an important role in imprinting. These interactions are discussed in more detail in the applications section, where the interactions of TPA and TBA templates in zeolites MFI and MEL are described. It is now established that an organic molecule is suitable to template a certain zeolite framework if it has a favorable host–guest interaction energy and if the organic molecules can be packed in the zeolite framework in a way that affords them a favorable guest–guest interaction energy.

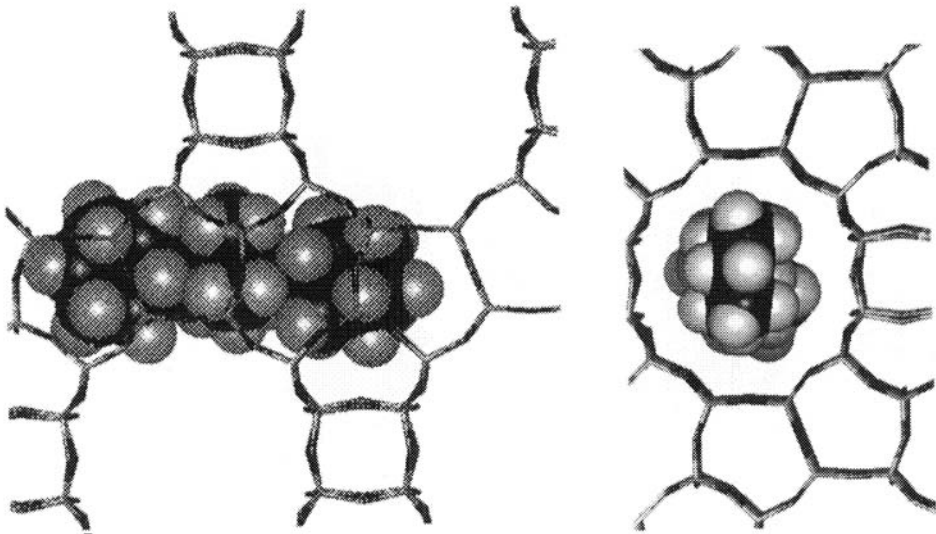


Figure 6 Geometry of the di(cyclohexylmethyl)dimethylammonium ion in zeolite beta.
From Ref. 42. Left: view along the *a*-axis of the crystal. Right: view along the *b*-axis of the crystal.

Initial configurations of more templates per unit cell can be created also by intuition or by a variation on the above-mentioned procedure as follows. Instead of a set of reasonable initial configurations containing one template per unit cell, only one initial configuration containing more than one template per unit cell is generated. One by one the templates are placed in the unit cell: a template is inserted into the zeolite framework in a random conformation at a random location. The energy of the configuration is calculated by taking into account host–guest as well as guest–guest interactions. The configuration is accepted if its energy is lower than a certain threshold; otherwise it is rejected and a new effort is made to insert the template. This process is repeated until the desired template loading (number of molecules per unit cell) has been reached. Then simulated annealing is applied to sample the whole configurational space, hopefully without getting trapped in a local energy minimum before the final energy minimization is done.⁴³

The knowledge obtained by studying known template–zeolite combinations was used by Willock et al. to develop a method to design new templates.⁴⁴ In their procedure, a template is allowed to grow in the zeolite framework, whereby a function based on overlap of van der Waals spheres is used to control the growth. New atoms are added to the template as fragments. In the beginning the configuration, conformation, and position of the template are manipulated in such a way that the template is located as far as possible from the framework to facilitate growth. When growth is no longer possible, the template is maneuvered into a position of optimum zeolite–template and template–template interaction. Energy minimization was one of the methods of manipulating the template using a classical or quantum mechanical description of the system. For example, TPA was successfully grown in ZSM-5.⁴⁴

Adsorption in Zeolites

Several computational approaches^{45–49} have been used to simulate binding of adsorbates in zeolites. To locate the preferred adsorption site, approaches similar to those used on templates in zeolites have been employed. Alternatively, Monte Carlo simulations can be carried out to study the adsorbate distribution in the zeolite and to calculate heats of adsorption. The adsorbates are allowed to move randomly in the zeolite framework, and the whole of configurational space is sampled. For small molecules, adsorption isotherms can be calculated with the grand-canonical Monte Carlo method,¹³ which allows the number of adsorbates in the zeolite to fluctuate. The determination of the heat of adsorption and the adsorption isotherm of larger adsorbates requires a special approach. Inserting a large molecule randomly into a zeolite often results in an energetically unfavorable configuration owing to overlap with the zeolite framework. Consequently, many MC steps are needed, not only to find a favorable configuration, but also to sample the whole configurational space. This sampling can become an endless task. The configurational bias MC method¹⁴ circumvents this problem by growing the adsorbate atom by atom in the micro-

pores, while avoiding overlap with the zeolite framework. By appropriate adjusting of the acceptance rules, it is possible to remove exactly the bias introduced by the growing. Molecular dynamics can also be used to assess the adsorbate distribution in a zeolite or to calculate heats of adsorption. Because the adsorbates are not allowed to move randomly in the zeolite, MD simulations generally take more computer time to sample an adequate amount of configuration space than MC simulations.

Diffusion in Zeolites

In principle, diffusion in zeolites can be studied directly with MD methods.^{2,3} Transport properties can be calculated, and an impression of how adsorbates migrate through the micropores can be obtained. A problem arises if the movements of the adsorbates are so small or rare that the system cannot be equilibrated in a reasonable amount of computer time. Most MD simulations, therefore, are on small adsorbates such as methane and Xe, which can be represented as spherical particles, or on small molecules like ethane and propane, with not too many rotational and internal degrees of freedom. Such studies have contributed to a better understanding of diffusion in zeolites. It has been shown that including the flexibility of the molecules can increase the diffusivity and that framework motions can also influence the behavior of the adsorbates. Furthermore, charge-compensating cations cannot be neglected.

In industry, however, zeolites are applied in catalytic and separation processes that involve larger and more complex molecules. Several alternative methods have been developed to study the behavior of these adsorbates in zeolites. A simple and cheap method is based on the construction of a “migration path” along which the adsorbate travels through the micropores of the zeolite. The adsorbate moves in steps along this predefined trajectory. At each step an energy minimization is carried out, resulting in a minimum energy profile that may be used to locate energy barriers. Benzene molecules in faujasite, for example, tend to hop from cage to cage rather than diffusing smoothly, because of the presence of energy barriers between the cages⁵⁰ (see Figure 7). Insight into shape selectivity may also be obtained if the assumption is made that the selectivity is controlled by translation diffusion. For example, the minimum energy profiles for diffusion of 2,6- and 2,7-dialkylnaphthalene were compared in several zeolites to evaluate which zeolite is selective toward the 2,6-isomer.⁵¹ Mordenite was shown to give the largest difference, and in practice mordenite does indeed show a preference for the 2,6-isomer.

Transition state theory can also be employed to calculate diffusion coefficients in hopping processes. Adsorbates prefer to reside at particular places in a zeolite and because an energy barrier is present between them, they do not transfer easily from one site to another. The possible adsorption sites are located via a Monte Carlo method, and the transition state via migration path analyses. A rate constant k_{ij} can be associated with jumps from site i to site j . A surface can be defined that separates sites i and j and contains the top of the energy

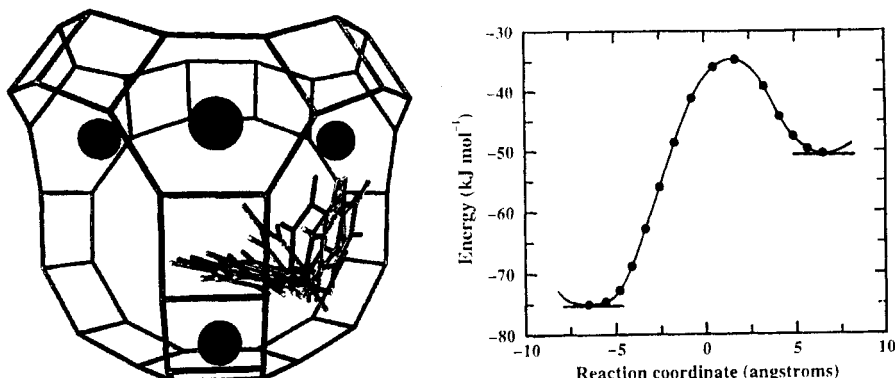


Figure 7 Migration path for benzene between sites S_{II} and W in faujasite and the energy profile along the migration path (reaction coordinate). Data from Ref. 50.

barrier, which can be considered to be the transition state between those sites. Rate constants can be then determined for all possible transitions in the lattice, which are then used to calculate the diffusion coefficient. In the original theory, the rate constants were obtained via a Monte Carlo technique, and the rate constant k_{ij} was assumed to be proportional to the ratio of the configuration integral of the dividing surface and site i . Dynamical corrections can be made from MD trajectories that start at the transition state. Initial configurations at the transition state are generated either via MC techniques or constrained reaction coordinate dynamics. Finally a kinetic Monte Carlo scheme⁵² is applied, whereby the zeolite framework is replaced by a three-dimensional lattice of adsorption sites to determine the diffusion coefficient. The molecules are allowed to hop randomly from site to site using the rate constants as frequency criteria. The diffusion coefficient is calculated from the mean-square displacements.^{53–55}

Zeolite-Catalyzed Reactions

Zeolites are applied on a large scale as solid acid catalysts in the petroleum and petrochemical industries; examples can be found in hydrocracking, fluidized catalytic cracking, catalytic dewaxing, aromatics processing, and reforming, and in the synthetic fuel area. Several computational studies have been carried out on these proton-catalyzed reactions.^{56–59} The methanol-to-gasoline (MTG) process has been investigated most extensively. Methanol is first dehydrated to form dimethyl ether, and subsequently olefins, aliphatics, and aromatics are formed. The reaction mechanism is still being debated, and many studies have been devoted to elucidating the first step in which methanol is adsorbed. No consensus has been reached yet on whether methanol is physisorbed, forming a hydrogen-bonded complex at a Brønsted acid site, or whether proton transfer occurs, yielding a chemisorbed methoxonium ion. We

Table 1 Zeolite Modeling Schemes

Application	Model/Method ^a							
	QM	CM	QM/CM	Cluster	Periodic	EM	MD	MC
Structure/dynamics	×	×		×	×	×	×	
Isomorphic substitution	×	×		×	×	×	×	×
Acidity	×	×	×	×	×	×	×	×
Template action		×			×	×		
Adsorption		×			×			×
Diffusion		×			×		×	
Reactivity	×		×	×	×	×	×	

^aQM, quantum mechanical model; CM, classical model; EM, energy minimization; MD, molecular dynamics; MC, Monte Carlo.

shall closely consider modeling results for the methanol–zeolite system in the section on applications.

Another important zeolite-catalyzed chemical reaction is the decomposition of NO. Cu-exchanged zeolites, especially Cu-ZSM-5, have been shown to catalyze the decomposition of NO_x in the presence of hydrocarbons and excess oxygen. The increasing awareness of the detrimental effects of automobile exhaust has prompted several theoretical studies on the active site and reaction mechanism.^{60–63} Cu-ZSM-5 was described using an empirical force field and energy minimization to locate the copper ions in ZSM-5. Isolated copper atoms and copper clusters were found in the micropores, mostly associated with framework aluminium species. A cluster of two copper ions bridged via an OH species not part of the zeolite framework (“extra-framework”) was proposed as the active site. Quantum mechanical cluster calculations were carried out to study the elementary steps in the NO_x decomposition. A single T-site model was used to represent the zeolite framework.

Table 1 gives a summary of the approaches applied in zeolite modeling.

MODELS

The choice of a theoretical model usually depends on the goals of the study, but sometimes other considerations, such as computer resources available, can also play a role in this selection process. A study of zeolite framework acidity or catalytic activity requires an explicit consideration of the electronic structure of the system, and quantum mechanical (QM) models are best suited for such investigations. Since the high CPU demands greatly limit the size of the systems that can be simulated with quantum mechanical models, the zeolite framework is often represented in these simulations by a cluster that presumably resembles the active site. The cluster approximation has the obvious drawback that influences of the crystal lattice are neglected.

Studies of adsorption and diffusion processes and of framework dynamics necessitate an explicit consideration of the periodicity of the system. For such studies, classical models involving force fields are generally used in which the interactions between the atoms in the system are represented by potential functions. The third class of models are hybrid models, which as mentioned previously try to combine the advantages of the quantum and classical approaches: explicit treatment of the electronic structure for certain parts of the system like the catalytic site and its direct environment, combined with a classical treatment of the rest of the system. Each of these models is now described in turn.

Quantum Mechanical Models

Wavefunction Model

Hartree–Fock (HF) theory⁶⁴ is the wavefunction model most often used to describe the electronic structure of atoms and molecules. When the Born–Oppenheimer approximation⁶⁴ can be made, one can find an approximation of the many-electron wavefunction Ψ of a system by a variety of quantum chemical methods. When Ψ is known, one calculates the expectation value A_{exp} of a quantity A from

$$A_{\text{exp}} = \frac{\int \Psi^* A \Psi dr}{\int \Psi^* \Psi dr} \quad [1]$$

where A denotes the operator for the quantity A . The many-electron wavefunction Ψ is sought as a solution of the time-independent Schrödinger equation

$$\mathbf{H}\Psi = E\Psi \quad [2]$$

where E is the electronic energy. In atomic units the Hamiltonian operator \mathbf{H} is given by

$$\mathbf{H} = -\frac{1}{2} \sum_i \nabla_i^2 - \sum_i \sum_A \frac{Z_A}{r_{iA}} + \sum_i \sum_{j>i} \frac{1}{r_{ij}} \quad [3]$$

The first term in Eq. [3] is the kinetic energy operator, the second term is the electron–nucleus attraction energy operator, and the third term stands for the electron–electron repulsion energy operator. In HF theory Eq. [2] is solved by means of the orbital approximation: (1) the many-electron wavefunction Ψ is represented with a determinant of one-electron wavefunctions ψ_i (Slater determinant) satisfying the antisymmetric behavior of the many-electron wavefunc-

tion; (2) the one-electron wavefunctions are written as a linear combination of atomic orbitals χ_k

$$\phi_i = \sum_{k=1}^m c_k^i \chi_k \quad [4]$$

where c_k^i are the expansion coefficients. The many-electron wavefunction Ψ is therefore defined by the set of the coefficients c_k^i . Use of the variational principle leads to a set of equations for the coefficients c_k^i that are solved iteratively [the self-consistent field (SCF) procedure]. A comprehensive discussion of Hartree–Fock theory is given in many quantum chemistry books including ones by McWeeny and Sutcliffe⁶⁴ and Pople and Beveridge.⁶⁵

The set of atomic orbitals $\{\chi_k\}$ is called a basis set, and the quality of the basis set will usually dictate the accuracy of the calculations.^{66a} For example, the interaction energy between an active site and an adsorbate molecule might be seriously overestimated because of excessive basis set superposition error (BSSE) if the number of atomic orbitals taken in Eq. [4] is too small.^{66b} Note that Hartree–Fock theory does not describe correlated electron motion. Models that go beyond the HF approximation and take electron correlation into account are termed post-Hartree–Fock models. Extensive reviews of post-HF models based on configurational interaction (CI) theory, Møller–Plesset (MP) perturbation theory, and coupled-cluster theory can be found in other chapters of this series.⁶⁷

Electron Density Model

Another model that describes the electronic structure of a system is provided by density functional theory (DFT).^{68,69} In DFT the electron density ρ of the system in the ground state plays the role of the many-electron wavefunction Ψ in the wavefunction model because it uniquely defines all ground state properties of a system.⁷⁰ An advantage of DFT is that Ψ , which is a function of both spatial and spin coordinates of all electrons in the system, is replaced by a function that depends only on a position in Cartesian space: $\rho = \rho(\mathbf{r})$. The electron density can be obtained by using the variational principle

$$\delta \left(E[\nu, \rho] - \mu \left(\int d\mathbf{r} \rho \nu - N \right) \right) = 0 \quad [5]$$

where ρ , ν , and μ stand for the electron density, nuclear–electron attraction potential, and Lagrange multiplier, respectively. The latter is used to preserve the number of electrons in the system and is in fact the chemical potential of the system.⁶⁸ $E[\nu, \rho]$ is a functional of both the electron density and the external potential. It is defined^{68,69} as

$$E[\rho, \nu] = T[\rho] + V_{ee}[\rho] + \int d\mathbf{r} \rho(\mathbf{r}) \nu(\mathbf{r}) \quad [6]$$

where $T[\rho]$ is the kinetic energy and $V_{ee}[\rho]$ is the electron–electron interaction energy comprising both the exchange-correlation energy and the Coulombic energy. The last term in Eq. [6] describes the interaction between the electron density and the electrostatic potential of the nuclei.

The electron density is generally represented as a sum of squares of occupied orthonormal orbitals called Kohn–Sham orbitals.⁷¹ The use of these orbitals leads to a set of equations that are solved iteratively. The orbitals are defined with a linear combination of basis functions, comparable to Eq. [4]. Note that the Kohn–Sham orbitals are not the DFT analogy of the HF orbitals ψ although the basis sets for both may be of the same functional form. The Kohn–Sham orbitals are a functional representation of the electron density, and they therefore cannot be viewed as effective orbitals.

Different DFT models apply different approximations for the $T[\rho]$ and $V_{ee}[\rho]$ functionals. Thus, the local density approximation (LDA) implies that for a density $\rho(\mathbf{r})$ the kinetic energy and exchange-correlation energy functionals in each point of the space \mathbf{r} are those of a homogeneous electronic system of the same density. For a discussion of these different DFT models, we refer the interested reader to earlier chapters in this series^{69,72} and to the indispensable book by Parr and Yang.⁶⁸

Semiempirical Models

In the discussion of the quantum mechanical models, it was implicitly assumed that the calculations with these models are carried out without simplifications. Such an approach is known as a first-principles or ab initio method. Simplifications in the equations of both HF and DF theory result in so-called semiempirical models. A common approach is to consider only valence electrons. Moreover, some of the terms in the Hamiltonian are either neglected (those that are believed not to contribute significantly to the properties of interest) or parameterized to ab initio or experimental data. A detailed discussion on semiempirical models is given elsewhere in this series.^{73,74}

A semiempirical model that has been particularly useful in zeolite studies is known as the electronegativity equalization method (EEM).⁷⁵ EEM is based on the following assumptions: (1) the electron density can be partitioned into spherical atomic contributions; (2) $T[\rho]$ and $V_{ee}[\rho]$ in Eq. [6] can be written as a second-order Taylor expansion of the effective charges; and (3) each atom i carries an effective charge $q_i = Z_i - N_i$, where Z_i and N_i are the charge on the nucleus and the number of electrons in the atom, respectively. Then the total energy is given⁷⁵ by:

$$E = \sum_{i=1}^N \left[E_i^* + \chi_i^* q_i + \eta_i^* q_i^2 + \frac{1}{2} \sum_{j \neq i}^N \frac{q_i q_j}{r_{ij}} \right] \quad [7]$$

where E_i^* , χ_i^* , and η_i^* are coefficients of the Taylor expansion. The χ_i^* and η_i^* are called the electronegativity and the hardness of a neutral atom in a molecule, respectively.

The partial derivatives of Eq. [7] with respect to the atomic charges q_i define the electronegativities χ_i of the atoms in the molecule. Sanderson's electronegativity equalization principle,⁷⁶ proven by DFT to be correct, states that $\chi_1 = \chi_2 = \dots = \chi_N = \bar{\chi}$, where $\bar{\chi}$ is the global molecular electronegativity.^{68,69} This results in a set of N equations for N atomic charges q_i and the global electronegativity of the system $\bar{\chi}$:

$$\bar{\chi} = \chi_i = \chi_i^* + 2\eta_i^* q_i + \sum_{j \neq i}^N \frac{q_j}{r_{ij}}, \quad i = 1, \dots, N \quad [8]$$

The missing equation necessary to find the charges and the global electronegativity is

$$\sum_{i=1}^N q_i = Q \quad [9]$$

where Q is the total charge of the system. Equations [8] and [9] can be rewritten in an $(N + 1) \times (N + 1)$ matrix equation:

$$\mathbf{A} \cdot \mathbf{q} = \mathbf{b} \quad [10]$$

where

$$\mathbf{A} = \begin{vmatrix} 2\eta_1^* & 1/r_{12} & \cdots & -1 \\ 1/r_{21} & 2\eta_2^* & \cdots & -1 \\ \vdots & \vdots & \ddots & \vdots \\ 1/r_{N1} & 1/r_{N2} & \cdots & -1 \\ 1 & 1 & \cdots & 0 \end{vmatrix}, \quad \mathbf{q} = \begin{pmatrix} q_1 \\ q_2 \\ \vdots \\ q_N \\ \bar{\chi} \end{pmatrix}, \quad \text{and } \mathbf{b} = \begin{pmatrix} -\chi_1^* \\ -\chi_2^* \\ \vdots \\ -\chi_N^* \\ Q \end{pmatrix}$$

Obviously, the charges are geometry dependent because of the last term in Eq. [8]. The EEM scheme derived for a molecule can be extended to macromolecular systems where equilibration of electronegativities occurs within parts of the system rather than in the system as a whole.⁷⁷ Such an extension leads to an $(N + M) \times (N + M)$ matrix equation, where N is the total number of atoms and M the number of separate parts in the system. Equation [8] can also be adapted to include the long-range character of the electrostatic interactions and the periodicity of zeolite structures.

The *atomic* parameters χ_i^* and η_i^* are usually calibrated to represent atomic charges calculated with ab initio QM methods. Mulliken charges⁷⁸ are generally used, although charges calculated with other partitioning schemes

(e.g., electrostatic potential derived charges) may also be chosen.⁷⁹ An extension of EEM called charge sensitivity analysis (CSA) is a promising development described in detail elsewhere.^{80,81}

A model related to EEM has been proposed by Rappé and Goddard⁸² and is called the charge equilibration method (QEeq). The main difference between EEM and QEeq lies in the treatment of the electrostatic interactions. In EEM these interactions are calculated using the point charge approximation assuming a $1/r$ dependence for the interaction energy, whereas in QEeq the interactions are calculated between ns Slater orbitals ($n = 1, 2, \dots$):

$$U_{\text{el}}(r) = \iint dr_i dr_j \phi^2(r_i) \frac{1}{|r_i - r_j - r|} \phi^2(r_j) \quad [11]$$

where r_i and r_j are the coordinates of atoms i and j , and

$$\phi(r) = N_n r^{n-1} e^{-\zeta r} \quad [12]$$

The orbital exponent ζ is related to the atomic covalent radius. In QEeq the value of parameter ζ for hydrogen depends on the charge on the H atom, a dependence that makes QEeq iterative, unlike EEM.

An extension of the EEM scheme proposed in 1998 that keeps the computational simplicity of the method while introducing a physically more correct description of the electrostatic interactions, similar to that in QEeq.^{79,93} This is achieved by substituting the $1/r$ dependence of the Coulomb law by

$$\frac{1}{(r^3 + 1/\gamma_{ij}^3)^{1/3}} \quad [13]$$

where $\gamma_{ij} = \sqrt{\gamma_{ii}\gamma_{jj}}$. The γ_{ii} parameters are added to the calibration procedure of the EEM scheme.

Potential Models for Framework Modeling

Owing to the complexity of zeolitic systems, most computational studies are still performed with the help of classical models. These methods use a set of potential functions to describe the potential energy surface (PES) in a many-dimensional space of geometrical parameters of the system. Although the PES can be tested in terms of observables such as equilibrium atom positions, vibrational frequencies, heats of formation, and other experimental information, the PES itself is not an observable quantity. Because of that, there is no unique representation of the PES, and several coordinate systems and parameteriza-

tions can be used to describe it. This point is of particular importance because the use of different coordinates implies a certain model of bonding. A specific representation of the potential energy in the system, i.e., a set of used potential functions together with their parameters, is therefore termed a “potential model.”

An early potential model used for zeolite framework modeling corresponds to a central force field model and was developed by Demontis et al.⁸⁴ In this model the framework potential energy U is expanded in a Taylor series with respect to interatomic distances

$$U = U_0 + \frac{1}{2} \sum_i \sum_{j \neq i} \sum_{k=2}^{\infty} \frac{1}{k!} \left(\frac{\partial^k U}{\partial r_{ij}^k} \right)_0 (r_{ij} - r_{ij}^0)^k \quad [14]$$

where r_{ij}^0 is the equilibrium value of the distance between atoms i and j . Only T–O and O–O interactions between the nearest atoms (T means a tetrahedrally coordinated atom, e.g., Si), and cation–oxygen interactions are considered in the harmonic ($k = 2$) and anharmonic ($k \geq 2$) versions of the force field.⁸⁴ The model has been widely employed in MD studies of zeolites.⁹ Although the force field reproduces the structure of zeolites well, the framework dynamics is described only approximately. This deficiency exists because atoms in a structure are kept at correct positions via a network of the T–O and O–O harmonic (or anharmonic) springs but fail to reproduce interactions relevant to the system dynamics. Later the model was extended, while retaining its central force field character, by changing the potential functions for specific interactions and by introducing additional terms for Si–Si nearest neighbors and electrostatic interactions.⁸⁵

Another early potential assumes that the character of the bonds in zeolite lattices is largely ionic and in line with a force field used for simulations of ionic solids, the potential energy is written in the form

$$U = \frac{1}{2} \sum_i \sum_{j \neq i} \left[A_{ij} \exp(-b_{ij} r_{ij}) - \frac{C_{ij}}{r_{ij}^6} + \frac{q_i q_j}{r_{ij}} \right] \quad [15]$$

Equation [15] is often referred as a rigid ion potential model.

An improvement of the rigid ion model is a shell model that describes an anion O^{-n} as a composite entity consisting of a positively charged core surrounded by a massless shell. The latter carries a negative charge and the total charge of the anion (the sum of the core and shell charges) is often constrained to a formal charge on an oxygen atom in a solid. The shell is considered to interact with its core via a harmonic spring, and the potential energy of a solid is then written as

$$U = \frac{1}{2} \sum_i \sum_{j \neq i} \left[A_{ij} \exp(-b_{ij} r_{ij}) - \frac{C_{ij}}{r_{ij}^6} \right] + \frac{1}{2} \sum_i \sum_{j \neq i} \frac{q_i q_j}{r_{ij}} + \sum_i K_i (r_i^{\text{core}} - r_i^{\text{shell}})^2 \quad [16]$$

In the first sum, indices i and j denote shells and cations, the second term runs over all point charges in the system, and the third term accounts for interactions of the shells with their cores. The shell model takes into account the polarization of the anions by the crystal field of the solid, which is an important feature. To better reproduce the characteristics of systems with partly covalent bonds, such as zeolites, Eqs. [15] and [16] are supplemented with a term

$$U = \frac{1}{2} \sum K_\theta (\theta - \theta_0)^2 \quad [17]$$

where θ represents the O–T–O and/or T–O–T bond angles. The shell coordinates of the oxygen atoms are used to compute the angles.

Both the rigid ion and shell potential models have been used in energy minimization studies of dense and microporous silica and molecular sieves. Kramer and coworkers^{86,87} reported parameters of the rigid ion potential model for silicates, aluminosilicates, and aluminophosphates. The model also includes parameters for extra-framework cations such as Na^+ and Cl^- . Both the rigid ion and shell models were used by Catlow and coworkers in modeling silicate and zeolite structures.^{88,89}

Another family of potential models takes into account the covalent character of chemical bonds in zeolite lattices more explicitly and uses for the PES representation a set of potential functions like those employed in molecular mechanics (MM) force fields for organic molecules. Such a force field describes the potential energy of the system in two terms:

$$U = U_I + U_S \quad [18]$$

where U_I is geometry independent and is composed of bond energy increments and some corrections,^{90,91} such as for the presence of the high energy conformations. Because the U_I term is geometry independent, it does not affect the dynamic characteristics of the system. The U_S part is often called the steric energy. In a typical MM force field, an expression for the steric energy reads

$$U_S = \sum U_{\text{bonds}} + \sum U_{\text{angles}} + \sum U_{\text{torsions}} + \sum U_{\text{cross}} + \sum U_{\text{nonbond}} \quad [19]$$

The first four terms on the right-hand side of Eq. [19] are termed the valence part of a force field and are intended to describe interactions among covalently bonded atoms. Therefore, these terms are written as functions of the bond

lengths, bond angles, and dihedral angles. The last sum in Eq. [19] accounts for interactions between nonbonded atoms, and it is usually assumed to have pairwise additivity. The nonbonded interactions are represented via Eq. [15] or by a sum of the Lennard-Jones,

$$U_{\text{LJ}} = \frac{1}{2} \sum_i \sum_{j \neq i} \left(\frac{A_{\alpha_i \alpha_j}}{r_{ij}^m} - \frac{B_{\alpha_i \alpha_j}}{r_{ij}^n} \right) \quad [20]$$

and Coulombic potentials. Typically, $m = 12$ and $n = 6$. In most MM force fields the nonbonded sum excludes 1-2 and 1-3 interactions, since these are already included in the valence part.

The main advantages of MM force field models are that the terms in the potential energy representation correlate with the usual chemical intuition and that such models can easily be combined with force fields for modeling organic molecules. The latter permits the use of a consistent approach for calculation of sorbate–zeolite systems. A drawback is that a large number of parameters must be determined on the basis of either experimental information or quantum chemical calculations (or by a combination of both).

In the early 1990s, Nicholas and coworkers proposed an MM force field for modeling siliceous zeolites.⁹² In their model the framework steric energy was described as a sum of a harmonic Si–O bond term, O–Si–O and Si–O–Si angle bending terms, and an Si–O–Si–O dihedral angle term. The Lennard-Jones (12-6) and Coulombic terms represented nonbonded interactions. Their force field was successfully applied for calculation of the structures and infrared spectra of the siliceous sodalite and silicalite lattices.⁹²

Simultaneously, de Vos Burchart and van de Graaf constructed a molecular mechanics force field for modeling silicate structures.⁹³ The Si–O bond potential was described by a Morse function, whereas a Urey–Bradley term

$$U = \frac{1}{2} F_{13} (r_{13} - r_{13}^0)^2, \quad r_{13} = r_{\text{O–O}}, r_{\text{Si–Si}} \quad [21]$$

was used for 1-3 interactions rather than the angle-bending harmonic function of Eq. [17]. The exp-6 and Coulombic terms (Eq. [15]) described the nonbonded interactions. This attempt resulted in a force field capable of reproducing and predicting the structures and relative stabilities of dense silicate and silica zeolite lattices. The vibrational spectra were also reproduced quite satisfactorily. Later on, this force field was extended to aluminosilicates and phosphates.⁹⁴

At normal temperatures the lattice dynamics involves predominantly low amplitude atomic motions that are well described in a harmonic approximation. Therefore, potential models widely used in the theory of molecular vibration, such as a generalized valence force field (GVFF) model,⁹⁵ may be of use for such studies. In a GVFF the potential energy of a system is described with a set

of internal coordinates Λ (bonds, bond angles, dihedral angles) and has the form

$$U = \frac{1}{2} \sum_i \sum_j F_{ij} (\lambda_i - \lambda_i^0)(\lambda_j - \lambda_j^0) \quad [22]$$

where λ_i^0 is the equilibrium value of the internal coordinate λ_i . Versions of GVFF are often used as a valence part of MM force fields. The main advantages of this model are its simplicity and low computational cost, since no long-range interactions are explicitly taken into account. In addition, the values of force constants F_{ij} can be taken from normal mode analysis (NMA) of related molecules. On the other hand, the harmonic approximation employed in this model restricts the possibility of studying structural changes in a system due to temperature changes. Therefore, this model is mostly employed for studying the framework dynamics (see below).

An empirical set of GVFF parameters for dense silicate structures has been proposed by Etchepare et al.⁹⁶ and another empirical parameterization of GVFF was proposed by Creighton et al.⁹⁷ Recently, Bärtsch et al.⁹⁸ derived values of force constants in Eq. [22] on the basis of experimental spectra of the $H_8Si_8O_{12}$ molecule and its deuterio-substituted derivative. Dropping the off-diagonal and torsional terms in Eq. [22] leads to a simplified version of the GVFF. Such a model was used by Deem et al. [18] in a study of zeolite aperture dynamics and by Smirnov and Bougeard⁹⁹ in an MD simulation of zeolite vibrational spectra. This simplified model was shown to reproduce well both infrared and Raman spectra of a number of silica zeolite structures with the use of only three force constants, and it was subsequently extended to aluminosilicate structures.¹⁰⁰

It is worthy of note that in MD studies of zeolites, the use of Eq. [17] for the T–O–T angle-bend potential conceals a pitfall as a result of the high degree of flexibility of these angles. Indeed, defining the T_1 –O– T_2 angle θ via $\theta = \arccos(\cos \theta)$ where

$$\cos \theta = \frac{\mathbf{r}_{OT_1} \cdot \mathbf{r}_{OT_2}}{|\mathbf{r}_{OT_1}| |\mathbf{r}_{OT_2}|}$$

one obtains

$$\frac{\partial \theta}{\partial \alpha_i} \propto \frac{1}{\sin \theta}, \quad \alpha = x, y, z, \quad i = T_1, O, T_2$$

and therefore the use of Eq. [17] leads to an infinite force as the angle approaches 180° . To avoid this result, one can use a cosine harmonic form for the T–O–T potential¹⁰¹

$$U_{\text{TOT}} = \frac{1}{2} C_\theta (\cos \theta - \cos \theta_0)^2 \quad [23]$$

where $C_\theta = K_\theta / \sin^2 \theta_0$, instead of the angle harmonic term of Eq. [17]. Such a form of the potential allows the linearity of the T-O-T angle.

So far there is no unambiguous answer to the question of which potential model is best suited for zeolite modeling. Moreover, there are many parameter sets for each of the potential models described above, though it would be highly desirable to define a unique set for a particular model. In the case of the rigid ion or shell models, comparison of different parameterizations is complicated by the use of either formal or partial charges for the atoms. Furthermore, values of parameters are often biased by the set of experimental data used in the fitting procedure. Use of different functional forms for specific interactions in MM force fields makes such a comparison difficult as well. Perhaps such a comparison can succeed only for a GVFF model with its simple form of the potential functions. Table 2 lists values for a set of selected force constants used in calculation of silicate structures: even in these structures, values of force constants vary from 15% for the Si-O stretching force constant to more than 300% for the O-Si/Si-O and Si-O/O-Si interaction force constants.

The example above reflects a fundamental problem for force field models that make use of internal coordinates to describe the PES of a system. The problem arises because some of the internal coordinates (mainly the angle-bending and torsional coordinates) can be represented as linear combinations of others, and thus the complete set of internal coordinates is *redundant*. One cannot say *a priori* which of the coordinates are more important for the “proper” description of the PES, and one is unable to separate the contributions of the corresponding terms to the steric energy in a simple way.

In the GVFF model used in NMA of molecules, the problem of redundancy is solved by the choice of independent linear combinations of the internal coordinates. This choice permits one to work with well-defined (nonredundant) sets of the coordinates and corresponding force constants, even though they may not reflect our view of the physics of the interatomic interactions in the system. If we wish to use the knowledge about the chemical bonding in the

Table 2 Values of Some Force Constants Used in Different Parameterizations of the GVFF Model (Eq. [22]) for Silicates

Force Constant	96	98	97
F_{SiO} , mdyn/Å	5.94	5.10	4.468
F_{OSiO} , mdyn·Å/rad ²	0.729	0.948	1.416
$F_{\text{Osi/Sio}}$, mdyn/Å	0.711	0.153	0.591
$F_{\text{SiO/osi}}$, mdyn/Å	0.843	0.275	
F_{SiOSi} , mdyn·Å/rad ²	0.126	0.091	

system, the force constants corresponding to specific internal coordinates will need to be determined from those obtained for the set of nonredundant coordinates. The task of finding these unknowns is usually complicated by the fact that the number of unknown force constants exceeds the number of equations available and, therefore, some of the unknowns must be assumed a priori to be equal to zero. Only experience (or a sufficiently large information database on related structures) can reveal whether the appropriate choice was made. The freedom in choosing the force constants to be set to zero leads to different values of the remaining force constants, as illustrated in Table 2. An additional problem appears because one can design several sets of the linearly independent coordinates from the given set of internal coordinates.

Until recently, the choice of parameters for potential functions was based mostly on empirical information. Significant developments in both computer hardware and quantum chemical calculation software during the past decade have made possible derivation of the force field parameters from first-principles calculations.¹⁰²

Kramer and co-workers⁸⁶ used ab initio calculations of H_4TO_4 ($T = Si, Al, P$) clusters to derive parameters for the rigid ion potential model. The potential energy surface of the clusters was scanned along two modes of distortion, and the resulting potential curves were fitted using Eq. [15]. The set of parameters was refined by the use of experimental data on α -quartz. This procedure resulted in a parameterization that well reproduced both structure and elastic moduli of silicates, aluminosilicates, and aluminophosphates. Subsequently, this approach was extended to protonated forms of zeolites.⁸⁷

De Boer and coworkers^{103,104} parameterized the shell model for silica polymorphs on the results of ab initio calculations of the potential energy surfaces, polarizabilities, and dipole moments of $Si(OH)_4$ and $(OH)_3Si-O(H)-Si(OH)_3$ clusters. The structural characteristics and elastic moduli calculated with this set of parameters for three structures compared well with results computed with the use of both the rigid ion⁸⁶ and the empirical shell models.⁸⁹

Parameters for MM and shell potential models have been recently derived on the basis of ab initio calculations by Hill and Sauer^{105,106} and by Schröder and Sauer.¹⁰⁷ The authors used a wide range of molecular models representing principal building blocks of zeolite structures ranging from disilicic acid $Si_2O_7H_6$ to the sodalite cage $Si_{24}O_{60}H_{24}$. Some of these molecules were used as a “training set” and computed at the Hartree–Fock level with a high quality basis set. The potential energy surface computed by distortion of these structures was then fitted by a set of molecular mechanics force field potential functions of Eq. [19]. The parameters derived were first tested by computing structures of the molecules that were not included in the “training set” and then by optimization of periodic models of zeolites and related crystals. Molecular mechanics force field parameters for dense and microporous silicates were obtained,¹⁰⁵ and subsequently the force field was extended to protonated aluminosilicate structures.¹⁰⁶ In its final version, the force field contained as

many as 336 adjusted parameters.¹⁰⁶ As a specific feature, the potential model included a scheme that uses geometry-dependent charges, which were calculated as follows:

$$q_i = \sum_{j=1}^{N_{\text{bonds on } i}} \delta_{ij}(r_{ij} - r_{ij}^0) - \delta_{ij}^0 \quad [24]$$

where δ_{ij} and δ_{ij}^0 are bond parameters, and r_{ij}^0 is an equilibrium value of the bond length between atoms i and j . The force field reproduced all-silica zeolite structures with an average error of 3%. Results obtained for protonated aluminosilicates were shown to be compatible with the experimental observations.

In an additional refinement, Schröder and Sauer carried out a parameterization of the shell model on the basis of ab initio data.¹⁰⁷ This model turned out to be more flexible than the MM force field in the description of the structure of the H-forms of zeolites. In addition, the authors¹⁰⁷ note that the vibrational spectra are substantially better simulated with the ab initio shell model potential than with the ab initio MM force fields.

Parameters of GVFF for silicates and aluminosilicates obtained from first-principles calculations were reported by Ermoshin et al.^{108,109} Having assumed that the dynamics of zeolite lattices can be described in terms of vibrations of the TO_4 tetrahedra ($\text{T} = \text{Si}, \text{Al}$) and shared $\text{O}_3\text{T}-\text{O}(\text{H})-\text{TO}_3$ tetrahedra, the authors calculated the matrix of second derivatives of the total energy in Cartesian coordinates, the Hessian matrix \mathbf{H} , for molecular models of such units. The matrix \mathbf{H} was then transformed¹¹⁰ into a matrix of force constants in internal coordinates \mathbf{F}

$$\mathbf{F} = \tilde{\mathbf{B}}^{-1} \mathbf{H} \mathbf{B}^{-1} \quad [25]$$

where matrix \mathbf{B} relates to the Cartesian displacement coordinates \mathbf{s} and the internal coordinates $\mathbf{\Lambda}$ (thus $\mathbf{\Lambda} = \mathbf{B} \cdot \mathbf{s}$), and the tilde signifies the transpose. Values of the force constants computed at the Hartree–Fock level with a 3-21G* basis set were corrected for systematic errors by reference calculations with a double-zeta basis at the second-order Moller–Plesset (MP2) level. Force constants obtained for silicate structures turned out to be close to those derived by Bärtsch et al.⁹⁸ Unconstrained geometry optimization showed useful correlations between the equilibrium values of the internal coordinates and the force constants: for example, between values of the T–O bond length and the T–O stretching force constant (Badger's rule¹¹¹). Application of the force field to the calculation of the vibrational spectra of siliceous and aluminated zeolite structures has shown that below 1000 cm⁻¹ the force field reproduces experimental positions of bands in the IR and Raman spectra with a mean-square error less than 16 cm⁻¹.

As a summary, Table 3 gathers potential models used in modeling the zeolite frameworks with their corresponding references.

Table 3 Potential Models Used in Zeolite Framework Modeling

Potential Model	Eq.	Parameterization	Ref.	Method ^a
Central FF	[14]	Empirical	84	MD
		Empirical	85	MD
Rigid ion	[15]	Ab initio	86	Energy minimization
		Ab initio	87	Energy minimization
Shell model	[16]	Empirical	89	Energy minimization
		Ab initio	103, 104	Energy minimization
		Ab initio	107	Energy minimization
		Ab initio	105, 106	Energy minimization
MMFF	[22]	Empirical	92	Energy minimization, MD, NMA
		Empirical	93, 94	Energy minimization
GVFF	[22]	Ab initio	96	NMA
		Empirical	97	NMA
		Empirical	98	NMA
		Ab initio	108, 109	MD

^aMD, molecular dynamics; NMA, normal mode analysis.

Force Field Models with Geometry-Dependent Charges

One of the deficiencies of the force fields in use today is that they commonly use the fixed charge approximation, whereas in reality the atomic charges vary in response to changes of both the molecular conformation and the environment. Obviously, a scheme with geometry-dependent charges would extend capabilities of the force field methods.

One of the force fields with geometry-dependent charges was mentioned above. A model with such charges (Eq. [24]) was employed by Hill and Sauer¹⁰⁶ within the ab initio parameterized MM force field model for protonated aluminosilicates. Deficiencies of the scheme originate from the absence of a solid theoretical background for the model; it is just a first-order Taylor expansion of atomic charges with respect to distances between bonded atoms, and it neglects the influence of the environment. In addition, its parameterization is hampered by the use of bond rather than atomic parameters.

In 1996 a force field model was proposed in which geometry-dependent charges are calculated by EEM.¹¹² This model, called consistent implementation of the electronegativity equalization method (CIEEM), combines a force field representation for the PES (e.g., Eq. [19]) with the EEM equation for the electronic energy (Eq. [7]) in such a way that the atomic terms of Eq. [7] explicitly enter the expression for the potential energy. Thus, within the CIEEM, the expression for the steric energy in the MM force field model will read

$$U_S = \sum_{i=1}^N [\chi_i^* q_i + \eta_i^* q_i^2] + \frac{1}{2} \sum_{i=1}^N \sum_{j \neq i}^N \frac{q_i q_j}{r_{ij}} + U_{NC} \quad [26]$$

In Eq. [26] U_{NC} is the potential energy that includes all charge-independent terms in Eq. [19]. Such a modification will, of course, make a reparameterization of the force field necessary. Now the atomic charges can be computed by means of Eq. [10] and then used in Eq. [26] to calculate an interaction energy.

CIEEM is straightforward to implement in a Monte Carlo method. In such calculations, the atomic charges derived by the EEM for a new geometry of the system are used to compute the intermolecular energy (Eq. [26]). When used in energy minimization or molecular dynamics calculations, Eq. [26] leads to a very modest increase in computational overhead, as we shall see. Also note that CIEEM allows charge sensitivity analysis to be applied to the results of the calculations.

Hybrid Models

The hybrid approach is a combination of the QM and classical models: a QM cluster is embedded in a non-QM environment. A detailed description of this approach, which was developed to include long-range effects in the cluster approximation, appeared earlier in this series.¹¹ Here some basic considerations are discussed.

Factors influencing the outcome of hybrid modeling include the scheme for division of the system into a quantum and a classical mechanical region, the theoretical models employed for both regions, the compatibility of the two models, the coupling of the regions, and the level of embedding. To save computer time, it is advantageous to make the quantum mechanical region as small as possible, but attention must be paid to ensuring that all features influencing the chemical reaction directly are included. The models employed should be consistent and applicable to the system of interest. A reasonable choice, for example, might be a force field that is parameterized using QM data obtained from calculations at the level of theory that is used to describe the reactive center. When the system is divided in such a way that chemical bonds extend across the border between the regions, problems might occur if the regions are not properly linked with one other. The linkage can be described either by adjusting the atomic orbitals on the atom in the classical mechanical region or by introducing a so-called link atom. The latter approach is commonly used in studies on zeolite-catalyzed chemical reactions.

Link atoms are used to terminate the cluster and are treated explicitly in the quantum mechanical part. They are however invisible to the classical mechanical part. Hydrogen atoms are often employed as link atoms. There are several possibilities for placement of the link atom: (1) fixed distance between the link atom and the quantum mechanical atom and a fixed bond length between the two real atoms of the system, (2) link atom on the bond plus fixed distance between the link atom and the quantum mechanical atom, (3) link atom on the bond, and (4) freely moving link atom. Careful bookkeeping is important to keep track of all the interactions between the regions.

Finally, there are three levels of embedding, of increasing sophistication to be considered: (1) mechanical embedding, where the interactions between the regions are restricted to classical bonded and nonbonded forces; (2) electrostatic embedding, which includes electrostatic interactions between the regions and allows polarization of the quantum mechanical region due to its surroundings, and (3) classical mechanical polarization, in which the electrostatic effects of the quantum mechanical region on the classical mechanical region are also accounted for.

METHODS

Structure and Periodicity

In all modeling studies, one needs a starting three-dimensional geometry. These geometries can be constructed with the information given in the *Atlas of Zeolite Structure Types*, a compilation of different internationally recognized zeolite framework types.¹ New structure types can be found on the World Wide Web site (<http://www-iza-sc.csb.yale.edu/IZA-SC/>). Generally, the structures are provided in unit cell fractional coordinates. Most computational software uses Cartesian coordinates, so one has to convert the fractional coordinates f to Cartesian coordinates r . This is done by multiplying the fractional coordinates with a transformation matrix T

$$r = T \cdot f \quad \text{and} \quad f = T^{-1} \cdot r \quad [27]$$

The Cartesian coordinate system is usually chosen such that the z axis and the yz plane are parallel to the c axis and the b axis of the crystal lattice, respectively. Then the elements of T are given by

$$T = \begin{pmatrix} a \sin \beta \sin \phi & 0 & 0 \\ a \sin \beta \cos \phi & b \sin \alpha & 0 \\ a \cos \beta & b \cos \alpha & c \end{pmatrix} \quad [28]$$

in which $\phi = \arccos[(\cos \gamma - \cos \alpha \cos \beta)/\sin \alpha \sin \beta]$ and a, b, c , and α, β, γ are the crystallographic lattice parameters, respectively.

There exist several ways to treat the zeolite framework structure in modeling. One can take into account either the periodicity of the full lattice or only a small part of the lattice, the latter sometimes being called the cluster approach. The cluster approach is often used in quantum chemistry studies because it requires less computer time. As long as specific properties connected with the framework topology (e.g., the dimensions of the channels) are not dominating the outcome of the calculations, this approach can provide valuable informa-

tion about zeolite acidity and zeolite catalysis, for example. If one wishes to take into account the full periodicity of the framework, limited computer performance compels one to restrict the number of atoms N used in modeling to a few thousands. This implies that the atoms in one or more zeolite unit cells are to be explicitly considered as a central simulation box, while the complete spatial periodicity of the solid is modeled by so-called periodic boundary conditions (PBC). The PBC replicate the central cell throughout space to form an “infinite” lattice: the atoms are in the same position in each image of the original box. If an atom leaves the central cell during a simulation, one of its images enters the box from an opposite side to conserve mass. One should realize that the use of PBC imposes some restrictions on the properties calculated in the simulation. Thus, structural characteristics cannot be computed at distances that exceed the length of a cell side, and no lattice vibrations with wavelength below a certain value can be reproduced in the simulation (see below).

Further, one has to decide whether to keep the framework fixed—the rigid framework approximation—or to treat the framework as flexible. The rigid framework approximation is, for reasons of computer time, often used in molecular dynamics and Monte Carlo studies, whereas for less CPU-intensive energy minimization studies the framework is usually treated as flexible.

In the flexible framework approach, one can, in principle, restrict the independent coordinates to the Cartesian coordinates of the atoms and keep the lattice parameters fixed. In general, however, one would also like to relax the lattice parameters. In energy minimization, one can use the six nonzero elements of T (Eq. [28]) as independent variables instead of the lattice parameters themselves.¹¹³ The advantage is that the first and second derivatives of T with respect to these independent variables are very simple: only six first derivatives, all equal to one (e.g., $\partial T_{11}/\partial T_{11} = 1$); all other first derivatives and all second derivatives are zero. During analysis of the modeling results, it is, of course, easy to change the six nonzero elements of T back to the crystallographic lattice parameters. Similarly, in molecular dynamics calculations, the elements of T may be treated as fictitious coordinates to allow the simulation box to change both shape and size (see below).

Summation of Long-Range Interactions

The use of force fields, as described in the preceding section, demands that their potentials be summed over all internal coordinates of the system of interest. Such a summation is straightforward for small molecules. For calculations on large systems (e.g., crystal structures, macromolecules), however, the summation of the long-range nonbonded interactions becomes a problem because their number increases rapidly (as N^2 for pair interaction potentials between N particles) with the size of the system. Therefore, one needs methods to minimize the range over which the summation of the nonbonded interactions is performed.

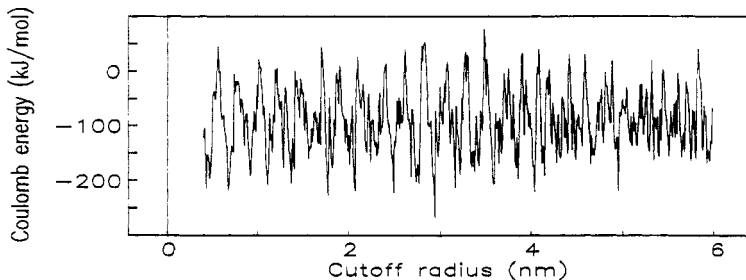


Figure 8 Coulomb energy for the α -quartz structure calculated as a function of a cutoff radius.

A simple but primitive method is to use a cutoff radius: the summation is carried out to a predefined interatomic distance only, the cutoff radius; beyond that distance, all interactions are neglected. This method works reasonably well with potentials that decrease regularly and rapidly with increasing interatomic distance, e.g., the Lennard-Jones potential. In the case of a periodic lattice, as is the case with zeolites, it is also easy to improve the overly simple cutoff treatment by implementing an approximation¹¹⁴ for the summation of the interactions beyond the cutoff radius:

$$\sum_{r_{ij} > R_C}^{\infty} -\frac{A_{ij}}{r_{ij}^6} = \frac{\pi N_j A_{ij}}{V_{uc} R_C^3} \quad [29]$$

in which R_C is the cutoff distance, $-A_{ij}/r_{ij}^6$ is the attractive term in the Lennard-Jones potential, N_j is the number of atoms of type j in a unit cell, and V_{uc} is the volume of the unit cell.

Electrostatic interactions, in contrast to dispersion or multipolar interactions, do not decrease rapidly with interatomic distance, and in a structure with alternating positive and negative charge the total electrostatic energy oscillates as a function of the cutoff radius (see Figure 8). This implies that the simple cutoff method can no longer be used and that a more sophisticated method is needed for the summation of the electrostatic interactions. Three methods that have been used in zeolite modeling will be discussed: Ewald summation, shifted-force method, and taper functions. The Ewald summation is the traditional method for the summation of the electrostatic interactions in a lattice. When properly executed, it accurately provides the Madelung sum^{115–117} for the lattice.

Ewald Summation

The Ewald method splits the summation into a summation in direct space and a summation in reciprocal space:

$$U_{\text{el}} = \frac{1}{2} \sum_{i=1}^N \sum_{j \neq i}^N \frac{q_i q_j}{r_{ij}} = \frac{1}{2} \sum_{i=1}^N q_i \sum_{j \neq i}^N \frac{q_j}{r_{ij}} \operatorname{erfc}(\zeta r_{ij}) \\ + \frac{1}{2} \sum_{i=1}^N q_i \left[\sum_{j=1}^N q_j \frac{4\pi}{V} \sum_{K \neq 0}^{K_{\max}} \exp\left(-\frac{K^2}{4\zeta^2}\right) K^{-2} \cos(K \cdot \mathbf{r}_{ij}) \right] - \frac{\zeta}{\sqrt{\pi}} \sum_{i=1}^N q_i^2$$
[30]

In Eq. [30], $\operatorname{erfc}(x)$ denotes the complementary error function, N is number of atoms in the simulation box of volume V , and q_i and q_j are charges of atoms i and j , respectively. $K = 2\pi H$, $K = |K|$, and H stands for a vector of the reciprocal lattice defined for the simulation box; ζ and K_{\max} are parameters controlling convergence of the direct and reciprocal sums.

Descriptions of the method and its physical background are given by Bertaut,¹¹⁶ by Jackson and Catlow,⁸⁹ and by Tosi.¹¹⁷ Jackson and Catlow⁸⁹ and Karasawa and Goddard¹¹⁸ have deduced optimal values of the parameters for the summations in direct and reciprocal spaces. Computer code for the Ewald summation is available from several sources.^{13,119}

Shifted-Force Method

In the shifted force method, both the potential and the force are smoothed out to zero at a certain cutoff distance R_C

$$U_{\text{sf}}(r) = U(r) - U(R_C) - \frac{r^3 - R_C^3}{3R_C^2} \left(\frac{\partial U(r)}{\partial r} \right)_{r=R_C}$$
[31]

The last two terms in Eq. [31] *shift* the original potential $U(r)$ to make both potential and its derivative zero at the cutoff distance. The cutoff distance R_C can be adjusted to suit the minimal image convention¹³ often used to make molecular dynamics calculations efficient. It has also been shown that the method can be easily combined with a shielded potential.¹²⁰ When the shielded electrostatic potential is represented by Eq. [13] so

$$U_{\text{sh}}(r_{ij}) = \frac{q_i q_j}{(r_{ij}^3 + 1/\gamma_{ij}^3)^{1/3}} = \frac{q_i q_j}{S}$$
[32]

the shifted-force potential is given by

$$U_{\text{sf}}(r) = C_{ij} \left[U_{\text{sh}}(r) - U_{\text{sh}}(R_C) - \frac{S^3 - S_C^3}{3S_C^2} \left(\frac{\partial U_{\text{sh}}(r)}{\partial r} \right)_{r=R_C} \right]$$
[33]

where

$$C_{ij} = \frac{\gamma_{ij}}{\gamma_{ij} - 1/S_C - R_C^3/3S_C^4}$$
[34]

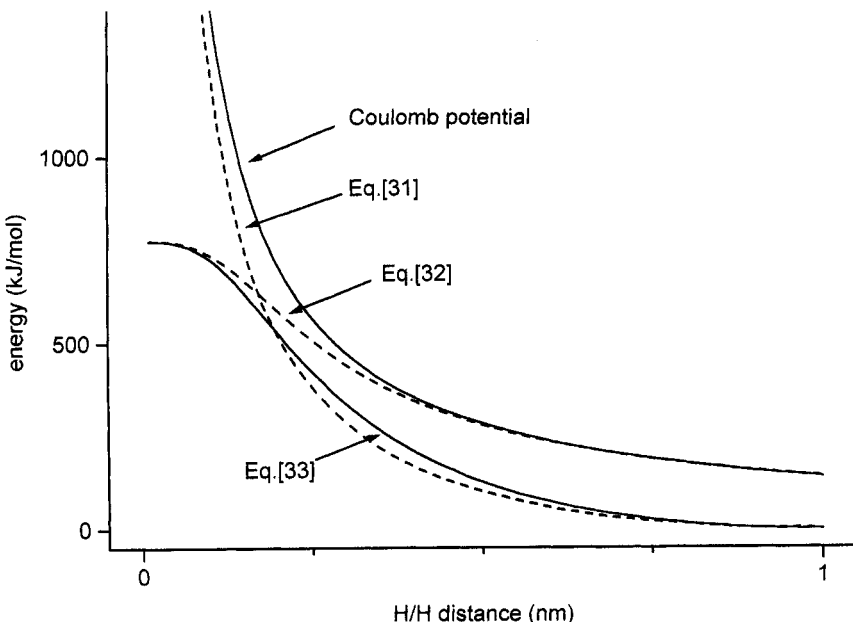


Figure 9 Electrostatic interaction energy between two hydrogen atoms represented by the shifted-force Coulomb and shielded Coulomb potentials.

Figure 9 shows the Coulomb potential, the shifted-force Coulomb potential (Eq. [31]), the shielded Coulomb potential (Eq. [32]), and the shielded shifted-force Coulomb potential (Eq. [33]) calculated for interaction between two hydrogen atoms with a charge $q_H = +1|el|$.

Taper Functions

Just as in the shifted-force method, the taper method replaces a strict cutoff radius by a cutoff region in which the interactions are smoothly tapered to zero.⁹³ This is done by multiplying the Coulomb potential from $r = A$ to $r = B$ with a taper function

$$S_m(r) = \sum_{n=0}^m C_n r^n \quad [35]$$

The coefficients C_n can be calculated from the conditions $S_m(A) = 1$ and $S_m(B) = 0$; $S'_m(r = A, B) = 0$ for $m > 2$; $S''_m(r = A, B) = 0$ for $m > 4$; and $S'''_m(r = A, B) = 0$ for $m > 6$, where S'_m signifies $\partial S_m(r)/\partial r$, etc. The coefficients for $m = 3, 5$, and 7 are collected in Table 4. The number of interactions to be calculated is determined by B , and $D = B - A$ determines the smoothness and the accuracy of the taper function.⁹³ Therefore, it is efficient to take $A = 0$. With $A = 0$ and $B = 15 \text{ \AA}$, it was found that the summation of the electrostatic interactions for a variety of systems is almost equal to the result of the Ewald method.¹²¹ Figure 10 com-

Table 4 Coefficients^a for Taper Functions of Eq. [35]

Coefficient	S_3	S_5^b	S_7
C_0	$(-3AB^2 + B^3)/D^3$	$(10A^2B^3 - 5AB^4 + B^5)/D^5$	$(-35A^3B^4 + 21A^2B^5 - 7AB^6 + B^7)/D^7$
C_1	$6AB/D^3$	$-30A^2B^2/D^5$	$140A^3B^3/D^7$
C_2	$-3(A + B)/D^3$	$30(A^2B + AB^2)/D^5$	$-210(A^3B^2 + A^2B^3)/D^7$
C_3	$2/D^3$	$-10(A^2 + 4AB + B^2)/D^5$	$140(A^3B + 3A^2B^2 + AB^3)/D^7$
C_4		$15(A + B)/D^5$	$-35(A^3 + 9A^2B + 9AB^2 + B^3)/D^7$
C_5		$-6/D^5$	$84(A^2 + 3AB + B^2)/D^7$
C_6			$-70(A + B)/D^7$
C_7			$20/D^7$

^a A , start of taper function; B , end of taper function; $D = B - A$.

^bCoefficients for S_5 were derived by Jay Ponder, Washington University, St. Louis, MO personal communication, 1990.

pares the potentials and the forces for the shifted-force and taper methods. It is clear that both the potentials and the forces resemble each other closely. However, this is not the case for the second derivative of the potential, as can be easily seen by taking the second derivative of the shifted-force potential. For reasons of continuity, this would give taper functions with $m = 5$ and $m = 7$ an advantage in energy minimization studies.

Finally, it should be noted that both the shifted-force method and the tapered method can be made more computer efficient by the construction of lookup tables¹³ for the potentials and their derivatives.

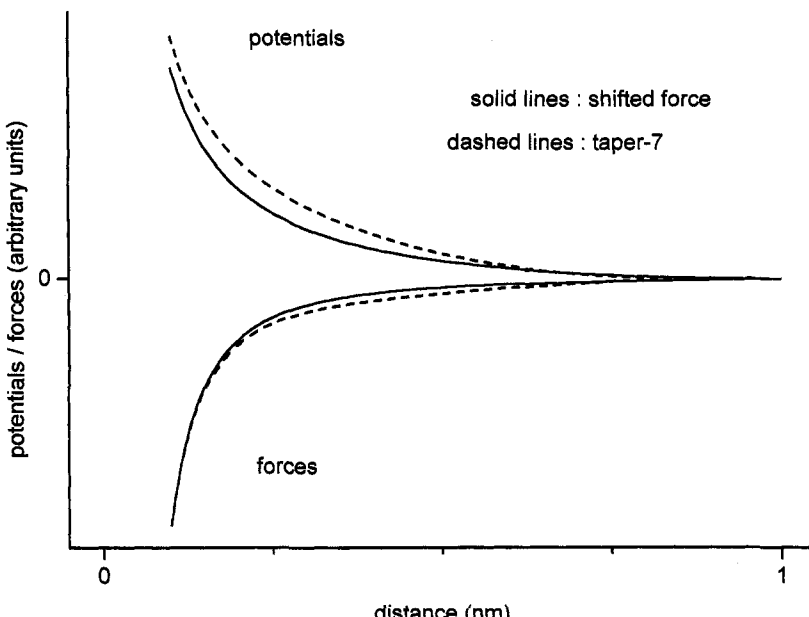


Figure 10 Potentials and forces calculated for the shifted-force potential and taper-7 potential ($A = 0$).

The question of which of the methods described above is appropriate for handling long-range interactions is, in our opinion, related to the system under study and the model that is used. Thus, in the modeling of adsorption and diffusion of relatively nonpolar molecules in zeolites with molecular-mechanics-type force fields, the less CPU-time-demanding shifted-force and taper function methods are in our opinion to be preferred. In contrast, in studies on extra-framework ions in zeolites with a rigid ion model, the more rigorous Ewald method is probably a better choice. However, there is still work that should be done for validation of either method for handling the long-range interactions in zeolite modeling.

Energy Minimization

Algorithms for energy minimization, optimizing the geometry till an energy minimum is reached, are generally more complex than algorithms for molecular dynamics. However, energy minimization is relatively inexpensive with respect to computer time and is, therefore, still an important tool in zeolite modeling. In some cases, the answers provided by energy minimization can be sufficient. In other cases, energy minimization can serve as a tool to obtain a reasonable starting geometry for a molecular dynamics study.

Techniques for energy minimization have been discussed extensively in this series.¹² Such a discussion is not repeated in this chapter, but a few experiences and tricks pertinent to zeolite modeling are presented.

Minimization and Lattice Dynamics

Contrary to intuition, zeolite frameworks are quite flexible, and the minima on the potential energy surface can be quite shallow. Accordingly, one needs an efficient minimizer. One can start minimization with a good conjugate gradient method (e.g., the method described in Ref. 122), but in our experience it is clearly advantageous to have a second-derivative minimizer available for the final stage of the minimization process. A full-matrix second-derivative minimizer is based on an expansion of the potential energy in a second-order Taylor series around a trial geometry:

$$U_S(r) = U_S(r_0) + \sum_i \left(\frac{\partial U_S}{\partial r_i} \right)_0 \Delta r_i + \frac{1}{2} \sum_j \sum_i \left(\frac{\partial^2 U_S}{\partial r_i \partial r_j} \right)_0 \Delta r_i \Delta r_j \quad [36]$$

Differentiation of Eq. [36] with respect to Δr_i gives

$$\sum_j \left(\frac{\partial^2 U_S}{\partial r_i \partial r_j} \right)_0 \Delta r_j = - \left(\frac{\partial U_S}{\partial r_i} \right)_0 \quad [37]$$

With proper care,¹²⁴ this set of equations can be solved for Δr_j , which, when added to the trial coordinates, should give a geometry closer to the mini-

mum. A second-derivatives minimizer is not only more efficient in locating the minimum, but by computing the vibrational frequencies⁹⁵ from the Hessian \mathbf{H} (the matrix containing the second derivatives of the potential energy at the minimum), one finds directly if a minimum has indeed been reached.

Once the equilibrium geometry has been reached, the right-hand term in Eq. [36] vanishes and the vibrational frequencies can be found by solving a matrix equation

$$\mathbf{M}^{-1/2}\mathbf{H}\mathbf{M}^{-1/2}\mathbf{L} = \Lambda\mathbf{L} \quad [38]$$

where $\mathbf{M}^{-1/2}$ is the diagonal matrix containing the inverse square roots of the atomic masses, Λ is the diagonal matrix containing the eigenvalues of the mass-weighted Hessian, and \mathbf{L} is the matrix of eigenvectors. Equation [38] can be solved by standard procedures.¹²³ From the eigenvalues λ_k one can calculate the vibrational frequencies

$$\bar{v}_k = \frac{1}{2\pi c} \sqrt{\lambda_k} \quad [39]$$

The elements of column k of the matrix \mathbf{L} are the normalized mass-weighted Cartesian amplitudes of the atoms in the k th vibrational mode with frequency \bar{v}_k . This procedure is the same as that used in normal mode analysis (NMA) with the difference that in NMA the matrix of the second derivatives of the energy is written in *internal coordinates*. When the minimization includes lattice parameters, one obtains $3N - 3$ real vibrational frequencies if a true minimum has been found, where N is the number of atoms in the simulation box.¹¹³ Finding an imaginary frequency indicates that the minimization ended on a saddle point on the potential energy surface instead of a minimum.

Multiple Minima

Some of the problems encountered in the simulation of large systems are also found in zeolite modeling. In particular, the potential energy surface can have more than one minimum. It is therefore advisable to explore the neighborhood around the minimum after an energy minimum has been found. A good trick for successfully accomplishing this is to vary the geometry by translating the atoms along one of the low frequency vibrational modes, or, if at a saddle point, by translating the atoms along the normal mode belonging to the imaginary frequency.

Constrained Minimization

Constraints are easy to implement in a second-derivative minimization.¹²⁴ For instance, in zeolite modeling it may be required to carry out an energy minimization under the constraint of constant volume. This could be done by adding to the set of equations an equation of constraint. Because the

volume of the unit cell is the product of the diagonal elements of the transformation matrix T , the equation of constraint is given by

$$\sum_{i \neq j \neq k}^3 (T_{ii} T_{jj} \Delta T_{kk}) = 0 \quad [40]$$

which is obtained from the condition $\Delta V = 0$.

Energy Minimization with Geometry-Dependent Charges

The use of a force field model with geometry-dependent charges implies that $\partial q / \partial \alpha$, where $\alpha = x, y, z$, must be evaluated in both energy minimization and MD calculations. Calculation of these charge derivatives can be avoided, however, in the CIEEM approach,¹¹² which also simplifies the calculations when using a second derivative minimizer.

Starting from Eq. [26], the α -component of the force acting on atom k is given by

$$\begin{aligned} F_{\alpha_k} = -\frac{\partial U_S}{\partial \alpha_k} &= -\sum_{i=1}^N \left(\left[\chi_i^* + 2\eta_i^* q_i + \sum_{j \neq i}^N \frac{q_j}{R_{ij}} \right] \frac{\partial q_i}{\partial \alpha_k} \right) \\ &\quad + q_k \sum_{i \neq k}^N \frac{q_i}{R_{ki}^2} \frac{\partial R_{ki}}{\partial \alpha_k} - \frac{\partial U_{NC}}{\partial \alpha_k} \end{aligned} \quad [41]$$

where χ_i^* and η_i^* are defined in Eq. [7], U_S is from Eq. [18], and U_{NC} is from Eq. [26]. The first sum in square brackets in Eq. [41] is equal to the electronegativity of atom i and thus, according to the Eq. [8], we may rewrite the first term as

$$\sum_{i=1}^N \left(\left[\chi_i^* + 2\eta_i^* q_i + \sum_{j \neq i}^N \frac{q_j}{R_{ij}} \right] \frac{\partial q_i}{\partial \alpha_k} \right) = \bar{\chi} \frac{\partial}{\partial \alpha_k} \sum_{i=1}^N q_i \quad [42]$$

Because of conservation of charge for the system, Eq. [41] may be rewritten as

$$F_{\alpha_k} = q_k \sum_{i \neq k}^N \frac{q_i}{R_{ki}^2} \frac{\partial R_{ki}}{\partial \alpha_k} - \frac{\partial U_{NC}}{\partial \alpha_k} \quad [43]$$

because the first sum in Eq. [41] vanishes. Note that within the CIEEM approach the forces acting on atoms are *identical* to those that would be obtained in the fixed charge approximation, and thus it is not necessary to calculate the derivatives of the charges in either gradient energy minimization or MD calculations.

Because $\partial U_S / \partial \alpha_k$ does not contain the first derivatives of the charges, one need not evaluate their second-derivatives when using a second derivatives

minimizer. However, in this case one needs to compute the first derivatives of the charges because $\partial U_S / \partial \beta_l^2$ contains nonvanishing $\partial q / \partial \beta_l$ quantities. Taking a partial derivative of Eq. [10] with respect to coordinate α of atom k gives

$$\frac{\partial \mathbf{A}}{\partial \alpha_k} \cdot \mathbf{q} + \mathbf{A} \cdot \frac{\partial \mathbf{q}}{\partial \alpha_k} = 0 \quad [44]$$

or

$$\mathbf{A} \cdot \mathbf{q}' = \mathbf{b}' \quad [45]$$

where $\mathbf{q}' = \partial \mathbf{q} / \partial \alpha_k$ and $\mathbf{b}' = -(\partial \mathbf{A} / \partial \alpha_k) \cdot \mathbf{q}$. Equation [45] is analogous to Eq. [10] and can effectively be solved with respect to \mathbf{q}' using the lower–upper triangle decomposition (LU) algorithm¹²³ because Eqs. [45] and [10] have the same matrix \mathbf{A} .

Method of Molecular Dynamics

Molecular dynamics uses classical mechanics to study the evolution of a system in time. At each point in time the classical equations of motion are solved for a system of particles (atoms), interacting via a set of predefined potential functions (force field), after which the solution obtained is applied to predict positions and velocities of the particles for a (short) step in time. This step-by-step process moves the system along a trajectory in phase space. Assuming that the trajectory has sampled a sufficiently large part of phase space and the ergodicity principle¹²⁵ is obeyed, all properties of interest can then be computed by averaging along the trajectory. In contrast to the Monte Carlo method (see below), the MD method allows one to calculate both the structural and time-dependent characteristics of the system. An interested reader can find a comprehensive description of the MD method in the books by Allen and Tildesley¹³ or Frenkel and Smit.¹⁴

Application of the MD method to zeolite systems was pioneered by Demontis and coworkers in 1986.¹²⁶ Since then, MD has been used in an increasing number of zeolite modeling studies. Those papers appearing before 1992 have been reviewed in Ref. 9, and a review of later studies can be found in Ref. 3; some recent examples are discussed in subsequent parts of this chapter.

A typical MD simulation protocol consists of the following steps: (1) assign the initial values to the atomic coordinates and velocities; (2) integrate the equations of motion (this is the heart of the MD method); and (3) analyze the results of the simulation. These steps are discussed below in relation to zeolite modeling.

Starting an MD Run

An initial set of coordinates and velocities of all particles in the system must be known to start a simulation. For the atoms of a zeolite framework, those initial coordinates are usually taken from experimental data, for example, from X-ray or neutron diffraction measurements collected in the *Atlas of Zeolite Structure Types*.¹

Placement of guest molecules into the zeolite framework can be done several ways, but it is important to avoid severe overlap of the van der Waals spheres because the large forces resulting from such an overlap can produce a numerically unstable system that “blows up” (the energy becomes excessively high). In a few cases, atomic coordinates of guest molecules are available from experimental data. Small molecules (diatomics, water, methane, etc.) can often be distributed easily in the zeolite channels. This distribution can be done uniformly, but the initial configuration will be destroyed during equilibration. For larger molecules, the best approach is to use either energy minimization or the Monte Carlo approach to dock the guest molecule in the zeolite; these approaches translate and rotate the molecule until it is trapped in an energy minimum. An advantage of using the docking procedure is that one starts close to the equilibrium structure, which means that the equilibration stage of the simulation demands somewhat less time.

Having defined the atomic coordinates, initial velocities must next be assigned. The atomic velocity components may be chosen randomly from either a Gaussian distribution at the desired temperature or from a uniform distribution in the interval $(-\nu_{\max}, \nu_{\max})$, where ν_{\max} can be chosen to be equal to the square root of the dispersion of that Gaussian distribution. In both cases, the velocities will be adjusted to the proper distribution during the equilibration stage of simulation. The same approaches may be applied to the center-of-mass velocities of guest molecules if these are treated as rigid bodies. In that case, the initial values for the angular velocity components are usually also chosen to be consistent with the desired temperature.

Integrating the Equations of Motion

Once the initial state of the system has been set up, the equations of motion (e.g., in the form of the Newton's equations) are solved numerically by means of the finite difference approach. Known atomic positions, velocities, and forces at time t are used to obtain the coordinates and velocities at time $t + \Delta t$, after which the procedure is repeated. The value of the time step Δt that can be used depends on the specific model of the system and the accuracy of the integration algorithm. In general, the time step should be smaller than $\tau/10$, where τ is the minimum characteristic time in the system, e.g., the period of the highest frequency vibration.

Many algorithms are available for integrating the equations of motion and several of them have been reviewed in Refs. 13 and 127. One of the most widely used schemes is the velocity form of the Verlet algorithm:

$$\mathbf{r}(t + \Delta t) = \mathbf{r}(t) + \mathbf{v}(t)\Delta t + \frac{1}{2m} \mathbf{F}(t)\Delta t^2 \quad [46]$$

$$\mathbf{v}(t + \Delta t) = \mathbf{v}(t) + \frac{1}{2m} [\mathbf{F}(t) + \mathbf{F}(t + \Delta t)]\Delta t \quad [47]$$

where \mathbf{r} , \mathbf{v} , and \mathbf{F} are vectors of coordinate, velocity, and force, respectively, for a particle of mass m . The algorithm is easy to program, and it requires only nine vectors of length N to be stored for each time step.

The choice of which integration algorithm is best suited for exploring the dynamics of guest molecules depends on how many intramolecular degrees of freedom must be accounted for. For rigid molecules in which all internal coordinates (bonds, angles, dihedrals) are fixed, the translational motion of the molecular center of mass (CoM) is separated from the rotational motion about the CoM. The CoM equations of motion for translation may be then integrated by means of, for example, the velocity Verlet scheme, whereas the quaternion algorithm¹²⁹ is normally used for integrating the equations of motion for the rotational degrees of freedom. In the quaternion algorithm, the three Euler angles that define the orientation of a body-fixed frame for each molecule with respect to a space-fixed frame are substituted by four parameters (quaternions). These are linked by one equation, and thus there are just three independent variables. Such a trick is needed because the equations of motion for the Euler angles contain a singularity, whereas the equations of motion for the quaternions are singularity free.¹³ The rigid molecule approximation for the guest molecules allows the use of a relatively large time step (typically 5–10 fs), especially when used together with a rigid zeolite framework approximation. This rigid body model can be adequate for some small molecules, but for more complex polyatomic molecules it is insufficient because it ignores all conformational transformations.

Large flexible molecules are better handled by the SHAKE or RATTLE schemes,^{130–132} in which bond-stretch (and often bond angle) coordinates are constrained, while torsional coordinates evolve in time according to intramolecular and intermolecular forces. If all intramolecular degrees of freedom are unconstrained, then a small time step (typically 0.5–1 fs) must be used for an accurate integration of the equations of motion. This obviously limits the length of the trajectory over which the dynamics of atoms can be computed. The reversible multiple-time-scale MD algorithm¹³³ provides an opportunity to speed up such simulations without loss of accuracy while keeping the appropriate length of the trajectory.

In MD simulations we are interested in obtaining the properties of the system at certain macroscopic conditions (temperature T , volume V , pressure P , etc.). These parameters act as constraints and determine a statistical ensemble that is sampled. For instance, one commonly used ensemble is the microcanonical or NVE ensemble, for which the number of particles N , volume of the

system V , and total energy E are constant. (It is commonly accepted that an abbreviation XYZ denotes macroscopic parameters X , Y , and Z that are conserved quantities in the simulation.)

The method proposed by Parrinello and Rahman^{134,135} is of special interest in studies of crystalline solids and zeolites in particular. The method allows a variation of both volume and shape of simulation box and therefore is suitable for studying phase transitions induced by sorption of molecules, isomorphic substitution, or change of temperature. In this method, the Lagrangian of a system with kinetic energy T and potential energy U

$$\mathcal{L} = T - U \quad [48]$$

is extended by additional terms that represent the kinetic T_V and potential energy U_V of the simulation box. The equation of motion, which is obtained from the extended Lagrangian,

$$\mathcal{L}_{\text{ext}} = T + T_V - U - U_V \quad [49]$$

samples the isobaric–isoenthalpic NPH ensemble.¹³⁵

A similar approach exists for performing constant temperature MD calculations. The Lagrangian (Eq. [48]) is extended by terms for additional (fictitious) degrees of freedom that couple the system to an external heat reservoir.¹³⁶ A combination of the Parrinello–Raman and Nosé schemes is possible to sample an isobaric–isothermal (NPT) ensemble. These methods as well as other techniques for performing calculations in different statistical ensembles are reviewed by Allen and Tildesley¹³ in detail.

Computing the interatomic forces is the most time-consuming part in an MD simulation. The use of a cutoff radius is a standard “trick of the trade” that reduces computational cost by neglecting interactions between atoms separated by a distance larger than the specified cutoff. As described earlier, this truncation results in a discontinuity of both the potential and the force at the cutoff distance, but the drawback thus entailed can be avoided by implementation of either the shifted-force potential or a taper function.

Equilibration is the first stage of any MD calculation. During this stage, the system comes to equilibrium at the desired values of the macroscopic parameters. In fact, there are two processes taking place during this stage. The first process is an adjustment of the macroscopic parameters (e.g., temperature, pressure) to the target values and then subsequent equilibration at these values. The second process is a redistribution of the energy among the available degrees of freedom in accordance to the equipartition principle.¹²⁵

The temperature may be adjusted by coupling the system to a thermal bath as described by Berendsen et al.¹³⁷ In this method the atomic velocities are scaled (multiplied) by a factor

$$\xi = \left[1 + \frac{\Delta t}{\tau} \left(\frac{T_0}{T} - 1 \right) \right]^{1/2} \quad [50]$$

where τ is the relaxation time, T_0 is the target temperature, and T is the instantaneous temperature of the system computed as

$$T = \frac{2}{(3N - N_C)k_B} \sum_{i=1}^N \frac{m_i v_i^2}{2} \quad [51]$$

in which N_C is the number of constrained degrees of freedom; for example, $N_C = 3$ if a condition of zero total linear momentum is applied. The ratio $\Delta t/\tau$ determines the degree of coupling, and one speaks of “soft” scaling if $\tau \gg \Delta t$. In “hard” coupling, $\tau = \Delta t$ is employed. A similar procedure exists for equilibrating the system at a desired value of pressure.¹³⁷ The redistribution between the kinetic and potential energies usually happens within hundreds of time steps, and thus the macroscopic parameters can be fitted to their desired values relatively fast.

The redistribution of energy between different degrees of freedom for the guest may span a long time, especially when one uses the rigid zeolite framework approximation, because then redistribution occurs only via collisions between guest molecules, and these are rather infrequent events, especially at low loadings. In contrast, a flexible zeolite lattice acts as a thermal bath,⁹ and collisions of molecules with the zeolite walls effectively redistribute the energy. A useful check is to compare the CoM translational and rotational kinetic energies of the molecules. These have to be equal within root-mean-square (rms) fluctuations if the equipartition principle is obeyed.

Following equilibration, the production phase of the simulation stores the coordinates and velocities of particles for later analysis.

Sample Calculations to Illustrate the Methodology

We now consider two specific examples to discuss the scope of MD modeling for zeolites. The first concerns a silica faujasite structure, the all-silica analog of zeolite Y, in which the simulation was carried out using the GVFF potential model¹⁰⁸ at a temperature of 300 K in the *NVE* ensemble with a simulation box consisting of one unit cell. The equations of motion were integrated using the velocity form of the Verlet algorithm (Eq. [47]) with a time step of 1 fs. The second example involves a simulation of methanol in silica faujasite using a flexible molecule–rigid framework approach. This system consisted of eight methanol molecules and one faujasite unit cell at 300 K. Again, atomic coordinates and velocities were followed by the velocity Verlet scheme with a time step of 0.4 fs. The calculation was carried out for this example using the CIEEM approach.^{112,120}

Does MD Work Properly?

Two tests are available to ensure that the equations of motion are solved correctly in an MD simulation. The first test assesses the conservation of energy. In the absence of terms explicitly dependent on time, the Hamiltonian of the system must be a conserved quantity, and integrating Newton's equations of motion should conserve the total energy of the system E . In fact, small fluctuations of the energy will result from the finite difference approach and round-off errors. Numerical criteria often used¹³³ for the energy fluctuations are

$$\Delta\hat{E} = \log\left(\frac{1}{N_{\text{steps}}} \sum_{k=1}^{N_{\text{steps}}} \left| \frac{E(0) - E(k\Delta t)}{E(0)} \right| \right) \quad [52]$$

$$R = \frac{\text{rms } E}{\text{rms } E_{\text{kin}}} \quad [53]$$

where $\text{rms } E$ and $\text{rms } E_{\text{kin}}$ are the root-mean-square fluctuations of the total and kinetic energies, respectively. Values of $\Delta\hat{E} < 3$ and $R < 0.01$ indicate that the integration algorithm and time step used for the simulation are sufficiently accurate. Figure 11 shows the kinetic energy and the total energy along the trajectory calculated for the all-silica faujasite. Values of -4.21 and 0.0063 obtained in this calculation for the $\Delta\hat{E}$ and R criteria, respectively, show that the integration algorithm was sufficiently accurate.

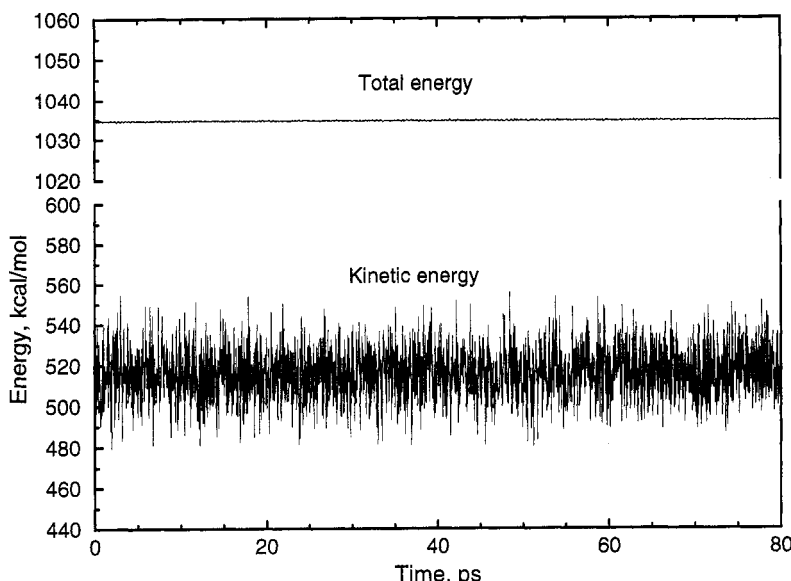


Figure 11 Time history of the kinetic and total energies in the NVE molecular dynamics simulation of silica faujasite.

A second test is to see if varying the time step Δt used in the simulation leads to the expected change in $\Delta\hat{E}$. The velocity Verlet algorithm is a second-order algorithm, and a decrease of the time step by a factor of 2 should lead to a decrease of the $\Delta\hat{E}$ value by a factor of 4.^{13,127}

Analyzing the Results

An MD simulation produces a file containing the time history of the coordinates and the velocities of atoms, the energies, and so on in the system. Assuming that a sufficient part of phase space has been sampled, the next step is to extract “observables” from this file by averaging instantaneous values of the quantity of interest, say A , over time

$$A_{\text{obs}} = \lim_{T \rightarrow \infty} \frac{1}{T} \int_0^T A(t) dt \quad [54]$$

Some of the more frequently computed properties of zeolites are structure, spectra, and transport characteristics, discussed in this order below.

Structural Characteristics The pair distribution function $g_2(\mathbf{r}_1, \mathbf{r}_2) \equiv g(\mathbf{r}_{12})$ [or simply $g(r)$] is perhaps the most commonly computed characteristic in zeolite modeling. The definition of $g(r_{12})$ for the canonical ensemble is¹²⁵

$$g(\mathbf{r}_{12}) = \frac{N(N-1)}{V^2 Z_{NVT}} \int d\mathbf{r}_3 d\mathbf{r}_4 \cdots d\mathbf{r}_N \exp\left(\frac{-U}{k_B T}\right) \quad [55]$$

and for isotropic systems $g(r) = g(r)$ because all directions in the space are equivalent to each other. The utility of $g(r)$ is that it is related, by Fourier transformation, to the elastic scattering amplitudes measured in X-ray or neutron diffraction experiments, and therefore the calculation of $g(r)$ makes it possible to predict and to check the results of these experiments.

To evaluate of $g(r)$ by computer modeling, one may redefine $g(r)$ as the ratio of the density $\rho(r)$ of atoms at distance r from a chosen reference atom to the mean density of atoms in the system $\bar{\rho} = N/V$

$$g(r) = \frac{\rho(r)}{\bar{\rho}} = \frac{N(r)V}{4\pi r^2 \Delta r N} \quad [56]$$

where $N(r)$ is the number of particles in a spherical shell of thickness Δr . This definition can be easily adapted to compute $g(r)$ between atoms of different types. Several other specific structural characteristics commonly derived include distribution functions of diameters of windows in zeolite structures, CoM/center-of-cage distribution functions for sorbed molecules, and density profiles of guest molecules along a selected direction (e.g., channel axis) in a zeolite.

Spectral Characteristics Computing spectral characteristics can provide a powerful tool for analyzing processes that occur in appropriate time scales.

Moreover, because spectroscopic methods are among the most widely used experimental techniques in zeolite studies, a direct comparison between theory and experiment is often possible.

The time scale of MD simulations is comparable to that probed by vibrational spectroscopies. The distribution of vibrational frequencies in the system $f(\omega)$, known as the power spectrum, is calculated by Fourier transformation of the velocity autocorrelation function¹²⁵

$$f(\omega) \propto \int_0^{\infty} \langle \mathbf{v}(0) \cdot \mathbf{v}(t) \rangle e^{i\omega t} dt \quad [57]$$

where the angle brackets denote averaging over all atoms and all time origins (see below). The power spectrum is directly related to the incoherent scattering function measured in inelastic neutron scattering experiments.¹²⁵

Although $f(\omega)$ is useful for assessing the dynamics of small molecules, it becomes unwieldy for the dynamics of large systems because of the large number of bands in the power spectrum. The infrared (IR) and Raman spectra are more useful for this purpose because the appearance of bands in these spectra is governed by selection rules that cut from $f(\omega)$ the vibrations with changing dipole moment and polarizability of system, respectively (Figure 12). These spectra depend on both the symmetry of the system and its potential energy

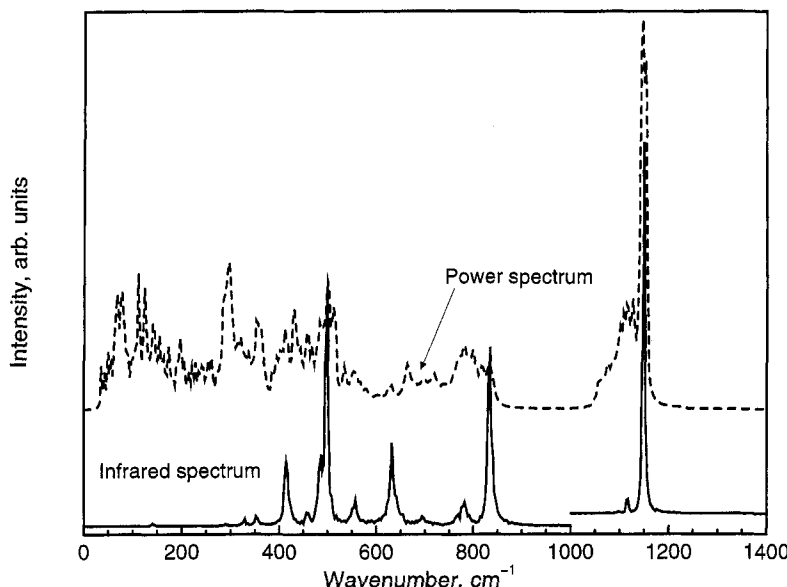


Figure 12 Power and infrared spectra of silica faujasite structure.

surface. Therefore, comparison between the computed and experimental spectra provides a test both of the structure and of the potential model.

The IR and Raman spectra are calculated by Fourier transformation of the dipole and polarizability tensor autocorrelation functions, respectively.^{125,138–140} A classical expression for the infrared absorption coefficient $\sigma(\omega)$ at frequency ω reads¹³⁹

$$\sigma(\omega) = \frac{4\pi^2\omega^2}{3cnk_B T} I(\omega) \quad [58]$$

where c is the velocity of light, n is the refraction index of the medium, and 4π , k_B , and T have their usual meanings. $I(\omega)$ denotes an absorption line shape and is the Fourier transform of the dipole moment autocorrelation function

$$I(\omega) = \int_0^\infty dt e^{i\omega t} \langle \mu(0) \cdot \mu(t) \rangle \quad [59]$$

where the time history of the dipole moment $\mu(t)$ is extracted from the time history of the atomic coordinates and atomic charges q_i ,

$$\mu_s(t) = \sum_i^N q_i s_i(t), \quad s = x, y, z \quad [60]$$

The dipole moment components $\mu_s(t)$ as a function of time are usually computed with a fixed charge approximation. Values of atomic charges are often taken from quantum chemical calculations of representative models, although absolute charge values play no role (other than influencing the MD trajectory) unless absolute infrared intensities are to be computed. However, the relative values of charges are of importance for reproducing relative band intensities.

Computing Raman spectra is complicated by the fact that the polarizability of the system \mathcal{P} is a tensor. Assuming that the polarizability can be represented as a sum of bond polarizabilities, one can write

$$\mathcal{P} = \sum_{i \in \text{bonds}} \mathbf{T}_i^{-1} \alpha_i \mathbf{T}_i \quad [61]$$

where α_i is the bond polarizability tensor in the principal axes and \mathbf{T}_i is the matrix of direction cosines of the principal axes of the bond in the Cartesian frame.¹⁴¹ The components of α_i can be expanded in a Taylor series with respect to the bond length displacement coordinate¹⁴²

$$\alpha_i = \alpha_i^0 + \frac{\partial \alpha_i}{\partial R_i} (R_i - R_i^0) + \dots \quad [62]$$

where R_i and R_i^0 are an instantaneous and equilibrium values of the bond length i , respectively. Therefore, the trajectories of the atoms can be used to compute \mathcal{P}

as a function of time. In a simple case, one may assume that one of the principal axes of the bond polarizability tensor is directed along the bond vector and only that component (the longitudinal polarizability) varies with bond length.¹⁴² A more sophisticated model would take into account variation of the transverse components of the polarizability tensor as well. Indeed, such models for calculating both infrared and Raman spectral intensities have been developed¹⁴¹ on the basis of electrooptical parameters.

Spectra of other dynamical variables like CoM velocities and zeolite window diameters can also be obtained by Fourier transformation of the appropriate time correlation functions. Calculation of spectra for different spatial components of a time dependent quantity provides useful information about the anisotropy of the corresponding motion.

It is important to note that no motion having a period in excess of L/v_s can be reproduced in the simulations, where L is the length of the simulation box and v_s is a velocity of sound in the medium.¹³ In addition, use of periodic boundary conditions together with a single structural unit cell as the simulation box restricts the calculation of spectral quantities to those at the center of the Brillouin zone: the periodic boundary conditions force atoms in all images of the simulation box to vibrate in-phase, that is, the definition of a motion at the center of Brillouin zone. When comparing results of the calculations with the experimental spectra, one must also bear in mind that the model used in the calculations implies a perfect crystal structure, whereas experiments are usually done with microcrystals having defects.

Transport Coefficients The reactivity of zeolites is determined by the ability of molecules (reactants and products) to diffuse to and from an active site. Therefore, knowledge about the diffusion process is essential for understanding zeolite chemical activity. The diffusion process is characterized by a diffusion coefficient which can be calculated two ways.¹²⁵ The first makes the use of the Einstein relationship that relates mean-square displacement of a molecular CoM position

$$\langle \Delta r^2(t) \rangle = \langle |\mathbf{r}(t) - \mathbf{r}(0)|^2 \rangle \quad [63]$$

to the diffusion coefficient D by

$$2Dt = \frac{1}{3} \langle \Delta r^2(t) \rangle \quad [64]$$

As in Eq. [57], the angle brackets signify averaging over atoms and time origins.

The second method is to compute the diffusion coefficient as the integral of the molecular CoM velocity autocorrelation function by using time correlation functions formalisms:

$$D = \frac{1}{3} \int \langle \mathbf{v}(0) \cdot \mathbf{v}(\tau) \rangle d\tau \quad [65]$$

Although in principle Eqs. [64] and [65] should lead to the same result, the former is more often used in calculations, because a plot of $\langle \Delta r^2(t) \rangle$ versus t provides a clear picture of the diffusion phenomenon. This issue is illustrated in Figure 13, which shows the $\langle \Delta r^2(t) \rangle$ and $\langle v(0) \cdot v(t) \rangle$ quantities as functions of time for the case of our reference system, methanol molecules adsorbed in all-silica faujasite. Calculating the diffusion coefficient by Eqs. [64] and [65] gives values of $D = 0.86$ and $0.96 \text{ \AA}^2/\text{ps}$, respectively. Note that in the estimation of D with Eq. [65], the fluctuating tail of the velocity autocorrelation function leads to slow convergence of the integral, which might be a cause of error. On the other hand, the slope of the $\langle \Delta r^2(t) \rangle$ curve may also vary, depending on the time interval used for calculation of the slope.

At this point it is important to ask how reliable the computed results are. More specifically, it should be determined whether phase space has been sampled sufficiently. To illustrate the issue of reliability, we point out that spectral intensities may vary from run to run owing to an improper distribution of energy among the vibrational degrees of freedom ($k_B T$ per normal mode) after the MD equilibration phase, even though the macroscopic parameters were equilibrated at the desired values. To avoid this pitfall, one should carry out as many MD runs as possible, starting with different initial conditions but with the same values of the macroscopic parameters. This practice will provide the data for averaging over multiple ensembles (as denoted by the angle brackets in Eqs. [57] and [63]). Ensembles can be considered to be a collection of points in phase space, and choosing different initial conditions allows one to explore different parts of phase space, parts that could be attained in the limit of infinitely long time sampling. However, if the system is sufficiently large and the

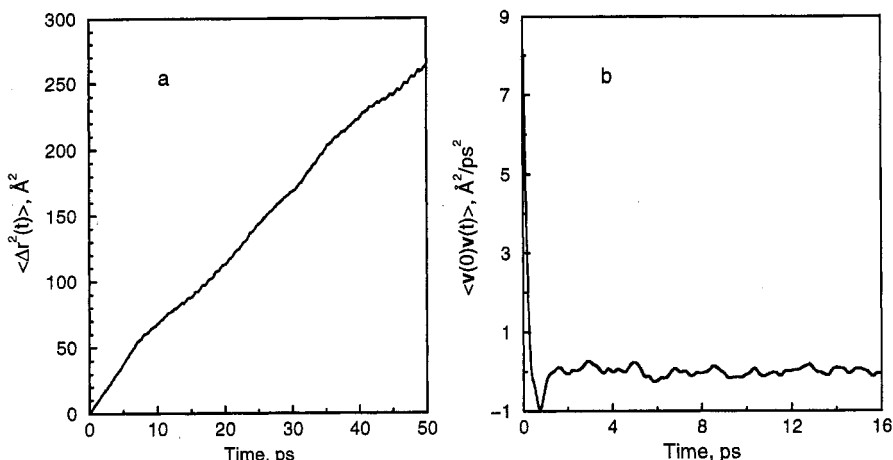


Figure 13 (a) Mean-square displacement (Eq. [63]) and (b) CoM velocity autocorrelation function (Eq. [65]) for methanol molecules adsorbed in silica faujasite structure.

computed trajectory is long enough, an averaging over multiple time origins may be carried out instead of using multiple runs.

Monte Carlo Methods

In contrast to the deterministic nature of the classical equations of the MD method, the Monte Carlo method makes use of a probabilistic picture of atomic motion. According to statistical mechanics,¹²⁵ an observable A_{obs} can be calculated from

$$A_{\text{obs}} = \int A(\Gamma) \rho(\Gamma) d\Gamma \quad [66]$$

where Γ denotes a point in phase space defined by a set of $3N$ positions and $3N$ conjugate momenta. The points Γ are distributed in the phase space non-uniformly, but according to a probability density $\rho(\Gamma)$ that depends on the statistical ensemble. Hence, to compute A_{obs} one needs *only* to evaluate the integral in Eq. [66]. For all real systems, such an evaluation is, of course, quite impossible by standard numerical integration methods because of the huge dimensionality of the integrals.

In MC methods the integrand in Eq. [66] is randomly sampled and the integral is approximated by a sum

$$A_{\text{obs}} = \int A(\Gamma) \rho(\Gamma) d\Gamma \approx \sum_{i=1}^{N_{\text{trials}}} A(\Gamma_i) \rho(\Gamma_i) \quad [67]$$

However, in the case of a simple sampling when trial configurations are uniformly distributed in phase space, many trials will fall into regions where the integrand has a negligible value and accordingly does not contribute significantly. The result is that sum in Eq. [67] converges very slowly because one is sampling unproductive regions of the phase space. A faster convergence of this sum can be achieved with importance sampling,¹³ whereby the trial configurations are chosen from a distribution p that mimics the probability density $\rho(\Gamma)$, and A_{obs} is then simply

$$A_{\text{obs}} = \lim_{N_{\text{trials}} \rightarrow \infty} \frac{1}{N_{\text{trials}}} \sum_{i=1}^{N_{\text{trials}}} A(\Gamma_i) \quad [68]$$

Importance sampling is central to Monte Carlo applications in statistical physics. In the subsections that follow, we describe the concepts of the schemes that are most frequently used in zeolite modeling.

Metropolis Scheme

A method with $\rho = \rho_{\text{NVT}} \approx e^{-H/k_B T}$, where H is the Hamiltonian of system, was proposed by Metropolis and coworkers in 1953.¹⁴³ Because the kinetic

energy of the system is fixed ($T = \text{const}$), this method samples the configurational part of phase space and the chain of states of the system are generated by the following algorithm:

1. Choose a particle (atom/molecule).
2. Translate/rotate it randomly to obtain a new configuration.
3. Compute the difference in energies $\Delta U = U_{\text{new}} - U_{\text{old}}$ between the new and old configurations.
4. Accept the new state of the system if $\Delta U < 0$ and go to step 1.
5. If $\Delta U > 0$, generate a random number ζ from a uniform distribution on the interval $[0,1]$; if $\zeta < e^{-\Delta U/k_B T}$, accept the new state; if $\zeta > e^{-\Delta U/k_B T}$, reject the new state and go to step 1.

Steps 4 and 5 are often summarized by the expression $P_{\text{accept}} = \min[1, \exp(-\Delta U/k_B T)]$. Step 2 is usually carried out in such way that about 50% of the trial moves are accepted. The Metropolis method allows calculation of the structural and energetic properties of a system.

Grand-Canonical Monte Carlo Method

In the grand-canonical Monte Carlo method, the system volume, temperature, and chemical potential are kept fixed, while the number of particles is allowed to fluctuate.¹³ There exist three types of trial move: (1) displacement of a particle, (2) insertion of a particle, and (3) removal of a particle. These trial moves are generated at random with equal probability. The acceptance probability of the Metropolis method can be used for the trial moves of type (1). For the two other types, the acceptance probabilities are different.¹³ Regarding zeolites, an adsorption isotherm can be calculated with the grand-canonical Monte Carlo method by running a series of simulations at varying chemical potentials.

Configurational-Bias Monte Carlo Method

The original Metropolis scheme cannot be used efficiently in simulations on adsorption of long chain molecules in zeolites because the acceptance ratio of trial moves resulting from random rotation and translation of the chain molecules is extremely low; almost all trial moves run the molecule into the wall of the zeolite channel or cage. This problem can be overcome by using the configurational bias Monte Carlo method.¹⁴⁴ In this method the trial moves are biased in a way calculated to avoid host–guest collisions. However, the probability that a particular state being generated is no longer proportional to its Boltzmann weight. To ensure proper sampling, the bias must be removed by adjusting the acceptance rules. The configurational bias MC method is based on a scheme developed by Rosenbluth and Rosenbluth¹⁴⁵ to study polymer conformations. The method has been extensively applied to adsorption of long chain hydrocarbons in zeolites by Smit et al.^{47,48}

Car–Parrinello Approach

Simulations using force fields are capable of exploring the properties of complex systems, but these methods cannot adequately describe the atomic dynamics in parts of configurational space that were omitted in the parameterization of the force field. In the force field methods, it is implicitly assumed that the valence electrons follow the atomic motion, and a redistribution of the valence electrons because of this motion is not taken into account. Thus, bond-making and bond-breaking processes are generally outside the scope of force field methods. It would be of great utility to have a method available that overcomes such restrictions where, for example, the forces acting on the atoms would be calculated according to the electronic state of the system having a particular atomic configuration. This can be accomplished by means of quantum mechanics because information on both the atomic dynamics and the electron–structure characteristics would be obtained. In an MD (or energy minimization) study based on quantum mechanics, the following steps are followed:

1. Select an initial atomic configuration.
2. Use one of the methods of quantum chemistry to perform an electronic structure calculation.
3. From the wavefunction Ψ , compute the forces on the atoms.
4. Move the atoms to new positions.
5. Go to step 2.

Note that these steps are equivalent to the force field–based method, but the forces are derived quantum mechanically. Accordingly, one can carry out simulations in the ground or electronically excited states as well as account for chemical reactions.

Despite the theoretical feasibility of the scheme, it is quite limited from the computational point of view. The electronic structure calculations are carried out by matrix diagonalization, which is iteratively repeated until a self-consistent solution is found. Even for small systems, this procedure is time-consuming, and because it must be repeated for each atomic configuration during a simulation, it is easy to see that such calculations are impractical. A way out was found by Car and Parrinello.¹⁴⁶

The Car–Parrinello (CP) approach is an extended energy minimization and MD scheme in which electronic degrees of freedom are treated explicitly on an equal footing with nuclear coordinates. Below we outline the conceptual scheme of the method and refer the interested reader elsewhere for a comprehensive discussion.^{147,148}

Let us describe the electronic state of a system by a set of one-electron wavefunctions (orbitals) $\phi_1 \dots \phi_n$, which are represented by expansion over some basis functions as in Eq. [4]. Formally, one may consider the set of coefficients $c_k^i \equiv C^i$ as a set of coordinates that specifies the “position” of the orbital i

in a space of the coefficients $\{\mathbf{C}^i\}$ exactly in the same way as x , y , and z coordinates determine the position of an ion I in the configurational space $\{\mathbf{R}_I\}$. Each atom is considered to be a positive ion in a sea of electrons.

Using the analogy between the ionic and electronic coordinates, one may assign to the “particles” \mathbf{C}^i a fictitious mass μ that controls the motion momentum of the “particles” through coefficient space, and one may define a “velocity” of the “particles” as

$$\dot{c}_k^i \equiv \frac{dc_k^i}{dt} \quad [69]$$

The system is thus uniquely defined by the sets of ionic \mathbf{R}_I and electronic coordinates \mathbf{C}^i and their conjugate momenta.

At this point, let us recall that the equations of motion for a particle i characterized by the generalized coordinate w_i and conjugate momentum \dot{w}_i are derived from a Lagrangian described in Eq. [48] as

$$\frac{d}{dt} \frac{\partial \mathcal{L}}{\partial \dot{w}_i} - \frac{\partial \mathcal{L}}{\partial w_i} = 0 \quad [70]$$

For the extended system of ions and “particles” \mathbf{C}^i , the Lagrangian may be obtained by extension of the classical Lagrangian for ionic dynamics by means of a (fictitious) kinetic energy term due to the particles \mathbf{C}^i

$$\mathcal{L} = \frac{1}{2} \mu \sum_{i=1}^n \sum_{k=1}^m (\dot{c}_k^i)^2 + \frac{1}{2} \sum_{I=1}^N \sum_{\alpha=x,y,z} M_I (\dot{\mathbf{R}}_I^\alpha)^2 - U(\mathbf{R}_I, \mathbf{C}^i) \quad [71]$$

The $U(\mathbf{R}_I, \mathbf{C}^i)$ is the Born–Oppenheimer energy, which now explicitly depends on the c_k^i coordinates and consists of the nucleus–nucleus, electron–nucleus, and electron–electron interaction energy terms. Note that the real electron kinetic energy is included in this last term. The equation of motion for the particles (both real and fictitious) are then obtained from the extended Lagrangian (Eq. [71]) and reads as follows:

$$M_I \ddot{\mathbf{R}}_I = - \frac{\partial U(\mathbf{R}_I, \mathbf{C}^i)}{\partial \mathbf{R}_I} \quad [72]$$

$$\mu \ddot{c}_k^i = - \frac{\partial U(\mathbf{R}_I, \mathbf{C}^i)}{\partial c_k^i} + \Lambda_k^i \quad [73]$$

where the second term Λ_k^i in the right-hand side of Eq. [73] is a constraint “force” that assures that the orbitals ϕ remain orthonormal:

$$\int \phi_l^* \phi_m d\mathbf{r} = \sum_{k=1}^m c_k^{l*} c_k^m = \delta_{lm} \quad [74]$$

Equation [73] has the same form as the equations of motion for molecules with constrained internal coordinates,¹³ and we already know that such equations can be solved effectively using the SHAKE algorithm.¹³⁰ Equations [72] and [73] play a key role in the Car–Parrinello method and enable one to run the dynamics for both ionic and electronic degrees of freedom in parallel. With carefully chosen effective mass μ and a small time step, the electronic state adjusts itself instantaneously to the nuclear configuration (Born–Oppenheimer principle), and, therefore, the atomic dynamics is computed along the system’s Born–Oppenheimer surface. Note that there is no need to carry out the costly matrix-diagonalization procedure for performing electronic structure calculations.

Up till now, we have not specified a way to calculate the forces acting on the particles in our extended system. For the ions, the forces are computed using the Hellmann–Feynman theorem, which states that if $\Psi(\mathbf{r})$ is a stationary wavefunction of the system, then

$$\mathbf{F}_I = -\frac{\partial U}{\partial \mathbf{R}_I} = \left\langle \Psi^*(\mathbf{r}) \left| \frac{\partial \mathbf{H}}{\partial \mathbf{R}_I} \right| \Psi(\mathbf{r}) \right\rangle \quad [75]$$

To calculate the forces on electronic coordinates, one has to specify the details of the electronic structure calculations. Although the CP scheme outlined above is by no means limited to a particular method of quantum chemistry, most of the CP studies performed so far have been carried out using DFT methods because these handle large systems fairly rapidly.^{147,148} The ion may be considered as either a bare nucleus or an atom minus valence electrons. The latter model simplifies the calculations but necessitates using pseudopotentials to describe the interaction between the valence electrons and ion.

SOME SELECTED APPLICATIONS

Framework Dynamics

Modeling of dynamics of zeolite frameworks has two main goals. The first is to test whether a particular force field is suitable for description of the dynamic characteristics of the lattice as well as to simulate the zeolite structure itself. Examples of such calculations were mentioned in the section on Potential Models for Framework Modeling. The second and most challenging goal is to provide a qualitative (quantitative would be even more desirable) interpretation of experimental data, in particular, data from spectroscopic experiments. Mod-

eling zeolite spectra can, in principle, help not only to explain spectral features in terms of specific atomic motion, but also to predict how this motion will manifest itself in the corresponding vibrational spectra of a given structure. Most of the examples that follow below have the second aim as their main goal.

Framework Local Modes

In 1971 Flaningen, Khatami, and Szymanski¹⁴⁹ proposed an empirical assignment of the vibrational bands in the spectra of zeolites. Structure-insensitive bands were attributed to intratetrahedral modes of TO_4 tetrahedra, whereas those showing dependence on framework topology were assigned to vibrations of secondary building units. Even though this classification had been used extensively in many vibrational spectroscopic studies of zeolites, several theoretical attempts were undertaken to elucidate whether particular structural subunits of the frameworks could actually be identified by a specific pattern in the spectra. In particular, much effort was applied to identify the bands resulting from vibrations of rings having different sizes. Indeed, the scheme of Flaningen et al.¹⁴⁹ implies a possibility of ascribing a normal mode of the lattice to a vibration (or vibrations) localized on particular substructures of the lattice.

De Man and van Santen¹⁵⁰ performed a normal mode analysis of both cluster and periodic models of zeolite lattices using the GVFF developed by Etchepare et al.⁹⁶ In an attempt to find a relation between specific normal modes and the presence of particular substructures, de Man and van Santen compared spectra of zeolite lattices with those of lattice substructures, projected eigenvectors of a substructure in the framework onto the eigenvectors of the molecular model of the structure, and constructed the difference and sum spectra of frameworks with and without particular structural units. The study concluded that there is no general justification for correlating the presence of large structural elements with particular features in the vibrational spectra.

Creighton, Deckman, and Newsam⁹⁷ simulated the infrared and Raman spectra of sodalite frameworks using the NMA method and a GVFF model. The number of bands observed in the sodalite spectra was smaller than expected from symmetry considerations, a finding the authors attributed to an overlapping of bands that fall into a narrow spectral interval. In addition, the intensity of many bands appeared to be less than 1% of that of the most intense band. The normal modes of cation-exchanged sodalites were analyzed in terms of symmetry coordinates for structural subunits (TO_4 tetrahedra, four- and six-membered rings). Confirming the results of de Man and van Santen, Creighton and coworkers found that no vibrations can be regarded as exclusively SiO_4 or AlO_4 tetrahedral modes. Nevertheless, it was shown that most of the normal modes involve only a few of the symmetry coordinates. For example, the Raman active mode computed at 471 cm^{-1} can be represented as a pore-opening vibration of a four-membered ring (4-R) that receives its main contributions from the symmetric bending coordinates of the 4-R structures. This work has also revealed relationships between the intensities and positions of spectral

bands with structural features of the frameworks. In particular, the intensity of the infrared-active band at 750 cm^{-1} was found to correlate with the value of the Si-O-Al angle in the structure.

Correlations between the spectrum of zeolite A and spectra of several $(\text{TO})_8\text{T}_8\text{O}_{12}$ models constructed to mimic double four-membered rings (D4-R) of the zeolite structure were studied by Bärtsch et al.⁹⁸ As above, this investigation used NMA and a GVFF derived by the authors from matching experimental data. Analysis of the potential energy distribution of normal modes revealed that the vibrational spectra of the models above can be divided into four regions corresponding to $\nu_{as}(\text{T}-\text{O}-\text{T})$, $\nu_s(\text{T}-\text{O}-\text{T})$, $\delta(\text{O}-\text{T}-\text{O})$, and $\delta(\text{T}-\text{O}-\text{T})$ modes. It was found that four vibrations can be attributed to breathing modes of zeolite subunits: 476 cm^{-1} to the D4-R unit; 288 and 271 cm^{-1} to the sodalite cage, and 214 cm^{-1} to pore openings of eight-membered ring windows in the structure. The frequency of the former Raman active vibration at 476 cm^{-1} compares well with the 4-R pore-opening vibrational frequency computed by Creighton, Deckman, and Newsam.⁹⁷

The study of ring-opening vibrations in spherosiloxanes was continued by Bornhauser and Calzaferri,¹⁵¹ who investigated the vibrational spectra of known and hypothetical molecules of general formula $(\text{HSiO}_{3/2})_{2n}$, $n = 2, 3, 4, \dots$. This study confirmed the group frequency scheme proposed in their earlier paper.⁹⁸ The pore-opening vibrations of the ring structures were calculated to occur in the 490 – 390 , 440 – 250 , and 340 – 210 cm^{-1} spectral regions for four-, five-, and six-membered rings, respectively. For example, for all the structures studied, the 4-R pore-opening Raman active mode appears in the interval 420 – 455 cm^{-1} . Bornhauser and Calzaferri also noticed that no pore-opening modes fit the above-mentioned group frequency scheme of the earlier paper.⁹⁸

Iyer and Singer^{152,153} designed a systematic procedure for assigning normal modes to local structural units by using spatial and energetic localization criteria. They applied this approach to the investigation of local modes in sodalite and zeolite A structures, using the shell model potential developed by Sanders et al.⁸⁸ Many vibrations localized on the 4-R, 6-R, and D4-R secondary building units were represented as a linear combination of normal modes, some of which fell within a narrow frequency interval. For example, a 4-R local mode at 448 cm^{-1} (breathing vibration of O atoms) is a linear combination of normal modes within a 30 cm^{-1} interval. Furthermore, the authors found a high degree of transferability between the 4-R local modes in sodalite and zeolite A structures. Thus, the above mentioned 4-R local mode at 448 cm^{-1} in the sodalite structure has a counterpart at 428 cm^{-1} in the framework of zeolite A.¹⁵³ The latter mode was also found to be localized on the D4-R unit. However, the authors stress that the character of the local modes found might be dependent on the force field used to obtain the normal modes of the lattices.

Figure 14 shows the atomic displacements and compares the vibrational frequencies of the 4-R pore-opening mode computed in Refs. 97, 98, and 153.

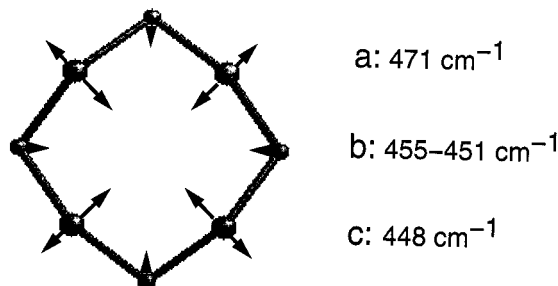


Figure 14 Atomic displacements and vibrational frequencies of the 4-R opening vibration computed in Refs. 97 (a), 98 (b), and 153 (c).

The frequencies calculated are similar even though the results of Refs. 97 and 98 were obtained with a GVFF model in contrast to a shell model used by Iyer and Singer.¹⁵³ The vibration might be related to the band at 489 cm^{-1} in the experimental Raman spectrum of zeolite A.¹⁵⁴

We now return to all-silica faujasite to examine the 4-R opening modes in this structure (which contains two kinds of 4-R subunit). The first kind of four-membered ring is located in the sodalite blocks, whereas the second forms side faces of the hexagonal prisms. Defining the ring opening as a fluctuation of the ring area, one can easily calculate the corresponding spectra using the MD method. Figure 15 compares the MD computed spectra¹⁵⁵ of the 4-R window-opening motions with the computed infrared and Raman spectra of the faujasite structure. The high frequency limit of the ring-opening modes occurs at ca. 520 cm^{-1} , in good agreement with the results of Bornhauser and Calzaferri.¹⁵¹ Despite the similarities in the power spectra of this motion for both kinds of ring, there is a noticeable difference between the spectral patterns. In fact, Figure 15 shows that (1) the simple pore opening is a linear combination of numerous normal modes of the lattice, and (2) no unambiguous attribution of an infrared or Raman active band to the ring opening may be made. Indeed, one may hardly attribute a particular band in the IR or Raman spectra of all-silica faujasite to the ring-opening vibration.

Although no band can be assigned to a specific vibration in the TO_4 tetrahedra, for aluminosilicate structures, a strong band at 960 cm^{-1} in the infrared spectra of Ti-substituted zeolites is used as the fingerprint of titanium incorporation into the frameworks. A number of assignments have been proposed for this feature; for example, it was attributed to a vibration in $\text{Si}-\text{O}^{\delta-}\cdots\text{Ti}^{\delta+}$ units,¹⁵⁶ a $\text{Ti}=\text{O}$ vibration,¹⁵⁷ or to a $\text{Si}=\text{O}_2$ mode.¹⁵⁸ Two more recent investigations have shown unambiguously that this band belongs to a vibration of the $\text{Si}-\text{O}-\text{Ti}$ bridges.^{21,26}

De Man and Sauer²⁶ performed ab initio quantum chemical calculations on Ti-containing molecular structures representing zeolite units. The calculations allowed them to assign the 960 cm^{-1} band to an antisymmetric $\text{Si}-\text{O}-\text{Ti}$

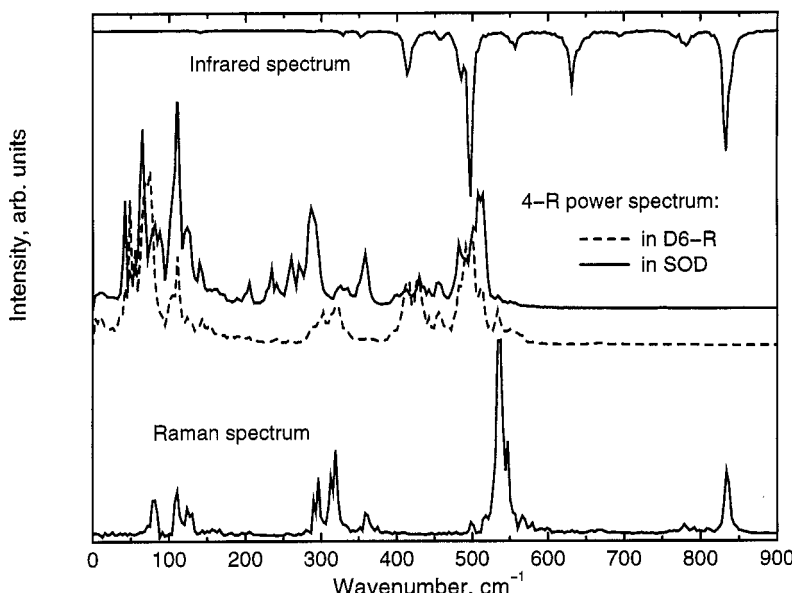


Figure 15 Power spectrum of opening motion of four-membered rings in silica faujasites compared to the infrared and Raman spectra of the structure. SOD and D6-R notations correspond to the rings situated in the sodalite blocks and hexagonal prisms, respectively.

stretching vibration. The red shift of the vibration, compared to the frequency of the corresponding Si—O—Si mode, is due to the decrease of the Ti—O stretching force constant, resulting from a 0.2 Å increase of the Ti—O bond length versus the Si—O bond length. The mass effect plays a minor role in the shift of the band.

Smirnov and van de Graaf²¹ carried out an MD study of Ti-substituted MFI structures by means of a simplified GVFF. Introducing Ti atoms into the framework led to the appearance of a band at 935 cm⁻¹ that resembles well the observed fingerprint band. Analysis of density of vibrational states for TO_4 tetrahedra ($\text{T} = \text{Si}, \text{Ti}$), computed by using different force constant values for the T—O bond, enabled the authors to attribute the band to a localized Si—O vibration in the Si—O—Ti bridges. The localization is caused by the inequivalence of the Si—O and Ti—O stretching force constants. The difference in masses of the Si and Ti atoms cannot account for the low frequency position of the band. Both conclusions agree with the results of de Man and Sauer.²⁶

Zeolite Aperture Fluctuations

Among pore-opening vibrations of zeolite structures, those resulting in fluctuations of window aperture are of great importance for the majority of zeolite applications, because the window openings dictate the molecular sieving

capabilities of the structures and control the access to active sites of the internal surface of the solids. Modeling the framework dynamics yields direct information about the dynamic size of the apertures in the structures. Insight into the frequencies involved in those aperture motions can be obtained by analyzing the Fourier transform of the window diameter (area) autocorrelation function.¹⁸

Deem and coworkers¹⁸ studied the variations in window aperture with temperature for six representative zeolite structures (SOD, RHO, TON, MFI, LTL, BEA) containing apertures as defined by the number of oxygen atoms ranging from 6 (SOD) to 12 (BEA). For all the structures, the window diameters, defined as the distance between the oxygen atoms located on opposite sides of the window, were found to have well-defined periodic fluctuations, with period and amplitude depending on which oxygen atoms were used to define the diameter and on the framework connectivity. The data obtained for the LTL structure (12-ring windows) showed that the frequencies of the window diameter fluctuations appear up to 400 cm^{-1} . The breathing motion of the window area in this structure was computed to occur at a frequency of ca. 200 cm^{-1} and varies slightly with temperature.

Figure 16 shows a 12-membered ring in the faujasite structure that forms a window between the big cavities. Not all the oxygens of the ring lie in a plane, so the window area may be defined here as a surface of the hexagon formed by the six O_1 atoms located in the same plane.¹⁵⁹ For the sodium form of zeolite Y, Schrimpf et al.¹⁵⁹ calculated that the largest window deformations arise from low frequency vibrations in the region $30\text{--}100\text{ cm}^{-1}$. Results of an MD calcula-

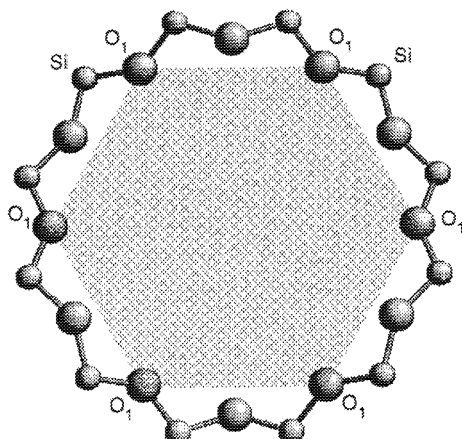


Figure 16 A 12-membered ring in faujasite that forms windows between large cavities in the structure. Surface of the hexagon formed by six O_1 atoms defines the window area.

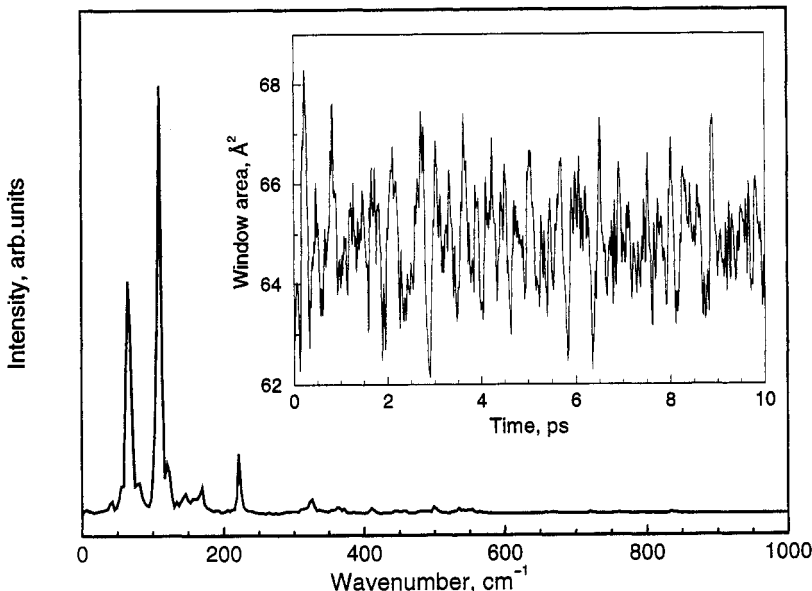


Figure 17 Fluctuations of the window area (inset) and spectrum of the fluctuations of the 12-R windows in silica faujasite structure.

tion¹⁵⁵ carried out for all-silica faujasite are presented in Figure 17, where periodic fluctuations of the window area with frequencies of ca. 65 and 112 cm^{-1} are shown to be in agreement with data of Schrimpf and coworkers.¹⁵⁹

An MD study of zeolite A¹⁹ with eight-membered ring windows showed that the mean window diameter and the mean-square amplitudes of the diameter fluctuations are affected by the nature of the charge-compensating cations in the structure (in this structure one type of cations is located in the windows). For both siliceous and aluminated structures, the spectrum of window diameter fluctuations has a well-defined pattern, with the most prominent band at ca. 100 cm^{-1} . This band was calculated to undergo a low frequency shift upon introduction of the extra-framework cation into the structure, and the band correlates strongly with an intense band in the computed Raman spectrum. A band at this frequency is also present in the experimental spectrum, and the band displays trends upon cation exchange similar to the calculated band.¹⁰⁰ Much higher values for the frequency of the window fluctuations in the siliceous form of zeolite A were computed by Demontis and Suffritti,¹⁶⁰ who obtained a low frequency limit of ca. 300 cm^{-1} for this motion.

Extra-Framework Cation Dynamics

Strictly speaking the extra-framework cations do not belong to the zeolite lattice; nevertheless, their dynamics is often considered along with those of the framework. The mobility of the extra-framework cations is of particular inter-

est. Faux, Smith, and Forester,¹⁶¹ who used the flexible framework approach to perform an MD study of both dehydrated and hydrated Na⁺ zeolite A, found that the mobility of the cations depends on the sites occupied by those cations, as shown in Figure 18. Thus, Na(2) cations situated in the eight-membered rings (windows) of the structure have the highest degree of mobility for motions both in the plane of the window and out of the plane. The computed amplitude of the out-of-plane motion for this kind of cation can be as large as 1 Å, and a migration between equivalent sites in the window plane occurs. In contrast, Na(1) cations in six-membered rings vibrate about the center of the rings but do not migrate away in the time scale of the simulation (300 ps).

The variation of the far-infrared and Raman spectra of zeolites, induced by the exchange of cations, clearly indicates that the cationic degrees of freedom manifest themselves in that frequency region where large-amplitude deforma-

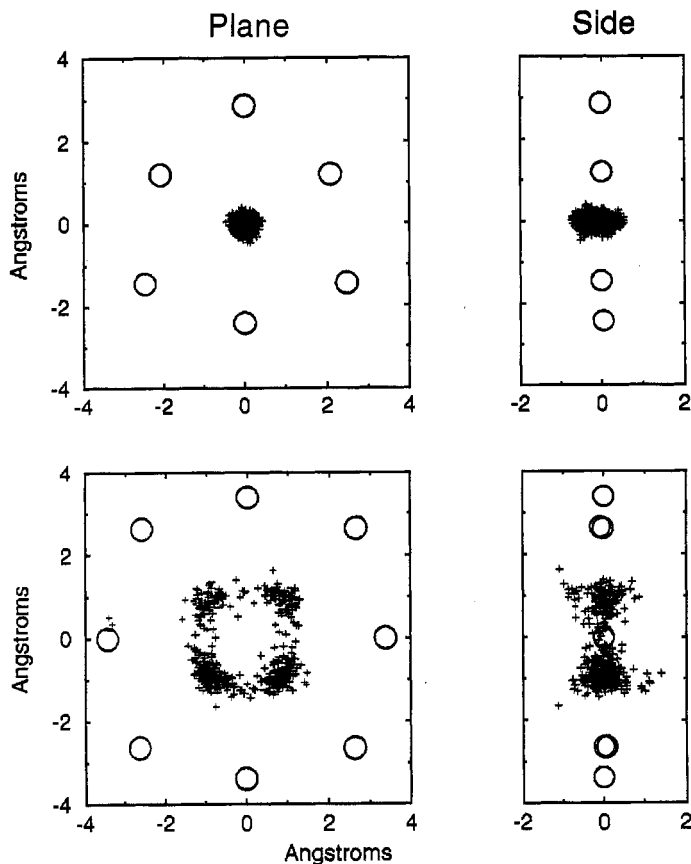


Figure 18 Motion of sodium cations in 6-rings and 8-rings of dehydrated zeolite A structure. Data from Ref. 161, reprinted with permission of the American Chemical Society.

tion motions of the framework are expected (see preceding section). Accordingly, the assignment of the low frequency bands in these zeolite spectra was a subject of discussion for a long time. The location of the charge-compensating cations in certain positions suggests that, in a simple interpretation, each feature appearing in the spectra may be assigned to the cationic motion at one particular site, whereas changes of the spectra due to different Si/Al ratios may be attributed to different partial occupancies of the sites.¹⁶²

Assuming an ionic-like interaction potential between the framework atoms and cations, Smirnov et al.¹⁰⁰ performed an MD study to assess the cation dynamics in zeolite A. The calculation of the power spectra for Na⁺ and K⁺ cations at each site revealed that no specific spectral pattern can be attributed to a particular cation position. Vibrations of cations in all sites occur over a frequency region of 30–300 cm⁻¹. In addition, the spectra calculated with a flexible framework showed a substantial coupling between the cationic and lattice degrees of freedom. The results of this work¹⁰⁰ have brought into question the assignments proposed for the bands in the far-infrared spectra of cationic forms of zeolites.

A comparative computational study of cation-exchanged zeolite Y¹⁶³ has confirmed the conclusions reached in Ref. 100. The infrared and Raman spectra of the Na and K forms of this structure were investigated by means of energy minimization and MD techniques. In both methods, the interaction between the cations and framework atoms was described by a rigid ion potential with the use of different functional forms. Figure 19 shows that the far-infrared spectra computed by both methods agree well with experiment. The contribution to the spectra of cations located at each cationic site has revealed unambiguously that no band can be assigned to vibrations of a cation in one specific position in the lattice.

Zeolite/Template Interactions: Tetrabutylammonium and Tetrapropylammonium in MEL and MFI Structures

To illustrate the uses of modeling for understanding zeolite-template interactions, some results are presented from a recent energy minimization study¹⁶⁴ on the interactions of tetrabutylammonium (TBA) and tetrapropylammonium (TPA) ions with the all-silica zeolites MEL and MFI. TPA is the template that is normally used to synthesize MFI, and TBA was used to synthesize MEL, but is now superseded by N,N-diethyl-3,5-diethylpiperidinium ions.^{165,166} MFI and MEL are closely related. Both zeolites are built from identical pentasil (consisting of five-membered rings) layers:^{167,168} in MFI these layers are related by inversion, but they have mirror symmetry in MEL. These different layer connections give rise to two different two-dimensional pore systems: in MFI one finds zigzag channels and straight channels parallel to the α

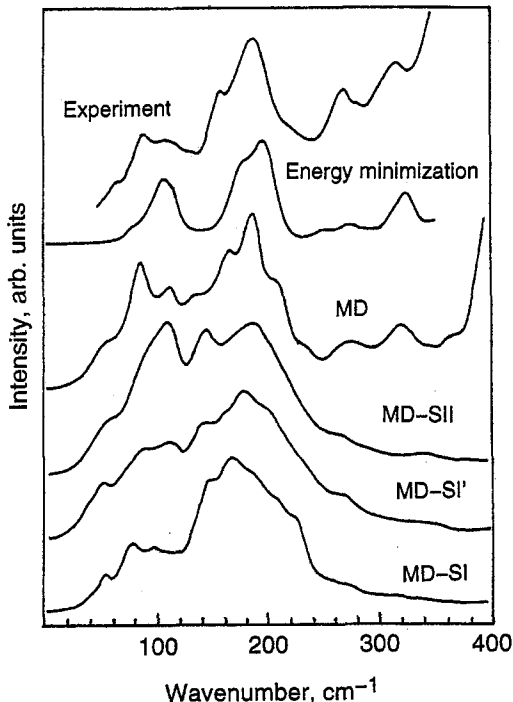


Figure 19 Comparison of the experimental and the MD and EM calculated far-infrared spectra of NaY zeolite. MD-SII, MD-SI', and MD-SI denote power spectra of Na^+ cations in cationic site II, site I', and site I, respectively. From Ref. 163.

and b axes, respectively, whereas in MEL there exist straight channels along the a and b axes. In both MFI and MEL, the channels intersect leading to four intersections per unit cell. MFI exhibits only one type of intersection, as shown in Figure 20(a). In MEL there are two types of intersection: one for which the overlap of crossing channels is large [Figure 20(b)], and one which is significantly smaller [Figure 20(c)]. At temperatures below 350 K, the MFI structure has a monoclinic unit cell that changes to an orthorhombic unit cell as temperature rises. The MEL structure has only one modification.

Both the template molecules and the zeolite frameworks were treated as flexible, using the zeolite force field developed in Delft⁹³ together with the MM3 force field developed by Allinger et al.^{169,170} Calculations were carried out on systems consisting of different combinations of templates (TBA and TPA) and zeolites (MFI and MEL). Salient results are given in Table 5.

The empty, monoclinic MFI structure is calculated to be 37.0 kJ/mol more stable than empty MEL. Both the monoclinic and the orthorhombic MFI structures are minima on the potential energy surface described by the force field¹⁷¹ and, in agreement with the experimental data, the monoclinic MFI structure has

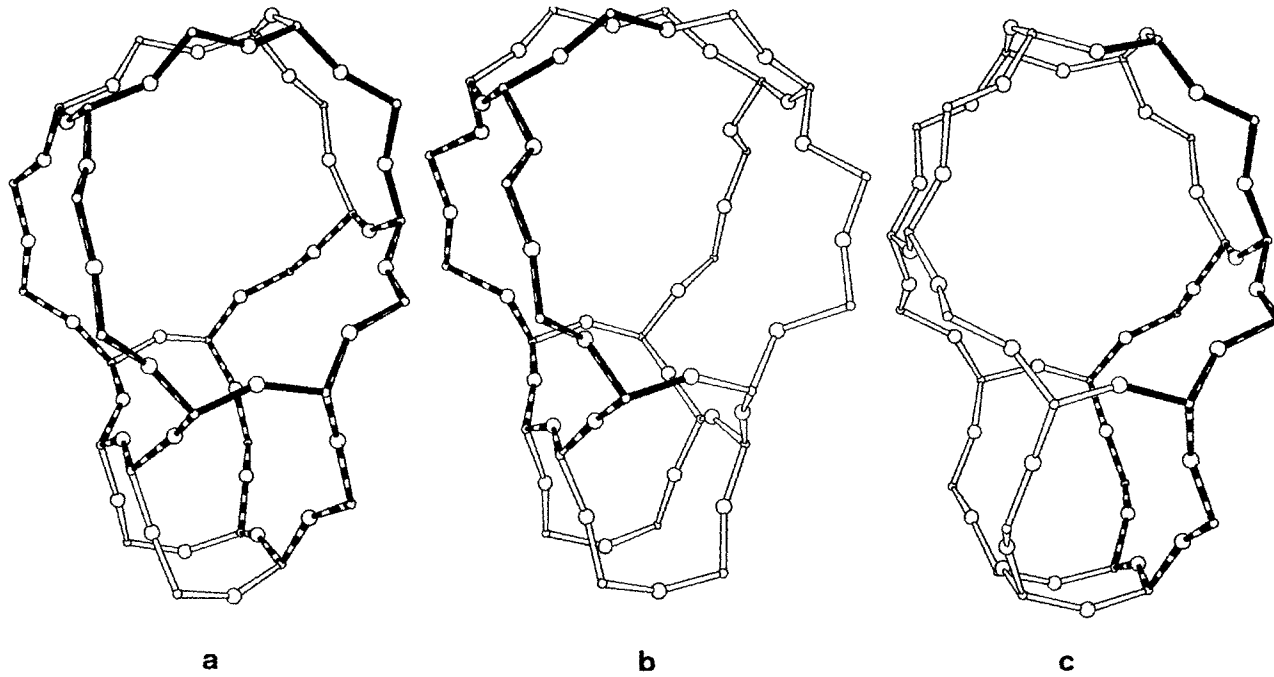


Figure 20 Intersections of the channels in the MFI structure (a) and the MEL structure (b, c). In the MFI intersection, one of the double 10-rings in the straight channel is indicated in black; the 10-rings in the sinusoidal channel are dashed. In MEL, one of the intersections (b) can be obtained by connecting the “left”-half of the MFI intersection with its mirror image; the other intersection (c) can be obtained by connecting the “right”-half of the MFI intersection with its mirror image.

Table 5 Energies Relative to Empty MFI and Isolated TPA and TBA

System	Energies in per unit cell (kJ/mol)			
	$\Delta E_{\text{zeolite}}$	$\Delta E_{\text{organic}}$	$\Delta E_{\text{host-guest}}$	ΔE_{total}
MEL	37.0			37.0
MEL1/1TPA	60.5	0.8	-166.5	-105.2
MEL2/1TPA	63.8	21.8	-139.7	-54.2
MEL/4TPA	277.6	128.4	-833.5	-427.4
MFI/1TPA	25.1	18.8	-164.0	-120.0
MFI/4TPA	228.4	144.3	-855.6	-482.8
MEL1/1TBA	59.6	1.7	-205.4	-144.1
MEL2/1TBA	63.8	27.2	-176.1	-85.1
MEL1/2TBA	101.5	7.5	-438.9	-329.9
MFI/1TBA	26.8	28.9	-191.6	-136.0
MFI/2TBA	84.5	95.4	-401.2	-221.3

the lower energy at room temperature.¹⁶⁸ Empty MEL relaxes in space group *Imm2*.

For the MEL–template systems, there are large differences between the two different types of intersection. Both TPA and TBA prefer MEL1 over MEL2 because in MEL2 the templates cannot adopt their most favorable conformation as they can in MEL1. Similarly, these most favorable conformations cannot be adopted in MFI (see Figure 21). Hence, both templates stabilize MEL more than MFI at loadings of one and two template molecules per unit cell. This explains why MEL is formed preferentially when TBA is used as the templating agent. Because of severe overcrowding (see Figure 22), neither MEL nor MFI will accommodate easily more than two TBA molecules per unit cell.

Since TPA is a smaller molecule than TBA, both MEL and MFI can accommodate four molecules of TPA per unit cell without overcrowding. However, at this loading MEL is forced to accommodate two template molecules at the MEL2 intersection. Therefore, MFI/4TPA has a lower energy than MEL/4TPA, in agreement with the experimental evidence that MFI is formed preferentially when TPA is used as the templating agent.

Isomorphic Substitution

Titanium silicalite-1 (TS-1), first synthesized in 1983,¹⁷² is well known for its outstanding ability to catalyze various oxidation and hydroxylation reactions.¹⁷³ This catalytic activity is ascribed to the presence of Ti atoms in the zeolite. Knowledge of the effect of the Ti atoms on the framework structure and of the location of the Ti atoms in the zeolite would be useful in understanding the catalytic properties of TS-1. Although TS-1 has been characterized extensively,¹⁷⁴ the location of the Ti atoms in the zeolite is still under discussion. The maximum amount of framework Ti has been reported to be 2.5 Ti atoms per

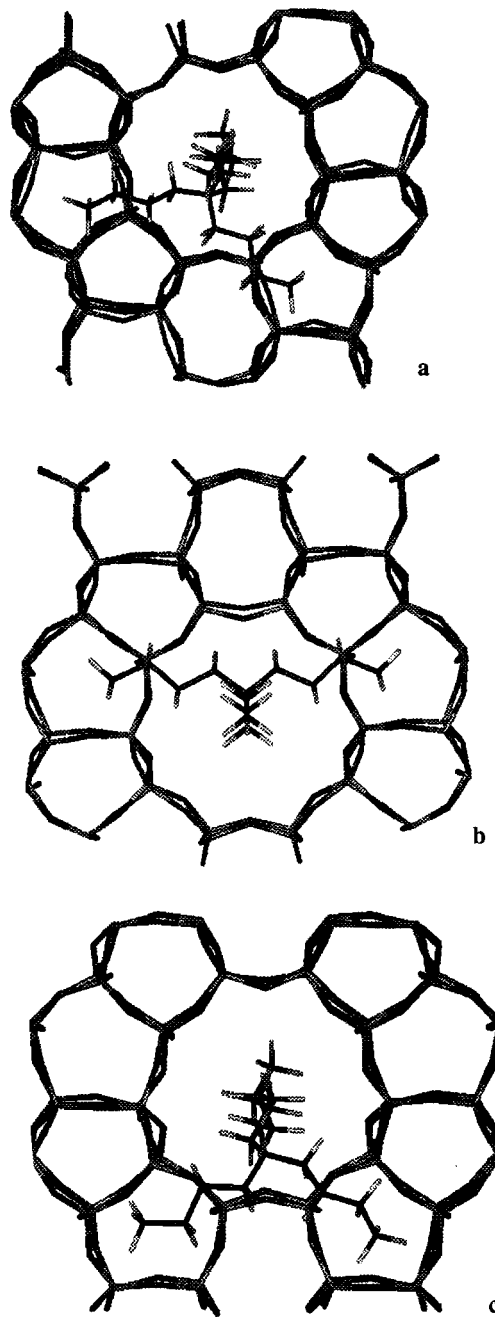


Figure 21 The template TBA located in the intersections of MFI (a) and MEL (b, c).

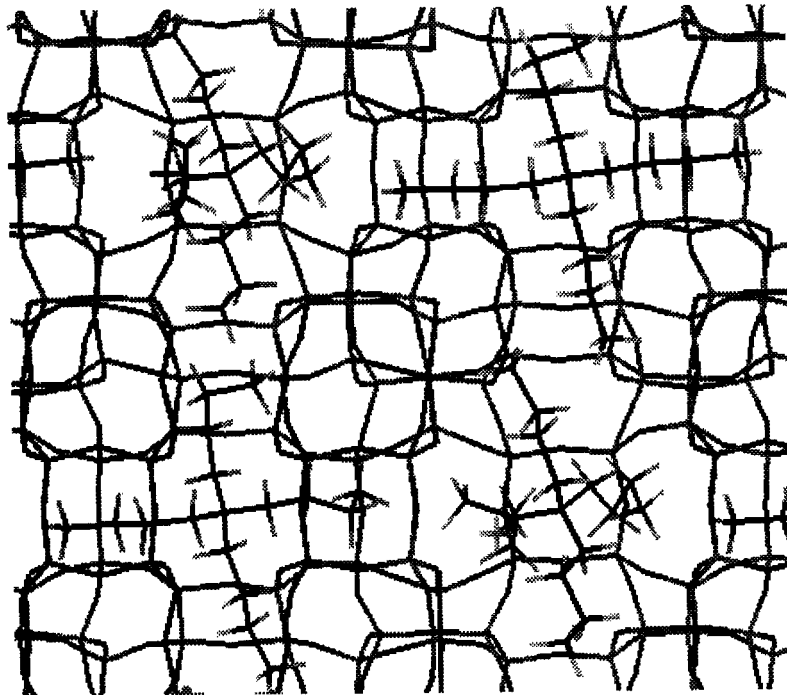


Figure 22 Overcrowding when four TBA ions per unit cell are loaded in MEL.

unit cell ($\text{Ti}/(\text{Si} + \text{Ti}) = 0.026$). Higher Ti loadings give rise to nonframework Ti.²⁷ It is supposed that only framework Ti(IV) is responsible for the catalytic properties of TS-1.¹⁷⁵ The actual location of the Ti atoms in the framework is difficult to determine experimentally. Therefore, information obtained from theoretical methods is of considerable interest.

In the orthorhombic MFI structure, substitution can take place at 12 crystallographically different tetrahedral (T) sites (numbered T1–T12). In the monoclinic MFI framework, the mirror symmetry is lost and 24 crystallographically different T-sites can be distinguished (see Figure 23).

Several computational studies have been conducted on the location of Ti in TS-1, including one by Jentys and Catlow,²⁸ who used defect energy minimization techniques and quantum mechanical cluster calculations to study the Ti substitution in monoclinic MFI. Their calculations showed that incorporation of Ti atoms into the zeolite lattice at T-sites is preferred over the formation of bridges consisting of a Ti atom bonded to four oxygen atoms, which are pairwise-bonded to Si atoms located in the lattice (see Figure 24). With respect to incorporation of Ti atoms at T-sites, it was found that although no site was clearly preferred, there were a slight preference for T6 and T19, whereas T18

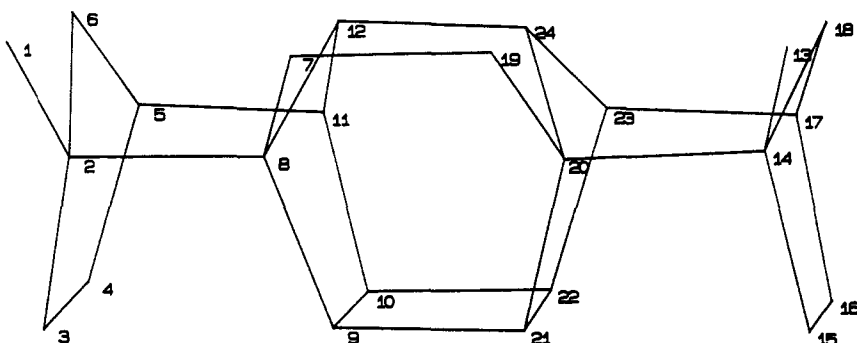


Figure 23 Crystallographically different T-sites in MFI. T1(T2, . . . , T12) and T13(T14, . . . , T24) are related by a mirror plane in orthorhombic MFI.

was least favored (note that T6 and T18 are related by mirror symmetry in the orthorhombic structure).

Millini, Perego, and Seiti²⁹ conducted local density functional quantum mechanical calculations on monomeric $\text{Ti}(\text{OH})_4$ and pentameric $\text{Ti}(\text{OSiO}_3\text{H}_3)_4$ clusters to study the Ti substitution patterns in orthorhombic MFI. They kept fixed the geometry of the cluster, which was abstracted from the orthorhombic MFI framework, while replacing a Si atom by a Ti atom. No clear preference for a substitution site was found, although sites T12 and T3 were energetically favored slightly, whereas T4 and T5 were preferred least. Oumi et al.³⁰ also investigated Ti substitution in orthorhombic MFI but used molecular dynamics calculations in their study. They evaluated the influence of substituting one Ti atom per unit cell on the lattice parameters and then compared their results with experimental X-ray diffraction data. Their comparison did not invoke thermodynamic equilibrium to predict the Ti distribution (in contrast to all other published studies). T8 was found to be the most probable site for Ti substitution. In contrast, Smirnov and van de Graaf²¹ did not find any correlation between the unit cell expansion and Ti location. The MD calculations,²¹ in which the Ti atoms are randomly placed in the framework, perfectly repro-

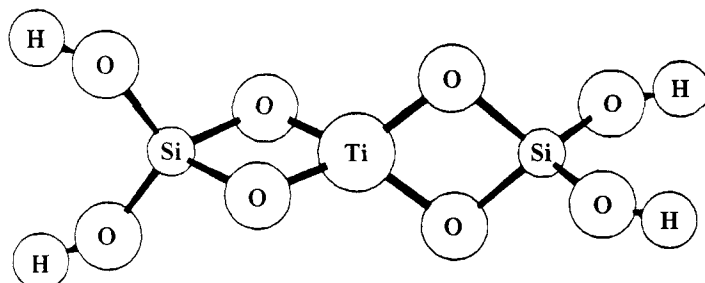


Figure 24 Extra-framework Ti-containing cluster.

duced the experimental unit cell expansion as a function of the Ti loading (see Figure 25).

De Man and Sauer²⁶ performed ab initio calculations on molecules containing Ti, Si, O and H which are meant to represent substructures of titanozolites. Their study showed that Ti atoms prefer a fourfold coordination in zeolites: their calculated relative energies and vibrational spectra make other forms of incorporation very unlikely. Njo, van Koningsveld, and van de Graaf³¹ used a combination of Metropolis Monte Carlo and energy minimization methods to investigate the Ti atom distribution over the T-sites in MFI. In their approach, trial configurations are created by exchanging a randomly chosen Ti atom with a randomly chosen Si atom, which is in contrast to all previously mentioned substitution studies, in which Ti atoms are incorporated at symmetry-related positions. With this combined computational scheme, information regarding the influence on the substitution of the T-sites themselves and on the distances between the T-sites can be obtained. The difference between this method and the plain Metropolis Monte Carlo scheme is that the trial configuration is energy-minimized before it is evaluated for acceptability.

Because modeling of the Ti distribution at loadings above the experimentally determined maximum limit (2.5 Ti atoms per unit cell) seems questionable,

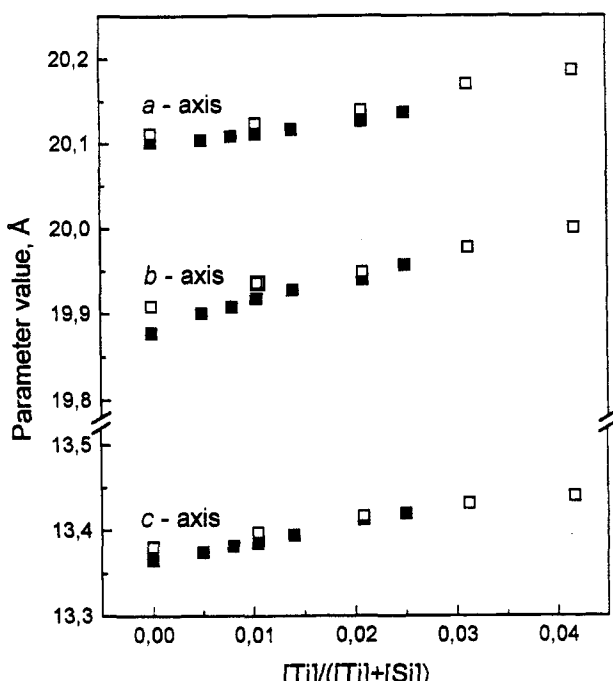


Figure 25 Lattice parameters as a function of the $\text{Ti}/(\text{Ti} + \text{Si})$ ratio. Open squares denote calculated values; solid squares are experimental values.

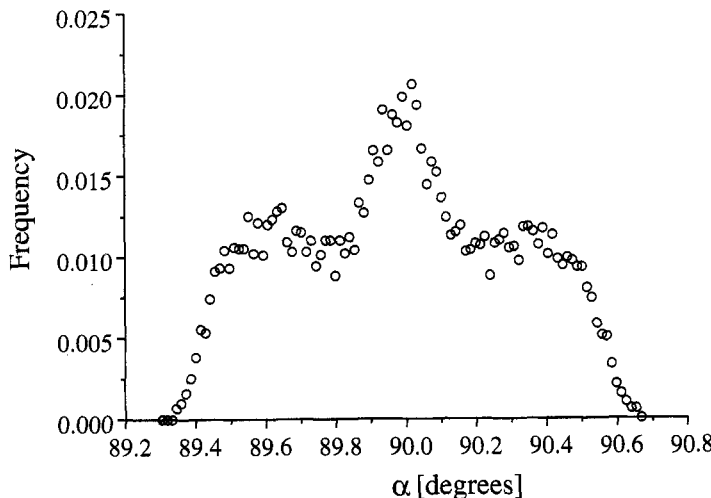


Figure 26 Lattice parameter α distribution.

a constant strain was maintained on a double unit cell containing 5 Ti, 187 Si, and 384 O atoms while the calculations were carried out. The results showed that the Ti atoms in TS-1 are distributed over all lattice positions rather than being located at one preferred T-site (see Figures 26 and 27). The distribution, however, is not random: T2 and T12 sites are clearly preferred. The framework symmetry is related to both the location of the Ti atoms and the Ti loading.

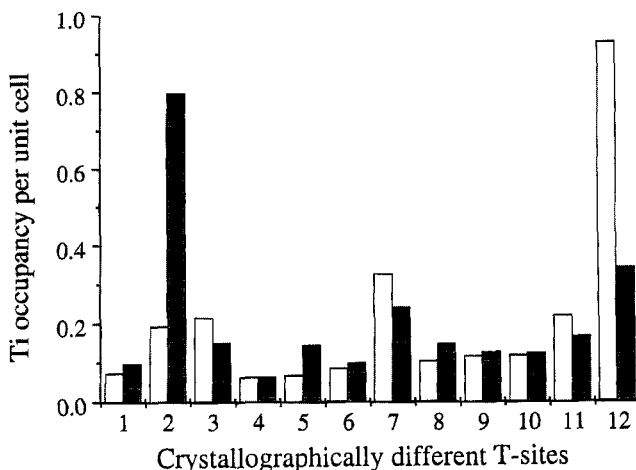


Figure 27 Ti distribution per unit cell over the crystallographically different T-sites for orthorhombic (T1-T12, white) and monoclinic (T1-T12, gray; T13-T24, black) structures.

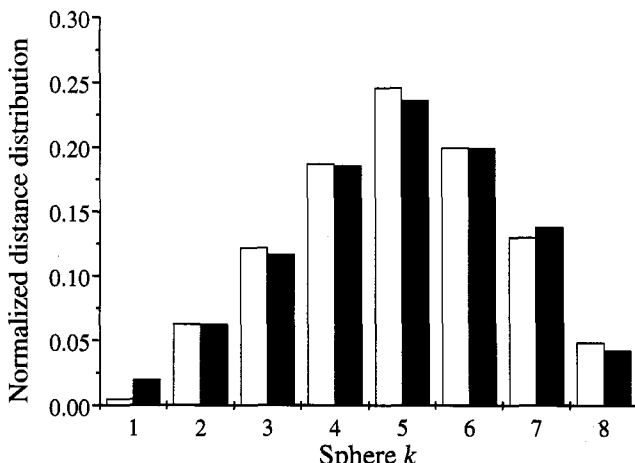


Figure 28 Normalized simulated (white) and random (black) distance distribution expressed in k spheres.

There are many fewer Ti atoms present as neighbors than can be expected from a random substitution, which might indicate that Loewenstein's rule is dependent not only on electrostatic effects, but also on framework deformations (see Figure 28).

Chemical Reactivity

Understanding chemical reactivity of zeolites is in fact the primary focus of interest of most zeolite studies. Modeling reactivity has formed the subject of many reviews that describe both the computational techniques and specific results in detail (see, e.g., Refs. 4, 6, 58).

We shall concentrate on computational studies of the interaction between the methanol molecule and the acidic proton of the bridging ($\text{Al} \cdots \text{O}-\text{H} \cdots \text{Si}$) hydroxyl group in zeolites to exemplify the contribution of simulation techniques in understanding chemical reactivity of zeolites. This interaction is the initial step of the industrially important conversion of methanol to gasoline. Therefore, understanding this primary step at the microscopic level has a direct impact on our understanding (and possibly rationalization) of the process. Before considering the results of calculations, let us outline the experimental information available for these systems.

Most of the experimental data on interaction of methanol molecules with H-zeolites were collected using NMR and IR spectroscopic techniques.^{176–179} The ^1H NMR data showed that, for low sorbate loadings, the interaction results in a proton signal at 12 ppm that gradually shifts to 8 ppm upon increasing the number of CH_3OH molecules per acid site.¹⁷⁶ For a loading of one

molecule per site in the $\text{CH}_3\text{OH}/\text{H-RHO}$ system, two bands at 10 and 12 ppm were observed.¹⁷⁶ A signal at 9.1–9.4 ppm has been observed in the ^1H NMR spectrum for the $\text{MeOH}/\text{H-ZSM-5}$ system.^{178,180} A characteristic pattern of three bands in the 2900–2800, 2500–2400, and 1700–1600 cm^{-1} regions is seen in the IR spectra of the methanol–zeolite systems.^{177,179} This pattern is supplemented by a band at 3545–3575 cm^{-1} . The ^{13}C NMR studies indicated the presence of several adsorbed methanol species¹⁸¹ that were also inferred on the basis of the infrared data.¹⁷⁹ The adsorption energy of the methanol was found to be in the range of 60–120 kJ/mol.^{182,183}

Two interpretations of the experimental data were put forward to explain the observed features. The first interpretation supposes the methanol molecule to be hydrogen-bonded via its O atom to the proton of the $\text{Al} \cdots \text{OH} \cdots \text{Si}$ bridge [hydrogen-bonded (HB) complex, Figure 29(a)]. The second assumes the formation of methoxonium ion CH_3OH_2^+ resulting from protonation of the adsorbed molecule by the acidic zeolite proton [ion-pair (IP) complex, Figure 29(b)]. For the latter interpretation, the infrared data are regarded as stretching and bending vibrations of the OH_2^+ moiety of the methoxonium ion.^{177,178} For the hydrogen-bonded MeOH –zeolite complex, the IR data are accounted for by Fermi resonance between vibrations of the zeolite OH group. Because of H-bond formation, the stretching O–H vibration undergoes a shift toward lower frequency, whereas the in-plane and out-of-plane bending vibrations of the hydroxyl are shifted to higher frequencies.^{184,185} Interaction of the OH stretching vibration and the first overtones of the bending vibrations (Fermi resonance) leads to two transition windows at the frequencies of the overtones and to a redistribution of the spectral intensity into the wings of the OH stretching band, a feature that is often called an A-B-C pattern.

As mentioned, the interaction between methanol and zeolite has been the subject of numerous theoretical studies. For example, the $\text{H}_3\text{SiOHAL}(\text{OH})_2\text{OSiH}_3$ cluster was studied by Gale, Catlow, and Carruthers¹⁸⁶ within a nonlocal spin density approximation with a DZP Gaussian basis set for non-hydrogen atoms. The HB complex was found to be a minimum at the potential energy surface with a binding energy (after zero-point energy correction) of 63.5 kJ/mol, whereas the methoxonium ion was found to be a transition state.

Another example is the extensive study by Haase and Sauer,¹⁸⁷ whose calculations were carried out for a methanol molecule with a number of cluster models, the most sophisticated of which was sufficiently large to represent a portion of the faujasite lattice formed by three 4-R rings and one 6-R. All structures were fully optimized at the SCF and/or MP2 level. The authors found that, for all cases studied, the IP complex was a transition state, whereas the HB complex corresponded to a minimum on the PES of the system. However, the adsorption energies for both structures were very close to one other, with a barrier for proton transfer of only a few kilojoules per mole. A strong H-bond between the Brønsted proton and the O atoms of methanol, and a long and weak H-bond between the H atom of the molecule and the O atom of the zeolite

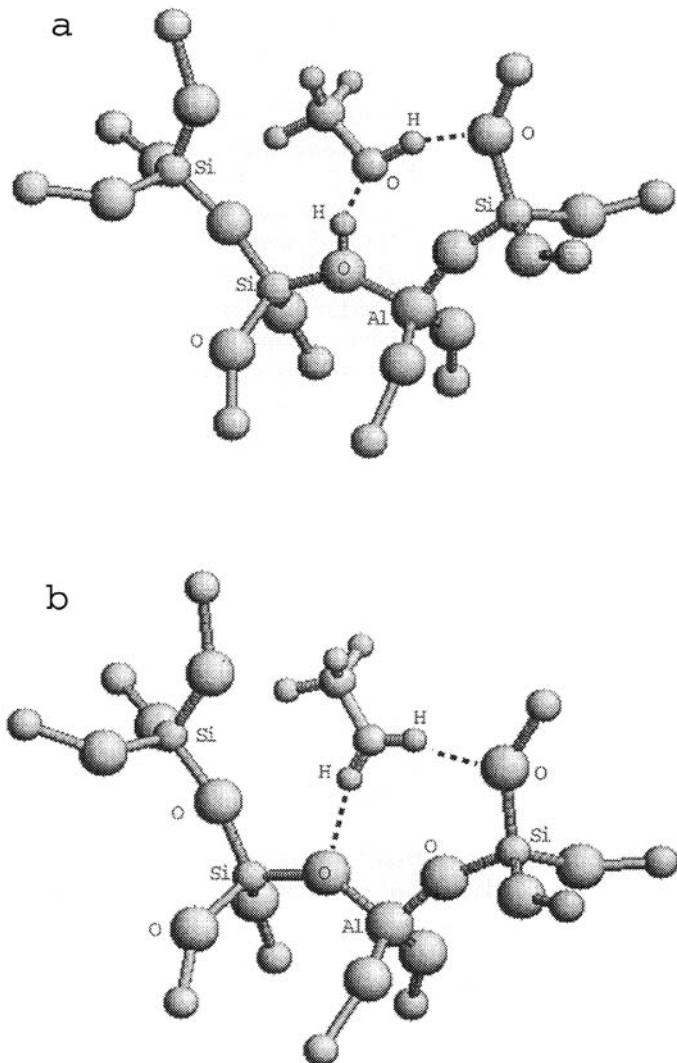


Figure 29 Hydrogen bonded (a) and ion-pair (b) complexes of methanol molecule and zeolite cluster.

model, were found to be characteristic for the HB complex, a feature also mentioned by Gale, Catlow, and Carruthers.¹⁸⁶

Calculations of the complexes' vibrational spectra were carried out by Haase and Sauer at the MP2 level with corrections for the basis set superposition error.¹⁸⁷ The frequencies calculated for the HB complex were consistent with the interpretation of the observed IR spectrum. This interpretation attributes the three observed bands to the A-B-C pattern arising from the Fermi

resonance between the zeolite OH stretching and bending vibrations. Inclusion of some electron correlation in their calculations was crucial for the realistic prediction of the vibrational frequencies and the NMR chemical shifts. The chemical shift calculated for the HB complex was found^{187,188} to be in better agreement with the experimental ¹H magic angle spinning (MAS) NMR data, whereas the chemical shift for the IP structure was in poor agreement with those NMR signals.^{176,178}

A DFT study of methanol activation by Brønsted zeolite protons was undertaken by Blaszkowski and van Santen,¹⁸⁹ who used the local density approximation with corrections for nonlocal effects. To ensure DZP quality for all nonhydrogen atoms, a linear combination of Gaussian orbitals was used as the basis set. No symmetry constraints were applied to the final optimization of complexes consisting of one methanol molecule and either H₃SiOHAl(OH)₂OSiH₃ or H₃SiOHALH₂OSiH₃ clusters. In agreement with the results of Haase and Sauer,¹⁸⁷ Blaszkowski and van Santen characterized the HB complex as a minimum, whereas the IP was found to be a transition state with an activation barrier for the proton transfer of 1–11 kJ/mol, the value depending on the cluster model used and the level of theory; the zero-point energy correction was applied. Calculation of the vibrational frequencies showed a significant decrease of the OH stretching energy, and an increase of both in-plane and out-of-plane bending vibration frequencies of the zeolitic OH group. In contrast, the OH stretching vibration of the methanol was only slightly perturbed. These results further support an origin for the observed IR pattern in the Fermi resonance between OH stretching and bending vibrations.

More recently, Shah et al. used periodic models to perform density functional calculations of the methanol adsorption in zeolites.^{190,191} A generalized gradient approximation and a plane waves basis were used for the electronic structure calculations. All atoms in the system were allowed to relax freely without any constraints except for the periodic boundary conditions applied to the system. The authors took as a model a methanol molecule interacting with a chabazite structure having one Brønsted site per unit cell (12 T-atoms). In contrast to studies relying on cluster models,^{186,187,189} the IP complex was found to represent the most stable adsorbed form, with no energy barrier for the proton transfer. Other structures corresponding to energy minima on the PES were also located. Analysis of the bonding between the methanol and the zeolite acidic proton showed that the proton is highly delocalized between the methanol and zeolite oxygens, with a full width at half-maximum in the computed probability distribution of 0.26 Å. Calculation of the vibrational frequencies led to an assignment of the observed IR bands in the 2000–2700 cm⁻¹ region to O–H stretching vibrations, whereas the experimental band at 1687 cm⁻¹ was ascribed to an H–O–H bending mode computed at 1700 cm⁻¹.

Shah and coworkers also studied methanol adsorption in sodalite and, in contrast to the case of chabazite, the HB complex with two hydrogen bonds between the methanol and the zeolite lattice was found to represent the mini-

mum on the PES of the system.^{190,191} This result agreed with the results of an ab initio MD calculation (see below).¹⁹² Shah et al. suggested that adsorption of methanol in structures with small rings, such as 6-R rings in sodalite, leads to an HB complex, whereas formation of a methoxonium ion is preferred in structures with rings large enough to permit the molecule to be placed in the plane of the rings. The results obtained by Shah et al. using periodic DFT calculations are qualitatively different from those derived with cluster models. The former results suggest that the IP complex can be stabilized by the electrostatic potential of the lattice and/or the interaction with atoms in the rings of the zeolite lattice, an effect that is omitted in the cluster calculations.

This conclusion is supported by results of Greatbanks et al.,¹⁹³ who used an embedding technique to calculate methanol–zeolite interactions. The following computational scheme was used: a Hartree–Fock (HF) calculation of purely siliceous zeolite Y with periodic boundary conditions was first performed. A T3 cluster was then excised from the structure and used to generate potential derived charges (PDC) that mimic the electrostatic potential of the lattice. Those charges were subsequently used in cluster calculations, in which the central Si atom was replaced by aluminium to create an $\text{H}_3\text{SiOHAl(OH)}_2\text{OSiH}_3$ cluster. The structure of the cluster interacting with the methanol molecule was optimized with and without PDC at the HF-SCF and MP2 levels, as well as by using DFT methods. Greatbanks and coworkers found that the inclusion of a point charge field and the presence of some electron correlation significantly affect both the structure and adsorption energies of the complexes. Inclusion of electron correlation resulted in a structure with two hydrogen bonds. Subsequent addition of the PDC led to more pronounced proton transfer to the methanol that more closely resembled an IP complex than an HB structure.

Table 6 summarizes all the pros and cons for assigning the adsorbed species as either the hydrogen-bonded complex or a methoxonium ion. One can see that no unambiguous assignment can be made in favor of either structure, but the HB complex seems to be preferred. Although the calculated adsorption energy is in the range of experimental values for both complexes, the observed IR spectra are naturally explained as the A-B-C pattern, assuming an HB structure with the experimental band at 3540 cm^{-1} attributed to the OH stretching vibration of the methanol molecule. The calculated ^1H NMR shift also seems to favor the hydrogen-bonded structure. However, this is still not the end of the story.

The data above are results of *static* calculations, whereas adsorption is a dynamic process. In addition, typical experimental conditions correspond to loadings higher than one molecule per active site. Although the high-loading issue complicates performing the static calculations due to the increase of degrees of freedom subject to variation, reality demands an *explicit* consideration of the atomic dynamics. Fortunately, because of substantial progress in both hardware and software, ab initio MD calculations using the Car-

Table 6 Experimental and Calculated Characteristics of Methanol-Zeolite Adsorption Complexes

Complex	Experiment					
	Vibrational frequencies ^a (cm ⁻¹)				¹ H NMR shift ^b (ppm)	<i>E</i> ^c _{ads} (kJ/mol)
	3540	2900	2450	1680	8–12	60–120
Calculations ^d						
Complex	Vibrational Frequencies (cm ⁻¹) ^a			¹ H NMR Shift (ppm) ^b		<i>E</i> _{ads} (kJ/mol) ^c
HB	2963	2378	1392			63.5
HB	3276	2548	1353	10.1		48.1
IP	2131	1689	1634	17.8		35
HB	3237	2398	1372	1055		73.2
IP ^e		2757	2009	1583		82
HB ^f	3565	2160	1420	1050		73
IP					13.9	103.8

^aRefs. 177, 179.

^bRefs. 176, 178, 180.

^cRefs. 182, 183.

^dResults for cluster models refer to interaction of methanol molecule with H₃SiOHAl(OH)₂OSiH₃ cluster. Data presented for highest level of theory reported.

^eCluster model, nonlocal spin density approximation.

^fCluster model, SCF+MP2//MP2.

^gCluster model, DFT LDA with non-local corrections.

^hChabazite structure.

ⁱDFT periodic calculations within GGA.

^jSodalite structure.

^kEmbedded cluster model PDC derived at 3-21G level.

Parrinello (CP-MD) approach are now feasible for periodic models as large as zeolitic systems.

A CP-MD study performed by Nusterer, Blöchl, and Schwarz¹⁹² for a single methanol molecule adsorbed in sodalite showed that no protonation of methanol occurred during the brief period of simulation (10 ps), although a strong hydrogen bond between the zeolite proton and the methanol was formed. It is interesting to note that, for the first time, the proton-exchange reaction between methanol and the zeolite could be seen directly. Figure 30 presents the calculated distance dependence between the zeolite's oxygen and the hydrogen atom of the methanol molecule and between the zeolite proton and the methanol's oxygen as functions of time. The proton transfer occurs within a 0.1 ps interval, and one can easily see that the methxonium ion (corresponding to the intersection of the curves) does not have any noticeable lifetime and is indeed a transition state. In their subsequent investigation,¹⁹⁴ the authors simulated the interaction of two methanols with a sodalite acid Brøn-

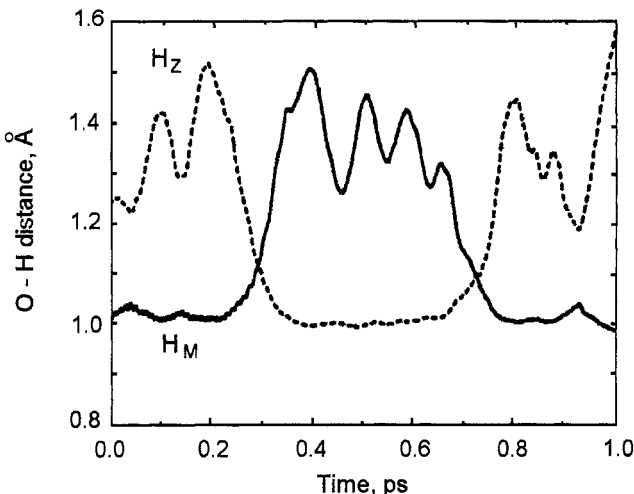


Figure 30 Proton-exchange reaction between methanol molecule and the Brønsted proton of sodalite lattice. Solid and dotted lines show distances between the methanol oxygen and the methanol and zeolite protons H_M and H_Z , respectively.

sted site and found formation of a protonated complex in which the acidic zeolite proton was transferred to one of the molecules that was then shared between the two methanols.

Haase, Sauer, and Hutter¹⁹⁵ have also carried out CP-MD calculations of methanol interacting with the Brønsted site of chabazite. Energy minimization calculations led to the location of two IP structures, which differ in the length of the H-bonds formed between methxonium ion and zeolite. However, results of their dynamic calculations showed that these ion-pair forms were stable only for a few oscillations of the Brønsted proton. Distortion of the eight-membered ring in the chabazite structure allowed the methanol's H atom to interact with the second next-nearest oxygen atom of aluminum, resulting in the formation of the HB complex. Energy minimization of the structure resulted in HB complexes that were more stable, by 18 kJ/mol, than the IP structures. Hence, these MD calculations revealed that the Brønsted proton is significantly delocalized between the methanol and framework oxygens, in agreement with the data of Shah et al.¹⁹⁰

Very recently, Stich and coworkers⁵⁷ reported an extensive CP-MD study of methanol interacting with chabazite, ferrierite, and ZSM-5 zeolite structures at different loadings and temperatures. Only an HB complex was found for the interaction of one methanol with the chabazite structure, in agreement with data of Haase and coworkers.¹⁹⁵ However, modeling the interaction with the ferrierite structure revealed the significance of zeolite topology for the relative stability of adsorbed complexes. It was found that if methanol resides on the 10-rings of the ferrierite, the HB complex is formed, although methxonium ion

formation occurs for short periods, and the IP form was calculated to be the predominant species for the molecule in the 8-rings of ferrierite. This surprising difference between the 8-rings in chabazite and ferrierite arises from an elliptical distortion of the rings in the latter structure that stabilizes the ion-pair complex. For the ZSM-5 structure, the formation of only an HB complex was computed.

For both chabazite and ferrierite, an increase of loading up to two molecules resulted in the formation of a methoxonium ion hydrogen-bonded both to the second methanol and to the zeolite lattice. This feature had already been computed for methanol in sodalite.¹⁹⁴ Adsorption in ferrierite was calculated to lead to an *elongation* in the C—O bond length that directly indicates *activation* of methanol. The difference between the two structures originates from the dynamics of the adsorbed complexes. Stich and coworkers⁵⁷ note that in chabazite, the two-methanol complex resembles a protonated methanol chain, whereas in ferrierite the methoxonium ion rotates with respect to the other. This rotation leads to a change in alignment of the methanol dipole moments that correlates with the elongation of the C—O bond. Calculations performed by Stich et al. for typical reaction conditions (four molecules per active site and $T = 700$ K) revealed even more pronounced activation of the molecules due to a strong anharmonicity of the PES of the adsorption complex.

Results from these CP-MD calculations show that we in fact have a more complicated situation than dealing with simple hydrogen bond or ion-pair complex formation as methanol interacts with a zeolite acidic proton. Stich and coauthors⁵⁷ conclude that the zeolite reactivity can be understood only by taking three factors into account simultaneously: zeolite topology, sorbate loading, and dynamic effects. The examples above illustrate that the capabilities of modern modeling techniques will allow us to accept this challenge.

FUTURE DEVELOPMENTS

When thinking about future developments, it is useful to consider again Figure 3. Just 15 years ago zeolite modeling was largely the visualization of the three-dimensional structures. Since then considerable progress has been made, and theoretical studies providing real insight in zeolite catalysis appear regularly. One might say that zeolite modeling during this 15-year period has steadily moved away from the origin in Figure 3, and our expectation is that this trend will continue.

Because of the continued development of both computer hardware and modeling software, it will be increasingly possible to use even more sophisticated models and methods for modeling of zeolites and related systems. The need to reduce the complexity of a system as much as possible will diminish, meaning, in general, that models used in the future can produce results that should be more comparable to experiment than is possible at this moment. Our

expectation is that this will attract experimentalists more and more to the field of zeolite modeling.

We also expect that more studies will use MD and the Car-Parrinello approach, while the share of studies based solely on energy minimization and cluster approximations will diminish. It seems reasonable to expect that some of the difficulties encountered with embedding will be solved in the next couple of years. If this becomes true, one might expect that embedding, in fierce competition with the Car-Parrinello approach, will be used extensively in studies on zeolite catalysis. For embedding to become a success, it will be necessary to develop force fields that are compatible with the quantum chemistry model that is used in the description of the catalytic site. Such a compatibility seems possible only if these force fields allow for polarization.

One might hope that some progress would also be made in areas barely touched upon at all in zeolite modeling at this time. Specifically we think here of synthesis of zeolites and by zeolites, and of zeolite design. Ideally, one would like to model zeolite synthesis by MD simulation; however, the time scale of zeolite synthesis, hours to many days, and the complexity of the synthesis mixture represent huge difficulties. Perhaps MC methods, for example, the configurational bias MC method, might be a way out; let us wait and see.

ACKNOWLEDGMENTS

KSS is deeply grateful to the Région Nord-Pas de Calais for a research fellowship, to the Laboratoire de Spectrochimie Infrarouge et Raman du CNRS for hospitality, and to Dr. Daniel Bougeard for many fruitful and stimulating discussions.

REFERENCES

1. W. M. Meier, D. H. Olson, and C. Baerlocher, *Atlas of Zeolite Structure Types*, 4th ed., Elsevier, London, 1996.
2. A. T. Bell, E. J. Maginn, and D. N. Theodorou, in *Handbook of Heterogeneous Catalysis*, G. Ertl, H. Knözinger, and J. Weitkamp, Eds., VCH Publishers, Weinheim, 1997, pp. 1165–1185. Molecular Simulation of Adsorption and Diffusion in Zeolites.
3. P. Demontis and G. B. Suffritti, *Chem. Rev.*, **97**, 2845 (1997). Structure and Dynamics of Zeolites Investigated by Molecular Dynamics.
4. J. B. Nicholas, *Top. Catal.*, **4**, 157 (1997). Density Functional Theory of Zeolite Structure, Acidity, and Reactivity.
5. R. A. van Santen, *Catal. Today*, **38**, 377 (1997). Quantum-Chemistry of Zeolite Acidity.
6. S. P. Bates and R. A. van Santen, *Adv. Catal.*, **42**, 1 (1998). The Molecular Basis of Zeolite Catalysis: A Review of Theoretical Simulations.
7. R. A. Jackson, S. C. Parker, and P. Tschaufeser, in *Computer Modeling of Structure and Reactivity of Zeolites*, C. R. A. Catlow, Ed., Academic Press, London, 1992, pp. 3–61. Lattice Energy and Free Energy Minimization of Zeolites.

8. A. K. Cheetham and J. D. Gale, in *Computer Modeling of Structure and Reactivity of Zeolites*, C. R. A. Catlow, Ed., Academic Press, London, 1992, pp. 63–78. Computer Simulation of the Structure, Thermochemistry and Dynamics of Adsorbed Molecules in Zeolites and Related Catalysts.
9. P. F. Demontis and G. Suffritti, in *Computer Modeling of Structure and Reactivity of Zeolites*, C. R. A. Catlow, Ed., Academic Press, London, 1992, pp. 79–132. Molecular Dynamics Studies on Zeolites.
10. J. Sauer, *Stud. Surf. Sci. Catal.*, **84**, 2039 (1994). Structure and Reactivity of Zeolite Catalysts: Atomistic Modeling Using Ab Initio Techniques.
11. J. Gao, in *Reviews in Computational Chemistry*, K. B. Lipkowitz and D. B. Boyd, Eds., VCH Publishers, New York, 1996, Vol. 7, pp. 119–185. Methods and Applications of Combined Quantum Mechanical and Molecular Mechanical Potentials.
12. T. Schlick, in *Reviews in Computational Chemistry*, K. B. Lipkowitz and D. B. Boyd, Eds., VCH Publishers, New York, 1992, Vol. 3, pp. 1–71. Optimization Methods in Computational Chemistry.
13. M. P. Allen and D. J. Tildesley, *Computer Simulation of Liquids*, Clarendon Press, Oxford, 1987.
14. D. Frenkel and B. Smit, *Understanding Molecular Simulation*, Academic Press, London, 1996.
15. J. M. Newsam, *Stud. Surf. Sci. Catal.*, **102**, 231 (1996). Computational Approaches in Zeolite Structural Chemistry.
16. A. P. Stevens and P. A. Cox, *J. Chem. Soc., Chem. Commun.*, **343** (1995). Postulated Mechanism for Faulting in Zeolite Beta.
17. E. de Vos Burchart, H. van Bekkum, and B. van de Graaf, *Zeolites*, **13**, 212 (1993). Molecular Mechanics Studies on MFI-Type Zeolites: 3. The Monoclinic–Orthorhombic Phase Transition.
18. M. W. Deem, J. M. Newsam, and J. A. Creighton, *J. Am. Chem. Soc.*, **114**, 7198 (1992). Fluctuations in Zeolite Aperture Dimensions Simulated by Crystal Dynamics.
19. K. S. Smirnov and D. Bougeard, *Zeolites*, **14**, 203 (1994). Molecular Dynamics Computer Study of Window Fluctuations in Zeolite A.
20. K. S. Smirnov and M. V. Kudryashova, *Microporous Mater.*, **5**, 9 (1995). Computer Simulation Study on Isomorphously Substituted Silicalites.
21. K. S. Smirnov and B. van de Graaf, *Microporous Mater.*, **7**, 133 (1996). On the Origin of the Band at 960 cm^{-1} in the Vibrational Spectra of Ti-Substituted Zeolites.
22. A. Chatterjee and A. K. Chandra, *J. Mol. Catal. A*, **119**, 51 (1997). Fe and B Substitution in ZSM-5 Zeolites: A Quantum-Mechanical Study.
23. M. E. Grillo and J. Carrazza, *J. Phys. Chem. B*, **101**, 6749 (1997). Computer Simulation Study of Aluminium Incorporation in the Microporous Titanosilicate ETS-10.
24. G. Ricchiardi and J. M. Newsam, *J. Phys. Chem. B*, **101**, 9943 (1997). Predicted Effects of Site-Specific Aluminium Substitution on the Framework Geometry and Unit Cell Dimensions of Zeolite ZSM-5 Materials.
25. H. van Bekkum, E. M. Flanigen, and J. C. Jansen, *Introduction to Zeolite Science and Practice*, Elsevier Science Publishers, Amsterdam, 1991.
26. A. J. M. de Man and J. Sauer, *J. Phys. Chem.*, **100**, 5025 (1996). Coordination, Structure, and Vibrational Spectra of Titanium in Silicates and Zeolites in Comparison with Related Molecules. An Ab Initio Study.
27. R. Millini, E. Previde Massara, G. Perego, and G. J. Bellussi, *J. Catal.*, **137**, 497 (1992). Framework Composition of Titanium Silicalite-1.
28. A. Jentys and C. R. A. Catlow, *Catal. Lett.*, **22**, 251 (1993). Structural Properties of Titanium Sites in Ti-ZSM5.
29. R. Millini, G. Perego, and K. Seiti, *Stud. Surf. Sci. Catal.*, **84**, 2123 (1994). Ti Substitution in MFI Type Zeolites: A Quantum Mechanical Study.

30. Y. Oumi, K. Matsuba, M. Kubo, T. Inui, and A. Miyamoto, *Microporous Mater.*, **4**, 53 (1995). Selective T-Site Substitution as a Cause of the Anisotropy of Lattice Expansion in Titanosilicalite-1 Investigated by Molecular Dynamics and Computer Graphics.
31. S. L. Njo, H. van Koningsveld, and B. van de Graaf, *J. Phys. Chem. B*, **101**, 10065 (1997). A Combination of the Monte Carlo Method and Molecular Mechanics Calculations: A Novel Way To Study the Ti(IV) Distribution in Titanium Silicalite-1.
32. C. P. Herrero, *J. Phys. Chem.*, **97**, 3338 (1993). Monte Carlo Simulation of the Si, Al Distribution in A-Type Zeolites.
33. D. Ding, P. Sun, Q. Jin, B. Li, and J. Wang, *Zeolites*, **14**, 65 (1994). Studies of Mordenite by the Monte Carlo Method.
34. P. Levitz, A. L. Blumenfeld, and J. J. Fripiat, *Catal. Lett.*, **38**, 11 (1996). Number of Isolated Aluminium Atoms in the Framework of Dealuminated Acid Zeolites.
35. W. Loewenstein, *Am. Mineral.*, **39**, 92 (1954). The Distribution of Aluminum in the Tetrahedra of Silicates and Aluminates.
36. M. V. Frash, M. A. Makarova, and A. M. Rigby, *J. Phys. Chem. B*, **101**, 2116 (1997). Quantum-Chemical Justification of the Zeolite Acid Strength Measurement by Infrared Spectroscopy.
37. A. K. Chandra, A. Goursot, and F. Fajula, *J. Mol. Catal. A*, **119**, 45 (1997). Proton Affinity Differences in Zeolite: A DFT Study.
38. N. Gonzales, A. T. Bell, and A. K. Chakraborty, *J. Phys. Chem. B*, **101**, 10058 (1997). Density Functional Theory Calculations of the Effects of Local Composition and Defect Structure on the Proton Affinity of H-ZSM-5.
39. U. Eichler, M. Brändle, and J. Sauer, *J. Phys. Chem.*, **101**, 10035 (1997). Predicting Absolute and Site-Specific Acidities for Zeolite Catalysts by a Combined Quantum Mechanics/Interatomic Potential Function Approach.
40. M. Brändle and J. Sauer, *J. Mol. Catal. A*, **119**, 19 (1997). Combining Ab Initio Techniques with Analytical Potential Functions. A Study of Zeolite–Adsorbate Interactions for NH₃ on H-Faujasite.
41. E. Fois and A. Gamba, *J. Phys. Chem. B*, **101**, 4487 (1997). Host/Guest Interactions and Femtosecond Scale Proton Exchange in a Zeolitic Cage.
42. J. C. van der Waal, P. J. Kooyman, J. C. Jansen, and H. van Bekkum, *Microporous Mesoporous Mater.*, **25**, 43 (1998). Synthesis and Characterization of Aluminium-Free Zeolite Titanium Beta Using Di(cyclohexylmethyl)dimethylammonium as a New and Selective Template.
43. A. P. Stevens, A. M. Gorman, C. M. Freeman, and P. A. Cox, *J. Chem. Soc., Faraday Trans.*, **92**, 2065 (1996). Prediction of Template Location Via a Combined Monte Carlo–Simulated Annealing Approach.
44. D. J. Willock, D. W. Lewis, C. R. A. Catlow, G. J. Hutchings, and J. M. Thomas, *J. Mol. Catal. A*, **119**, 415 (1997). Designing Templates for the Synthesis of Microporous Solids Using De Novo Molecular Design Methods.
45. G. Vitale, C. F. Mellot, and A. K. Cheetham, *J. Phys. Chem. B*, **101**, 9886 (1997). Localization of Adsorbed Cyclohexane in the Acid Form of Zeolite Y. A Powder Neutron Diffraction and Computational Study.
46. E. J. Maginn, A. T. Bell, and D. N. Theodorou, *J. Phys. Chem.*, **99**, 2057 (1995). Sorption Thermodynamics, Siting, and Conformation of Long n-Alkanes in Silicalite as Predicted by Configurational-Bias Monte Carlo Integration.
47. B. Smit, *Phys. Scripta*, **T66**, 80 (1996). Computational Physics in Petrochemical Industry.
48. B. Smit, L. D. J. C. Loyens, and G. L. M. M. Verbist, *Faraday Discuss., Chem Soc.*, **106**, 93 (1997). Simulation of Adsorption and Diffusion of Hydrocarbons in Zeolites.
49. V. Lachet, A. Boutin, B. Tavitian, and A. H. Fuchs, *Faraday Discuss. Chem. Soc.*, **106**, 307 (1997). Grand Canonical Monte Carlo Simulations of Adsorption of Mixtures of Xylene Molecules in Faujasite Zeolites.

50. S. M. Auerbach, *J. Chem. Phys.*, **106**, 7810 (1997). Analytical Theory of Benzene Diffusion in Na-Y Zeolite.
51. J. A. Horsley, J. D. Fellmann, E. G. Derouane, and C. M. Freeman, *J. Catal.*, **147**, 231 (1994). Computer-Assisted Screening of Zeolite Catalysts for the Selective Isopropylation of Naphthalene.
52. K. A. Fichthorn and W. H. Weinberg, *J. Chem. Phys.*, **95**, 1090 (1991). Theoretical Foundations of Dynamical Monte Carlo Simulations.
53. T. Mosell, G. Schrimpf, and J. Brickmann, *J. Phys. Chem. B*, **101**, 9485 (1997). Diffusion and Aromatic Molecules in Zeolite NaY. 2. Dynamical Corrections.
54. F. Jousse and S. M. Auerbach, *J. Chem. Phys.*, **107**, 9629 (1997). Activated Diffusion of Benzene in NaY Zeolite: Rate Constants from Transition State Theory with Dynamical Corrections.
55. R. C. Runnebaum and E. J. Maginn, *J. Phys. Chem. B*, **101**, 6394 (1997). Molecular Dynamics Simulations of Alkanes in the Zeolite Silicalite: Evidence for Resonant Diffusion Effects.
56. K. Schwarz, E. Nusterer, P. Margl, and P. E. Blöchl, *Int. J. Quant. Chem.*, **61**, 369 (1997). Ab Initio Molecular Dynamics Calculations to Study Catalysis.
57. I. Stich, J. D. Gale, K. Terakura, and M. C. Payne, *Chem. Phys. Lett.*, **283**, 402 (1998). Dynamical Observation of the Catalytic Activation of Methanol in Zeolites.
58. S. R. Blaszkowski and R. A. van Santen, *Top. Catal.*, **4**, 145 (1997). Quantum Chemical Studies of Zeolite Proton Catalyzed Reactions.
59. M. V. Frash, V. B. Kanzansky, A. M. Rigby, and R. A. van Santen, *J. Phys. Chem. B*, **101**, 5346 (1997). Density Functional and Hartree-Fock Calculations on the Cyclopropane Ring Intermediates Involved in the Zeolite-Catalyzed Skeletal Isomerization of Hydrocarbons and in the Carbon Isotope Scrambling in 2-Propyl Cation.
60. R. Ramprasad, K. C. Hass, W. F. Schneider, and J. B. Adams, *J. Phys. Chem. B*, **101**, 6903 (1997). Cu-Dinitrosyl Species in Zeolites: A Density Functional Molecular Cluster Study.
61. D. C. Sayle, C. R. A. Catlow, J. D. Gale, M. A. Perrin, and P. Nortier, *J. Phys. Chem. A*, **101**, 3331 (1997). Computer Modeling of the Active-Site Configurations Within the NO Decomposition Catalyst Cu-ZSM-5.
62. K. Teraishi, M. Ishida, J. Irisawa, M. Kume, Y. Takahashi, T. Nakano, H. Nakamura, and A. Miyamoto, *J. Phys. Chem. B*, **101**, 8079 (1997). Active Site Structure of Cu/ZSM-5: Computational Study.
63. H. V. Brand, A. Redondo, and P. J. Hay, *J. Phys. Chem. B*, **101**, 7691 (1997). Theoretical Studies of CO and NO Adsorption on Cu⁺-ZSM-5 Zeolite.
64. R. McWeeny and B. T. Sutcliffe, *Methods of Molecular Quantum Mechanics*, Academic Press, London and New York, 1969.
65. J. A. Pople and D. L. Beveridge, *Approximate Molecular Orbital Theory*, McGraw-Hill, New York, 1970.
66. (a) D. Feller and E. R. Davidson, in *Reviews in Computational Chemistry*, K. B. Lipkowitz and D. B. Boyd, Eds., VCH Publishers, New York, 1990, Vol. 1, pp. 1–43. Basis Sets for Ab Initio Molecular Orbital Calculations and Intermolecular Interactions. (b) N. R. Kestner and J. E. Combariza, in *Reviews in Computational Chemistry*, K. B. Lipkowitz and D. B. Boyd, Eds., Wiley-VCH, New York, 1999, Vol. 13, pp. 99–132. Basis Set Superposition Errors: Theory and Practice.
67. (a) R. J. Bartlett and J. F. Stanton, in *Reviews in Computational Chemistry*, K. B. Lipkowitz and D. B. Boyd, Eds., VCH Publishers, New York, 1994, Vol. 5, pp. 65–169. Applications of Post-Hartree-Fock Methods: A Tutorial. (b) T. D. Crawford and H. F. Schaefer III, in *Reviews in Computational Chemistry*, K. B. Lipkowitz and D. B. Boyd, Eds., Wiley-VCH, New York, 1999, Vol. 14, pp. 33–136. An Introduction to Coupled Cluster Theory for Computational Chemists.
68. R. G. Parr and W. Yang, *Density-Functional Theory of Atoms and Molecules*, Oxford University Press, New York, 1989.

69. L. J. Bartolotti and K. Flurhick, in *Reviews in Computational Chemistry*, K. B. Lipkowitz and D. B. Boyd, Eds., VCH Publishers, New York, 1995, Vol. 7, pp. 187–216. An Introduction to Density Functional Theory.
70. P. Hohenberg and W. Kohn, *Phys. Rev. B*, **136**, 864 (1964). Inhomogeneous Electron Gas.
71. W. Kohn and L. J. Sham, *Phys. Rev. A*, **140**, 1133 (1965). Self-Consistent Equations Including Exchange and Correlation Effects.
72. A. St-Amant, in *Reviews in Computational Chemistry*, K. B. Lipkowitz and D. B. Boyd, Eds., VCH, New York, 1995, Vol. 7, pp. 217–259. Density Functional Methods in Biomolecular Modeling.
73. J. J. P. Stewart, in *Reviews in Computational Chemistry*, K. B. Lipkowitz and D. B. Boyd, Eds., VCH Publishers, New York, 1990, Vol. 1, pp. 45–81. Semiempirical Molecular Orbital Methods.
74. M. C. Zerner, in *Reviews in Computational Chemistry*, K. B. Lipkowitz and D. B. Boyd, Eds., VCH Publishers, New York, 1991, Vol. 2, pp. 313–365. Semiempirical Molecular Orbital Methods.
75. W. J. Mortier, S. K. Ghosh, and S. Shankar, *J. Am. Chem. Soc.*, **108**, 4315 (1986). Electronegativity Equalization Method for the Calculation of Atomic Charges in Molecules.
76. R. T. Sanderson, *Chemical Bonds and Bond Energy*, 2nd ed., Academic Press, New York, 1976.
77. H. Toufar, B. G. Baekelandt, G. O. A. Janssens, W. J. Mortier, and R. A. Schoonheydt, *J. Phys. Chem.*, **99**, 13876 (1995). Investigation of Supramolecular Systems by a Combination of the Electronegativity Equalization Method and a Monte Carlo Simulation Technique.
78. R. S. Mulliken, *J. Chem. Phys.*, **23**, 2343 (1955). Electronic Population Analysis on LCAO-MO Molecular Wave Functions. IV. Bonding and Antibonding in LCAO and Valence-Bond Theories.
79. S. L. Njo, J. Fan, and B. van de Graaf, *J. Mol. Catal. A*, **134**, 79 (1998). Extending and Simplifying the Electronegativity Equalization Method. See also: M. M. Franci and L. E. Chirlian, in *Reviews in Computational Chemistry*, K. B. Lipkowitz and D. B. Boyd, Eds., Wiley-VCH, New York, Vol. 14, pp. 1–31. The Pluses and Minuses of Mapping Atomic Charges to Electrostatic Potentials.
80. B. G. Baekelandt, W. J. Mortier, and R. A. Schoonheydt, *Struct. Bonding*, **80**, 187 (1992). The EEM Approach to Chemical Hardness in Molecules and Solids: Fundamentals and Applications.
81. B. G. Baekelandt, G. O. A. Janssens, W. J. Mortier, H. Toufar, and R. A. Schoonheydt, in *Acidity and Basicity in Solids*, J. Fraissard and L. Petrakis, Eds., NATO ASI Series C444, Kluwer Academic Publishers, New York, 1994, pp. 95–127. Acidity and Basicity Concepts: The Density Functional View Point Based on an Atom-in-Molecules Sensitivity Analysis—A Tutorial.
82. A. K. Rappé and W. A. Goddard III, *J. Phys. Chem.*, **95**, 3358 (1991). Charge Equilibration for Molecular Dynamics Simulations.
83. J. N. Louwen and E. T. C. Vogt, *J. Mol. Catal. A*, **134**, 63 (1998). Semi-Empirical Atomic Charges for Use in Computational Chemistry of Molecular Sieves.
84. P. Demontis, G. B. Suffritti, S. Quartieri, E. S. Fois, and A. Gamba, *J. Phys. Chem.*, **92**, 867 (1988). Molecular Dynamics Studies on Zeolites. 3. Dehydrated Zeolite A.
85. P. Demontis, G. B. Suffritti, S. Bordiga, and R. Buzzoni, *J. Chem. Soc., Faraday Trans.*, **91**, 525 (1995). Atom Pair Potential for Molecular Dynamics Simulations of Structural and Dynamical Properties of Aluminosilicates: Test on Silicalite and Anhydrous Na-A and Ca-A Zeolites and Comparison with Experimental Data.
86. G. J. Kramer, N. P. Farragher, B. W. H. van Beest, and R. A. van Santen, *Phys. Rev. B*, **43**, 5068 (1991). Interatomic Force Fields for Silicas, Aluminophosphates, and Zeolites: Derivation Based on Ab Initio Calculations.
87. G. J. Kramer, A. J. M. de Man, and R. A. van Santen, *J. Am. Chem. Soc.*, **113**, 6435 (1991). Zeolites Versus Aluminosilicate Clusters: The Validity of a Local Description.
88. M. L. Sanders, M. Leslie, and C. R. A. Catlow, *J. Chem. Soc., Chem. Commun.*, **1271** (1984). Interatomic Potentials for SiO_2 .

89. R. A. Jackson and C. R. A. Catlow, *Mol. Simul.*, **1**, 207 (1988). Computer Simulation Studies of Zeolites Structure.
90. A. C. T. van Duin, J. M. A. Baas, and B. van de Graaf, *J. Chem. Soc., Faraday Trans.*, **90**, 2881 (1994). Delft Molecular Mechanics: A New Approach to Hydrocarbon Force Fields. Inclusion of a Geometry-Dependent Charge Calculation.
91. A. C. T. van Duin, J. M. A. Baas, and B. van de Graaf, *J. Chem. Soc., Faraday Trans.*, **92**, 353 (1996). Molecular Mechanics Force Fields for Tertiary Carbocations.
92. J. B. Nicholas, A. J. Hopfinger, F. R. Trouw, and L. E. Iton, *J. Am. Chem. Soc.*, **113**, 4792 (1991). Molecular Modeling of Zeolite Structure. 2. Structure and Dynamics of Silica Sodalite and Silicalite Force Field.
93. E. de Vos Burchart, V. A. Verheij, H. van Bekkum, and B. van de Graaf, *Zeolites*, **12**, 183, (1992). A Consistent Molecular Mechanics Force Field for All-Silica Zeolites.
94. E. de Vos Burchart, E. T. C. Vogt, H. van Bekkum, and B. van de Graaf, *J. Chem. Soc., Faraday Trans.*, **88**, 2761 (1992). A Consistent Molecular Mechanics Force Field for Aluminophosphates.
95. S. Califano, *Vibrational States*, Wiley, London, 1976.
96. J. Etchepare, M. Merian, and L. Smetankine, *J. Chem. Phys.*, **60**, 1873 (1974). Vibrational Normal Modes of SiO_2 . I. α and β Quartz.
97. J. A. Creighton, H. W. Deckman, and J. M. Newsam, *J. Phys. Chem.*, **98**, 448 (1994). Computer Simulation and Interpretation of the Infrared and Raman Spectra of Sodalite Frameworks.
98. M. Bärtsch, P. Bornhauser, G. Calzaferri, and R. Imhof, *J. Phys. Chem.*, **98**, 2817 (1994). $\text{H}_8\text{Si}_8\text{O}_{12}$: A Model for the Vibrational Structure of Zeolite A.
99. K. S. Smirnov and D. Bougeard, *J. Phys. Chem.*, **97**, 9434 (1993). Molecular Dynamics Study of the Vibrational Spectra of Siliceous Zeolites Built from Sodalite Cages.
100. K. S. Smirnov, M. Le Maire, C. Brémard, and D. Bougeard, *Chem. Phys.*, **179**, 445 (1994). Vibrational Spectra of Cation-Exchanged Zeolite A. Experimental and Molecular Dynamics Study.
101. S. L. Mayo, B. D. Olafson, and W. A. Goddard III, *J. Phys. Chem.*, **94**, 8897 (1990). DREIDING: A Generic Force Field for Molecular Simulations.
102. U. Dinur and A. T. Hagler, in *Reviews in Computational Chemistry*, K. B. Lipkowitz and D. B. Boyd, Eds., VCH Publishers, New York, 1991, Vol. 2, pp. 99–164. New Approaches to Empirical Force Fields.
103. K. de Boer, A. P. J. Jansen, and R. A. van Santen, in *Zeolites and Related Microporous Materials: State of the Art 1994*, J. Weitkamp, H. G. Karge, H. Pfeifer, and W. Hölderich, Eds., Elsevier Science Publishers, Amsterdam, 1994, pp. 2083–2087. Interatomic Potentials for Zeolites. Derivation of an Ab Initio Shell Model Potential.
104. K. de Boer, A. P. J. Jansen, and R. A. van Santen, *Chem. Phys. Lett.*, **223**, 46 (1994). Ab Initio Approach to the Development of Interatomic Potentials for the Shell Model of Silica Polymorphs.
105. J.-R. Hill and J. Sauer, *J. Phys. Chem.*, **98**, 1238 (1994). Molecular Mechanics Potential for Silica and Zeolite Catalysts Based on Ab Initio Calculations. 1. Dense and Microporous Silica.
106. J.-R. Hill and J. Sauer, *J. Phys. Chem.*, **99**, 9536 (1995). Molecular Mechanics Potential for Silica and Zeolite Catalysts Based on Ab Initio Calculations. 2. Aluminosilicates.
107. K.-P. Schröder and J. Sauer, *J. Phys. Chem.*, **100**, 11043 (1996). Potential Functions for Silica and Zeolite Catalysts Based on Ab Initio Calculations. 3. A Shell Model Ion Pair Potential for Silica and Aluminosilicates.
108. V. A. Ermoshin, K. S. Smirnov, and D. Bougeard, *Chem. Phys.*, **202**, 53 (1996). Ab Initio Generalized Force Field for Zeolite Modeling. 1. Siliceous Zeolites.
109. V. A. Ermoshin, K. S. Smirnov, and D. Bougeard, *Chem. Phys.*, **209**, 41 (1996). Ab Initio Generalized Force Field for Zeolite Modeling. 2. Aluminosilicates.

110. A. Allouche and J. Pourcin, *Spectr chim. Acta*, **49A**, 571 (1993). Ab Initio Calculation of Vibrational Force Fields: Determination of Non-Redundant Symmetry Coordinates by Least-Square Component Analysis.
111. R. M. Badger, *J. Chem. Phys.*, **2**, 128 (1934). A Relation Between Internuclear Distances and Bond Force Constants.
112. K. S. Smirnov and B. van de Graaf, *J. Chem. Soc., Faraday Trans.*, **92**, 2469 (1996). A Consistent Implementation of the Electronegativity Equalization Method in Molecular Mechanics and Molecular Dynamics.
113. B. van de Graaf and E. de Vos Burchart, *Comput. Chem.*, **17**, 81 (1993). Simplification and Acceleration of Crystal Energy Calculations Under Constant Pressure.
114. M. Born and K. Huang, *Dynamical Theory of Crystal Lattices*, Clarendon Press, Oxford, 1954.
115. P. P. Ewald, *Ann. Phys.*, **64**, 253 (1921). Die Berechnung optischer und electrostatischer Gitterpotentiale.
116. F. Bertaut, *J. Phys. Radium*, **13**, 499 (1952). L'Énergie Électrostatique de Réseaux Ioniques.
117. M. P. Tosi, *Solid State Phys.*, **16**, 1 (1964). Cohesion of Ionic Solids in the Born Model.
118. N. Karasawa and W. A. Goddard III, *J. Phys. Chem.*, **93**, 7320 (1989). Acceleration of Convergence for Lattice Sums.
119. R. Fischer, FORTRAN program BERTAU, Institute for Mineralogy and Crystallography, Vienna University; see also Ref. 13.
120. K. S. Smirnov and B. van de Graaf, *J. Chem. Soc., Faraday Trans.*, **92**, 2475 (1996). Study of Methane Adsorption in MFI and MEL Zeolites by Combination of the Electronegativity Equalization Method and Molecular Dynamics.
121. E. de vos Burchart, PhD thesis, Delft University of Technology, The Netherlands, 1992. Studies on Zeolites: Molecular Mechanics, Framework Stability, and Crystal Growth.
122. S. J. Watowich, E. S. Meyer, R. Hagstrom, and R. Josephs, *J. Comput. Chem.*, **9**, 650 (1988). A Stable, Rapidly Converging Conjugate Gradient Method for Energy Minimization.
123. W. H. Press, B. P. Flannery, S. A. Teukolsky, and W. T. Vetterling, *Numerical Recipes, The Art of Scientific Computing*, Cambridge University Press, Cambridge, 1986.
124. B. van de Graaf and J. M. A. Baas, *J. Comput. Chem.*, **5** 314 (1984). Empirical Force Field Calculations. 23. The Lagrange Multiplier Method for Manipulating Geometries. Implementation and Applications in Molecular Mechanics.
125. D. A. McQuarrie, *Statistical Mechanics*, Harper & Row, New York, 1976.
126. P. F. Demontis, G. B. Suffritti, A. Alberti, S. Quartieri, E. S. Fois, and A. Gamba, *Gazz. Chim. Ital.*, **116**, 459 (1986). Molecular Dynamics Studies on Zeolites. I. Water in Natrolite.
127. H. J. C. Berendsen and W. F. van Gunsteren, in *Molecular Dynamics Simulation of Statistical-Mechanical Systems*, (Proceedings of the International School of Physics, "Enrico Fermi" Course XCVII), G. Cicotti and W. G. Hoover, Eds., North-Holland, Amsterdam, 1986, pp. 43–65. Practical Algorithms for Dynamic Simulations.
128. W. C. Swope, H. C. Andersen, H. C. Berens, and K. R. Wilson, *J. Chem. Phys.*, **76**, 637 (1982). A Computer Simulation Method for the Calculation of Equilibrium Constants for the Formation of Physical Clusters of Molecules: Application to Small Water Clusters.
129. D. J. Evans and S. Murad, *Mol. Phys.*, **34**, 327 (1977). Singularity-Free Algorithm for Molecular Dynamics Simulation of Rigid Polyatomics.
130. J. P. Ryckaert, G. Ciccotti, and H. J. C. Berendsen, *J. Comput. Phys.*, **23**, 327 (1977). Numerical Integration of the Cartesian Equations of Motion of a System with Constraints: Molecular Dynamics of *n*-Alkanes.
131. H. C. Andersen, *J. Comput. Phys.*, **52**, 24 (1983). RATTLE: A "Velocity" Version of the SHAKE Algorithm for Molecular Dynamics Calculations.
132. R. Kutteh and T. P. Straatsma, in *Reviews in Computational Chemistry*, K. B. Lipkowitz and D. B. Boyd, Eds., Wiley-VCH, New York, 1998, Vol. 12, pp. 75–136. Molecular Dynamics with General Holonomic Constraints and Application to Internal Coordinate Constraints.

133. M. Tuckerman, B. J. Berne, and G. J. Martyna, *J. Chem. Phys.*, **97**, 1990 (1992). Reversible Multiple Time Scale Molecular Dynamics.
134. M. Parrinello and A. Rahman, *Phys. Rev. Lett.*, **45**, 1196 (1980). Crystal Structure and Pair Potentials: A Molecular Dynamics Study.
135. M. Parrinello and A. Rahman, *J. Appl. Phys.*, **52**, 7182 (1981). Polymorphic Transitions in Single Crystals: A New Molecular Dynamics Method.
136. S. Nosé, *Mol. Phys.*, **52**, 255 (1984). A Molecular Dynamics Method for Simulations in the Canonical Ensemble.
137. H. J. C. Berendsen, J. P. M. Postma, W. F. van Gunsteren, A. DiNola, and J. R. Haak, *J. Chem. Phys.*, **81**, 3684 (1984). Molecular Dynamics with Coupling to an External Bath.
138. R. G. Gordon, in *Advances in Magnetic Resonance*, J. S. Waugh, Ed., Academic Press, New York, 1968, pp. 1–42. Correlation Functions for Molecular Motions.
139. P. H. Berens and K. R. Wilson, *J. Chem. Phys.*, **74**, 4872 (1981). Molecular Dynamics and Spectra. I. Diatomic Rotation and Vibration.
140. P. H. Berens, S. R. White, and K. R. Wilson, *J. Chem. Phys.*, **75**, 515 (1981). Molecular Dynamics and Spectra. II. Diatomic Raman.
141. M. Gussoni, in *Advances in Infrared and Raman Spectroscopy*, R. J. Clark and R. Hester, Eds., Heyden, London, 1979, pp. 61–126. Infrared and Raman Intensities from Electro-Optical Parameters.
142. K. S. Smirnov and D. Bougeard, *J. Raman Spectrosc.*, **24**, 255 (1993). Raman and Infrared Spectra of Siliceous Faujasite. A Molecular Dynamics Study.
143. N. Metropolis, A. W. Rosenbluth, M. N. Rosenbluth, A. H. Teller, and E. Teller, *J. Chem. Phys.*, **21**, 1087 (1953). Equation of State Calculations by Fast Computing Machines.
144. J. I. Siepmann and D. Frenkel, *Mol. Phys.*, **75**, 59 (1992). Configurational Bias Monte Carlo: A New Sampling Scheme for Flexible Chains.
145. M. N. Rosenbluth and A. W. Rosenbluth, *J. Chem. Phys.*, **23**, 356 (1955). Monte Carlo Calculation of the Average Extension of Molecular Chains.
146. R. Car and M. Parrinello, *Phys. Rev. Lett.*, **55**, 2471 (1985). Unified Approach for Molecular Dynamics and Density-Functional Theory.
147. D. K. Remler and P. A. Madden, *Mol. Phys.*, **70**, 921 (1990). Molecular Dynamics Without Effective Potentials Via the Car–Parrinello Approach.
148. M. C. Payne, M. P. Teter, D. C. Allan, T. A. Arias, and J. D. Joannopoulos, *Rev. Mod. Phys.*, **64**, 1045 (1992). Iterative Minimization Techniques for Ab Initio Total-Energy Calculations: Molecular Dynamics and Conjugate Gradients.
149. E. M. Flaningen, H. Khatami, and H. A. Szymanski, *Adv. Chem. Ser.*, **101**, 201 (1971). Infrared Structural Studies of Zeolite Frameworks.
150. A. J. M. de Man and R. A. van Santen, *Zeolites*, **12**, 269 (1992). The Relation Between Zeolite Framework Structure and Vibrational Spectra.
151. P. Bornhauser and G. Calzaferri, *J. Phys. Chem.*, **100**, 2035 (1996). Ring-Opening Vibrations of Spherosiloxanes.
152. K. A. Iyer and S. J. Singer, *J. Phys. Chem.*, **98**, 12670 (1994). Local Mode Analysis of Complex Zeolite Vibrations: Sodalite.
153. K. A. Iyer and S. J. Singer, *J. Phys. Chem.*, **98**, 12679 (1994). Local Mode Analysis of Complex Zeolite Vibrations: Zeolite-A.
154. P. K. Dutta and B. Del Barco, *J. Phys. Chem.*, **92**, 354 (1988). Raman Spectroscopy of Zeolite A: Influence of Si/Al Ratio.
155. K. S. Smirnov, unpublished results.
156. M. R. Boccuti, K. M. Rao, A. Zecchina, G. Leofanti, and G. Petrini, *Stud. Surf. Sci. Catal.*, **48**, 133 (1989). Spectroscopic Characterization of Silicalite and Titanium-Silicalite.
157. D. R. C. Huybrechts, I. Vassen, H. X. Li, and P. A. Jacobs, *Catal. Lett.*, **8**, 237 (1991). Factors Influencing the Catalytic Activity of Titanium Silicalites in Selective Oxidations.

158. G. Deo, A. M. Turek, I. E. Wachs, D. R. C. Huybrechts, and P. A. Jacobs, *Zeolites*, **13**, 365 (1993). Characterization of Titania Silicates.
159. G. Schrimpf, M. Schlenkrich, J. Brickmann, and P. Bopp, *J. Phys. Chem.*, **96**, 7404 (1992). Molecular Dynamics Simulation of Zeolite NaY. A Study of Structure, Dynamics, and Thermalization of Sorbates.
160. P. Demontis and G. B. Suffritti, in *Zeolites and Related Microporous Materials: State of the Art 1994*, J. Weitkamp, H. G. Karge, H. Pfeifer, and W. Hölderich, Eds., Elsevier Science Publishers, Amsterdam, 1994, pp. 2107–2113. Molecular Dynamics Simulations of Diffusion in a Cubic Symmetry Zeolite.
161. D. A. Faux, W. Smith, and T. R. Forester, *J. Phys. Chem.*, **101**, 1762 (1997). Molecular Dynamics Studies of Hydrated and Dehydrated Na^+ -Zeolite-4A.
162. J. Godber, M. D. Baker, and G. A. Ozin, *J. Phys. Chem.*, **93**, 1409 (1989). Far-IR Spectroscopy of Alkali-Metal and Alkaline-Earth Cations in Faujasite Zeolites.
163. K. Krause, E. Geidel, J. Kindler, H. Förster, and K. S. Smirnov, *Vib. Spectrosc.*, **12**, 45 (1996). A Comparative Computer Modeling Study of Spectral Characteristics of Cation Exchanged Zeolite Y.
164. E. de Vos Burchart, H. van Koningsveld, and B. van de Graaf, *Microporous Mater.*, **8**, 215 (1997). Molecular Mechanics Studies of TBA and TPA in MEL and MFI.
165. S. L. Njo, J. H. Koegler, H. van Koningsveld, and B. van de Graaf, *Microporous Mater.*, **8**, 223 (1997). Molecular Mechanics Calculations on the N,N-Diethyl-3,5-dimethyl-piperidinium ions in MEL and MFI.
166. O. Terasaki, T. Ohsuna, H. Sakuma, D. Watanabe, Y. Nakagawa, and R. C. Medrud, *Chem. Mater.*, **8**, 463 (1996). Direct Observation of “Pure MEL Type” Zeolite.
167. H. van Koningsveld, J. C. Jansen, and H. van Bekkum, *Zeolites*, **10**, 235 (1990). The Monoclinic Framework Structure of Zeolite H-ZSM-5. Comparison with the Orthorhombic Framework of As-Synthesized ZSM-5.
168. C. A. Fyfe, H. Gies, G. T. Kokotailo, C. Pasztor, H. Strobl, and D. E. Cox, *J. Am. Chem. Soc.*, **111**, 2470 (1989). Detailed Investigation of the Lattice Structure of Zeolite ZSM-11 by a Combination of Solid-State NMR and Synchrotron X-Ray Diffraction Techniques.
169. N. L. Allinger, Y. H. Yuh, and J.-H. Lii, *J. Am. Chem. Soc.*, **111**, 8551 (1989). Molecular Mechanics. The MM3 Force Field for Hydrocarbons. 1.
170. E. de Vos Burchart, B. van der Linden, H. van Bekkum, and B. van de Graaf, *Collect. Czech. Chem. Commun.*, **57**, 675 (1992). Molecular Mechanics Studies on MFI Type Zeolites. 1. Effect of *p*-Xylene Adsorption on Zeolite Structure.
171. E. de Vos Burchart, H. van Bekkum, and B. van de Graaf, *Zeolites*, **13**, 212 (1993). Molecular Mechanics Studies on MFI Type Zeolites. 3. The Monoclinic–Orthorhombic Phase Transition.
172. M. Taramaso, G. Perego, and B. Notari, U.S. Patent 4,410,501 (1983). Preparation of Porous Crystalline Synthetic Materials Comprised of Silicon and Titanium Oxides.
173. G. Bellussi and M. S. Rigutto, *Stud. Surf. Sci. Catal.*, **85**, 177 (1994). Metal Ions Associated to the Molecular Sieve Framework: Possible Catalytic Oxidation Sites.
174. E. Astorino, J. B. Peri, R. J. Willey, and G. J. Busca, *J. Catal.*, **157**, 482 (1995). Spectroscopic Characterization of Silicalite-1 and Titanium Silicalite-1.
175. S. Bordiga, S. Coluccia, C. Lamberti, L. Marchese, A. Zecchina, F. Boscherini, F. Buffa, F. Genoni, G. Leofanti, G. Petrini, and G. J. Vlaic, *J. Phys. Chem.*, **98**, 4125 (1994). XAFS Study of Ti-Silicalite: Structure of Framework Ti(IV) in the Presence and Absence of Reactive Molecules (H_2O , NH_3) and Comparison with Ultraviolet-Visible and IR Results.
176. Z. Luz and A. J. Vega, *J. Chem. Phys.*, **91** (1987) 374. Interaction of H-RHO Zeolite with Water and Methanol Studied by Multinuclear NMR Spectroscopy.
177. G. Mirth, J. A. Lercher, M. W. Anderson, and J. Klinowski, *J. Chem. Soc., Faraday Trans.*, **86**, 3039 (1990). Adsorption Complexes of Methanol on Zeolite ZSM-5.
178. M. W. Anderson, P. J. Barrie, and J. Klinowski, *J. Chem. Phys.*, **95**, 235 (1991). ^1H Magic-Angle-Spinning NMR Studies of the Adsorption of Alcohols on Molecular Sieve Catalysts.

179. L. Kubelková, J. Nováková, and K. Nedomová, *J. Catal.*, **124**, 441 (1990). Reactivity of Surface Species on Zeolites in Methanol Conversion.
180. J. Klinowski, *Chem. Rev.*, **91**, 1459 (1991). Solid State NMR Studies of Molecular Sieves Catalysts.
181. C. Tsai, D. R. Corbin, and C. Dybowski, *J. Am. Chem. Soc.*, **112**, 7140 (1990). Investigation of Methanol Adsorbed on Zeolite H-ZSM-5 by ^{13}C NMR Spectrometry.
182. U. Messow, K. Quitzsch, and H. Herden, *Zeolites*, **4**, 255 (1984). Heats of Immersion of ZSM-5 Zeolite in *n*-Alkanes, 1-Alkenes and 1-Alcohols at 30° C.
183. J. Sauer, P. Ugliengo, E. Garrone, and V. R. Saunders, *Chem. Rev.*, **94**, 2095 (1994). Theoretical Study of van der Waals Complexes at Surface Sites in Comparison with the Experiment.
184. A. G. Pelmentschikov and R. A. van Santen, *J. Chem. Phys.*, **97**, 10678 (1993). Water Adsorption on Zeolites: Ab-Initio Interpretation of IR Data.
185. A. G. Pelmentschikov, J. H. M. C. van Wolput, J. Jänen, and R. A. van Santen, *J. Chem. Phys.*, **99**, 3612 (1995). (A,B,C) Triplet of Infrared OH Bands of Zeolitic H-Complexes.
186. J. D. Gale, C. R. A. Catlow, and J. R. Carruthers, *Chem. Phys. Lett.*, **216**, 155 (1993). An Ab Initio Study of Methanol Adsorption in Zeolites.
187. F. Haase and J. Sauer, *J. Am. Chem. Soc.*, **117**, 3780 (1995). Interaction of Methanol with Brønsted Acid Sites of Zeolite Catalysts: An Ab Initio Study.
188. F. Haase and J. Sauer, *J. Phys. Chem.*, **98**, 3083 (1994). ^1H NMR Chemical Shifts of Ammonia, Methanol, and Water Molecules Interacting with Brønsted Acid Sites of Zeolite Catalysts: Ab-Initio Calculations.
189. S. R. Blaszkowski and R. A. van Santen, *J. Phys. Chem.*, **99**, 11728 (1995). Density Functional Theory Calculations of the Activation of Methanol by a Brønsted Zeolitic Proton.
190. R. Shah, M. C. Payne, M.-H. Lee, and J. D. Gale, *Science*, **271**, 1395 (1996). Understanding the Catalytic Behavior of Zeolites: A First-Principles Study of the Adsorption of Methanol.
191. R. Shah, J. D. Gale, and M. C. Payne, *J. Phys. Chem.*, **100**, 11688 (1996). Methanol Adsorption in Zeolites—A First-Principles Study.
192. E. Nusterer, P. E. Blöchl, and K. Schwarz, *Angew. Chem., Int. Ed. Engl.*, **35**, 175 (1996). Structure and Dynamics of Methanol in a Zeolite.
193. S. P. Greatbanks, I. W. Hillier, N. A. Burton, and P. Sherwood, *J. Chem. Phys.*, **105**, 3770 (1996). Adsorption of Water and Methanol on Zeolite Brønsted Acid Sites: An Ab Initio, Embedded Cluster Study Including Electron Correlation.
194. E. Nusterer, P. E. Blöchl, and K. Schwarz, *Chem. Phys. Lett.*, **253**, 448 (1996). Interaction of Water and Methanol with Zeolite at High Coverages.
195. F. Haase, J. Sauer, and J. Hutter, *Chem. Phys. Lett.*, **266**, 397 (1997). Ab Initio Molecular Dynamics Simulation of Methanol Adsorbed in Chabazite.

CHAPTER 4

Toward More Accurate Model Intermolecular Potentials for Organic Molecules

Sarah L. Price

*Centre for Theoretical and Computational Chemistry,
University College London, 20 Gordon Street, London WC1H
0AJ, United Kingdom*

INTRODUCTION

Computer simulations of the behavior of organic molecules in the solid, liquid, and gas and in complexes, including ligands binding in active sites of proteins,¹ have added greatly to our understanding of these systems. Such simulations are increasingly being used in the design of new materials, such as pharmaceuticals.² A fundamental scientific input into such simulations is the quantitative mathematical model for the interaction between the molecules—the model intermolecular potential (often also referred to as the nonbonded potential in force fields for flexible molecules when the same terms are used for both inter- and intramolecular interactions^{3,4}). Early intermolecular potentials, often based on an atom–atom Lennard-Jones model, were usually constructed to be “good enough” for a specific type of simulation of a molecule, or type of molecule, in a given phase. The emphasis was on simplicity because of the limitations of the available computers. Indeed, in developing molecular dynamics simulations, there will always be a trade-off between the size of the

Reviews in Computational Chemistry, Volume 14
Kenny B. Lipkowitz and Donald B. Boyd, Editors
Wiley-VCH, John Wiley and Sons, Inc., New York, © 2000

molecular system, the length of time being simulated, and the time required to evaluate the intermolecular potential energy of the system in each configuration. However, in recent years computer power has increased considerably, and with it our ambitions for the range of properties to be calculated, and their accuracy. This results in a desire for more realistic and reliable model potentials. The literature does not reflect the number of simulation projects that have been abandoned for lack of a suitable model potential or when the best potential available from the literature (or suite of modeling software) did not reproduce the basic experimental properties of the system. However, many quality computer simulation papers do include comments about aspects of the simulation results that may be artifacts of, or reflect inadequacies in, the model potential. Thus, although current model potentials are “good enough” and validated for many purposes, there is a continuing interest in being able to derive more realistic models to increase the confidence that can be placed in the simulations.

Intermolecular forces have been studied extensively for closed-shell atoms,⁵ such as helium and argon, and for small polyatomic molecules. Quite detailed model intermolecular potentials, specific to each molecule, are used for small polyatomics, such as HF, Cl₂, and water.⁶ These model potentials are often derived, at least in part, from ab initio calculations and are tested for their ability to reproduce the spectra of van der Waals dimers or molecular beam experiments, which are direct measures of the intermolecular potential. The potentials are also tested on condensed phase systems. The intermolecular forces have been so accurately tuned for argon that it is possible to calculate within experimental error a wide range of experimental properties of this element in the solid, liquid, and gaseous states, and in van der Waals complexes.⁵ Although there is no model intermolecular pair potential yet for a polyatomic molecule that is as definitively accurate as for argon, or other intermolecular atom–atom or atom–diatomic potentials, considerable progress has been made toward this goal. This has largely been based on developments in the theory of intermolecular forces that relate the intermolecular forces to the distribution of charge within each molecule. In contrast, the models for intermolecular forces used to simulate organic and biochemical interactions are mainly derived by assuming that each intermolecular atom–atom interaction is transferable between different molecules. Such models are usually derived empirically, by fitting to a range of experimental data such as molecular crystal structures. Thus, the route to improving the model potentials for organic molecules is to apply the ideas and techniques that are used to develop accurate potentials for small polyatomics.

This tutorial focuses on the lessons that can be learned from the current intermolecular potentials of small polyatomics for the development of more accurate potentials for organic molecules. The electrostatic component is emphasized because the methodology for accurate electrostatic models is already being applied to organic molecules with considerable impact. This chapter also considers other contributions to the intermolecular potential and aims to give

an awareness of the approximations that are in current models and the prospects for estimating these effects in the future. This review can be used by researchers who wish to assess the model potential they are using in simulations at two levels. First, the material may suggest an idea of which approximations in the current force fields are likely to be least harmful for a given molecule and type of simulation. Second, for those who wish to improve the model potentials, the chapter outlines the theoretical basis of how this can be done. However, for a more detailed assessment of the theoretical basis, formalisms, and techniques used in the theory of intermolecular forces, and the use of spherical tensor theory, one should refer to the book by Stone.⁶

This chapter starts with some basic definitions and then discusses the physical origins of the different contributions to the intermolecular forces, and their different properties. Dividing the intermolecular potential into contributions of different types is the basis of the functional form of all model intermolecular potentials. The survey of different methods of determining model intermolecular potentials described in this chapter emphasizes the advantages, as well as limitations, of these divisions. The further divisions of the intermolecular potential into atom–atom contributions is both essential for a practical model for organic molecules and attractive as a basis for constructing model potentials for larger related organic molecules by assuming transferability. However, some of the limitations of the transferability assumptions require careful consideration, as will be highlighted in the penultimate section of this chapter. A significant limitation of the traditional isotropic atom–atom model potential for organic molecules is the assumption that the atoms in the different molecules interact as if they were spherical. It is in getting away from this assumption, leading to anisotropic atom–atom potentials, that the studies on small polyatomics have contributed most to improving model potentials for organic molecules. However, it is this flexibility to describe the interactions of a realistic molecular charge distribution that requires additional mathematical complexity in the potential model and therefore in the computer codes. These issues, too, are described in this chapter.

DEFINITIONS AND LIMITATIONS OF INTERMOLECULAR POTENTIAL THEORY

The intermolecular pair potential $U(R, \Omega)$ is defined as the difference between the energy of a pair of molecules (at a given separation R and relative orientation Ω) and their energy when completely separated; that is, $U(R, \Omega) = E(R, \Omega) - E(\infty)$. The pair potential is used to describe the weak interactions between closed-shell molecules, so that the effect of the interaction on the charge distributions of the individual molecules is very small and does not

change the vibrational or electronic states of the interacting molecules. The theories of intermolecular forces and model intermolecular pair potentials have been heavily developed⁵ for the spherical (or approximately spherical) molecules such as argon, methane, and nitrogen. (In this chapter, closed-shell atoms like argon that interact by intermolecular forces are referred to as “molecules,” to provide a clear distinction from atoms that are part of polyatomic molecules.) For such small polyatomic molecules, the distinction between intermolecular forces and the internal covalent forces is clear-cut because the intermolecular interactions are less than about 25 kJ/mol, whereas a typical chemical bond has a dissociation energy of over 200 kJ/mol, and so the geometry of polyatomic molecules can be assumed to be unaffected by the interaction. Since, however, the approach of another strongly interacting molecule can influence the conformation of a flexible organic molecule, it is more of an approximation to separate the intermolecular and intramolecular forces (see the penultimate section and Ref. 6). It also becomes questionable whether the theory should be used for stronger interactions when significant charge transfer exists between the molecules, blurring the distinction between inter- and intramolecular interactions.

The intermolecular pair potential for two closed-shell spherical molecules, such as $\text{Ar} \cdots \text{Ar}$, is only a function of the separation R and will have the qualitative form shown in Figure 1(a), with a minimum energy $-\epsilon$ at $R = R_m$ and steeply rising repulsive wall. For two polyatomic molecules, this curve will also depend on the relative orientation of the two molecules, even for approximately spherical molecules such as N_2 , with some orientations having much deeper wells than others [Figure 1(b)]. For organic molecules, the orientation dependence can be marked, with sharp deep wells for orientations in which hydrogen bonds form, and possibly completely repulsive curves for orientations where two electronegative atoms approach each other. It is because of this complexity that a molecule–molecule potential $U(R, \Omega)$ is really helpful only for comparing small-molecule interactions. A suitable coordinate system and set of orientation-dependent functions must be used to describe the orientational dependence of the intermolecular potential for polyatomic molecules, whether in the molecule–molecule or atom–atom form. An explanation of this choice is essential for the development of model potentials, but the rest of this section may be skipped by those with less interest in the associated mathematical formulation.

Coordinate Systems

In general, the position of a nonlinear rigid polyatomic molecule relative to a global axis system (fixed in space) can be defined by six coordinates: three to define the position of the center of mass and three (usually the Euler angles⁷ α, β, γ) to define the orientation of its local or molecule-fixed axis system relative to the global axis system. The local axis system is defined by the bonds within the molecule and should be chosen to reflect any symmetry because this simplifies the model potential. For example, a water molecule with C_{2v} symme-

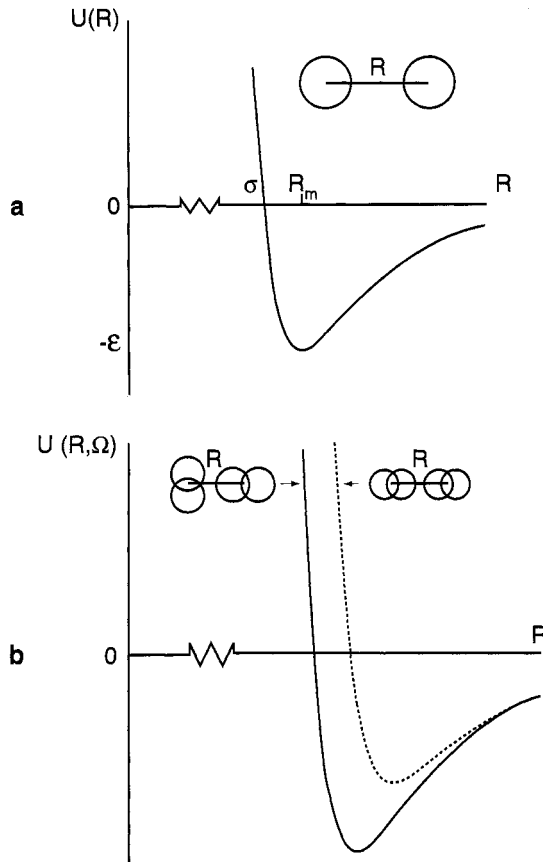


Figure 1 (a) A typical intermolecular potential energy function $U(R)$ for two closed-shell atoms, such as $\text{Ar} \cdots \text{Ar}$. Note the scale break along the R axis: the width of the region in which there is a significant attractive intermolecular energy is generally smaller than the sterically forbidden region. (b) Two sections of a simple potential energy surface for two homonuclear diatomic molecules $\text{X}_2 \cdots \text{X}_2$, corresponding to a fixed T-shaped or linear relative orientation. This is just the surface for a repulsion-dispersion atom–atom interaction. The orientational dependence will depend considerably on the diatomic molecule, because its charge distribution will determine the balance between the electrostatic and repulsion–dispersion forces, and so different diatomic molecules have different minimum energy dimer structures.

try would have the z axis bisecting the $\text{H}—\text{O}—\text{H}$ bond angle and lie in the xz plane, whereas the choice for uracil would be more arbitrary, but might take the x axis parallel to $\text{N}1 \cdots \text{C}4$ and have the z axis perpendicular to the plane of the molecule (Figure 2).

Unless there is a macroscopic feature, such as an external electric field, defining the global axis system, the coordinate system is just an abstract frame of reference, and $U(R, \Omega)$ cannot depend on the relative orientation of the two

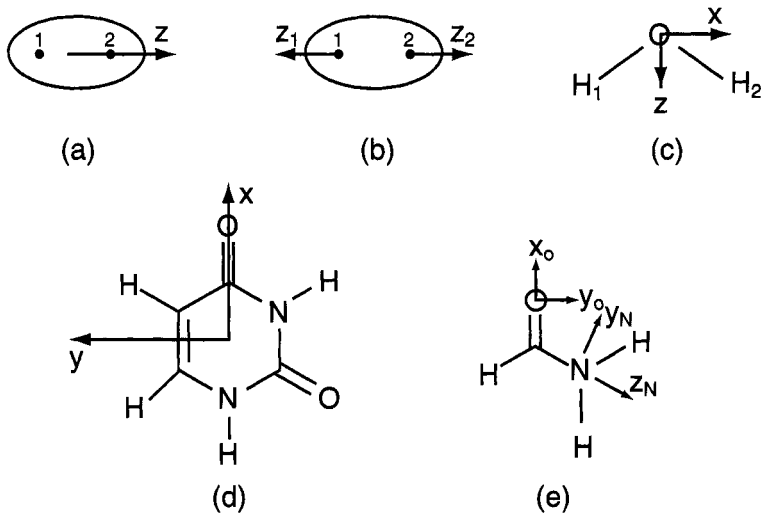


Figure 2 Examples of global and local axis systems. (a) Molecular axis system for a homonuclear diatomic. With this system, all central multipoles Q_{lk} with $k \neq 0$ or l odd will be zero, and no S functions with $k \neq 0$ or l odd can appear in a molecule-molecule expansion of $U(R, \Omega)$. The atomic multipoles Q_{10} (all $l \neq 0$ allowed) on the two atoms will be related by $Q_{10}^1 = (-1)^l Q_{10}^2$. (b) Local atomic axis system for a homonuclear diatomic molecule. With this definition $Q_{10}^1 = Q_{10}^2$. (c) Molecular axis system for water. The nonzero atomic multipole moments for the O atom would be Q_{00} , Q_{10} , Q_{20} , $Q_{22c} = (Q_{22} + Q_{2-2})/\sqrt{2}$, Q_{30} , $Q_{32c} = (Q_{32} + Q_{3-2})\sqrt{2}$, etc., and on the hydrogen atoms $Q_{00}^1 = Q_{00}^2$, $Q_{10}^1 = Q_{10}^2$, $Q_{11c}^1 = (-Q_{11}^1 + Q_{1-1}^1)/\sqrt{2} = -Q_{11c}^2$, $Q_{20}^1 = Q_{20}^2$, $Q_{21c}^1 = (-Q_{21}^1 + Q_{2-1}^1)/\sqrt{2} = Q_{21c}^2$, $Q_{22c}^1 = (Q_{22}^1 + Q_{2-2}^1)/\sqrt{2} = Q_{22c}^2$, etc. (d) Molecular axis system for uracil. With this system, all nonzero atomic, or central multipoles have $l + k$ even. (e) Local atomic axis system for the O and N atoms in formamide. Any comparison of the multipoles on a given atom, say, the carbonyl oxygen atom, in different compounds, must have the atomic multipoles referred to the same local axis system (e.g., x_o , y_o , z_o) defined by the covalent bonds.

molecules to the global axis system, but instead only on the relative positions of the atoms in the two molecules. Thus, $U(R, \Omega)$ depends on only six independent variables, which are usually chosen as the intermolecular separation R [with one molecule at the origin of the global axis system and the other at $(0, 0, R)$] and five angles, often taken as the Euler angles $(\alpha_1 - \alpha_2, \beta_1, \beta_2, \gamma_1, \text{ and } \gamma_2)$.⁶ We also know that the intermolecular potential $U(R, \Omega)$ is a scalar quantity, which must be invariant under the rotation of the entire system, a requirement that considerably constrains the functions of the orientational variables that can appear in $U(R, \Omega)$. However, the tensor properties of the individual molecules, such as the dipole moment components or p orbitals relative to the global axis, change with rotations of the molecule. Vector properties ($l = 1$) have different components (labeled $m = 1, 0, -1$) according to orientation. Similarly, second-rank tensors ($l = 2$), such as quadrupole moments or d orbitals, have different components ($m =$

$-2, -1, 0, 1, 2)$ according to the relative orientation of the object and the axis system. Angular momentum theory⁷ can be used to handle the effects of rotations on such tensor properties. One general set of expansion functions for the orientational dependence of $U(R, \Omega)$ are the normalized \tilde{S} functions

$$\begin{aligned} \tilde{S}_{l_1 l_2 j}^{k_1 k_2} = i^{l_1 - l_2 - j} & \left[\begin{pmatrix} l_1 & l_2 & j \\ 0 & 0 & 0 \end{pmatrix} \right]^{-1} \\ & \times \sum_{m_1 m_2 m} [D_{m_1 k_1}^l(\alpha_1, \beta_1, \gamma_1)]^* [D_{m_2 k_2}^l(\alpha_2, \beta_2, \gamma_2)]^* C_{jm}(\theta, \phi) \begin{pmatrix} l_1 & l_2 & j \\ m_1 & m_2 & m \end{pmatrix} \quad [1] \end{aligned}$$

where the orientation dependence is contained in the Wigner rotation matrices $D_{mk}^l(\Omega)$ for the orientations of molecules 1 and 2, which describe how the components (m and k) of angular momentum l are transformed between each other by the rotation; the spherical harmonic functions C_{jm} of the polar angles θ and ϕ describe the orientation of the intermolecular vector R . The Wigner 3-j symbol ensures that the three orientation-dependent functions are combined to give a scalar as required. The division by the Wigner 3-j symbol with zero m values ensures that the maximum magnitude of each \tilde{S} function is 1, the bar over the S denoting this normalization. The angular momentum theory behind these functions is well explained in many texts (e.g. Ref. 7), and Ref. 6 covers the application of these functions to intermolecular potentials. This is a general set of expansion functions, which can be expressed for different choices of coordinate system. The first few terms have often been tabulated, at least for simple systems, such as atom-linear molecule (where they reduce to the spherical harmonics) or for two linear molecules.⁸ One of the useful features of these functions is that the symmetry of the molecules (reflected in the choice of axes), as well as the constraints on the coupling of the angular momenta, severely restrict which \tilde{S} functions can appear in the intermolecular potentials. For example, k is always restricted to one of the integer values between $-l$ and l , but for linear molecules (with the z axis along the molecular axis) only $k = 0$ is allowed. For molecules with a plane of symmetry perpendicular to the z axis (σ_h), $l + k$ must be even. Further restrictions of the allowed \tilde{S} functions according to the symmetry of both the system as a whole and the individual molecules have been given.⁹ Some examples appear in Figure 2.

In many applications, it is more computationally convenient to express the \tilde{S} functions in terms of the scalar products between the unit local axis vectors (x_1, y_1, z_1 and x_2, y_2, z_2) and the unit intermolecular vector \hat{R} . This set of variables is highly redundant, but easily calculated from the local axis vector information in most simulations. As an illustration, Table 1 gives the \tilde{S} functions¹⁰ that are important in describing the anisotropy of the atom-atom repulsion between an N atom in pyridine and a hydrogen-bonding proton of methanol.

Table 1 Examples of a Few of the \tilde{S} Functions That Can Be Used to Express the Orientational Dependence of the Intermolecular Potential^a

$\tilde{S}_{101}^{00} = +\mathbf{z}_1 \cdot \hat{\mathbf{R}}$	$\tilde{S}_{011}^{00} = -\mathbf{z}_2 \cdot \hat{\mathbf{R}}$
$\tilde{S}_{202}^{00} = \frac{1}{2}[3(\mathbf{z}_1 \cdot \hat{\mathbf{R}})^2 - 1]$	$\tilde{S}_{022}^{00} = \frac{1}{2}[3(\mathbf{z}_2 \cdot \hat{\mathbf{R}})^2 - 1]$
$\tilde{S}_{303}^{00} = -\frac{1}{2}[3(\mathbf{z}_1 \cdot \hat{\mathbf{R}}) - 5(\mathbf{z}_1 \cdot \hat{\mathbf{R}})^3]$	$\tilde{S}_{033}^{00} = -\frac{1}{2}[5(\mathbf{z}_2 \cdot \hat{\mathbf{R}})^3 - 3(\mathbf{z}_2 \cdot \hat{\mathbf{R}})]$
$\tilde{S}_{404}^{00} = \frac{1}{8}[3 - 30(\mathbf{z}_1 \cdot \hat{\mathbf{R}})^2 + 35(\mathbf{z}_1 \cdot \hat{\mathbf{R}})^4]$	$\tilde{S}_{044}^{00} = \frac{1}{8}[3 - 30(\mathbf{z}_2 \cdot \hat{\mathbf{R}})^2 + 35(\mathbf{z}_2 \cdot \hat{\mathbf{R}})^4]$
	$\tilde{S}_{011}^{0\pm 1} = \pm \frac{1}{\sqrt{2}}(\mathbf{x}_2 \cdot \hat{\mathbf{R}} \mp i\mathbf{y}_2 \cdot \hat{\mathbf{R}})$
	$\tilde{S}_{022}^{0\pm 1} = \mp \frac{\sqrt{6}}{2}(\mathbf{x}_2 \cdot \hat{\mathbf{R}} \mp i\mathbf{y}_2 \cdot \hat{\mathbf{R}})(\mathbf{z}_2 \cdot \hat{\mathbf{R}})$
$\tilde{S}_{202}^{\pm 20} = \frac{\sqrt{6}}{4}(\mathbf{x}_1 \cdot \hat{\mathbf{R}} \mp i\mathbf{y}_1 \cdot \hat{\mathbf{R}})^2$	$\tilde{S}_{022}^{0\pm 2} = \frac{\sqrt{6}}{4}(\mathbf{x}_2 \cdot \hat{\mathbf{R}} \mp i\mathbf{y}_2 \cdot \hat{\mathbf{R}})^2$
$\tilde{S}_{404}^{\pm 20} = \frac{\sqrt{10}}{24}(\mathbf{x}_1 \cdot \hat{\mathbf{R}} \mp i\mathbf{y}_1 \cdot \hat{\mathbf{R}})^2[7\{3(\mathbf{z}_1 \cdot \hat{\mathbf{R}})^2 - 1\} + 4]$	
$\tilde{S}_{404}^{\pm 40} = \frac{\sqrt{70}}{16}(\mathbf{x}_1 \cdot \hat{\mathbf{R}} \mp i\mathbf{y}_1 \cdot \hat{\mathbf{R}})^4$	

^aThese are expressed in terms of scalar products between the unit axis system vectors on sites 1 and 2 (on different molecules) and the unit vector $\hat{\mathbf{R}}$ from site 1 to 2. The \tilde{S} functions that can have nonzero coefficients in the intermolecular potential depend on the symmetry of the site. This table includes the first few terms that would appear in the expansion of the atom–atom potential for linear molecules. The second set illustrate the types of additional functions that can occur for sites with other than $C_{\infty v}$ symmetry. These additional terms happen to be those required to describe the anisotropy of the repulsion between the N atom in pyridine (with \mathbf{z}_1 in the direction of the conventional lone pair on the nitrogen and \mathbf{y}_1 perpendicular to the ring) and the H atom in methanol (with \mathbf{z}_2 along the O–H bond and \mathbf{x}_2 in the COH plane, with C in the direction of positive \mathbf{x}_2). The important \tilde{S} functions reflect the different symmetries of the two molecules.¹⁰ Note that coefficients of \tilde{S} functions with values of k of opposite sign are always related so that purely real combinations of \tilde{S} functions appear in the intermolecular potential.

Molecule-Centered Expansions Versus Atom–Atom Models

The intermolecular potential between two small molecules is traditionally expanded in terms of the intermolecular separation R and orientation-dependent functions. An example of this is

$$U(R, \Omega) = \sum f_{l_1 l_2 j}^{k_1 k_2}(R) \tilde{S}_{l_1 l_2 j}^{k_1 k_2}(\Omega) \quad [2]$$

where Ω denotes the orientational coordinates of the two molecules with respect to each other. Indeed this form is the most convenient for scattering calculations. As will be discussed later, the intermolecular potential at large

separations comes out naturally in this form, with the coefficients being properties of the isolated molecules. An example of this is the formula for the dipole-dipole electrostatic energy. However, since this is an expansion in terms of the deviations of the molecule from a sphere, it is rapidly convergent for even the more spherical molecules only at large separations. In contrast, it would take many, many terms to adequately describe how the uracil–uracil potential varies from attractive to repulsive with rotation of the molecules about their centers of mass, as hydrogen bonds are formed and broken.

The usual method of expressing the intermolecular potential for a pair of organic molecules is to use the isotropic atom–atom model, where the total interaction between the two molecules is assumed to be the sum of intermolecular type interactions between all the intermolecular pairs of atoms, for example:

$$U(R, \Omega) = \sum_{i \in A, k \in B} U_{ik}(R_{ik}) \quad [3]$$

where atom i belonging to molecule A is at a distance R_{ik} from atom k belonging to molecule B. This is clearly an excellent first approximation, recognizing that molecules are composed of atoms. Equation [3] gives a potential that automatically reflects the shape of the interacting molecules, at least at the level of a superposition of spherical atoms. However, this is only a first approximation because the charge distribution of a molecule is not a superposition of spherical atomic charge distributions. The formation of the covalent bonds within the molecules redistributes the valence electron density to give bonding, lone pair, and π -electron density, and so on. Considerable effort has gone into developing qualitative and quantitative models of chemical bonding, and nobody believes that upon bonding, charge is redistributed from the electropositive to electronegative atoms such that the charge distribution around each atom is spherical. Nevertheless, the existing popular isotropic atom–atom model is based on this assumption!

Thus, it is reasonable to assume that the intermolecular forces between the atoms of polyatomic molecules will depend on the relative orientation of the atoms (as defined by local axes within the molecule that reflect the directions of the covalent bonds to that atom). Hence a more general form of the atom–atom model potential would be

$$U(R, \Omega) = \sum_{i \in A, k \in B} U_{ik}(R_{ik}, \Omega_{ik}) \quad [4]$$

where the orientation dependence could be expanded in the appropriate \hat{S} functions for the approximate local symmetry of the atom. For example, an anisotropic atom–atom potential for HCN ··· HCN could not contain any terms with $k_1, k_2 \neq 0$, for any atom–atom contributions, because HCN is linear.

By analogy, the $N \cdots N$ terms in a $\text{CH}_3\text{CN} \cdots \text{CH}_3\text{CN}$ potential could have only negligible contributions with $k_1, k_2 \neq 0$, because the methyl group will not distort the charge distribution around the N atoms much. This formulation has the important advantage that the orientational dependence of the potential around each atom is easier to describe in terms of S functions than that of the entire molecule, because an atom is a closer approximation to a sphere than most molecules. Thus an obvious way to improve the description of the intermolecular potential between polyatomic molecules is to combine the traditional one-center anisotropic potentials for small molecules, with the isotropic atom-atom model traditionally used for organic molecules to produce anisotropic atom-atom potentials. The next stage is to consider the physical origins and characteristic properties of the different terms in the intermolecular potential, and to address how model potentials can be derived for use in studying molecules in the solid, liquid, and gaseous states.

THE PAIRWISE ADDITIVE APPROXIMATION

When one is calculating the lattice energy of a molecular crystal, or the potential energy of a liquid, or indeed the energy of any ensemble of N molecules relative to their energy when completely separated, it is usual to assume that the energy is equal to the sum of the interactions between every pair of molecules in the ensemble (*the pairwise additive approximation*):

$$U = \sum_{A < B}^N U_{AB} \quad [5]$$

However, this energy should be expressed formally as an expansion

$$\varepsilon = 1 + \frac{4\pi}{3} \frac{\langle \mathbf{M}^2 \rangle}{V k_B T} \quad [6]$$

where U_{AB} is the energy of the pair of molecules A and B, and the three-body term U_{ABC} is the difference between the energy of the three molecules and the sum of the pair potentials $U_{AB} + U_{AC} + U_{BC}$, and likewise for the four-body term, and so on. The different contributions to the intermolecular potential differ markedly in whether they are additive—that is, in whether they are correctly represented by the pairwise additive approximation. An extreme example of nonadditivity involves Li^+ interacting with argon. One Li^+ will polarize the charge distribution of a nearby Ar atom to induce a dipole moment. However, when a second Li^+ is placed symmetrically on the opposite side of the

argon, no dipole can be induced, and so the interaction energy of the two ions with the induced quadrupole is much less than the interaction of one ion with the induced dipole. Thus the importance of the many-body terms will depend on the deficiencies of the nonadditive contributions to the pair potential.

One consequence of using the pairwise additive approximation is that if a true pair potential is used to calculate the properties of a liquid or solid, there will be an error due to the omission of the nonadditive contributions. Conversely, if the pairwise additive approximation is made in deriving the pair potential U_{AB} , the latter will have partially absorbed some form of average over the many-body forces present, producing an error in the calculated properties of the gas phase where only two-body interactions are important. Because the effective pair potential U_{AB} cannot correctly model the orientation and distance dependence of the absorbed nonadditive contributions, there will also be errors in transferring the effective potential to other condensed phases with different arrangements of molecules.

CONTRIBUTIONS TO THE INTERMOLECULAR PAIR POTENTIAL

All the important contributions to the forces between molecules arise ultimately from the electrostatic interactions between the particles that make up the two molecules. Thus our main theoretical insight into the nature of intermolecular forces comes from perturbation theory,^{8,11} using these interactions as the perturbation operator $H' = \sum e_i e_j / (4\pi\epsilon_0 r_{ij})$, where e_i is the charge on particle i in one molecule, r_{ij} is the distance between particles i and j in different molecules, and ϵ_0 is permittivity of a vacuum. The definitions of the contributions, such as the repulsion, dispersion, and electrostatic terms, which are normally included in model potentials, correspond to different terms in the perturbation series expansion.

When two molecules are sufficiently separated such that there is no overlap of the molecular charge distributions (long range), the interaction can be treated by ordinary nondegenerate Rayleigh–Schrödinger perturbation theory.⁶ This provides analytical expressions that can be quantified in terms of the properties of the individual molecular charge distributions. However, this approach breaks down when there is overlap between the two molecular charge distributions, so there is no rigorous analytical theory for the interaction energy at short range, where the repulsion dominates both the quantum mechanical exchange effects and the contributions corresponding to the long-range terms as modified by the overlap. The main terms are described below and summarized in Table 2.

Table 2 Contributions to the Energy of Interaction Between Nonspherical Molecules at a Distance R Apart

Contribution	Additive?	Sign	Comment	Form in Model U_{ij}^a
Long-range $U \approx R^{-n}$				
Electrostatic	Yes	\pm	Strong orientational dependence	Atomic multipoles
Induction	No	—		
Dispersion	Approx.	—	Always present	$-C/R^6$
Resonance	No	\pm	Degenerate states only	
Magnetic	Yes	\pm	Very small	
Short-range $U \approx e^{-\alpha R}$				
Exchange	No	—		
Repulsion	No	+	Dominates	$Ae^{-\alpha R}$
Charge Transfer	No	—	Donor–acceptor interaction	
Penetration	Yes	—	Can be repulsive at very short range	
Damping	Approx.	+	Modification of dispersion and induction	

^aTerms normally explicitly included in models for the forces between organic molecules.

Long-Range Contributions to the Intermolecular Energy

The Electrostatic Energy

The electrostatic energy is the first-order term in long-range perturbation theory and is usually the interaction that persists over the longest range. The Coulombic interaction between the undistorted molecular charge distributions is:

$$U_{\text{electrostatic}} = \int_{\text{all space}} \frac{\rho^A(\mathbf{r}_1)\rho^B(\mathbf{r}_2)}{|\mathbf{r}_1 - \mathbf{r}_2|} d^3\mathbf{r}_1 d^3\mathbf{r}_2 = \langle 0^A 0^B | H' | 0^A 0^B \rangle \quad [7]$$

where ρ^A is the charge distribution corresponding to the ground state wavefunction 0^A of molecule A in isolation, and H' is the perturbation operator. Although zero for spherical neutral molecules (atoms), the electrostatic term is significant for almost all organic molecules, except possibly the saturated hydrocarbons. It is the only major contribution to the intermolecular potential that can be either attractive or repulsive. Indeed the rapid variation of the electrostatic term with orientation for organic molecules means that it usually determines the most favorable relative orientations of the molecules. It is strictly pairwise additive, as it is defined in terms of the charge densities of the isolated molecules.

The traditional description of the electrostatic interactions between small polyatomics is in terms of the first nonvanishing multipole moment—the total charge for ions, dipole for most neutral molecules, or the quadrupole for neutral molecules with a center of symmetry. An expression for the electrostatic energy in terms of these multipole moments can be derived from the integral of Eq. [7] over the molecular charge distributions, by expanding $1/|\mathbf{r}_1 - \mathbf{r}_2|$, the inverse of the distance between the charges in the different molecules, in terms of a vector \mathbf{R} between the centers of the two molecules, and the vectors from these centers to the charges in each molecule, and expressing this as a multipole expansion. This converts the expression into an infinite sum over the multipole moments of the isolated molecules, plus terms defining the dependence of the interaction on the relative geometry of the two molecules. The result is the familiar multipole expansion of the electrostatic energy, which can be expressed in terms of Cartesian or spherical tensor permanent multipole moments Q_{lk} of the isolated molecules: the charge ($l = 0$), dipole ($l = 1$), quadrupole ($l = 2$), octopole ($l = 3$), hexadecapole ($l = 4$), and so on. The electrostatic energy expressed in spherical tensor form is:

$$U_{\text{electrostatic}}(R, \Omega) = \frac{1}{4\pi\epsilon_0} \sum_{l_1 l_2} \sum_{k_1 k_2} \binom{l_1 + l_2}{l_1} Q_{l_1 k_1}^A Q_{l_2 k_2}^B \bar{S}_{l_1, l_2, l_1 + l_2}^{k_1 k_2}(\Omega) R^{-l_2 - l_2 - 1} \quad [8]$$

where the factor in parentheses is a binomial coefficient. Thus the interaction between multipole l_1 on molecule A and l_2 on molecule B decays as R^{-n} , where $n = l_1 + l_2 + 1$. The relative orientation of the molecular axes systems (used to define the molecular multipoles) appears in the orientation-dependent \bar{S} functions.

Before the advent of ab initio calculations for determining the molecular charge density, it was usually possible to measure experimentally only the first nonvanishing total multipole moment of the molecule. Hence, only the longest range term in the electrostatic energy, (e.g., the dipole–dipole term involving Q_{10}^A, Q_{10}^B and varying as R^{-3}) could be used in the model potential. However, current models for the electrostatic energy use more accurate representations of the molecular charge distribution, with many multipoles Q_{lk} in the series (see, e.g., Figure 2), and hence use many terms in Eq. [8].

The Polarization Energy

Second-order perturbation theory provides expressions for the polarization or induction energy. This is the attractive energy term arising from the distortions of the charge density of each molecule due to the field arising from the other (undistorted) molecule:

$$U_{\text{induction}}^A = - \sum_{n^A \neq 0^A} \frac{|\langle 0^A 0^B | H' | n^A 0^B \rangle|^2}{E_n^A - E_0^A} \quad [9]$$

This term represents the additional energy from the changes in the charge density of A (a molecule whose excited state wavefunctions n^A are of energy E_n^A) caused by the presence of B, interacting with the undistorted ground state charge distribution of B. The sum is thus over all the excited states of molecule A. There is a corresponding term that likewise represents the induction energy for the first-order changes in the charge density of B induced by A. This energy is always attractive, because the distortions occur only to lower the energy of the pair.

The application of the multipole expansion allows the induction energy of A to be expressed in terms of the permanent multipole moments of B and the polarizabilities of A, plus the orientation-dependent functions. For all molecules, the first polarizability is the dipole–dipole polarizability, which describes the ease of changing the total dipole moment of the molecule. Thus, for any atom or molecule in the presence of a charge, the first term in the induction energy changes as R^{-4} . However, if another charge is symmetrically placed on the opposite side of the molecule, there is no induced dipole by symmetry, and the leading induction energy term is then determined by the quadrupolar polarizability. Thus the induction energy is nonadditive. The induction energy is very important for the intermolecular interactions of ions, but the leading term for the induction energy arising from the presence of a dipolar molecule changes as R^{-6} and so will often be very small for ensembles of neutral molecules, and zero for neutral spherical molecules.

The Dispersion Energy

There are no electrostatic or induction forces between spherical molecules, such as argon, and yet there is clearly a long-range attractive force that causes the liquefaction of argon at low temperatures. This is the dispersion energy, the universal long-range force, which appears at second-order perturbation theory as:

$$U_{\text{dispersion}} = - \sum_{n^A \neq 0^A, n^B \neq 0^B} \frac{|\langle 0^A 0^B | H' | n^A n^B \rangle|^2}{E_n^A - E_0^A + E_n^B - E_0^B} \quad [10]$$

The dispersion forces arise from a purely quantum mechanical effect, and thus are difficult to envisage. The sum over all the excited states of both A and B shows that the dispersion arises from correlated distortions in the two molecular charge densities. Application of the central multipole expansion produces the usual series,

$$U_{\text{dispersion}} = - \frac{C_6}{R^6} - \frac{C_8}{R^8} - \frac{C_{10}}{R^{10}} - \dots \quad [11]$$

The leading R^{-6} dispersion term is often described as the correlation in the instantaneous dipolar fluctuations in the charge density of the two molecules.

The higher terms describe more complicated fluctuations. For polyatomic molecules, the dispersion coefficients depend on orientation, and for noncentro-symmetric molecules, there are anisotropic dispersion coefficients of odd powers, starting at R^{-7} . However, the average of the C_7 coefficient over all orientations is zero, if all orientations have equal weight.

The C_n coefficients can be obtained from the properties of the isolated molecules in favorable cases, either by means of the energies of transition from the ground to all excited states and the probabilities for these transitions (oscillator strengths)¹² or from the polarizabilities of the two molecules calculated at imaginary frequencies.⁶ An approximation that considers average excitation energies and static isotropic polarizabilities α^A and α^B and a rather ill-defined effective number of valence electrons N_A and N_B ¹³ gives the Slater-Kirkwood approximation, which is frequently used for organic molecules:

$$U_{\text{dispersion}} = - \frac{3\alpha_A \alpha_B}{2R^6[(\alpha_A/N_A)^{1/2} + (\alpha_B/N_B)^{1/2}]} \quad [12]$$

where the numeric factor arises from the averaging over the polarizability tensors and their associated orientational dependence.⁶

The dispersion energy is the universal attractive glue that leads to the formation of condensed phases. It is additive at second order in perturbation theory, and the form of the three-body term that arises at third order (the triple-dipole dispersion term) is also well known from perturbation theory. This Axilrod-Teller term¹⁴ was the only addition to the pair potential for argon that was required to quantitatively account for its solid and liquid state properties. This may be grounds for optimism that other nonadditive dispersion terms are negligible. Whether this can be extended to less symmetrical organic molecules and their typical crystalline and liquid environments has not yet been established however.

Unusual Long-Range Terms

If both molecules have unpaired electrons (such as O_2), then there are long-range magnetic interactions, albeit of very small magnitude. The energies associated with magnetic interactions between nuclei with nonzero spin in different molecules are several orders of magnitude weaker still and considered to be absolutely insignificant.

If one of the molecules is in a degenerate state, or if they are identical and one is in an excited state, then there will be resonance interactions, which are long range. This intermolecular force may cause the dimer in which one molecule is excited (an *excimer*) to be much more strongly bound than when both are in the ground state. Resonance is important in excited states of molecular crystals.¹⁵

Contributions to the Intermolecular Potential from Molecular Overlap

Exchange–Repulsion

As two molecules approach, the new first-order terms arising from the overlap of the charge distributions result in net intermolecular repulsion. The overlapping charge densities cannot occupy the same space (Pauli exclusion principle), reducing the electron density in the overlap region and thus deshielding the approaching nuclear charges, producing a repulsive force. This repulsion force dominates the attractive exchange force arising from the electron motions extending over both molecules. The two terms are usually taken together and for atoms can be represented as $f(R)\exp(-\alpha R)$, where $f(R)$ is a slowly varying polynomial function of the separation R . The exchange–repulsion energy is approximately additive, at the level of overlap normally found in molecular crystals and van der Waals complexes.

Charge Transfer

A further term that arises at second order in perturbation theory is the transfer of charge from the occupied orbitals of one molecule to the unoccupied orbitals of the other. These charge transfer, or intermolecular bonding, effects can be evaluated by perturbation theory¹⁶ or by Morokuma decomposition of self-consistent field (SCF) supermolecule calculations¹⁷ and have been shown to decay approximately exponentially with separation. The values of the charge transfer contribution will depend on the definition one uses to distinguish it from the exchange–repulsion and the long-range polarization term. However, a far more important problem is that its magnitude can be grossly overestimated because of contamination from basis set superposition error (BSSE). BSSE involves the use of orbitals based on one molecule to describe the charge distribution on the other, which can improve the description of the intramolecular interactions within one molecule (i.e., give a spurious energy lowering because of the inadequate basis sets of the isolated molecules) as well as describe the real transfer of charge between the molecules. This BSSE problem can be overcome,^{18,19} but early estimates of charge transfer effects must be viewed with considerable caution. Charge transfer is intrinsically nonadditive. If the charge transfer is genuinely a major contribution to the interaction, it should be modeled at the electronic level, because the charge distribution of the complex is no longer a small perturbation on the sum of the isolated molecule distributions.

Damping of Long-Range Terms

A final effect that occurs when the molecular charge distributions overlap is that this overlap modifies the long-range electrostatic, induction, and dispersion contributions, damping down the R^{-n} separation dependence and thus avoiding the singularity as $R \rightarrow 0$. These effects are not negligible in the van der Waals region. The damping terms are usually absorbed into any empirical short-

range exponential repulsive potential. Therefore their form and strength, comprising a subject of current research for atomic intermolecular interactions,²⁰ are important when a potential is being constructed by summing up models for each of the other contributions. Several different functional forms of damping function have been proposed,⁶ which exponentially reduce the dispersion energy as the molecules approach. These forms are mainly based on fitting to accurate calculations of the dispersion interaction between two H atoms with parallel spins (H_2 in the repulsive $b\ ^3\Sigma_u^+$ state), with parameters that allow the form to be adapted for different atoms. Work toward an accurate intermolecular potential for $(N_2)_2$ ²¹ showed that the assumed damping function can have a significant effect on the intermolecular potential in the van der Waals region. Hence, such terms will have an effect on solid state properties.

METHODS OF DERIVING MODEL INTERMOLECULAR POTENTIALS

Empirical Model Potentials for Organic Molecules

Because many experimental properties of molecules in the solid, liquid, and gaseous states depend on the intermolecular potential, accurate experimental data can be used to derive model potentials. This is analogous to the methods used to construct empirical intramolecular force fields.^{3,4,22,23} There exist several traditional methods of “inverting” experimental data, such as using a set of second virial coefficients over a wide temperature range⁵ or extracting pertinent information from the dimer rotation–vibration microwave spectrum⁵ to define a reasonable region of the intermolecular pair potential numerically, but such methods of obtaining $U(R)$ are limited to the simplest systems. Extension to the intermolecular potentials of polyatomics is prevented by the complexity of the anisotropy of the potential, inasmuch as most experimental data depend on some complex average over orientations, and also because the collisions between polyatomic molecules can be inelastic.

Thus, the usual approach to deriving intermolecular potentials from experimental data is to choose a functional form for the model potential, for example, the Lennard-Jones 12–6 potential:⁵

$$U(R) = 4\epsilon \left[\left(\frac{\sigma}{R} \right)^{12} - \left(\frac{\sigma}{R} \right)^6 \right] = \epsilon \left[\left(\frac{R_m}{R} \right)^{12} - 2 \left(\frac{R_m}{R} \right)^6 \right] \quad [13]$$

which is defined so that $U(\sigma) = 0$ and $U(R_m) = -\epsilon$, as shown in Figure 1. The potential parameters (in this case ϵ and either σ or R_m) are then adjusted until the calculated properties are as close as possible to the experimental properties.

This process is limited by the experimental errors and the approximations in the theory used to calculate the properties from the potential, as well as the assumed functional form. Insufficient experimental data can lead to a variety of correlated sets of parameters that reproduce the data acceptably, but may give potentials that are very different except in the feature that determines the property being calculated. For example, a variety of potentials having the same potential well area will give similar second virial coefficients.⁵ Hence, the wider the range of experimental data sensitive to different regions of the potential energy surface used in fitting the potential, the more realistic the potential is likely to be.

Early work on intermolecular forces concentrated on spherical molecules, such as argon, where the pair potential is only a function of the separation, R , of the two molecules, and there are no electrostatic or induction forces. That work was intimately associated with the development of quantitative theories relating the experimental properties of such molecules in the solid, liquid, and gaseous states, and in their van der Waals complexes, to the intermolecular potential.⁵ Indeed, the success in the 1930s of the Lennard-Jones potential model for reconciling different properties of the solid and gas (and later the liquid in simulations) had such an intellectual impact that it is sometimes forgotten that the model was designed as the most mathematically tractable form for the general shape of the actual potential curve.

The search for a quantitative model intermolecular pair potential for argon was based on empirically fitting the potential to a wide range of experimental data. To accomplish this, a far more realistic and flexible functional form than the Lennard-Jones potential was constructed, using perturbation theory for the form and estimated coefficients for the long-range contribution; then the potential parameters were fitted to optimize the agreement between calculated and experimental properties. A model intermolecular pair potential that can reproduce a wide range of experimental data of the gas (including scattering data and the dimer vacuum ultraviolet absorption spectra), the liquid, and the solid (with the addition of the Axilrod-Teller term for the three-body dispersion contribution) was finally obtained in the early 1970s, through a long process that is described in Ref. 5. The functional form used was:

$$\frac{U(R)}{\varepsilon} = \exp\left[\alpha\left(1 - \frac{R}{R_m}\right)\right] \sum_{i=0}^5 A_i \left(\frac{R}{R_m} - 1\right)^i + \sum_{j=0}^2 \frac{C_{2j+6}^*}{(\delta + (R/R_m)^{2j+6})} \quad [14]$$

In this multiparameter form, the exponential term is multiplied by a fifth-order polynomial with coefficients A_i , to give a sufficiently accurate representation of the overlap contributions. The sum over j provides the C_6 , C_8 , and C_{10} terms in the dispersion series. The modification of the dispersion, due to overlap, is absorbed into the approximately exponential short-range repulsion term, with the minor parameter $\delta = 0.01$ used just to prevent a nonphysical maximum in

the potential at short range. Thus a functional form flexible enough to represent the true pair potential energy curve required almost a dozen parameters (within a theoretically justified functional form and with theoretical calculations to support the dispersion coefficients). The complexity of Eq. [14] illustrates the difficulties associated with obtaining intermolecular potentials by empirical fitting. It also shows that the ability to reproduce a wide range of experimental data is a severe test of a model potential. Note, too, that it is possible that potentials with different anisotropies can give a good account of a range of properties that average over the orientational dependence, as has been found for the spectral and transport properties of He ··· CO.²⁴

The usual model intermolecular potential for organic molecules is based on the assumption that the interaction between the molecules is the sum of the interactions between their constituent atoms. For example, the interaction energy between molecules M and N can be given by

$$U(R, \Omega) = \sum_{i \in M, k \in N} \left[A_{ik} \exp(-B_{ik} R_{ik}) - \frac{C_{ik}}{R_{ik}^6} + \frac{q_i q_k}{R_{ik}} \right] \quad [15]$$

where atom i in molecule M is of type ι and a distance R_{ik} from atom k in N of type κ . Atoms can be classified into types by just their atomic number, though more usually their hybridization type (sp^3 C and so on) is used, and for hydrogen atoms by the nature of its covalent bond. This model for the atom–atom repulsion and dispersion between the atoms is much simpler than that required for argon, and therefore even the radial form is approximate. The additional electrostatic interaction that arises for polyatomic molecules is modeled by an atomic point charge model. The entire model assumes that the molecule is a superposition of spherical atoms, ignoring the redistribution of the valence electron density on bonding.

Even with these assumptions, there are a considerable number of parameters to be determined, depending on the number of types of atom in the molecule. The atomic charges are almost always determined independently, using ab initio or, for large molecules, semiempirical calculations. Even for a hydrocarbon, there are nine other parameters to be determined (three each for C ··· C, H ··· H and C ··· H interactions using the first two terms of Eq. [15]), and so for a typical organic molecule containing C, H, N, and O atoms there are a minimum of 10×3 repulsion–dispersion parameters. This number would have to be increased with additional parameters for any of the hydrogen atoms bonded to O or N, if the model is to give reasonable estimates of both hydrogen bond lengths and C–H van der Waals contact separations. It might also be a poor assumption to use the same parameters for a nitrogen in an aromatic ring and for a nitro or amine nitrogen atom, because this is assuming that their intermolecular repulsion–dispersion properties are the same. Hence there exists a conflict between the number of atom types that are to be chosen and the additional effort associated with increasing the number of parameters, and hence the

amount of reference data required to fit them. In practice, the number of atom types is limited to as many as are found necessary to obtain a reasonable reproduction of the data. In some situations reproduction of the data cannot be done well because of ill-determined fits or problems with highly correlated parameters.

Another common approach to reduce the number of parameters is to assume some form of combining rules, so that the hetero-interaction parameters are given by “homo-parameters”:

$$A_{ik} = (A_{ii} A_{kk})^{1/2} \quad B_{ik} = \frac{B_{ii} + B_{kk}}{2} \quad C_{ik} = (C_{ii} C_{kk})^{1/2} \quad [16]$$

With these, only 4×3 parameters are required for molecules containing four atom types (e.g., nitrobenzenes with types C, H, O, N). The geometric mean combining rule for the dispersion coefficients C_{ik} can be loosely justified by approximations for the dispersion energy, such as ignoring the variations in the denominator in Eq. [12]. However the combining rules for the repulsion parameters A_{ik} and B_{ik} come from assuming that the interaction energy also obeys the geometric mean rule [$U_{ik} = (U_{ii} U_{kk})^{1/2}$], which is a crude approximation, and many other forms of combining rule have been investigated.^{5,25} It is worth noting that in many simulations some of the repulsive interactions may not be sampled—for example, when the electrostatic repulsion between like atoms makes such orientations unfavorable. Hence the approximate values given by the combining rules are usually adequate. If, for example, N, C, H parameters are fitted to crystal structures of azahydrocarbons where there are no short N ··· N contacts, the nitrogen parameters will be determined solely through the N ··· H and N ··· C interactions. The accuracy of the combining rules for the N repulsion will not be relevant unless the potential is tested on a crystal structure such as *s*-tetrazine $C_2H_2N_4$, where close N ··· N contacts are inevitable.

Many sets of parameters for this type of model potential have been derived by empirical fitting to different choices of experimental data. Pertsin and Kitaigorodsky's book on the atom–atom potential method²⁶ reviews the problems and describes a variety of models derived prior to 1981 for organic molecules. Their tabulated values of 6-exp parameters for hydrocarbons in the literature eloquently demonstrate the problems with empirical parameterization of such a potential. When a simplified functional form is fitted to experimental data, with its associated errors, using an approximate theory, the parameters will inevitably absorb many of the errors in an ill-defined manner. The fitted C parameters will thus be a crude approximation to the genuine C_6 induced-dipole–induced-dipole dispersion coefficient, because they will have absorbed the omitted higher order terms in the dispersion series, errors in the electrostatic or repulsion potential, and other neglected effects such as nonadditivity and polarization. This approximation may be adequate when the model potential is being used as a form of extrapolation to calculate the same proper-

ties for closely related molecules, but, if too much confidence is placed in the correspondence of the terms to a true intermolecular potential—for example, by mixing parameters from different potential schemes, or for using them to calculate properties that depend on different regions of the molecules' potential energy surface—the results can be very disappointing. Even empirical force field models having less drastic changes can require reoptimizing the parameters. For example, parameters for the aliphatic CH_n united atoms in the GROMOS force field, designed for simulating the enthalpies of vaporization, vapor pressures, and densities of alkanes at 298 K, required reparameterization²⁷ when the cutoff radius used in evaluating the intermolecular energy was increased from 8 Å to 16 Å, since the nonnegligible dispersion energy contribution between 8 Å and 16 Å had been empirically absorbed in the earlier set of parameters.

Crystal structures of organic molecules are commonly used for developing atom–atom potentials, partly because these data are readily available for a wide range of organic molecules, and also because the structures can be very sensitive to the potential in the important van der Waals contact region (at least for the contacts that are found in the crystal structures). The model potentials most widely used for crystal structure modeling are therefore those that have been developed by fitting a wide range of crystal structures and heats of sublimation for common atomic types. Examples are the Hagler–Lifson²⁸ Lennard-Jones potentials for amides and carboxylic acids and the C, H, N,²⁹ O,³⁰ Cl,³¹ and F³² potentials of Williams and coworkers; the repulsion–dispersion parameters are derived in conjunction with an externally derived electrostatic model.³³

More recently, Gavezzotti and Filipinni used a large quantity of crystallographic data and heats of sublimation to parameterize a 6-exp potential for C, H, N, O, S³⁴ and certain hydrogen-bonding protons³⁵ to produce the UNI force field specifically for crystal structure modeling. The UNI parameters appear to be successful for estimating heats of sublimation and for reproducing many crystal structures, though with some limitations. The UNI model effectively absorbed the electrostatic term into the 6-exp parameters, which resulted in considerable deviations of the parameters from those expected under the usual combining rules.

The nonbonded parameters that make up the intermolecular potential in the commonly used force fields for biomolecular simulations are derived by different means, though not always independently, and usually tested as “good enough” for the purpose at hand. For example, the nonbonded parameters in AMBER³⁶ have evolved empirically³⁷ from the Hagler–Lifson 12–6 amide parameters as a starting point. The CHARMM potential originally³⁸ derived its repulsion–dispersion parameters from the van der Waals radii of the atoms and the atomic polarizabilities and effective number of outer shell electrons, using the Slater–Kirkwood approach to the dispersion energy. Even when the nonbonded parameters have not been fitted, they are justified by tests of the total force field against the experimental data one is seeking to reproduce.

Although these model potentials are adequate for many modeling studies, the limitations imposed by their empirical nature, assumptions of transferability, and limited functional form mean that they may be inadequate for some simulations outside the range of interpolation between the data used in their validation. Hence, we need to develop more accurate models, learning from the lessons of small-molecule potentials.

Ab Initio Potential Energy Surfaces

Supermolecule Calculations

The conceptually simplest method of evaluating the intermolecular interaction energy between a pair of molecules is to use an ab initio method of calculating the total energy of the molecules at a given relative orientation (the supermolecule) and then subtract the energies of the isolated molecules. Because all the significant intermolecular forces arise from the Coulombic interaction term in the Hamiltonian, if we could solve the Schrödinger equation exactly for both the supermolecule and the isolated molecules, this would provide the total interaction energy directly, without the need for any subdivision into the different contributions. In practice, this is very demanding of the ab initio method^{39,40} because the intermolecular energy is so tiny compared with the total electronic energies of the molecules. For example, the total energy of a molecule like uracil is several hundred atomic units, whereas a typical hydrogen bond energy (~ 25 kJ/mol) corresponds to about 10^{-2} atomic unit. Moreover, since the dispersion energy arises from the instantaneous correlation of the electron fluctuations, it is not included at all in an SCF calculation. Large basis sets⁴¹ and a correlated (post-Hartree–Fock) method⁴² are required to calculate a significant fraction of the dispersion energy. This problem is compounded by the basis set superposition error (BSSE), where the intermolecular interaction energy and charge transfer are overestimated. This error can be corrected by the counterpoise procedure,^{18,19} but this adds to the expense of the calculation. Considerable progress is being made with such calculations for the intermolecular interactions of small polyatomics, such as the water dimer. However, supermolecule calculations are usually done to find the energy of only a few selected geometries, because the calculation at each point is too expensive to permit the calculation at sufficient geometries to define fully the potential energy surface that would be sampled in a condensed phase simulation. The number of points required should not be underestimated: a full six-dimensional intermolecular potential surface for the water dimer was recently obtained by performing density functional calculations at 20,480 numerical quadrature points,⁴³ defined by an expansion of $U(R, \Omega)$ in terms of Wigner rotation matrices (cf. Eq. [2]).

Intermolecular Perturbation Theory Methods

Because methods providing an equivalent description of the intramolecular effects in the supermolecule and the isolated molecules is a major problem with the supermolecule approach, the notion of evaluating the components of the interaction energy directly from the wavefunctions of the isolated molecules is very attractive. This perturbation approach provides the analytical form for the long-range potential, in terms of the properties of the isolated molecules, using the products of the isolated molecule wavefunctions to describe the interacting molecules as shown in Eqs. [7], [9], and [10]. In orientations characterized by overlapping molecular charge distributions, the electrons can no longer be assigned to a specific molecule, and so the wavefunction for the interacting molecules must be constructed from the isolated molecule wavefunctions such that it is antisymmetric with respect to interchange of any two electrons. This antisymmetrization produces the exchange energy, a significant attractive contribution to the total energy, as well as the repulsion arising from the overlap of the electrons from the two molecules. The requirement for antisymmetry produces many complications in developing a short-range perturbation theory, including nonorthogonality of the antisymmetrized zeroth-order wavefunctions and a lack of definition of the zeroth-order Hamiltonian. As a result, many different methods⁶ can be used, with different detailed partitions of the energy. For example, although all methods yield a quantity that becomes the induction energy at long range, the modifications of the induction energy at short range differ between methods, and short-range effects such as charge transfer can be viewed as a separate effect or considered to be part of the short-range induction energy. Nevertheless, despite these caveats, the division of the interaction energy into components is an attractive aspect of these calculations because it gives some insights into the nature of the intermolecular interactions. The division is also helpful in fitting model intermolecular potentials, which is more easily done for each contribution separately.

The method that has been most widely applied to organic molecules is the nonorthogonal intermolecular perturbation theory (IMPT) of Hayes and Stone,⁴⁴ which evaluates the intermolecular interactions to second order of perturbation theory between the SCF charge densities. It enables a separation to be made between the charge transfer¹⁶ and the induction energy, which gives a charge transfer component free of basis set superposition error. More accurate calculations, corresponding to the interactions between the correlated charge densities of the molecules, are possible for small systems using symmetry-adapted perturbation theories.⁴⁵

Thus perturbation theory calculations currently suffer from the same disadvantage of supermolecule calculations for defining the intermolecular potential between organic molecules at short range. They are so expensive when used to obtain results of reasonable accuracy that are converged with respect to basis set, even for small molecules, that it is impossible to calculate the energies at a sufficient number of points to define the potential energy surface. Calcula-

tion of the dispersion energy is the most time-consuming and basis-set-dependent aspect of this approach, so it is possible to use IMPT calculations of individual first-order contributions for a selected set of orientations and use them to fit or to test models for these contributions. This scheme has proved very useful in the development of systematic potentials, described later. However, perhaps the most important use of these calculations, particularly the subdivision into components, is to provide some insights into the intermolecular forces between organic molecules, which complement experimental observations, and provide some lessons for the construction of model potentials. An example of an IMPT analysis of a hydrogen-bonding interaction between pyridazine and methanol is shown in Figure 3. This plot emphasizes that at a typical hydrogen bond length, the minimum energy is the balance between very large exchange-repulsion and attractive electrostatic energies, with the dispersion, polarization, and charge transfer all making nonnegligible contributions. The orientational dependence of the hydrogen bond energy with changes in the angle at the acceptor N atom parallels that of the electrostatic energy until the repulsive interaction with the neighboring C-H bond becomes significant. Plots of this type, containing information on limited parts of the potential energy surface, have been utilized to gain some understanding about specific intermolecular interactions of organic molecules.

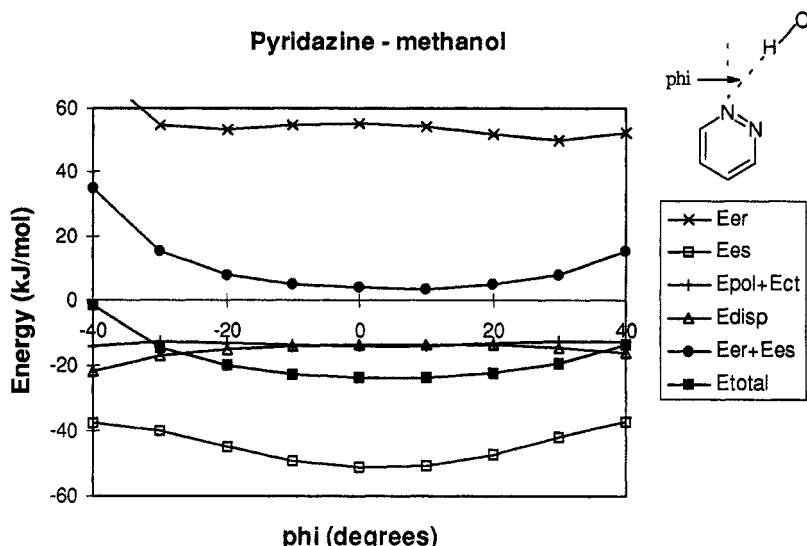


Figure 3 The components of the interaction energy between pyridazine and methanol for a coplanar, linear $\text{N} \cdots \text{H}-\text{O}$ hydrogen bond of length $d(\text{N} \cdots \text{H}) = 1.85 \text{ \AA}$. Values are for the exchange-repulsion E_{er} , electrostatic E_{es} , dispersion E_{disp} , induction E_{pol} , and charge transfer E_{ct} contributions to the total energy E_{total} estimated by IMPT calculations using a 6-31G** basis set.

Lessons from Intermolecular Perturbation Theory Calculations on Organic Molecules

Dominance of the Electrostatic Energy

One of the most important observations derived from intermolecular perturbation theory calculations on small polyatomics is that the orientational dependence of the intermolecular potential parallels that of the electrostatic interaction quite closely around the minimum. These calculations confirmed the implication of the computer experiment by Buckingham et al.,⁴⁶ who found the minima in the electrostatic energy (within sterically accessible orientations) for over two dozen van der Waals complexes. The researchers obtained excellent reproductions of the experimental structures of these, mainly hydrogen-bonded, complexes. Their model potential was an accurate, distributed multipole model for the electrostatic interaction, derived from the wavefunctions of the isolated molecules. The only other term in the intermolecular potential was a hard-sphere repulsion. The sterically accessible orientations were thus defined by the spherical van der Waals radii of the atoms, with a zero radius on the hydrogen atoms, reflecting the normal length of hydrogen bonds. Thus the directionality of the electrostatic interaction was able to account for the proposed "rules"⁴⁷ that the hydrogen bond forms in the direction of the conventional lone pair density on the acceptor, or, in the absence of lone pair density, toward π -bonding density. For example, H—C≡N ··· H—F is linear, but (H—F)₂ is bent by about 70° (i.e., H—F ··· (H)F = 120–130°) and H—C≡C—H ··· HF is T-shaped. The IMPT calculations carried out on several small specific hydrogen-bonded systems⁴⁸ accounted for this empirical observation. Those calculations showed that the total energy curve was usually approximately parallel to the electrostatic energy for angular displacements of the hydrogen bond because the orientational variation of the other terms, although significant, tended to cancel. The few cases in which the simple Buckingham-Fowler model⁴⁶ was not successful were also explained: the inversion of the relative stability of the hydrogen-bonded and anti-hydrogen-bonded complexes involving Cl atoms, for example, was an artifact of the assumed spherical repulsion of Cl, and in cases such as H₂O ··· H—F both the electrostatic and total potential energy surfaces were very flat, and vibrational averaging had to be considered in interpreting the experimental structure. The charge transfer component was generally rather small in all the van der Waals complexes of neutral polyatomic molecules considered.⁴⁸ Hence, hydrogen bonding is now generally described in terms of the electrostatic interaction, an interpretation that has largely replaced the older HOMO/LUMO picture.⁴⁹

Apart from this detailed orientational dependence in the region of a hydrogen-bonding contact, the electrostatic energy is such a strong orientation-dependent force that minimizing the electrostatic energy (calculated accurately,

e.g., from a distributed multipole model) with a simple model for the other terms (hard sphere or empirical isotropic atom–atom repulsion–dispersion potential) has become a useful means of scanning the potential energy surface to find favorable regions. The major advantage of this method is that it can find some unexpected low energy structures. For example, it correctly found two minima in the relative orientation of two *s*-tetrazine molecules: the obvious hydrogen-bonded coplanar structure and a T-shaped dimer.⁵⁰ Both have been observed spectroscopically,⁵¹ illustrating the need to search the entire potential energy surface for low energy structures, not just assume that they will be hydrogen-bonded.

Providing an Understanding of Functional Group Interactions

The interactions between organic molecules are usually thought of in terms of the interactions between the various functional groups in the molecules. For example, we would expect to find a hydrogen bond between a molecule containing a hydrogen bond donor and a molecule containing a hydrogen bond acceptor. If there was only one donor, with a choice of acceptors, like an ester group and an amide group, it is less obvious which hydrogen bond would be formed. There now exists considerable interest in being able to classify the strength and directionality of different functional group interactions. For example, scoring functions used in drug design are based on identifying potentially strong interactions, such as hydrogen bonding, between the protein receptor site and the possible ligand.² Crystal engineering,^{52,53} the attempt to design molecular crystal structures with specific intermolecular motifs, uses the concept of “intermolecular synthons,” which are known combinations of functional groups that tend to associate in given ways and are therefore likely to be found in the crystal structure. These ideas about the intermolecular forces between organic molecules are usually derived by observation and supported by surveys of crystallographic databases such as the Cambridge Structural Database⁵⁴ and the Protein Data Bank (PDB),⁵⁵ which contain organic molecule and protein crystal structures, respectively.

Knowledge of how two molecular fragments interact in crystal structures can be derived by first finding all crystal structures that contain the two fragments (e.g., a C—OH group and a histidine ring), and then analyzing their relative positions. This comparison can be done graphically after each interacting pair has been rotated to superimpose one group (e.g., the histidine ring), resulting in a scatter plot for the positions of the other fragment. The Cambridge Crystallographic Data Centre ISOSTAR library⁵⁶ provides rotatable three-dimensional scatter plots for many pairs of organic functional groups, particularly those common in protein–ligand interactions. Also, the *Atlas of Protein Side-Chain Interactions*⁵⁷ gives the relative orientations of protein side chains, complementing the many publications surveying individual interactions.^{58,59} The plots can reveal a preferred directionality of some interactions,

such as hydrogen bonds, or avoided relative orientations, such as showing that phenyl rings do not stack vertically like a sandwich. Rarely will a statistically significant sample portray the random distribution of interactions that would be expected if only steric repulsion existed between the fragments. It is worth noting that considerable care must be taken in such surveys to avoid incorporation of homologous proteins and other biases, and to take the correct function of the orientational variables for comparison with a proper random distribution. For example, the volume of space that can be occupied by D—H · · · A bonds with angles of approximately 180° is smaller than that for angles around 170° ; hence comparisons should be based on $\sin\theta$. These surveys give straightforward information about probable relative orientations for sufficiently strong interactions; the information can be exploited in chemical design or protein structure predictions. These applications range from providing a qualitative feel for likely packing motifs or ligands for specific binding sites, to being used statistically in computer-aided prediction of crystal structures.⁶⁰

The distributions derived from such database searches give information on intermolecular forces between the fragments, if we assume that the observed preferred orientation of the two fragments corresponds to an optimal interaction, or at least that the observed relative orientations are the more energetically favorable. Thus, these distributions provide guidelines for model intermolecular potentials—at least, if the model does not broadly correspond to the observed distributions, you need to know why, and whether this lack of correspondence is showing that the model potential is inadequate. For example, any isotropic atom–atom repulsion–dispersion potential for benzene will predict that the minimum energy structure is a stacked, sandwichlike structure, because this optimizes the number of close, intermolecular contacts, and hence the attractive dispersion energy. However, surveys of the relative orientations of phenyl rings in protein structures⁵⁷ show a marked absence of such sandwich structures. If the planes of the two aromatic rings are nearly parallel, they are displaced relative to each other so there is little overlap of the rings. On the other hand, many crystal structures have phenyl rings in van der Waals contact in an approximately T-shaped relative orientation. These configurations originate from the electrostatic repulsion between the π electrons when the rings are stacked in the sandwich orientation. Therefore electrostatic forces have to be included in any model potential for simulating benzene, phenyl groups, or other aromatic π – π interactions. This can be done either by distributed multipoles,⁶¹ or more approximately by a set of point charges above and below the plane of the benzene ring,⁶² or more crudely still, by overestimating the polarity of the C–H bond.⁵⁰

IMPT calculations have often been used to rationalize the favored relative orientations of functional groups found in molecular and protein crystal structures^{63–65} revealing the variation in the strengths of hydrogen bonds to a given atom (O or N) with the bonding environment of that atom. For example, the strength of methanol hydrogen bonded to various oxygen and nitrogen

acceptors in aromatic heterocycles⁶⁶ varied from around -27 kJ/mol for pyridine to -16 kJ/mol for furan, predominantly (but not exclusively) because of the variation in the electrostatic interaction. This explains the observed scarcity of hydrogen bonds to furan fragments in molecular crystal structures. The weakness of the furan oxygen as a hydrogen bond acceptor is a result of its bonding environment;⁶⁷ in contrast, methanol forms relatively strong hydrogen bonds to tetrahydrofuran (about -25 kJ/mol). Thus the IMPT estimates of relative interaction energies for different molecular fragments in the ISOSTAR library are useful for evaluating ligand binding and for assessing the effect of functional group replacement on protein binding energies.⁵⁶ Such variations of hydrogen bond strength with the hybridization and bonding environment of the acceptor atom have major implications for the design of force fields for organic molecules.⁶⁸ They emphasize the gross limitations of assuming that explicit hydrogen-bonding potentials are fully transferable. The dominance of the electrostatics in determining the strength and orientation dependence of the hydrogen bonds shows the need to use a realistic electrostatic model. Indeed a recent assessment of empirical force fields, based on ab initio calculations of the relative energetics of peptide conformations, suggested that future force fields will need to employ a representation for the electrostatics that goes beyond the use of atom-centered partial charges.⁶⁹

Understanding Specific Interactions: Cl . . . Cl

Experimental information reflects only the total intermolecular potential. However, a potential energy function that correctly models one phase must accurately subdivide the potential into its additive and nonadditive components if it is to model the same molecule in different environments. The case of Cl . . . Cl interactions illustrates this problem. It is clear that the isotropic atom–atom model potential is inadequate for Cl . . . Cl interactions: it cannot account for the observed layered herringbone crystal structure of Cl₂, or the marked anisotropy in the effective van der Waals radii of Cl in crystal structures,⁷⁰ nor for the structures of van der Waals complexes involving Cl atoms.⁷¹ These inadequacies led to the suggestion that there exists some sort of specific attraction involving the chlorine lone pair density.⁷² The addition of weak intermolecular bonds (represented by a Morse potential) will certainly stabilize the observed crystal structure of Cl₂, but this raises the issue of how many Morse potential weak hydrogen bonds should be applied to Cl atoms in different coordination environments, especially since the charge transfer or weak intermolecular bonding interaction is nonadditive. An alternative explanation is that repulsion and electrostatic interactions of Cl atoms are markedly anisotropic, and indeed, the crystal structure of Cl₂ has been quantitatively reproduced by an empirical,⁷³ and more recently by a systematic ab initio based potential,⁷⁴ for Cl₂ with anisotropic repulsion and electrostatic atom–atom potentials. These findings are consistent with the electron density difference map of Cl₂,⁷⁵

which shows the lone pair electron density from one molecule fitting into the depression in the repulsive wall at the end of the intramolecular bond, giving the shorter van der Waals contact distance. The more general proposal that the frequent occurrence of short intermolecular contacts in chlorine–chlorine interactions in molecular crystal structures is evidence for a significant specific attractive force⁷² has been countered⁷⁶ by IMPT calculations, electrostatic modeling, and a reanalysis of the database evidence. The charge transfer term is very small, and the observed anisotropy of the Cl · · · Cl interactions, which can be mildly attractive for some van der Waals contact orientations, is sufficiently accounted for by the anisotropy of the exchange–repulsion and electrostatic terms. Fortunately, since the charge transfer term is small, a reasonably transferable Cl atom–atom potential should be obtainable, though it will have to include both anisotropic electrostatic and repulsion terms if it is to reflect the orientational preference of intermolecular Cl interactions.

Competition Effects

The expectation that the preferred relative orientation of two functional groups seen in the analysis of crystal structures should correspond to the most favorable intermolecular interaction (as shown by the structure of the van der Waals complex of simple model molecules) is probably valid only when the interaction is dominant. When one is considering weaker types of hydrogen bond, theoretical calculations are extremely useful in disentangling energetic influences from competition effects. For instance, both the water · · · benzene⁷⁷ and the ammonia · · · benzene⁷⁸ van der Waals complexes show hydrogen bonding to the benzene π -electron density, but hydrogen bonds between water or N–H groups and aromatic rings do not seem to be favored in proteins. Electrostatic modeling⁷⁹ of the interactions of water with various conformations of the phenylalanine dipeptide [$\text{CH}_3\text{CONHCH}(\text{CH}_2\text{Ph})\text{CONHCH}_3$] showed that there are favorable interaction sites above the phenylalanine ring, but the protein backbone atoms would often block such sites or perturb them by providing stronger alternative hydrogen-bonding sites. The solvent accessibility of phenylalanine residues in the PDB collection is low, with more protein residues blocking the faces and less at the edges of the phenylalanine than would be expected statistically, thus explaining why water molecules are rarely found above and below the plane of the aromatic ring. The amino–aromatic hydrogen bond is found in some proteins, but only about 10% of observed interactions between sp^2 -hybridized nitrogen atoms and phenylalanine or tyrosine rings have the nitrogen positioned above the ring, and of these, the hydrogen bonds are outnumbered about 5:2 by stacked orientations with the N–H parallel to the ring.^{80,81} Since a statistical distribution would have far more hydrogen-bonded than stacked geometries, the amino–aromatic hydrogen bonds appear to be less favored than stacked interactions. Ab initio IMPT calculations on guanidinium · · · benzene, formamide · · · benzene, and imidazolium · · · ben-

zene models⁸¹ for the relative orientations representative of those found in protein structures confirmed that the hydrogen-bonded structures were more stable; but the stacked geometries were surprisingly not much less stable. Indeed, in all three cases, there was at least one experimental hydrogen-bonded structure less favorable than at least one stacked structure. However, the stacked sp^2 nitrogen atoms are more accessible to form conventional hydrogen bonds with other fragments than those involved in an N—H \cdots aromatic hydrogen bond. Thus, the rarity of amino \cdots aromatic hydrogen bonds in proteins appears to be the consequence of the ability of the stacked conformation to be stabilized simultaneously by the aromatic interaction and by conventional hydrogen bonds to other atoms. The overall conclusion seems to be that weak hydrogen bonds to π -electron density are generally outcompeted by stronger interactions within proteins, where there are usually a variety of strong hydrogen bond donors and acceptors available, including waters of hydration.

The situation is often different with small organic molecules, particularly in neat liquids and crystals of one molecule, because there are fewer functional groups available. However, the condensed phase structure will be dominated by the need to achieve close packing (generated by the dispersion), produce the strongest electrostatic stabilization through any conventional hydrogen bonds, and, if possible, produce further stabilization by forming other weaker directional interactions such as C—H \cdots O⁸² or hydrogen bonds to π -electron density. Thus the weaker functional group interactions may not occur or may show a broader distribution of relative orientations, though the interactions are still somewhat directional, as when polar C—H groups interact with O

It is clearly not possible to assign anything more than a rough estimate of the energy to each functional group interaction, partly because the charge density on each atom depends on the other functional groups in the molecule; hence the major electrostatic contribution is influenced by those neighboring functional groups. Identifying the different hydrogen bonds in a crystal structure or ligand–protein complex can allow one to estimate binding energies only roughly. (For example, the many sterically accessible doubly hydrogen-bonded complexes involving two of the nucleic acid bases can vary in intermolecular binding energy from being just less stable than the triply hydrogen-bonded guanine–cytosine base pairing found in DNA to being completely unstable.⁸⁴) Since the experimental structures of supramolecular complexes are a balance of the competing functional group interactions, it is vital that we model them all on an equal footing in terms of accuracy in order to predict the forces that govern the competition between those various interactions.

After this digression into the lessons about organic nonbonded interactions that can be learned from limited IMPT calculations in conjunction with experimental results, we should return to considering how to derive accurate intermolecular potentials in a way that can be applied systematically to a range of organic molecules.

SYSTEMATIC POTENTIALS

Because the number of points on a potential energy surface that can be calculated ab initio will always be rather limited, deriving model potentials by fitting to a set of ab initio points suffers from the same disadvantage as empirical fitting: that is, one must assume a priori the functional form of the model potential. In the case of small polyatomics, it is possible to include a wide range of relative orientations, which may reveal that the surfaces are inadequately modeled by an isotropic atom–atom repulsion, as happened for $(HF)_2^{85}$ and $(N_2)_2^{86}$. However, calculating sufficient points to sample adequately the repulsive wall, the attractive well, and the long-range interactions around several different atomic types in a potential energy surface for an organic system (i.e., to test empirically the form of the atom–atom anisotropy and radial dependence) will be prohibitively expensive in the foreseeable future for an acceptable level of accuracy at each point. Consequently, a more promising route is to derive the functional form and as many of the parameters as possible from the quantitative theory of intermolecular forces. This is the idea behind the systematic potential approach,⁸⁷ where each contribution is represented and quantified separately, and then added to give the total potential. This approach is now providing reliable potentials for atom–diatom interactions,⁸⁸ has already resulted in a considerable improvement in the accuracy of potentials for small polyatomics, and is behind the advances in model potentials for organic molecules. However, as discussed earlier, some contributions are easier to quantify than others. Most effort has been put into developing the electrostatic contribution for organic molecules, where that contribution dictates the orientational dependence, in contrast to atom–diatom systems, which have no long-range electrostatic term. Thus, to understand the possibilities, and current limitations, of the approach requires the separate consideration of each contribution, which follows.

Table 3 summarizes for each contribution the types of model and size of molecule being studied in the mid 1990s.^{16,20,25,89–99} This summary and account are intended to give just an entry into the often large literature on each contribution and to encourage the extension of these methods to larger molecules.

Electrostatic Contribution: Distributed Multipoles

The electrostatic interaction, which is defined as the classical Coulombic interaction between the undistorted charge distributions of the isolated molecules, is the easiest to derive from wavefunctions. When there is no overlap of the charge distributions of the molecules, all that is required is a representation of the molecular charge density. The traditional, and simplest, representation of the molecular charge distribution is in terms of the total multipole moments. The first nonvanishing multipole moment could often be derived from experi-

Table 3 Anisotropic Atom–Atom Models for the Intermolecular Pair Potential, Which Can Be Quantified Using Ab Initio Monomer Properties, and Lead References

Contribution	Theory and Lead References	Applied to
Long-range R^{-n}	Perturbation theory	
Electrostatic	Distributed multipoles e.g., DMA, ⁸⁹ CAMM, ⁹⁰ Topologically partitioned electric properties ⁹¹	Polyatomics, up to polypeptides
Induction	Distributed polarizabilities ^{92,93} Topologically partitioned polarizabilities ⁹⁴	Small polyatomics <i>n</i> -Alkanes
Dispersion	Distributed dispersion ⁹⁵ Topologically partitioned dispersion energies ⁹⁶	Linear molecules, e.g., N ₂ , C ₂ H ₂ Small polyatomics, up to urea
Short range $\sim Ae^{-\alpha R}$	No rigorous analytical expressions for $U(R, \Omega)$	
Exchange–repulsion	Overlap model ⁹⁷ Penetration model ⁹⁸	Diatomics, small organic molecules Atom–diatomic
Electrostatic penetration	Test particle model ²⁵ Gaussian multipoles ⁹⁹	Diatomics, HCCH, H ₂ S Organic molecules, e.g., benzene–guanidinium complex
Dispersion damping	Dispersion damping ²⁰	H, He, Li
Charge transfer/induction damping	Fitting IMPT charge transfer energies ¹⁶	H ₂ O

ment.¹⁰⁰ Only the first nonvanishing total multipole moment is independent of the choice of the origin of the molecule-fixed axes system used to define the multipole moments. Thus, this origin, which is often chosen as the center of mass, is the only interaction site in each molecule, giving an expansion of the electrostatic energy in the form of Eq. [2], termed the *central multipole expansion*.

The central multipole series is useful for estimating the electrostatic interaction at very long range, where only the first nonzero term is significant, but this approach cannot be used in modeling molecules in van der Waals contact. It is now known from accurate ab initio calculations¹⁰¹ that the central multipole series is very slowly convergent, even for small polyatomic molecules. A central multipole series for, say, nitrobenzene, would be required to contain a large number of terms of the spherical harmonic expansion of the molecular shape before it included even an approximate shape for the nitro group, let alone its detailed charge distribution. (Contrast nitrobenzene with the multipolar charge distributions in Figure 4.) Even for diatomic molecules, the first term of the central multipole expansion is poor. The lowest energy crystal packing for homonuclear diatomics can depend on whether the same central quadrupole moment is modeled by atomic dipoles or quadrupoles.¹⁰² The central multipole expansion is invalid in many molecular crystal structures, as demonstrated empirically for pyrazine,¹⁰³ because there is overlap of the spheres that contain all the molecular electron density being represented by each multipole series in the solid state.

The usual method of representing the charge density for organic molecules is by a partial charge at each atomic nucleus. This is clearly an approximation because it assumes that the charge distribution around each atom is spherical. However, it does at least give a reasonable approximation to the spatial extent of the regions of high and low electrostatic potential around the molecule through the relative position of the polar atoms, and it is computationally fast and convenient when combined with the isotropic atom-atom model potential. A more complete alternative to either the central multipole model or the atomic

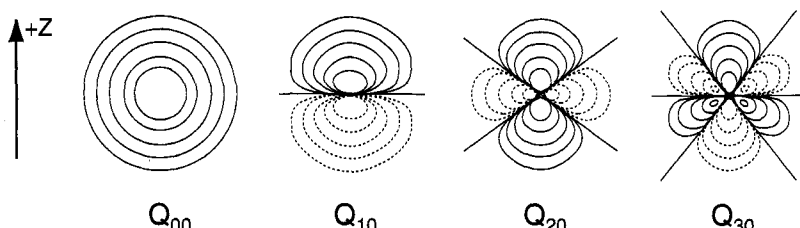


Figure 4 Contours of the charge distributions corresponding to the pure multipolar moments: Q_{00} , charge; Q_{10} , dipole; Q_{20} , quadrupole; Q_{30} , octopole. The solid contours are positive and dashed negative (buildup of electron) charge density.

point charge model is to combine the advantages of both approaches and represent the molecular charge distribution by a set of multipoles at each atomic center. Distributing the multipole centers around the molecule provides a good way of describing the molecular shape, and the multipoles at each atom can represent the nonspherical features in the atomic charge distribution, such as lone pairs and π -electron density. The contour maps for the charge distributions that can be represented by just one point multipole are given in Figure 4. The features of the experimental molecular charge density that give rise to the electrostatic interactions are shown on the molecular charge density difference maps (e.g., Refs. 75, 104), where the superposition of spherical atomic charge densities (having no long-range electrostatic interaction) has been subtracted from the total charge density. A comparison of such experimental charge density difference maps and Figure 4 makes it clear that an atomic dipole moment gives a good initial description of axial lone pair density, whereas an atomic quadrupole could represent either axial lone pair density (as in a chlorosubstituent) or π -electron density. Thus, an atomic multipole series seems a natural method of representing the valence electron density of a molecule.

Actually quantifying a distributed multipole model requires a method for dividing up the molecular charge density between the sites. This can be done^{105,106} rigorously by the Atoms-in-Molecules partitioning scheme, but this is computationally demanding, and the shapes of the atoms defined by this method are not necessarily readily represented by a low order multipole expansion. Hirshfeld partitioning,¹⁰⁷ which is based on differences from a superposition of spherical neutral atoms, has also been used.¹⁰⁸ Other methods have the partitioning defined by the basis set,¹⁰⁹ including an optimized method for linear molecules,¹¹⁰ and the cumulative atomic multipole moments (CAMM) method,¹¹¹ which extends Mulliken analysis¹¹² to give the higher moments. Partitioning can also be done by fitting the atomic multipole moments directly to the electrostatic potential surface.^{33,113}

The method that is used in most of the work described in this chapter is the distributed multipole analysis (DMA) of Stone,^{89,114} which is implemented in the CADPAC¹¹⁵ ab initio suite. DMA is based on the density matrix ρ_{ij} of the ab initio wavefunction of the molecule, expressed in terms of the Gaussian primitives η that comprise the atomic orbital basis set:

$$\rho(\mathbf{r}) = \sum_{ij} \rho_{ij} \eta_i \eta_j \quad [17]$$

Each contribution to the charge density can be exactly represented (outside itself) by a series of point multipoles located at the overlap center. The position of the overlap center is determined by the origins (atomic sites) and exponents of the two Gaussian primitives η_i and η_j involved, using the usual formulas for representing the product of two Gaussian functions by a single Gaussian. If both orbitals are s orbitals, the contribution is represented by a charge; if two p orbitals, then a charge, dipole, and quadrupole at the overlap center. (The series

terminates at the l^{th} multipole, where l is the sum of the angular momenta of the basis functions involved.) Thus, for example, the π -electron density in aromatic compounds is represented by out-of-plane quadrupole moments (Q_{20} if the z axis is perpendicular to the molecular plane). If both Gaussian functions are on the same atom, the analysis generates the corresponding limited multipole series on that atom. If they are on different atoms, the analysis "moves" the contribution from the overlap center to the nearest atom, using the relationship between a point multipole at one site to an infinite series of the same and higher order multipoles at another point. This series converges rapidly, provided the distance moved is not too great. Thus for a molecule that is well described by an sp basis set, the atomic charges, dipoles, and quadrupoles are fundamental to the description of the valence density, whereas the higher moments arise from the displacement of the overlap density to the atoms and improves the quantitative accuracy of the description.

All the partitioning methods should be able to describe the electrostatic potential outside the molecular charge distribution to essentially the accuracy of the wavefunction, provided sufficient expansion sites and orders of multipole are included. (Some partitioning schemes have multipole sites between as well as on the nuclei, either by definition or as an option.) Thus, several different distributed multipolar expansions for $(\text{HF})_2$ gave values for the electrostatic interaction energy in excellent agreement with each other, provided terms up to quadrupole were included.¹¹⁶ The DMA method of moving the contribution to the nearest site optimizes this convergence, by minimizing the magnitude of the higher multipole moments generated by moving the multipole contributions onto an interaction site. The use of distributed sites, each representing the charge distribution around an atom (or smaller fragment), also ensures that the expansion is valid for almost all relative orientations where an intermolecular potential model is appropriate.⁶

The use of distributed multipoles inevitably involves a large number of parameters. A charge distribution with no symmetry is described by a point charge Q_{00} , three dipole components ($Q_{10}, Q_{1,-1}, Q_{11}$), five quadrupole moments ($Q_{2k}, k = -2, -1, 0, +1, +2$), seven octopole moments ($Q_{3k}, k = -3, \dots, +3$), nine hexadecapole components ($Q_{4k}, k = -4, \dots, +4$) etc. (It is more convenient to use the real combinations $Q_{lk_c} = [(-1)^k Q_{lk} + Q_{l,-k}] / \sqrt{2}$ and $i Q_{lk_s} = [(-1)^k Q_{lk} - Q_{l,-k}] / \sqrt{2}$ for $k > 0$, where the subscripts c and s allude to the trigonometric functions associated with complex algebra). Some of these components will be zero if the atomic charge distribution has elements of symmetry. This can be deduced as described earlier, though each atomic site usually has less symmetry, and thus more nonzero multipoles, than the entire molecule.

The electrostatic interaction energies are evaluated using the multipole expansion formulas for each intermolecular pair of sites. Explicit expressions for all terms up to R^{-5} are given in Ref. 117, and for terms up to R^{-6} in Ref. 118. Stone⁶ has provided a general formulation and discussion of the spherical tensor and Cartesian tensor approaches. The program ORIENT¹¹⁹ incorporates

these expressions and is widely used for gas phase modeling of molecular complexes using distributed multipole electrostatic models. To illustrate the types of equation involved, consider two homonuclear diatomic (X_2) molecules. The electrostatic energy, U_{es} , can be expressed in terms of the atomic dipole (Q_{10}), quadrupole (Q_{20}), and octopole (Q_{30}), which are defined relative to the vector \mathbf{z}_1 on atom 1 pointing away from the second atom in one molecule, and \mathbf{z}_2 on atom 2 also pointing out from the intramolecular bond, though on the other molecule, as in Figure 2(b). The orientational dependence of the electrostatic interaction is expressed in terms of the scalar products of the molecule-fixed vectors \mathbf{z}_1 and \mathbf{z}_2 and the vector \mathbf{R} from atom 1 to atom 2 (as shown in Figure 5):

$$\begin{aligned}
 (4\pi\epsilon_0)U_{es} = & Q_{10}^1 Q_{10}^2 R^{-5} [(\mathbf{z}_1 \cdot \mathbf{z}_2) R^2 - 3(\mathbf{z}_1 \cdot \mathbf{R})(\mathbf{z}_2 \cdot \mathbf{R})] \\
 & + Q_{20}^1 Q_{10}^2 R^{-7} \frac{3}{2} [-5(\mathbf{z}_1 \cdot \mathbf{R})^2 (\mathbf{z}_2 \cdot \mathbf{R}) + 2R^2(\mathbf{z}_1 \cdot \mathbf{R})(\mathbf{z}_1 \cdot \mathbf{z}_2) \\
 & + R^2(\mathbf{z}_2 \cdot \mathbf{R})] + Q_{10}^1 Q_{20}^2 R^{-7} \frac{3}{2} [+5(\mathbf{z}_1 \cdot \mathbf{R})(\mathbf{z}_2 \cdot \mathbf{R})^2 \\
 & - 2R^2(\mathbf{z}_2 \cdot \mathbf{R})(\mathbf{z}_1 \cdot \mathbf{z}_2) - R^2(\mathbf{z}_1 \cdot \mathbf{R})] \\
 & + Q_{30}^1 Q_{10}^2 R^{-9} \frac{1}{2} [-35(\mathbf{z}_1 \cdot \mathbf{R})^3 (\mathbf{z}_2 \cdot \mathbf{R}) \\
 & + 15R^2(\mathbf{z}_1 \cdot \mathbf{R})^2(\mathbf{z}_1 \cdot \mathbf{z}_2) + 15R^2(\mathbf{z}_1 \cdot \mathbf{R})(\mathbf{z}_2 \cdot \mathbf{R}) - 3R^4(\mathbf{z}_1 \cdot \mathbf{z}_2)] \quad [18] \\
 & + Q_{10}^1 Q_{30}^2 R^{-9} \frac{1}{2} [-35(\mathbf{z}_2 \cdot \mathbf{R})^3 (\mathbf{z}_1 \cdot \mathbf{R}) + 15R^2(\mathbf{z}_2 \cdot \mathbf{R})^2(\mathbf{z}_1 \cdot \mathbf{z}_2) \\
 & + 15R^2(\mathbf{z}_1 \cdot \mathbf{R})(\mathbf{z}_2 \cdot \mathbf{R}) - 3R^4(\mathbf{z}_1 \cdot \mathbf{z}_2)] \\
 & + Q_{20}^1 Q_{20}^2 R^{-9} \frac{3}{4} [35(\mathbf{z}_1 \cdot \mathbf{R})^2 (\mathbf{z}_2 \cdot \mathbf{R})^2 - 5R^2[(\mathbf{z}_1 \cdot \mathbf{R})^2 + (\mathbf{z}_2 \cdot \mathbf{R})^2] \\
 & - 20R^2(\mathbf{z}_1 \cdot \mathbf{R})(\mathbf{z}_2 \cdot \mathbf{R})(\mathbf{z}_1 \cdot \mathbf{z}_2) + 2R^4(\mathbf{z}_1 \cdot \mathbf{z}_2)^2 + R^4] + \dots
 \end{aligned}$$

A multipole series should strictly be truncated at a given power, $n = -(l_1 + l_2 + 1)$, of the intersite separation R , rather than by only using the multipoles Q_{lk} up to a given value of l on each molecule. Hence, to include the important quadrupole–quadrupole interactions (the terms in $Q_{2k}^1 Q_{2k}^2$), the series should be taken up to R^{-5} and thus also should include the hexadecapole charge ($Q_{4k}^1 Q_{60}^2$ and $Q_{60}^1 Q_{4k}^2$) and octopole–dipole ($Q_{3k}^1 Q_{1k}^2$ and $Q_{1k}^1 Q_{3k}^2$) terms.

The contribution to the predicted electrostatic potential of the anisotropic atomic multipoles (Q_{lk} , $l > 0$), which represent the lone pair and π -electron density, rapidly become less important as the distance between the molecules increases. This not only results from the inverse power of R increasing with l , but also from the cancellation between the contributions from different multipoles and different atoms. For example, there is generally an atomic dipole component along a bond that opposes the polarity implied by the atomic charges, as shown in the results of distributed multipole analyses (DMAs) of the azabenzenes.¹²⁰ Thus, the accuracy gained by using a distributed multipole model is very dependent on the relative separation and orientation of the molecules, as well as the actual distribution of charge in the molecule.

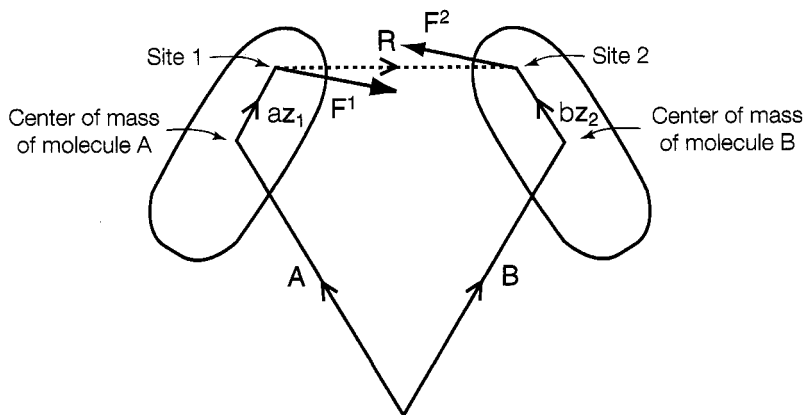


Figure 5 Illustration of the forces F^1 and F^2 (Eq. [23]) arising from the interaction between two dipole moments situated at (atomic) site 1 at $A + az_1$ and site 2 at $B + bz_2$, where molecules A and B have their centers of mass at A and B, respectively, and the dipoles are parallel to the local axes z_1 and z_2 , respectively. There is a torque at each center of mass arising from these forces and the dipole-dipole interaction torque (Eq. [24]), which is perpendicular to the plane of the page, if z_1 , z_2 , and R are all in the plane of the paper.

Limitations to the Accuracy of Distributed Multipole Electrostatic Energies

The accuracy of a distributed multipole representation can always be tested by evaluating the effect on the calculated electrostatic energies in the region of interest of increasing the number of interaction sites (e.g., by adding sites at the midpoints of bonds) or the order of multipoles. Similarly, simplifications of the model, such as removing small multipole components, can be evaluated. However, the accuracy of the calculated electrostatic energies is inevitably limited by the quality of the wavefunction and the absence of penetration effects.

Increasingly high quality wavefunctions can be used to calculate the distributed multipoles, with near-definitive charge distributions being possible for small polyatomics, and split-valence and better basis set SCF calculations being feasible for quite large organic molecules. Fortunately, it seems possible that the approximations in the wavefunction, for split-valence or better basis sets, will primarily produce a scaling of the electrostatic interactions, rather than any significant change in the orientational dependence of the electrostatic interaction. At least this was the case in a comparison of the electrostatic potential on a grid of points outside N-acetylalanine-N'-methylamide, as calculated from the DMAs of various wavefunctions differing in the basis set and inclusion of electron correlation.¹²¹ Thus for large molecules, where only a SCF 6-31G** wavefunction can be calculated, the overestimated polarity of the molecular charge distribution can be corrected by multiplying the atomic multi-

poles by a 0.9 fudge factor to approximate for the effect of electron correlation. This results in a 20% [$\sim (1 - (0.9 \times 0.9))$] reduction in the estimated electrostatic energies. The 0.9 factor is based on an average of the ratio of the calculated to experimental total dipole moments of eight small polyatomic molecules, ranging from 0.78 for NH₃ to 0.96 for CH₃CN.¹²² However, the necessity of making such assumptions is likely to vanish as higher quality wavefunctions become routinely available for organic molecules.

A second approximation (or matter of definition) is that the electrostatic energies calculated from any of the point multipolar representations of the molecular charge distribution do not include the effect of any interpenetration of the molecular charge distributions (i.e., the damping of the electrostatic interaction). This penetration energy is defined as the difference between the exact electrostatic energy involving the full spatial extent of charge distribution and a converged distributed point–multipolar representation. The penetration energy decays exponentially with separation, reflecting how the charge density of a molecule decreases in going from within the molecule toward the van der Waals contact region and beyond. The penetration energy can be significant at the van der Waals separations involved in hydrogen bonding, but generally does not alter the orientational dependence significantly, as shown by the comparison of the electrostatic energy evaluated by perturbation theory and from DMAs for various van der Waals complexes.⁴⁸ A method developed⁹⁹ for calculating electrostatic energies using Gaussian multipoles, which have an appropriate spatial extent, was used to estimate that the penetration energy contributes 25% to the electrostatic energy of the formamide · · · formaldehyde complex. Nevertheless, the penetration energy is a short-range, exponentially decaying effect that is often empirically absorbed into the repulsion potential.

Importance of the Electrostatic Energy in Intermolecular Interactions

The distributed multipole model incorporates a nearly exact description of the molecular charge distribution into the evaluation of the electrostatic energy. Is the increase in accuracy gained by representing the effects of lone pair and π -electron density worth the extra complexity in the potential model? Even if there is a significant enhancement, is it worth using such an elaborate model when only crude models, such as the isotropic atom–atom 6-exp potential, are available for the other contributions?

There have been many studies that contrast the accuracy of various atomic charge and distributed multipole models. These studies include the extensive tests provided when various distributed multipole methods were first proposed. For example, there are published contour plots of the potential around a water molecule,¹²³ the amino acid histidine,⁹⁰ and variations in the electrostatic energies of nucleic acid bases,¹²⁴ which confirm the significance of the atomic anisotropy shown in the color three-dimensional displays of the electrostatic field around uracil and pyrimidine.¹²⁵ It is clear that the difference

made when going from an atomic point charge model to a distributed multipole model depends considerably on the molecule and region of the intermolecular potential being sampled, often more than on the precise variant of the atomic charge and distributed multipole model used. The distributed multipole model is most important in the regions close to atoms with marked nonspherical features in their charge distributions, such as lone pair and π -electron density. The practical importance of accurate electrostatic models has been demonstrated extensively,^{123,126} with the most well-known need being that of using distributed multipole models to account for the structure of van der Waals complexes of small polyatomics.⁴⁶

The atomic point charge model, which is commonly used in simulating organic systems, is a severely truncated distributed multipole expansion. The now common practice of deriving these atomic charges by fitting to the electrostatic potential, as calculated by integration over the wavefunction at a grid of points around the molecule, allows the charges to partially absorb the effects properly represented by the anisotropic atomic multipoles, and to thus give the best possible atomic point charge model (though care is needed in choice of method^{127,128}). However, a survey¹²⁹ of different methods of deriving atomic charges concluded that no atomic charge model was capable of giving a completely satisfactory representation of the electrostatic potential around all molecules. Nevertheless, there exist computational disadvantages to the use of a distributed multipole model which requires special computer programs. So, there is considerable merit behind the pragmatic approach of using point charges situated away from the nuclear sites to represent the effects of the atomic dipoles and quadrupoles on atoms. This approach is gradually being adopted in some molecular mechanics force fields.^{130,131}

Induction and Dispersion Contributions: Distributed Polarizabilities

Long-range induction energy can be expressed⁶ in terms of the permanent multipoles and polarizabilities of the individual molecules, as well as the separation and orientation of the molecules, by a multipole expansion of the second order long range perturbation theory expression (Eqs. [9] and [10]). Similarly, the coefficients in the perturbation theory expansion of the dispersion energy can be related to the integrals over the individual molecular polarizabilities at imaginary frequency. These properties can be derived from experimental data for atoms⁵ and small molecules in favorable cases, but quantum mechanical calculations are often the best source. Since polarizabilities measure the ease of distortion of the molecular charge density, their calculation requires a basis set with high angular momentum basis functions and the inclusion of electron correlation. Thereby quantifying these long-range contributions to the intermolecular energy from the charge distributions of the isolated molecules is

possible, but the methods have yet to become routine for use with organic molecules.

Such reluctance to use long-range perturbation methods exists partly because the polarization and dispersion properties must be distributed, usually to atomic centers, for the perturbation theory expressions to be valid and useful.⁹¹ This is intrinsically more demanding of the method of dividing the molecule into atoms than it is for the distribution of charge of a distributed multipole model, because an applied field can result in charge density moving between the atomic sites. An accurate treatment must therefore allow for the movement of charge between the atoms under the influence of the electric field arising from another nearby molecule.⁹² This treatment involves a double sum over all intermolecular pairs of sites in the molecule. Such model potentials are too complex for most applications, but the successes of empirical models suggest that some form of localization, to keep the potential in the form of Eq. [4], should be possible without an unreasonable loss in accuracy. Such models are being developed and tested (Table 3). It already appears that partial localization schemes, which maintain the charge flow polarizabilities but localize the other polarization terms on the atoms, hold promise for quite accurate calculations.⁹³ Thus the development of practical schemes for deriving accurate models for the induction and dispersion interactions of organic molecules, using atom–atom polarizabilities and dispersion coefficients,⁶ should be possible in the near future.

Short-Range Terms

As already noted, there is no rigorous analytical theory for deriving the short-range energy terms (except penetration energy) from the charge densities of the individual molecules. Nevertheless, there is considerable evidence that for some atoms,¹³² the anisotropy of the atom–atom repulsion gives rise to experimentally observable effects, as discussed earlier for chlorine.⁷⁶ The anisotropy of the repulsive wall is important in determining the van der Waals contact distance in a crystal, and this affects the lattice energy mainly through the long-range contributions. Certainly, plausible variations in atomic shape (as represented by anisotropic atom–atom potentials) can lead to significant changes in the relative stability of the crystal structures of X_2 molecules.¹⁰² For small polyatomics, such as $(N_2)_2$ and $(HF)_2$, where it has been possible to calculate a sufficiently extensive ab initio potential surface to test fully the form of the repulsive wall, it is clear that the anisotropy is important. For example, the fit⁸⁶ to an $(N_2)_2$ ab initio potential energy surface with the atom–atom potential

$$U = \sum_{i \in A} \sum_{k \in B} \frac{\epsilon}{(\alpha \rho_0 - 6)} \left[6 \exp[-\alpha(R_{ik} - \rho(\Omega_{ik}))] - \frac{\alpha \rho_0^7}{(R_{ik} - \rho(\Omega_{ik}) + \rho_0)^6} \right] + U_{es} \quad [19]$$

was found to be far superior when the shape of the atoms was explicitly included by making the minimum energy separation ρ of the repulsion-dispersion atom-atom term depend on the orientation of the two atoms, than when it was isotropic [$\rho(\Omega) = \rho_0$]. (The first two atom-atom terms in Eq. [19] are a 6-exp potential with minimum energy $-\epsilon$ at $R_{ik} = \rho(\Omega)$ and a repulsive wall slope of α .) Almost a fivefold reduction in the rms error in the representation of the ab initio SCF surface points was obtained with the form

$$\begin{aligned}\rho(\Omega) &= \rho_0 + \rho_{101}[\bar{S}_{101}^{00}(\Omega) + \bar{S}_{011}^{00}(\Omega)] + \rho_{202}[\bar{S}_{202}^{00}(\Omega) + \bar{S}_{022}^{00}(\Omega)] \\ &= \rho_0 + \rho_1(z_1 \cdot \hat{R} - z_2 \cdot \hat{R}) + \rho_2 \frac{1}{2}[3(z_1 \cdot \hat{R})^2 + 3(z_2 \cdot \hat{R})^2 - 2]\end{aligned}\quad [20]$$

Here the orientational dependence is expressed in terms of scalar products between the unit intersite vector \hat{R} and unit bond vectors z_1 and z_2 , defined to point from the center of molecules 1 and 2, respectively, toward the atoms whose interactions are being calculated (see Table 1). The combination of anisotropy of these two sets of symmetry-related \bar{S} functions shifts the repulsive wall outward at the end of the molecule and close to the intramolecular bond, allowing closer approach in the plane through the atom perpendicular to the intramolecular bond. Thus this picture of the effective shape of the N_2 molecule is compatible with its charge distribution.

This polyatomic example illustrates the need for a method of determining the functional form of the atomic repulsion anisotropy, which will depend on the orientation of the nonspherical features in the atomic charge density, such as lone pairs, relative to the intramolecular bonds. One approach is to use an ab initio potential energy surface for the molecule interacting with a test particle (a spherical atom such as helium or 4S nitrogen) and to fit an anisotropic form to these points. Then one can assume combining rules to estimate the repulsion between atoms in the two molecules. Since the test particle is spherical, only terms of the form \bar{S}_{l0l}^{k0} and \bar{S}_{0ll}^{0k} (i.e., functions of $z_1 \cdot R$ and $z_2 \cdot R$ but not $z_1 \cdot z_2$ for linear molecules) can appear in the resulting potential. Tests of this approach for N_2 , Cl_2 , C_2H_2 , and H_2S^{25} all show that it is a promising methodology to use, though a recent detailed analysis of models for the exchange-repulsion for methane¹³³ suggests that the test particle model can be refined with the help of a few calculations on the dimer. A second method assumes that the repulsion is proportional to the overlap of the undistorted molecular charge distributions. Analytical expressions can be obtained for the overlap between Gaussian functions centered on two atoms, and thus it is possible to analyze molecular charge densities (calculated using Gaussian basis sets) to give the overlap in an analytical atom-atom form for each atom-atom separation. This has been shown to give a reasonable model for the repulsion anisotropy for F_2 , Cl_2 , and N_2 ,⁹⁷ and the method is currently being extended to organic molecules.¹⁰

Damping Terms

Modification of the long-range terms due to overlap, though dwarfed by the exchange–repulsion energy, is still significant in the van der Waals region of the potential sampled in simulations on condensed phases or van der Waals complexes. Comparisons of IMPT and distributed point multipolar estimates of the electrostatic energy are providing experience with electrostatic damping (penetration energy), but the damping of the dispersion energy has been investigated only for very small systems,²⁰ mainly atoms, and so there is little guidance on how the empirically based isotropic forms could be modified. This is a pity, because when a model potential is systematically constructed from good models for all the component sections, the experimental predictions can be disappointingly sensitive to the choice of damping function.²¹

Examples of Systematic Potentials

A major example of this systematic construction of a model potential, aimed at achieving the best accuracy in each component, is the water potential of Millot and Stone.¹³⁴ This potential used distributed multipoles, up to quadrupole on oxygen, charge and dipole on hydrogen, along with central polarizabilities up to quadrupole–quadrupole, and central anisotropic dispersion coefficients up to C_{10} which are damped. The repulsion was described by an anisotropic atom–atom exponential function, fitted to the exchange–repulsion plus penetration energy calculated by IMPT. The model was subsequently re-parameterized by improving the electrostatic model, including a charge transfer term, and using more accurate dispersion coefficients.¹³⁵ This potential gives a good account of the equilibrium geometry, energy, and harmonic frequencies of the water dimer (compared with the best ab initio calculations) and is one of the few potentials that can successfully account for the second virial coefficient of steam over a wide temperature range (373–973 K). A breakdown of the various contributions to the minimum energy of the water dimer, estimated from this potential, is given in Table 4. Like the results in Figure 3, Table 4 emphasizes that the net energy of a hydrogen–bonding interaction is a delicate balance between two large terms—electrostatic and exchange–repulsion—with significant contributions from induction, dispersion, charge transfer, and damping.

The minimum energy structure is clearly sensitive to the electrostatic model, though it has long been established that no atomic-charge-only model will be adequate for water,¹³⁶ and so a model using only the atomic charge component of the DMA is ridiculous. Modifying the other contributions to the potential, by omitting the anisotropy or other unusual terms for model potentials (Table 4), has a modest effect on the energy and also on the minimum energy structure. Although modest, these terms are significant for some applications. For example, the relative stability of the different water clusters was

Table 4 Importance of Relative Terms in the Millot–Stone Potential for $(\text{H}_2\text{O})_2^a$

Energy Contributions at the Minimum Energy Structure			
Full Model	Energy (kJ/mol)	Modified Model	Energy (kJ/mol)
Electrostatic	-25.19	Only charges on atoms	-3.86
Induction	-3.44	Only charges on atoms	-0.53
Dispersion	-8.49	Only C_6 isotropic dispersion ^b	-3.56
Exchange–repulsion	+18.50	Only isotropic terms	+22.16
Charge transfer	-2.24	Only isotropic terms	-3.17
Total	-20.87	Without short range damping	-25.66

Sensitivity of Minimum Energy Structure of $(\text{H}_2\text{O})_2$ to Various Approximations in the Model Potential			
	O · · · O separation (Å)	O · · · H separation (Å)	Angle O—H · · · O (°)
Full potential	2.97	2.02	176.95
Δ if charge only electrostatic model	+0.33	+0.80	-64.78
Δ if charge-transfer omitted	+0.07	+0.07	-0.02
Δ if polarization omitted	+0.07	+0.09	-8.20
Δ if only isotropic repulsion	+0.09	+0.09	-2.84
Δ if only isotropic C_6^b	+0.12	+0.11	+1.51

^a Δ = structure for modified potential minus structure for full potential. Each modified model is the full potential with the parameters and model of just one contribution modified.

^bCentral multipole expansion term like in Eq. [11].

found to be sensitive to the inclusion of the induction term, to the extent that its inclusion is necessary for the observed tetramer structure to be the global energy minimum.¹³⁷

The Millot–Stone water potential¹³⁴ is an example of applying the theory of intermolecular forces as accurately as possible, to get the best possible model potential. It is an approach that is being extended to other small polyatomics, such as $(HF)_2$.¹³⁸ The resulting model potential is far too complicated to be used in any molecular dynamics simulation. Indeed the input data set of all the parameters (available from <http://fandango.ch.cam.ac.uk>) is a couple of pages long, and the formulas for evaluating the energy, programmed into ORIENT, are likewise extensive. This is an intermolecular potential for a polyatomic molecule with only one nonhydrogenic atom, thus allowing a one-site description of the induction and dispersion. Thus, future applications of the systematic approach will result in potentials that will be used for constructing simpler models for use in simulations, for example, using only the most important anisotropic terms. Ideally, these simpler models will have the advantage of using a minimal number of assumptions in their derivation, and the errors in the potential will be known.

Another simpler systematic potential was derived for chlorine,⁷⁴ using the two atomic sites for the distributed multipoles and dispersion coefficients. The anisotropic atom–atom repulsion potential was derived from the overlap model, with the proportionality constant and one major anisotropic coefficient being adjusted by empirical fitting to the crystal structure. This empirical adjustment appeared to effectively absorb the missing contributions, including the many-body effects, because the potential was able to reproduce a wide range of properties of the solid and liquid from Monte Carlo simulations.

There have been several other examples of the systematic approach that have varied in the models used to both derive and represent the different contributions, including some in which the isotropic atom–atom form has been assumed for certain terms. For example, there is a nonempirical method, called NEMO by its authors,^{136,139,140} which is mainly used for producing potentials for studying hydration effects by molecular dynamics. The SIBFA (sum of interactions between fragments ab-initio-computed) approach has been used for studying biomolecular protein–ligand binding.^{141–144} In general, most emphasis has been placed on using an accurate model for the electrostatic term. For example, Spackman combined isotropic atom–atom potentials derived from electron gas theory with a distributed multipole type electrostatic model to model hydrogen-bonded dimers.¹¹⁶ Sokalski et al.¹⁴⁵ used ab initio calculations on small model molecules to derive isotropic atom–atom repulsion–dispersion parameters for use in combination with their CAMM electrostatic model. Systematic model potentials, based on DMA electrostatics and isotropic overlap model repulsion terms, have been successfully applied to explain the spectroscopy of hydrazine clusters¹⁴⁶ and methanol.¹⁴⁷

Model Potentials for Organic Molecules Constructed from Ab Initio Charge Distributions and Empirical Fitting

The use of theoretical methods for contributions that can be accurately estimated, combined with empirical fitted potentials for the other main contributions (and thereby to some extent absorbing the missing contributions and nonadditivity errors), seems to be the most accurate, feasible approach for a diverse set of organic molecules at this moment. This is the method that we have been using for modeling molecular crystal structures. The electrostatic term is represented by a DMA of an ab initio charge distribution of the molecule, with a set of multipoles up to hexadecapole at every atom. This accurately represents the electrostatic forces around each atom and includes the variations due to differing hybridization and neighboring functional groups. The repulsion-dispersion potential is empirical, using Williams's parameters^{29,30} for C/H/N/O and specifically fitted parameters for polar hydrogen atoms H_N(—N), and assuming the usual combining rules. Thus, the model atom–atom potential differs only from the traditional model (Eq. [15]) in the electrostatic term

$$U(R, \Omega) = \sum_{i \in M, k \in N} A_{ik} \exp(-B_{ik} R_{ik}) - \frac{C_{ik}}{R_{ik}^6} + U_{es}(\text{DMA}, \bar{S}_{l_2 l_2}^{k_1 k_2}(\Omega_{ik}) R_{ik}^{-l_2 - l_2 - 1}, l_1 + l_2 \leq 4) \quad [21]$$

where the last term implies the full atom–atom electrostatic expansion (i.e., the generalization of Eq. [18] for atomic sites of arbitrary symmetry) including all terms up to R^{-5} , using the atomic multipoles for the molecule obtained by the DMA of a suitable wavefunction. This potential reasonably reproduces,¹⁴⁸ via static minimization, the room temperature crystal structures of over 40 simple rigid organic molecules (mainly aromatic and heterocyclic rings, with amine, nitro, or amide substituents). The electrostatic forces represented by the anisotropic multipole moments play an important role in many crystal structures; several of these molecular crystal structures minimized to qualitatively incorrect structures when the atomic dipoles and higher multipoles were removed, signifying that the extra computational expense and program development required in using a realistic electrostatic model seem well justified for molecular crystal structure modeling. Although computationally more expensive than the traditional models, the minimizations are still sufficiently fast that such model potentials have been used to “predict” organic crystal structures^{149,150} via searches for the global minimum in the lattice energy. Because these lattice energies include a theoretically rigorous model for the dominant electrostatic interactions, the relative lattice energies of both the known and hypothetical structures of possible polymorphs should be more reliable than those of searches using empirical force fields.¹⁵¹

COMPUTER CODING OF ANISOTROPIC POTENTIALS

Although there are problems in deriving accurate anisotropic atom–atom potentials, the lack of simulation programs using such potentials has probably been the major disincentive to their use. The great advantage of the isotropic atom–atom potential is that each atom–atom interaction produces forces between the two atoms along the vector between them. The introduction of anisotropic terms in the potential, in contrast, generates torques about the atomic sites in addition to noncentral forces. For example, the energy of interaction between two dipole moment components Q_{10}^1 and Q_{10}^2 on (atomic) sites 1 and 2 of molecules A and B, defined relative to the unit atomic/molecular axes \mathbf{z}_1 and \mathbf{z}_2 on molecules A and B, respectively [cf. Figure 2(b)] and separated by an intersite vector \mathbf{R} (Figure 5), is

$$U_{10,10}^{\text{electrostatic}} = (4\pi\epsilon_0)^{-1} Q_{10}^1 Q_{10}^2 R^{-5} [R^2(\mathbf{z}_1 \cdot \mathbf{z}_2) - 3(\mathbf{z}_1 \cdot \mathbf{R})(\mathbf{z}_2 \cdot \mathbf{R})] \quad [22]$$

The interaction between the two dipole moments will produce a force at the site 2 on molecule B

$$\begin{aligned} \mathbf{F}_{10,10}^{2,\text{electrostatic}} &= (4\pi\epsilon_0)^{-1} Q_{10}^1 Q_{10}^2 R^{-7} \{3[R^2(\mathbf{z}_1 \cdot \mathbf{z}_2) - 5(\mathbf{z}_1 \cdot \mathbf{R})(\mathbf{z}_2 \cdot \mathbf{R})]\mathbf{R} \\ &\quad + 3R^2(\mathbf{z}_2 \cdot \mathbf{R})\mathbf{z}_1 + 3R^2(\mathbf{z}_1 \cdot \mathbf{R})\mathbf{z}_2\} \end{aligned} \quad [23]$$

which is clearly noncentral (i.e., not parallel to \mathbf{R}), and also a force at the dipole site 1 on molecule B $\mathbf{F}_{10,10}^{1,\text{electrostatic}} = -\mathbf{F}_{10,10}^{2,\text{electrostatic}}$ (see Figure 5). The torques arising from this interaction can be expressed about the centers of mass A of molecule A and B of molecule B, assuming that the dipole site 1 on molecule A is at position $\mathbf{a} = a\mathbf{z}_1$, and the dipole site 2 on molecule B is at $\mathbf{b} = b\mathbf{z}_2$ from their respective centers of mass:

$$\begin{aligned} \mathbf{G}_{10,10}^{1,\text{electrostatic}} &= (4\pi\epsilon_0)^{-1} Q_{10}^1 Q_{10}^2 R^{-7} \{[-15a(\mathbf{z}_1 \cdot \mathbf{R})(\mathbf{z}_2 \cdot \mathbf{R}) + 3aR^2(\mathbf{z}_1 \cdot \mathbf{z}_2) \\ &\quad - 3R^2(\mathbf{z}_2 \cdot \mathbf{R})]\mathbf{R} \times \mathbf{z}_1 - [3aR^2(\mathbf{z}_1 \cdot \mathbf{R}) + R^4]\mathbf{z}_1 \times \mathbf{z}_2\} \\ \mathbf{G}_{10,10}^{2,\text{electrostatic}} &= (4\pi\epsilon_0)^{-1} Q_{10}^1 Q_{10}^2 R^{-7} \{[15b(\mathbf{z}_1 \cdot \mathbf{R})(\mathbf{z}_2 \cdot \mathbf{R}) - 3bR^2(\mathbf{z}_1 \cdot \mathbf{z}_2) \\ &\quad - 3R^2(\mathbf{z}_1 \cdot \mathbf{R})]\mathbf{R} \times \mathbf{z}_2 - [3bR^2(\mathbf{z}_2 \cdot \mathbf{R}) - R^4]\mathbf{z}_1 \times \mathbf{z}_2\} \end{aligned} \quad [24]$$

Note that there are torques on each molecule from the interaction, even if the interaction sites are the centers of mass ($a = b = 0$). The sum of the torques is usually not zero. Rather, it is the total torque on the system, arising from all the torques and forces that must sum to zero [i.e., $\mathbf{G}^1 + \mathbf{G}^2 + (\mathbf{A} \times \mathbf{F}^1) + (\mathbf{B} \times \mathbf{F}^2) = 0$ in this example] in the absence of external fields.

Equations [22]–[24] illustrate why the derivation and programming of the forces and torques, and second derivatives for all the terms up to R^{-5} in the atom–atom multipole expansion of the electrostatic energy is a nontrivial exercise in classical mechanics. It has been described in detail by Popelier and Stone,¹⁵² and, with the additional derivatives required for modeling molecular crystal structures, by Willock et al.¹⁵³

Calculations on the gas phase interactions of most pairs (or small clusters) of molecules have been possible using ORIENT for some time. This program is available on request from the author's web site (<http://fandango.ch.cam.ac.uk/>). The latest version ORIENT3 not only can determine the minimum energy structures of van der Waals clusters, their transition states, and other stationary points, it also can calculate their vibrational modes,¹¹⁹ and it has the ability to use anisotropic repulsion, dispersion, and induction energy models.

Codes to model the condensed phases using anisotropic potentials are gradually being developed. The general molecular crystal structure relaxation program DMAREL,¹⁵³ minimizes the lattice energy of a crystal, including the DMA electrostatic model, with respect to the position and orientation of the molecules and distortions of the unit cell, without being constrained by the initial space group symmetry. This program required the development of Ewald summation techniques to evaluate the charge–dipole and dipole–dipole contributions to the lattice energy. It also handles another complication in using distributed multipoles, namely, that they are defined using a right-handed coordinate system. Hence, if an ensemble of molecules is generated using crystallographic symmetry elements that invert this axis system, this must be corrected and reflected in the multipoles. Thus DMAREL automatically has two sets of multipoles stored for use (simply related by appropriate sign reversals) for crystal structures in which the molecules are related by an inversion type operator.

There have been some molecular dynamics simulations with anisotropic atom–atom potentials, the earliest being simulations with chlorine potentials.^{154,155} Those simulations demonstrated that the computer time requirements were quite reasonable, and the results were effective compared with the inclusion of additional isotropic sites. The technique¹⁵⁶ has also been extended to butane by means of a four-site anisotropic carbon model.¹⁵⁷ A general DMA based potential model is being implemented into the new CCP5 molecular simulation program DL_POLY.¹⁵⁸ Monte Carlo simulations can use anisotropic atom–atom potentials readily,^{74,159} since the calculations require the evaluation of only the energy.

DMA models have also been incorporated into the molecular modeling force field program MOMO,¹⁶⁰ which was used to study host–guest complexes, such as benzene in a hexaoxacyclophe host. The difficult problem of accurately modeling the intramolecular electrostatic energy of proteins has also used distributed-multipole-type models.¹⁶¹

Most of these programs are based on the assumption that spherical tensor distributed multipoles to be used are defined as in Ref. 6. The large number of parameters involved (25 per atom to include all multipoles needed to evaluate all atom–atom terms in the electrostatic energy up to R_{ik}^{-5}) can be conveniently transferred using the “punchfile” produced after the distributed multipole analysis has been performed on the wavefunction within the program CADPAC.¹¹⁵ The developers of other forms of distributed multipoles, such as CAMM¹¹¹ or SIBFA,¹⁴² have used their own software. It is worth emphasizing that care must be taken to ensure that the same definition of multipole moments is used in the generation and applications programs. The relationship between Cartesian and spherical tensor definitions is straightforward and given explicitly in an appendix to Ref. 6. However, given that Debye’s convention for the dipole moment pointing from positive to negative may still be encountered, although almost all the recent literature defines the dipole from negative to positive, one must remain cognizant of possible confusion of definitions. The next generation of simulation codes, which can use anisotropic atom–atom potentials, is emerging, and this will lead to an increased use of such potentials.

TRANSFERABILITY OF POTENTIALS FOR ORGANIC MOLECULES

Virtually all models for intermolecular forces between organic molecules are based on assumptions about transferability of the models and their associated parameters. These assumptions are both necessary and desirable to keep the calculations tractable. We can derive and test model potentials and parameters on small model systems such as amides, where there are sufficient experimental data and high quality theoretical calculations are possible, and then we can use the validated parameters to simulate and understand larger related systems, such as polypeptides and proteins, for which it would not be possible to derive a model potential directly. The accuracy of the resulting potential will depend on the realism of the transferability assumptions, which should always be known and questioned. For example, is formamide (HCONH_2) a suitable model for the amide group (NHCO) potentials in polypeptides? Or, is it better to consider *N*-methylacetamide ($\text{CH}_3\text{CONHCH}_3$), or even *N*-acetyl, *N'*-methylamide blocked peptide residues (i.e., $\text{CH}_3\text{CONHCHRCONHCH}_3$)? Alternatively, (going to the other extreme), would the best nitrogen isotropic atom–atom repulsion–dispersion parameters from an N_2 or pyridine model be adequate for describing amide nitrogen atoms? In addition to assuming that potential parameters are transferable between molecules, it is also usual to assume that they are transferable between different conformations of the same flexible molecule. Recent studies indicate that both types of assumption could limit the accuracy of the intermolecular potentials quite seriously.

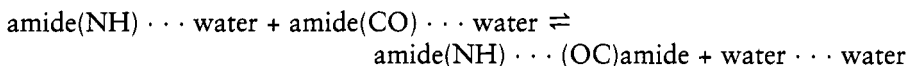
Transferability of Atom–Atom Nonbonded Parameters Between Molecules

Transferability assumptions inevitably involve some approximation. Chemical intuition tells us that changing the hybridization state of an atom will make a huge difference to its atomic charge distribution and intermolecular interactions, so that nitrogen parameters from pyridine or the nitrogen molecule will be very poor for an amide nitrogen. However, replacing a hydrogen by a methyl group will surely have a negligible effect on the electron density of an amide nitrogen several peptide residues away, unless the conformation brings the two groups so close together that there is a through-space polarization between them. Hence, invoking the transferability assumption depends on the accuracy required in the calculation, and there is no point in seeking a more accurate potential for a model system than the intrinsic errors associated with the transferability assumption.

It is worth noting that repulsion–dispersion parameters can be assumed to be widely transferable, in contrast to the electrostatic parameters, which must be calculated separately for chemically distinct atoms. [Indeed, transferring any (nonzero) atomic charges between atoms in different hybridization states usually results in a nonphysical net charge on the molecule.] Thus many force fields use an electrostatic model calculated specifically for the molecule being studied, but use “generic” repulsion–dispersion parameters that may depend only on the atomic number of the atoms concerned. This approximation is adequate for many molecular modeling studies and indeed is often the only option when the molecule under investigation does not belong to one of the families of compounds for which specific force fields are available (such as amides and peptides, nucleic acids, or carbohydrates). While this limitation is often expected during the modeling of compounds containing less common atoms, such as Se or Br, where there has been little model potential development, it can also occur for first-row atoms in less common functional groups. For example, a transferable 6-exp potential plus a distributed multipole electrostatic model underestimated the hydrogen bond length to various nitrogen atoms with an error of usually 0.1 to 0.2 Å relative to that optimized in IMPT calculations. Even larger errors have been observed for some unusual nitrogen atoms: for example, an error of 0.29 Å in the hydrogen bond length between dimethylamide and *trans*-diazabutene.¹⁶² This difference is because the difference in the exchange–repulsion energy can be quite significant amounting to about 7 kJ/mol at the same hydrogen-bonded geometry for methanol with pyridine or methylcyanide.¹⁰ Hence the assumption of transferable repulsion potentials becomes inadequate when we require this level of accuracy in intermolecular contact distances and energies. It seems reasonable, then, that different types of nitrogen atoms, with different valence electron distributions, should have differ-

ent repulsion potentials with different anisotropies for accurate modeling of the intermolecular atom–atom separations in complexes.

Even within the limits of maintaining chemically similar atoms, care is needed when one is invoking transferability. IMPT calculations on amide–amide and amide–water systems indicated¹⁶³ that the change in the intermolecular interaction energy associated with the hydrogen bond exchange process



varied by almost 5 kJ/mol, producing a variation in sign for the range of models formamide, acetamide, N-methylformamide, and N-methylacetamide. The differences in the electrostatic and exchange–repulsion terms both contributed to this, reflecting the changes in the charge distribution of both the NH and CO groups involved in the hydrogen bonds. Thus, there is little point in calculating accurate formamide–formamide and formamide–water ab initio surfaces, to derive a model potential for studying protein hydration by assuming transferability.

To test the transferability of the moments, and to suggest a method of building up distributed multipole electrostatic models for polypeptides without needing to calculate the wavefunction for the entire molecule, an analysis of the atomic multipoles for a range of several amides and dipeptides with hydrocarbon side chains was performed.¹⁶⁴ The model molecule structures had standardized bond lengths and angles, and a fixed basis set SCF method was used throughout to eliminate some factors that would otherwise cause changes in the calculated atomic charge distributions. The atomic dipoles, quadrupoles, et cetera were referred to corresponding local axis systems [see Figure 2(e)] for comparison. The results clearly showed that an atomic charge distribution was dependent on the nature of the bonded atoms, but that it was reasonably transferable if the bonded atom types were the same. For example, the charge on an amide nitrogen atom varied from $-0.805 \pm 0.015\text{ e}$ for CONH_2 to $-0.289 \pm 0.018\text{ e}$ for $\text{CON}(\text{CH}_3)_2$. The higher multipole moments showed a similar pattern of large variations between atoms in different bonding environments, but reasonable transferability if the bonded atoms were the same. The importance of nearest-neighbor atoms and their varying short-range inductive effects in determining the atomic charge distributions are also seen in the distributed multipole analysis of the azabenzenes molecules. In these aromatic six-membered rings, there is a marked pattern of each CH group donating about a quarter of an electron to any neighboring nitrogen atom.¹²⁰ Thus, the net charges on the CH groups varied from just over $+0.5\text{ e}$ in s-triazine and s-tetrazine to approximately zero for benzene and the CH groups not bonded to any nitrogens in pyridine, pyridazine, and pyrimidine. This rough rule of thumb, that the charge distribution of an atom is only approximately transferable if

bonded to the same functional groups, seems to hold for other partitioning schemes and molecules, such as stockholder partitioning of purines and pyrimidines,¹⁶⁵ or Bader partitioning of $\text{CH}_3(\text{CH}_2)_m\text{CH}_3$ ¹⁶⁶ and CHF compounds.¹⁶⁷ This rule of thumb is also the basis of other methods of building up different types of model charge distribution^{168,169} from ab initio calculations, and a method for analyzing experimental X-ray charge densities.¹⁷⁰

A major problem with assuming the transferability of atomic charges or multipoles is that the electrostatic interaction is very sensitive to those charges. A charge of 0.01 e produces an electrostatic potential of 5 kJ/mol at a point 3 Å away. Therefore, although the atomic multipoles for a given atom may appear reasonably transferable between different molecules when the bonded neighbors are the same, the variations of hundredths of an electron, caused by the changes in the more distant functional groups, are not negligible. Consequently, although the transferable atomic multipoles model can be used to build up a model charge distribution for other amides and even peptides, it gives only moderate predictions of the potential outside the molecule.¹⁶⁴ (Nevertheless, the errors from assuming transferability of atomic multipoles between model molecules with a larger target peptide were significantly less¹⁶⁴ than those resulting from assuming that a Mulliken analysis of a wavefunction of the target peptide could provide charges needed to adequately represent its electrostatic interactions.) Significantly better predictions can be made by using larger model molecules, such as the N-acetyl, N'-methylamide blocked peptides.¹⁷¹ [see Figure 6(a)] to construct a polypeptide charge distribution. It should be noted that successes in building up model charge distributions have been based on using molecular fragments with the same conformation as in the target molecule.

Transferability Between Conformations

The issue of transferability of atomic charge models between conformations has been more vigorously discussed in the last decade. Most force fields assume that the charge distribution associated with each atom is independent of conformation. However, it has been noted that potential derived atomic charges do vary with the conformation of the molecule used to derive them^{172,173} and that these variations have a significant effect on computed properties such as the free energy of hydration of alcohols.¹⁷⁴

In discussing the conformational variation in an electrostatic model used for calculating intermolecular interactions, it is worth separating those effects that are artifacts of the method used to construct the model charge distribution,¹⁷⁵ from those that reflect the genuine physical changes in the molecular charge distribution. Potential-derived charges are fitted to the electrostatic potential calculated at a grid of points around the molecule, and since the electrostatic potential is long range, the potential at most grid points will include contributions from many neighboring atoms. The partitioning of the potential

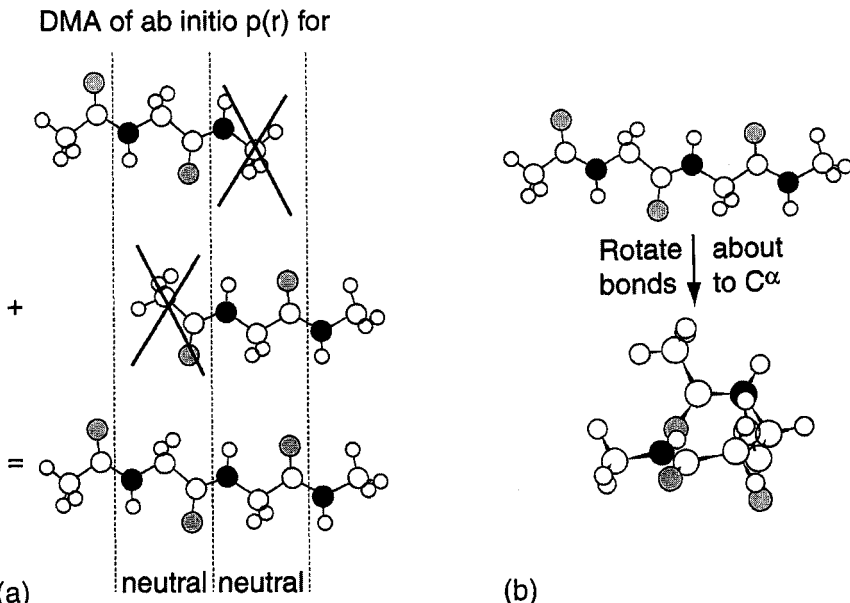


Figure 6 Schematic diagram for the construction of a DMA model to test transferability. (a) To test transferability between molecules, a DMA for $\text{CH}_3\text{CO}(\text{NHCH}_2\text{CO})_2\text{NHCH}_3$ is constructed from the DMAs of ab initio calculations on $\text{CH}_3\text{CO}(\text{NHCH}_2\text{CO})\text{NHCH}_3$ in the same conformation, but discarding the multipoles on the fragments that have been crossed out. The charge on the C^α atoms should be adjusted to ensure that each residue and the entire molecule is exactly neutral, but the required change in the charge should be very small. (b) Note that when a DMA calculated in one conformation is used to represent the charge distribution in another, Q_{lk} ($l > 0$) must be transformed according to their rank l , so that the local atomic charge distribution remains the same. For example, the dipoles along the $\text{C}=\text{O}$ bond remain the same relative to the new $\text{C}=\text{O}$ bond orientation, but because they are in a different orientation in space, the components relative to the global or molecule-fixed axes will differ.

between atoms in the fitting of the charges is far from unique¹²⁸ but can be done to optimize the reproduction of the potential in that conformation. Hence, when these charges are used to represent another conformation, a cancellation of errors in the charges between two atoms that were nearby in the original conformation may no longer occur for the new conformation in which they are well separated. Thus, a proportion of the observed conformational dependence of potential-derived charges can be an artifact based on their method of determination. The change in conformation of a molecule undoubtedly does alter its charge distribution, both through local changes in the bonding and also by changing the mutual through-space polarization of atoms. The key question then becomes whether these effects contribute significantly to the intermolecu-

lar potential for a given molecule. If so, then the best method of representing these effects will depend on the electrostatic and polarization model (if any) being used.

The transferability of charge distributions between conformations has been investigated by means of DMA methods of partitioning the molecular charge distribution and representing the intermolecular electrostatic forces. There is a degree of arbitrariness in the division of charge density contributions arising from orbitals on adjacent atoms, which, if the atoms are nonbonded, may affect the transferability with conformation. However, although such studies strictly monitor only the transferability of DMA models with conformation, the relative completeness of the representation of the charge density and electrostatic effects (and the more rigorously defined partitioning) means that these studies will give a closer approximation to the genuine physical limits to the transferability of atomic charge distributions with conformation than point charge models. To test the transferability approximation for modeling protein backbones,¹⁷¹ the DMAs of N-acetyl, N'-methylamine diglycine [$\text{CH}_3\text{CO}(\text{NHCH}_2\text{CO})_2\text{NHCH}_3$] were calculated from SCF 6–31G* wavefunctions in four conformations using standard bond lengths and angles (thus eliminating errors due to the choice of charge distribution or other changes in molecular structure). Two conformations served as models for the β -sheet and α -helical secondary structure in proteins: the extended conformation ($\phi_1 = \psi_1 = \phi_2 = \psi_2 = 180^\circ$) and α -helix conformation ($\phi_1 = \phi_2 = -57^\circ$, $\psi_1 = \psi_2 = -47^\circ$). The structure with three amide groups is too small to display the intramolecular hydrogen bonds that stabilize these conformations. The other two model conformations were type I ($\phi_1 = -60^\circ$, $\psi_1 = -30^\circ$, $\phi_2 = -90^\circ$, $\psi_2 = 0^\circ$) and type II ($\phi_1 = -60^\circ$, $\psi_1 = 120^\circ$, $\phi_2 = 80^\circ$, $\psi_2 = 0^\circ$) β -turns, commonly adopted when a protein main chain reverses direction at the surface. These latter conformers do include an internal hydrogen bond. Model DMA charge distributions can be constructed by taking the atomic multipoles calculated for one conformation and transforming them by the appropriate rotational transformations of spherical tensors⁷ to represent another conformation [Figure 6(b)]. The transferability assumption could then be evaluated by comparing the electrostatic properties for a given test conformation as calculated from the transformed DMAs calculated from another conformation, with those calculated from the DMA evaluated for the same type of wavefunction for the test conformation.

The errors in assuming transferability of a peptide charge distribution with changes in the backbone torsional angle were found to be significant compared with the variations in the electrostatic potential around each molecule.¹⁷¹ For example, the typical root-mean-square (rms) error in the electrostatic potential on the water-accessible surface (1.4 Å from the van der Waals surface) was around 10 kJ/mol, rising to over 20 kJ/mol when the multipoles determined in the internally hydrogen bonded conformations were used to model the extended and helical conformations. The errors varied considerably over the grids, with a maximum magnitude of 75 kJ/mol near a terminal N

group when a type I β -turn charge distribution was used to model the extended conformation. The relative electrostatic energies of the various structures for a water hydrogen-bonded to each peptide were also poorly estimated, and sometimes wrongly ordered, by the electrostatic models that assumed transferability between conformations.

In contrast, the errors involved in assuming transferability between molecules, by constructing a model for the blocked diglycine from the DMAs of the wavefunctions of blocked glycine [$\text{CH}_3\text{CO}(\text{NHCH}_2\text{CO})\text{NHCH}_3$] with the corresponding ϕ, ψ angles [see Figure 6(a)] were significantly smaller.¹⁷¹ In this case the rms errors on the water-accessible surface were 6 kJ/mol or less (a maximum absolute error of 12 kJ/mol on any surface), and only a few kilojoules per mole for the water-binding energy. This suggests that the effects on the charge density of the interactions between residues, including the intramolecular hydrogen bonds in the β -turns, were relatively small and indeed were found to be comparable to the estimated polarization effects on the amide group in formamide.¹⁷¹ Thus, the large errors that arose under the assumption that the electrostatic model could be transferred between conformations were mainly associated with the changes in the ϕ, ψ torsional angles, rather than any intramolecular hydrogen bonding.

This approach can be used to establish whether the electrostatic model one intends to use is conformation dependent. The next practical question is, How can one represent this dependence? A completely accurate method of representing the changes in the distribution of charge within a molecule as a function of conformation would require an ab initio calculation at each conformation; but this is what model intermolecular potentials are intended to avoid. However, any conformational change that produced a major rearrangement of the valence electron density, such as rotation around formal double bonds or buckling of aromatic rings, would have such a high intramolecular energy that those conformations would not be sampled in simulations anyway. Hence, there is a natural compensating influence such that the conformation-dependent charge distributions relevant for simulating conformationally flexible molecules under reasonable conditions will not change drastically. Various methods have been proposed for producing conformation-dependent charges,^{176,177} and they have been included in some force fields.^{177,178} However, these charges are inevitably based on a quickly estimated, and therefore crude, representation of the charge distribution in each conformation. So, it is important to assess whether the errors in the model charge distribution in each conformation (relative to an accurate representation of a reasonable quality wavefunction) are less important than the errors inherent in neglecting the conformational dependence of the charge distribution for the particular molecule and application. In particular, any approach that is successful for conformational studies (which test validity of the intramolecular force field) may not work well for properties that are more sensitive to the intermolecular forces (and vice versa). Both the charge distributions and their variation with confor-

mation can be represented accurately^{179,180} by calculating the wavefunction for a set of conformations and fitting the corresponding distributed multipoles to a Fourier series in the torsional angle. Such studies of ethanol, acrolein, *N*-methylacetamide, *N,N*-dimethylacetamide, and *N*-acetyl, *N'*-methylamide blocked peptides led to a clear conclusion that the Fourier series technique does well in modeling the modest changes in charge distribution with conformation, as well as the corresponding substantial effect on the rotational barriers of the hydrated molecules.¹⁸⁰ However, this method is expensive to implement—both in calculating the wavefunction for a sufficient number of conformations to establish the Fourier coefficients and also in actually performing the simulations.

In many instances it may be more appropriate, or even pragmatically necessary, to use a fixed set of atomic charges or multipoles. Then, the fixed electrostatic model should be carefully chosen to minimize the errors inherent in neglecting their conformational variations. Reynolds, Essex, and Richards proposed that the atomic charges used should be a Boltzmann-weighted average over the important conformations that will be sampled in the simulation.¹⁸¹ Alternatively, if one conformation is used to determine the electrostatic model parameters, it should be chosen judiciously. For example, the extended conformation of a blocked model peptide, $\text{CH}_3\text{CO}(\text{NHCH}_2\text{CO})\text{NHCH}_3$ with $\phi = \psi = 180^\circ$, gives a worse prediction of the potential around the other conformations than does the α -helical conformation¹⁷¹ (the former has a tendency to overestimate the extremes of the potential). This inadequacy may be rationalized by noting that in the extended geometry, the neighboring $\text{O}=\text{C}—\text{N}$ groups are coplanar, and their π -systems can interact hyperconjugatively through the intervening C^{α} . Accordingly, the extended conformation may be the worst choice of model for a simulation of a peptide lacking a predominantly β -sheet structure.

Thus, accurate electrostatic models capable of representing a genuine physical effect will be conformation dependent, whereas approximate models may overestimate this effect. We are still at an early stage in developing methods for dealing with this for intermolecular interactions, and it becomes terribly complicated when the same charges are also involved in the intramolecular force fields that determine the molecular conformation. A significant amount of work will be needed because of the problems associated with separating out the changes in charge distributions that can be reasonably modeled by an intermolecular type of polarization (e.g., in an intramolecular hydrogen bond between two functional groups separated by many single bonds) and an intramolecular effect resulting from a redistribution of the valence density due to local changes in conformation (e.g., loss of π -bonding due to torsion around a bond with partial multiple-bond character) where the intermolecular type functional form is not likely to be adequate. This is clearly going to be an important area for future developments for modeling flexible molecules.^{161,182} However, we should be aware that this may be pushing too far the assumption that nonbonded intramolecular forces can be adequately represented by the models for intermolecular forces.

FUTURE MODEL POTENTIALS

Empirical isotropic atom–atom potentials have been widely used for modeling the crystal structures of organic molecules and in the simulation of biological interactions. However, for molecules and simulations for which these potentials are inadequate, or when the scientific argument requires the best possible estimate of the intermolecular interaction energies, there are now alternatives, derived from the molecular wavefunction using the theory of intermolecular forces. Using distributed multipole electrostatic models leads to substantial improvements in our ability to predict the structures of van der Waals complexes and molecular crystal structures. However, to further improve our model intermolecular potentials, we need to put both the repulsion and dispersion models on a better theoretical footing, both in allowing an anisotropic form and in obtaining the requisite parameters. This will not be an easy task, but the work on small polyatomics suggests that it will be possible.

Thus, in the future, there will be far more accurate, and complex, models available for the intermolecular forces between organic molecules. The anisotropic atom–atom form is expected to provide an accurate representation of the molecular charge distribution and to provide a satisfactory assessment of the resultant intermolecular forces. The model potential should be consonant with the chemist’s picture of a molecules’ valence electrons, which in turn determine the hydrogen bonding and other interactions associated with that molecule. Hence decisions regarding which approximations can be made in the model potential will become more complicated because we will need to ask: What terms can be neglected? Can the atoms be treated as spherical? Can the atom–atom potential parameters be assumed transferable? And so on. Moreover, deciding which model potential will be good enough for a given study will become a more important issue than it now is. Resolution of that issue will be determined by the goals of the simulation and the molecular system under study, and less by computational limitations requiring the simplest physical model.

ACKNOWLEDGMENTS

The author wishes to thank current members of her group, Irene Nobeli, Helen Tsui, Theresa Beyer, and Tanja van Mourik, for providing material and assisting with the production of this chapter, and all the numerous collaborators who have helped develop the ideas represented here, particularly Anthony Stone (University of Cambridge), who laid much of the theoretical (and computer coding) foundation on which this was based. Financial support from EPSRC and Cambridge Crystallographic Data Centre is also gratefully acknowledged.

REFERENCES

1. T. P. Lybrand, in *Reviews in Computational Chemistry*, K. B. Lipkowitz and D. B. Boyd, Eds., VCH Publishers, New York, 1990, Vol. 1, pp. 295–320. Computer Simulation of Biomolecular Systems Using Molecular Dynamics and Free Energy Perturbation Methods.
2. L. M. Balbes, S. W. Mascarella, and D. B. Boyd, in *Reviews in Computational Chemistry*, K. B. Lipkowitz and D. B. Boyd, Eds., VCH Publishers, New York, 1994, Vol. 5, pp. 337–379. A Perspective of Modern Methods in Computer-Aided Drug Design.
3. E. Ōsawa and K. B. Lipkowitz, in *Reviews in Computational Chemistry*, K. B. Lipkowitz and D. B. Boyd, Eds., VCH Publishers, New York, 1995, Vol. 6, pp. 355–381. Published Force Field Parameters. See also: M. Jalaie and K. B. Lipkowitz, this volume.
4. I. Pettersson and T. Liljefors, in *Reviews in Computational Chemistry*, K. B. Lipkowitz and D. B. Boyd, Eds., VCH Publishers, New York, 1996, Vol. 9, pp. 167–189. Molecular Mechanics Calculated Conformational Energies of Organic Molecules: A Comparison of Force Fields.
5. G. C. Maitland, M. Rigby, E. B. Smith, and W. A. Wakeham, *Intermolecular Forces. Their Origin and Determination*, Clarendon Press, Oxford, 1981.
6. A. J. Stone, *The Theory of Intermolecular Forces*, Clarendon Press, Oxford, 1996.
7. D. M. Brink and G. R. Satchler, *Angular Momentum*, Clarendon Press, Oxford, 1967.
8. A. J. Stone and R. J. A. Tough, *Chem. Phys. Lett.*, **110**, 123 (1984). Spherical Tensor Theory of Long-Range Intermolecular Forces.
9. A. J. Stone, in *The Molecular Physics of Liquid Crystals*, G. R. Luckhurst and G. W. Gray, Eds., Academic Press, London, 1979, pp. 31–50. Intermolecular Forces.
10. I. Nobel, S. L. Price, and R. J. Wheatley, *Mol. Phys.*, **95**, 525 (1998). Use of Molecular Overlap to Predict Intermolecular Repulsion in N · · · H—O Hydrogen Bonds.
11. A. D. Buckingham, *Adv. Chem. Phys.*, **12**, 107 (1967). Permanent and Induced Multipole Moments and Long-Range Intermolecular Forces.
12. A. Kumar and W. J. Meath, *Mol. Phys.*, **75**, 311 (1992). Dipole Oscillator Strength Properties and Dispersion Energies for Acetylene and Benzene.
13. K. S. Pitzer, *Adv. Chem. Phys.*, **11**, 59 (1959). Inter- and Intramolecular Forces and Molecular Polarizabilities.
14. P. M. Axilrod and E. Teller, *J. Chem. Phys.*, **11**, 299 (1943). Interaction of the van der Waals Type Between Three Atoms.
15. A. S. Davydov, *Theory of Molecular Excitons*, McGraw-Hill, New York, 1962.
16. A. J. Stone, *Chem. Phys. Lett.*, **211**, 101 (1993). Computation of Charge-Transfer Energies by Perturbation Theory.
17. K. Morokuma and K. Kitaura, in *Chemical Applications of Atomic and Electrostatic Potentials*, P. Politzer and D. G. Truhlar, Eds., Plenum Press, London, New York, 1981, pp. 215–242. Energy Decomposition Analysis of Molecular Interactions.
18. F. B. van Duijneveldt, J. G. C. M. van Duijneveldt-van de Rijdt, and J. H. van Lenthe, *Chem. Rev.*, **94**, 1873 (1994). State-of-the-Art in Counterpoise Theory.
19. N. R. Kestner and J. E. Combariza, in *Reviews in Computational Chemistry*, K. B. Lipkowitz and D. B. Boyd, Eds., Wiley-VCH, New York, 1999, Vol. 13, p. 99–132. Basis Set Superposition Errors: Theory and Practice.
20. R. J. Wheatley and W. J. Meath, *Mol. Phys.*, **80**, 25 (1993). Dispersion Energy Damping Functions, and Their Relative Scale with Interatomic Separation, for (H, He, Li)–(H, He, Li) Interactions.
21. M. S. H. Ling and M. Rigby, *Mol. Phys.*, **51**, 855 (1984). Towards an Intermolecular Potential for Nitrogen.
22. J. P. Bowen and N. L. Allinger, in *Reviews in Computational Chemistry*, K. B. Lipkowitz and D. B. Boyd, Eds., VCH Publishers, New York, 1991, Vol. 2, pp. 81–97. Molecular Mechanics: The Art and Science of Parameterization.

23. U. Dinur and A. T. Hagler, in *Reviews in Computational Chemistry*, K. B. Lipkowitz and D. B. Boyd, Eds., VCH Publishers, New York, 1991, Vol. 2, pp. 99–164. New Approaches to Empirical Force Fields.
24. A. K. Dham and W. J. Meath, *Mol. Phys.*, **88**, 339 (1996). Multi-Property Predictions from Recent He–CO Potential-Energy Surfaces and Related Comments on the Nature of Heteronuclear Rare Gas Interactions.
25. A. J. Stone and C. S. Tong, *J. Comput. Chem.*, **15**, 1377 (1994). Anisotropy of Atom–Atom Repulsions.
26. A. J. Pertsin and A. I. Kitaigorodsky, *The Atom–Atom Potential Method: Applications to Organic Molecular Solids*, Springer-Verlag, Berlin, 1987.
27. X. Daura, A. E. Mark, and W. F. van Gunsteren, *J. Comput. Chem.*, **19**, 535 (1998). Parameterization of Aliphatic CH_n United Atoms of GROMOS96 Force Field.
28. A. T. Hagler, E. Huler, and S. Lifson, *J. Am. Chem. Soc.*, **96**, 5319 (1974). Energy Functions for Peptides and Proteins. I. Derivation of a Consistent Force-Field Including the Hydrogen Bond from Amide Crystals.
29. D. E. Williams and S. R. Cox, *Acta Crystallogr. B*, **40**, 404 (1984). Nonbonded Potentials for Azahydrocarbons: The Importance of the Coulombic Interaction.
30. S. R. Cox, L. Y. Hsu, and D. E. Williams, *Acta Crystallogr. A*, **37**, 293 (1981). Nonbonded Potential Function Models for Crystalline Oxohydrocarbons.
31. L.-Y. Hsu and D. E. Williams, *Acta Crystallogr. A*, **36**, 277 (1980). Intermolecular Potential Function Models for Crystalline Perchlorohydrocarbons.
32. D. E. Williams and D. J. Houpt, *Acta Crystallogr. B*, **42**, 286 (1986). Fluorine Nonbonded Potential Parameters Derived from Crystalline Perfluorocarbons.
33. D. E. Williams, in *Reviews in Computational Chemistry*, K. B. Lipkowitz and D. B. Boyd, Eds., VCH Publishers, New York, 1991, Vol. 2, pp. 219–271. Net Atomic Charge and Multipole Models for the Ab Initio Molecular Electric Potential.
34. G. Filippini and A. Gavezzotti, *Acta Crystallogr. B*, **49**, 868 (1993). Empirical Intermolecular Potentials for Organic-Crystals: The “6-Exp” Approximation Revisited.
35. A. Gavezzotti and G. Filippini, *J. Phys. Chem.*, **98**, 4831 (1994). Geometry of the Intermolecular X–H · · · Y (X, Y = N, O) Hydrogen-Bond and the Calibration of Empirical Hydrogen-Bond Potentials.
36. W. D. Cornell, P. Cieplak, C. I. Bayly, I. R. Gould, K. M. Merz Jr., D. M. Ferguson, D. C. Spellmeyer, T. Fox, J. W. Caldwell, and P. A. Kollman, *J. Am. Chem. Soc.*, **117**, 5179 (1995). A Second Generation Force-Field for the Simulation of Proteins, Nucleic Acids, and Organic Molecules.
37. S. J. Weiner, P. A. Kollman, D. A. Case, U. C. Singh, C. Ghio, G. Alagona, S. Profeta Jr., and P. Weiner, *J. Am. Chem. Soc.*, **106**, 765 (1984). A New Force Field for Molecular Mechanical Simulation of Nucleic Acids and Proteins.
38. B. R. Brooks, R. E. Brucolieri, B. D. Olafson, D. J. States, S. Swaminathan, and M. Karplus, *J. Comput. Chem.*, **4**, 187 (1983). CHARMM: A Program for Macromolecular Energy, Minimization and Dynamics Calculations.
39. J. G. C. M. van Duijneveldt-van de Rijdt and F. B. van Duijneveldt, in *Theoretical Treatments of Hydrogen Bonding*, D. Hadzi, Ed., Wiley, Chichester, 1997, pp. 13–47. Ab Initio Methods Applied to Hydrogen-Bonded Systems.
40. S. Scheiner, in *Reviews in Computational Chemistry*, K. B. Lipkowitz and D. B. Boyd, Eds., VCH Publishers, New York, 1991, Vol. 2, pp. 165–218. Calculating the Properties of Hydrogen Bonds by Ab Initio Methods.
41. D. Feller and E. R. Davidson, in *Reviews in Computational Chemistry*, K. B. Lipkowitz and D. B. Boyd, Eds., VCH Publishers, New York, 1990, Vol. 1, pp. 1–43. Basis Sets for Ab Initio Molecular Orbital Calculations and Intermolecular Interactions.
42. R. J. Bartlett and J. F. Stanton, in *Reviews in Computational Chemistry*, K. B. Lipowitz and D. B. Boyd, Eds., VCH Publishers, New York, 1994, Vol. 5, pp. 65–169. Applications of Post-Hartree–Fock Methods: A Tutorial.

43. D. K. W. Mok, N. C. Handy, and R. D. Amos, *Mol. Phys.*, **92**, 667 (1997). A Density Functional Water Dimer Potential Surface.
44. I. C. Hayes and A. J. Stone, *Mol. Phys.*, **53**, 83 (1984). An Intermolecular Perturbation Theory for the Region of Moderate Overlap.
45. B. Jeziorski, R. Moszynski, and K. Szalewicz, *Chem. Rev.*, **94**, 1887 (1994). Perturbation Theory Approach to Intermolecular Potential Energy Surfaces of van der Waals Complexes.
46. A. D. Buckingham, P. W. Fowler, and A. J. Stone, *Int. Rev. Phys. Chem.*, **5**, 107 (1986). Electrostatic Predictions of Shapes and Properties of van der Waals Molecules.
47. A. C. Legon and D. J. Millen, *Acc. Chem. Res.*, **20**, 39 (1987). Directional Character, Strength, and Nature of the Hydrogen Bond in Gas Phase Dimers.
48. G. J. B. Hurst, P. W. Fowler, A. J. Stone, and A. D. Buckingham, *Int. J. Quantum Chem.*, **29**, 1223 (1986). Intermolecular Forces in van der Waals Dimers.
49. K. R. Leopold, G. T. Fraser, S. E. Novick, and W. Klempner, *Chem. Rev.*, **94**, 1807 (1994). Current Themes in Microwave and Infrared-Spectroscopy of Weakly-Bound Complexes.
50. S. L. Price and A. J. Stone, *J. Chem. Phys.*, **86**, 2859 (1987). The Electrostatic Interactions in van der Waals Complexes Involving Aromatic Molecules.
51. C. A. Haynam, D. V. Brumbaugh, and D. H. Levy, *J. Chem. Phys.*, **79**, 1581 (1983). Dimers in Jet-Cooled *s*-Tetrazine Vapor: Structure and Electronic Spectra.
52. G. R. Desiraju, *Angew. Chem., Int. Ed. Eng.*, **34**, 2311 (1995). Supramolecular Synths in Crystal Engineering—A New Organic Synthesis.
53. C. B. Aakeroy, *Acta Crystallogr. B*, **53**, 569 (1997). Crystal Engineering: Strategies and Architectures.
54. F. H. Allen, J. E. Davies, J. J. Galloy, O. Johnson, O. Kennard, C. F. Macrae, E. M. Mitchell, G. F. Mitchell, J. M. Smith, and D. G. Watson, *J. Chem. Info. Comput. Sci.*, **31**, 187 (1991). The Development of Version 3 and Version 4 of the Cambridge Structural Database System.
55. F. C. Bernstein, T. F. Koetzle, G. J. B. Williams, E. F. Meyer, M. D. Brice, J. R. Rodgers, O. Kennard, T. Shimanouchi, and M. Tasumi, *J. Mol. Biol.*, **112**, 535 (1972). The Protein Databank.
56. I. J. Bruno, J. C. Cole, J. P. M. Lommerse, R. S. Rowland, R. Taylor, and M. L. Verdonk, *J. Comput.-Aided Mol. Des.*, **11**, 525 (1997). IsoStar: A Library of Information About Non-bonded Interactions.
57. J. Singh and J. M. Thornton, *Atlas of Protein Side-Chain Interactions*, IRL Press, Oxford, 1992. See also: R. A. Laskowski, J. Singh, and J. M. Thornton, <http://biochem.ucl.ac.uk/bsm/sidechains>.
58. R. Taylor, O. Kennard, and W. Versichel, *J. Am. Chem. Soc.*, **105**, 5761 (1983). Geometry of the N—H · · · O=C Hydrogen-Bond. 1. Lone-Pair Directionality.
59. J. D. Dunitz and R. Taylor, *Chem. Euro. J.*, **3**, 89 (1997). Organic Fluorine Hardly Ever Accepts Hydrogen Bonds.
60. D. W. M. Hofmann and T. Lengauer, *J. Mol. Model.*, **4**, 132 (1998). Crystal Structure Prediction Based on Statistical Potentials.
61. J. B. O. Mitchell, C. L. Nandi, J. M. Thornton, S. L. Price, J. Singh, and M. Snarey, *J. Chem. Soc., Faraday Trans.*, **89**, 2619 (1993). A Comparison of Three Theoretical Approaches to the Study of Side-Chain Interactions in Proteins.
62. C. A. Hunter, J. Singh, and J. M. Thornton, *J. Mol. Biol.*, **218**, 837 (1991). π – π Interactions: The Geometry and Energetics of Phenylalanine–Phenylalanine Interactions in Proteins.
63. J. P. M. Lommerse, A. J. Stone, R. Taylor, and F. H. Allen, *J. Am. Chem. Soc.*, **118**, 3108 (1996). The Nature and Geometry of Intermolecular Interactions Between Halogens and Oxygen or Nitrogen.
64. J. P. M. Lommerse, S. L. Price, and R. Taylor, *J. Comput. Chem.*, **18**, 757 (1997). Hydrogen Bonding of Carbonyl, Ether, and Ester Oxygen Atoms with Alkanol Hydroxyl Groups.
65. F. H. Allen, J. P. M. Lommerse, V. J. Hoy, J. A. K. Howard, and G. R. Desiraju, *Acta Crystallogr. B*, **53**, 1006 (1997). Halogen · · · O(Nitro) Supramolecular Synthon in Crystal

- Engineering: A Combined Crystallographic Database and Ab Initio Molecular Orbital Study.
- 66. I. Nobel, S. L. Price, J. P. M. Lommerse, and R. Taylor, *J. Comput. Chem.*, **18**, 2060 (1997). Hydrogen Bonding Properties of Oxygen and Nitrogen Acceptors in Aromatic Heterocycles.
 - 67. I. Nobel, S. L. Yeoh, S. L. Price, and R. Taylor, *Chem. Phys. Lett.*, **280**, 196 (1997). On the Hydrogen Bonding Abilities of Phenols and Anisoles.
 - 68. H. J. Bohm, S. Brode, U. Hesse, and G. Klebe, *Chem. Euro. J.*, **2**, 1509 (1996). Oxygen and Nitrogen in Competitive Situations: Which Is the Hydrogen-Bond Acceptor?
 - 69. M. D. Beachy, D. Chasman, R. B. Murphy, T. A. Halgren, and R. A. Friesner, *J. Am. Chem. Soc.*, **119**, 5908 (1997). Accurate Ab Initio Quantum Chemical Determination of the Relative Energetics of Peptide Conformations and Assessment of Empirical Force Fields.
 - 70. S. C. Nyburg and C. H. Faerman, *Acta Crystallogr. B*, **41**, 274 (1985). A Revision of van der Waals Atomic Radii for Molecular Crystals—N, O, F, S, Cl, Se, Br and I Bonded to Carbon.
 - 71. S. A. Peebles, P. W. Fowler, and A. C. Legon, *Chem. Phys. Lett.*, **240**, 130 (1995). Anisotropic Repulsion in Complexes $B \cdots Cl_2$ and $B \cdots HCl$: the Shape of the Chlorine Atom in a Molecule.
 - 72. G. R. Desiraju and R. Parthasarathy, *J. Am. Chem. Soc.*, **111**, 8725 (1989). The Nature of Halogen \cdots Halogen Interactions. Are Short Halogen Contacts Due to Specific Attractive Forces or Due to Close Packing of Nonspherical Atoms?
 - 73. S. L. Price and A. J. Stone, *Mol. Phys.*, **47**, 1457 (1982). The Anisotropy of the $Cl_2 \cdots Cl_2$ Pair Potential as Shown by the Crystal Structure. Evidence for Intermolecular Bonding or Lone Pair Effects?
 - 74. R. J. Wheatley and S. L. Price, *Mol. Phys.*, **71**, 1381 (1990). A Systematic Intermolecular Potential Method Applied to Chlorine.
 - 75. E. D. Stevens, *Mol. Phys.*, **37**, 27 (1979). Experimental Electron Density Distribution of Molecular Chlorine.
 - 76. S. L. Price, A. J. Stone, J. Lucas, R. S. Rowland, and A. E. Thornley, *J. Am. Chem. Soc.*, **116**, 4910 (1994). The Nature of $—Cl \cdots Cl—$ Intermolecular Interactions.
 - 77. S. Suzuki, P. G. Green, R. E. Bumgarner, S. Dasgupta, W. A. Goddard III, and G. A. Blake, *Science*, **257**, 942 (1992). Benzene Forms Hydrogen Bonds with Water.
 - 78. D. A. Rodham, S. Suzuki, R. D. Suenram, F. J. Lovas, S. Dasgupta, W. A. Goddard III, and G. A. Blake, *Nature*, **362**, 735 (1993). Hydrogen Bonding in the Benzene Ammonia Dimer.
 - 79. K. Flanagan, J. Walshaw, S. L. Price, and J. M. Goodfellow, *Protein Eng.*, **8**, 109 (1995). Solvent Interactions with π Ring Systems in Proteins.
 - 80. J. B. O. Mitchell, C. L. Nandi, S. Ali, I. K. McDonald, J. M. Thornton, S. L. Price, and J. Singh, *Nature*, **366**, 413 (1993). Amino Aromatic Interactions.
 - 81. J. B. O. Mitchell, C. L. Nandi, I. K. McDonald, J. M. Thornton, and S. L. Price, *J. Mol. Biol.*, **239**, 315 (1994). Amino/Aromatic Interactions in Proteins—Is the Evidence Stacked Against Hydrogen-Bonding?
 - 82. G. R. Desiraju, *Acc. Chem. Res.*, **24**, 290 (1991). The C—H \cdots O Hydrogen-Bond in Crystals—What Is It?
 - 83. T. Steiner and G. R. Desiraju, *J. Chem. Soc., Chem. Commun.*, 891 (1998). Distinction Between the Weak Hydrogen Bond and the van der Waals Interaction.
 - 84. S. L. Price, F. Lo Celso, J. A. Treichel, J. M. Goodfellow, and Y. Umrania, *J. Chem. Soc., Faraday Trans.*, **89**, 3407 (1993). What Base Pairings Can Occur in DNA? A Distributed Multipole Study of the Electrostatic Interactions Between Normal and Alkylated Nucleic Acid Bases.
 - 85. J. T. Brobjer and J. N. Murrell, *Mol. Phys.*, **50**, 855 (1983). The Intermolecular Potential of HF.
 - 86. S. L. Price, *Mol. Phys.*, **58**, 651 (1986). The Limitations of Isotropic Site–Site Potentials to Describe a N_2 – N_2 Intermolecular Potential Surface.
 - 87. S. L. Price, *Philos. Mag. B*, **73**, 95 (1996). Anisotropic Atom–Atom Potentials.

88. C. Bissonnette, C. E. Chuaqui, K. G. Crowell, R. J. Leroy, R. J. Wheatley, and W. J. Meath, *J. Chem. Phys.*, **105**, 2639 (1996). A Reliable New Potential-Energy Surface for H₂ . . . Ar.
89. A. J. Stone and M. Alderton, *Mol. Phys.*, **56**, 1047 (1985). Distributed Multipole Analysis—Methods and Applications.
90. W. A. Sokalski and A. Sawaryn, *THEOCHEM (J. Mol. Struct.)* **88**, 91 (1992). Cumulative Multicenter Multipole Moment Databases and Their Applications.
91. G. Jansen, C. Hattig, B. A. Hess, and J. G. Angyan, *Mol. Phys.*, **88**, 69 (1996). Intermolecular Interaction Energies by Topologically Partitioned Electric Properties. 1. Electrostatic and Induction Energies in One-Center and Multicenter Multipole Expansions.
92. C. R. Le Sueur and A. J. Stone, *Mol. Phys.*, **78**, 1267 (1993). Practical Schemes for Distributed Polarizabilities.
93. C. R. Le Sueur and A. J. Stone, *Mol. Phys.*, **83**, 293 (1994). Localization Methods for Distributed Polarizabilities.
94. A. J. Stone, C. Hattig, G. Jansen, and J. G. Angyan, *Mol. Phys.*, **89**, 595 (1996). Transferability of Topologically Partitioned Polarizabilities—The Case of *n*-Alkanes.
95. A. J. Stone and C. S. Tong, *Chem. Phys.*, **137**, 121 (1989). Local and Non-Local Dispersion Models.
96. C. Hattig, G. Jansen, B. A. Hess, and J. G. Angyan, *Mol. Phys.*, **91**, 145 (1997). Intermolecular Interaction Energies by Topologically Partitioned Electric Properties. 2. Dispersion Energies in One-Centre and Multicentre Multipole Expansions.
97. R. J. Wheatley and S. L. Price, *Mol. Phys.*, **69**, 507 (1990). An Overlap Model for Estimating the Anisotropy of Repulsion.
98. R. J. Wheatley and W. J. Meath, *Mol. Phys.*, **79**, 253 (1993). On the Relationship Between First Order Exchange and Coulomb Interaction Energies for Closed-Shell Atoms and Molecules.
99. R. J. Wheatley and J. B. O. Mitchell, *J. Comput. Chem.*, **15**, 1187 (1994). Gaussian Multipoles in Practice—Electrostatic Energies for Intermolecular Potentials.
100. C. G. Gray and K. E. Gubbins, *Theory of Molecular Fluids*, Clarendon Press, Oxford, 1984.
101. C. E. Dykstra, J. D. Augspurger, B. Kirtman, and D. J. Malik, in *Reviews in Computational Chemistry*, K. B. Lipkowitz and D. B. Boyd, Eds., VCH Publishers, New York, 1990, Vol. 1, pp. 83–118. Properties of Molecules by Direct Calculation.
102. S. L. Price, *Mol. Phys.*, **62**, 45 (1987). The Structure of the Homonuclear Diatomic Solids Revisited. A Distorted Atom Approach to the Intermolecular Potential.
103. F. Mulder and C. Huiszoon, *Mol. Phys.*, **34**, 1215 (1977). The Dimer Interaction and Lattice Energy of Ethylene and Pyrazine in the Multipole Expansion; A Comparison with Atom-Atom Potentials.
104. R. Wiest, V. Pichon-Pesme, M. Benard, and C. Lecomte, *J. Phys. Chem.*, **98**, 1351 (1994). Electron Distributions in Peptides and Related Molecules: Experimental and Theoretical Study of Leu-Enkephalin Trihydrate.
105. D. L. Cooper and N. C. J. Stutchbury, *Chem. Phys. Lett.*, **120**, 167 (1985). Distributed Multipole Analysis from Charge Partitioning by Zero-Flux Surfaces: The Structure of HF Complexes.
106. K. E. Laidig, *J. Phys. Chem.* **97**, 12760 (1993). General Expression for the Spatial Partitioning of the Moments and Multipole Moments of Molecular Charge Distributions.
107. F. L. Hirshfeld, *Theor. Chim. Acta*, **44**, 129 (1977). Bonded-Atom Fragments for Describing Molecular Charge Densities.
108. J. P. Ritchie, *J. Am. Chem. Soc.*, **107**, 1829 (1985). Electron Density Distribution Analysis for Nitromethane, Nitromethide, and Nitramide.
109. F. Vigne-Maeder and P. Claverie *J. Chem. Phys.*, **88**, 4934 (1988). The Exact Multicenter Multipolar Part of a Molecular Charge-Distribution and Its Simplified Representations.
110. R. J. Wheatley, *Chem. Phys. Lett.*, **208**, 159 (1993). A New Distributed Multipole Procedure for Linear Molecules.

111. W. A. Sokalski and A. Sawaryn, *J. Chem. Phys.*, **87**, 526 (1987). Correlated Molecular and Cumulative Atomic Multipole Moments.
112. R. S. Mulliken, *J. Chem. Phys.*, **23**, 1833 (1955). Electron Population Analysis on LCAO-MO Molecular Wavefunctions.
113. C. Chipot, J. G. Angyan, and C. Millot, *Mol. Phys.*, **94**, 881 (1998). Statistical Analysis of Distributed Multipoles Derived from Molecular Electrostatic Potentials.
114. A. J. Stone, *Chem. Phys. Lett.*, **83**, 233 (1981). Distributed Multipole Analysis, or How to Describe a Molecular Charge Distribution.
115. R. D. Amos, with contributions from I. L. Alberts, J. S. Andrews, S. M. Colwell, N. C. Handy, D. Jayatilaka, P. J. Knowles, R. Kobayashi, N. Koga, K. E. Laidig, P. E. Maslen, C. W. Murray, J. E. Rice, J. Sanz, E. D. Simandiras, A. J. Stone, and M. D. Su, CADPAC5: The Cambridge Analytical Derivatives Package, 5.0 ed., Cambridge, UK, 1992.
116. M. A. Spackman, *J. Chem. Phys.*, **85**, 6587 (1986). A Simple Quantitative Model of Hydrogen Bonding.
117. S. L. Price, A. J. Stone, and M. Alderton, *Mol. Phys.*, **52**, 987 (1984). Explicit Formulas for the Electrostatic Energy, Forces and Torques Between a Pair of Molecules of Arbitrary Symmetry.
118. C. Hattig and B. A. Hess, *Mol. Phys.*, **81**, 813 (1994). Calculation of Orientation-Dependent Double-Tensor Moments for Coulomb-Type Intermolecular Interactions.
119. P. L. A. Popelier, A. J. Stone, and D. J. Wales, *Faraday Discuss., Chem. Soc.*, **243** (1994). Topography of Potential-Energy Surfaces for van der Waals Complexes.
120. S. L. Price and A. J. Stone, *Chem. Phys. Lett.*, **98**, 419 (1983). A Distributed Multipole Analysis of the Charge Densities of the Azabenzenes Molecules.
121. S. L. Price, J. S. Andrews, C. W. Murray, and R. D. Amos, *J. Am. Chem. Soc.*, **114**, 8268 (1992). The Effect of Basis Set and Electron Correlation on the Predicted Electrostatic Interactions of Peptides.
122. S. R. Cox and D. E. Williams, *J. Comput. Chem.*, **2**, 304 (1981). Representation of the Molecular Electrostatic Potential By a Net Atomic Charge Model.
123. C. E. Dykstra, *Chem. Rev.*, **93**, 2339 (1993). Electrostatic Interaction Potentials in Molecular-Force Fields.
124. J. P. Ritchie and A. S. Copenhaver, *J. Comput. Chem.*, **16**, 777 (1995). Comparison of Potential-Derived Charge and Atomic Multipole Models in Calculating Electrostatic Potentials and Energies of Some Nucleic Acid Bases and Pairs.
125. S. L. Price and N. G. J. Richards, *J. Comput.-Aided Mol. Des.*, **5**, 41 (1991). On the Representation of Electrostatic Fields Around Ab Initio Charge Distributions.
126. G. Naray-Szabo and G. G. Ferenczy, *Chem. Rev.*, **95**, 829 (1995). Molecular Electrostatics.
127. E. Sigfridsson and U. Ryde, *J. Comput. Chem.*, **19**, 377 (1998). Comparison of Methods for Deriving Atomic Charges from the Electrostatic Potential and Moments.
128. M. M. Franci and L. E. Chirlian, in *Reviews in Computational Chemistry*, K. B. Lipkowitz and D. B. Boyd, Eds., Wiley-VCH, New York, 1999, pp. 1–31. The Pluses and Minuses of Mapping Atomic Charges to Electrostatic Potentials.
129. K. B. Wiberg and P. R. Rablen, *J. Comput. Chem.*, **14**, 1504 (1993). Comparison of Atomic Charges Derived Via Different Procedures.
130. J. G. Vinter, *J. Comput.-Aided Mol. Des.*, **10**, 417 (1996). Extended Electron Distributions Applied to the Molecular Mechanics of Some Intermolecular Interactions. 2. Organic Complexes.
131. R. W. Dixon and P. A. Kollman, *J. Comput. Chem.*, **18**, 1632 (1997). Advancing Beyond the Atom-Centered Model in Additive and Nonadditive Molecular Mechanics.
132. A. J. Stone and S. L. Price, *J. Phys. Chem.*, **92**, 3325 (1988). Some New Ideas in the Theory of Intermolecular Forces: Anisotropic Atom–Atom Potentials.
133. E. Fraschini and A. J. Stone, *J. Comput. Chem.*, **19**, 847 (1998). H–H Model Potential for Exchange Repulsion Energy of Methane Dimer.

134. C. Millot and A. J. Stone, *Mol. Phys.*, **77**, 439 (1992). Towards an Accurate Intermolecular Potential for Water.
135. C. Millot, J.-C. Soetens, M. T. C. Martins Costa, M. P. Hodges, and A. J. Stone, *J. Phys. Chem. A*, **102**, 754 (1998). Revised Anisotropic Site Potentials for the Water Dimer and Calculated Properties.
136. A. Wallqvist and R. D. Mountain, in *Reviews in Computational Chemistry*, K. B. Lipkowitz and D. B. Boyd, Eds., Wiley-VCH, New York, 1999, Vol. 13, pp. 132–182. Molecular Models of Water, Derivation and Description.
137. J. K. Gregory and D. C. Clary, *J. Phys. Chem.*, **100**, 18014 (1996). Structure of Water Clusters—The Contribution of Many-Body Forces, Monomer Relaxation, and Vibrational Zero-Point Energy.
138. M. P. Hodges, A. J. Stone, and E. C. Lago, *J. Phys. Chem. A*, **102**, 2455 (1998). Analytical Potentials for HF Dimer and Larger HF Clusters from Ab Initio Calculations.
139. A. Wallqvist, P. Ahlstrom, and G. Karlstrom, *J. Phys. Chem.*, **94**, 1649 (1990). A New Intermolecular Energy Calculation Scheme: Applications to Potential Surface and Liquid Properties of Water.
140. P. O. Astrand, A. Wallqvist, and G. Karlstrom, *J. Chem. Phys.*, **100**, 1262 (1994). Nonempirical Intermolecular Potentials for Urea–Water Systems.
141. N. Gresh, P. Claverie, and A. Pullman, *Theor. Chim. Acta*, **66**, 1 (1984). Theoretical Studies of Molecular Conformation. Derivation of an Additive Procedure for the Computation of Intramolecular Interaction Energies; Comparison with Ab Initio SCF Computations.
142. N. Gresh, A. Pullman, and P. Claverie, *Theor. Chim. Acta*, **67**, 11 (1985). Theoretical Studies of Molecular Conformation. 2. Application of the SIBFA Procedure to Molecules Containing Carbonyl and Carboxylate Oxygens and Amide Nitrogens.
143. N. Gresh, P. Claverie, and A. Pullman, *Int. J. Quantum Chem.*, **29**, 101 (1986). Intermolecular Interactions: Elaboration on an Additive Procedure Including an Explicit Charge-Transfer Contribution.
144. N. Gresh and D. R. Garner, *J. Comput. Chem.*, **17**, 1481 (1996). Comparative Binding Energetics of Mg^{2+} , Ca^{2+} , Zn^{2+} , and Cd^{2+} to Biologically Relevant Ligands—Combined Ab-Initio SCF Supermolecule and Molecular Mechanics Investigation.
145. W. A. Sokalski, A. H. Lowrey, S. Roszak, V. Lewchenko, J. Blaisdell, P. C. Hariharan, and J. J. Kaufman, *J. Comput. Chem.*, **7**, 693 (1986). Nonempirical Atom–Atom Potentials for Main Components of Intermolecular Interaction Energy.
146. T. A. Beu, U. Buck, J. G. Siebers, and R. J. Wheatley, *J. Chem. Phys.*, **106**, 6795 (1997). A New Intermolecular Potential for Hydrazine Clusters: Structures and Spectra.
147. U. Buck, J. G. Siebers, and R. J. Wheatley, *J. Chem. Phys.*, **108**, 20 (1998). Structure and Vibrational Spectra of Methanol Clusters from a New Potential Model.
148. D. S. Coombes, S. L. Price, D. J. Willock, and M. Leslie, *J. Phys. Chem.*, **100**, 7352 (1996). Role of Electrostatic Interactions in Determining the Crystal Structures of Polar Organic Molecules. A Distributed Multipole Study.
149. D. S. Coombes, G. K. Nagi, and S. L. Price, *Chem. Phys. Lett.*, **265**, 532 (1997). On the Lack of Hydrogen Bonds in the Crystal Structure of Alloxan.
150. S. L. Price and K. S. Wibley, *J. Phys. Chem. A*, **101**, 2198 (1997). Predictions of Crystal Packings for Uracil, 6-Azauracil, and Allopurinol: The Interplay Between Hydrogen Bonding and Close Packing.
151. P. Verwer and F. J. J. Leusen, in *Reviews in Computational Chemistry*, K. B. Lipkowitz and D. B. Boyd, Eds., Wiley-VCH, New York, 1998, Vol. 12, pp. 327–365. Computer Simulation to Predict Possible Crystal Polymorphs.
152. P. L. A. Popelier and A. J. Stone, *Mol. Phys.*, **82**, 411 (1994). Formulas for the 1st and 2nd Derivatives of Anisotropic Potentials with Respect to Geometrical Parameters.
153. D. J. Willock, S. L. Price, M. Leslie, and C. R. A. Catlow, *J. Comput. Chem.*, **16**, 628 (1995). The Relaxation of Molecular Crystal Structures Using a Distributed Multipole Electrostatic Model.

154. P. M. Rodger, A. J. Stone, and D. J. Tildesley, *J. Chem. Soc., Faraday Trans. II*, **83**, 1689 (1987). Atomic Anisotropy and the Structure of Liquid Chlorine.
155. P. M. Rodger, A. J. Stone, and D. J. Tildesley, *Mol. Phys.*, **63**, 173 (1988). The Intermolecular Potential of Chlorine—A Three Phase Study.
156. P. M. Rodger, A. J. Stone, and D. J. Tildesley, *Chem. Phys. Lett.*, **145**, 365 (1988). Intermolecular Interactions in Halogens—Bromine and Iodine.
157. P. M. Rodger, A. J. Stone, and D. J. Tildesley, *Mol. Simul.*, **8**, 145 (1992). Anisotropic Site-Site Potentials in Molecular Dynamics.
158. W. Smith and T. R. Forester, *J. Mol. Graphics*, **14**, 136 (1996). DL_Poly 2.0—A General Purpose Parallel Molecular Dynamics Simulation Package.
159. S. Yashonath, S. L. Price, and I. R. McDonald, *Mol. Phys.*, **64**, 361 (1988). A 6-Site Anisotropic Atom–Atom Potential Model for the Condensed Phases of Benzene.
160. U. Koch and E. Egert, *J. Comput. Chem.*, **16**, 937 (1995). An Improved Description of the Molecular Charge Density in Force Fields with Atomic Multipole Moments.
161. M. J. Dudek and J. W. Ponder, *J. Comput. Chem.*, **16**, 791 (1995). Accurate Modeling of the Intramolecular Electrostatic Energy of Proteins.
162. J. P. M. Lommerse, personal communication, 1997.
163. J. B. O. Mitchell and S. L. Price, *Chem. Phys. Lett.*, **180**, 517 (1991). On the Relative Strengths of Amide · · · Amide and Amide · · · Water Hydrogen Bonds.
164. C. H. Faerman and S. L. Price, *J. Am. Chem. Soc.*, **112**, 4915 (1990). A Transferable Distributed Multipole Model for the Electrostatic Interactions of Peptides and Amides.
165. M. Eisenstein, *Int. J. Quantum Chem.*, **33**, 127 (1988). SCF Deformation Densities and Electrostatic Potentials of Purines and Pyrimidines.
166. R. F. W. Bader, A. Larouche, C. Gatti, M. T. Carroll, P. J. Macdougall, and K. B. Wiberg, *J. Chem. Phys.*, **87**, 1142 (1987). Properties of Atoms in Molecules. Dipole Moments and Transferability of Properties.
167. J. Cioslowski and A. Nanayakkara, *J. Am. Chem. Soc.*, **115**, 11213 (1993). Similarity of Atoms in Molecules.
168. P. G. Mezey, *Int. Rev. Phys. Chem.*, **16**, 361 (1997). Quantum Chemistry of Macromolecular Shape.
169. P. D. Walker and P. G. Mezey, *J. Am. Chem. Soc.*, **115**, 12423 (1993). Molecular Electron-Density Lego Approach to Molecule Building.
170. V. Pichon-Pesme, C. Lecomte, and H. Lacheckar, *J. Phys. Chem.*, **99**, 6242 (1995). On Building a Data-Bank of Transferable Experimental Electron Density Parameters. Application to Polypeptides.
171. S. L. Price and A. J. Stone, *J. Chem. Soc., Faraday Trans.*, **88**, 1755 (1992). Electrostatic Models for Polypeptides: Can We Assume Transferability?
172. J. W. Essex, C. A. Reynolds, and W. G. Richards, *J. Am. Chem. Soc.*, **114**, 3634 (1992). Theoretical Determination of Partition Coefficients.
173. T. R. Stouch and D. E. Williams, *J. Comput. Chem.*, **13**, 622 (1992). Conformational Dependence of Electrostatic Potential Derived Charges of a Lipid Headgroup Glycerylphosphorylcholine.
174. C. A. Reynolds, J. W. Essex, and W. G. Richards, *Chem. Phys. Lett.*, **199**, 257 (1992). Errors in Free-Energy Perturbation Calculations Due to Neglecting the Conformational Variation of Atomic Charges.
175. T. R. Stouch and D. E. Williams, *J. Comput. Chem.*, **14**, 858 (1993). Conformational Dependence of Electrostatic Potential-Derived Charges: Studies of the Fitting Procedure.
176. W. J. Mortier, S. K. Ghosh, and S. Shankar, *J. Am. Chem. Soc.*, **108**, 4315 (1986). Electronegativity Equalization Method for the Calculation of Atomic Charges in Molecules.
177. A. K. Rappé and W. A. Goddard, *J. Phys. Chem.*, **95**, 3358 (1991). Charge Equilibration for Molecular-Dynamics Simulations.

178. A. C. T. van Duin, J. M. A. Baas, and B. van de Graaf, *J. Chem. Soc., Faraday Trans.*, **90**, 2881 (1994). Delft Molecular Mechanics—A New Approach to Hydrocarbon Force Fields: Inclusion of a Geometry-Dependent Charge Calculation.
179. U. Koch, P. L. A. Popelier, and A. J. Stone, *Chem. Phys. Lett.*, **238**, 253 (1995). Conformational Dependence of Atomic Multipole Moments.
180. U. Koch and A. J. Stone, *J. Chem. Soc., Faraday Trans.*, **92**, 1701 (1996). Conformational Dependence of the Molecular Charge Distribution and Its Influence on Intermolecular Interactions.
181. C. A. Reynolds, J. W. Essex, and W. G. Richards, *J. Am. Chem. Soc.*, **114**, 9075 (1992). Atomic Charges for Variable Molecular Conformations.
182. G. G. Ferenczy, P. J. Winn, and C. A. Reynolds, *J. Phys. Chem. A*, **101**, 5446 (1997). Toward Improved Force Fields. 2. Effective Distributed Multipoles.

CHAPTER 5

Nonequilibrium Molecular Dynamics

Christopher J. Mundy,^{*†} Sundaram Balasubramanian,[‡]
Ken Bagchi,^{*} Mark E. Tuckerman,[¶] Glenn J.
Martyna,[§] and Michael L. Klein^{*}

**Center for Molecular Modeling and the Department of Chemistry, University of Pennsylvania, Philadelphia, Pennsylvania 19104, †(present address): Max-Planck-Institut, für Festkörperforschung, Heisenbergstrasse 1, D-70569 Stuttgart, Germany, [‡]Chemistry and Physics of Materials Unit, Jawaharlal Nehru Center for Advanced Scientific Research, Jakkur P.O., Bangalore 560 064, India, [¶]Department of Chemistry and Courant Institute of Mathematical Sciences, New York University, New York, New York 10003, and [§]Department of Chemistry, Indiana University, Bloomington, Indiana 47405*

INTRODUCTION

Why Nonequilibrium Molecular Dynamics?

We begin this chapter by making it clear that equilibrium molecular dynamics techniques are important. The methodology of dynamics, per se, has

Reviews in Computational Chemistry, Volume 14
Kenny B. Lipkowitz and Donald B. Boyd, Editors
Wiley-VCH, John Wiley and Sons, Inc., New York, © 2000

been around since the time of Sir Isaac Newton, but only in the last 40 years, with the advent of fast computers, could one conceive of computing physical properties of fluids from empirical force fields. The impact of computer simulation on our understanding of condensed matter systems is almost without measure. Besides being able to explain interesting experimental phenomena with the aid of a microscopic picture, it has also provided predictive power. As the name suggests, equilibrium molecular dynamics finds its success by being able to explain the equilibrium state. One can also learn about the dynamical nature of a system through equilibrium molecular dynamics.^{1,2} In fact, the first calculation of a dynamical property (diffusion constant) of a fluid was calculated with equilibrium molecular dynamics methods by Alder and Wainwright.^{3,4}

One easy extension of equilibrium molecular dynamics is the computation of the properties of condensed matter systems in the presence of external fields. Many experiments are done by applying an external field, whether it be an electric field, heat gradient, or some type of flow. Usually, the experimentalist waits some time for the system under investigation to reach a “steady state” in the presence of the applied field. Measurements are then performed to deduce structural or dynamical information. Performing this task on a computer is what is commonly known as nonequilibrium molecular dynamics (NEMD). It is nonequilibrium in the sense that, in the presence of an external field, the system at the steady state will be in a state of lower entropy. Upon removing the external field, the system will return to the state of maximum entropy or the equilibrium state.

NEMD provides the framework to perform simulations in the way that the experiment is done in the laboratory. Further, it can provide structural information as a function of the external field strength, clearly a task that equilibrium dynamics is incapable of accomplishing. One of the prominent applications of the NEMD method has been the calculation of the shear viscosity of fluids. Besides being of general interest to physical chemists, methods used to obtain accurate physical properties of fluids are of great importance to industry, where the methodology could aid in the design of new lubricants as an example. Lees and Edwards provided the framework to simulate a fluid in the presence of a flow.⁵ Using linear phenomenological relations (to be discussed later), one can obtain the shear viscosity of simple atomic fluids with relatively little computational effort. The issue of whether NEMD methods or equilibrium methods are “better” for computing dynamical properties of fluids is still unresolved. It is our hope that this chapter will provide the necessary background to permit the interested reader to reach an independent conclusion on this subject.

Equilibrium molecular dynamics was put on a firm theoretical ground with Andersen’s seminal paper on extended system dynamics (to be discussed in great detail later).⁶ NEMD found its first success in this area with the advent of the so-called DOLL’s (not an acronym) algorithm by Hoover and coworkers.⁷

This was the first time that Hamiltonian methods could be used to rigorously relate NEMD to the linear phenomenological transport relations. However, even with the immediate success of the DOLL's algorithm, its rigor could not be extended outside of the linear regimes. The extension of the DOLL's algorithm to the so-called SLLOD (DOLL's spelled backward, or transposed) algorithm by Evans and Morriss provided the missing link.⁸ It will be shown later that the SLLOD algorithm provides the correct behavior in both the linear and non-linear regime starting from equations of motion that are not derivable from an underlying Hamiltonian. The consequences of non-Hamiltonian dynamics on the thermodynamics of nonequilibrium steady states comprise a recent topic of debate. Hopefully, this chapter will provide insights into this issue.

Finally, with the advent of high speed computers, parallel architecture, and the popularity of extended system methods, NEMD has seen yet another resurgence. Researchers are beginning to access the resources that allow one to compute the physical properties of real lubricants. The aim of this chapter is to provide the theoretical and technical foundations to enable simulators to model realistic systems under nonequilibrium conditions.

Homogeneous Versus Inhomogeneous Methods

Whereas it is clear that nonequilibrium simulations are important in some circumstances, it is not clear that one needs to develop any special NEMD techniques. For example, imagine chemical engineers who wish to understand the behavior of a prototypical lubricant under shear. The most straightforward simulation would mimic the real experimental setup and would require only standard equilibrium MD methods. The fluid could be placed between two surfaces, and these surfaces could be given equal and opposite velocities, as shown in Figure 1. Standard Newtonian equations of motions would be sufficient to evolve the system in time.

Although intuitive, this approach suffers from two important drawbacks, the first of which deals with time scales. In the simulation described above, both the solid and the fluid atoms are initially at rest. At the start, the surfaces begin to move with the prescribed velocities, and the fluid particles will collide with the atoms of the walls. Through these collisions, momentum will be imparted to the fluid. Through secondary collisions between these "first-layer" fluid particles and other fluid particles, a velocity gradient will slowly be created. As can be guessed, the time needed to establish this gradient grows as the distance from the wall increases. Hence, a prohibitively long time may be spent developing a steady state.

The second drawback will be spatial inhomogeneities. In general, most simulations are concerned with "bulk" properties of a fluid. The presence of a surface, however, introduces some anisotropic behavior to the fluid. For exam-

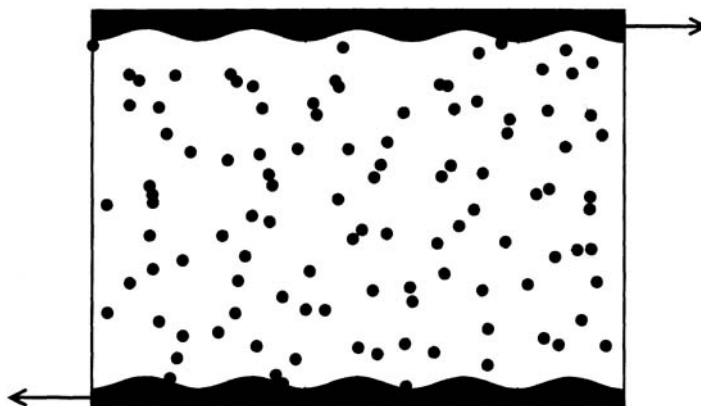


Figure 1 Intuitive simulation of two surfaces separated by a lubricant or other material. This model is designed to mimic experimental conditions.

ple, most interatomic interactions are highly repulsive at close distances. Hence, all the fluid particles that would otherwise be found within a few angstroms of a solid surface are pushed away from the wall. This leads to an abnormally high density of fluid particles just outside this “repulsive” region. To a lesser extent, other fluid particles are kept away from this first fluid layer, thereby creating a second layer, and so on. The effect on the density is shown in Figure 2. For prototypical lubricant fluids, this effect can be seen up to 30 Å from the wall. In experimental setups, in contrast, this effect is quite small. If we consider a one-cubic-centimeter cell filled with water, we can make a rough estimate of the number of water molecules that are within this distance from the wall. Each face of the cube perturbs a volume of $1 \text{ cm} \times 1 \text{ cm} \times 30 \text{ \AA}$. Neglecting some overlapping regions, the total from the six faces of the cube is then $6 \times 1 \text{ cm} \times 1 \text{ cm} \times 30 \text{ \AA}$. By using the ratio of this volume to the total volume of the cube (1 cm^3), we estimate that only one molecule in 10^6 will be affected by the walls. Hence, most properties that will be measured will reflect “bulk behavior.” By comparison, simulation system sizes are much smaller. With the use of parallel computers, it is now possible to do a simulation with 10^6 water molecules. Even at that size, only slightly more than half of the water molecules will be unaffected by walls.

Other kinds of inhomogeneity can also arise with this approach. For example, in experiments the container is placed in contact with a heat bath that regulates the temperature of the system. Shear motion tends to generate viscous heating, which is then conducted through the container wall and out to the heat bath. Hence, fluid particles closer to the wall will be colder than those farther away. If we limit ourselves to atomistic length scales, a simple hydrodynamic theory predicts that the maximum local temperature depends quadratically on the distance from the wall.⁹ The combination of these and other inhomogene-

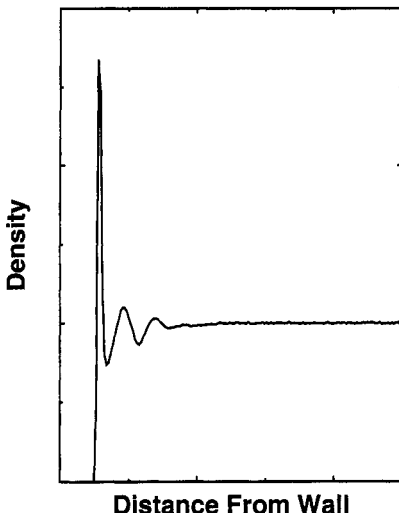


Figure 2 The effect of surfaces on fluid density as a function of distance from the wall.

ties means that prohibitively large simulations will be needed to obtain bulk behavior. Hence, such an approach must be limited to simulations that focus on the effects of extreme confinement on a fluid and not on bulk properties.

Thus, the “intuitive” inhomogeneous simulations require both excessively large system sizes and run times. Given these complications, the remainder of this chapter focuses on the use of homogeneous methods to study nonequilibrium systems. Examples of such methods include the use of fields to induce flows and uniform thermostats to control temperature. Because these approaches are no longer an atomistic mimic of the true experimental conditions, it is reasonable to ask whether these homogeneous runs will in fact give the “correct” answer that would have been found had we the computer power to do the inhomogeneous simulations in the first place.

To address this, Liem, Brown, and Clarke¹⁰ simulated in excess of 40,000 particles interacting via a Weeks–Chandler–Andersen (WCA) potential.¹¹ While the x and z directions were treated normally, the y direction was divided into three regions: two atomistic walls separated by a fluid region. The walls consisted of three hexagonally close-packed layers of particles. The wall atoms interacted with the fluid particles and with each other through the same WCA potential used for the fluid–fluid interactions. Additionally, each wall particle felt a harmonic potential centered at its triangular lattice site. This setup allowed heat transfer from the fluid to the wall while allowing the wall to remain crystalline. The momenta of the wall particles were rescaled to keep the total

instantaneous kinetic energy of the wall fixed. This effectively created a boundary with infinite heat capacity.

A velocity gradient in the y direction was induced by uniformly translating all the atoms in the top wall in the $+x$ direction and all the atoms in the bottom wall in the $-x$ direction, at a velocity set by the prescribed shear rate. Liem, Brown, and Clarke found that several key properties, such as temperature and viscosity, strongly depended on y , that is, the distance from the wall. For a few values of y that were far from the walls, the authors computed the local temperature, shear rate, and density. These three parameters were used to do homogeneous simulations (SLLOD dynamics,¹² to be discussed later). The pressure tensor computed globally from the SLLOD runs and the values locally computed in the “wall” setup agreed within error bars. Hence, for small to moderate shear rates, the results of the homogeneous and inhomogeneous methods are comparable. In addition to this empirical evidence, we will shortly demonstrate that the homogeneous methods also enjoy a strong theoretical foundation.

Hopefully, we have hinted that there are interesting nonequilibrium systems that can be explored using homogeneous, field-driven simulations. Because these approaches are often extensions of equilibrium methods, it is natural to first present the equilibrium foundation, as is done in the next section. From there, we will be able to develop the theoretical basis for NEMD simulations and practical guidelines for implementing them. Once the tools are in place, we will discuss applications and the kinds of question that can be tackled by NEMD methods.

MOLECULAR DYNAMICS AND EQUILIBRIUM STATISTICAL MECHANICS

Microscopic Motion and Macroscopic Observables

Perhaps one of the greatest successes of the molecular dynamics (MD) method is its ability both to predict macroscopically observable properties of systems, such as thermodynamic quantities, structural properties, and time correlation functions, and to allow modeling of the microscopic motions of individual atoms. From modeling, one can infer detailed mechanisms of structural transformations, diffusion processes, and even chemical reactions (using, for example, the method of ab initio molecular dynamics).¹³ Such information is extremely difficult, if not impossible, to obtain experimentally, especially when detailed behavior of a local defect is sought. The variety of different experimental conditions that can be mimicked in an MD simulation, such as

constant temperature T , constant volume V , constant pressure P , or constant stress, corresponding to the different statistical ensembles, further enhances the predictive power of MD. Often, these conditions are controlled through the use of *continuous* dynamical evolution by the introduction of non-Hamiltonian equations of motion. Although this concept was introduced nearly two decades ago,^{6,14} a proper understanding of the connection between non-Hamiltonian dynamics and statistical mechanics is only now emerging.¹⁵ This section discusses and reviews various aspects of both Hamiltonian and non-Hamiltonian dynamics and their connection to equilibrium statistical mechanics. It will be seen how non-Hamiltonian evolution affects the geometry of phase space and thereby the calculation of observable properties. Examples of the use of both Hamiltonian and non-Hamiltonian equations of motion in the generation of different statistical ensembles will be presented.

Hamiltonian Dynamics

Consider a classical N -particle system in d dimensions in isolation from any external influences. The system is considered to have N_f total degrees of freedom, which, in general, can differ from dN . If, for example, there are N_c constraints on the system, then $N_f = dN - N_c$. The physical state of such a system is defined by specifying at any time t the complete set of coordinates $\mathbf{q}(t) \equiv \{\mathbf{q}_1(t), \dots, \mathbf{q}_N(t)\}$ and momenta $\mathbf{p}(t) \equiv \{\mathbf{p}_1(t), \dots, \mathbf{p}_N(t)\}$, with $\mathbf{p}_i = (m_i d\mathbf{q}_i / dt)$. If the system is truly in isolation, then the time evolution of the coordinates and momenta is normally prescribed by Hamilton's equations of motion

$$\dot{\mathbf{q}}_i = \frac{\partial H}{\partial \mathbf{p}_i} \quad \text{and} \quad \dot{\mathbf{p}}_i = \frac{\partial H}{\partial \mathbf{q}_i} \quad [1]$$

where $H(\mathbf{p}, \mathbf{q})$, the Hamiltonian, is the total energy of the system expressed as a function of the coordinates and momenta of the particles in the system. For an isolated (nonrelativistic) classical system, $H(\mathbf{p}, \mathbf{q})$ takes the form

$$H(\mathbf{p}, \mathbf{q}) = \sum_{i=1}^N \frac{\mathbf{p}_i^2}{2m_i} + U(\mathbf{q}_1, \dots, \mathbf{q}_N) \quad [2]$$

where $U(\mathbf{q}_1, \dots, \mathbf{q}_N) \equiv U(\mathbf{q})$ is the N -particle interaction potential. Hamilton's equations then become

$$\dot{\mathbf{q}}_i = \frac{\mathbf{p}_i}{m_i} \quad \text{and} \quad \dot{\mathbf{p}}_i = \frac{\partial U}{\partial \mathbf{q}_i} \quad [3]$$

or

$$m_i \ddot{\mathbf{q}}_i = -\frac{\partial U}{\partial \mathbf{q}_i} = \mathbf{F}(\mathbf{q}_1, \dots, \mathbf{q}_N) \equiv \mathbf{F}_i(\mathbf{q}) \quad [4]$$

where $\mathbf{F}_i(\mathbf{q}) = -\partial U/\partial \mathbf{q}_i$ is just the force on the i th particle due to all other particles in the system. Equations [3] and [4] illustrate explicitly the equivalence between Hamilton's and Newton's equations of motion. The equations of motion must be solved subject to a set of initial conditions on the coordinates and momenta, $\{\mathbf{q}(0), \mathbf{p}(0)\}$, which then determines a *unique* solution.

Note that the Hamiltonian is conserved by the classical equations of motion; that is, $H(\mathbf{p}(0), \mathbf{q}(0)) = H(\mathbf{p}(t), \mathbf{q}(t))$, or $dH/dt = 0$. The proof of this statement follows straightforwardly from the chain rule:

$$\begin{aligned} \frac{dH}{dt} &= \sum_{i=1}^N \left[\frac{\partial H}{\partial \mathbf{p}_i} \cdot \dot{\mathbf{p}}_i + \frac{\partial H}{\partial \mathbf{q}_i} \cdot \dot{\mathbf{q}}_i \right] \\ &= \sum_{i=1}^N \left[-\frac{\partial H}{\partial \mathbf{p}_i} \cdot \frac{\partial H}{\partial \mathbf{q}_i} + \frac{\partial H}{\partial \mathbf{q}_i} \cdot \frac{\partial H}{\partial \mathbf{p}_i} \right] \\ &= 0 \end{aligned} \quad [5]$$

where the second line follows from Hamilton's equations (Eqs. [1]).

Each coordinate and momentum vector is a d -dimensional vector, where d is the number of spatial dimensions. If the complete set of coordinates and momenta are collected into a single vector $\boldsymbol{\Gamma}_t = (\mathbf{q}_1(t), \dots, \mathbf{q}_N(t), \mathbf{p}_1(t), \dots, \mathbf{p}_N(t))$ a $2dN$ -dimensional vector results. This vector can be thought of as existing in an abstract $2dN$ -dimensional space, which is known as *phase space*. The axes of phase space are labeled by the Cartesian directions of each of coordinate and momentum vectors. Hamilton's equations prescribe the evolution of the phase space vector $\boldsymbol{\Gamma}_t$ in time. This evolution traces out a parametric curve or *trajectory* in the phase space. Conservation of the Hamiltonian by the dynamics, however, implies that not all of phase space is accessible to the system, but only the *constant energy hypersurface*, that is, the surface defined by $H(\mathbf{p}(t), \mathbf{q}(t)) = \text{constant}$. As an example, consider a one-dimensional harmonic oscillator with coordinate $q(t)$ and momentum $p(t)$, with $H(p, q) = p^2/2m + m\omega^2 q^2/2$. The phase space is two-dimensional with axes labeled by p and q . The condition, $H(\mathbf{p}(t), \mathbf{q}(t)) = \text{constant}$, defines an ellipse in phase space, shown in Figure 3. By solving the equations of motion, $\dot{q} = p/m$, $\dot{p} = -m\omega^2 q$, subject to the initial conditions $p(0)$ and $q(0)$, and plotting $p(t)$ versus $q(t)$, it can be seen that the dynamics does indeed generate this ellipse.

Hamilton's equations can be cast in the form of an equation for $\boldsymbol{\Gamma}_t$ by introducing the Poisson bracket $\{f, g\}$ between two functions on the phase space $f(\boldsymbol{\Gamma})$ and $g(\boldsymbol{\Gamma})$ ¹⁶:

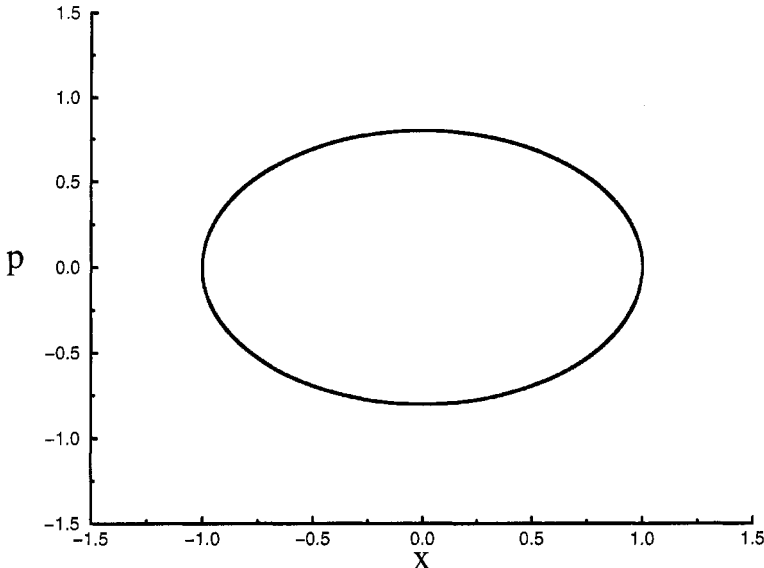


Figure 3 Phase space of a harmonic oscillator with Hamiltonian $H = p^2/2m + mw^2q^2/2$ for $m = 1$, $w = 0.8$, and initial conditions $x(0) = 1$, $p(0) = 0$.

$$\{f, g\} = \sum_{i=1}^N \left[\frac{\partial f}{\partial q_i} \cdot \frac{\partial g}{\partial p_i} - \frac{\partial f}{\partial p_i} \cdot \frac{\partial g}{\partial q_i} \right] \quad [6]$$

Then, it is straightforward to show that the phase space vector Γ_t evolves according to

$$\dot{\Gamma}_t = \{\Gamma_t, H\} \quad [7]$$

where the derivatives are taken to act at the phase space point $\Gamma_t = (q_1(t), \dots, q_N(t), p_1(t), \dots, p_N(t))$. Moreover, by defining an operator, $iL = \{\dots, H\}$, which acts on functions of the phase space variables, the equations of motion can be cast in the form

$$\dot{\Gamma}_t = iL\Gamma_t \quad [8]$$

Equation [8] can be solved, in principle, to yield the time evolution

$$\Gamma_t = e^{iLt}\Gamma_0 \quad [9]$$

where Γ_0 denotes the initial conditions on the phase space vector. The operator $\exp(iLt)$ is known as the classical propagator, and since operators such as $-i\partial/\partial q$

and $i\partial/\partial p$ are Hermitian, \mathbf{L} is also Hermitian. Thus, it follows that the propagator is unitary. Finally, by defining a gradient operator on the phase space

$$\frac{\partial}{\partial \Gamma} = \left(\frac{\partial}{\partial q_1}, \dots, \frac{\partial}{\partial q_N}, \frac{\partial}{\partial p_1}, \dots, \frac{\partial}{\partial p_N} \right) \quad [10]$$

the Liouville operator can be expressed as $i\mathbf{L} = \dot{\Gamma} \cdot \partial/\partial \Gamma$.

Consider now a large collection of systems, characterized by the same Hamiltonian, evolving in time according to Hamilton's equations. The initial conditions of each member of the group, or ensemble, are different and are assumed to be distributed according to a function $f(\Gamma, 0)$. Such a function is known as a phase space *distribution function*, and $f(\Gamma, 0)d\Gamma$ represents the number of ensemble members having an initial phase space vector $\Gamma_0 = \Gamma$ in a volume element $d\Gamma$ about the phase space point Γ . Given that each member of the ensemble evolves according to Hamilton's equations of motion, it is instructive to ask what the phase space distribution function $f(\Gamma, t)$ will be at a time t later.

To answer this, note that the total number of ensemble members, given by

$$\mathcal{N}(t) = \int d\Gamma f(\Gamma, t) \quad [11]$$

is constant; that is, systems are neither added to nor deleted from the ensemble. If Ω represents an arbitrary volume in phase space and S represents its surface, then the flux of members leaving the volume through the surface (i.e., in the direction \mathbf{n} of the surface normal) must be equal to the rate of decrease in the number of members in the volume, itself. Mathematically, this is expressed as:

$$-\frac{d}{dt} \int_{\Omega} d\Gamma f(\Gamma, t) = \int_S dS \mathbf{n} \cdot \dot{\Gamma} f(\Gamma, t) \quad [12]$$

where the expression on the left is the rate of decrease of the number of members in the volume and the expression on the right is the flux through the surface in the direction of the surface normal.^{17,18} Using the divergence theorem on the $6N$ -dimensional phase space, the surface integral can be converted into a volume integral of the divergence of $\dot{\Gamma}f(\Gamma, t)$, so that Eq. [12] becomes

$$\int_{\Omega} d\Gamma \left[\frac{\partial f}{\partial t} + \frac{\partial}{\partial \Gamma} \cdot [\dot{\Gamma} f(\Gamma, t)] \right] = 0 \quad [13]$$

Since the volume element in Eq. [13] is arbitrary, the expression in brackets, itself, must vanish:

$$\frac{\partial f}{\partial t} + \frac{\partial}{\partial \Gamma} \cdot [\dot{\Gamma} f(\Gamma, t)] = \frac{\partial f}{\partial t} + \dot{\Gamma} \cdot \frac{\partial f(\Gamma)}{\partial \Gamma} + f(\Gamma, t) \frac{\partial}{\partial \Gamma} \cdot \dot{\Gamma} = 0 \quad [14]$$

The quantity $\partial/\partial\Gamma \cdot \dot{\Gamma}$ is known as the *phase space compressibility*. For systems evolving according to Hamilton's equations of motion, the phase space compressibility vanishes:

$$\frac{\partial}{\partial\Gamma} \cdot \dot{\Gamma} = \sum_{i=1}^N \left[\frac{\partial}{\partial q_i} \cdot \dot{q}_i + \frac{\partial}{\partial p_i} \cdot \dot{p}_i \right] = \sum_{i=1}^N \left[\frac{\partial}{\partial q_i} \cdot \frac{\partial H}{\partial p_i} - \frac{\partial}{\partial p_i} \cdot \frac{\partial H}{\partial q_i} \right] = 0 \quad [15]$$

where Eqs. [1] have been used. Therefore, the equation of motion for $f(\Gamma, t)$ becomes

$$\frac{\partial f}{\partial t} + \dot{\Gamma} \cdot \frac{\partial f(\Gamma, t)}{\partial\Gamma} = \frac{df}{dt} = 0 \quad [16]$$

Equation [16] is known as the *Liouville equation* and is, in fact, a statement of the conservation of the phase space probability density. Indeed, it can be seen that the Liouville equation takes the form of a continuity equation for a flow field on the phase space satisfying the incompressibility condition $\partial/\partial\Gamma \cdot \dot{\Gamma} = 0$. Thus, given an initial phase space distribution function $f(\Gamma, 0)$ and some appropriate boundary conditions on the phase space satisfied by f , Eq. [16] can be used to determine $f(\Gamma, t)$ at any time t later.

Another important property of Hamiltonian systems can be deduced by considering the change in the volume element of phase space $d\Gamma$ as the ensemble evolves from an initial time $t = 0$ to a time t . Hamilton's equations of motion can be viewed as generating a transformation from an initial set of coordinates and momenta $\{q_1(0), \dots, q_N(0), p_1(0), \dots, p_N(0)\}$ to a set of coordinates and momenta $\{q_1(t), \dots, q_N(t), p_1(t), \dots, p_N(t)\}$ via the evolution operator $\exp(iLt)$ in Eq. [9]. We can, therefore, use this transformation to calculate the Jacobian that results when the volume element $d\Gamma_t$ for the phase space coordinates at time t is transformed into the volume element $d\Gamma_0$ for the phase space coordinates at $t = 0$. The volume element will transform according to

$$d\Gamma_t = \det\left(\frac{\partial\Gamma_t}{\partial\Gamma_0}\right) d\Gamma_0 = \mathcal{J}(\Gamma_t; \Gamma_0) d\Gamma_0 \quad [17]$$

where the determinant $\det(\partial\Gamma_t/\partial\Gamma_0) = \mathcal{J}(\Gamma_t; \Gamma_0)$ is the Jacobian of the transformation. An equation of motion for $\mathcal{J}(\Gamma_t; \Gamma_0)$ can be derived directly from the transformation and is given by

$$\frac{d\mathcal{J}(\Gamma_t; \Gamma_0)}{dt} = \mathcal{J}(\Gamma_t; \Gamma_0) \frac{\partial}{\partial\Gamma_t} \cdot \dot{\Gamma}_t \quad [18]$$

The details of this derivation can be found in Appendix 1. Note that the inverse Jacobian $\mathcal{J}(\Gamma_0; \Gamma_t)$ will satisfy an equation of motion of the form

$$\frac{d\mathcal{J}(\boldsymbol{\Gamma}_0; \boldsymbol{\Gamma}_t)}{dt} = -\mathcal{J}(\boldsymbol{\Gamma}_0; \boldsymbol{\Gamma}_t) \frac{\partial}{\partial \boldsymbol{\Gamma}_t} \cdot \dot{\boldsymbol{\Gamma}}_t \quad [19]$$

as a consequence of the fact that $\mathcal{J}(\boldsymbol{\Gamma}_0; \boldsymbol{\Gamma}_t)\mathcal{J}(\boldsymbol{\Gamma}_t; \boldsymbol{\Gamma}_0) = 1$. Equations [18] and [19] have the obvious initial condition that $\mathcal{J}(\boldsymbol{\Gamma}_0; \boldsymbol{\Gamma}_0) = 1$.

Since, for Hamiltonian systems, the phase space compressibility vanishes, Eqs. [18] and [19] have the solutions $\mathcal{J}(\boldsymbol{\Gamma}_0; \boldsymbol{\Gamma}_t) = \mathcal{J}(\boldsymbol{\Gamma}_t; \boldsymbol{\Gamma}_0) = 1$, from which it follows that the phase space volume element is the same at $t = 0$ as at an arbitrary time t :

$$d\boldsymbol{\Gamma}_t = d\boldsymbol{\Gamma}_0 \quad [20]$$

Thus, Hamilton's equations preserve the volume element on the phase space. In fact, this result is a statement of Liouville's theorem. Combining Eq. [16] with Eq. [20] leads to a statement that the probability of finding a member of the ensemble in a volume element $d\boldsymbol{\Gamma}$ about the point $\boldsymbol{\Gamma}$, which is just $f(\boldsymbol{\Gamma}, t)d\boldsymbol{\Gamma}$, is a conserved quantity:

$$f(\boldsymbol{\Gamma}_t, t)d\boldsymbol{\Gamma}_t = f(\boldsymbol{\Gamma}_0, 0)d\boldsymbol{\Gamma}_0 \quad [21]$$

The notion that there is a conserved probability is an important conclusion for relating the collection of systems evolving according to Hamilton's equations to a statistical ensemble that can be used to describe thermodynamic observables. If, in Eq. [16], $\partial f / \partial t = 0$, then the general solution of the Liouville equation is $f(\boldsymbol{\Gamma}) = f(H(\boldsymbol{\Gamma}))$, that is, any arbitrary function of the Hamiltonian. This assertion can be verified by direct substitution. In this case, $f(\boldsymbol{\Gamma})$ describes an *equilibrium ensemble*. Equilibrium ensembles are characterized by fixed values of certain thermodynamic control variables, such as the total energy E , total particle number N , temperature T , volume V , pressure P , or chemical potential μ . Well known examples are the *microcanonical* (NVE), the *canonical* (NVT), the *isothermal-isobaric* (NPT), and *grand-canonical* (μ VT) ensembles. The fundamental postulate upon which equilibrium statistical mechanics is based is that all microstates that give rise to the same set of macroscopic observables are equally probable. In the next section, we shall see how the conservation of probability in Hamiltonian systems allows one to use a dynamical trajectory in phase space to generate an equilibrium ensemble.

Relation to Microcanonical Ensemble

The microcanonical ensemble is characterized by fixed values of the thermodynamic variables: N , the total particle number, V , the volume of the system, and E , the total energy. The phase space distribution function for the microcanonical ensemble is

$$f(\Gamma) = \frac{1}{N! h^{N_f} \Omega(N, V, E)} \delta(H(\Gamma) - E) \quad [22]$$

where h is a constant having units of action (energy \times time), N_f is $d \times N$ with d being the number of spatial dimensions (it has been assumed that there are no constraints on the system, so $N_c = 0$), $\Omega(N, V, E)$ is the microcanonical partition function

$$\Omega(N, V, E) = \frac{1}{N! h^{N_f}} \int d\Gamma \delta(H(\Gamma) - E) \quad [23]$$

It can be seen from Eq. [22] that the microcanonical partition function is the totality of only those points in phase space (ensemble members) that belong to the constant energy surface defined by the condition $H(\Gamma) = E$. Indeed, an infinite collection of systems with initial conditions chosen from the constant energy surface constitutes a microcanonical ensemble, and to calculate $\Omega(N, V, E)$, one need only integrate over all the initial conditions corresponding to the individual members. On the other hand, since phase space probability is conserved under Hamiltonian evolution, a single dynamical system evolving according to Hamilton's equations of motion can also be used to generate this ensemble; that is, it can be viewed as generating a sampling of configurations on the constant energy hypersurface, each with the same probability weighting. A fundamental assumption is required, however, and it is that the phase space trajectory of this system is *ergodic*; that is, it visits *all* points of the constant energy surface given an infinite amount of time. If this basic assumption of ergodicity holds, then the microcanonical ensemble average of a physical observable $A(\Gamma)$:

$$\langle A \rangle = \frac{\int d\Gamma A(\Gamma) \delta(H(\Gamma) - E)}{\int d\Gamma \delta(H(\Gamma) - E)} \quad [24]$$

can be related to the time average of the same observable taken over the trajectory of the single dynamical system:

$$\bar{A} \equiv \lim_{T \rightarrow \infty} \frac{1}{T} \int_0^T dt A(\Gamma_t) \rightarrow \langle A \rangle \quad [25]$$

The same dynamical system can also be used to generate an equilibrium time correlation function $C_{AB}(t) \equiv \langle A(0)B(t) \rangle$. Since any physical observable can be shown to evolve according to

$$\frac{dA}{dt} = \{A, H\} = i\mathbf{L}A$$

$$A(t) = e^{i\mathbf{L}t}A(0) \quad [26]$$

the expression for $C_{AB}(t)$ is

$$C_{AB}(t) = \frac{\int d\Gamma A(\Gamma) e^{i\mathbf{L}t} B(\Gamma) \delta(H(\Gamma) - E)}{\int d\Gamma \delta(H(\Gamma) - E)} \quad [27]$$

In terms of a trajectory average, the time correlation function can be written as

$$C_{AB}(t) = \lim_{T \rightarrow \infty} \frac{1}{T-t} \int_0^{T-t} ds A(\Gamma_s) B(\Gamma_{t+s}) \quad [28]$$

In practice, Eqs. [25] and [28] are evaluated for a finite value of T that is long enough to ensure sufficient sampling of the constant energy surface, hence to converge averages and time correlation functions of properties under consideration. In addition, Eq. [23] should be evaluated only for $t \ll T$, to ensure the sampling of a large number of correlation times. However, t should be large enough that the time correlation function decays according to the well-known long-time result:^{17,19}

$$C_{AB}(t) \rightarrow \langle A \rangle \langle B \rangle \quad [29]$$

The ability to generate an equilibrium ensemble from a dynamical trajectory has a number of useful features. One can obtain not only ordinary static equilibrium properties from Eq. [25], but also dynamical information. In fact, dynamical information is available on two levels. On the one hand, equilibrium time correlation functions can be calculated, leading to the prediction of vibrational spectra, transport coefficients and so on. On the other, the trajectory allows access to the microscopic detailed motion of individual atoms. Therefore, one can, in a sense, “visualize” at an atomistic level the dynamical behavior of the system as a function of time, which can lead to valuable insights about chemical reaction mechanics, structural rearrangements, and other details of the system that can be captured only by visualization at this level of detail.

Non-Hamiltonian Dynamics

Given the possibility of generating the microcanonical ensemble from a dynamical trajectory, it is natural to ask whether other equilibrium ensembles can be generated in a similar manner. For many such ensembles, it cannot be

assumed that the system is in isolation. Rather, one assumes the presence of some external influence, such as a heat bath (thermostat) or a mechanical piston (barostat), which maintains the system at a constant temperature, pressure, and so on. These effects must somehow be accounted for in any set of dynamical equations proposed to generate these other ensembles and might, therefore, be best formulated in terms of *non-Hamiltonian* equations of motion. Similarly, the coupling of a system to an external field in order to drive a system away from equilibrium and establish a flow pattern within the system might also be expected to give rise to non-Hamiltonian equations of motion. Specific examples are given later in this and subsequent sections. First, however, it is instructive to examine certain aspects of non-Hamiltonian dynamical systems and to consider how they relate to the concepts of phase space and continuity.

Consider a general dynamical system described by the equations of motion

$$\dot{\Gamma} = \mathcal{F}(\Gamma) \quad [30]$$

where \mathcal{F} is a vector function on the phase space. The non-Hamiltonian nature of these equations means that the compressibility does not, in general, vanish:

$$\frac{\partial}{\partial \Gamma} \cdot \dot{\Gamma} = \frac{\partial}{\partial \Gamma} \cdot \mathcal{F} \equiv \kappa(\Gamma) \neq 0 \quad [31]$$

Accordingly, Eqs. [18] and [19] no longer have nontrivial [$\mathcal{J}(\Gamma_0; \Gamma_t) = \mathcal{J}(\Gamma_t; \Gamma_0) = 1$] solutions. In fact, since

$$\frac{d\mathcal{J}(\Gamma_t; \Gamma_0)}{dt} = \frac{\partial \mathcal{J}(\Gamma_t; \Gamma_0)}{\partial t} + \dot{\Gamma}_t \cdot \frac{\partial \mathcal{J}(\Gamma_t; \Gamma_0)}{\partial \Gamma_t} \quad [32]$$

the equation for the Jacobian becomes

$$\frac{\partial \mathcal{J}(\Gamma_t; \Gamma_0)}{\partial t} + \dot{\Gamma}_t \cdot \frac{\partial \mathcal{J}(\Gamma_t; \Gamma_0)}{\partial \Gamma_t} = \kappa(\Gamma_t) \mathcal{J}(\Gamma_t; \Gamma_0) \quad [33]$$

If $\mathcal{J}(\Gamma_t; \Gamma_0)$ has no explicit time dependence, as is expected in equilibrium, then the partial derivative with respect to time vanishes, and Eq. [33] becomes

$$\left(\dot{\Gamma}_t \cdot \frac{\partial}{\partial \Gamma_t} - \kappa(\Gamma_t) \right) \mathcal{J} = 0 \quad [34]$$

Since d/dt and $\dot{\Gamma}_t \cdot \partial/\partial \Gamma_t$ are now interchangeable, the general solution to Eq. [33] can be shown to be

$$\mathcal{J}(\Gamma_t; \Gamma_0) = \exp \left[\int_0^t \kappa(\Gamma_s) ds \right] \quad [35]$$

which clearly satisfies the initial condition $\mathcal{J}(\Gamma_0; \Gamma_0) = 1$. Note that the solution can also be written in the form

$$\begin{aligned} \mathcal{J}(\Gamma_t; \Gamma_0) &= e^{W(\Gamma_t) - W(\Gamma_0)} \\ &= e^{W(\Gamma_t)} e^{-W(\Gamma_0)} \end{aligned} \quad [36]$$

where $W(\Gamma)$ is a function on the phase space satisfying

$$\dot{W} = \kappa \quad [37]$$

The Jacobian tells how the volume element $d\Gamma$ transforms:

$$\begin{aligned} d\Gamma_t &= \frac{\partial \Gamma_t(\Gamma_0)}{\partial \Gamma_0} d\Gamma_0 \\ &= \mathcal{J}(\Gamma_t; \Gamma_0) d\Gamma_0 \\ &= e^{W(\Gamma_t)} e^{-W(\Gamma_0)} d\Gamma_0 \end{aligned} \quad [38]$$

Arranging Eq. [38] so that functions of Γ_t appear on one side and functions of Γ_0 appear on the other yields:

$$d\Gamma_t e^{-W(\Gamma_t)} = d\Gamma_0 e^{-W(\Gamma_0)} \quad [39]$$

Equation [39] implies that for a system with nonvanishing compressibility, the invariant volume is $d\Gamma e^{-W(\Gamma)}$. The number of ensemble members is given by integrating $f(\Gamma, t)$ over this volume element:

$$\mathcal{N}(t) = \int d\Gamma e^{-W(\Gamma)} f(\Gamma, t) \quad [40]$$

The function $e^{-W(\Gamma)}$ can be interpreted in the following way. Consider phase space to be a general space that is not necessarily Euclidean. Then, the measure on this space will be $d\Gamma \sqrt{g(\Gamma)}$, where $g(\Gamma)$ is the metric determinant. The requirement that there be an invariant measure on this space is tantamount to the condition

$$d\Gamma_0 \sqrt{g(\Gamma_0)} = d\Gamma_t \sqrt{g(\Gamma_t)} \quad [41]$$

Comparing Eqs. [41] and [39] leads to an identification of the metric determinant as

$$\sqrt{g(\Gamma)} = e^{-W(\Gamma)} \quad [42]$$

Thus, following the same steps that lead to Eqs. [13] and [14] leads to a new generalization of the Liouville equation:

$$\frac{\partial(f\sqrt{g(\Gamma)})}{\partial t} + \frac{\partial}{\partial \Gamma} \cdot (f\sqrt{g(\Gamma)}\dot{\Gamma}) = 0 \quad [43]$$

Equation [43] was first derived in Ref. 15, where we represented $\sqrt{g(\Gamma)}$ by a generic Jacobian function $J(\Gamma)$, and it represents a correct generalization of the Liouville equation to account for the nonvanishing compressibility of phase space. Equation [43] can be derived in many ways. A general approach starts with a statement of continuity valid for a space with *any* metric (see Appendix 2). One can examine the transformation from one set of phase space coordinates Γ to another Γ' . The metric determinant transforms²⁰ according to

$$\sqrt{g(\Gamma')} = \sqrt{g(\Gamma)} J(\Gamma; \Gamma') \quad [44]$$

Therefore, the transformation of the metric in time is given by

$$\sqrt{g(\Gamma_t)} = \sqrt{g(\Gamma_0)} J(\Gamma_0; \Gamma_t) \quad [45]$$

where $J(\Gamma_0; \Gamma_t)$ is the dynamical Jacobian satisfying Eq. [19]. Taking the time derivative of both sides shows that $\sqrt{g(\Gamma_t)}$ satisfies the differential equation

$$\frac{d\sqrt{g(\Gamma_t)}}{dt} = \sqrt{g(\Gamma_0)} \frac{dJ(\Gamma_0; \Gamma_t)}{dt} = -\sqrt{g(\Gamma_0)} J(\Gamma_0; \Gamma_t) \frac{\partial}{\partial \Gamma_t} \cdot \dot{\Gamma}_t = -\sqrt{g(\Gamma_t)} \frac{\partial}{\partial \Gamma_t} \cdot \dot{\Gamma}_t \quad [46]$$

where Eq. [19] has been used. Combining Eqs. [46] and [43] shows that by properly accounting for the effect of compressibility on the geometry (curvature) of phase space, a conserved probability density $f(\Gamma_t, t)$ can be defined on this space. Thus, since $df/dt = 0$, the following conservation law follows from Eq. [39]:

$$\begin{aligned} f(\Gamma_t, t)\sqrt{g(\Gamma_t)} d\Gamma_t &= f(\Gamma_0, 0)\sqrt{g(\Gamma_0)} d\Gamma_0 \\ f(\Gamma_t, t)e^{-W(\Gamma_t)} d\Gamma_t &= f(\Gamma_0, 0)e^{-W(\Gamma_0)} d\Gamma_0 \end{aligned} \quad [47]$$

The integration of any function $A(\Gamma)$ over the phase space must include the metric in the measure:

$$\int d\Gamma \sqrt{g(\Gamma)} A(\Gamma) \quad [48]$$

Thus, for example, the expectation value of A over the distribution function $f(\Gamma, t)$ would be

$$\langle A \rangle = \frac{\int d\Gamma \sqrt{g(\Gamma)} A(\Gamma) f(\Gamma, t)}{\int d\Gamma \sqrt{g(\Gamma)} f(\Gamma, t)} \quad [49]$$

The profound consequences of the microscopic formulation become manifest in nonequilibrium molecular dynamics and provide the mathematical structure to begin a theoretical analysis of nonequilibrium statistical mechanics. As discussed earlier, the equilibrium distribution function f_{eq} contains no explicit time dependence and can be generated by an underlying set of microscopic equations of motion. One can define the Gibbs entropy as the integral over the phase space of the quantity $f_{\text{eq}} \ln f_{\text{eq}}$. Since Eq. [48] shows how functions must be integrated over phase space, the Gibbs entropy must be expressed^{15,21,22} as follows:

$$S = -k_B \int d\Gamma \sqrt{g(\Gamma)} f_{\text{eq}} \ln f_{\text{eq}} \quad [50]$$

It follows trivially that $dS/dt = 0$ for all time in the equilibrium state. Thus, there is no purely microscopic mechanism that will give rise to entropy production, $dS/dt \geq 0$. The reason for this is that the phase space density f_{eq} accounts for all of the microstructure of phase space. In reality, we can never know this full microstructure, as was recognized by Ehrenfest, who suggested that one should work with a coarse-grained density, \hat{f}_{eq} , obtained by averaging over suitably small cells in phase space. Then one can define an entropy in analogy with Eq. [50], but in terms of \hat{f}_{eq} . In this way, entropy production can be realized microscopically, as discussed in detail in Ref. 23. Thus, the “fine-grained” entropy as defined in Eq. [50] always has a zero time derivative.

Now consider a situation of an equilibrium state that is subjected to a time-dependent field and allowed to come to a steady state in the presence of this field. One can imagine that this circumstance can be realized with a set of microscopic equations of motion coupled to a time-dependent external field (more details about this are given later in the chapter). These microscopic equations of motion will in general be more complicated and could have a time-dependent phase space compressibility that will lead to a time-dependent metric determinant. Thus, in general, both the distribution function generated by the dynamics and the metric determinant will have explicit time dependence, namely, $f(\Gamma, t)$ and $\sqrt{g(\Gamma, t)}$, respectively. The Gibbs entropy for a system coupled to a time-dependent field, $S(t)$, is defined to be the integral over the phase space of the quantity $f(\Gamma, t) \ln f(\Gamma, t)$. Again, Eq. [48] makes clear how functions must be integrated over the phase space, so the Gibbs entropy must be expressed^{15,21,22} as follows:

$$S(t) = -k_B \int d\Gamma \sqrt{g(\Gamma)} f(\Gamma, t) \ln f(\Gamma, t) \quad [51]$$

Equation [51] represents a fine-grained entropy and should therefore satisfy $dS/dt = 0$. Differentiating Eq. [51] with respect to time, one finds¹⁵

$$\begin{aligned} \frac{dS}{dt} &= -k_B \frac{d}{dt} \int d\Gamma \sqrt{g(\Gamma)} f(\Gamma, t) \ln f(\Gamma, t) \\ &= -k_B \int d\Gamma \frac{\partial \sqrt{g(\Gamma)}}{\partial t} f(\Gamma, t) \ln f(\Gamma, t) - k_B \int d\Gamma \sqrt{g(\Gamma)} [1 + \ln f(\Gamma, t)] \frac{\partial f(\Gamma, t)}{\partial t} \\ &= -k_B \int d\Gamma \frac{\partial \sqrt{g(\Gamma)}}{\partial t} f(\Gamma, t) \ln f(\Gamma, t) - k_B \int d\Gamma [1 + \ln f(\Gamma, t)] \frac{\partial}{\partial t} (f(\Gamma, t) \sqrt{g(\Gamma)}) \\ &\quad + k_B \int d\Gamma [1 + \ln f(\Gamma, t)] f(\Gamma, t) \frac{\partial \sqrt{g(\Gamma)}}{\partial t} \\ &= -k_B \int d\Gamma [1 + \ln f(\Gamma, t)] \frac{\partial}{\partial t} (f(\Gamma, t) \sqrt{g(\Gamma)}) + k_B \int d\Gamma f(\Gamma, t) \frac{\partial \sqrt{g(\Gamma)}}{\partial t} \end{aligned} \quad [52]$$

Then we use Eq. [43] to obtain

$$\begin{aligned} \frac{dS}{dt} &= k_B \int d\Gamma [1 + \ln f(\Gamma, t)] \frac{d}{d\Gamma} \cdot (\dot{\Gamma} f(\Gamma, t) \sqrt{g(\Gamma)}) + k_B \int d\Gamma f(\Gamma, t) \frac{\partial \sqrt{g(\Gamma)}}{\partial t} \\ &= -k_B \int d\Gamma \frac{\partial}{\partial \Gamma} [1 + \ln f(\Gamma, t)] \cdot (\dot{\Gamma} f(\Gamma, t) \sqrt{g(\Gamma)}) + k_B \int d\Gamma f(\Gamma, t) \frac{\partial \sqrt{g(\Gamma)}}{\partial t} \\ &= -k_B \int d\Gamma \frac{\partial}{\partial \Gamma} f(\Gamma, t) \cdot (\dot{\Gamma} \sqrt{g(\Gamma)}) + k_B \int d\Gamma f(\Gamma, t) \frac{\partial \sqrt{g(\Gamma)}}{\partial t} \\ &= k_B \int df(\Gamma, t) \left[\frac{\partial}{\partial \Gamma} \cdot \dot{\Gamma} \sqrt{g(\Gamma)} + \dot{\Gamma} \cdot \frac{\partial}{\partial \Gamma} \sqrt{g(\Gamma)} + \frac{\partial \sqrt{g(\Gamma)}}{\partial t} \right] \\ &= 0 \end{aligned} \quad [53]$$

where the final step was obtained by means of Eq. [46]. This result holds for a nonequilibrium system as well, once again, as a result of the fine-grained nature of Eq. [51].²³ It is well known that a suitable coarse-graining procedure applied to a fine-grained entropy yields an entropy that is consistent with Boltzmann's H -theorem.²³ Equation [51], therefore, gives an appropriate starting point for developing such a coarse-graining procedure.

Dynamical Generation of the NVT Ensemble

In a series of papers,^{24,25} Nosé showed that a Hamiltonian mechanics could be written down that would generate the distribution function for the NVT or canonical ensemble. The basic approach involves extending the phase space of the system, in a manner similar to that originally laid out by Andersen⁶ and by Parrinello and Rahman.¹⁴ Namely, in addition to the dN coordinates and dN momenta, where d is the number of spatial dimensions, an additional variable s , representing a heat bath, and its conjugate momentum p_s are included. The Hamiltonian for the extended system is given by

$$\begin{aligned} H_N(\mathbf{p}, p_s, \mathbf{q}, s) &= H(\mathbf{p}/s, \mathbf{q}) + \frac{p_s^2}{2Q} + (N_f + 1)k_B T \ln s \\ &= \sum_{i=1}^N \frac{\mathbf{p}_i^2}{2m_i s^2} + U(\mathbf{q}_1, \dots, \mathbf{q}_N) + \frac{p_s^2}{2Q} + (N_f + 1)k_B T \ln s \end{aligned} \quad [54]$$

where Q is a “mass parameter” (having units of energy \times time²) that determines the time scale on which the heat bath evolves. The variable s is referred to as the *Nosé thermostat*. The form of the Hamiltonian H_N is such that the microcanonical distribution generated by it is equivalent to a canonical distribution in H . To see this, consider the microcanonical partition function generated by H_N :

$$\begin{aligned} \Omega(N+1, V, E) &= C_{N+1} \int d\mathbf{p} d\mathbf{q} dp_s ds \delta(H_N - E) \\ &= C_{N+1} \int d\mathbf{p} d\mathbf{q} dp_s ds \delta\left(H(\mathbf{p}/s, \mathbf{q}) + \frac{p_s^2}{2Q} + (N_f + 1)k_B T \ln s - E\right) \end{aligned} \quad [55]$$

where $C_{N+1} = 1/[(N+1)!h^{N_f+1}]$. To perform the integrations over s and p_s in Eq. [55] analytically, we first change variables in the particle momenta integration according to $\mathbf{p}'_i = \mathbf{p}_i/s$. Then $d\mathbf{p} = s^{N_f} d\mathbf{p}'$, and Eq. [55] becomes

$$\Omega(N+1, V, E) = C_{N+1} \int d\mathbf{p}' d\mathbf{q} dp_s ds s^{N_f} \delta\left(H(\mathbf{p}', \mathbf{q}) + \frac{p_s^2}{2Q} + (N_f + 1)k_B T \ln s - E\right) \quad [56]$$

The integration over s can now be performed using the δ function and the identity

$$\delta(f(s)) = \frac{\delta(s - s_0)}{|f'(s_0)|} \quad [57]$$

where $f(s)$ is a function having a single zero at $s = s_0$. According to Eq. [56],

$$\begin{aligned}
 f(s) &= H(\mathbf{p}', \mathbf{q}) + \frac{p_s^2}{2Q} + (N_f + 1)k_B T \ln s - E \\
 f'(s) &= \frac{(N_f + 1)k_B T}{s} \\
 s_0 &= \frac{1}{(N_f + 1)k_B T} \left[E - H(\mathbf{p}', \mathbf{q}) - \frac{p_s^2}{2Q} \right]
 \end{aligned} \tag{58}$$

Substituting Eq. [58] into Eq. [56] gives^{24,25}

$$\begin{aligned}
 \Omega(N+1, V, E) &= \frac{C_{N+1}}{k_B T} \int d\mathbf{p}' d\mathbf{q} dp_s ds s^{N_f+1} \delta(s - s_0) \\
 &= \frac{C_{N+1}}{(N_f + 1)k_B T} \int d\mathbf{p}' d\mathbf{q} dp_s \exp \left[\frac{1}{k_B T} \left(E - H(\mathbf{p}', \mathbf{q}) - \frac{p_s^2}{2Q} \right) \right] \\
 &= \frac{C_{N+1} \sqrt{2\pi Q \beta}}{(N_f + 1)} e^{\beta E} \int d\mathbf{p}' d\mathbf{q} e^{-\beta H(\mathbf{p}', \mathbf{q})} \\
 &= \frac{C_{N+1} \sqrt{2\pi Q \beta} e^{\beta E}}{(N_f + 1) C_N} Q(N, V, T)
 \end{aligned} \tag{59}$$

where $\beta = 1/k_B T$, $Q(N, V, T)$ is the canonical partition function. Note that Eq. [59] is still a representation of the microcanonical partition function for the extended system. However, it depends parametrically on the desired temperature T through the Hamiltonian. Thus, one can regard it as an additional control variable. The temperature-dependent constants multiplying $Q(N, V, T)$ will not affect any averages of observable properties. They do affect thermodynamic derivatives with respect to β such as occur in the expressions for the total energy and heat capacity at constant volume. However, their effect can be determined analytically. Consider taking the derivative with respect to β to obtain an expression for the total internal energy of the canonical system:

$$U_\Omega = - \frac{\partial}{\partial \beta} \ln \Omega(N+1, V, E; \beta) \tag{60}$$

Then, using Eq. [59], one finds

$$\begin{aligned}
 U_\Omega &= - \frac{\partial}{\partial \beta} \ln Q(N, V, T) - E - \frac{k_B T}{2} \\
 - \frac{\partial}{\partial \beta} \ln Q(N, V, T) &= U_\Omega + E + \frac{k_B T}{2}
 \end{aligned} \tag{61}$$

The interpretation of this result is that to obtain the canonical energy of the system, one computes the thermodynamic derivative with respect to β of the extended-system microcanonical partition function and adds back $k_B T/2$ for the thermostat kinetic energy and a constant E , which merely changes the energy scale. Similarly, the heat capacity at constant volume is given by

$$\begin{aligned} C_\Omega &= -k_B \beta^2 \frac{\partial^2}{\partial \beta^2} \ln \Omega(N, V, E; \beta) \\ &= -k_B \beta^2 \frac{\partial^2}{\partial \beta^2} \ln Q(N, V, T) - \frac{k_B}{2} \quad [62] \\ -k_B \beta^2 \frac{\partial^2}{\partial \beta^2} \ln Q(N, V, T) &= C_\Omega + \frac{k_B}{2} \end{aligned}$$

where again the first term is the heat capacity of the true canonical ensemble. Thus, one only need add $k_B/2$ for the thermostat kinetic energy to the heat capacity that results from thermodynamic differentiation. The implication of the foregoing analysis is that the canonical distribution of H can be obtained by performing a dynamical simulation based on Eq. [54]. If the trajectory obtained is ergodic, then it will cover the constant energy surface, thus generating the microcanonical distribution of H_N , and hence the canonical distribution of H .

The equations of motion generated by H_N are:

$$\begin{aligned} \dot{\mathbf{q}}_i &= \frac{1}{s} \frac{\partial H}{\partial (\mathbf{p}_i/s)} \\ \dot{\mathbf{p}}_i &= - \frac{\partial H}{\partial \mathbf{q}_i} \\ \dot{s} &= \frac{p_s}{Q} \\ \dot{p}_s &= \frac{1}{s} \left[\left(\sum_{i=1}^N \frac{\partial H}{\partial (\mathbf{p}_i/s)} \cdot \frac{\mathbf{p}_i}{s} \right) - \frac{N_f + 1}{\beta} \right] \quad [63] \end{aligned}$$

The difficulty inherent in Eqs. [63] is the presence of \mathbf{p}_i/s . The analysis carried out above shows that a canonical distribution in $\mathbf{p}'_i = \mathbf{p}_i/s$ results. However, if we introduce such a noncanonical transformation into the equations of motion, the result is

$$\begin{aligned}
 \frac{d\mathbf{q}'_i}{dt/s} &= \frac{\partial H}{\partial \mathbf{p}'_i} \\
 \frac{\partial \mathbf{p}'_i}{dt/s} &= -\frac{\partial H}{\partial \mathbf{q}'_i} - \frac{1}{s} \frac{ds}{dt/s} \mathbf{p}'_i \\
 \frac{1}{s} \frac{ds}{dt/s} &= \frac{p_s}{Q} \\
 \frac{dp_s}{dt/s} &= \sum_{i=1}^{N_f} \frac{\partial H}{\partial \mathbf{p}'_i} \cdot \mathbf{p}'_i - \frac{N_f + 1}{\beta}
 \end{aligned} \tag{64}$$

which suggests an unusual time scaling by the variable s . To circumvent this problem, Hoover⁶ introduced a time scaling transformation $dt' = dt/s$ and a change of variables $\ln s = \eta$, resulting in the following non-Hamiltonian set of equations of motion:

$$\begin{aligned}
 \dot{\mathbf{q}}_i &= \frac{\partial H}{\partial \mathbf{p}_i} \\
 \dot{\mathbf{p}}_i &= -\frac{\partial H}{\partial \mathbf{q}_i} - \frac{p_\eta}{Q} \mathbf{p}_i \\
 \dot{\eta} &= \frac{p_\eta}{Q} \\
 \dot{p}_\eta &= \sum_{i=1}^{N_f} \frac{\partial H}{\partial \mathbf{p}_i} \cdot \mathbf{p}_i - N_f k_B T
 \end{aligned} \tag{65}$$

where, for simplicity, the primes have been dropped. p_η is the momentum corresponding to the variable η . These equations, known as the Nosé–Hoover equations, are non-Hamiltonian in form; however, they have the conserved energy:

$$H' = H(\mathbf{p}, \mathbf{q}) + \frac{p_\eta^2}{2Q} + N_f k_B T \eta \tag{66}$$

Although H' is conserved by the equations of motion, it clearly is not a Hamiltonian for Eqs. [65]. Since non-Hamiltonian systems tend to be more difficult than Hamiltonian systems to integrate stably numerically, the existence of a conserved energy for a non-Hamiltonian system is of vital importance as a check on the stability of the numerical integration scheme employed.

The basic mechanism inherent in the Nosé–Hoover equations of motion is that the variable p_η acts as a dynamic friction coefficient that controls the

fluctuations in the particle momenta, thereby allowing the total kinetic energy $\sum_i \mathbf{p}_i^2/2m$, to fluctuate but on the average to equal $N_f k_B T/2$. Indeed, one can see from Eqs. [65] that

$$\langle \dot{\mathbf{p}}_\eta \rangle = \left\langle \sum_{i=1}^{N_f} \frac{\partial H}{\partial \mathbf{p}_i} \right\rangle = 0 \quad [67]$$

so that the kinetic energy is guaranteed to have $N_f k_B T/2$ as its average if the trajectory is ergodic.

The phase space compressibility corresponding to Eqs. [65] can be seen to be

$$\frac{\partial}{\partial \Gamma} \cdot \dot{\Gamma} = \sum_{i=1}^{N_f} \left[\frac{\partial}{\partial \mathbf{p}_i} \cdot \dot{\mathbf{p}}_i + \frac{\partial}{\partial \mathbf{q}_i} \cdot \dot{\mathbf{q}}_i \right] = -N_f \frac{\dot{p}_\eta}{Q} \quad [68]$$

from which it follows that

$$\mathcal{J}(\Gamma_t; \Gamma_0) = e^{-N_f(n_t - n_0)} \quad [69]$$

and

$$\sqrt{g(\Gamma)} = e^{-W(\Gamma)} = e^{N_f n} \quad [70]$$

Equation [70] combined with the distribution function $f(\Gamma) = \delta(H' - E)$ gives a canonical distribution function in $H(\mathbf{p}, \mathbf{q})$:

$$\begin{aligned} & \frac{1}{N! h^{N_f}} \int d\mathbf{p}; d\mathbf{q}; d\eta \, dp_\eta \, e^{N_f n} \delta\left(H(\mathbf{p}, \mathbf{q}) + \frac{p_\eta^2}{2Q} + N_f k_B T \eta - E\right) \\ &= \frac{\beta e^{\beta E}}{N! h^{N_f} N_f} \int d\mathbf{p} \, d\mathbf{q} \, dp_\eta \, e^{-\beta H} e^{-\beta p_\eta^2/2Q} = \frac{\sqrt{2\pi Q \beta} e^{\beta E}}{N! h^{N_f} N_f} \int d\mathbf{p} \, d\mathbf{q} \, e^{-\beta H} \quad [71] \\ &= \frac{\sqrt{2\pi Q \beta} e^{\beta E}}{N_f} Q(N, V, T) \end{aligned}$$

It is, moreover, straightforward to show that $\sqrt{g(\Gamma)}$ together with $f(\Gamma) = \delta(H' - E)$ satisfies the time-independent form of Eq. [43]:

$$\frac{\partial}{\partial \Gamma} \cdot (\sqrt{g} f \dot{\Gamma}) = 0 \quad [72]$$

It was noted by Hoover²⁶ that Eqs. [65] are not guaranteed to yield ergodic trajectories, in which case a dynamical simulation based on these equations of motion would not generate a canonical distribution in $H(\mathbf{p}, \mathbf{q})$. This was seen most dramatically in the example of a single harmonic oscillator coupled to a Nosé–Hoover thermostat, where a distribution radically different from the correct canonical distribution was generated as a result of nonergodicity. Thus far, two different solutions to this problem based on continuous dynamics have been proposed.

The first of these, proposed by Martyna, Tuckerman, and Klein (MTK),²⁷ was based on the notion that the variable p_η , itself, has a canonical (Gaussian) distribution $\exp(-\beta p_\eta^2/Q)$. However, there is nothing in the equations of motion to control its fluctuations. MTK proposed that the Nosé–Hoover thermostat should, itself, be connected to a thermostat, and that this thermostat should also be connected to a thermostat. The result is that a “chain” of thermostats is introduced whereby each element of the chain controls the fluctuations of the element just preceding it. The equations of motion for such a thermostat chain are:

$$\begin{aligned}\dot{\mathbf{q}}_i &= \frac{\partial H}{\partial \mathbf{p}_i} \\ \dot{\mathbf{p}}_i &= -\frac{\partial H}{\partial \mathbf{q}_i} - \frac{p_{\eta_1}}{Q_1} \mathbf{p}_i \\ \dot{\eta}_i &= \frac{p_{\eta_i}}{Q_i} \\ \dot{p}_{\eta_i} &= \sum_{i=1}^N \frac{\partial H}{\partial \mathbf{p}_i} \cdot \mathbf{p}_i - N_f k_B T - \frac{p_{\eta_2}}{Q_2} p_{\eta_i} \\ \dot{p}_{\eta_i} &= \frac{p_{\eta_{i-1}}^2}{Q_{i-1}} - k_B T - \frac{p_{\eta_{i+1}}}{Q_{i+1}} p_{\eta_i} \quad i = 2, \dots, M-1 \\ \dot{p}_{\eta_M} &= \frac{p_{\eta_{M-1}}^2}{Q_{M-1}} - k_B T\end{aligned}\tag{73}$$

Equations [73], known as the Nosé–Hoover chain (NHC) or MTK equations, have the conserved energy:

$$H' = H(\mathbf{p}, \mathbf{q}) + \sum_{i=1}^N \frac{p_{\eta_i}^2}{2Q_i} + N_f k_B T \eta_1 + \sum_{i=2}^N k_B T \eta_i\tag{74}$$

The NHC equations of motion, which can be seen to describe a system of M thermostats “chained” together in succession, have been shown to give a correct

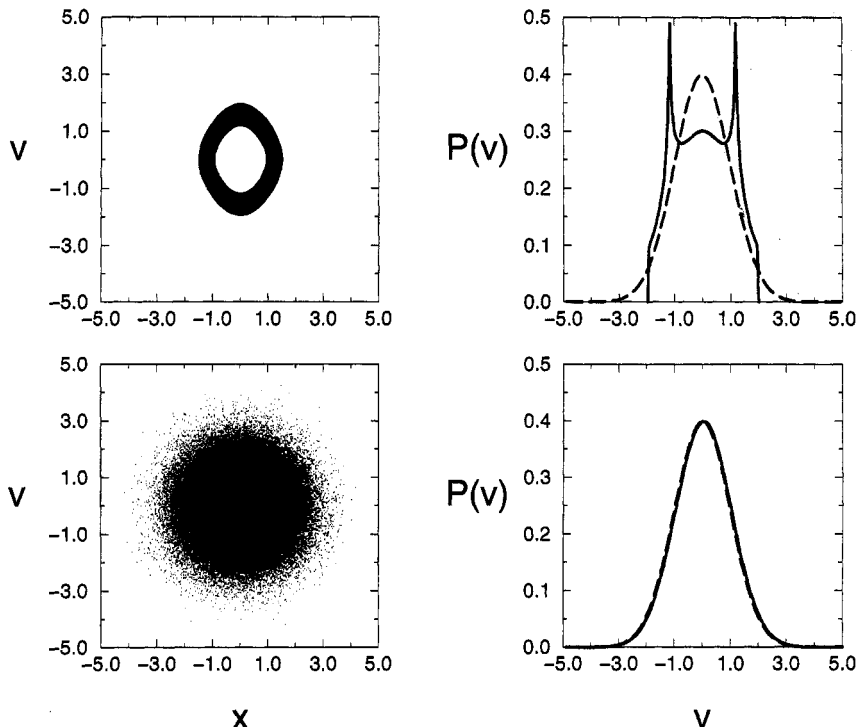


Figure 4 The left-hand column shows the Poincaré section v versus x of the phase space of a harmonic oscillator $H = p^2/2m + mw^2q^2/2$ with $m = 1$, $\omega = 1$ for Nosé-Hoover dynamics (top) (cf. Eqs. [65]) and for MTK dynamics (bottom) (cf. Eqs. [73]). The right-hand column shows the corresponding velocity distribution function. The solid curve in each plot is the distribution generated by the dynamics, and the dashed line is the analytical result.

canonical distribution both for systems containing large numbers of particles and for systems containing only a few degrees of freedom, including a single harmonic oscillator. Figure 4 demonstrates this fact, whereas Figure 5 shows that the equations of motion are being integrated accurately using the methods to be described in the later section on Numerically Integrating the SLLOD Equations.²⁸ Equations [73] have proved vital in simulations of proteins in the canonical ensemble,²⁹ as well as in implementations of path integral molecular dynamics.^{30,31} An example of the implementation for a simple atomic system is shown in Figure 6. All these examples, however, constitute equilibrium ensemble calculations, where $\langle \dot{p}_{\eta 1} \rangle = 0$. Hoover and Holian have pointed out³² that away from equilibrium, the NHC equations are not guaranteed to exhibit precise temperature control because $\langle \dot{p}_{\eta 1} \rangle$ may not average to zero. These authors have cited several examples of small nonequilibrium systems in which this

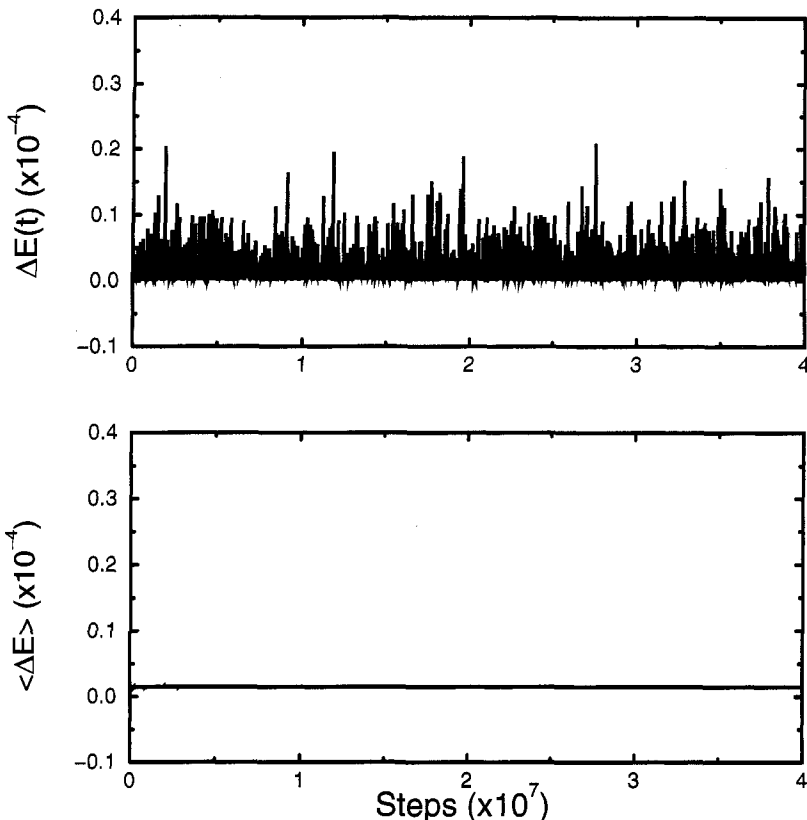


Figure 5 The instantaneous (*top*) and cumulative average (*bottom*) of the quantity $\Delta E = |E(t) - E(0)|/|E(0)|$ for the canonical harmonic oscillator of Figure 4 integrated with the Martyna–Tuckerman–Klein (MTK) thermostat using the integration techniques of Ref. 28.

has been the case. In large-scale systems, however, the NHC equations have exhibited satisfactory temperature control for all examples considered thus far.

Dynamical Generation of the *NPT* Ensemble

The original work of Andersen⁶ and of Parrinello and Rahman¹⁴ on the generation of the *NPT* or isothermal–isobaric ensemble using an extended phase space predates Nosé’s work on the *NVT* ensemble, as noted above. Applying the extended system method to generate the *NPT* ensemble involves the inclusion of the volume into the phase space as a dynamical variable along

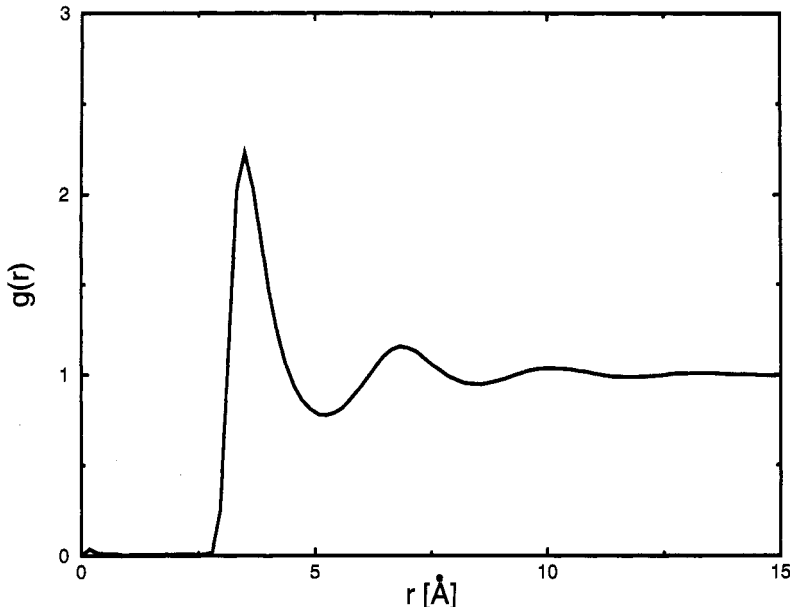


Figure 6 The radial distribution function for a Lennard-Jones model of liquid argon at a temperature $T = 300$ K. A simulation cell of 35 \AA containing 864 atoms with periodic boundary conditions was used. The simulation was carried out by coupling each degree of freedom to an MTK thermostat, and the equation of motion was integrated using the methods discussed in Ref. 28.

with a corresponding momentum. As such, it acts as a kind of barostat that maintains constant average pressure. However, it is necessary to incorporate a thermostat as well, so that the average temperature is kept fixed. Because of this, any Hamiltonian formulation of the problem will suffer from the same time scaling problems exhibited by the Nosé Hamiltonian. Although various non-Hamiltonian formulations of the *NPT* ensemble have been proposed, only recently has one been formulated that generates the correct phase space distribution for the *NPT* ensemble.

Recall that the partition function for the *NPT* ensemble is

$$\Delta(N, P, T) = \int_0^{\infty} dV e^{-\beta PV} Q(N, V, T) \quad [75]$$

where P is the applied pressure. To generate the distribution function corresponding to Eq. [75] Martyna, Tobias, and Klein³³ proposed the following equations of motion:

$$\begin{aligned}
 \dot{\mathbf{q}}_i &= \frac{\mathbf{p}_i}{m_i} + \frac{p_\epsilon}{W} \mathbf{q}_i \\
 \dot{\mathbf{p}}_i &= \mathbf{F}_i - \left(1 + \frac{d}{N_f}\right) \frac{p_\epsilon}{W} \mathbf{p}_i - \frac{p_\eta}{Q} \mathbf{p}_i \\
 \dot{V} &= \frac{dV p_\epsilon}{W} \\
 \dot{p}_\epsilon &= dV(P_{\text{int}} - P) + \frac{d}{N_f} \sum_{i=1}^N \frac{\mathbf{p}_i^2}{m_i} - \frac{p_\eta}{Q} p_\epsilon \\
 \dot{\eta} &= \frac{p_\eta}{Q} \\
 \dot{p}_\eta &= \sum_{i=1}^N \frac{\mathbf{p}_i^2}{m_i} + \frac{p_\epsilon^2}{W} - (N_f + 1)k_B T
 \end{aligned} \tag{76}$$

where $\epsilon = \ln V$, p_ϵ is a momentum corresponding to ϵ , and P_{int} is the internal pressure given by

$$P_{\text{int}} = \frac{1}{dV} \left[\sum_{i=1}^N \left(\frac{\mathbf{p}_i^2}{m_i} + \mathbf{q}_i \cdot \mathbf{F}_i \right) - dV \frac{\partial U}{\partial V} \right] \tag{77}$$

Note that the last term in Eq. [77] involves a derivative of the potential with respect to the explicit volume dependence. Such an explicit dependence comes about when employing, for example, long range corrections to Lennard-Jones potentials³⁴ or when Ewald summation is used to obtain energies and forces from electrostatic interactions. Equations [76] have the conserved energy

$$H' = H(\mathbf{p}, \mathbf{q}, V) + \frac{p_\epsilon^2}{2W} + \frac{p_\eta^2}{2Q} + (N_f + 1)k_B T \eta + PV \tag{78}$$

For simplicity, Eqs. [76] show the coupling of the system to an ordinary Nosé-Hoover thermostat. However, in practice, any desired thermostating scheme can be used. In addition, the system variables $\{\mathbf{p}, \mathbf{q}\}$ as well as the volume are shown coupled to the same thermostat. In practice, it is useful to couple the system and the volume to separate thermostats, because the time scales of their fluctuations are usually considerably different.

The phase space compressibility corresponding to Eqs. [76] can be expressed as follows:

$$\begin{aligned} \frac{\partial}{\partial \Gamma} \cdot \dot{\Gamma} &= \sum_{i=1}^N \left[\frac{\partial}{\partial \mathbf{p}_i} \cdot \dot{\mathbf{p}}_i + \frac{\partial}{\partial \mathbf{q}_i} \cdot \dot{\mathbf{q}}_i \right] + \frac{\partial \dot{V}}{\partial V} + \frac{\partial \dot{p}_\epsilon}{\partial p_\epsilon} + \frac{\partial \dot{\eta}}{\partial \eta} + \frac{\partial \dot{p}_\eta}{\partial p_\eta} \\ &= N_f \frac{p_\epsilon}{W} - N_f \left(1 + \frac{d}{N_f} \right) \frac{p_\epsilon}{W} - N_f \frac{p_\eta}{Q} + d \frac{p_\epsilon}{W} - \frac{p_\eta}{Q} \\ &= -(N_f + 1) \frac{p_\eta}{Q} \end{aligned} \quad [79]$$

from which it is clear that the metric/Jacobian $\sqrt{g(\Gamma)} = e^{-W(\Gamma)}$ is²⁸:

$$\sqrt{g(\Gamma)} = e^{-W(\Gamma)} = e^{-(N_f+1)\eta} \quad [80]$$

Therefore, it can be shown by the same techniques discussed above that

$$\begin{aligned} &\int dV dp_\epsilon dp dq d\eta dp_\eta \delta \left(H(\mathbf{p}, \mathbf{q}, V) + \frac{p_\epsilon^2}{2W} + \frac{p_\eta^2}{2Q} + (N_f + 1)k_B T \eta + PV \right) \\ &\approx \int dV dp dq e^{-\beta PV} e^{-\beta H(\mathbf{p}, \mathbf{q})} \end{aligned} \quad [81]$$

where δ is the Kronecker delta, the integral on the left represents the micro-canonical partition function of the extended system, and the integral on the right is obtained by integrating over η , p_η , and p_ϵ . Note that the ensemble average of \dot{p}_ϵ is

$$\langle \dot{p}_\epsilon \rangle = d[k_B T + \langle (P_{\text{int}} - P)V \rangle] = 0 \quad [82]$$

where the term in brackets is precisely the work-virial theorem obeyed by the *NPT* ensemble.

Equations [76] only allow for isotropic fluctuations in the volume. However, it is sometimes useful to allow the lengths and angles of the simulation box all to vary separately. Fully flexible cell simulations of this type, first carried out by Parrinello and Rahman, can also be formulated in terms of a non-Hamiltonian dynamical scheme. In such a scheme, the matrix \mathbf{h} representing the cell, which contains the cell vectors in its columns, is incorporated as a dynamical variable. That is, nine extra variables are added to the phase space along with an additional nine from its corresponding momentum \vec{p}_g matrix. In terms of the box matrix, the partition function $\Delta(N, P, T)$ is given by

$$\Delta(N, P, T) = \int d\vec{\mathbf{h}} e^{-\beta P \det(\vec{\mathbf{h}})} Q(N, \vec{\mathbf{h}}, T) [\det(\vec{\mathbf{h}})]^{1-d} \quad [83]$$

where the exponent $1 - d$ appearing in the $\det(\vec{\mathbf{h}})$ factor is one minus the number of spatial dimensions. The distribution function corresponding to Eq. [83] can be generated by the following equations of motion:

$$\begin{aligned}
 \dot{\mathbf{q}}_i &= \frac{\mathbf{p}_i}{m_i} + \frac{\overset{\leftrightarrow}{\mathbf{p}}_{\mathbf{g}}}{W} \mathbf{q}_i \\
 \dot{\mathbf{p}}_i &= \mathbf{F}_i - \frac{\overset{\leftrightarrow}{\mathbf{p}}_{\mathbf{g}}}{W} \mathbf{p}_i - \frac{1}{N_f} \frac{\text{Tr}(\overset{\leftrightarrow}{\mathbf{p}}_{\mathbf{g}})}{W} \mathbf{p}_i - \frac{p_{\eta}}{Q} \mathbf{p}_i \\
 \dot{\overset{\leftrightarrow}{\mathbf{h}}} &= \frac{\overset{\leftrightarrow}{\mathbf{p}}_{\mathbf{g}} \overset{\leftrightarrow}{\mathbf{h}}}{W} \\
 \dot{\overset{\leftrightarrow}{\mathbf{p}}_{\mathbf{g}}} &= V(\overset{\leftrightarrow}{\mathbf{P}}_{\text{int}} - \overset{\leftrightarrow}{\mathbf{P}}) + \frac{d}{N_f} \sum_{i=1}^N \frac{\mathbf{p}_i^2}{m_i} \overset{\leftrightarrow}{\mathbf{I}} - \frac{p_{\eta}}{Q} \overset{\leftrightarrow}{\mathbf{p}}_{\mathbf{g}} \\
 \dot{\eta} &= \frac{p_{\eta}}{Q} \\
 \dot{p}_{\eta} &= \sum_{i=1}^N \frac{\mathbf{p}_i^2}{m_i} + \frac{\text{Tr}(\overset{\leftrightarrow}{\mathbf{p}}_{\mathbf{g}}^t \overset{\leftrightarrow}{\mathbf{p}}_{\mathbf{g}})}{W} - (N_f + d^2) k_B T
 \end{aligned} \tag{84}$$

where $\overset{\leftrightarrow}{\mathbf{p}}_{\mathbf{g}}^t$ is the transpose of $\overset{\leftrightarrow}{\mathbf{p}}_{\mathbf{g}}$, and $\overset{\leftrightarrow}{\mathbf{P}}_{\text{int}}$ is the internal pressure tensor given by

$$\overset{\leftrightarrow}{\mathbf{P}}_{\text{int}} = \frac{1}{V} \left[\sum_{i=1}^N \left(\frac{p_i p_i}{m} + \mathbf{q}_i \mathbf{F}_i \right) - \frac{\partial U}{\partial \overset{\leftrightarrow}{\mathbf{h}}} \overset{\leftrightarrow}{\mathbf{h}}^t \right] \tag{85}$$

Equations [84] have the conserved energy

$$H' = H(\mathbf{p}, \mathbf{q}, V) + \frac{\text{Tr}(\overset{\leftrightarrow}{\mathbf{p}}_{\mathbf{g}}^t \overset{\leftrightarrow}{\mathbf{p}}_{\mathbf{g}})}{2W} + \frac{p_{\eta}^2}{2Q} + (N_f + d^2) k_B T \eta + P \det(\overset{\leftrightarrow}{\mathbf{h}}) \tag{86}$$

where P is the pressure. The metric tensor $\sqrt{g(\Gamma)}$ corresponding to Eqs. [84] is²⁸

$$\sqrt{g(\Gamma)} = [\det(\overset{\leftrightarrow}{\mathbf{h}})]^{1-d} e^{(N_f + d^2)\eta} \tag{87}$$

Once again, Eqs. [84] utilize only a single Nosé–Hoover thermostat, although in practice, one should couple separate thermostats to the cell matrix and to the system variables. The ensemble average of $\overset{\leftrightarrow}{\mathbf{p}}$ is, from Eqs. [84],

$$\langle \overset{\leftrightarrow}{\mathbf{p}}_{\mathbf{g}} \rangle = \langle k_B T \overset{\leftrightarrow}{\mathbf{I}} + V(\overset{\leftrightarrow}{\mathbf{P}}_{\text{int}} - \overset{\leftrightarrow}{\mathbf{P}}) \rangle = 0 \tag{88}$$

which is just the tensorial form of the work-virial theorem. Taking the trace of both sides of Eq. [88] gives back the standard work-virial theorem:

$$\frac{1}{d} \text{Tr}(\langle \overset{\leftrightarrow}{\mathbf{p}}_{\mathbf{g}} \rangle) = k_B T + \langle V(P_{\text{int}} - P) \rangle = 0 \tag{89}$$

The argument by which one shows that Eqs. [84] generate the correct phase space distribution is similar to that employed previously and will not be given in detail. However, one need only to compute the compressibility, use it to solve for the metric determinant, and then carry out the integration over η , p_η , and the nine components of \vec{p}_g of $\sqrt{g(\Gamma)}\delta(H' - E)$. As an illustration of the NPT ensemble, consider the simple problem of a single particle in three dimensions subject to an external potential of the form

$$U(\mathbf{q}) = \frac{m\omega^2}{k^2} [1 - \cos (\mathbf{k} \cdot \mathbf{q})] \quad [90]$$

where $\mathbf{k} = (2\pi/L, 2\pi/L, 2\pi/L)$, with L the length of a side of the cubic cell containing the particle. Figure 7 shows the velocity and volume distribution functions obtained for this potential using Eqs. [76]. Figure 7 suggests a wide

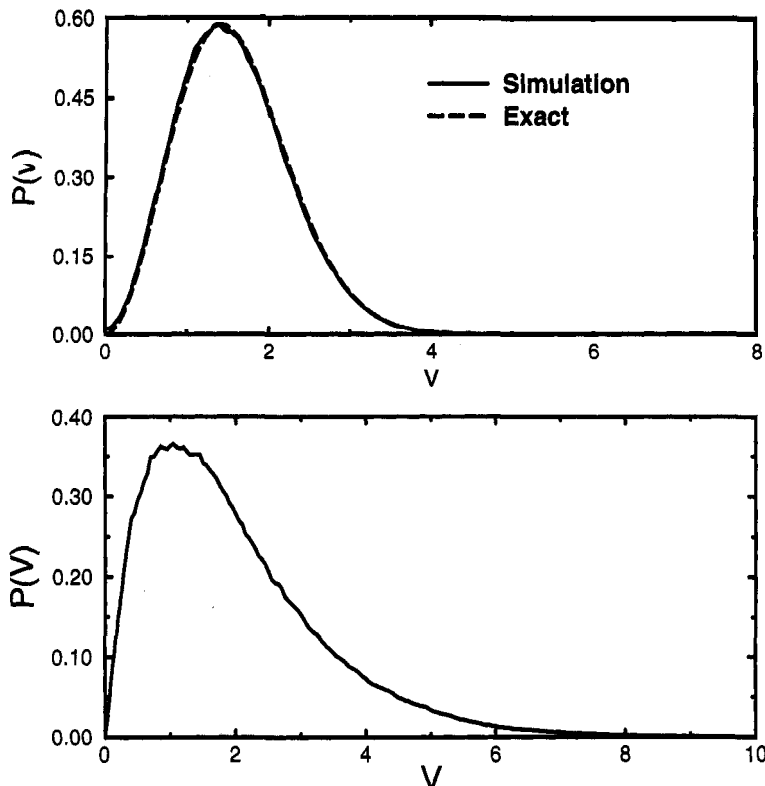


Figure 7 The velocity (*top*) and volume (*bottom*) distribution functions for a simple particle in three dimensions subject to the potential of Eqs. [90]. The solid line in the velocity distribution function plot is the result obtained from Eqs. [76]; the dashed line is the analytical result.

distribution of volumes for this problem. In more realistic examples, fluctuations of the volume are considerably smaller.

The next section discusses in detail linear response theory for homogeneous methods that allow direct coupling of the system to the external field via the equations of motion. As was alluded to in the introduction, a homogeneous method has no direct way of dissipating energy generated by coupling to the external field. The extended system methods of thermostating and barostating, which are typically applied to equilibrium systems, are used to allow temperature and pressure control in systems coupled to an external field.

NONEQUILIBRIUM MOLECULAR DYNAMICS AND LINEAR RESPONSE

Generalized Equations of Motion

In this section we present the concept of a generalized set of equations of motion that will describe a system coupled to an external field (e.g., shear flow, electric field, etc.). This general set of equations of motion will also describe coupling to the extended phase space (e.g., thermostats, barostats) and is of the form:

$$\begin{aligned}\dot{\mathbf{q}}_i &= \frac{\mathbf{p}_i}{m_i} + \mathbf{C}_i(\mathbf{p}, \mathbf{q})f_e(t) + \mathbf{g}_i(\mathbf{p}, \mathbf{q}, \boldsymbol{\Gamma}_{\text{ext}}) \\ \dot{\mathbf{p}}_i &= \mathbf{F}_i + \mathbf{D}_i(\mathbf{p}, \mathbf{q})f_e(t) + \mathbf{h}_i(\mathbf{p}, \mathbf{q}, \boldsymbol{\Gamma}_{\text{ext}}) \\ \dot{\boldsymbol{\Gamma}}_{\text{ext}} &= \mathbf{k}(\mathbf{p}, \mathbf{q}, \boldsymbol{\Gamma}_{\text{ext}})\end{aligned}\quad [91]$$

where the functions \mathbf{g} and \mathbf{h} represent the coupling to the extended part of the phase space, and the last equation gives the evolution of the extended system variables. The functions \mathbf{C} and \mathbf{D} represent a coupling to an external time-dependent field $f_e(t)$ and are assumed to be independent of the extended system.¹² We learned in the preceding section that equations of motion will in general have a phase space distribution function that allows one to define averages of phase variables (or observables). It is then of interest to discover what one can learn from computing averages of phase variables with respect to the steady state distribution function generated by Eqs. [91]. Equations [91] can, in general, possess a phase space compression factor $\partial/\partial\boldsymbol{\Gamma} \cdot \dot{\boldsymbol{\Gamma}}$. The earlier section on non-Hamiltonian dynamics taught us that compressible phase space leads to dynamical metric $\sqrt{g(\boldsymbol{\Gamma}, t)}$ that must be included in the phase space measure to specify unambiguously the average of any property $B(\boldsymbol{\Gamma})$ ^{15,35,36}

$$\langle B \rangle(t) = \int d\Gamma \sqrt{g(\Gamma, t)} B(\Gamma) f(\Gamma, t) \quad [92]$$

The notation $\langle B \rangle(t)$ reminds us that the phase variable B has no explicit time dependence. However, its average in the nonequilibrium steady state explicitly depends on time through the distribution function $f(\Gamma, t)$ generated by Eqs. [91].

Thus, we have a set of equations of motion given by Eqs. [91] that describe a general coupling to an external field. Our objective is to compute averages of functions of the phase space when the system coupled to the external field has reached a steady state. This is the procedure of nonequilibrium molecular dynamics (NEMD) simulations. An illustrative example to consider is the computation of the shear viscosity from Newton's law of viscosity, which reads³⁷

$$\sigma_{xy} = \eta \gamma \quad [93]$$

Here, σ_{xy} is the xy component of the stress tensor, η is the shear viscosity, and γ is the shear rate (or strain). A salient feature of Eq. [93] is that it is a linear phenomenological equation that relates a stress to a strain. The proportionality constant, in this case, is the shear viscosity. In this formulation of the problem, η is assumed to be independent of γ . Clearly, there are interesting regimes of η where the stress and strain are not linearly related. We will discuss this phenomenon in the section on Applications of Shear Flow. The present aim is to construct a set of equations of motion in the form of Eqs. [91] that produce the strain (e.g., shear), that will allow the simulator to then compute the response (e.g., stress) and obtain the transport coefficient (e.g., shear viscosity) via the simple quotient of Eq. [93]. Thus, the average stress will be computed via Eq. [92] by making the identification of $B(\Gamma) = \sigma_{xy}$. However, the right-hand side of Eq. [93] is linear in γ , and it is imperative that the right-hand side of Eq. [92] be linear in γ as well. We must develop the machinery to treat the coupling of the system to the field given by Eq. [91] perturbatively. We now turn our attention to this development.

Linear Response Theory

In this section we develop a general linear response theory for which the coupling of the system to the field in Eqs. [91] is small [i.e., $f_e(t) \ll 1$]. Linear response theory should, in general, take into account the possibility of phase space compression coming from either the coupling to the external field or from the extended phase space variables. In traditional formulations of linear response theory, phase space compression has not been carefully considered.¹ The present formulation treats the first level of compressibility exactly, for example, the compressibility due to the presence of an extended system (such as ther-

mostats and barostats) necessary for the system to reach a well-defined steady state. The time-dependent compressibility arising from the coupling to the extended system will be neglected. More precisely, we assume

$$\sum_i \frac{\partial}{\partial \mathbf{q}_i} \cdot \mathbf{C}_i(\mathbf{p}, \mathbf{q}) + \frac{\partial}{\partial \mathbf{p}_i} \cdot \mathbf{D}_i(\mathbf{q}, \mathbf{p}) = 0 \quad [94]$$

It will be shown that the restriction above allows one to consider the linear response of a phase variable coupled to nearly all the NEMD algorithms in the literature to date. The one known exception is the thermal conductivity algorithm due to Gillan and Dixon.³⁸ Thus, the present formulation will provide a template for the computation of the linear response of any phase variable coupled to an external field of the form given by Eqs. [91] under the conditions specified by Eq. [94].

Recall from the section on non-Hamiltonian dynamics that the phase space distribution function satisfies a generalized Liouville equation:¹⁵

$$\frac{\partial(f\sqrt{g})}{\partial t} = - \frac{\partial}{\partial \Gamma} \cdot (f\sqrt{g}\dot{\Gamma}) \quad [95]$$

Equation [95] is capable of predicting the phase space distribution function of a system on a general manifold by incorporating a dynamical metric $\sqrt{g(\Gamma, t)}$. Recall also from prior sections that Eq. [95] must be supplemented with the equation of motion for the metric

$$\frac{d\sqrt{g}}{dt} = -\sqrt{g} \frac{\partial}{\partial \Gamma} \cdot \dot{\Gamma} \quad [96]$$

The simultaneous solution of Eqs. [95] and [96] gives all the information about the phase space necessary to compute the average in Eq. [92].

In linear response theory, the coupling of the system to the external field is assumed to be weak and is treated as a perturbation.¹² The problem, therefore, is to solve Eqs. [95] and [96] in this regime. To accomplish this task in a rigorous fashion, we first must resolve how $f(\Gamma, t)$ evolves. By substituting the expression for \sqrt{g} given by Eq. [96] into Eq. [95], we obtain

$$\begin{aligned} \frac{\partial f}{\partial t} + \dot{\Gamma} \cdot \frac{\partial}{\partial \Gamma} f &= \frac{df}{dt} = 0 \\ \frac{\partial f}{\partial t} &= -i\mathbf{L}(t)f(\Gamma, t) \end{aligned} \quad [97]$$

Here $i\mathbf{L}(t) = \dot{\Gamma}(t) \cdot \partial/\partial\Gamma$ is the *fully* time dependent Liouvillian that evolves $f(\Gamma, t)$ in accordance with Eqs. [91]. Furthermore, it is the *same* Liouvillian used for

an ordinary phase variable (i.e., no contribution from the compressibility) under the dynamics given by Eqs. [91] as described earlier. All the information of the phase space compression is contained in the metric \sqrt{g} .

We can now proceed to linearize Eq. [92]. First we rewrite Eq. [92] in a more suggestive form, namely,

$$\langle B \rangle(t) = \int d\Gamma_t \sqrt{g(\Gamma_t)} B(\Gamma_t) f(\Gamma_t, t) \quad [98a]$$

Here we have explicitly introduced a dummy label for the variable of integration Γ_t , and we have noted that the only contribution to the evolution of the metric comes from the extended system, and this formulation contains no explicit time dependence. We then proceed by considering the time evolution of $f(\Gamma, t)$

$$\langle B \rangle(t) = \int d\Gamma_t \sqrt{g(\Gamma_t)} B(\Gamma_0) U_R^\dagger(0, t) f_{eq} \quad [98b]$$

where the symbol \dagger represents the operation of complex conjugation (*) and transposition (t). Here we have introduced $f_{eq} \equiv f(\Gamma_{t=0}, 0)$ to denote the as-yet unspecified equilibrium (field-independent) distribution function as the initial condition. f_{eq} is propagated forward to time t by the action of $U_R^\dagger(0, t)$, which is a *time-dependent* operator given by¹²

$$U_R^\dagger(0, t) = \sum_{n=0}^{\infty} (-1)^n \int_0^t ds_1 \int_0^{s_1} ds_2 \cdots \int_0^{s_{n-1}} ds_n iL(s_n) \cdots iL(s_2)L(s_1) \quad [99]$$

Here $iL(t)$ is the Liouvillian corresponding to the fully time-dependent dynamics of Eqs. [91], and the subscript R denotes a right-time-ordered product, with later times appearing to the right.¹²

The challenge is to linearize the field in Eq. [99]. We can perform this task by making use of operator identities. Namely, consider decomposing U_R^\dagger in terms of a time-*independent* reference propagator U_{R0}^\dagger . It follows that¹²

$$U_R^\dagger(0, t) = U_{R0}^\dagger(0, t) - \int_0^t ds U_{R0}^\dagger(s, t) [iL(s) - iL_0(s)] U_R^\dagger(0, s) \quad [100]$$

Now, we can choose our reference propagator iL_0 to be the Liouvillian corresponding to the field-free equations of motion (Eqs. [91] with $f_e(t) = 0$). Then, substituting Eq. [100] into Eq. [99], we obtain

$$\begin{aligned} \langle B \rangle(t) &= \int d\Gamma_t \sqrt{g(\Gamma_t)} B(\Gamma_t) U_{R0}^\dagger(0, t) f_{eq} \\ &\quad - \int d\Gamma_t \sqrt{g(\Gamma_t)} B(\Gamma_t) \int_0^t ds U_{R0}^\dagger(s, t) [iL(s) - iL_0] U_R^\dagger(0, s) f_{eq} \end{aligned} \quad [101]$$

If we consider the external field $f_e(t)$ to be small, we can define the term in brackets in Eq. [101] to be linear in the field strength, namely,

$$i\mathbf{L}(t) = i\mathbf{L}_0 + i\Delta\mathbf{L}(t) \quad [102]$$

From the definition in Eq. [102], Eq. [101] becomes

$$\begin{aligned} \langle B \rangle(t) &= \int d\Gamma_t \sqrt{g(\Gamma_t)} B(\Gamma_t) U_{R0}^\dagger(0, t) f_{eq} \\ &\quad - \int d\Gamma_t \sqrt{g(\Gamma_t)} B(\Gamma_t) \int_0^t ds U_{R0}^\dagger(s, t) i\Delta\mathbf{L}(s) f_{eq} \end{aligned} \quad [103]$$

Because we are working to linear order in $i\Delta\mathbf{L}$, we have used the fact that $U_R^\dagger(0, s)$ can contribute only higher powers of $i\mathbf{L} = i\mathbf{L}_0 + i\Delta\mathbf{L}$. Higher powers of $i\Delta\mathbf{L}$ must be dropped in the linear approximation. Effectively, it can be seen that the operator $U_R^\dagger(0, s) = e^{-i\mathbf{L}_0 t} + O(i\Delta\mathbf{L})$, where $O(i\Delta\mathbf{L})$ indicates terms of order $i\Delta\mathbf{L}$ and where we have used Eq. [99] and the time independence of $i\mathbf{L}_0$. We also note that by definition, $i\mathbf{L}_0 f_{eq} = 0$. Thus only the first term in the Taylor series expansion of $U_R^\dagger(0, s)$ survives, yielding $e^{-i\mathbf{L}_0 t} f_{eq} = f_{eq}$, and we obtain Eq. [103].

We can now systematically investigate each term in Eq. [103]. Consider the term

$$\int d\Gamma_t \sqrt{g(\Gamma_t)} B(\Gamma_t) U_{R0}^\dagger(0, t) f_{eq} \quad [104]$$

Because our reference propagator U_{R0}^\dagger is time independent, we know that its analytic form is given by (see earlier section on Non-Hamiltonian Dynamics)

$$U_{R0}^\dagger(0, t) = e^{-i\mathbf{L}_0 t} \quad [105]$$

It thus follows that

$$\int d\Gamma_t \sqrt{g(\Gamma_t)} B(\Gamma_t) e^{-i\mathbf{L}_0 t} f_{eq} \quad [106]$$

The operator $e^{-i\mathbf{L}_0 t}$ now operates on everything to its left in Eq. [106]. It should be noted that $e^{-i\mathbf{L}_0 t}$ will not operate on the integration measure, which is defined to be $d\Gamma_t \sqrt{g(\Gamma_t)}$. This is yet another example of why one should treat f and \sqrt{g} separately. Using the Hermitian property of the propagator, we can write

$$e^{i\mathbf{L}_0 t} B(\Gamma_0) = B(\Gamma_0) e^{-i\mathbf{L}_0 t} = B(\Gamma_t) \quad [107]$$

Equation [106] then takes the form

$$\int d\Gamma_t \sqrt{g(\Gamma_t)} B(\Gamma_{2t}) f_{eq} \quad [108]$$

Because the variables of integration and the phase variables are at different times, a change of variables from $d\Gamma_t \rightarrow d\Gamma_{2t}$ must be performed. The transformation of the metric is always accompanied by a Jacobian, namely, $\sqrt{g(\Gamma_t)} \mathcal{J}(\Gamma_t; \Gamma_{2t}) = \sqrt{g(\Gamma_{2t})}$. Also, phase variables at different times are not independent since they are connected through the dynamics generated by Eqs. [91]. It is implicit that $f_{eq} = f(\Gamma_{t=0}(\Gamma_{2t}))$. So, we finally obtain for the first term in Eq. [101]:

$$\int d\Gamma_{2t} \sqrt{g(\Gamma_{2t})} B(\Gamma_{2t}) f_{eq} \equiv \langle B \rangle_0 \quad [109]$$

We now examine the second term in Eq. [103]

$$\int d\Gamma_t \sqrt{g(\Gamma_t)} B(\Gamma_t) \int_0^t ds e^{-iL_0(t-s)} i\Delta L(s) f_{eq} \quad [110]$$

Here, again, we have substituted in the analytic form for $U_{R0}^\dagger(s, t)$. We first consider the action of $i\Delta L(s)f_{eq}$. The final form will be expressed in terms of the quantity $H_0(\Gamma)$ that is conserved by Eqs. [91] when $f_e(t) = 0$. This conservation law is expressed as follows:

$$\begin{aligned} \frac{dH_0}{dt} &= \sum_i \left[\left(\frac{\mathbf{p}_i}{m_i} + \mathbf{g}_i(\mathbf{p}, \mathbf{q}, \Gamma_{ext}) \right) \cdot \frac{\partial H_0}{\partial \mathbf{r}_i} + (\mathbf{F}_i + \mathbf{h}_i(\mathbf{p}, \mathbf{q}, \Gamma_{ext})) \cdot \frac{\partial H_0}{\partial \mathbf{p}_i} \right] \\ &\quad + \mathbf{k}(\mathbf{p}, \mathbf{q}, \Gamma_{ext}) \cdot \frac{\partial H_0}{\partial \Gamma_{ext}} = 0 \end{aligned} \quad [111]$$

Note that H_0 need not be a proper Hamiltonian for the unperturbed equations of motion, it merely needs to be conserved by them.

We proceed by noting

$$\begin{aligned} i\Delta L(s)f_{eq} &= \left[\dot{\Gamma}(s) \cdot \frac{\partial}{\partial \Gamma} - \dot{\Gamma}_0 \cdot \frac{\partial}{\partial \Gamma} \right] f_{eq} \\ &= \dot{\Gamma}(s) \cdot \frac{\partial}{\partial \Gamma f_{eq}} \\ &= \frac{\partial f_{eq}}{\partial H_0} \dot{\Gamma}(s) \cdot \frac{\partial}{\partial \Gamma} H_0|_{t=0} \end{aligned} \quad [112]$$

where we remember that f_{eq} , hence H_0 , is a function of the phase variables at $t = 0$. By virtue of Eq. [111], the result above becomes

$$\begin{aligned} i\Delta L(s)f_{eq} &= \frac{\partial f_{eq}}{\partial H_0} f_e(s) \sum_i \left[D_i(\mathbf{p}, \mathbf{q}) \cdot \frac{\partial H_0}{\partial \mathbf{p}_i} + C_i(\mathbf{p}, \mathbf{q}) \cdot \frac{\partial H_0}{\partial \mathbf{q}_i} \right]_{t=0} \\ i\Delta L(s)f_{eq} &= \frac{\partial f_{eq}}{\partial H_0} j(\Gamma|_{t=0})f_e(s) \end{aligned} \quad [113]$$

where the quantity $j(\Gamma|_{t=0})$ is known as the dissipative flux.¹² Again, in deriving Eq. [113], it is assumed that f_{eq} is a pure function of the conserved quantity H_0 . We then substitute Eq. [113] into Eq. [110] to obtain

$$\int_0^t ds \int d\Gamma_t \sqrt{g(\Gamma_t)} B(\Gamma_t) e^{-iL_0(t-s)} \frac{\partial f_{eq}}{\partial H_0} j(\Gamma|_{t=0})f_e(s) \quad [114]$$

Here we have switched the order of integration because the measure and the phase variable are independent of s . Using the same analysis that led to Eq. [109], we propagate everything to the left of $e^{-iL_0(t-s)}$ and perform the appropriate variable transformation $\Gamma_i \rightarrow \Gamma_{t-s}$ to finally obtain

$$\begin{aligned} &\int_0^t ds \int d\Gamma_{t-s} \mathcal{J}(\Gamma_t; \Gamma_{t-s}) \sqrt{g(\Gamma_t)} B(\Gamma_{t-s}) \frac{\partial f_{eq}}{\partial H_0} j(\Gamma|_{t=0})f_e(s) \\ &= \int_0^t ds \langle B(\Gamma_{t-s}) j(\Gamma|_{t=0}) \rangle_{\partial_0} f_e(s) \end{aligned} \quad [115]$$

Here, $\langle \dots \rangle_{\partial_0} = \int d\Gamma \sqrt{g} (\partial f_{eq}/\partial H_0)(\dots)$ (e.g., $\partial f_{eq}/\partial H_0$ is the probability distribution with respect to which all averages are to be taken), and again it is implicit that one can express $\Gamma_{t=0}(\Gamma_{t-s})$.

We now consolidate Eqs. [109] and [115] to obtain the average of any phase variable as a function of time:

$$\langle B \rangle(t) = \langle B \rangle_0 - \int_0^t ds \langle B(\Gamma_{t-s}) j(\Gamma|_{t=0}) \rangle_{\partial_0} f_e(s) \quad [116]$$

Equation [116] is the central result of this section and is one of the most important equations in nonequilibrium statistical mechanics. It is from this point that one makes contact with the more familiar relations relating transport coefficients to time correlation functions under the guise of the so-called Green–Kubo formulas.^{12,39,40}

Recall that we started with a general set of dynamics given by Eqs. [91] and derived the time-dependent average of *any* phase variable to linear order in field coupling. It is also important to note that at no point have we assumed the form of the distribution function through which the averages are computed. This is also a very important result. Namely, the dynamics (in this case, Eqs. [91]) determine the distribution function. We will now demonstrate how one

understands the average over the distribution function $\partial f_{\text{eq}}/\partial H_0$. In general, we would like the average appearing in Eq. [116] to be canonical. In the earlier section on the *NVT* ensemble, we learned how to generate the canonical ensemble from a set of continuous dynamics, namely, Nosé–Hoover dynamics.²⁶ This corresponds to $\mathbf{g}_i = 0$ and $\mathbf{h}_i = -p_\eta \mathbf{p}_i$ in Eqs. [91]. In this case,

$$H_0 = H(\mathbf{p}, \mathbf{q}) + \frac{p_\eta^2}{2Q} + N_f k_B T \eta \quad [117]$$

where $H(\mathbf{p}, \mathbf{q}) = \sum_i (\mathbf{p}_i^2/2m_i) + V(\mathbf{q})$, η and p_η are the thermostat position and momentum variables, and D is the spatial dimension. Recall from the earlier section on the *NVT* ensemble that the unperturbed distribution function f_{eq} and the invariant measure for Nosé–Hoover dynamics are²⁸

$$f_{\text{eq}}(H_0) = \frac{\delta(H_0 - E)}{\Omega} \quad [118]$$

$$d\Gamma \sqrt{g(\Gamma)} = d\Gamma e^{N_f \eta}$$

Here we have computed the square root of the metric determinant by means of Eq. [42]. We proceed by substituting Eq. [118] into Eq. [116], recognizing that

$$\frac{\partial f_{\text{eq}}}{\partial H_0} = \frac{1}{N_f k_B T} \frac{\partial f_{\text{eq}}}{\partial \eta} \quad [119]$$

Using the formula $\int dx f(x)\delta'(x) = -f'(0)$ (or equivalently integrating by parts) gives the familiar result

$$\langle B \rangle(t) = \langle B \rangle_0 + \beta \int_0^t ds \langle B(\Gamma_{t-s}) \rangle_0 f_e(s) \quad [120]$$

where $\beta = 1/k_B T$. It has been assumed that B does not depend on the thermostat variables. Equation [120] is the linear response result for the canonical ensemble. It should be pointed out that the average denoted by $\langle \cdot \cdot \cdot \rangle$ refers to the average at the steady state with respect to the nonequilibrium ensemble. For notational convenience we define this average to be $\langle \cdot \cdot \cdot \rangle_{\text{NE}}$, and this notation is used from this point onward.

The SLLOD Equations of Motion

As stated in the earlier section on Generalized Equations of Motion, we would ultimately like to find a set of equations of motion in the form of Eq. [91] to compute transport coefficients such as the shear viscosity and self diffusion

constants. Before we embark on this, it is useful to refamiliarize ourselves with the standard results relating transport phenomena to equilibrium averages, commonly called Green–Kubo relations. These so-called fluctuation dissipation relations, in a sense, eliminate the need to perform nonequilibrium molecular dynamics simulations because all the transport properties can be related to equilibrium time correlation functions. For example, the Green–Kubo relations for shear–viscosity and self-diffusion coefficient are, respectively,^{12,39,40}

$$\eta = \beta V \int_0^t ds \langle P_{xy}(\Gamma_0) P_{xy}(\Gamma_s) \rangle_0 \quad [121]$$

$$D = \frac{3}{m\beta} \int_0^t ds \frac{\langle \mathbf{v}_0 \cdot \mathbf{v}_s \rangle_0}{\langle \mathbf{v}_0 \cdot \mathbf{v}_0 \rangle_0} \quad [122]$$

Here, $\beta = 1/k_B T$, V is the volume, P_{xy} is the xy component of the pressure tensor, \mathbf{v} is the velocity, m is the mass, η is the shear viscosity, D is the diffusion constant, and $\langle \cdot \cdot \cdot \rangle_0$ denotes an ensemble average (as defined in Eq. [120]) over the equilibrium distribution. The salient feature of these relations is that a transport coefficient, an inherently dynamical property, is related to an *equilibrium* time correlation function. A physical interpretation of this, known as the Onsager regression hypothesis,⁴ states that the relaxation of the fluctuations of a phase variable (say the velocity or the xy component of the pressure tensor) at equilibrium is indistinguishable from *long-time* relaxation of a phase variable perturbed from equilibrium by an external field.¹² Thus, although at equilibrium there will be no stress on a system ($\langle P_{xy} \rangle_0 = 0$), correlations of the instantaneous deviations of P_{xy} from zero will give us the same information (in the small-field limit) as the one obtained if we induced a stress on the system (with the presence of a velocity field) and measured the average stress ($\langle P_{xy} \rangle_{NE} \neq 0$) in the nonequilibrium steady state. This is precisely what Eq. [120] states in mathematical terms. One can compute the shear viscosity and diffusion constants for molecular fluids such as water. The results are shown in Figures 8 and 9.^{42,43}

Earlier we introduced Newton's law of viscosity (Eq. [93]), which relates the xy component of the stress (σ) to the strain (γ) via the shear viscosity (η). The method of nonequilibrium molecular dynamics allows us to compute the shear viscosity *directly* by coupling the system to a shear field and calculating the steady state average of the stress. The shear viscosity thus becomes a simple quotient instead of the relatively complicated time correlation function defined in Eq. [121]. The final ingredient will be a set of equations of motion allowing one to compute the average of the xy component of the stress in a steady state while undergoing planar Couette flow (see Figure 1). These equations of motion fall under the general form of Eqs. [91] and are the celebrated SLLOD equa-

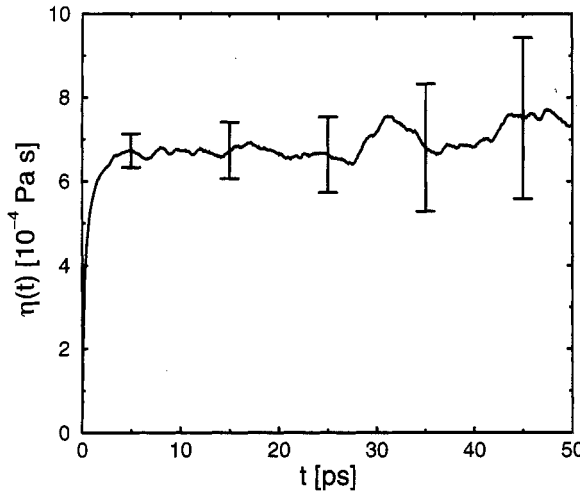


Figure 8 The integrated stress–stress autocorrelation function as described in Eqs. [121] for SPC/E water at 303.15 K as described in Ref. 42. Note the convergence of the integral over time deteriorates owing to insufficient data sampling. The experimental value of the shear viscosity is 7.97×10^{-4} Pa · s, whereas the calculated value from this curve $6.6 \pm 0.8 \times 10^{-4}$ Pa · s.

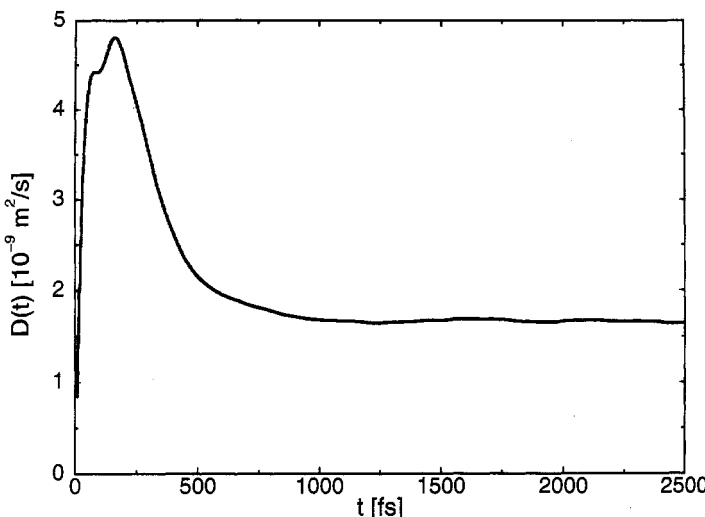


Figure 9 The integrated velocity–velocity autocorrelation function as described in Eqs. [122] for SPC/E water at 277.2 K and 1 atm as described in Ref. 43. Note the convergence of the integral over time. The experimental value of the diffusion constant is 10^{-9} m²/s, whereas the calculated value from this curve is $1.6 \pm 0.08 \times 10^{-9}$ m²/s.

tions.^{8,12} The SLLOD equations coupled to a Nosé–Hoover thermostat are written in the following form:

$$\begin{aligned}\dot{\mathbf{q}}_i &= \frac{\mathbf{p}_i}{m_i} + \hat{\mathbf{i}}\gamma q_{y_i} \\ \dot{\mathbf{p}}_i &= \mathbf{F}_i - \hat{\mathbf{i}}\gamma q_{y_i} - \mathbf{p}_i \frac{p_\eta}{Q} \\ \dot{\eta} &= \frac{p_\eta}{Q} \\ \dot{p}_\eta &= \sum_{i=1}^N \frac{\mathbf{p}_i^2}{m_i} - N_f k_B T\end{aligned}\quad [123]$$

Here, γ is the shear rate, and $\hat{\mathbf{i}}$ is a unit vector in the x direction. Thus, Eqs. [123] describe a system coupled to a shear field in the x direction with a gradient in the shear field along the y . Note that there is no explicit time dependence from the external field [$f_e(t) = \gamma = \text{constant}$], and the compressibility due to the coupling to the velocity field satisfies Eq. [94]. Equations [123] are not derivable from an underlying Hamiltonian; however, one can provide some physical insight by examining the individual equations of motion comprising Eqs. [123].

The equation for $\dot{\mathbf{q}}_i$ (Eq. [123]) can be thought of as the velocity of the particle in the laboratory frame. This can be understood more completely by noting that the laboratory velocity, $\dot{\mathbf{q}}_i$ is a sum of a thermal (or peculiar) velocity \mathbf{p}_i/m_i and a component due to the velocity field $\hat{\mathbf{i}}\gamma q_{y_i}$. At the steady state, the laboratory velocity profile will be linear as in Figure 10, with the slope (the

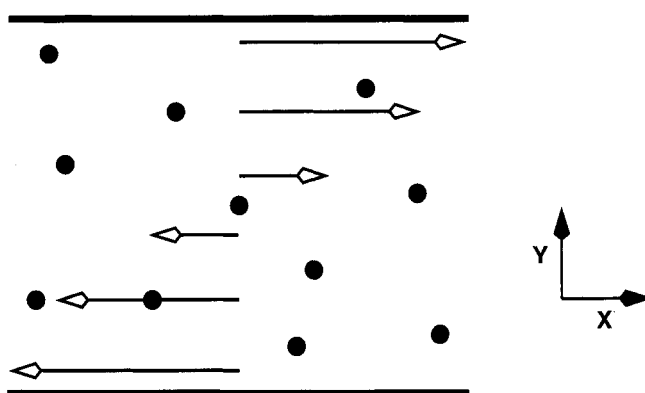


Figure 10 A schematic of a linear velocity profile. The gradient of the flow (γ) is in the y direction and denoted by arrows of varying lengths. The direction of the flow is in the x direction ($\hat{\mathbf{i}}$).

gradient) being equal to γ . It is important to note that the momentum and position in SLLOD equations (Eqs. [123]) are in two different reference frames. The position q_i is in the laboratory frame, whereas the equation for the momentum p_i is in the frame of the fluid or the peculiar frame. This mixed representation is very convenient for coupling the system to thermostats. Thermostats are imperative when one is performing nonequilibrium molecular dynamics simulations. Without the presence of the thermostat, the coupling to the external field would cause the system to heat up, and a steady state would never be achieved. Indeed, if one examines the third term in the equation of motion for p_i in Eqs. [123], it is the peculiar momentum that is coupled to the thermostat. Thus, in the SLLOD equations of motion, the contribution to the velocity from the shear field is not interpreted as “heat.” A distinction must be made between the thermal velocity and the laboratory velocity. For example, if one drops a closed container of water, prior to impact there will be an increase in the laboratory velocity without an increase in the “heat” of the water. If one were to thermostat the laboratory velocity, any deviation from a purely Maxwellian velocity distribution would be interpreted as “heat” by the thermostats and thus quenched. A linear velocity profile (or any profile for that matter) would be prohibited. Instead, with the peculiar velocity being thermostated, any deviation in the velocity from an *exact linear profile*, given by $\hat{i}q_{y_i}$, is interpreted by the thermostat as “heat” and quenched. Thus a perfect linear velocity profile is stabilized, and any viscous heating is removed via the thermostats.

It is also interesting to examine Eqs. [123] within the linear response theory developed in the preceding subsection. Thus, we would like to treat the coupling to the velocity field as perturbation and examine the consequences of this. We then invoke Eq. [120]. As our phase variable B , we will choose to examine P_{xy} , the xy component of the pressure tensor. Thus, Eq. [120] reads

$$\langle P_{xy} \rangle_{\text{NE}}(t) = \langle P_{xy} \rangle_0 + \beta\gamma \int_0^t ds \langle P_{xy}(\Gamma_{t-s}) j(\Gamma_{t=0}) \rangle_0 \quad [124]$$

where again, the subscript NE denotes an average to be taken with respect to the nonequilibrium steady state distribution function. The next step is to evaluate the dissipative flux, $j(\Gamma_{t=0})$ appearing in Eq. [124]. Recall the definition for the dissipative flux given by the bracketed expression in Eq. [113]. Also recall that H_0 for Nosé–Hoover dynamics is given by Eq. [117]. We can now proceed by noting that within the SLLOD equations of motion, $D_i(\Gamma) = -\hat{i}p_{y_i}$ and $C_i(\Gamma) = \hat{i}q_{y_i}$. It is clear that the dissipative flux $j(\Gamma_{t=0}) = -\sum_i (p_x p_{y_i}/m_i + F_x q_{y_i})$. Recall from section on the Dynamical Generation of the NPT Ensemble that this is the microscopic definition for $P_{xy}V$. So, Eq. [124] becomes

$$\langle P_{xy} \rangle_{\text{NE}}(t) = \langle P_{xy} \rangle_0 - V\beta\gamma \int_0^t ds \langle P_{xy}(\Gamma_{t-s}) P_{xy}(\Gamma_{t=0}) \rangle_0 \quad [125]$$

It should be clear that at equilibrium, $\langle P_{xy} \rangle_0 = 0$. We can compare the result of Eq. [125] to the Green–Kubo expression for the shear viscosity given by Eq. [121]. We can equate the left-hand side of Eq. [125] to η , and we then obtain the following remarkable result:

$$\langle P_{xy} \rangle_{\text{NE}}(t) = -\gamma \eta \quad [126]$$

Making use of the fact that the stress is equal to the negative of the pressure, we finally obtain

$$\langle \sigma_{xy} \rangle_{\text{NE}}(t) = \gamma \eta \quad [127]$$

We have thus demonstrated that Newton's law of viscosity, an inherently macroscopic result, can be obtained via linear response theory as the non-equilibrium average in the steady state. Furthermore, the distribution function for the steady state average is determined by microscopic equations of motion. Hence, the SLLOD equations, in the linear regime, reduce to the linear phenomenological law proposed by Newton. Moreover, all the quantities that are needed to compute the shear viscosity can be obtained from a molecular dynamics simulation.

The choice between using Eq. [127] or Eq. [121] for computing the shear viscosity depends on the system of interest, as well as the questions be addressed. From the formal point of view, Eq. [127] is equivalent to Eq. [121]. One, however, must be concerned with the practical implementations of Eqs. [127] and [121]. Equation [121] is a correlation function that must be converged. To assure this, long simulations must be performed to gather the appropriate amount of statistics such that the error bars in the shear viscosity become small. In general, the more complicated the system, the more difficult it will be to converge the correlation function. Namely, argon will be less difficult than water, which will be less difficult than decane. Equation [127], at first sight, is much easier to implement. One picks a shear rate γ , computes the steady state average of the stress, and takes their quotient to obtain the shear viscosity. The trick to using Eq. [127] is to ensure that the linear regime is reached. Thus, many independent simulations must be performed, using different values of the shear rate, until η becomes *independent* of γ (see Figure 11). The results of this procedure as well as the implementation specifics are discussed later. Suffice it to say that both methods are perfectly valid. However, Eq. [127] is fundamentally the equation of choice when the simulations are performed under constant pressure conditions and when one is interested in structural properties as a function of shear rate. Equation [121] is derived in the canonical ensemble, and the extension to the isobaric–isothermal ensemble, to our knowledge has not been considered. The structural properties under flow, a major topic in this chapter, are discussed in detail in the section on Applications of Shear Flow.

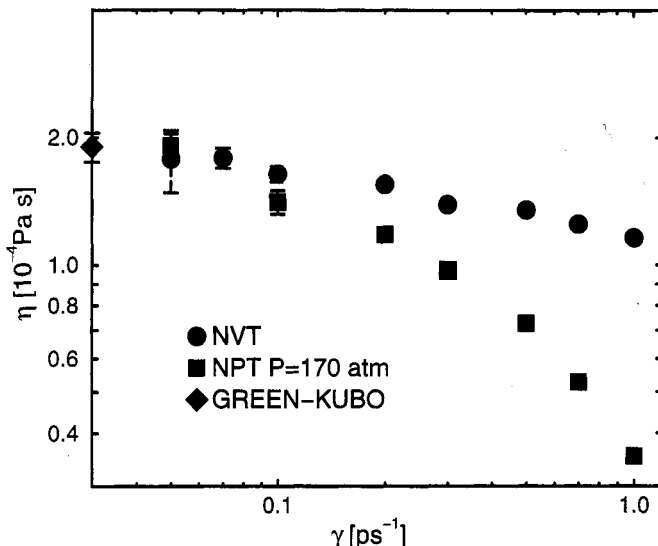


Figure 11 The shear viscosity for liquid decane at $T = 480\text{ K}$ and $P = 170\text{ atm}$ calculated three different ways: NEMD-NVT, NEMD-NPT, and by means of the Green-Kubo formula (Eqs. [198]). The Green-Kubo value is actually at $\gamma = 0$ but is placed on the y axis as a guide to the eye. The linear regime is reached when $\gamma \approx 0.005\text{ ps}^{-1}$. Note the ensemble-dependent results in the shear thinning regime.

Other Types of Flow: GSLLOD Equations of Motion

The SLLOD equations of motion presented in Eqs. [123] are for the specific case of planar Couette flow. It is interesting to consider how one could write a version of Eqs. [123] for a general flow. One way to do this is introduce a general strain tensor, denoted by ∇u . For the case of planar Couette flow, $\nabla u = \hat{j}\hat{i}\gamma$ in dyadic form, where \hat{i} and \hat{j} denote the unit vector in the x and y directions, respectively. The matrix representation is

$$\nabla u = \begin{pmatrix} 0 & 0 & 0 \\ \gamma & 0 & 0 \\ 0 & 0 & 0 \end{pmatrix} \quad [128]$$

With $\nabla u = \hat{j}\hat{i}\gamma$, the SLLOD equations in the unthermostated form become

$$\begin{aligned} \dot{q}_i &= \frac{\mathbf{p}_i}{m_i} + \mathbf{q}_i \cdot \nabla u \\ \dot{\mathbf{p}}_i &= \mathbf{F}_i - \mathbf{p}_i \cdot \nabla u \end{aligned} \quad [129]$$

It is interesting to analyze Eqs. [129] further to point out interesting features of SLLOD dynamics.

If one assumes that $\nabla \mathbf{u}$ has explicit time dependence, we can construct $\ddot{\mathbf{q}}$ from Eqs. [129] to obtain

$$\ddot{\mathbf{q}}_i = \frac{\dot{\mathbf{p}}_i}{m_i} + \dot{\mathbf{q}}_i \cdot \nabla \mathbf{u} + \mathbf{q}_i \cdot \frac{d}{dt} \nabla \mathbf{u} \quad [130]$$

Substituting Eqs. [129] for $\dot{\mathbf{p}}_i$ and $\dot{\mathbf{q}}_i$ gives

$$\ddot{\mathbf{q}}_i = \mathbf{F}_i/m_i + \dot{\mathbf{q}}_i \cdot \nabla \mathbf{u} \cdot \nabla \mathbf{u} + \mathbf{q}_i \cdot \frac{d}{dt} \nabla \mathbf{u} \quad [131]$$

To proceed, one assumes that the time dependence of $\nabla \mathbf{u}$ is given by $\Theta(t) \nabla \mathbf{u}$ where $\Theta(t)$ is the Theta function [i.e., $\Theta(t) = 0$ for $t < 0$ and $\Theta(t) = 1$ for $t \geq 0$]. With this definition for the time dependence of the strain rate, Eq. [131] becomes

$$\ddot{\mathbf{q}}_i = \frac{\mathbf{F}_i}{m_i} + \mathbf{q}_i \cdot \nabla \mathbf{u} \cdot \nabla \mathbf{u} + \delta(t) \mathbf{q}_i \cdot \nabla \mathbf{u} \quad [132]$$

where $\delta(t)$ is the time derivative of $\Theta(t)$. For the case of planar Couette flow, $\nabla \mathbf{u} \cdot \nabla \mathbf{u} = 0$, and the result simplifies to

$$\ddot{\mathbf{q}}_i = \frac{\mathbf{F}_i}{m_i} + \delta(t) \mathbf{q}_i \cdot \nabla \mathbf{u} \quad [133]$$

The interpretation of Eq. [133] for planar Couette flow is as follows: at $t < 0$, the system evolves under normal NVE dynamics (i.e., $\nabla \mathbf{u} = 0$). At $t = 0$, the impulsive force $\delta(t) \mathbf{q}_i \cdot \nabla \mathbf{u}$ is applied, after which the system continues to evolve under NVE dynamics for $t > 0$, but the “memory” of the flow is contained in the definition of $\dot{\mathbf{q}}_i$ and $\dot{\mathbf{p}}_i$ as specified in Eq. [129]. When periodic boundary conditions are applied on the simulation cell, they must be treated in a way that preserves the flow. This in general will lead to time-dependent boundary conditions for the case of planar Couette flow to be discussed in detail shortly.

However, it is clear that for a general tensor $\nabla \mathbf{u}$, trajectory analysis based on the SLLOD dynamics in Eqs. [129] will yield incorrect results. Equation [132] has an extra term in the “force,” which is equivalent to saying that the momenta in Eqs. [129] are not “peculiar” with respect to a *general* flow (indeed, Eqs. [129] yield peculiar velocities for the case of planar Couette flow), and therefore the flow profile produced will not be $\mathbf{q} \cdot \nabla \mathbf{u}$ as expected. Equations [129] also lead to problems when one is considering definitions of pressure

and temperature based on the Irving–Kirkwood procedure,² which assume that the velocities are peculiar. Thus, when simulations are done by means of planar elongational, three-dimensional elongational, uniaxial stretching, and biaxial stretching flows,⁴⁴ a new set of equations of motion must be considered. For a general strain rate tensor to describe flow pattern of other types, the SLLOD equations can be generalized to the so-called GSLLOD equations:⁴⁵

$$\begin{aligned}\dot{\mathbf{q}}_i &= \frac{\mathbf{p}_i}{m_i} + \mathbf{q}_i \cdot \nabla \mathbf{u} \\ \dot{\mathbf{p}}_i &= \mathbf{F}_i - \mathbf{p}_i \cdot \nabla \mathbf{u} - m_i \mathbf{q}_i \cdot \nabla \mathbf{u} \cdot \nabla \mathbf{u} - \frac{p_\eta}{Q} \mathbf{p}_i \\ \dot{\eta} &= \frac{p_\eta}{Q} \\ \dot{p}_\eta &= \sum_{i=1}^N \frac{\mathbf{p}_i^2}{m_i} - N_f k_B T\end{aligned}\quad [134]$$

Here, we have coupled the GSLLOD equations to a Nosé–Hoover thermostat. It is simple to show that the computation of $\ddot{\mathbf{q}}_i$ in the unthermostated form of the GSLLOD equations will yield Eq. [133].

It was also shown in Ref. 45 that the addition of the dummy variable

$$\dot{I} = \sum_{i=1}^N \mathbf{q}_i \cdot \nabla \mathbf{u} \cdot \mathbf{p}_i \frac{p_\eta}{Q} \quad [135]$$

in conjunction with the GSLLOD equations of motion conserves the following energy:

$$H' = \sum_{i=1}^N \frac{(\mathbf{p}_i + m_i \mathbf{q}_i \cdot \nabla \mathbf{u})^2}{2m_i} + V(\mathbf{q}) + \frac{p_\eta^2}{2Q} + N_f k_B T \eta + I \quad [136]$$

From the earlier section on Molecular Dynamics and Equilibrium Statistical Mechanics, we hope that we have made clear that a conserved quantity is the starting point for phase space analysis and the derivation of a probability distribution function. Following the same analysis that led to the distribution functions for NVE, NVT, and NPT dynamics, the new distribution $f(\mathbf{q}, \mathbf{p}, p_\eta, I)$ for GSLLOD coupled to a Nosé–Hoover thermostat is given by

$$f(\mathbf{p}, \mathbf{q}, p_\eta, I) \approx \exp \left\{ \frac{-1}{k_B T} \left[\sum_{i=1}^N \frac{(\mathbf{p}_i + m_i \mathbf{q}_i \cdot \nabla \mathbf{u})^2}{2m_i} + V(\mathbf{q}) + \frac{p_\eta^2}{2Q} + I \right] \right\} \quad [137]$$

The distribution of Eq. [137] is canonical in laboratory momentum and positions for a general strain rate tensor ∇u ; this is the expected form for a system subject to an external field. Equation [137] is the first distribution function to be derived for SLLOD-type dynamics and has provided impetus for studies concerning the nature of the distribution function in the nonequilibrium steady state.

NUMERICAL IMPLEMENTATION OF SLLOD DYNAMICS

Numerically Integrating the SLLOD Equations

Up to this point, the majority of the ideas we have developed entail formal methodology making contact with the theory of ensembles in classical statistical mechanics through microscopic equations of motion. In this section, we develop the tools for numerically integrating the equations of motion introduced in the preceding sections. These integration schemes have a rigorous mathematical foundation and are shown to be extremely stable. A detailed introduction to the theory of reversible integration and an explicit derivation of the reversible integrator for the SLLOD equations motion under *NVT* and *NPT* conditions are provided.

The Theory of Reversible Integration

Let us consider the time evolution of phase space variable Γ , that is,

$$\Gamma_0 \rightarrow \Gamma_t \quad [138]$$

Once again, Γ is an abstract vector in the full phase space (i.e., including extended system variables). The majority of this section is devoted to how one mathematically represents the “ \rightarrow .” Formally, this is quite simple. Suppose that we want to evolve a phase variable $B(\Gamma)$. We can write differential equations for B :

$$\begin{aligned} \frac{dB}{dt} &= \dot{\Gamma} \cdot \frac{\partial}{\partial \Gamma} B \\ \frac{dB}{dt} &= iLB \end{aligned} \quad [139]$$

Here again, we have introduced the Liouville operator for the phase variables and have also noted that the phase variable does not have any explicit time dependence. We can solve Eqs. [139] to obtain

$$B(\Gamma_t) = e^{i\mathbf{L}t} B(\Gamma_0) \quad [140]$$

Again, we have assumed that the Liouville operator has no explicit time dependence. To proceed further, we need to specify the equations of motion so that we can explicitly write out \mathbf{L} . The simplest nontrivial dynamics for an isolated system are Hamilton's equations of motion, which read

$$\dot{\mathbf{q}}_i = \frac{\mathbf{p}_i}{m_i} \quad \text{and} \quad \dot{\mathbf{p}}_i = \mathbf{F}_i \quad [141]$$

Here, \mathbf{q} is the position, \mathbf{p} is the conjugate momentum, m is the mass, and \mathbf{F} is the force. Thus, the phase space vector Γ has two components:

$$\Gamma_t = \begin{pmatrix} \mathbf{q}(t) \\ \mathbf{p}(t) \end{pmatrix} \quad [142]$$

We can also write the Liouville operator for Hamiltonian dynamics, where again, the particle index has been suppressed:

$$\begin{aligned} i\mathbf{L} &= \dot{\Gamma} \cdot \frac{\partial}{\partial \Gamma} = \dot{\mathbf{q}} \cdot \frac{\partial}{\partial \mathbf{q}} + \dot{\mathbf{p}} \cdot \frac{\partial}{\partial \mathbf{p}} \\ &= \frac{\mathbf{p}}{m} \cdot \frac{\partial}{\partial \mathbf{q}} + \mathbf{F} \cdot \frac{\partial}{\partial \mathbf{p}} \end{aligned} \quad [143]$$

In the last line of Eq. [143], we have utilized Eq. [141]. For Hamiltonian dynamics, Eq. [140] takes the following form,

$$B(\Gamma_t) = \exp \left[t \left(\frac{\mathbf{p}}{m} \cdot \frac{\partial}{\partial \mathbf{q}} + \mathbf{F} \cdot \frac{\partial}{\partial \mathbf{p}} \right) \right] B(\Gamma_0) \quad [144]$$

If we could analytically evaluate the action of the operator in Eq. [144] for any potential energy function or force field, there would be no need for molecular dynamics simulation. Since that is generally not possible, we need to devise a numerical scheme that will solve Eq. [144] to a desired accuracy, while preserving the symmetry of the equations of motion (e.g., time-reversal symmetry).

To proceed, it will be useful to review some formulas from the theory of operators. Suppose one has an operator of the form $e^{t(\hat{A}+\hat{B})}$, where \hat{A} and \hat{B} are noncommuting operators. When one encounters the exponential of a sum of operators, it is usually desirable to decompose the expression into a more manageable form. This is done through use of the Baker–Campbell–Hausdorff theorem⁴⁶ and the Trotter-type factorizations.⁴⁷ One can decompose the operator expression to linear order in t , namely

$$e^{t(\hat{A}+\hat{B})} = e^{t\hat{A}}e^{t\hat{B}} + O(t) \quad [145]$$

Equation [145] is certainly more useful than the full operator expression, but there is a very important element missing: the left-hand side of this equation is time reversible, whereas the right-hand side is not. One can see this by changing t to $-t$ and multiplying the two expressions, remembering that the order of the operations must remain intact because the two operators do not commute. This is certainly an undesirable side effect. In any approximate scheme, one would like to preserve the symmetry of the original operator. The Trotter type factorizations allow one to circumvent this problem while gaining accuracy in the approximations. The Trotter factorization for the right-hand side of Eq. [145] is

$$\begin{aligned} e^{t(\hat{A}+\hat{B})} &= e^{(t/2)\hat{A}}e^{t\hat{B}}e^{(t/2)\hat{A}} + O(t^2) \\ &= e^{(t/2)\hat{B}}e^{t\hat{A}}e^{(t/2)\hat{B}} + O(t^2) \end{aligned} \quad [146]$$

Equation [146] is clearly time reversible, with the desirable side effect of being more accurate. We will now proceed with examining Eq. [144]. We can apply the Trotter factorization introduced in Eq. [146] to Eq. [144] to obtain

$$B(\Gamma_i) = \exp\left(\frac{t}{2}\mathbf{F} \cdot \frac{\partial}{\partial \mathbf{p}}\right) \exp\left(t\frac{\mathbf{p}}{m} \cdot \frac{\partial}{\partial \mathbf{q}}\right) \exp\left(\frac{t}{2}\mathbf{F} \cdot \frac{\partial}{\partial \mathbf{p}}\right) B(\Gamma_0) + O(t^2) \quad [147]$$

The actual order that was chosen for the decomposition in Eq. [147] has a special significance that is elucidated later. For the error to be sufficiently small, it is imperative to have a time that is sufficiently small, whereas we are most often interested in trajectories that, relatively speaking, span a rather long period of time. However, we can apply the operator in Eq. [138] successively for some small time step, thereby minimizing the error. So, we define $\Delta t = t/P$ and write

$$B(\Gamma_i) = \prod_{i=1}^P \left[\exp\left(\frac{\Delta t}{2}\mathbf{F} \cdot \frac{\partial}{\partial \mathbf{p}}\right) \exp\left(\Delta t\frac{\mathbf{p}}{m} \cdot \frac{\partial}{\partial \mathbf{q}}\right) \exp\left(\frac{\Delta t}{2}\mathbf{F} \cdot \frac{\partial}{\partial \mathbf{p}}\right) \right]^P B(\Gamma_0) + O(P\Delta t^2) \quad [148]$$

Two questions must now be addressed: How does one translate Eq. [148] into a computer algorithm? and How will the error grow as P increases? For the case of the Hamiltonian dynamics of Eq. [141], we are interested in the trajectories of \mathbf{p} and \mathbf{q} , namely, $B(\Gamma) = \Gamma$. We will examine in detail one time-slice of the operator in Eq. [148]:

$$\Gamma_{\Delta t} = \exp\left(\frac{\Delta t}{2}\mathbf{F} \cdot \frac{\partial}{\partial \mathbf{p}}\right) \exp\left(\Delta t\frac{\mathbf{p}}{m} \cdot \frac{\partial}{\partial \mathbf{q}}\right) \exp\left(\frac{\Delta t}{2}\mathbf{F} \cdot \frac{\partial}{\partial \mathbf{p}}\right) \Gamma_0 \quad [149]$$

The first thing to note is that each operator represents a differential equation that can be solved analytically. Consider the first operation on the initial state

$$\exp\left(\frac{\Delta t}{2} \mathbf{F} \cdot \frac{\partial}{\partial \mathbf{p}}\right) \begin{pmatrix} \mathbf{q}(0) \\ \mathbf{p}(0) \end{pmatrix} \quad [150]$$

It should be clear that the operator will act only on the momentum, since the derivative is with respect to the momentum. If the operator is going to have an effect on the initial state, the operator itself must be evaluated at $t = 0$:

$$\exp\left(\frac{\Delta t}{2} \mathbf{F}(0) \cdot \frac{\partial}{\partial \mathbf{p}(0)}\right) \begin{pmatrix} \mathbf{q}(0) \\ \mathbf{p}(0) \end{pmatrix} \quad [151]$$

The differential equation representation of the operator can be deduced from Eq. [138], namely,

$$\frac{dp(0)}{dt} = F(0) \frac{\partial p(0)}{\partial p(0)} = F(0) \quad [152]$$

Here we have used only one dimension for clarity. Equation [152] is solved by straight-forward integration, with the limits of integration being from $0 \rightarrow \Delta t/2$. Everything on the right-hand side is independent of time and the solution is

$$p\left(\frac{\Delta t}{2}\right) = p(0) + \frac{\Delta t}{2} F(0) \quad [153]$$

The careful reader will notice that we have derived via differential equations the result of the “shift” operator, $e^{a(\partial/\partial x)} f(x) = f(x + a)$. Since we must operate on \mathbf{p} a final time before its full evolution is complete, we adopt the convenient notation and define this evolution up to $\Delta t/2$. One can prove the shift operator by expanding both sides in a Taylor series expansion. We choose the differential equation approach because there will in general be operators that appear more complicated than the simple shift operator. With the methods outlined, one will be able to deduce the action of any operator. So, often generalizing to three dimensions by noting that there is no coupling between the x , y , and z components, we can write out the first step toward the solution of Equation [149]:

$$\begin{aligned} \Gamma_{\Delta t} &= \exp\left(\frac{\Delta t}{2} \mathbf{F} \cdot \frac{\partial}{\partial \mathbf{p}}\right) \exp\left(\Delta t \frac{\mathbf{p}}{m} \cdot \frac{\partial}{\partial \mathbf{q}}\right) \begin{pmatrix} \mathbf{q}(0) \\ \mathbf{p}(\Delta t/2) \end{pmatrix} \\ &= \exp\left(\frac{\Delta t}{2} \mathbf{F} \cdot \frac{\partial}{\partial \mathbf{p}}\right) \exp\left(\Delta t \frac{\mathbf{p}}{m} \cdot \frac{\partial}{\partial \mathbf{q}}\right) \begin{pmatrix} \mathbf{q}_1 \\ \mathbf{p}_1 \end{pmatrix} \end{aligned} \quad [154]$$

For the next evolution step of Γ_1 the same steps outlined above apply, but the next step in the evolution will affect \mathbf{q} . Reverting to one dimension for clarity, the following differential equation is generated:

$$\frac{dq_1}{dt} = \frac{p_1}{m} \quad [155]$$

The solution is

$$\begin{aligned} q_1(\Delta t) &= q_1(0) + \Delta t \frac{p_1}{m} \\ q_1(\Delta t) &= q_1(0) + \Delta t \frac{p(\Delta t/2)}{m} \\ &= q(0) + \frac{\Delta t}{m} p(0) + \frac{\Delta t^2}{2m} F(0) \end{aligned} \quad [156]$$

We have adopted the notation $q(\Delta t)$ to denote the full evolution of \mathbf{q} . We now look at the third and final operation,

$$\begin{aligned} \Gamma_{\Delta t} &= \exp\left(\frac{\Delta t}{2} \mathbf{F} \cdot \frac{\partial}{\partial \mathbf{p}}\right) \begin{pmatrix} \mathbf{q}(0) + \Delta t \frac{p(\Delta t/2)}{m} \\ p(\Delta t/2) \end{pmatrix} \\ &= \exp\left(\frac{\Delta t}{2} \mathbf{F} \cdot \frac{\partial}{\partial \mathbf{p}}\right) \begin{pmatrix} \mathbf{q}_2 \\ \mathbf{p}_2 \end{pmatrix} \end{aligned} \quad [157]$$

This operation is equivalent to the first operation considered except that now the operator must be evaluated at \mathbf{q}_2 and \mathbf{p}_2 . Because the force, \mathbf{F} , is a function of \mathbf{q} , $\mathbf{F}(\mathbf{q}_2) = \mathbf{F}(\Delta t)$. Thus, we finally obtain

$$\Gamma_{\Delta t} = \begin{pmatrix} \mathbf{q}(0) + \Delta t \frac{p(\Delta t/2)}{m} \\ \mathbf{p}(\Delta t/2) + \Delta t / 2 \mathbf{F}(\Delta t) \end{pmatrix} \quad [158]$$

Equation [158] is the velocity Verlet algorithm. We now have a way to transcribe the operator notation to computer code:

```
p=p+.5*dt*f ! shift p to the half time step
q=q+dt*p ! shift q to the full time step using Equation [153]
call force ! update the force at the full time step using q of
               ! Equation [156]
p=p+.5*dt*f ! shift p to the full time step using Equation [157]
```

The reader must now put the particle index back into the equations, and the velocity Verlet integrator for the Hamiltonian dynamics in Equation [141] is derived. It is reversible in time and accurate to $O(P\Delta t^2)$.

The last question that must be addressed is this: How does one obtain a stable integrator when P exceeds, say, 10^6 steps? The answer to this question is due to a remarkable theorem in the theory of reversible integrators. We will simply quote the theorem here and interpret it. The interested reader can pursue the details in Refs. 48 and 49. If the Jacobian of the map (integrator)

$$J = \det \begin{pmatrix} \partial/\partial \mathbf{q}(0) \cdot \mathbf{q}(\Delta t) & \partial/\partial \mathbf{p}(0) \cdot \mathbf{q}(\Delta t) \\ \partial/\partial \mathbf{q}(0) \cdot \mathbf{p}(\Delta t) & \partial/\partial \mathbf{p}(0) \cdot \mathbf{p}(\Delta t) \end{pmatrix} \quad [159]$$

is unity, then there is a conserved quantity H' that is preserved exactly by the map (integrator). For the one-dimensional simple harmonic oscillator, the Hamiltonian is $H = \frac{1}{2}(p^2 + q^2)$. The quantity that is exactly preserved by the map is $H' = \frac{1}{2}(q^2 + p^2)/[1 - (\Delta t/2)^2]$. As one can see, $H = H' + O(\Delta t^2)$. Thus, H will never deviate from the constant energy surface by more than Δt^2 assuming perfect integration no matter what the value of P . It is now clear why the velocity Verlet integrator is so successful. In the next section, we use the tools developed here to derive explicit reversible integrators for SLLOD dynamics.

SLLOD Dynamics for Planar Couette Flow in the Canonical Ensemble

The underlying theory for deriving an integrator was introduced in the preceding subsection. Now we outline the essential details of applying these concepts to obtain an integrator scheme for NVT dynamics. For simplicity, the treatment contains only one Nosé–Hoover thermostat attached to the system. The generalization to chains is straightforward and has been presented in Refs. 28 and 50. The SLLOD equations of motion coupled to one Nosé–Hoover (NH) thermostat are those presented in Eqs. [123]. The time evolution of phase space variable Γ is given by

$$\Gamma_{\Delta t} = e^{(iL_{\text{SLLOD}})\Delta t} \Gamma_0 \quad [160]$$

where Γ denotes the set of phase space variables $\{\mathbf{q}_i, \mathbf{p}_i, \eta, p_\eta\}$ and iL_{SLLOD} is given by

$$iL_{\text{SLLOD}} = \dot{\Gamma} \cdot \frac{\partial}{\partial \Gamma} = iL_{\text{NH}} - \hat{i}\gamma v_{y_i} \cdot \frac{\partial}{\partial \mathbf{v}_i} + iL_{\text{mvV}} \quad [161]$$

with

$$\begin{aligned} i\mathbf{L}_{\text{mvV}} &= \frac{\mathbf{F}_i}{m_i} \cdot \frac{\partial}{\partial \mathbf{v}_i} + (\mathbf{v}_i + \hat{\mathbf{i}}\gamma q_{y_i}) \cdot \frac{\partial}{\partial \mathbf{q}_i} \\ i\mathbf{L}_{\text{NH}} &= - \sum_{i=1}^N \nu_\eta \mathbf{v}_i \cdot \frac{\partial}{\partial \mathbf{v}_i} + G \frac{\partial}{\partial \nu_\eta} + \nu_\eta \frac{\partial}{\partial \eta} \end{aligned} \quad [162]$$

The subscripts mvV and NH refer to modified velocity Verlet and Nosé-Hoover, respectively, and G is the force on the thermostat as given by

$$G = \sum_{i=1}^N m_i \mathbf{v}_i^2 - N_f k_B T \quad [163]$$

where N_f is the number of system degrees of freedom. A short-time approximation to Eq. [160] can be found using the Trotter factorization as

$$\Gamma_{\Delta t} = \exp\left[\frac{\Delta t}{2}\left(i\mathbf{L}_{\text{NH}} - \hat{\mathbf{i}}\gamma q_{y_i} \cdot \frac{\partial}{\partial \mathbf{v}_i}\right)\right] \exp[\Delta t(i\mathbf{L}_{\text{mvV}})] \exp\left[\frac{\Delta t}{2}\left(i\mathbf{L}_{\text{NH}} - \hat{\mathbf{i}}\gamma q_{y_i} \cdot \frac{\partial}{\partial \mathbf{v}_i}\right)\right] \Gamma_0 \quad [164]$$

Similarly, the mvV operator can be factorized as

$$\exp t(i\mathbf{L}_{\text{mvV}}) = \exp\left(\frac{\Delta t}{2} \frac{\mathbf{F}_i}{m_i} \cdot \frac{\partial}{\partial \mathbf{v}_i}\right) \left\{ \exp\left[\Delta t(\mathbf{v}_i + \hat{\mathbf{i}}\gamma q_{y_i}) \cdot \frac{\partial}{\partial \mathbf{q}_i}\right] \right\} \exp\left(\frac{\Delta t}{2} \frac{\mathbf{F}_i}{m_i} \cdot \frac{\partial}{\partial \mathbf{v}_i}\right) \quad [165]$$

Notice that the term in braces, which evolves the particle positions, is different from the one encountered under equilibrium conditions as described earlier. The q_x and q_y components of this operator do not commute owing to the term involving the shear rate. Thus, the central operator has to be factorized further to yield

$$\exp\left(\frac{\Delta t}{2} \nu_{y_i} \frac{\partial}{\partial q_{y_i}}\right) \exp\left[\Delta t(\nu_{x_i} + \gamma q_{y_i}) \frac{\partial}{\partial q_{x_i}}\right] \exp\left(\Delta t \nu_{z_i} \frac{\partial}{\partial q_{z_i}}\right) \exp\left(\frac{\Delta t}{2} \nu_{y_i} \frac{\partial}{\partial q_{y_i}}\right) \quad [166]$$

The \mathbf{L}_{mvV} operator evolves the particle positions and velocities at time 0 to time Δt . Using the general methodology already introduced for representing the action of the operators as differential equations, the evolution equation for q_x can be written as

$$q_{x_i}(\Delta t) = q_{x_i}(0) + \Delta t \left[\nu_{x_i} \left(\frac{\Delta t}{2} \right) + \gamma q_{y_i} \left(\frac{\Delta t}{2} \right) \right] \quad [167]$$

Here,

$$\nu_{x_i}\left(\frac{\Delta t}{2}\right) = \nu_{x_i}(0) + \Delta t \frac{F_{x_i}(0)}{2m_i} \quad [168]$$

and

$$q_{y_i}\left(\frac{\Delta t}{2}\right) = q_{y_i}(0) + \frac{\Delta t}{2} \nu_{y_i}\left(\frac{\Delta t}{2}\right) \quad [169]$$

with

$$\nu_{y_i}\left(\frac{\Delta t}{2}\right) = \nu_{y_i}(0) + \Delta t \frac{F_{y_i}(0)}{2m_i} \quad [170]$$

The evolution of q_y , q_z , and \mathbf{v} is unaffected by shear rate and is the same as the usual velocity Verlet equations introduced earlier. The operator expression for the action of $i\mathbf{L}_{mvV}$ can be translated to computer code as follows:

```
subroutine LmvV
  v = v + .5 * dt * f/m          ! shift v to the half time step
  qy = qy + .5 * dt * vy         ! shift qy to the half time step
  qz = qz + dt * vz              ! shift qz to the full time step
  qx = qx + dt * (vx + gamma * qy) ! shift qx to the full time step
  qy = qy + .5 * dt * vy         ! shift qy to the full time step
  call force                      ! update the force at the full time step
  v = v + .5 * dt * f            ! shift v to the full time step
end subroutine LmvV
```

Let us now consider the action on the phase space variables of the operator $\exp[(\Delta t/2)[i\mathbf{L}_{NH} - i\gamma\nu_{y_i} \cdot (\partial/\partial v_i)]]$ from Eq. [164]. The purpose of this operator is to evolve the extended system variables η , and ν_η and the particle velocities \mathbf{v}_i in time.

It should be noted that in practice one should use a multiple-time step approach in conjunction with higher order integrator schemes to numerically integrate the extended system variables.^{51,52} To understand the reason, we must examine the error that occurs in the breakup. As stated earlier, the prefactor of the error, P , is effectively rendered to unity because the Jacobian of the map (integrator) is unity, or volume preserving. As discussed in the earlier section on equilibrium molecular dynamics, Nosé–Hoover dynamics do not preserve the volume of phase space; hence the Jacobian for the map (integrator) will in general not be unity. Accordingly, one is not able to construct a conserved quantity, H' , that is related to the conserved quantity of the dynamics as in

Hamiltonian systems. Thus, one has to treat this “non-volume-preserving piece” of the integrator a bit more carefully. To ensure numerical stability, higher order reversible integration schemes in conjunction with multiple time step methods are preferred. The details of implementing this scheme are provided in Ref. 28.

The operator considered in the preceding paragraph can be represented as follows:

$$\exp\left[\frac{\Delta t}{2}\left(iL_{NH} - \hat{i}\gamma\nu_{y_i} \cdot \frac{\partial}{\partial v_i}\right)\right] = \exp\left[\frac{\Delta t}{2}(-\nu_\eta v_i - \hat{i}\gamma\nu_{y_i}) \cdot \frac{\partial}{\partial v_i} + \nu_\eta \frac{\partial}{\partial \eta} + G \frac{\partial}{\partial \nu_\eta}\right] \quad [171]$$

Because the update of ν_η depends on the velocities (through the force on the thermostat G), the two operators involving the evolution of v_i and ν_η do not commute. Thus, Eq. [171] must be factorized to

$$\exp\left(\frac{\Delta t}{4} G \frac{\partial}{\partial \nu_\eta}\right) \exp\left[\frac{-\Delta t}{2}(\nu_\eta v_i - \hat{i}\gamma\nu_{y_i}) \cdot \frac{\partial}{\partial v_i}\right] \exp\left(\frac{\Delta t}{2} \nu_\eta \frac{\partial}{\partial \eta}\right) \exp\left(\frac{\Delta t}{4} G \frac{\partial}{\partial \nu_\eta}\right) \quad [172]$$

From the preceding discussion, it can be seen that the $\nu_\eta(\Delta t/2)$ and $\eta(\Delta t/2)$ are given by

$$\begin{aligned} \eta(\Delta t) &= \eta(0) + \frac{\Delta t}{2} \nu_\eta\left(\frac{\Delta t}{2}\right) \\ \nu_\eta(\Delta t) &= \nu_\eta\left(\frac{\Delta t}{2}\right) + \frac{\Delta t}{4} G(\Delta t) \\ \nu_\eta\left(\frac{\Delta t}{2}\right) &= \nu_\eta(0) + \frac{\Delta t}{4} G(0) \end{aligned} \quad [173]$$

The update of the particle velocities v is addressed by the term in square brackets in Eq. [172]. At equilibrium, $\gamma = 0$ and the action of the operator is to scale v by $\exp[-(t/2)\nu_\eta]$, as can be seen from the differential equation

$$\begin{aligned} \dot{v} &= -\nu_\eta\left(\frac{\Delta t}{2}\right)v \\ v\left(\frac{\Delta t}{2}\right) &= v(0) \exp\left[\left(\frac{\Delta t}{2}\right)(-\nu_\eta)\left(\frac{\Delta t}{2}\right)\right] \end{aligned} \quad [174]$$

Equation [172] shows that the shear-rate-dependent term affects the update of only v_{x_i} . As a result, the v_x and v_y components in the bracketed term in Eq. [172] do not commute, and a Trotter factorization of this term must be performed:

$$\begin{aligned} & \exp\left(\frac{-\Delta t}{4} (\nu_\eta v_{x_i} + \gamma v_{y_i}) \frac{\partial}{\partial v_{x_i}}\right) \exp\left(\frac{-\Delta t}{2} \nu_\eta v_{y_i} \frac{\partial}{\partial v_{y_i}}\right) \\ & \times \exp\left(\frac{-\Delta t}{2} \nu_\eta v_{z_i} \frac{\partial}{\partial v_{z_i}}\right) \exp\left(\frac{-\Delta t}{4} (\nu_\eta v_{x_i} + \gamma v_{y_i}) \frac{\partial}{\partial v_{x_i}}\right) \end{aligned} \quad [175]$$

The term involving the update of v_x yields a first-order inhomogeneous differential equation. This could be solved analytically or, alternatively, it could be Trotter-factorized further to obtain an approximation to the inhomogeneous differential equation. As discussed at the beginning of this section, one usually incorporates a multiple-time-step procedure in conjunction with higher order reversible integrators to integrate the extended system variables. This is a simpler route, and, because the extended system is being treated more accurately, the approximation is fine. Further discussion on this can be found in Refs. 28 and 50. The operator can thus be written as follows:

$$\begin{aligned} & \exp\left(\frac{-\Delta t}{8} \nu_\eta v_{x_i} \frac{\partial}{\partial v_{x_i}}\right) \exp\left(\frac{-\Delta t}{4} \gamma v_{y_i} \frac{\partial}{\partial v_{x_i}}\right) \exp\left(\frac{-\Delta t}{8} \nu_\eta v_{x_i} \frac{\partial}{\partial v_{x_i}}\right) \exp\left(\frac{-\Delta t}{2} \nu_\eta v_{y_i} \frac{\partial}{\partial v_{y_i}}\right) \\ & \times \exp\left(\frac{-\Delta t}{2} \nu_\eta v_{z_i} \frac{\partial}{\partial v_{z_i}}\right) \exp\left(\frac{-\Delta t}{8} \nu_\eta v_{x_i} \frac{\partial}{\partial v_{x_i}}\right) \exp\left(\frac{-\Delta t}{4} \gamma v_{y_i} \frac{\partial}{\partial v_{x_i}}\right) \exp\left(\frac{-\Delta t}{8} \nu_\eta v_{x_i} \frac{\partial}{\partial v_{x_i}}\right) \end{aligned} \quad [176]$$

The operators have to be applied on the initial state $v_x(0)$, $v_y(0)$, $v_z(0)$ to yield the state $v_x(\Delta t/2)$, $v_y(\Delta t/2)$, $v_z(\Delta t/2)$. These are given by

$$\begin{aligned} v'_x &= \exp\left[\frac{-\Delta t}{4} \nu_\eta \left(\frac{\Delta t}{2}\right)\right] v_x(0) + \frac{-\Delta t}{4} \gamma v_y(0) \exp\left[\frac{-\Delta t}{8} \nu_\eta \left(\frac{\Delta t}{2}\right)\right] \\ v_y &= \exp\left[\frac{-\Delta t}{2} \nu_\eta \left(\frac{\Delta t}{2}\right)\right] v_y(0) \\ v_z &= \exp\left[\frac{-\Delta t}{2} \nu_\eta \left(\frac{\Delta t}{2}\right)\right] v_z(0) \\ v_x &= \exp\left[\frac{-\Delta t}{4} \nu_\eta \left(\frac{\Delta t}{2}\right)\right] v'_x + \frac{-\Delta t}{4} \gamma v_y \left(\frac{\Delta t}{2}\right) \exp\left[\frac{-\Delta t}{8} \nu_\eta \left(\frac{\Delta t}{2}\right)\right] \end{aligned} \quad [177]$$

We now convert the action of Eq. [172] into computer code:

```

subroutine LNH
call getG
vη=vη+.25*dt*G
η=η+.5*dt*vη
! compute force on thermostat using
! Equation [163]
! shift vη to the quarter time step
! shift η to the half time step
! begin the update of v's using Equation
! [176]
vx=vx*exp(-.125*dt*vη)
vx=vx-γ*.25*vy
vx=vx*exp(-.125*dt*vη)
vy=vy*exp(-.5*dt*vη)
vz=vz*exp(-.5*dt*vη)
vx=vx*exp(-.125*dt*vη)
vx=vx-γ*.25*vy
vx=vx*exp(-.125*dt*vη)
! scale vx
! shift vx
! scale vx. vx now updated to quarter
time step
! scale vy to half time step
! scale vz to half time step
! scale vx
! shift vx
! scale vx. vx now updated to half time
step
! all the v's updated to half time step
! compute force on thermostat using
Equation [163]
! shift vη to half time step
call getG
vη=vη+.25*dt*G
end subroutine LNH

```

The full time evolution to $\Gamma_{\Delta t} = e^{(iL_{SLLOD})\Delta t}$ is then summarized as follows

```

subroutine LSLLOD
call LNH
call Lmvv
call LNH
! update vη; update η to half time step;
scale v
! update v; update q to full time step
! update vη; update η to full time step;
scale v
end subroutine LSLLOD

```

SLLOD Dynamics for Planar Couette Flow in the Isothermal–Isobaric Ensemble

In the earlier subsection on the Dynamical Generation of the NPT Ensemble, we introduced equations of motion to perform equilibrium MD under constant temperature and pressure conditions. These equations of motion can be augmented with terms involving the shear rate from the SLLOD equations and can be written⁵⁰ as follows:

$$\begin{aligned}
\dot{\mathbf{q}}_i &= \frac{\mathbf{p}_i}{m_i} + \hat{\mathbf{i}}\gamma q_{y_i} + \frac{p_\epsilon}{W} \mathbf{q}_i \\
\dot{\mathbf{p}}_i &= \mathbf{F}_i - \hat{\mathbf{i}}\gamma p_{y_i} - \mathbf{p}_i \frac{p_\eta}{Q} - \left(1 + \frac{d}{N_f}\right) \frac{p_\epsilon}{W} \mathbf{p}_i \\
\dot{V} &= \frac{dVp_\epsilon}{W} \\
\dot{p}_\epsilon &= dV(P_{\text{int}} - P_{\text{ext}}) + \frac{d}{N_f} \sum_{i=1}^N \frac{\mathbf{p}_i^2}{m_i} - \frac{p_{\eta_\epsilon}}{Q_\epsilon} p_\epsilon \\
\dot{\eta} &= \frac{p_\eta}{Q} \\
\dot{\eta}_\epsilon &= \frac{p_{\eta_\epsilon}}{Q} \\
\dot{p}_\eta &= \sum_{i=1}^N \frac{\mathbf{p}_i^2}{m_i} - N_f k_B T \\
\dot{p}_{\eta_\epsilon} &= \frac{p_\epsilon^2}{W} - k_B T
\end{aligned} \tag{178}$$

These equations assume isotropic cell fluctuations, whereas Eqs. [84] allow anisotropy in cell dynamics. Note that different thermostats are coupled to the system and barostat variables in Eq. [178]. The total Liouvillian governing the evolution of the phase space variables, $\{\mathbf{q}, \mathbf{p}, \eta, \nu_\eta, V, \nu_\epsilon, \eta_\epsilon\}$, is given by

$$\begin{aligned}
i\mathcal{L}_{\text{NPT-SLLOD}} &= i\mathcal{L}_{\text{SLLOD}} + \nu_\epsilon \mathbf{q}_i \cdot \frac{\partial}{\partial \mathbf{q}_i} + dV \nu_\epsilon \frac{\partial}{\partial V} - \left(1 + \frac{d}{N_f}\right) \nu_\epsilon \mathbf{v}_i \cdot \frac{\partial}{\partial \mathbf{v}_i} \\
&\quad + (G_\epsilon - \nu_\epsilon \nu_{\eta_\epsilon}) \frac{\partial}{\partial \nu_\epsilon} + \nu_{\eta_\epsilon} \frac{\partial}{\partial \eta_\epsilon} + G_{\eta_\epsilon} \frac{\partial}{\partial \nu_{\eta_\epsilon}}
\end{aligned} \tag{179}$$

where

$$G_{\eta_\epsilon} = W\nu_\epsilon^2 - k_B T \tag{180}$$

$$G_\epsilon = dV(P_{\text{int}} - P_{\text{ext}}) + \frac{d}{N_f} \sum_i^N m_i \mathbf{v}_i^2 \tag{181}$$

Here P_{int} is the internal pressure given by Eq. [77] and P_{ext} is the pressure set by the simulator. We proceed in the same fashion as detailed in the earlier subsec-

tion where the extended propagators are brought to the outside using the Trotter factorization (see Eq. [164]). We can modify $i\mathbf{L}_{\text{mvV}}$ presented in Eq. [162] for the isobaric–isothermal ensemble. Thus the modified velocity Verlet Liouville propagator becomes

$$\begin{aligned} \exp(i\mathbf{L}_{\text{mvV}}) = & \exp\left(\frac{\Delta t}{2} \frac{\mathbf{F}_i}{m_i} \cdot \frac{\partial}{\partial \mathbf{v}_i}\right) \left\{ \exp\left[\Delta t (\mathbf{v}_i + \hat{i}\gamma q_{y_i} + \nu_\epsilon \mathbf{q}_i) \cdot \frac{\partial}{\partial \mathbf{q}_i}\right] \right\} \exp\left(\frac{\Delta t}{2} \frac{\mathbf{F}_i}{m_i} \cdot \frac{\partial}{\partial \mathbf{v}_i}\right) \\ & \times \exp\left(\Delta t dV \nu_\epsilon \frac{\partial}{\partial V}\right) \end{aligned} \quad [182]$$

Here we have used the fact that the volume V commutes with the positions and velocities. As described earlier, because of the presence of the external fields, different components of the position are coupled and thus do not commute. The term in square brackets must be factorized again to become

$$\begin{aligned} & \exp\left[\frac{\Delta t}{2} (\nu_{y_i} + \nu_\epsilon q_{y_i}) \frac{\partial}{\partial q_{y_i}}\right] \exp\left[\Delta t (\nu_{x_i} + \gamma \nu_\epsilon q_{y_i} + \nu_\epsilon q_{x_i}) \frac{\partial}{\partial q_{x_i}}\right] \\ & \times \exp\left[\Delta t (\nu_{z_i} + \nu_\epsilon q_{z_i}) \frac{\partial}{\partial q_{z_i}}\right] \exp\left[\frac{\Delta t}{2} (\nu_{y_i} + \nu_\epsilon q_{y_i}) \frac{\partial}{\partial q_{y_i}}\right] \end{aligned} \quad [183]$$

The equivalent differential equation for the operators given in Eq. [183] in generic form reads:

$$\dot{x} = Ax + B \quad [184]$$

The careful reader should have realized that we choose not to break up this operator with another Trotter factorization, as was done for the extended system case. In practice, one does not multiple-time-step the modified velocity Verlet algorithm because it will, in general, have a unit Jacobian. Thus, one would like the best representation of the operator that can be obtained in closed form. However, even in the case of a modified velocity Verlet operator that has a nonunit Jacobian, multiple-time-stepping this procedure can be costly because of the multiple force evaluations. Generally, if the integrator is stable without multiple-time-step procedures, avoid them. The solution to this first-order inhomogeneous differential equation is standard and can be found in texts on differential equations (see, e.g., Ref. 53).

$$x(t) = x(0)e^{At} + \frac{2B}{A} e^{At/2} \sinh \frac{At}{2} \quad [185]$$

We now translate the action of the operator expression Eq. [182] into computer code:

```

subroutine Lmvv
  v=v+.5*dt*f/m
  ! shift v to the half
  ! time step
  ! update q's using
  ! Equation [183]
  qy=qy*exp(v_e*dt*.5)
  +4.*vy*exp(v_e*dt*.25)*sinh(.25*v_e*dt) ! shift qy to the
                                               ! halftime step
  qx=qx*exp(v_e*dt)
  +2.*(vx+gamma*qy)*exp(v_e*dt*.5)*sinh(.5*v_e*dt) ! shift qx to the
                                               ! fulltime step
  qz=qz*exp(v_e*dt)
  +2.*vz*exp(v_e*dt*.5)*sinh(.5*v_e*dt) ! shift qz to the
                                               ! fulltime step
  qy=qy*exp(v_e*dt*.5)
  +4.*vy*exp(v_e*dt*.25)*sinh(.25*v_e*dt) ! shift qy to the
                                               ! fulltime step
  ! q's updated to
  ! fulltime step
  v=v*exp(dv_e*dt)
  ! shift V to the full
  ! time step
  call force
  ! updating force at
  ! fulltime step
  v=v+.5*dt*f/m
  ! shift v to the full
  ! time step
end subroutine Lmvv

```

The proper numerical representations of the hyperbolic sine function (\sinh) can be found in Ref. 28. The extended system propagator must be modified from the definition in Eq. [162] to include the additional barostat variables as well as the extra thermostat that is attached to the barostat degree of freedom.

$$\exp\left(\frac{\Delta t}{2} i \mathbf{L}_{\text{NHP}}\right) = \exp\left[\frac{\Delta t}{2} \left[i \mathbf{L}_{\text{NH}} + i \mathbf{L}_{\text{NH}_e} - \left(1 + \frac{d}{N_f}\right) \nu_e \mathbf{v}_i \cdot \frac{\partial}{\partial \mathbf{v}_i} + (G_e - \nu_e \nu_{\eta_e}) \right] \frac{\partial}{\partial \nu_e}\right] \quad [186]$$

where the Liouville operator $i \mathbf{L}_{\text{NH}_e}$ denotes the Nosé–Hoover thermostat for the barostat and is given by

$$i \mathbf{L}_{\text{NH}_e} = \nu_{\eta_e} \frac{\partial}{\partial \eta_e} + G_{\eta_e} \frac{\partial}{\partial \nu_{\eta_e}} \quad [187]$$

As was done previously, we perform successive Trotter factorizations to Eq. [186] and obtain

$$\begin{aligned} \exp\left(\frac{\Delta t}{2}iL_{NHP}\right) &= \exp\left(\frac{\Delta t}{4}G\frac{\partial}{\partial v_\eta}\right)\exp\left(\frac{\Delta t}{4}G_{\eta_\epsilon}\frac{\partial}{\partial v_{\eta_\epsilon}}\right)\left\{\exp\left(\frac{\Delta t}{4}(G_\epsilon - v_\epsilon v_{\eta_\epsilon})\frac{\partial}{\partial v_\epsilon}\right)\right\} \\ &\times \exp\left[\frac{-\Delta t}{2}\left(\left(v_\eta + \left(1 + \frac{d}{N_f}\right)v_\epsilon\right)v_i + \hat{i}\gamma v_{y_i}\right)\cdot\frac{\partial}{\partial v_i}\right]\exp\left(\frac{\Delta t}{2}v_{\eta_\epsilon}\frac{\partial}{\partial \eta_\epsilon}\right)\exp\left(\frac{\Delta t}{2}v_\eta\frac{\partial}{\partial \eta}\right) \\ &\times \left\{\exp\left(\frac{\Delta t}{4}(G_\epsilon - v_\epsilon v_{\eta_\epsilon})\frac{\partial}{\partial v_\epsilon}\right)\right\}\exp\left(\frac{\Delta t}{4}G_{\eta_\epsilon}\frac{\partial}{\partial v_{\eta_\epsilon}}\right)\exp\left(\frac{\Delta t}{4}G\frac{\partial}{\partial v_\eta}\right) \end{aligned} \quad [188]$$

The salient features of Eq. [188] are that the term in brackets is handled in exactly the same fashion as the bracketed term in Eq. [172]. The terms in curly braces will be factorized to avoid the inhomogeneous differential equation to yield

$$\exp\left(\frac{\Delta t}{4}(G_\epsilon - \nu_\epsilon \nu_{\eta_\epsilon}) \frac{\partial}{\partial \nu_\epsilon}\right) = \exp\left(-\frac{\Delta t}{8} \nu_\epsilon \nu_{\eta_\epsilon} \frac{\partial}{\partial \nu_\epsilon}\right) \exp\left(\frac{\Delta t}{4} G_\epsilon \frac{\partial}{\partial \nu_\epsilon}\right) \exp\left(-\frac{\Delta t}{8} \nu_\epsilon \nu_{\eta_\epsilon} \frac{\partial}{\partial \nu_\epsilon}\right) \quad [189]$$

We are now ready to translate Eq. [188] into computer code:

```

subroutine LNHP
call getGε
call getG
call getGηε
vη=vη+.25*dt*G
vηε=vηε+.25*dt*Gηε
vε=vε*exp(-.125*vηε)
vε=vε+.25*dt*Gε
vε=vε*exp(-.125*vηε)
η=η+.5*dt*vη
ηε=ηε+.5*dt*vηε
vx=vx*exp(-.125*dt*(vη+(1+d/Nf)*vε))
vx=vx-γ*.25*vy
! compute force on barostat
using Equation [181]
! compute force on
thermostat using Equation
[163]
! compute force on
thermostat using Equation
[180]
! shift vη to the quarter
timestep
! shift vηε to the quarter
timestep
! scale vε
! shift vε
! scale vε to quartertime
step
! shift η to the halftime
step
! shift ηε to the halftime
step
! begin the update of v's
using Equation [176]
! scale vx
! shift vx

```

```

vx=vx*exp(-.125*dt*(vη+(1+d/Nf)*vε)) ! scale vx. vx now updated to
                                                       quarter timestep
vy=vy*exp(-.5*dt*(vη+(1+d/Nf)*vε)) ! scale vy to half timestep
vz=vz*exp(-.5*dt*(vη+(1+d/Nf)*vε)) ! scale vz to half timestep
vx=vx*exp(-.125*dt*(vη+(1+d/Nf)*vε)) ! scale vx
vx=vx-γ*.25*vy ! shift vx
vx=vx*exp(-.125*dt*(vη+(1+d/Nf)*vε)) ! scale vx. vx now updated to
                                                       half timestep
                                                       all the v's updated to half
                                                       timestep
call getGε ! compute force on barostat
               using Equation [181]
vε=vε*exp(-.125*vηε) ! scale vε
vε=vε+.25*dt*Gε ! shift vε
vε=vε*exp(-.125*vηε) ! scale vε to half timestep
call getGηε ! compute force on
                   thermostat using Equation
                   [163]
call getGηε ! compute force on
                   thermostat using Equation
                   [180]
vηε=vηε+.25*dt*Gηε ! shift vηε to the half time
                                           step
vη=vη+.25*dt*G ! shift vη to half timestep
endsubroutine LNHP

```

The full time evolution to $\Gamma_{\Delta t} = e^{(iL_{NPT-SLLOD})\Delta t} \Gamma_0$ is then summarized as follows:

```

subroutine LNPT - SLLOD
call LNHP ! update vη, vε, and η to half time
           step; scale v
call Lmvv ! update v, v, and q to full time step.
call LNHP ! update vη, vε, and η to full time
           step; scale v
endsubroutine LNPT - SLLOD

```

We thus conclude the section on the numerical implementation of SLLOD dynamics for two very important and useful ensembles. However, our work is not yet complete. The use of periodic boundary conditions in the presence of a shear field must be reconsidered. This is explained in detail in the next section. Furthermore, one could imagine a situation in which SLLOD dynamics is executed in conjunction with constraint algorithms for the internal degrees of freedom and electrostatic interactions. An immediate application of this extension would be the simulation of polar fluids (e.g., water) under shear. This extension has been performed, and the integrator is discussed in detail in Ref. 42.

Boundary Conditions

Equilibrium

The earlier section on Nonequilibrium Molecular Dynamics and Linear Response Theory discussed in detail the general equations of motion in the presence of an external field. Methods to integrate these systems of equations and thereby generate a trajectory were presented in the preceding subsection. Atomistic simulations with currently available computing power can be performed for systems containing 10,000 interacting particles to a time length of about 1 ns. This sample will contain a sizable number of atoms at the surface. To understand the bulk properties of condensed phase systems that contain on the order of Avogadro's number of atoms, methods to eliminate surface effects must be developed.

The commonly employed methods are known in the literature as "periodic boundary condition" (PBC) and "minimum imaging."³⁴ Essentially, the way to remove surfaces is to allow the atoms near opposite surfaces to interact as if they were near neighbors, that is, to create a flat torus in $d + 1$ dimensions, where d is the dimension of a space. A pictorial representation of minimum imaging can be found in Figure 12. In this section, we discuss the application of these boundary conditions for a simulation cell of arbitrary shape.

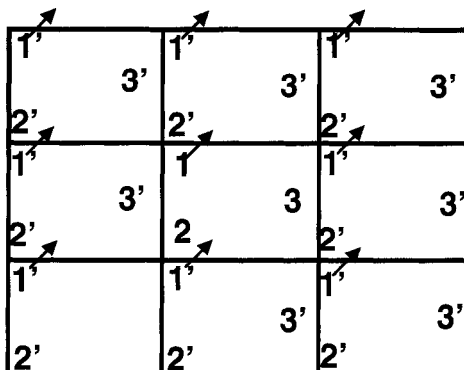


Figure 12 Schematic to illustrate minimum imaging of interparticle distances in a square box. Particles 1, 2, and 3 represent real coordinates in the central box, whereas the primed numbers represent image positions obtained by translations of real coordinates by a box length in each direction. The distance between particles 1 and 2 and between 1 and 2' are calculated. Assuming that the latter is smaller than the former, particle 1 interacts with particle 2' and not with 2. Hence particle 1 does not suffer from lack of neighbors; that is, surface effects arising from a finite size system are eliminated. During the dynamics, if particle 1 leaves the box (see arrow), it can be brought back into the central box from the opposite edge, if necessary.

The operational methodology of minimum imaging for equilibrium systems can be summarized as follows. Let \hat{h} represent the $d \times d$ matrix of unit cell vectors. For a cubic box, this matrix will be diagonal, and the elements will each be L , the box length. In general, \hat{h} can describe a parallelepiped. To perform minimum imaging in such a general noncubic box, it is common practice to scale the physical coordinates of the particles (i.e., q_i) by \hat{h}^{-1} to give coordinates s_i . This set of atomic coordinates is contained in a unit cube, and the methods of imaging presented in Ref. 34 can be used. Once the image distance in the scaled system has been identified, the “real” distance vectors are computed by scaling to the original cell with the action of \hat{h} .

This operation thus consists of four parts: scale particle coordinates, compute scaled interparticle distances, perform minimum imaging, and unscale the interparticle distances. This procedure is performed inside the subroutine to compute the forces on each particle as described in the following code:

```

 $s_i = \hat{h}^{-1} \cdot q_i$            ! getting to scaled coordinates
 $s_{ij} = s_i - s_j$              ! scaled interparticle distances
 $s_{ij} = s_{ij} - dnint(s_{ij})$  ! Minimum imaging in unit cube
 $q_{ij} = \hat{h} \cdot s_{ij}$          ! Real interparticle distances

```

Here, the function `dnint` is a FORTRAN intrinsic function that returns the nearest integer of the argument. The procedure above, called *minimum imaging*, allows one to compute the closest neighbors to any particle, taking into account that interparticle distances between particles close to opposite faces of the box are computed “through” the boundary. It is pertinent to note that it is not necessary for all the particles to be in the central box during the MD run. Minimum imaging will compute the correct interparticle distances irrespective of the actual location of a particle.

Thus, during dynamics, the particles could leave the central box. At equilibrium, it is not necessary for the particles to be brought back into the central box. However, when this must be done, the PBC procedure, which is similar to minimum imaging, can be performed. In this procedure, the particle coordinates q_i are converted to scaled coordinates s_i . These are then brought into the central cubic box by means of the `dnint` operation, and then unscaled using \hat{h}^{-1} to give back q_i in the central cell. Because unshifted particle coordinates along the trajectory are often required (to calculate, e.g., mean-squared displacements), it is not necessary to perform PBC under equilibrium conditions.

Thus, the essential philosophy of removing surfaces is to maintain continuity of the particle coordinates and momenta across boundaries. Although the particle coordinates can be in any image box, the size and shape of the central box are always taken into account in the computation of interparticle distances. Thus, in a molecular dynamics simulation, the density of the sample is determined only by the minimum imaging procedure.

Generalized Flows

To construct the condition for minimum imaging for systems under an external field, let us reexamine the GSLLOD equations of motion (Eqs. [134]) without thermostats:

$$\begin{aligned}\dot{\mathbf{q}}_i &= \frac{\mathbf{p}_i}{m_i} + \mathbf{q}_i \cdot \nabla \mathbf{u} \\ \dot{\mathbf{p}}_i &= \mathbf{F}_i - \mathbf{p}_i \cdot \nabla \mathbf{u} - m_i \mathbf{q}_i \cdot \nabla \mathbf{u}\end{aligned}\quad [190]$$

The coordinates \mathbf{q}'_i and momenta \mathbf{p}'_i of the image particles can be written as follows:

$$\begin{aligned}\dot{\mathbf{q}}'_i &= \mathbf{q}_i + \overleftrightarrow{\mathbf{h}} \cdot \boldsymbol{\Lambda} \\ \dot{\mathbf{p}}'_i &= \mathbf{p}_i\end{aligned}\quad [191]$$

where $\boldsymbol{\Lambda}$ is a three-dimensional vector of arbitrary integers, λ_1 , λ_2 , and λ_3 . Note that \mathbf{p}_i is independent of λ . This implies that p_i is an intrinsic (also called peculiar) momentum of the particle (as discussed in connection with planar Couette flow) and thus is the same irrespective of the image box in which the particle resides. From Eq. [191] we see that the peculiar momenta of particles are continuous across boundaries between image boxes, whereas the laboratory coordinates \mathbf{q}_i are not. This is fully consistent with the nature of shear flow that one would expect in an ideal system of infinite extent with no boundaries.

At equilibrium, the box matrix $\overleftrightarrow{\mathbf{h}}$ evolves to respond to the internal stresses with respect to an externally set pressure in the *NPT* ensemble (Eqs. [84]) in both the isotropic and flexible cell cases. The application of the external field contributes an additional term to its evolution. It is important to apply appropriate boundary conditions that are consistent with the nature of the dynamics. The contribution of the field to the time evolution of the simulation box can be represented⁵⁴ as follows:

$$\dot{\overleftrightarrow{\mathbf{h}}} = (\nabla \mathbf{u})^t \cdot \overleftrightarrow{\mathbf{h}} \quad [192]$$

where the superscript denotes the transpose of the matrix. Equation [192] preserves the time evolution of the coordinates of the image particles also. By taking the time derivative of Eq. [191], and by using Eq. [192], one can obtain an equation of motion for the image particles (\mathbf{q}'_i , \mathbf{p}'_i) that is identical in form to Eq. [190]. This is shown as follows:

$$\begin{aligned}
 \dot{\mathbf{q}}'_i &= \frac{\mathbf{p}_i}{m_i} + \mathbf{q}_i \cdot \nabla \mathbf{u} + \nabla \mathbf{u}^t \cdot \vec{\mathbf{h}} \cdot \boldsymbol{\Lambda} \\
 &= \frac{\mathbf{p}_i}{m_i} + \mathbf{q}_i \cdot \nabla \mathbf{u} + \vec{\mathbf{h}} \cdot \boldsymbol{\Lambda} \cdot \nabla \mathbf{u} \\
 &= \frac{\mathbf{p}_i}{m_i} + \dot{\mathbf{q}}'_i \cdot \nabla \mathbf{u}
 \end{aligned} \tag{193}$$

This exercise, which validates Eq. [192], can also be performed to see the validity of the evolution of \mathbf{h} in the *NPT* ensemble, (Eqs. [84]). To simulate flows in bulk systems, Eq. [192] must be used in conjunction with SLLOD or GSLLOD equations. We call Eq. [192] the *box dynamics method*.

Equation [192] is a linear first-order differential equation, so its integration in time is straightforward. It can be integrated along with the particle coordinates in the *NVT* ensemble. While calculating the forces on particles, minimum imaging must then be performed with the evolved \mathbf{h} matrix. It is also essential that PBC on particle coordinates be performed at every time step during NEMD. This is because the rate of change of laboratory coordinate, \mathbf{q}_i , depends on the coordinate itself. Hence, if the particle is found several image boxes away from the central one, $\dot{\mathbf{q}}_i$ will be large, necessitating smaller and smaller time steps as the dynamics proceeds. The easy alternative to this nightmarish scenario is to apply periodic boundary conditions as described in the preceding subsection on equilibrium boundary conditions. In the following, we illustrate the use of Eq. [192] for the case of planar Couette flow.

Planar Couette Flow

We wish to study the effects of planar Couette flow on a system that is in the *NPT* (fully flexible box) ensemble.²⁹ In this section, we consider the effects of the external field alone on the dynamics of the cell. The intrinsic cell dynamics arising out of the internal stress is assumed implicitly.²⁸ The constant *NPT* ensemble can be employed in simulations of crystalline materials, so as to perform dynamics consistent with the cell geometry. In this section, we assume that the shear field is applied to anisotropic systems such as liquid crystals, or crystalline polytetrafluoroethylene. For an anisotropic solid, we assume that the shear field is oriented in such a way that different weakly interacting planes of atoms in the solid slide past each other. The methodology presented is quite general; hence it is straightforward to apply for simulations of shear flow in liquids in a cubic box, as well.

For planar Couette flow, the gradient of the strain rate tensor is given by

$$\nabla \mathbf{u}^t = \begin{pmatrix} 0 & \gamma & 0 \\ 0 & 0 & 0 \\ 0 & 0 & 0 \end{pmatrix} \tag{194}$$

where γ is the shear rate. The flow is in the x direction and its gradient is in the y direction.

One can use Eq. [192] to see that only certain elements of \vec{h} evolve in time. Their time evolution is given by

$$\begin{aligned}\dot{h}_{11} &= \gamma h_{21} \\ \dot{h}_{12} &= \gamma h_{22} \\ \dot{h}_{13} &= \gamma h_{23}\end{aligned}\quad [195]$$

We now concentrate on the evolution of h_{11} and h_{13} , postponing a consideration of the evolution of h_{12} until later.

Although the box matrix has nine elements, only six of them are independent. Thus, in setting up a box matrix for equilibrium simulations from crystal cell parameters, three of the off-diagonal elements can be arbitrarily chosen to be zero. This choice cannot be arbitrary for planar Couette flow. This is because, if the initial values of h_{21} and h_{23} are chosen to be nonzero, h_{11} and h_{13} will evolve boundlessly in time. On the other hand, if h_{21} and h_{23} were to be zero at $t = 0$, then during *NPT* dynamics they would oscillate around zero, and thus the average rate of change of h_{11} and h_{13} would be zero.

In contrast to h_{21} and h_{23} , h_{22} averages around a nonzero value. (For a cubic box under constant volume conditions, h_{22} would be the box length.) Thus, h_{12} , which is the projection of the cell vector \mathbf{b} on the x axis, would evolve in time without bound. If the simulated system is liquidlike in the x direction (which it must be, to be shearable), this would lead to a “pancaking” of the box, which is not desirable. Since the simulated system is periodic, we can reset h_{12} to zero whenever $\gamma\Delta t = h_{11}/h_{22}$ without loss of generality; that is, the minimum image distances along the x direction are identical for the two boxes illustrated in Figure 13.

Thus we can use Eq. [191] to write the x coordinate of an image particle in both representations (in two dimensions) as follows:

$$\begin{aligned}q_{i,x} &= q_{i,x} + \gamma_1 h_{11} && \text{Representation A} \\ q_{i,x} &= q_{i,x} + \gamma_1 h_{11} + \gamma_2 \gamma \Delta t h_{22} && \text{Representation B}\end{aligned}\quad [196]$$

When $\gamma\Delta t = h_{11}/h_{22}$, representation B provides image positions that are equivalent to that obtained from representation A. Thus, one can “reset” h_{12} to zero and still maintain the continuity of the dynamics. The range of h_{12} is thus restricted between zero and h_{11} .

Although the prescription to reset h_{12} discussed above is quite general, it can be made more efficient as applied to systems of finite size.^{42,55} For any molecular dynamics simulation, the cutoff distance of the potential, r_c , should be smaller than half of the smallest distance between any two opposite faces of

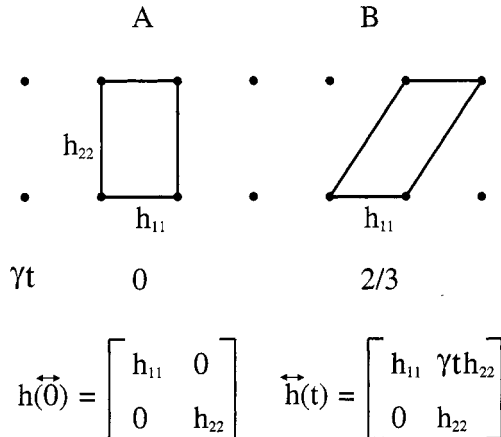


Figure 13 Minimum imaging under cell representations where cases A and B are equivalent. The box in B is skewed owing to the planar Couette shear field, and resetting it to representation A is consistent with the dynamics. \vec{h} is the matrix representing the box size and shape, γ is the shear rate, and t denotes time.

the box. When $\gamma\Delta t = h_{11}/h_{22}$, the simulation box is skewed to the largest extent. This, consequently, restricts r_c . Note that h_{12} can, in general, be allowed to change between $-h_{11}/2$ and $h_{11}/2$ instead of between 0 and h_{11} . It is thus possible to use a large cutoff without increasing the system size. This choice of r_c is illustrated schematically in Figure 14.

The treatment of applying periodic boundary conditions discussed here is markedly different from that traditionally employed in simulations of planar Couette flow. The PBC method that is commonly used is called the Lees–Edwards boundary condition.⁵ In its simplified form applied to cubic boxes, it represents a translation of the image boxes in the y direction, at a rate equal to γ . Further details on this method can be found elsewhere.^{12,34} In contrast to the method involving the dynamical evolution of \vec{h} presented here, the Lees–Edwards method is much harder to develop and implement for noncubic simulation cells. Also, in simulations involving charged particles, the Coulombic interaction is handled in both real and reciprocal spaces. The reciprocal space vectors \mathbf{k} of the simulation cell represented by \vec{h} can be written^{24,42,56} as follows:

$$\mathbf{k} = 2\pi(\vec{h}^{-1})^t \begin{pmatrix} l \\ m \\ n \end{pmatrix}, \quad l^2 + m^2 + n^2 \leq k_{\max}^2 \quad [197]$$

where l, m, n are integers, and the k_{\max} is used to incorporate a spherical cutoff in the reciprocal space sum (also called the Ewald sum). With Lees–Edwards

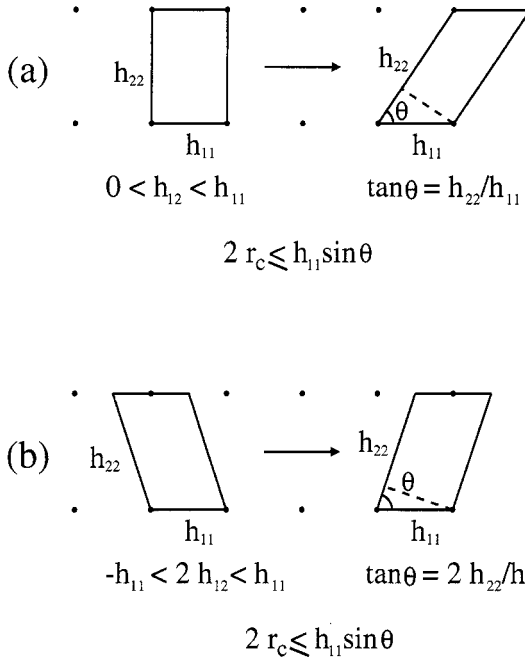


Figure 14 An efficient way of resetting h_{12} is to note that the evolutions of the periodic box in (a) and (b) lead to identical dynamics of the particles. Method a is inefficient because it necessitates the use of a larger interaction cutoff, r_c , (thus, a larger system size) than method b.

boundary conditions, the periodicity of the system is not as unambiguous as in box dynamics. Hence, a rigorous definition of reciprocal space is not known.

We have thus far discussed the basic foundations of nonequilibrium molecular dynamics, its methodology, and the details of numerically integrating the equations of motion for SLLOD dynamics. The next section presents applications of these methods.

APPLICATIONS OF SHEAR FLOW

Viscosity

As discussed in the Introduction, considerable effort has been devoted to the study of transport properties. Specifically, viscosity estimates are of potential importance in the rational design of lubricants. In these simulations, two main approaches have been used. The earlier of the two focused on a linear response theory based Green–Kubo formula:

$$\eta(t) = \frac{V}{k_B T} \int_0^t \langle P_{xy}(\Gamma_0) P_{xy}(\Gamma_s) \rangle ds \quad [198]$$

where V is the volume, k_B is Boltzmann's constant, T is temperature, and P_{xy} is the xy component of the pressure tensor. A second approach used NEMD algorithms, such as SLLOD,¹² to shear the system at a given rate γ and then apply another linear-response-based formula:

$$\eta(\gamma) = -\frac{\langle P_{xy} \rangle}{\gamma} \quad [199]$$

The application of the first method is fairly straightforward. A standard equilibrium calculation is performed until enough data have been collected to converge the integral shown in Eq. [198]. There are some additional complexities involved in the second approach. Equation [199] is based on a linear response theory, and hence is valid at shear rates for which the fluid behavior is Newtonian (i.e., the viscosity is independent of shear rate). As described in connection with homogeneous flows, limited computer power often forces NEMD simulations to operate at shear rates that can be 10 orders of magnitude higher than experiment.⁵⁷ Under these extreme modeling conditions, the fluid may no longer be Newtonian and could exhibit "shear thinning." Physically speaking, molecules find it preferential to both align themselves and decrease the density of the fluid to reduce the number of shear induced collisions. The net effect is that the resistance to shear drops, thereby producing an effective viscosity that is lower than the Newtonian value. Since such a nonlinear regime offers little insight into experimentally relevant behavior, care must be taken to demonstrate that the shear rate is sufficiently gentle to remain in the linear regime.

To this end, SLLOD simulations for a given value of γ are started from an equilibrium configuration. The effective viscosity is then calculated via Eq. [199] once the average has converged. This process must then be repeated for successively lower values of the γ until the effective viscosity becomes independent of shear rate. A demonstration of this procedure was given in Figure 11, where for low values of γ , the effective viscosity calculated via Eq. [199] can be seen to be statistically the same as the value calculated via the Green-Kubo approach (Eq. [198]). It is interesting to note that this limiting behavior is seen for values of the shear rates that are roughly below 0.005 ps^{-1} . Such a γ is still seven orders of magnitude faster than the top speed of an experimental viscometer.⁵⁷ Hence, most moderate molecular weight fluids will exhibit little nonlinear behavior under experimental conditions.

As can be seen from Figure 11, significant shear thinning is observed for a shear rate of 1 ps^{-1} . Given the 10-order-of-magnitude difference with experiment, this regime is mainly of academic interest in this case. In certain large molecular weight systems, however, shear thinning may occur at experimentally

accessible shear rates.⁵⁸ In such cases, it is interesting to note that there are measurable differences between constant pressure and constant volume simulations. It is fairly easy to understand this origin. In one case, the simulation cells can expand if the pressure rises, thereby allowing both the density to drop and the molecules to align themselves as needed. In the constant volume case, such rearrangements are hindered and molecules suffer significant collisions as they slide past one another. Hence, we see markedly different shear viscosities.

After the above-mentioned methods were successfully applied to simple atomic systems, several research groups simulated various models of butane.^{59–62} Work in this direction was important because increasing molecular complexity introduces nonnegligible long time tails in stress autocorrelation function. *n*-Butane was a very reasonable molecular system for these tests because it contains all the basic intramolecular interactions—bond stretches, bends, and torsions. Although the agreement between calculation and experiment was reasonable, quantitative comparisons could not be made because the methods, temperatures, and system sizes were different. Further, the lubricant stocks are generally made of much longer alkanes.

If one desires to make quantitative comparisons with experimentally relevant viscosities, however, it is not sufficient to simply extend the length of the molecules studied. Usually, systems needing lubrication, such as car engines, are under high pressures and temperatures. The potential model should be valid over a wide range of conditions. To this end, Siepmann and coworkers⁶³ used configuration-biased Monte Carlo techniques to develop model potential parameters for a range of alkanes that were capable of reproducing the experimentally known liquid–vapor coexistence curves. The quality of these parameters was also independently tested by Cummings and coworkers using Gibbs ensemble Monte Carlo and molecular dynamics;⁶⁴ these investigators came to similar conclusions regarding the effectiveness of the parameters. Because it was well established that this potential model⁶³ gave solid equilibrium results (e.g., coexistence densities and critical temperatures), a very good test of the model would be to see whether the transport properties could be reproduced. When applied to *n*-decane, the Green–Kubo and NEMD methods both give quantitative agreement with experiment at elevated state points (480 K and 170 atm) for nonequilibrium properties, such as the viscosity.⁶⁵ As these and earlier works have shown, potential parameters that are carefully determined to reproduce equilibrium features can then be used successfully in the computation of decidedly nonequilibrium properties.

Given this prescription for parameterization, prototypical lubricants were then explored. One of the first concerns was the investigation of the effects of molecular architecture on viscosity. Such tests were performed by comparing linear alkanes, such as tetracosane (C_{24}) and triacontane (C_{30}), versus a branched alkane squalane (C_{30} , with a 24-carbon-atom backbone).^{66–69} Intuitively, one would expect linear alkanes to have a lower viscosity. Not surprisingly, the simulations showed that the linear alkanes may form layers that

align with high shear fields. This allows them to slide past each other, thereby lowering the viscosity.

Hence, reliable simulations of long alkanes typically found in lubricants are attainable. Industrial lubricants may contain many additives, and some of the additives are polar. This introduces another technical challenge for the computational chemist. Electrostatic interactions are long-ranged and cannot be simply truncated. The Ewald summation method³⁴ is often employed because it efficiently handles the Coulombic energies by dividing them into real and Fourier space components, a feat that requires the ability to unambiguously define reciprocal lattice vectors. Hence, one is forced to use the box dynamics method instead of the more traditional Lees–Edwards method, as discussed in the section on Boundary Conditions. A test study was undertaken by shearing⁴² the extended special point charge (SPC/E) model⁷⁰ of water. This work⁴² found good agreement between NEMD and Green–Kubo results, with a viscosity that was approximately 18% below the experimental value. This discrepancy is consistent with expectations, since the model is known to give a similarly high value for the diffusion constant. Although possibly pointing to a shortcoming of the model, this work primarily demonstrates that the technical difficulties for shearing polar fluids can be easily handled. Hence, the simulation technology needed to use computer simulation as a predictive tool in industrial lubricant design exists.

Hydrodynamic Boundary Conditions

Confined Fluids under Shear

In the preceding sections, we have presented simulation methodologies to study systems away from equilibrium. In particular, we have concentrated on the problem of shear flow in bulk systems. In the present section, we illustrate the effectiveness of the SLLOD dynamics coupled with the robustness of the extended system approach to initiate and sustain a shear flow in a fluid in the absence of moving boundary conditions.

The physical problem we consider is the characterization of the boundary for a liquid flow over a stationary solid surface.^{71–5} The fluid flow can be studied by means of the Navier–Stokes equation

$$\frac{\partial \mathbf{v}}{\partial t} + (\mathbf{v} \cdot \nabla) \mathbf{v} = \nabla P + \eta \nabla^2 \mathbf{v} \quad [200]$$

where \mathbf{v} is the laboratory velocity, P the pressure tensor, and η the shear viscosity. Given appropriate boundary conditions, this equation can be solved for any particular geometry of the fluid flow. The issue then is the choice of the boundary condition at the interface. Traditionally, two extreme choices have been made. These are the slip and no-slip conditions. These conditions can be better visualized in the case of a fluid flow induced by moving the boundaries

(i.e., inhomogeneous methodology). The complete slip condition occurs for an ideally flat surface with no corrugation in the flow direction. The momentum transfer from the surface to the fluid will be zero, and hence the fluid will be unaltered from the equilibrium state. No slip occurs when a surface with corrugation is able to impart momentum to the fluid at the boundary as the fluid moves at the same speed as the boundary; that is, the relative velocity of the moving boundary and the fluid at the boundary is zero. In essence, the crucial parameter that controls the nature of the boundary condition is the degree of momentum transfer between the solid and the fluid. More generally, situations with varying amounts of slip at the interface necessitate the need for a general boundary condition. The most general boundary condition in the planar Couette geometry is due to Bocquet and Barrat (BB).^{73,74,76}

$$\frac{\partial v_x(\mathbf{q}, t)}{\partial y} \Big|_{y=y_{\text{wall}}} = \frac{1}{\delta_{\text{wall}}} v_x(\mathbf{q}, t) \Big|_{y=y_{\text{wall}}} \quad [201]$$

Here, x is the direction of the fluid flow and y is the direction of the velocity gradient. δ_{wall} and y_{wall} are the “slipping length” and the “hydrodynamic thickness,” respectively. The former is a measure of the slip, as described above, and y_{wall} is an average position from the boundary at which hydrodynamics breaks down. Recall from the Introduction that inhomogeneous methods will in general have an inhomogeneous density profile as shown in Figure 2. It should be clear that the viscosity η will not be uniform throughout the system, and thus Eq. [200], which *assumes* a uniform shear viscosity, will not be valid in these regions. Hence, y_{wall} measures the distance from the boundary where hydrodynamics (Eq. [200]) is valid. Real-world situations of slip include gas flows over metal surfaces and polymer flows through extrusion pipes.^{77,78}

Equation [201], when multiplied on both sides by the bulk shear viscosity, resembles a stress–strain relation with the factor $(\eta\delta)$ identified as the friction coefficient, λ . Thus, when the stress (left-hand side of Eq. [201]) is zero, δ is infinity, which is the “slip” condition. And the relative fluid velocity v_x is zero in the “no-slip” limit, making δ zero. Using the phenomenological relation $\lambda = \eta\delta$, it is thus possible to obtain the friction coefficient from microscopic simulations. In the approach of BB, the hydrodynamic boundary parameters (HBP) are treated as transport coefficients. A schematic of the methodology used here is shown in Figure 15. In the following sections, we delineate the linear response theory (LRT) of a confined fluid undergoing shear and follow this up with the necessary simulation methodology to be adopted to calculate the hydrodynamic boundary parameters.

SLLOD Dynamics for Confined Fluids

In the section on nonequilibrium molecular dynamics, the equations of motion for field-driven dynamics were introduced. We have also noted that for bulk fluids, the field must be accompanied by boundary conditions that are

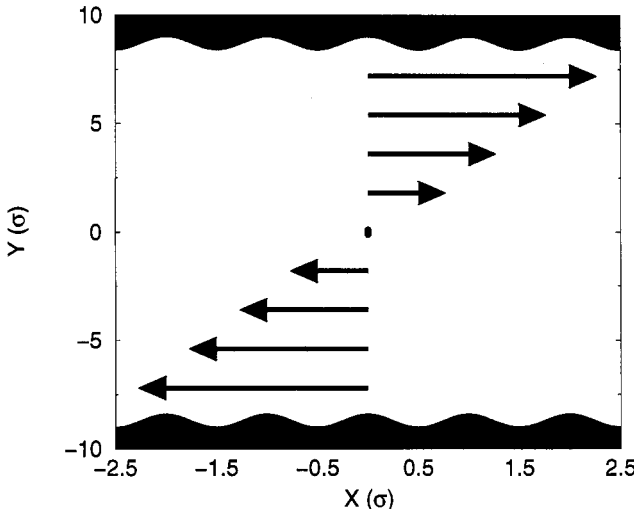


Figure 15 Schematic of the method employed to calculate friction coefficient. The corrugated surfaces are immobile, and a shear flow is generated in the confined fluid using SLLOD equations of motion. The difference in momentum between the fluid and the surfaces results in a frictional force, which is the response function.

consistent with the flow geometry. In this section, we address issues of SLLOD dynamics for confined fluids under shear.

In the absence of shearing periodic boundary conditions (of the type introduced earlier) the system is totally *isolated*; that is, all the degrees of freedom of the system are explicitly accounted for in the equations of motion. In this case, it is possible to obtain a conserved quantity for field-driven dynamics in general and SLLOD in particular.⁴⁵ The approach we employ is similar to that introduced in the section on Molecular Dynamics and Equilibrium Statistical Mechanics. The SLLOD equations of motion are

$$\begin{aligned}\dot{\mathbf{q}}_i &= \frac{\mathbf{p}_i}{m_i} + \hat{i}\gamma(q_{y_i} - q_0) \\ \dot{\mathbf{p}}_i &= \mathbf{F}_i - \hat{i}\gamma p_{y_i} - \frac{p_\eta}{Q} \mathbf{p}_i \\ \dot{\eta} &= \frac{p_\eta}{Q} \quad [202] \\ \dot{p}_\eta &= \sum_{i=1}^N \frac{\mathbf{p}_i^2}{m_i} - N_f k_B T \\ \dot{I} &= \gamma \sum_{i=1}^N (q_{y_i} - q_0) p_{x_i} \frac{p_\eta}{Q}\end{aligned}$$

and mass parameter $Q = N_f k_B T \tau^2$. Note that the equation of motion of the particle coordinate \mathbf{q} has a slight modification from the one introduced for bulk simulations in Eqs. [123]. In a bulk system, there are no surfaces, whereas in the case of a confined fluid, one can locate the shear field with respect to the surfaces, arbitrarily. The parameter q_0 represents the zero of the shear flow.

Also, note that in Eq. [202] we have introduced a variable, I , which although inconsequential to the dynamics of the variables representing the fluid (i.e., p , \mathbf{q}) is essential to obtain a conserved energy for SLLOD dynamics with time-independent boundary conditions. The conserved energy for the dynamics in Eqs. [202] is given by

$$H' = \sum_{i=1}^N \frac{(\mathbf{p}_i + \hat{\mathbf{i}} m_i \gamma (q_{y_i} - q_0))^2}{2m_i} + V(\mathbf{q}) + \frac{p_\eta^2}{2Q} + N_f k_B T \eta + I \quad [203]$$

An immediate use for this conserved quantity is obvious; it can (and should) be used to check the NEMD code for algorithmic and programming errors. It is also possible to use the conserved energy in obtaining a knowledge of the phase space. The approach proceeds in the same fashion as presented in the section on equilibrium molecular dynamics. Let Γ denote the full phase space of the variables, \mathbf{p}_i , \mathbf{q}_i , η , p_η , I . We now make the assumption of equal a priori probability for each of the microstates Γ with energy H' . This assumption has traditionally been applied to equilibrium systems only. In the isolated system we consider, this assumption is the most obvious one to make. Thus, one can write the phase space distribution function $f(\Gamma)$ as

$$f(\Gamma) = \delta(H' - E) \quad [204]$$

where E is the energy specified by the initial conditions, $\Gamma(0)$. The probability of finding the system between phase space points Γ and $\Gamma + d\Gamma$ is given by $f(\Gamma) \sqrt{g(\Gamma)} d\Gamma$. Here $\sqrt{g(\Gamma)}$ is the metric determinant that arises from the compressibility of Nosé–Hoover dynamics and is equal to $e^{N_f \eta}$. The corresponding microcanonical partition function is

$$\begin{aligned} Z &= \int \sqrt{g(\Gamma)} d\Gamma \delta(H' - E) \\ &= \int d^N \mathbf{p} d^N \mathbf{q} d\eta dp_\eta dI e^{N_f \eta} \delta \left[\sum_{i=1}^N \frac{(\mathbf{p}_i + \hat{\mathbf{i}} m_i \gamma (q_{y_i} - q_0))^2}{2m_i} + V(\mathbf{q}) \right. \\ &\quad \left. + \frac{p_\eta^2}{2Q} + N_f k_B T \eta + I - E \right] \end{aligned} \quad [205]$$

Performing the integral over the variable η , one obtains

$$Z = \int d^N \mathbf{p} d^N \mathbf{q} dp_\eta dI \tilde{f}(\mathbf{p}, \mathbf{q}, p_\eta, I) \quad [206]$$

where

$$\tilde{f}(\mathbf{p}, \mathbf{q}, p_\eta, I) \approx \exp \left\{ \frac{-1}{k_B T} \left[\sum_{i=1}^N \frac{(\mathbf{p}_i + i \mathbf{m}_i \gamma (q_{y_i} - q_0))^2}{2m_i} + V(\mathbf{q}) + \frac{p_\eta^2}{2Q} + I \right] \right\} \quad [207]$$

The form of $\tilde{f}(\mathbf{p}, \mathbf{q}, p_\eta, I)$ suggests that the particle momenta are distributed in the same fashion as in an equilibrium canonical ensemble, but with the peculiar momenta shifted by the drift momenta from the external field, $m_i \gamma (q_{y_i} - q_0)$. In the following section, we employ the methodology just discussed to evaluate the hydrodynamic boundary conditions of a fluid confined between two surfaces.

Linear Response Theory for Confined Fluid Under Shear

The treatment of LRT for confined fluids proceeds in the same fashion as that for deriving transport coefficients of bulk fluids.⁷⁴ We consider a fluid confined between two planar surfaces (or “walls”) at equilibrium at $t = 0$. The surfaces are parallel to the xz plane.

Following Eqs. [202], the equation of motion for the particle coordinate in a planar Couette flow can be written as follows:

$$\dot{\mathbf{q}}_i = \frac{\mathbf{p}_i}{m_i} + i \hat{\gamma} (q_{y_i} - q_0) \quad [208]$$

A difference between the perturbation considered here and that in the section on LRT considered earlier is the term involving \mathbf{q}_0 , the position at which the drift velocity (i.e., the velocity contribution from the external field) of the fluid is zero. This term was chosen to be zero in the treatment for bulk fluids for simplicity; it must be used here because confinement has broken the translational invariance of the system. The perturbation generates a planar Couette flow in the fluid between two surfaces:

$$v_x(y) = \gamma (q_{y_i} - q_0) \quad [209]$$

We have seen in the section on Linear Response Theory that the nonequilibrium average of any phase variable B is given by

$$\langle B \rangle_{\text{NE}}(t) = \langle B \rangle_0 + \beta \int_0^t ds \langle B(\Gamma_{t-s}) j(\Gamma_{t=0}) \rangle_0 f_e(s) \quad [210]$$

The subscript NE represents the steady state average in the nonequilibrium ensemble given by Eq. [207]. f_e is the external field as in Eq. [91]. The dissipative flux j is easily evaluated and is given by $P_{xy}V - F_x q_{y_0}$ for the SLLOD equations of motion, Eqs. [123] and [208]. Again, P_{xy} is the xy component of

the pressure tensor, V is the volume of the system, and F_x is the x component of the total force acting on the fluid particles. It is important to realize that F_x has two contributions: one from the fluid–fluid interactions and the other from the fluid–wall interactions. The sum over all particles of the former is zero, and thus $F_x = F_x^w$, where the superscript w is to denote the nonzero contribution from the walls.

To obtain the friction coefficient λ as the transport coefficient in LRT, we would like to take a nonequilibrium steady state average of the frictional force. Thus we identify F_x^w with the phase variable B . The frictional force in our system is the force exerted by the surface on the fluid. At equilibrium, the average of this force will be zero, because there is equal likelihood of fluid particles flowing in any given direction. Thus, the first term in Eq. [210] will be zero. Under shear, the surface will exert on average a nonzero force on the fluid due to the directionality of the flow. The frictional force is given by

$$\langle F_x^w \rangle_{\text{NE}}(t) = -\gamma \beta \int_0^t ds \langle F_x^w(\Gamma_t) [P_{xy}(\Gamma_s)V - F_x^w(\Gamma_s)q_{y_0}] \rangle_0 \quad [211]$$

We now define the hydrodynamic parameters λ_{wall} and y_{wall} as follows:

$$\lambda_{\text{wall}} = \frac{\beta}{S} \int_0^\infty ds \langle F_x^w(\Gamma_t) F_x^w(\Gamma_s) \rangle_0 \cdot y_{\text{wall}} = \frac{V \int_0^\infty ds \langle F_x^w(\Gamma_t) P_{xy}(\Gamma_s) \rangle_0}{\int_0^t ds \langle F_x^w(\Gamma_t) F_x^w(\Gamma_s) \rangle_0} \quad [212]$$

where s is the surface area of the wall. These are similar to the Green–Kubo expressions for bulk transport coefficients. Thus, using Eqs. [209] and [212], Eq. [211] can be rewritten as

$$\langle F_x^w \rangle_{\text{NE}}(t) = -S \lambda_{\text{wall}} \nu_x(y_{\text{wall}}) \quad [213]$$

Equation [213] can be equivalently obtained using the Mori–Zwanzig formalism.⁷⁴ It is also seen that, in contrast to LRT developed for shear flow in bulk fluids, the one presented here has two coefficients, λ_{wall} (which is similar to the shear viscosity η) and y_{wall} , which has no parallel in bulk fluids. y_{wall} should be interpreted as an average location at which hydrodynamics is found to be nominally invalid. Note that although the surface may have corrugations in the x as well as the y direction, the corrugation in the x direction alone matters to the frictional force in the planar Couette geometry.

Although the linear response expression for the frictional force parallels that for the shear viscosity used for bulk systems, there are some crucial differences between the two. In bulk NEMD simulations, the only independent parameter is the shear rate γ , whereas for confined fluids, both γ and q_{y_0} are independent variables. Hence one must find the set $\{\gamma, q_{y_0}\}$ such that Eq. [213] holds. Beyond the linear regime represented in Eq. [213], the results of the

boundary parameters are no longer comparable to the Green–Kubo results (Eq. [212]).

Calculation of Friction Coefficient

The model system we consider here is 300 soft sphere particles interacting via a purely repulsive potential of the form⁷⁵

$$U(r_{ij}) = \epsilon \left(\frac{\sigma}{q_{ij}} \right)^{12} \quad [214]$$

where ϵ and σ are energy and length parameters, respectively, and q_{ij} denotes the distance between two particles, i and j . The soft sphere fluid is confined between two walls, and the wall–fluid interaction is represented as follows:

$$U_{wf} = \epsilon \left\{ \left[\frac{\sigma}{q_y - q_y^l(x)} \right]^{12} + \left[\frac{\sigma}{L_y - q_y - q_y^u(x)} \right]^{12} \right\} \quad [215]$$

L_y is the box length in the y direction. The corrugation in U_{wf} is in the x direction and is given by $q_y^u(x) = q_y^l(x) = a \cos(kx)$, where the superscripts u and l denote the upper and lower walls, respectively, a is the corrugation amplitude, and the corrugation period is given by $2\pi/k$.

NEMD simulations were started from well-equilibrated, independent, equilibrium configurations. The potential parameters ϵ and σ were chosen to be 480 K and 3.405 Å, respectively. The simulations were performed at a reduced temperature of $k_B T/\epsilon = 1$ and at a density of $\rho\sigma^3 = 0.64$. The equations of motion (Eqs. [202]) were integrated with the additional variable I with a time step of 0.5 fs to ensure an “energy” conservation (see Eq. [203]) of one part in 10^5 .

Although we have assumed in Eq. [209] that the velocity profile in the confined fluid is linear, it is not immediately obvious that this is technically possible in the absence of moving boundary conditions. A parallel to this situation is the comparison between Nosé–Hoover (NH) thermostats and Nosé–Hoover chain (NHC) thermostats. Although the Nosé–Hoover equations of motion can be shown to generate the canonical phase space distribution function, for a pedagogical problem like the simple harmonic oscillator (SHO), the trajectory obtained from the NH equations of motion has been found not to fill up the phase space, whereas the NHC ones do. The SHO is a stiff system and thus to make it ergodic, one needs additional degrees of freedom in the form of an NHC.²⁷

In the confined fluid problem, in the absence of time-dependent shearing boundary conditions, we needed a “massive” thermostating scheme to stabilize the shear flow. In this scheme, each degree of freedom represented in Eqs. [202] is attached to a separate thermostat, to make the p_i of every particle truly peculiar with respect to the flow profile. The use of one global thermostat for

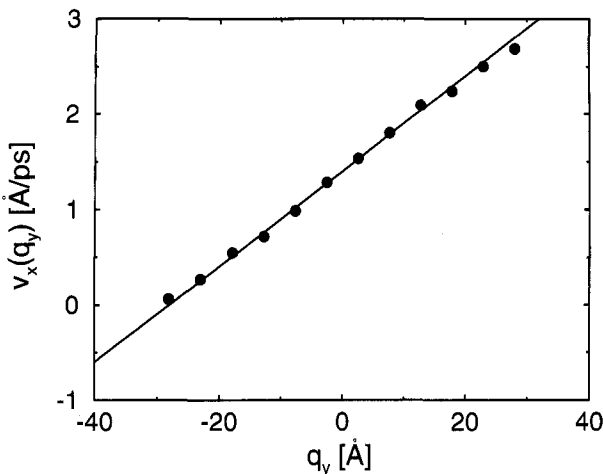


Figure 16 Velocity profile generated in the confined fluid by SLLOD equations. The circles correspond to simulation results, and the line is the expected behavior. The simulation was performed at a shear rate, $\gamma = 0.05 \text{ ps}^{-1}$, with a corrugation amplitude, $a = 0.02 \sigma$, and the zero of the shear field, $q_y^0 = -28 \text{ \AA}$.

the whole system led to a zero velocity profile. The velocity profile at a representative shear rate is shown in Figure 16.

The essence of the approach to obtaining the boundary parameters is as follows. One chooses a shear rate γ and a zero shear position $q_{y_0}^1$. This sets the velocity profile $v_x^1(q_y)$. Let us assume that we would like to characterize the hydrodynamic boundary parameters (HBP) for the lower wall. After reaching steady state (which is monitored by the generation of the linear velocity profile), the total force from the lower wall, $F_x^{l,1}$, on all the particles is calculated and averaged over 100 ps. Since we have only one equation, Eq. [213] from LRT, with two unknown parameters, two simulations with differing $v_x(y_{\text{wall}})$ must be performed. One can change $v_x(y_{\text{wall}})$ by changing q_{y_0} . Thus, we perform another simulation with the same shear rate γ , but with a different zero shear position, $q_{y_0}^2$. This will lead to a new average force $F_x^{l,2}$. The ratio of the forces $F_x^{l,1}$ and $F_x^{l,2}$ gives the ratio of the velocities at y_{wall} , which determines y_{wall} . The calculation of λ_{wall} is straightforward. It is to be borne in mind that not all choices of q_{y_0} yield sensible values of the HBPs. Only those that obey the linearity in Eq. [213] can give values that can be compared to those obtained at equilibrium. So, to find out the values of $\{\gamma, q_{y_0}\}$ that fall in the linear region, it is crucial that $\langle F_x^w \rangle_{\text{NE}}$ be plotted against $v_x(y_{\text{wall}})$. Typically y_{wall} is a couple of atomic layers away from the physical location of the wall. Hence, it is a good practice to choose the two values of q_{y_0} just below and above the “nominal” y_{wall} . This would lead to a sign reversal in the response $\langle F_x^w \rangle_{\text{NE}}$, which then can be used to bracket the exact value of y_{wall} .

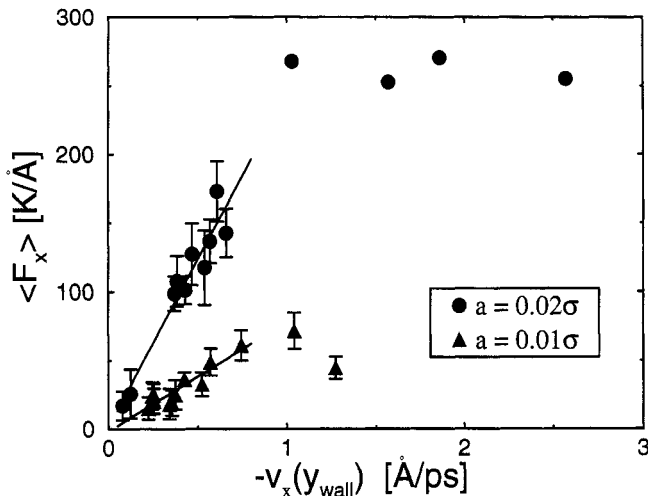


Figure 17 The frictional force, $\langle F_x^w \rangle_{NE}$, versus the velocity of the fluid at y_{wall} . The lines are a guide to the eye in the linear response regime.

The variation of $\langle F_x^w \rangle$ with $v_x(y_{wall})$ is shown in Figure 17 for two values of the corrugation amplitude. For small values of the flow velocity, we observe a linear evolution of the frictional force, in accordance with Eq. [213]. The slope of the line gives the friction coefficient in accordance with linear response. For larger values of the field, it is clear from Figure 17 that linear response theory is violated. Thus, nothing can be concluded from the outlying data.

Profile-Unbiased Thermostat and String Phases

As we have already demonstrated, the SLLOD equations have been highly successful for studying moderate shear rate systems. To review, the equations of motion for planar Couette flow, with Nosé–Hoover thermostats,^{25–27} are:

$$\begin{aligned} \dot{\mathbf{q}}_i &= \frac{\mathbf{p}_i}{m_i} + \hat{i}\gamma q_{y_i} \\ \dot{\mathbf{p}}_i &= \mathbf{F}_i - \hat{i}\gamma p_{y_i} - \mathbf{p}_i \frac{p_\eta}{Q} \\ \dot{\eta} &= \frac{p_\eta}{Q} \\ \dot{p}_\eta &= \sum_{i=1}^N \frac{\mathbf{p}_i^2}{m_i} - N_f k_B T \end{aligned} \quad [216]$$

It is important to realize that in these equations of motion, the \mathbf{q} 's are in the laboratory frame, whereas the $\mathbf{p}_{x,i}$'s are thermal momenta in a moving frame of γq_{y_i} ; that is, $\mathbf{p}_i/m_i = \dot{\mathbf{q}}_i - i\gamma q_{y_i}$. Evans and Morriss⁷² correctly pointed out that the true thermal momenta should be written with respect to the local drifting velocity $\mathbf{u}_s(\mathbf{r})$; thus, $\mathbf{p}_i/m_i = \dot{\mathbf{q}}_i - \mathbf{u}_s(\mathbf{q}_i)$. In Eqs. [216], we have assumed that $\mathbf{u}_s(\mathbf{q}_i) = (\gamma q_y, 0, 0)$. For modest shear rates, this is a reasonable assumption. At values of γ for which $\gamma\tau_r \geq 1$, where τ_r is the characteristic relaxation time of the system,⁸⁰ it is possible that secondary flows may develop. The thermostat will interpret any deviation from the assumed linear velocity profile as the generation of heat, and the thermostat will compensate by adjusting the momenta of the system in an attempt to reestablish a linear profile. (Actually, it cannot truly restore the linear profile, because a global thermostat can scale uniformly only the “kinks” in the profile.) The method is therefore referred to as a “profile-biased” thermostat (PBT). It has been shown that PBTs artificially stabilized a two-dimensional microstructure, the so-called string phase, in a hard disk system at high shear rates.⁷⁹

Evans and Morriss⁷⁹ wrote a new set of equations of motion for NEMD that allow for secondary flows:

$$\begin{aligned}\dot{\mathbf{q}}_i &= \frac{\mathbf{p}_i}{m_i} + \hat{i}\gamma q_{y_i} \\ \dot{\mathbf{p}}_i &= \mathbf{F}_i - \hat{i}\gamma p_{y_i} + (\mathbf{p}_i - m_i \mathbf{u}_{sl}(\mathbf{q}_i)) \frac{p_\eta}{Q} \\ \dot{p}_\eta &= \sum_i \frac{(\mathbf{p}_i - m_i \mathbf{u}_{sl}(\mathbf{q}_i))^2}{m_i} - N_f k_B T \\ \dot{\eta} &= \frac{p_\eta}{Q}\end{aligned}\quad [217]$$

The original scheme utilized Gaussian isokinetic thermostats,⁷⁹ whereas in Eqs. [217] we have replaced it with a Nosé–Hoover thermostat. In this equation, the true local streaming velocity is given by $i\gamma y_i + \mathbf{u}_{sl}(\mathbf{q}_i)$. In principle, there are no restrictions on \mathbf{u}_{sl} , so the steady state velocity can be of any form; hence, Evans and Morriss refer to Eqs. [217] as “profile-unbiased” thermostats (PUT). The PUT scheme requires only a reasonable prescription for determining the true local streaming velocity.

In most of the early PUT attempts,^{79,81–83} the streaming velocities did not evolve continuously over time; instead, they were instantaneous quantities that were freshly reassigned at each time step of the simulation. Such PUT procedures, however, might introduce other problems. At one extreme, PBTs interpret all secondary flows as thermal fluctuations and therefore weaken them. In the other extreme, if the \mathbf{u}_{sl} 's in a PUT scheme are heavily influenced by the

instantaneous momenta, thermal fluctuations can be seen as “instantaneous” secondary flows, which then remain unthermostated. In the past, researchers have made an effort to avoid this latter extreme. Some authors used only long wave vectors in a truncated Fourier series representation of the streaming velocity, whereas other authors average \mathbf{u}_{sl} over previous molecular dynamics time steps. Unfortunately, such methods did not provide satisfactory solutions, because the \mathbf{u}_{sl} 's fluctuate rapidly and often on time scales similar to the thermal fluctuations on which they were based. It is thus desirable to have an algorithm that can distinguish between a thermal fluctuation and a persistent attempt by the system to establish a secondary flow.

It is interesting to observe that the original Evans–Morriss PUT equations of motion [Eqs. (217)] place the momenta in an unusual frame; the \mathbf{p} 's are neither in the laboratory frame, nor are they truly thermal. The quantity being thermostated, hence the true thermal momentum, is $\mathbf{p} - m\mathbf{u}_{\text{sl}}$. Since it is at least aesthetically desirable to have direct access to the peculiar momenta, a simple change of variables can be applied. In the process, the phase space is extended to include a dynamical variable for the local streaming velocity. The new equations of motion become:⁵⁶

$$\begin{aligned}\dot{\mathbf{q}}_i &= \frac{\mathbf{p}_i}{m_i} + \hat{i}\gamma q_{y_i} - \mathbf{u}_{\text{sd}}(\mathbf{q}_i) \\ \dot{\mathbf{p}}_i &= \mathbf{F}_i - \hat{i}\gamma(p_{y_i} + m_i u_{\text{sd},y}) - m_i \frac{\mathbf{p}_u}{Q_u} + \mathbf{p}_i \frac{\dot{p}_\eta}{Q} \\ \dot{\eta} &= \frac{\dot{p}_\eta}{Q} \\ \dot{p}_\eta &= \sum_{i=1}^N \frac{\mathbf{p}_i^2}{m_i} - N_f k_B T \\ \dot{\mathbf{p}}_{u,i} &= (\mathbf{u}_{g,i} - \mathbf{u}_{\text{sd},i}) - \mathbf{p}_{u,i} \frac{p_{\eta u}}{Q_{\eta u}} \\ \dot{\mathbf{u}}_{\text{sd},i} &= \frac{\mathbf{p}_{u,i}}{Q_u} \\ \dot{p}_{\eta u} &= \sum_i \frac{m_i \mathbf{p}_{u,i}^2}{Q_u} - N_f k_B T_u \\ \dot{\eta}_u &= \frac{\dot{p}_{\eta u}}{Q_{\eta u}}\end{aligned}\quad [218]$$

In doing so, $\mathbf{u}_{\text{sd},i}$ was introduced as a dynamical variable for the local streaming velocity at q_i ($\mathbf{u}_{\text{sd},i} \equiv \mathbf{u}_{\text{sd}}(\mathbf{q}_i)$). The quantities $\mathbf{p}_{u,i}$ and Q_u serve as the correspond-

ing conjugate momentum and the effective mass, respectively. (Although Q_u serves a role similar to mass in the equations of motion, it actually has units of time squared.) As shown in the $\dot{p}_{u,i}$ equation, the force on the streaming velocity is given by the difference between u_g , a “guiding” streaming velocity, and the current value of $u_{sd,i}$. In principle, u_g can be obtained by any reasonable prescription for approximating the local streaming velocity.^{82,83} By adjusting the mass parameter Q_u in our new approach, the u_{sd} ’s can evolve slowly enough to ignore short-lived thermal noise while still responding to systematic and long-lived trends in the u_g ’s.

As can be seen in the last four lines of Eqs. [218], it is necessary to attach a single NH thermostat, with its position and momentum given by η_u and $p_{\eta u}$, to all the streaming velocities. If the temperature of this thermostat T_u is set equal to the simulation temperature T , too much “kinetic” energy is imparted to the streaming velocities. The resultant large-amplitude fluctuations then significantly disturb the particle velocity autocorrelation function. However, by arbitrarily lowering the temperature of the extended variables so that $T_u = T/N_f$, one can preserve the autocorrelation function.

To construct a reversible integrator for Eqs. [218] with a NH thermostat, we write the total Liouvillian in the form

$$\begin{aligned} i\mathbf{L}_{\text{total}} &= i\mathbf{L}_{\text{mvV}} + i\mathbf{L}_{\text{NH}} + i\mathbf{L}_{\text{PUT}} \\ i\mathbf{L}_{\text{mvV}} &= \sum_{i=1}^N (\mathbf{v}_i + \hat{\mathbf{i}}\gamma q_{y_i} + \mathbf{u}_{sd,i}) \cdot \frac{\partial}{\partial \mathbf{q}_i} + \sum_{i=1}^N \left(\frac{\mathbf{F}_i}{m_i} - m_i \frac{\mathbf{p}_u}{Q_u} \right) \cdot \frac{\partial}{\partial \mathbf{v}_i} \\ i\mathbf{L}_{\text{NH}} &= -\sum_{i=1}^N (\hat{\mathbf{i}}\gamma(v_{y_i} + u_{sd,y_i}) + v_\eta v_i) \cdot \frac{\partial}{\partial \mathbf{v}_i} + v_\eta \frac{\partial}{\partial \eta} \\ &\quad + G \frac{\partial}{\partial v_\eta} - \sum_{i=1}^N \left(\mathbf{p}_{u,i} \frac{p_{\eta u}}{Q_{\eta u}} \right) \cdot \frac{\partial}{\partial \mathbf{p}_{u,i}} + \frac{p_{\eta u}}{Q_{\eta u}} \frac{\partial}{\partial \eta_u} + G_u \frac{\partial}{\partial p_{\eta u}} \\ i\mathbf{L}_{\text{PUT}} &= \sum_{i=1}^N \frac{\mathbf{p}_{u,i}}{Q_u} \cdot \frac{\partial}{\partial u_{sd,i}} + \sum_{i=1}^N (\mathbf{u}_g - \mathbf{u}_{sd,i}) \cdot \frac{\partial}{\partial \mathbf{p}_{u,i}} \end{aligned} \quad [219]$$

where

$$\begin{aligned} \mathbf{v}_i &= \mathbf{p}_i/m_i \\ v_\eta &= p_\eta/Q \\ G &= \frac{1}{Q} \left(\sum_{i=1}^N m_i \mathbf{v}_i^2 - N_f k_B T \right) \\ G_u &= \sum_i \frac{m_i \mathbf{p}_{u,i}^2}{Q_u} - N_f k_B T_u \end{aligned}$$

We employed the following Trotter factorization^{47,84} to approximate the evolution operator to $O(\Delta t^3)$:

$$\begin{aligned} \exp iL\Delta t = & \exp\left(i \frac{\Delta t}{4} L_{\text{PUT}}\right) \exp\left(i \frac{\Delta t}{2} L_{\text{NH}}\right) \exp\left(i \frac{\Delta t}{4} L_{\text{PUT}}\right) \\ & \times \exp\left(i \Delta t L_{\text{mvV}}\right) \\ & \times \exp\left(i \frac{\Delta t}{4} L_{\text{PUT}}\right) \exp\left(i \frac{\Delta t}{2} L_{\text{NH}}\right) \exp\left(i \frac{\Delta t}{4} L_{\text{PUT}}\right) \end{aligned} \quad [220]$$

It is then a straightforward task to construct the action of this operator on the phase space variables. Details can be found in Refs. 46 and 84. The algorithm is called a reversible profile-unbiased thermostat (RPUT).

As a demonstration of the effectiveness of this approach, 500 Lennard-Jones particles were simulated using the RPUT technique; during this simulation, the velocity time autocorrelation function was computed along with the normalized time autocorrelation function for u_{sd} and for u_{sl} . Each of the simulations was run 50–100 times longer than the time it takes for the correlation

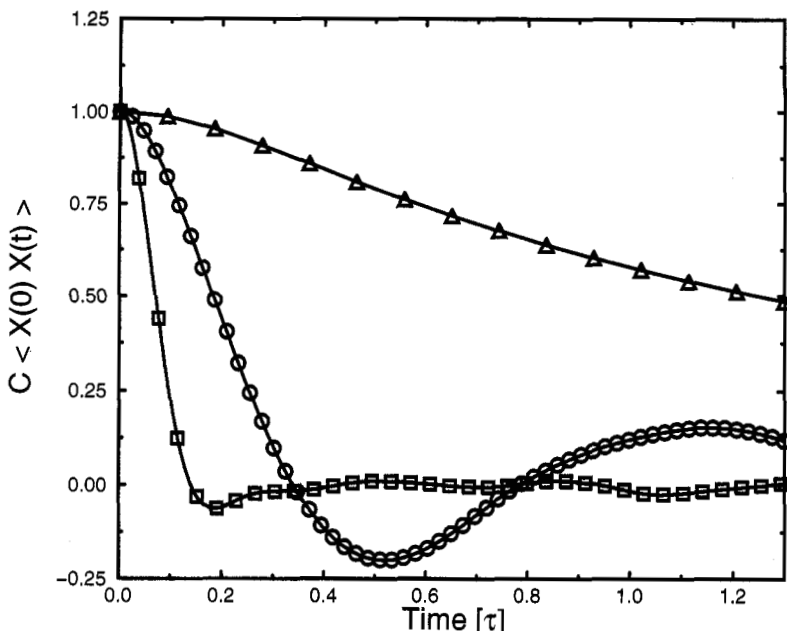


Figure 18 Various time autocorrelation functions. The curve with the triangles is for $X = u_{\text{sd}}$, the circles are for $X = u_{\text{sl}}$ with $Q_u \tau^2 = 2.15 \times 10^5$, and the squares represent $X = p$. C is the appropriate normalization constant, and τ is the fundamental unit of time.

function to decay to a value of e^{-1} ; we denote this decay time as τ_d . A plot of these correlation functions (Figure 18) demonstrates the clear separation of time scales between the dynamical streaming velocities and the thermal momenta. $\tau_d(u_{sd}) \approx 25\tau_d(p)$ and $\tau_d(u_{sl}) \approx 3\tau_d(p)$. This clearly shows that it is better to dynamically evolve the streaming velocities than to instantaneously assign them. The latter would result in unphysically fast changes in the streaming velocity. Further, the effective mass variable Q_u can be adjusted to ensure $\tau_d(u_{sd}) \gg \tau_d(p)$ for each system studied. As a second benefit, this approach restores conservation of total momenta, which was lacking in earlier efforts.⁵⁶

The development of PUT algorithms was encouraged by the desire to understand the phenomenon known as shear-induced microstructure. For low shear rate systems, we can project the particle coordinates onto a plane (yz , for example) perpendicular to the direction of flow (x , for example). In Figure 19 we show such a projection for a system consisting of 500 WCA (Weeks-Chandler-Andersen) particles.¹¹ As can be seen, there is little order that can be detected. It has been suggested however, that as the shear rate increases, particles will tend to form “strings” along the direction of flow to minimize collisions as particles slide past each other. If we increase the shear rate by a factor of 5 for the same WCA system, we can now see a partial alignment of particles into strings in Figure 20. This type of system is said to have a two-phase coexistence between string and liquid phases.

Whereas this behavior is both intuitive and reproducible in several simulations, there is a fair amount of controversy. Erpenbeck⁸⁵ first reported a “string

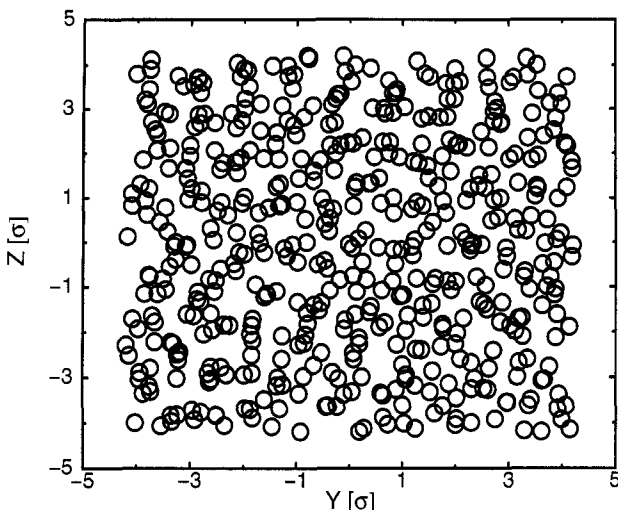


Figure 19 Shear-induced microstructure in a Weeks-Chandler-Andersen fluid of 500 particles under low shear ($T^* = 0.722$, $\rho^* = 0.844$, and $\gamma^* = 0.6$). The unit of length is the WCA potential σ . The direction of flow (x) is out of the page, and the particles are projected on the yz plane.

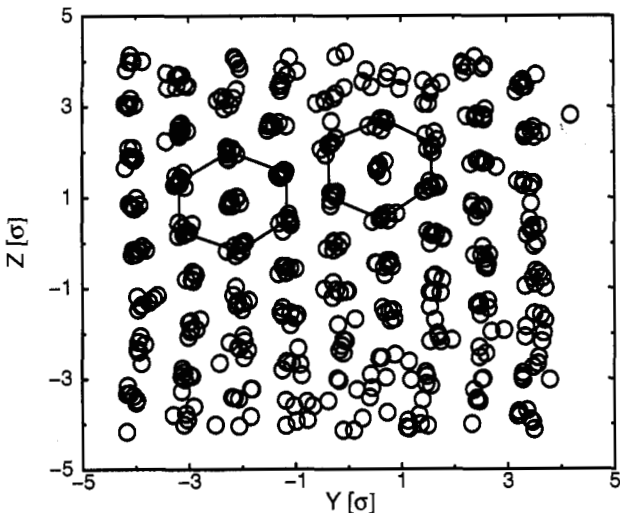


Figure 20 The Weeks–Chandler–Andersen fluid under high shear ($T^* = 0.722$, $\rho^* = 0.844$, $\gamma^* = 3.0$); outlines of hexagonal structure are used to guide the eye.

phase” for a two-dimensional system of hard disks flowing at high shear rates. Later, several groups claimed the existence of a “reentrant solid phase” in three-dimensional liquids at higher shear rates.^{86–90} Evans and coworkers^{79,81} claimed that a proper application of a PUT thermostat proved that these string phases were artifacts of biased thermostating systems.

Some recent work has demonstrated some of the pitfalls that arise in the study of string phases. It has long been known that computer simulations of phase transitions can suffer from system size artifacts. Small cells and periodic boundary conditions can unnaturally reinforce a regular solid structure preferentially over liquid phases. Such effects generally diminish with increasing cell dimensions. As such, strings may exist only in small systems. To test this hypothesis, Rastogi and coworkers⁹¹ compared systems smaller than 500 particles with larger systems (up to 43,000 particles). They concluded that the string phases were not an artifact of system size. A second concern is that the orientation of a string phase may be strongly influenced by the boundary conditions. In fact, Wilemski and coworkers^{92,93} found that geometrically based packing arguments could be used to explain how the structure of order phase adjusted to fit the periodic boundary conditions of the simulation cell. Although this appears to be a significant concern, its implications should be judged in the context of the work of Yamada and Nosé.⁹⁴ These authors performed an interesting set of simulations to test the robustness of string phase orientations. In systems with coexistence between liquid and string phases, the boundary is found to be parallel to the direction of the shear flow gradient (generally y in the examples we have given in the text). The authors started a simulation with the

boundary along the z direction and saw the system reorganize itself, through highly disordered intermediates stages, to a boundary that was along the y axis. They concluded that this final alignment was robust and stable. When we reconsider the results of Wilemski and coworkers, we find that although very small systems yielded the incorrect orientations, the 256-particle system was oriented in the “correct” manner. The combination of results tells us that gross structural features of string phases could be reproduced only with a few hundred particles, and finer details will be correctly rendered in simulations involving on the order of 10^4 particles.

There is a final word of caution regarding PUT and string phases. For certain systems, such as colloids, the shear rates studied are not deemed to be excessively high. But, for most other systems, the shear rates for which string phases and PUT become a factor are orders of magnitude higher than rates found in experiments. The rate of viscous heating can become prohibitively large. One must be careful that the system does not “melt” as a result and that the thermostat used to prevent this does not artificially alter the dynamics.

Small-Field Methods

Up to this point, we have primarily discussed two methods for calculating nonequilibrium properties: the Green–Kubo relations and direct simulation (e.g., SLLOD equations). The Green–Kubo relations are based on the idea that the relaxations of a system, whether from a sufficiently small nonequilibrium perturbation or from an equilibrium fluctuation, are indistinguishable. Hence, the Green–Kubo relations provide transport properties of the system, such as the viscosity, even though they are calculated from equilibrium simulations. These relations are derived from a linear response theory and cannot be used to calculate any nonlinear behavior, such as the variation of transport coefficients with the intensity of the nonequilibrium field. For this reason, Green–Kubo formulas are used in the limit as the perturbing field approaches zero. This regime is sometimes called the linear response or Newtonian regime.

Alternatively, one could use SLLOD equations to do direct simulations, such as shear a system under planar Couette flow and measure the shear stress. As we have already discussed, this approach has been used successfully to calculate a host of transport properties. It is important to remember, however, that direct simulation is often unable to simulate realistic materials at experimentally accessible shear rates. At low shear rates, the nonequilibrium response becomes small compared to the magnitude of the equilibrium fluctuations that naturally arise. The extremely small signal-to-noise ratio would demand prohibitively long simulations before any meaningful answers could be obtained.

The combined limitations of direct and Green–Kubo simulations mean that neither may be satisfactory if one is interested in the small, but nonzero, field limit. To accomplish this, two simulation techniques have been developed. The first is commonly known as the subtraction method because it is based on

differences between equilibrium and nonequilibrium trajectories.^{95,96} The second employs correlations functions that analyze the initial nonequilibrium responses temporally, and hence is called the transient time correlation functions method.^{97–99}

Subtraction Method

Ciccotti and coworkers^{95,96} developed a fairly straightforward scheme that significantly reduces the noise associated with small-field nonequilibrium simulations. If two trajectories, one equilibrium and one nonequilibrium, are started from the same point in phase space, their fluctuations will remain strongly correlated for a finite amount of time. This knowledge is useful because the major difficulty in small-field simulations is distinguishing the systematic response to the field from the noise of the simulation. The method, described below, subtracts the fluctuations found in the equilibrium trajectory from the signal obtained from the nonequilibrium one, thereby greatly enhancing the signal-to-noise ratio.

First, we denote averages taken over equilibrium trajectories with the notation $\langle \cdot \cdot \cdot \rangle_0$ and those in the presence of an external field with $\langle \cdot \cdot \cdot \rangle_e$. Imagine needing to calculate $\langle B \rangle_e$, with the condition that $\langle B \rangle_0 = 0$, where B is a quantity of interest. In the event that B does not satisfy this condition, one can always define a quantity B' , such that $B' = B - \langle B \rangle_0$, thereby making $\langle B' \rangle_0 = 0$.

As we showed in Eq. [9], we can calculate the time evolution of a phase variable via $B(\Gamma(t)) = e^{iL_e t} B(\Gamma(0))$. If we denote the equilibrium and non-equilibrium propagators with $e^{iL_0 t}$ and $e^{iL_e t}$, respectively, we can write:

$$\begin{aligned}\langle B(t) \rangle_e &= \langle B(t) \rangle_e - \langle B(t) \rangle_0 \\ &= \frac{1}{N} \sum_{i=1}^N [e^{iL_e t} - e^{iL_0 t}] B(\Gamma_i(0))\end{aligned}\quad [221]$$

In practice, the first step is to perform a long equilibrium simulation and pick N independent states to obtain $B(\Gamma_i)$, with $i = 1, \dots, N$. From each of these starting points, one commences a nonequilibrium trajectory of length N_{sub} steps. From the first step, we already have the corresponding equilibrium trajectory starting from this same point. We can then take the difference in the dynamical variable B along these two trajectories. This process is repeated N times, and the corresponding averages can be obtained.

There are two practical drawbacks to this approach. At larger values of t , the fluctuations in the two trajectories become uncorrelated, thereby nullifying the noise reduction ability of the method. Second, the equality in Eq. [221] requires that the last term on the first line equal zero. For finite N , this will not rigorously hold. For very small fields, a large number of trajectories must be run to decrease the noise in the calculation of the second term below that of the systematic response due to the field.

Transient Time Correlation Functions (TTCF)

Evans and Morris^{97–99} later derived a method that employs transient time correlations to study systems under small external fields. To start, if we want the average of a property B at time t over a given phase space distribution f , we can express that as follows:

$$\langle B \rangle(t) = \int d\Gamma \sqrt{g(\Gamma)} B(\Gamma) f(\Gamma, t) \quad [222]$$

This would be the Schrödinger representation. Alternatively, we could use the equivalent Heisenberg form, as in:

$$\langle B(t) \rangle = \int d\Gamma \sqrt{g(\Gamma)} B(\Gamma_t, t) f_{eq} \quad [223]$$

Here we have followed the notation of Ref. 12 and also noted that the time evolution operator will also act on the metric determinant. As described earlier, a change of variables is performed from $\Gamma \rightarrow \Gamma_t$. Henceforth, the change of variables will be implicit and the subscript dropped for simplicity. If we assume that the external field and metric determinant have no explicit time dependence, we can take the derivative of both sides with respect to time to obtain:

$$\frac{d\langle B(t) \rangle}{dt} = \int d\Gamma \sqrt{g(\Gamma)} f_{eq} \dot{\Gamma} \cdot \frac{\partial B(\Gamma, t)}{\partial \Gamma} \quad [224]$$

where we have noted that because the right-hand side is a pure function of time, the full time derivative becomes a partial derivative. We can then integrate the right-hand side by parts to obtain:

$$\frac{d\langle B(t) \rangle}{dt} = f_{eq} \sqrt{g(\Gamma)} B(\Gamma, t) |_{\Gamma} - \int d\Gamma B(\Gamma, t) \frac{\partial}{\partial \Gamma} \cdot (\dot{\Gamma} \sqrt{g(\Gamma)} f_{eq}) \quad [225]$$

At the limits of phase space, the momentum will be infinite; in all reasonable ensembles, f will be zero. Hence, the first term on the right-hand side will drop from the expression. We can then integrate both sides with respect to time to get:

$$\langle B(t) \rangle - \langle B(0) \rangle - \int_0^t ds \int d\Gamma B(\Gamma, s) \frac{\partial}{\partial \Gamma} \cdot (\dot{\Gamma} \sqrt{g(\Gamma)} f_{eq}) \quad [226]$$

At this point, we will assume that we are shearing a system in the canonical ensemble using the SLLOD equations of motion. Hence,

$$\begin{aligned}\dot{\mathbf{q}}_i &= \frac{\mathbf{p}_i}{m_i} + \hat{i}\gamma q_{y,i} \\ \dot{\mathbf{p}}_i &= \mathbf{F}_i - \hat{i}\gamma p_{y,i} - \frac{p_\eta}{Q} \mathbf{p}_i \\ \dot{p}_\eta &= \sum_i \frac{\mathbf{p}_i^2}{m_i} - N_f k_B T \\ \dot{\eta} &= \frac{p_\eta}{Q}\end{aligned}\quad [227]$$

$$f_{eq} = \frac{\delta(H' - E)}{\Omega} \quad [228]$$

where H' is given by H_0 in Eq. [117]. For the phase space integral in Eq. [226], we proceed to evaluate

$$\frac{\partial}{\partial \Gamma} \cdot (\dot{\Gamma} \sqrt{g(\Gamma)} f_{eq}) = \sqrt{g(\Gamma)} f_{eq} \frac{\partial}{\partial \Gamma} \cdot \dot{\Gamma} + \sqrt{g(\Gamma)} \dot{\Gamma} \cdot \frac{\partial f_{eq}}{\partial \Gamma} + f_{eq} \dot{\Gamma} \cdot \frac{\partial \sqrt{g(\Gamma)}}{\partial \Gamma} \quad [229]$$

For SLLOD dynamics coupled to a Nosé–Hoover thermostat, the metric determinant is given by $e^{N_f \eta}$. The first and third terms in Eq. [229] become $N_f e^{N_f \eta} f_{eq} p_\eta / Q$ with opposite signs and thus cancel. We are left with the expression

$$\langle B(t) \rangle = \langle B(0) \rangle - \int_0^t ds \int d\Gamma B(\Gamma, s) (\sqrt{g(\Gamma)} \frac{\partial f_{eq}}{\partial \Gamma} \cdot \dot{\Gamma}) \quad [230]$$

To proceed with evaluating Eq. [230], we first note that

$$\frac{\partial f_{eq}}{\partial \Gamma} = \frac{\partial f_{eq}}{\partial \eta} \frac{\partial \eta}{\partial H'} \frac{\partial H'}{\partial \Gamma} \quad [231]$$

Thus, Eq. [230] becomes

$$\begin{aligned}\int ds \int d\mathbf{p} d\mathbf{q} dp_\eta B(s) \int d\eta \left[\frac{\partial f_{eq}}{\partial \eta} e^{N_f \eta} \frac{1}{N_f k_B T} \left(N_f k_B T \frac{p_\eta}{Q} + \sum_i \frac{\mathbf{p}_i^2}{m_i} \frac{p_\eta}{Q} - N_f k_B T \frac{p_\eta}{Q} \right. \right. \\ \left. \left. - \sum_i \frac{\mathbf{p}_i^2}{m_i} \frac{p_\eta}{Q} + \sum_i \mathbf{F}_i \cdot \frac{\mathbf{p}_i}{m_i} - \gamma \sum_i \frac{p_{x_i} p_{y_i}}{m_i} - \sum_i \mathbf{F}_i \cdot \frac{\mathbf{p}_i}{m_i} - \gamma \sum_i F_{x_i} q_{y_i} \right) \right]\end{aligned}\quad [232]$$

After the cancellation we are left with

$$-\gamma V \int ds \int d\mathbf{p} d\mathbf{q} dp_\eta B(s) \int d\eta \left[\frac{1}{N_f k_B T} \frac{\partial f_{eq}}{\partial \eta} P_{xy}(0) \right] \quad [233]$$

where once again we have used our earlier definition of the pressure tensor. Again using the formula, $\int dx f(x)\delta'(x) = -f'(0)$, we obtain

$$\begin{aligned} \langle B(t) \rangle &= \langle B(0) \rangle - \beta \gamma V \int_0^t ds \int d\mathbf{p} d\mathbf{q} B(s) P_{xy}(0) f_{eq} \\ &= \langle B(0) \rangle - \beta \gamma V \int_0^t ds \langle B(s) P_{xy}(0) \rangle_0 \end{aligned} \quad [234]$$

and we have once again assumed that the phase variable B does not depend on the extended system variables. It is interesting to contrast this result with Eq. [124]. Note that all terms in Eq. [124] have been propagated with the field-independent Liouvilian. In Eq. [235] all time-dependent variables have been propagated with the full dynamics. In systems with more than a few degrees of freedom, most variables $B(t')$ will eventually become uncorrelated with $P_{xy}(0)$ at sufficiently long times. Hence, for large t' , $\langle B(t') P_{xy}(0) \rangle = \langle B(t') \rangle \langle P_{xy}(0) \rangle$ and will vanish because the off-diagonal components of the pressure tensor average to zero at equilibrium. We can then use $B(t') = \Delta B(t') + \langle B(t') \rangle$ to rewrite Eq. [234]:

$$\langle B(t) \rangle = \langle B(0) \rangle - \beta \gamma V \int_0^t dt' \langle \Delta B(t') P_{xy}(0) \rangle \quad [235]$$

Equation [235] requires two types of simulation. First, one needs to generate a set of sufficiently uncorrelated equilibrium states to calculate $P_{xy}(0)$ and $\langle B(0) \rangle$. Second, these states are then used as initial configurations for non-equilibrium runs to calculate $\Delta B(t')$. The latter runs should be long enough for the system to reach a steady state. In principle, Eq. [235] is exact, and the aforementioned procedure could be employed as stated. For sufficiently complicated systems, the B and $P_{xy}(0)$ become uncorrelated at long times, as we have mentioned. Hence the integral should converge because $\langle P_{xy}(0) \rangle = 0$ at equilibrium. However, statistical fluctuations that arise in finite length runs mean that this will not rigorously hold.

Evans and Morrissey employed a clever phase space mapping trick to avoid this problem.⁸ The purpose of the equilibrium runs is to generate starting states according to the canonical ensemble's distribution function. From the canonical distribution function, it is easy to see that reflections about either position or momentum axes do not affect the value of the equilibrium Hamiltonian H_0 , assuming the usual periodic boundary conditions. Hence, if through MD we generate a state $\Gamma = (\mathbf{q}_x, \mathbf{q}_y, \mathbf{p}_x, \mathbf{p}_y)$, then we know that all the following

combinations of states also exist with equal probability: $\Gamma' = (\pm q_x, \pm q_y, \pm p_x, \pm p_y)$. (As we will see shortly, the q_z and p_z will not play a role and have been dropped from the discussion.) In principle, 2^4 total states can be generated from a single phase point. However, we must eliminate some states because certain combinations, such as $\Gamma = (q_x, q_y, p_x, p_y)$ and $\Gamma' = (-q_x, -q_y, -p_x, -p_y)$, lead to identical nonequilibrium trajectories. If we further require that the shear stresses be equal in magnitude, we are left with the following four combinations:

$$\begin{aligned}\Gamma_1 &= (q_x, q_y, p_x, p_y) \\ \Gamma_2 &= (-q_x, -q_y, p_x, p_y) \\ \Gamma_3 &= (-q_x, q_y, -p_x, p_y) \\ \Gamma_4 &= (-q_x, q_y, p_x, -p_y)\end{aligned}\quad [236]$$

These states have the nice property that $P_{xy}(\Gamma_1) = P_{xy}(\Gamma_2) = -P_{xy}(\Gamma_3) = -P_{xy}(\Gamma_4)$. Hence, $\langle P_{xy}(0) \rangle$ is *exactly* zero, thereby eliminating the statistical difficulties at long times.

Evans and Morriss compared the TTGF method to Green–Kubo, direct NEMD simulation, and the subtraction method at various shear field strengths. Direct NEMD is the most efficient method to use with larger shear rates and is inferior to all other methods for small fields. In comparisons between the small field methods, TTGF was found to be more efficient with regard to statistical uncertainties. This efficiency is likely due to the clever use of symmetric starting states and the subtraction method's reliance on a strong correlation between the equilibrium and perturbed trajectories. Hence, if one wishes to calculate a nonlinear property in the small-field limit, the TTGF method will be the most promising approach to employ. Linear properties can, of course, be calculated by means of the straightforward Green–Kubo method.

Crack Propagation

An important application of NEMD simulation methods is in the study of material failure. Progress in this field can play a role in the development of new high strength materials. Crack propagation is one of most studied failure mechanisms. Although continuum fracture theory has been used successfully to describe the long-ranged strain fields that result from these defects, it has been less successful in predicting the atomistic details. Typically, such an approach assumes that cracks are smooth and approach a limiting velocity close to the Rayleigh speed⁸⁰ of the material. However, experiments inform us about three main crack propagation features: the limiting crack speed is about two-thirds the Rayleigh speed (c_r), the instantaneous crack velocity becomes erratic after reaching one-third the Rayleigh speed, and the propagation surface can be rough. Further, a crack may even evolve with a wiggle motion that maintains a

characteristic wavelength. A fundamental understanding of crack propagation requires atomistic simulations.

The first such simulations were performed more than 20 years ago by Ashurst and Hoover.¹⁰⁰ Unfortunately, limited computer power at that time presented two significant problems for an accurate assessment of crack stability. First, in analogy to shear rates in viscosity calculations, experimental strain rates are too low to permit observation of a fracture on a molecular dynamics time scale. Hence, fast computers are needed to close that gap as best they can. Second, the reflection of sound waves and defects off the boundaries of small systems can artificially alter the failure dynamics. Fortunately, the recent widespread availability of parallel computing power¹⁰¹ has spawned numerous long-time-scale studies on multimillion-particle systems. In 1994 Abraham and coworkers¹⁰² studied two-dimensional systems of Lennard-Jones particles. The reduced dimensionality allowed them to make comparisons with “mode one” loading experiments of Fineberg and coworkers.^{103–105} The largest model system contained 2 million particles and spanned roughly 0.5 μm per side in length. On the bottom face, a triangular patch of Lennard-Jones particles was removed to create a notch that would serve as the starting point for the crack propagation, as represented schematically in Figure 21. The left and right outermost columns of atoms were subjected to a strain rate of $-\dot{\epsilon}_x$ and $+\dot{\epsilon}_x$, respectively. The magnitude of the strain rate strongly influences the types of failure that occur. Most interatomic potentials, including Lennard-Jones, become less attractive as the separation distances increases. Therefore, the energy of the system tends to increase as the material gets stretched. Eventually, it becomes energetically favorable for fractures to develop. However, if the strain rate is too high, a large number of void sites arise, leading to multiple internal fractures. Abraham used a reduced strain rate of $\dot{\epsilon}_x = 0.0001$, which was sufficiently small that fracture was induced at the notch only when the system had stretched by ≈ 3%.

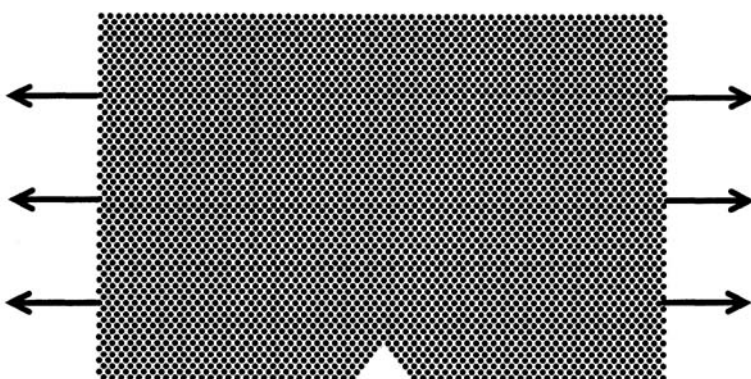


Figure 21 Schematic representation of Abraham's crack simulation.

Despite the shortcoming with regard to short simulation time, small sample size, and a strain rate that is an order of magnitude larger than experiment, several known features were observed.¹⁰² First, the crack velocity became erratic after reaching $0.32c_r$ ($\approx \frac{1}{3}c_r$) with a concomitant deceleration of the tip. At the same time, the crack started propagating in new directions that are $\pm 30^\circ$ to the formerly straight direction. The system periodically alternated between these two directions by making local 60° turns. This motion created an oscillatory crack pattern with a characteristic wavelength, similar to what is found experimentally. While the crack tip speed along these 30° segments was close to the Rayleigh velocity,⁸⁰ the effective “forward” crack speed was about $0.57c_r \approx \frac{2}{3}c_r \ll c_r$. Given that multiple experimental features were reproduced, Abraham and coworkers concluded that fracture may have “universal” properties that are independent of the material since this simplistic Lennard-Jones model was so successful.

Reflections off the boundaries of the simulation cell are a primary concern given the small system sizes used. The earlier work¹⁰² had reflected dislocations present before the crack had propagated three-quarters of the way across the system. Zhou and coworkers¹⁰⁶ undertook a similar study with viscous damping boundaries. A crack was created in the center of a rectangular simulation cell containing 400,000 particles interacting via a Morse potential $\phi(r) = e^{-2\alpha(r-1)} - 2e^{-\alpha(r-1)}$, where r is a distance and α is an inverse screening length. For an elliptical region surrounding the crack, the particles obeyed the following equations of motion:

$$\begin{aligned}\dot{\mathbf{q}}_i &= \frac{\mathbf{p}_i}{m_i} + \dot{\epsilon} q_{x,i} \hat{\mathbf{i}} \\ \dot{\mathbf{p}}_i &= \mathbf{F}_i - \dot{\epsilon} p_{x,i} \hat{\mathbf{i}}\end{aligned}\quad [237]$$

where $\hat{\mathbf{i}}$ is the unit vector in the x direction and $\dot{\epsilon}$ is the strain rate. In the limit of $\dot{\epsilon} = 0$, we recover Newtonian motion. This was done to prevent thermostating from altering the dynamics near the crack. For the elliptical region far from the crack, the velocities obeyed a new set of equations:

$$\dot{\mathbf{p}}_i = \mathbf{F}_i - \dot{\epsilon} p_{x,i} \hat{\mathbf{i}} - \gamma p_f \hat{\mathbf{i}} \quad [238]$$

A viscous damping term was added that depended on a “stadium function” f , which smoothly increased from 0 to 1 with increasing distance from the center of the simulation cell, and γ is a friction coefficient. The goal was to adsorb sound waves and emitted dislocations and prevent them from reflecting back into the main region. The central conclusion of the work¹⁰⁶ challenged the traditional concept that crack tip velocity was the single most important factor

to understanding propagation and branching. The authors¹⁰⁶ found that branching depends more strongly on the accumulation of energy near the crack tip and can occur at velocities less than the maximum. Since this branching arises from energy released from bond breaking Zhou et al. concluded that crack branching is essentially an atomistic phenomenon.

It is interesting to note that many experimental effects could be reproduced with fairly generic interatomic potentials, such as Lennard-Jones or Morse-type functions. Simulations involving more complicated potentials were undertaken in an effort to realistically mimic specific materials. Li and coworkers¹⁰⁷ for example, used pairwise repulsion, screened Coulombic, charge-dipole, and three-body covalent interactions to simulate the fracture of SiSe₂ nanowires. Chains ranging from 10 to 60 Å in diameter and 3500 Å in length were extracted from a three-dimensional crystalline structure and then subjected to a lengthwise strain in the wires via a uniform scaling of the particle coordinates. The investigators discovered that single bond breaking caused local cross-linking of the chains, leading to a regionalized amorphization; fracture at this point soon followed.

The more sophisticated potentials used in the nanowire study¹⁰⁷ point to an important consideration in modeling such systems. Simple potentials are parameterized under bulk homogeneous conditions and may give poor descriptions of the inhomogeneous environment near a crack tip. In an effort to employ a classical potential that is responsive to a rapidly changing environment, Omelchenko and coworkers¹⁰⁸ simulated a graphite sheet modeled by more than a million particles. The authors used a reactive bond order potential developed by Brenner.¹⁰⁹ In this approach, the total potential energy can be written as follows:

$$V_T = \sum_i^N \sum_{j>1}^N [\phi_{ij}^R(r_{ij}) - b_{ij}\phi_{ij}^A(r_{ij})] \quad [239]$$

where R and A label a repulsive and an attractive term, respectively. The *b* factor represents the difference in strength between single, double, and triple bonds, and it depends on a variety of parameters such as local coordination and bond angles. As such, the Brenner potential can reflect the changing environment near a crack tip. Two orientations were tested. If the strain is parallel to some of the C—C bonds, the system exhibits simple cleavage fracture. In the case of some C—C bonds being perpendicular to the strain, the system underwent multiple crack branches at speeds close to two-thirds the Rayleigh wave speed. These simulations have shown that simulations of micrometer-sized systems with realistic potentials are capable of providing an atomistic explanation of several experiment observables.

CONCLUSIONS AND FUTURE PROSPECTS

We conclude with a summary of the important issues that have been described, followed by discussion of some of the open and unresolved research areas to which the aforementioned methods and ideas could be applied. First, the point we hope to have made clear is that NEMD (as well as equilibrium molecular dynamics) is not a black box. All the important concepts have a firm theoretical basis, which allows one to connect Hamiltonian and non-Hamiltonian dynamics to classical statistical mechanics and phenomenology. Without this connection, there is no way to know whether a simulation has any relation to thermodynamic reality. Furthermore, even at the level of numerical implementation, theory is used to guide the scientist in producing accurate and stable algorithms that can be employed to investigate systems in nontrivial ensembles. This chapter may seem overwhelming at first reading. However, we believe that we have presented the theory, implementation, and applications in a self-consistent format that should serve as a reference guide for the interested reader in future endeavors in NEMD.

State-of-the-art NEMD simulations include calculating the physical properties of prototypical hydrocarbon lubricants typically consisting of 30–50 carbon units. Because of the advent of supercomputers and parallel architecture, these calculations are being performed in a timely manner.

One of the strengths of NEMD simulations that has yet to be exploited is the calculation of rheological properties of other materials. What distinguishes these real materials from the model lubricants? Typically, one is interested in the Newtonian regime of these prototypical lubricants. The non-Newtonian or rheological properties of typical lubricants (e.g., C₃₀), although interesting, are accessible only by computer simulation. That is, the maximum shear rates at which the experiments are being performed and the shear rates at which interesting rheological behavior is observed in computer simulation are typically four to five orders of magnitude out of range. The one area in which experimental shear rates can access interesting rheological behavior is the area of polymers. The polymers of interest typically consist of hundreds or thousands of monomer units. One such polymer that has received attention in the literature is polytetrafluoroethylene, or Teflon, whose rich phase diagram has already been explored by equilibrium molecular dynamics.¹¹⁰ The partially disordered phase of Teflon is known experimentally to exhibit non-Newtonian behavior with the log–log plot of the stress (σ_{xy}) versus strain (γ) showing a slope of one-fourth.⁵⁸ Newtonian behavior would show a slope of unity. Moreover, at constant shear rate (strain) in the disordered region, the stress as a function of temperature goes through a minimum before exhibiting a precipitous rise in the vicinity of the disorder transition. This is an ideal candidate for a NEMD simulation. To initiate such a study, the ideas presented in this chapter must be extended to

include SLLOD dynamics in the ensemble where the cell parameters are allowed to fluctuate.

The microscopic origin of friction is also a recent topic of study with hopes of designing better lubricants. The surface force apparatus (SFA) is an instrument that is providing a way to gain experimental insight on the phenomenon of friction. In the section on confined fluids under shear, we presented a systematic approach to compute the slipping length of a model fluid confined between model walls. Recently, it has been found that toluene between mica plates exhibit the “no-slip” boundary condition.¹¹¹ However, with the addition of small amounts of C₆₀, the boundary condition showed the “complete slip” boundary condition, indicating that C₆₀ could be used as an additive to help reduce friction.¹¹¹ With the methodology presented in the section on confined fluids under shear, a computation of the slipping length under experimental conditions could be possible.

It is clear that the future of NEMD simulation lies in the computation of physical properties in real materials. To date, this has been accomplished only in model systems. With the theory and implementation discussed in this chapter, we hope to spark the interest of some young (or even not so young) scientists to pursue these future endeavors.

APPENDIX 1: Time Evolution of the Jacobian

Note that the Jacobian is the determinant of a matrix $\mathbf{M}(\boldsymbol{\Gamma}_t; \boldsymbol{\Gamma}_0)$

$$\mathcal{J}(\boldsymbol{\Gamma}_t; \boldsymbol{\Gamma}_0) = \det(\mathbf{M}(\boldsymbol{\Gamma}_t; \boldsymbol{\Gamma}_0)) = e^{\text{Tr}(\ln \mathbf{M}(\boldsymbol{\Gamma}_t; \boldsymbol{\Gamma}_0))} \quad [240]$$

where

$$\mathbf{M}_{ij} = \frac{\partial \boldsymbol{\Gamma}_t^i}{\partial \boldsymbol{\Gamma}_0^j} \quad [241]$$

$\boldsymbol{\Gamma}_t^i$ represents the i th component of the phase space vector. Taking the time derivative of both sides of Eq. [240] gives

$$\frac{d\mathcal{J}(\boldsymbol{\Gamma}_t; \boldsymbol{\Gamma}_0)}{dt} = \mathcal{J}(\boldsymbol{\Gamma}_t; \boldsymbol{\Gamma}_0) \text{Tr}\left(\mathbf{M}^{-1}(\boldsymbol{\Gamma}_t; \boldsymbol{\Gamma}_0) \frac{d\mathbf{M}(\boldsymbol{\Gamma}_t; \boldsymbol{\Gamma}_0)}{dt}\right) \quad [242]$$

The inverse of the matrix M is just

$$(\mathbf{M}^{-1})^{ij} = \frac{\partial \Gamma_0^i}{\partial \Gamma_t^j} \quad [243]$$

Substituting Eq. [243] into Eq. [242] gives

$$\begin{aligned} \frac{d\mathcal{J}(\boldsymbol{\Gamma}_t; \boldsymbol{\Gamma}_0)}{dt} &= \mathcal{J}(\boldsymbol{\Gamma}_t; \boldsymbol{\Gamma}_0) \sum_{i,j} \left(\frac{\partial \Gamma_0^i}{\partial \Gamma_t^j} \frac{\partial \dot{\Gamma}_t^j}{\partial \Gamma_0^i} \right) \\ &= \mathcal{J}(\boldsymbol{\Gamma}_t; \boldsymbol{\Gamma}_0) \sum_{i,j,k} \left(\frac{\partial \Gamma_0^i}{\partial \Gamma_t^j} \frac{\partial \dot{\Gamma}_t^j}{\partial \Gamma_t^k} \frac{\partial \Gamma_t^k}{\partial \Gamma_0^i} \right) \\ &= \mathcal{J}(\boldsymbol{\Gamma}_t; \boldsymbol{\Gamma}_0) \sum_{j,k} \delta_{jk} \frac{\partial \dot{\Gamma}_t^j}{\partial \Gamma_t^k} \\ &= \mathcal{J}(\boldsymbol{\Gamma}_t; \boldsymbol{\Gamma}_0) \sum_j \frac{\partial \dot{\Gamma}_t^j}{\partial \Gamma_t^j} \\ &= \mathcal{J}(\boldsymbol{\Gamma}_t; \boldsymbol{\Gamma}_0) \nabla_{\boldsymbol{\Gamma}_t} \cdot \dot{\boldsymbol{\Gamma}}_t \end{aligned} \quad [244]$$

Thus,

$$\frac{d\mathcal{J}(\boldsymbol{\Gamma}_t; \boldsymbol{\Gamma}_0)}{dt} = \mathcal{J}(\boldsymbol{\Gamma}_t; \boldsymbol{\Gamma}_0) \nabla_{\boldsymbol{\Gamma}_t} \cdot \dot{\boldsymbol{\Gamma}}_t \quad [245]$$

which states that a nontrivial Jacobian will result if the phase space compressibility is nonvanishing.

APPENDIX 2: Geometric Derivation of the Generalized Liouville Equation

A set of points M is said to be a n -dimensional manifold if each point of M has an open neighborhood, which has a continuous 1:1 map onto an open set of R^n , the set of all n -tuples of real numbers.¹¹² Consider an n -dimensional Riemannian manifold with metric G . In an arbitrary coordinate system x^1, \dots, x^n , the volume n -form is generally given by $\tilde{w} = \sqrt{g} dx^1 \wedge \dots \wedge dx^n$. Here, g is the determinant of the metric in this basis, and \wedge denotes the “wedge” or antisymmetric tensor product. For a flow field on the manifold prescribed by $\dot{x}^i = \xi^i(x)$ with density $f(x, t)$, a continuity equation for $f(x, t)$ can be obtained by considering the number of ensemble members $\mathcal{N}(t)$ within a volume Ω of phase space given by

$$\mathcal{N}(t) = \int_{\Omega} \tilde{w} f \quad [246]$$

The continuity condition states that the rate of change of the number of ensemble members within Ω must be balanced by the flux of members through the surface, a condition that is stated mathematically as

$$-\frac{d}{dt} \int_{\Omega} \tilde{w} f = \int_{\partial\Omega} \tilde{\sigma} \hat{n} \cdot \xi f \quad [247]$$

where $\tilde{\sigma}$ is the surface ($n - 1$) form corresponding to the $\partial\Omega$ of Ω , and \hat{n} is the unit normal to the surface. The divergence theorem on a general manifold states that

$$\int_{\partial\Omega} \tilde{\sigma} \hat{n} \cdot \xi f = \int_{\Omega} \mathcal{L}_{\xi}(f \tilde{w}) \quad [248]$$

where \mathcal{L}_{ξ} is the Lie derivative in the direction of the vector ξ (see, e.g., Eq. 5.68 of Ref. 112). Equation [248] can be used to convert the surface integral in Eq. [247] into a volume integral, giving the condition

$$\int_{\Omega} \left(\frac{\partial}{\partial t} + \mathcal{L}_{\xi} \right) (f \tilde{w}) \quad [249]$$

which must hold, independent of the choice of Ω , and can thus be expressed as a local condition

$$\left(\frac{\partial}{\partial t} + \mathcal{L}_{\xi} \right) (f \tilde{w}) = 0 \quad [250]$$

From the Leibniz rule,²⁰ $\mathcal{L}_{\xi}(f \tilde{w}) = \tilde{w} \mathcal{L}_{\xi} f + f \mathcal{L}_{\xi} \tilde{w}$. The action of the Lie derivative on the scalar f and on the volume form \tilde{w} is known:

$$\begin{aligned} \mathcal{L}_{\xi} f &= \xi^i \frac{\partial f}{\partial x^i} \\ \mathcal{L}_{\xi} \varepsilon_{i_1 \dots i_n} &= \xi^k \frac{\partial \sqrt{g(x)}}{\partial x^k} \varepsilon_{i_1 \dots i_n} + \sqrt{g(x)} \left(\varepsilon_{k i_2 \dots i_n} \frac{\partial \xi^k}{\partial x^{i_1}} + \dots + \varepsilon_{i_1 \dots i_{n-1} k} \frac{\partial \xi^k}{\partial x^{i_n}} \right) \\ &= x^k \frac{\partial \sqrt{g(x)}}{\partial x^k} \varepsilon_{i_1 \dots i_n} + \sqrt{g(x)} \frac{\partial \xi^i}{\partial x^i} \varepsilon_{i_1 \dots i_n} \end{aligned} \quad [251]$$

where the tensorial representation of the wedge product is given by $\varepsilon_{i_1 \dots i_n}$, which is called the Levi-Civita tensor.²⁰ (The Einstein summation convention has been adopted.) The last line follows from the properties of the $\varepsilon_{i_1 \dots i_n}$ (see, e.g., Chapter 3 of Ref. 20). Combining the results of Eq. [251] with Eq. [250] gives the general form for the continuity equation

$$\left[\frac{\partial}{\partial t} (f \sqrt{g(x)}) + \frac{\partial}{\partial x^k} (f \sqrt{g(x)} \xi^k) \right] dx^1 \wedge \cdots \wedge dx^n = 0 \quad [252]$$

Since the volume element is not zero, the term in brackets must vanish, yielding

$$\begin{aligned} \frac{\partial}{\partial t} (f \sqrt{g(x)}) + \frac{\partial}{\partial x^k} (f \sqrt{g(x)} \xi^k) &= 0 \\ \frac{\partial}{\partial t} (f \sqrt{g(x)}) + \nabla \cdot (f \sqrt{g(x)} \xi) &= 0 \end{aligned} \quad [253]$$

Equation [253] is a general form of the Liouville equation, valid on a curved manifold.

REFERENCES

1. T. P. Lybrand, in *Reviews in Computational Chemistry*, K. B. Lipkowitz and D. B. Boyd, Eds., VCH Publishers, New York, 1990), Vol. 1, pp. 295–320. Computer Simulation of Biomolecular Systems Using Molecular Dynamics and Free Energy Perturbation Methods. T. P. Straatsma, in *Reviews in Computational Chemistry*, K. B. Lipkowitz and D. B. Boyd, Eds., VCH Publishers, New York, 1996, Vol. 9, pp. 81–127. Free Energy by Molecular Simulation.
2. R. Kutteh and T. P. Straatsma, in *Reviews in Computational Chemistry*, K. B. Lipkowitz and D. B. Boyd, Eds., Wiley-VCH, New York, 1998, Vol. 13, pp. 75–136. Molecular Dynamics with General Holonomic Constraints and Applications to Internal Coordinate Constraints. J. C. Shelley and D. R. Bérard, in *Reviews in Computational Chemistry*, K. B. Lipkowitz and D. B. Boyd, Eds., Wiley-VCH, New York, 1998, Vol. 12, pp. 137–205. Computer Simulation of Water Physisorption at Metal-Water Interfaces.
3. B. Alder and T. Wainwright, *Phys. Rev. Lett.*, **18**, 988 (1967). Velocity Autocorrelations for Hard Spheres.
4. B. Alder, D. Gass, and T. Wainwright, *J. Chem. Phys.*, **53**, 3813 (1970). Studies in Molecular Dynamics. VIII. The Transport Coefficients of a Hard-Sphere Fluid.
5. A. W. Lees and S. F. Edwards, *J. Phys. C*, **5**, 1921 (1972). The Computer Study of Transport Processes Under Extreme Conditions.
6. H. C. Andersen, *J. Chem. Phys.*, **72**, 2384 (1980). Molecular Dynamics Simulations at Constant Pressure and/or Temperature.
7. W. Hoover, D. Evans, R. Hickman, A. Ladd, W. Ashurst, and B. Moran, *Phys. Rev. A*, **22**, 1690 (1980). Lennard-Jones Triple-Point Bulk and Shear Viscosities. Green-Kubo Theory, Hamiltonian Mechanics, and Nonequilibrium Molecular Dynamics.
8. D. Evans and G. Morriss, *Phys. Rev. A*, **30**, 1528 (1984). Nonlinear-Response Theory for Steady Planar Couette Flow.
9. S.-I. Pai, *Viscous Flow Theory*, Vol. 1, *Laminar Flow*, Van Nostrand, Princeton, NJ, 1956.
10. S. Y. Liem, D. Brown, and J. H. R. Clarke, *Phys. Rev. A*, **45**, 3706 (1992). Investigation of the Homogeneous Shear Nonequilibrium Molecular Dynamics Method.
11. J. D. Weeks, D. Chandler, and H. C. Andersen, *J. Chem. Phys.*, **54**, 5237 (1971). Role of Repulsive Forces in Determining the Equilibrium Structure of Simple Liquids.
12. D. J. Evans and G. P. Morriss, *Statistical Mechanics of Nonequilibrium Liquids*, Academic Press, London, 1990.

13. R. Car and M. Parrinello, *Phys. Rev. Lett.*, **55**, 2471 (1985). Unified Approach for Molecular Dynamics and Density Functional Theory.
14. M. Parrinello and A. Rahman, *Phys. Rev. Lett.*, **45**, 1196 (1980). Crystal Structure and Pair Potentials: A Molecular Dynamics Study.
15. M. E. Tuckerman, C. J. Mundy, and M. L. Klein, *Phys. Rev. Lett.*, **78**, 2042 (1997). Towards a Statistical Thermodynamics of Steady States.
16. H. Goldstein, *Classical Mechanics*, Addison-Wesley, Reading, MA, 1981.
17. D. A. McQuarrie, *Statistical Mechanics*, HarperCollins, New York, 1976.
18. K. Huang, *Statistical Mechanics*, 2nd ed., Wiley, New York, 1987.
19. B. J. Berne and G. D. Harp, *Adv. Chem. Phys.*, **17**, 63 (1970). On the Calculation of Time Correlation Functions.
20. B. A. Dubrovin, A. T. Fomenko, and S. P. Novikov, *Modern Geometry—Methods and Applications Part I: The Geometry of Surfaces Transformation Groups and Fields*, Springer Verlag, New York, 1984.
21. G. Gerlich, *Physica*, **69**, 458 (1973). The Generalised Liouville Equation.
22. L. Andrey, *Nuovo Cimento*, **69B**, 136 (1982). Ideal Gas in Empty Space.
23. J. R. Waldram, *The Theory of Thermodynamics*, Cambridge University Press, Cambridge, U.K., 1985.
24. S. Nosé and M. L. Klein, *Mol. Phys.*, **50**, 1055 (1983). Constant Pressure Molecular Dynamics for Molecular Systems.
25. S. Nosé, *J. Chem. Phys.*, **81**, 511 (1984). A Unified Formulation of the Constant Temperature Molecular Dynamics Methods.
26. W. G. Hoover, *Phys. Rev. A*, **31**, 1695 (1985). Canonical Dynamics: Equilibrium Phase Space Distributions.
27. G. J. Martyna, M. L. Klein, and M. E. Tuckerman, *J. Chem. Phys.*, **97**, 2635 (1992). The Canonical Ensemble Via Continuous Dynamics.
28. G. J. Martyna, M. E. Tuckerman, D. J. Tobias, and M. L. Klein, *Mol. Phys.*, **87**, 1117 (1996). Explicit Reversible Integrators for Extended System Molecular Dynamics.
29. D. J. Tobias, G. J. Martyna, and M. L. Klein, *J. Phys. Chem.*, **97**, 12959 (1993). Molecular Dynamics Simulations of a Protein in the Canonical Ensemble.
30. M. E. Tuckerman, B. J. Berne, G. J. Martyna, and M. L. Klein, *J. Chem. Phys.*, **99**, 2796 (1993). Efficient Molecular Dynamics and Hybrid Monte Carlo Algorithms for Path Integrals.
31. M. E. Tuckerman, D. Marx, M. L. Klein, and M. Parrinello, *J. Chem. Phys.*, **104**, 5579 (1996). Efficient and General Algorithms for Path Integral Car-Parrinello Molecular Dynamics.
32. W. G. Hoover and B. L. Holian, *Phys. Lett. A*, **211**, 253 (1996). Kinetic Moments Method for the Canonical Ensemble Distribution.
33. G. J. Martyna, D. J. Tobias, and M. L. Klein, *J. Chem. Phys.*, **101**, 4177 (1994). Constant Pressure Molecular Dynamics Algorithms.
34. M. P. Allen and D. J. Tildesley, *Computer Simulation of Liquids*, Clarendon Press, Oxford, 1987.
35. C. J. Thompson, *Mathematical Statistical Mechanics*, Princeton University Press, Princeton, NJ, 1972.
36. V. I. Arnold, *Mathematical Methods of Classical Mechanics*, Springer-Verlag, New York, 1978.
37. S. Whitaker, *Introduction to Fluid Dynamics*, Englewood Cliffs, NJ, 1986.
38. M. Gillan and M. Dixon, *J. Phys. C*, **16**, 869 (1983). The Calculation of Thermal Conductivities by Perturbed Molecular Dynamics Simulation.
39. R. Kubo, *J. Phys. Soc. Jpn.*, **12**, 570 (1957). Statistical Mechanical Theory of Irreversible Processes. I. General Theory and Simple Application to Magnetic and Conduction Problems.

40. M. Green, *J. Chem. Phys.*, **22**, 398 (1954). Markoff Random Processes and the Statistical Mechanics of Time-Dependent Phenomena.
41. D. Chandler, *Modern Statistical Mechanics*, Oxford University Press, New York, 1987.
42. S. Balasubramanian, C. J. Mundy, and M. L. Klein, *J. Chem. Phys.*, **105**, 11190 (1996). Shear Viscosity of Polar Fluids: Molecular Dynamics Calculations of Water.
43. K. Bagchi, S. Balasubramanian, and M. L. Klein, *J. Chem. Phys.*, **107**, 8561 (1997). The Effects of Pressure on Structural and Dynamical Properties of Associated Liquids: Molecular Dynamics Calculations for the Extended Simple Point Charge Model of Water.
44. G. Ciccotti, C. Pierleoni, and J. P. Ryckaert, in *Microscopic Simulations of Complex Hydrodynamic Phenomena*, M. Mareschal and B. L. Holian, Eds., Plenum Press, New York, 1992.
45. M. E. Tuckerman, C. J. Mundy, S. Balasubramanian, and M. L. Klein, *J. Chem. Phys.*, **106**, 5615 (1997). Modified Nonequilibrium Molecular Dynamics for Fluid Flows with Energy Conservation.
46. M. Kaku, *Quantum Field Theory: A Modern Introduction*, Oxford University Press, New York, 1993.
47. H. F. Trotter, *Proc. Amer. Math. Soc.*, **10**, 545 (1959). On the Product of Semi-Groups and Operators.
48. A. Friedman and S. P. Auerbach, *J. Comput. Phys.*, **93**, 171 (1991). Numerically Induced Stochasticity.
49. S. P. Auerbach and A. Friedman, *J. Comput. Phys.*, **93**, 189 (1991). Long Time Behaviour of Numerically Computed Orbits: Small and Intermediate Timestep Analysis of One Dimensional Systems.
50. C. J. Mundy, J. I. Siepmann, and M. L. Klein, *J. Chem. Phys.*, **103**, 10192 (1995). Decane Under Shear—A Molecular Dynamics Study Using Reversible NVT-SLLOD and NPT-SLLOD Algorithms. *Ibid.*, **104**, 7797 (1996). Correction.
51. H. Yoshida, *Phys. Lett. A*, **150**, 262 (1990). Construction of Higher Order Symplectic Integrators.
52. M. Suzuki, *J. Math. Phys.*, **32**, 400 (1991). General Theory of Fractal Path Integrals with Applications to Many Body Theories and Statistical Physics.
53. G. Arfken and H. Weber, *Mathematical Methods for Physicists*, Academic, San Deigo, 1995.
54. J. P. Ryckaert, A. Bellemans, G. Ciccotti, and G. V. Paolini, *Phys. Rev. A*, **39**, 259 (1989). Evaluation of Transport Coefficients of Simple Fluids by Molecular Dynamics: Comparison of Green-Kubo and Nonequilibrium Approaches for Shear Viscosity.
55. R. Bhupathiraju, P. T. Cummings, and H. D. Cochran, *Mol. Phys.*, **88**, 1665 (1996). An Efficient Parallel Algorithm for Non-Equilibrium Simulations of Very Large Systems in Planar Couette Flow.
56. K. Bagchi, S. Balasubramanian, C. J. Mundy, and M. L. Klein, *J. Chem. Phys.*, **105**, 11183 (1996). Profile Unbiased Thermostat with Dynamical Streaming Velocities.
57. K. Stephan and K. Lucas, *Viscosity of Dense Fluids*, Plenum, New York, 1979.
58. B. Wunderlich, M. Moeller, J. Grebowicz, and H. Baur, *Adv. Polym. Sci.*, **87**, 50 (1988). Conformational Motion and Disorder in Low and High Molecular Mass Crystals.
59. M. Mareschal, J. P. Ryckaert, and A. Bellemans, *Mol. Phys.*, **61**, 33 (1987). The Shear Viscosity of *n*-Butane by Equilibrium and Non-equilibrium Molecular Dynamics.
60. R. Edberg, G. P. Morriss, and D. J. Evans, *J. Chem. Phys.*, **86**, 4555 (1987). Rheology of *n*-Alkanes by Nonequilibrium Molecular Dynamics.
61. S. Chynoweth, U. C. Klomp, and Y. Michopoulos, *J. Chem. Phys.*, **95**, 3024 (1991). Rheology of *n*-Alkanes by Nonequilibrium Molecular Dynamics—Comment.
62. H. Luo and C. Hoheisel, *Phys. Rev. E*, **47**, 3956 (1993). Thermodynamics and Transport Properties of *n*-Butane Computed by Molecular Dynamics and a Rigid Interaction Model.
63. J. I. Siepmann, S. Karaborni, and B. Smit, *Nature*, **365**, 330 (1993). Simulating the Critical Behaviour of Complex Fluids.

64. S. T. Cui, P. T. Cummings, and H. D. Cochran, *Fluid Phase Equilibria*, **141**, 45 (1997). Configurational Bias Gibbs Ensemble Monte Carlo Simulation of Vapor–Liquid Equilibria of Linear and Short-Branched Alkanes.
65. C. J. Mundy, J. I. Siepmann, and M. L. Klein, *J. Chem. Phys.*, **102**, 3376 (1995). Calculation of the Shear Viscosity of Decane Using a Reversible Multiple Time-Step Algorithm.
66. C. J. Mundy, S. Balasubramanian, K. Bagchi, J. I. Siepmann, and M. L. Klein, *Faraday Discuss. Chem. Soc.*, **104**, 17 (1996). Equilibrium and Non-equilibrium Simulation Studies of Fluid Alkanes in Bulk and at Interfaces.
67. S. A. Gupta, H. D. Cochran, and P. T. Cummings, *J. Chem. Phys.*, **107**, 10316 (1997). Shear Behavior of Squalane and Tetraicosane Under Extreme Confinement. 1. Model, Simulation Method, and Interfacial Slip.
68. S. A. Gupta, H. D. Cochran, and P. T. Cummings, *J. Chem. Phys.*, **107**, 10327 (1997). Shear Behavior of Squalane and Tetraicosane Under Extreme Confinement. 2. Confined Film Structure.
69. S. A. Gupta, H. D. Cochran, and P. T. Cummings, *J. Chem. Phys.*, **107**, 10335 (1997). Shear Behavior of Squalane and Tetraicosane Under Extreme Confinement. 3. Effect of Confinement on Viscosity.
70. A. Wallqvist and R. D. Mountain, in *Reviews in Computational Chemistry*, K. B. Lipkowitz and D. B. Boyd, Eds., Wiley-VCH, New York, 1999, Vol. 13, pp. 183–247. Molecular Models of Water: Derivation and Description.
71. P. A. Thompson and M. O. Robbins, *Phys. Rev. A*, **41**, 6830 (1990). Shear Flow Near Solids—Epitaxial Order and Flow Boundary Conditions.
72. P. A. Thompson, G. S. Grest, and M. O. Robbins, *Phys. Rev. Lett.*, **68**, 3448 (1992). Phase Transitions and Universal Dynamics in Confined Films.
73. L. Bocquet and J. L. Barrat, *Phys. Rev. Lett.*, **70**, 2726 (1993). Hydrodynamic Boundary Conditions and Correlation Function of Confined Fluids.
74. L. Bocquet and J. L. Barrat, *Phys. Rev. E*, **49**, 3079 (1994). Hydrodynamic Boundary Conditions, Correlation Functions and Kubo Relations for Confined Fluids.
75. C. J. Mundy, S. Balasubramanian, and M. L. Klein, *J. Chem. Phys.*, **105**, 3211 (1996). Hydrodynamic Boundary Conditions for Confined Fluids Via a Nonequilibrium Molecular Dynamics Simulation.
76. P. G. Wolynes, *Phys. Rev. A*, **13**, 1235 (1976). Hydrodynamic Boundary Conditions and Mode-Mode Coupling Theory.
77. M. K. Kogan, *Rarefied Gas Dynamics*, Plenum Press, New York, 1959.
78. P. G. De Gennes, *C.R. Acad. Sci. Paris B*, **288**, 219 (1979). Viscometric Flows of Tangled Polymers.
79. D. J. Evans and G. P. Morriss, *Phys. Rev. Lett.*, **56**, 2172 (1986). Shear Thickening and Turbulence in Simple Fluids.
80. D. J. Barber and R. Loudon, *An Introduction to the Properties of Condensed Matter*, Cambridge University Press, Cambridge, 1989.
81. D. J. Evans, S. T. Cui, H. J. M. Hanley, and G. C. Straty, *Phys. Rev. A*, **46**, 6731 (1992). Conditions for the Existence of a Reentrant Solid Phase in a Sheared Atomic Fluid.
82. K. P. Travis, P. J. Daivis, and D. J. Evans, *J. Chem. Phys.*, **103**, 10638 (1995). Thermostats for Molecular Fluids Undergoing Shear Flow: Applications to Liquid Chlorine. *Ibid.*, **105**, 3893 (1996). Addition/Correction: Thermostats for Molecular Fluids Undergoing Shear Flow: Applications to Liquid Chlorine.
83. P. Padilla and S. Toxvaerd, *J. Chem. Phys.*, **103**, 716 (1995). Shear Flow at the Liquid–Liquid Interface.
84. M. E. Tuckerman, G. J. Martyna, and B. J. Berne, *J. Chem. Phys.*, **97**, 1990 (1992). Reversible Multiple Time Scale Molecular Dynamics.
85. J. J. Erpenbeck, *Phys. Rev. Lett.*, **52**, 1333 (1984). Shear Viscosity of the Hard-Sphere Fluid Via Nonequilibrium Molecular Dynamics.

86. W. Loose and S. Hess, *Rheol. Acta*, **28**, 91 (1989). Rheology of Dense Model Fluids Via Nonequilibrium Molecular Dynamics: Shear Thinning and Ordering Transition.
87. W. Loose and G. Ciccotti, *Phys. Rev. A*, **15**, 3859 (1992). Temperature and Temperature Control in Nonequilibrium Molecular Dynamics Simulations of the Shear Flow in Dense Fluids.
88. W. Xue and G. Grest, *Phys. Rev. Lett.*, **64**, 419 (1990). Shear Induced Alignment of Colloidal Particles in the Presence of a Shear Flow.
89. M. J. Stevens , M. O. Robbins, and J. F. Belak, *Phys. Rev. Lett.*, **66**, 3004 (1991). Shear Melting of Colloids—A Nonequilibrium Phase Diagram.
90. D. M. Heyes and P. J. Mitchell, *Mol. Phys.*, **84**, 261 (1995). Nonequilibrium Molecular and Brownian Dynamics Simulations of Shear Thinning of Inverse Power Fluids.
91. S. R. Rastogi, N. J. Wagner, and S. R. Lustig, *J. Chem. Phys.*, **104**, 9234 (1996). Rheology, Self-Diffusion, and Microstructure of Charge Colloids Under Simple Shear by Massively Parallel Nonequilibrium Brownian Dynamics.
92. A. A. Rigos and G. Wilemski, *J. Phys. Chem.*, **96**, 3981 (1992). Brownian Dynamics Simulations of An Order–Disorder Transition in Sheared Sterically Stabilized Colloidal Suspension.
93. R. Cook and G. Wilemski, *J. Phys. Chem.*, **96**, 4023 (1992). Packing Constraints and Number Dependence in Simulations of Sheared Colloidal Suspensions.
94. T. Yamada and S. Nosé, *Phys. Rev. A*, **42**, 6282 (1990). Two-Phase Coexistence of String and Liquid Phases: Nonequilibrium Molecular-Dynamics Simulations of Couette Flow.
95. G. Ciccotti and G. Jacucci, *Phys. Rev. Lett.*, **35**, 789 (1975). Direct Computation of Dynamical Response by Molecular Dynamics: the Mobility of a Charged Lennard-Jones Particle.
96. G. Ciccotti, G. Jacucci, and I. R. McDonald, *J. Stat. Phys.*, **21**, 1 (1979). “Thought-Experiments” by Molecular Dynamics.
97. G. P. Morriss and D. J. Evans, *Phys. Rev. A*, **35**, 792 (1987). Application of Transient Correlation Functions to Shear Flow Far From Equilibrium.
98. D. J. Evans and G. P. Morriss, *Phys. Rev. A*, **36**, 4119 (1987). Asymptotic Nonlinear Stress Tensor in Small Periodic Systems Undergoing Couette Flow.
99. D. J. Evans and G. P. Morriss, *Phys. Rev. A*, **38**, 4142 (1988). Transient-Time-Correlation Functions and the Rheology of Fluids.
100. W. T. Ashurst and W. G. Hoover, *Phys. Rev. B*, **14**, 1465 (1976). Microscopic Fracture Studies in the Two-Dimensional Triangular Lattice.
101. R. A. Kendall, R. J. Harrison, R. J. Littlefield, and M. F. Guest, in *Reviews in Computational Chemistry*, K. B. Lipkowitz and D. B. Boyd, Eds., VCH Publishers, New York, 1995, Vol. 6, pp. 209–316. High Performance Computing in Computational Chemistry: Methods and Machines.
102. F. F. Abraham, D. Brodbeck, R. A. Rafey, and W. E. Rudge, *Phys. Rev. Lett.*, **73**, 272 (1994). Instability in Fracture—A Computer Simulation Investigation.
103. J. Fineberg, S. P. Gross, M. Marder, and H. L. Swinney, *Phys. Rev. Lett.*, **67**, 457 (1991). Instability on Dynamic Fracture.
104. J. Fineberg, S. P. Gross, M. Marder, and H. L. Swinney, *Phys. Rev. B*, **45**, 5146 (1992). Instability in Propagation of Fast Cracks.
105. S. P. Gross, J. Fineberg, M. Marder, W. D. McCormick, and H. L. Swinney, *Phys. Rev. Lett.*, **71**, 3162 (1993). Acoustic Emissions From Rapidly Moving Cracks.
106. S. J. Zhou, D. M. Beazley, P. S. Lomdahl, and B. L. Holian, *Phys. Rev. Lett.*, **78**, 479 (1997). Large-Scale Molecular Dynamics Simulations of Three-Dimensional Ductile Failure.
107. W. Li, R. K. Kalia, and P. Vashishta, *Phys. Rev. Lett.*, **77**, 2241 (1996). Amorphization and Fracture in Silicon Diselenide Nanowires—A Molecular Dynamics Study.
108. A. Omelchenko, J. Yu, R. K. Kalia, and P. Vashishta, *Phys. Rev. Lett.*, **78**, 2148 (1997). Crack Front Propagation and Fracture in a Graphite Sheet: A Molecular-Dynamics Study on Parallel Computers.

109. D. W. Brenner, O. A. Shenderova, and D. A. Areshkin, in *Reviews in Computational Chemistry*, K. B. Lipkowitz and D. B. Boyd, Eds., Wiley-VCH, New York, 1998, Vol. 12, pp. 207–239. Quantum-Based Analytic Interatomic Forces and Materials Simulation.
110. M. Sprik, U. Roethlisberger, and M. Klein, *J. Phys. Chem. B*, **101**, 2745 (1997). Structure of Solid Poly(tetrafluoroethylene): A Computer Simulation Study of Chain Orientational, Translational, and Conformational Disorder.
111. S. Campbell, G. Luengo, V. Srdanov, F. Wudl, and J. Israelachvili, *Nature*, **382**, 520 (1996). Very Low Viscosity at the Solid–Liquid Interface Induced by C₆₀ Monolayers.
112. B. Schutz, *Geometrical Methods of Mathematical Physics*, Cambridge University Press, Cambridge, 1980.

CHAPTER 6

History of the Gordon Research Conferences on Computational Chemistry

Donald B. Boyd and Kenny B. Lipkowitz

Department of Chemistry, Indiana University-Purdue University at Indianapolis (IUPUI), Indianapolis, Indiana 46202-3274

INTRODUCTION

The Gordon Research Conferences (GRCs) have a distinguished history that may not be familiar to all readers of this book series. Of particular interest to theoretical and computational chemists are the biennial GRCs on computational chemistry. The Gordon Research Conference on Computational Chemistry is a relatively young conference, having been founded in 1986. The computational chemistry conference has been exceedingly successful based on interest in attending the meetings as well as the quality of the talks, audience participation, and discussions. We thought it would be of interest to document the origins of this conference, describe some of the reasons for its success, and present a photo album of participants.

The originator of the GRCs, Dr. Neil E. Gordon, was a professor of chemistry at the Johns Hopkins University when he convened his first chemistry conference in the summer of 1931 in Baltimore, Maryland. The basic idea for that conference is still practiced today: to bring together under one roof a group of scientists working at the frontiers of research and to allow them to discuss the most recent advances of their work in an uninhibited and fruitful manner. The

Reviews in Computational Chemistry, Volume 14
Kenny B. Lipkowitz and Donald B. Boyd, Editors
Wiley-VCH, John Wiley and Sons, Inc., New York, © 2000

conferences were meant to stimulate new directions for research. From this genesis, the conference series evolved and expanded. From 1931 to 1946 the conferences were held in the Chesapeake Bay region of Maryland and were known as the Gibson Island Research Conferences. To have a cooler place to meet in the summer, the conferences moved to what is now Colby-Sawyer College in New London, New Hampshire. The conferences were named in honor of Dr. Gordon when he retired in 1946.

In the summer of 1947 there were 10 GRCs, each on a different subject. In 1956 the GRC effort was incorporated as a nonprofit, tax-exempt organization devoted to scientific and educational purposes and over the years expanded both the number of topical conferences as well as the locations of those conferences. About 10 other boarding schools in New Hampshire became hosts to the meetings. Currently, about 110 conferences are held annually during the warm months at the New Hampshire sites and at a site in Newport, Rhode Island. The Polymers Conference was moved to Santa Barbara, California, to begin the West Coast winter series in 1963. Those winter conferences moved to Ventura, California, in 1980, and approximately 25–30 conferences are held each year in the months of January–March at that site. In 1990 the GRC transcended international boundaries by establishing sites in Europe: first in Italy and then also England. In 1996 the GRC office established two meetings in Japan, and other foreign sites are starting or being considered. The scheduling of the conferences is almost year-round now.

Approximately 14,000 American and international scientists participate in the GRCs each year. There now exist more than 130 conferences covering various topics, and more are on the horizon. Although originally started as chemistry conferences, additional topics of interest to molecular scientists in biology, biomedicine, physics, and materials have been added over the years.

For the last several decades, the entire organization has been managed from the GRC office at the University of Rhode Island. The director is advised by a board of trustees and a council. The members of these bodies are scientists appointed by the director for short terms, so that fresh perspectives are continually brought in. Among those members have been the computational chemists William A. Goddard III, Barry Honig, and Mark Ratner.

The GRCs are preeminent scientific meetings because of the high quality of the science being discussed and because of the format of the meetings. Many features distinguish the GRCs: (1) the subject matter is at the forefront of some focused area of research, (2) attendance is limited to maximize interaction among the participants, (3) attendance is subject to approval by a democratically elected chair (or co-chairs), so that participants are qualified to contribute to progress of the field, (4) participants at each conference vote on who will be the chair(s) at the next conference, thereby implicitly selecting the emphasis for the next meeting, (5) the research presented at each conference is supposed to include previously unpublished work, even preliminary work, (5) no proceedings are published; the authors are free to disseminate their work through normal publication channels if they choose, (7) the invited talks are generally

informative and substantive,¹ (8) scientific sessions are held in the mornings and evenings; plenty of time is available after each lecture to allow relatively unrestricted discussion, (9) the conference sites are usually in small, remote towns, where expenses are low and participants can recreate in the afternoons, (10) there are no concurrent sessions, so everyone can hear each talk, (11) the participants sleep in dormitories and eat together in a dining hall, thus affording plenty of opportunities to meet the other participants, to form friendships and collaborations, to cross-fertilize scientific perspectives, to rub elbows with distinguished research leaders and graduate students alike, or just to relax and socialize in a secure and productive environment, (12) the meeting auditorium is not too large and is conducive to interactive discussion,² and (13) all conferences are subject to the careful oversight of a director of the GRC office and a board of trustees to ensure that the conferences retain vitality, harmony, and usefulness. Because of the effectiveness of the GRC format, organizers of other scientific meetings have occasionally tried to emulate various aspects of the format.

LAYING THE GROUNDWORK FOR A GORDON RESEARCH CONFERENCE ON COMPUTATIONAL CHEMISTRY

The history of the computational chemistry GRC begins in 1982.³ But first, we give additional background. In the 1960s the term “computational chemistry” had not come into use. Back then, a theoretical (quantum) chemistry GRC series existed, but the leaders of that group wanted to have a larger attendance than the GRC would allow (ca. 140 maximum), and they wanted to be able to publish the proceedings as books. Hence the theoretical chemists parted ways with the GRC organization to become the American Theory Conferences. In addition to this conference, there were other highly respected and long-standing regular conferences, such as the annual Sanibel Symposia (then held off the west coast of Florida) and triennial Canadian Symposia on Theoretical Chemistry, again focusing mainly on quantum chemistry. Thus, the need for meetings in the field of quantum chemistry was very well satisfied. But what about other facets of what we now consider the field of computational chemistry?

A part of the culture of the 1960s and 1970s was that molecular scientists doing calculations were roughly divided into two groups: (1) “*ab initio*-ists” including chemical physicists, and (2) chemists using approximate semiempirical and empirical approaches to understanding molecular behavior.⁴ Whereas there were many meetings catering to the first group, there was no real home in terms of a regular meeting for the “semiempiricists,” “molecular modelers,” and scientists doing molecular mechanics or macromolecular simulations.

The idea for a GRC on computational chemistry was conceived by one of us (DBB) at the March 1982 National Meeting of the American Chemical

Society in Las Vegas, Nevada, where he had been invited to give a paper.⁵ His vision was that quantum chemistry was only one part of an emerging field of computational chemistry, whereas molecular graphics, molecular modeling, molecular mechanics, molecular simulations, computer-aided drug design, polymer and materials design, chemical information, molecular structure databases, chemistry software development, computer-aided chemical education, computer-aided structure determination, organic synthesis planning, and other computational technologies were bound to become increasingly important to molecular science. All these topics fit under the umbrella of computational chemistry. The reason for founding a GRC on computational chemistry was to bring together all facets of the field in a balanced manner and in an atmosphere ideal for collegial exchange of ideas.

The vision of a computational chemistry conference of this type received a trial run of sorts the next year when the authors co-organized the world's first Symposium on Molecular Mechanics. It was held in Indianapolis June 23–24, 1983, and 140 scientists from the United States, Europe, and Japan attended. We were gratified by how enthusiastic the participants were about having a forum in which to describe their work and to debate the best ways of developing and applying potential functions for molecular mechanics. In addition, it was obvious that the same potential functions would underlie the growing field of molecular simulations, which is applicable to a variety of disciplines. The overwhelming success of that meeting led many of the attendees to urge us to organize a similar meeting in the future. In fact, looking back at the abstract booklet for the Indianapolis symposium, one can see many of the names of computational chemists who became frequent participants at the computational chemistry GRCs: well-known names such as Harold R. Almond Jr., Gerhard Barnickel, Frank K. Brown, Robert E. Carter, Tom A. Darden, Mark Froimowitz, Jiali Gao, Kendall N. Houk, Peter A. Kollman, Tommy Liljefors, Jeffry D. Madura, John McKelvey, Frank A. Momany, Terry R. Stouch, and William J. Welsh, among others.

In 1984, the authors of this chapter coauthored a proposal to the GRC Board of Trustees for a new conference on computational chemistry. At that time, Boyd was a theoretical chemist doing computer-aided ligand design at Eli Lilly and Company, and Lipkowitz was an associate professor of organic chemistry at IUPUI. We considered this collaboration of industrial perspective and academic perspective a key feature of our proposal. In the early 1980s, computational chemists in industry were few in number, but their numbers were growing rapidly to become a significant fraction of all computational chemists.⁵ For healthy development of the whole field, the authors felt it was very important to have balanced participation of both industrial and academic/governmental scientists in the conference. Some of the most interesting advances in computational chemistry methodologies and applications were (and still are) being made in industry. To assure vibrant interchange of ideas and respective needs, the conference should appeal to both industrial and academic researchers. In the proposal submitted August 17, 1984, the authors wrote:

For many years the focus of a large number of theoretical chemists was on the development of better computational methods and approximations. There was a small, but growing number of chemists who were interested in applying these methods to practical questions of concern to experimentalists. Computational chemistry has now achieved de facto recognition as a discipline through formation of the Division of Computers in Chemistry of the American Chemical Society and through the publications of *Journal of Computational Chemistry*, *Journal of Molecular Structure*, *Computers and Chemistry*, and *Journal of Molecular Graphics*.

Software companies specializing in computational chemistry have entered the marketplace in recent years, and new companies are emerging yearly. Laboratory chemists are finding the computational tools helpful to their research and want to learn how to use them better. At present there is no conference that concentrates, as we intend this conference to, on applications of computational chemistry.

To complement the existing theoretical chemistry conferences, the proposal for the new GRC called for balanced coverage of all the computational tools in use by researchers. No area of computational chemistry should be overemphasized, and no area should be ignored. The new conference should not infringe on the core interests of other conferences. Already in existence—and with a distinguished history—was a GRC on Quantitative Structure–Activity Relationships in Biology (QSAR) founded in 1975. That conference focused at that time mainly on statistical methods and the study of pharmaceutically interesting molecules. The QSAR GRC met in odd-numbered years, so the plan called for the computational chemistry conference to meet in even-numbered years, again complementing the existing conference.

Seconding letters to the authors' proposal were kindly provided by Nobel laureates William N. Lipscomb (Harvard University) and Roald Hoffmann (Cornell University), as well as Norman L. Allinger (University of Georgia), Richard W. Counts (QCPE), Kendall N. Houk (University of Pittsburgh), Daniel A. Kleier (Shell), and Peter A. Kollman (University of California, San Francisco). On October 15, 1984, the proposal was approved by the GRC Board of Trustees, and Dr. Alexander M. Cruickshank, then director of the Gordon Research Conferences, scheduled the first conference for the summer of 1986.

THE FIRST GORDON RESEARCH CONFERENCE ON COMPUTATIONAL CHEMISTRY

The topics covered in the first conference were selected to be as representative of the whole field as possible. Prominent scientists were willing to accept our

invitation to speak. We were also gratified by the financial backing obtained from various sponsors. These funds plus those from the GRC office and the generous cooperation of certain of our invited speakers to obtain their own travel funds permitted the conference to occur. We had the plan, we had the money, and we had the ambition. . . , all we needed were the participants. We publicized the meeting widely. The response was rewarding. There were more than 255 applications for the available openings. Applications could have reached 300, but we disseminated word in the months immediately before the meeting that applications had exceeded the size limit set by the GRC office. The high interest was all the more remarkable in light of the more than 25 other meetings and symposia held in 1986 covering one or more aspects of computational chemistry.⁷ The GRC office allowed us to expand beyond the recommended size of about 120 attendees, and we were able to accept 150 participants. We found ourselves in a bittersweet situation: as co-chairs we were required to turn down applications from some of the respected people in the field as well as from friends.

This aside, the first conference was extraordinarily encouraging, with electric enthusiasm and optimism being felt and expressed by the participants. Attendees sensed that they were part of history in the making. The success of the conference was due to the participants, carefully selected to achieve a balance in terms of research interests, geography, and affiliation. The GRC office sends to the chairmen weekly lists of people who have applied to attend. Applicants for that first meeting represented 183 organizations. By careful management, we achieved representation from 56 colleges and universities, 52 companies, and 15 government and private labs. Participation levels were exactly representative of those who applied to attend: 50% from academia, 40% from industry, and 10% from government and private laboratories. One of the perennial issues facing GRCs in general is being able to achieve what colleagues from overseas consider is fair representation. At our conference, 19% of the applicants were from outside the United States, and 19% of those attending represented 11 countries other than the United States. This was quite balanced, since so many computational chemists at that time lived or studied in the United States.

In the welcoming remarks, Boyd, speaking for both of us, discussed the demographics of the attendees and the scope of the conference vis-à-vis the definitions of computational chemistry. He pointed out that although numerous journals and books had been published that mentioned computational chemistry, few authors and editors had attempted to offer an explicit definition. The gist of Boyd's remarks about the definition and scope of computational chemistry was recorded and discussed further in the first volume of this book series.⁸

The participants at the first conference exhibited a high level of positive excitement throughout the week. The 19 talks and two poster paper sessions were excellent.⁹ It is interesting to look back at the original program (see Appendix 1 for a reproduction) and see the names of the established investigators, as well as their students, many of whom are now prominent leaders in the

field. The affiliations of many of the computational chemists have also changed over the years, as these individuals flowed toward newly created jobs.¹⁰

Besides the regular program, one of the “free” afternoons in 1986 was devoted to an open roundtable discussion of force fields. Interest in the topic was high, and about half the attendees came to the roundtable. An outcome of the discussions was that a committee of volunteers formed to promulgate guidelines for developing and evaluating force field parameters and for setting standards for energy minimizations. Unfortunately, the committee, like many committees, had trouble implementing its good intentions.

The principles we adopted to make the conference a success are simple: we wanted the content of the conference to be truly representative of all aspects of what computational chemistry could encompass, without being limited to one area of this discipline or being overwhelmed by a clique of scientists with a specialized interest. Additionally, we realized that many scientists working in industrial laboratories were pushing back the frontiers of computational chemistry by developing new algorithms and, because of the computing machinery they could afford to buy, were making unprecedented use of computers to solve practical problems. So, it was decided from the start that the conference would try to maintain a nearly equal mix of industrial and academic researchers. To set the tone, we decided that the conference would be run by co-chairs, one from industry and one from academia. Indeed, that is how the first two conferences were co-chaired.

The authors greatly enjoyed organizing the conference and decided during the trip from Indianapolis to New Hampshire that we would stand as candidates in the election to be held for the co-chairs of the second conference, which we hoped would take place. At the conference, additional nominees were put forward. A free and open election (with ballots managed by an independent election committee consisting of participants) resulted in Boyd (then in industry) and Peter Kollman (representing academia) being chosen by a majority of the participants to organize a second conference.

The GRC office often sends observers to the conferences to assess the general tenor of the meetings and to see if the conference guidelines are being adhered to. In addition, to measure the quality of the meeting, the GRC office asks all participants to fill out a short evaluation form. Longer evaluation forms are also filled out by randomly selected participants. Because of the very positive ratings for the computational chemistry conference, the Gordon Conference Board of Trustees gave approval to its continuation. After each conference, the chair(s) turn in a final report to the GRC office in which they can request preferred places and weeks for the next conference, but the final decision is made by the director according to the availability of site and date. As the authors wrote in their final report:

Although a number of theoretical chemistry meetings were being held each year, there was no forum for the rapidly evolving field of practical or applied computational chemistry. . . . Based on the responses received

both verbally and in the form of the questionnaires used at the conference, the meeting was highly worthwhile and beneficial to the participants. . . . Several people commented that they liked the way the program was organized in regard to the number of speakers and the two formal poster sessions. The discussions were very good both in and out of the lecture hall. . . . A foundation was laid for a successful and useful conference series.

THE SECOND GORDON RESEARCH CONFERENCE ON COMPUTATIONAL CHEMISTRY

Boyd and Kollman collaborated in planning the 1988 conference. Funding sources were found that gave the meeting an even larger budget than in 1986. As the organizers wrote in their proposals:

Computational chemistry is the study of chemistry using computer-based methods. Advances in both method development and applications to chemistry have been catalyzed by the computer revolution. They have also been stimulated by the ever-increasing realizations by chemists that computer simulation is becoming a full partner with experimental work in chemistry.

In the past, computational chemistry has been considered to be mainly synonymous with quantum chemistry. However, exciting developments of computational chemistry include molecular mechanics and dynamics applications to organic and biological molecules, computer graphics to study the properties of complex molecules, and distance geometry methods. . . . It is clear that a combination [of approaches] is more powerful than each is alone.

The co-chairs set about their task to create a program of excellent speakers, who would cover fresh topics. Information about the program was disseminated to the community of computational chemists. Again interest was high. About 240 scientists applied to attend the second conference in 1988; 150 could be accepted. Participants who were accepted represented over 100 organizations, including many universities, several government laboratories, 28 pharmaceutical companies, 7 agrochemical companies, and 13 other industrial organizations. Fifty percent of the participants were from academia, 35% from industry, and the remaining from government and private laboratories. Fifteen percent of the participants, representing 14 countries, were from outside the United States. The high attraction was again remarkable, in light of over 30 other meetings and symposia held in 1988 that covered at least one aspect of computational chemistry.

In his opening remarks at the GRC, Boyd pointed out that computational chemistry is not just quantum chemistry, not just molecular dynamics, or not just molecular modeling. Each approach has an appropriate and valuable role. The conference was intended to achieve a fair balance of various aspects of computational chemistry. A key feature of the conference, as at the first one, was a vigorous mix of academic and industrial scientists. A melding of these scientists advances the science in interesting, useful directions most quickly.

Besides the 19 full lectures and discussions, the session chairs were allowed to give short talks. More than 55 poster papers were presented at the two evening poster sessions. The original program is reproduced in Appendix 2. Again it is interesting to see the names and the work under way about 10 years ago.

RECENT DEVELOPMENTS

The first two GRCs on Computational Chemistry (1986 and 1988) had co-chairmen, one from industry and one from academia. The GRC office's standard advice is that it is better to have a chair plus a vice-chair who will succeed to the chair's position at the next meeting. Such an arrangement ensures a clear chain of command. Hence the more common GRC practice of having chairs and vice-chairs was adopted starting with the 1990 conference. In the new arrangement, the vice-chair moves up to become chair four years after election (the conferences being held in even-numbered years to alternate with the QSAR GRCs). To keep the critically important industrial/academic balance, the conferences alternate the chair's job between someone from industry and someone from academia or a government laboratory. An industrial chair can bring to the conference an appreciation of "real-world" research questions, whereas a chair from an academic or government laboratory can bring an appreciation of basic research questions. The vice-chair has responsibility for the poster sessions, and the chair has overall responsibility of inviting speakers, raising money, and accepting attendees. The topics and speakers invited to a conference usually reflect the interests of the chair, modulated to some degree by the influence of past chairs and the industrial/academic stewardship which ensures both fairness and diversity of interests at the meetings. Past chairs continue their service by automatic appointment to an executive steering committee, which has a responsibility to advise and assist the new chairs.

Since 1986, the GRC on Computational Chemistry has succeeded in having a turnover of those attending. This infusion of fresh faces and ideas is keeping the conference up to date and moving according to the dictates of the field. The conferences, the most recent of which was in 1998, are well attended. The recent chairs have somewhat avoided the problem of over-subscription by not publicizing the meetings as heavily as were the early con-

ferences. Whereas the conferences still touch on the many facets of computational chemistry, the recent conferences have given increased emphasis to molecular simulations research. This is partly because the molecular dynamics participants have outnumbered participants working in other areas of computational chemistry.

At the 1998 conference, repeated ties in the voting for the next vice-chair were broken when a quantum chemist, Prof. Michael Zerner, teamed up with a molecular simulations chemist, Dr. Bernard Brooks, to serve as co-vice-chairs in 2000.

Table 1 records the chairs of the conferences. Each chair brought to the conference their wisdom, enthusiasm, and work effort needed to perpetuate the conference. Table 2 records the organizations that provided financial support to

Table 1 Record of the Gordon Research Conferences on Computational Chemistry

Date	Organizers ^a	Site
August 18–22, 1986	Donald B. Boyd (Lilly) and Kenneth B. Lipkowitz (IUPUI), Co-Chairmen	Colby-Sawyer College, New London, New Hampshire
July 4–8, 1988	Donald B. Boyd (Lilly) and Peter A. Kollman (UCSF), Co-Chairmen	Plymouth State College, Plymouth, New Hampshire
June 18–22, 1990	William L. Jorgensen (Yale), Chair; John M. McKelvey (Kodak), Vice-Chair	Plymouth State College, Plymouth, New Hampshire
June 29–July 3, 1992	John M. McKelvey (Kodak), Chair; Kendall N. Houk (UCLA), Vice-Chair	New Hampton School, New Hampton, New Hampshire
July 4–8, 1994	Kendall N. Houk (UCLA), Chair; Thomas A. Halgren (Merck), Vice-Chair	New Hampton School, New Hampton, New Hampshire
June 30–July 5, 1996	Thomas A. Halgren (Merck), Chair; Jeffry D. Madura (University of South Alabama), Vice-Chair	New Hampton School, New Hampton, New Hampshire
June 28–July 3, 1998	Jeffry D. Madura (Duquesne), Chair; Terry R. Stouch (Bristol-Myers Squibb), Vice-Chair	Tilton School, Tilton, New Hampshire
2000	Terry R. Stouch (Bristol-Myers Squibb), Chair; and Bernard Brooks (NIH) and Michael Zerner (University of Florida), Co-Vice-Chairs	Not yet announced

^aAffiliations are shown at the time of service.

Table 2 Financial Supporters of Past Gordon Research Conferences on Computational Chemistry^a

Year	Sponsors
1986	GRC Board of Trustees, Eli Lilly and Company, IUPUI, Air Force Office of Scientific Research, QCPE, and Hoffmann-LaRoche
1988	GRC Board of Trustees, Air Force Office of Scientific Research, Office of Naval Research, QCPE, Eli Lilly and Company, and University of California, San Francisco
1990	GRC Board of Trustees, Eastman-Kodak, QCPE, Digital Equipment Corporation, Hoffmann-LaRoche, Eli Lilly and Company, and Tripos Associates
1992	GRC Board of Trustees, Eastman-Kodak, IBM, Stirling-Winthrop, and Tektronix
1994	GRC Board of Trustees, Cray Research, IBM, Tripos Associates, Ciba-Geigy, DuPont Merck Pharmaceutical, Eli Lilly and Company, MDL Information Systems, Merck, and Chiron
1996	GRC Board of Trustees, Astra-Hässle, Bristol-Myers Squibb, Chiron, Ciba-Geigy, DuPont Merck Pharmaceutical, Eastman Kodak, Glaxo Wellcome, IBM, MDL, Merck, Molecular Simulations Inc., Rohm and Haas, Sandoz, SmithKline Beecham, and Zeneca
1998	GRC Board of Trustees, Bristol-Myers Squibb, Chemical Computing Group, DuPont Merck Pharmaceutical, IBM, R. W. Johnson Pharmaceutical Research Institute, Molecular Simulations Inc., Novartis, Rohm and Haas, Tripos, Inc., and Zeneca

^aThis table may be incomplete; if there are other donors who made contributions after the conference began, their names may have been omitted because we were unaware of their generosity. We apologize to any such donors.

the conferences. These organizations were willing to invest in the field and in the professional development of computational chemists.

PICTORIAL HISTORY

Figures 1–7 are the group portraits that were taken at the conferences in New Hampshire by local professional photographers under contract with the GRC office. Many of the leaders in the field are pictured. In the photographs can also be found some novitiates to computational chemistry who have become today's "stars." Also pictured are some former colleagues who have retired from the profession or who regrettably have passed away.

In looking at Figures 1–7, it is obvious that the "rows" formed by the assemblage of attendees were a bit free-form. The names in the figure captions are based on the sign-up sheets that were distributed at the time of the photography. A row-by-row correspondence between the distribution on faces and the linear list of names is impossible in many cases. However, the faces and names



Figure 1 Group photo taken at the Gordon Research Conference on Computational Chemistry, Donald B. Boyd (Lilly) and Kenneth B. Lipkowitz (IUPUI), Co-Chairmen, August 18–22, 1986, Colby-Sawyer College, New London, New Hampshire.

Kneeling in front (left to right): K. B. Lipkowitz and D. B. Boyd.

Row 1 (left to right): R. W. Harper, B. R. Brooks, R. R. Holmes, S. Topiol, W. N. Lipscomb, R. Langridge, N. L. Allinger, J. W. Ponder, J. A. McCammon, W. A. Goddard III, L. C. Allen, P. A. Kollman, W. L. Jorgensen, N. S. Ostlund, K. N. Houk, A. P. Johnson, D. N. J. White, J. J. P. Stewart, J. M. McKelvey, C. E. Dykstra, T. Lilje fors, H. Kashiwagi, D. G. Watson.

Row 2 (left to right): T. M. Ford, T. Schlick, T. P. Lybrand, J. M. Blaney, A. M. Treasurywala, M. Renzel, V. Buss, C. F. Wong, P. R. Laurence, S. Grigoras.

Row 3 (left to right): M. T. Marron, M. Gall, M. M. Teeter, S. Scheiner, D. A. Kleier, A. M. Naylor, J. A. Deiters, A. Y. Meyer, M. L. Connolly, A. R. Srinivasan, D. A. Pearlman, D. P. Gieschen, V. Cody, B. van de Graaf, D. M. Walker, T. Gund, D. L. Beveridge, I. V. Pettersson, Y. C. Martin, G. Barnickel.

Row 4 (left to right): H. Luecke, J. H. Noordik, W. C. Herndon, M. Froimowitz, D. M. Gange, S. N. Rao, V. N. Balaji, R. L. Des Jarlais, W. E. Reiher III, M. Frisch, R. Counts, F. K. Brown, R. P. Sheridan, D. A. Case, M. Whitlow, M. A. Pleiss, D. F. DeTar, R. Voets, E. Ōsawa, T. Hirano, A. Buda.

Row 5 (left to right): R. L. Hilderbrandt, G. V. Nelson, M. L. McKee, C. Tosi, M. Ragazzi, F. A. Momany, N. Gensmantel, W. J. Welsh, G. Trummlitz, B. E. Hingerty, K. M. Merz Jr., L. E. Chirlian, T. Pierce, H. Almond Jr., G. P. Purvis III, K. E. Gilbert, W. Thiel, O. E. Millner, C. M. Cook, L. Kuyper, E. G. Maliski, P. R. Menard, M. M. Marsh.

Row 6 (left to right): E. Chamot, J. Lauher, F. H. Clarke, G. P. Ford, L. P. Davis, L. D. Strawser, J. D. Goddard, P. C. Jurs, D. E. Walters, R. W. Strozier, J. R. Damewood Jr., S. G. Wierschke, M. Waldman, C. J. Manly, R. B. Nachbar, E. M. Bellott, D. Cremer, E. Kraka, G. Frenking, D. P. Vercauteren, C. Venanzi, W. F. Head.

Row 7 (left to right): R. D. Cramer III, G. M. Smith, D. M. Storch, R. C. Glen, N. C. J. Stutchbury, T. R. Stouch, P. Dwyer-Hallquist, T. K. Dickens, K. F. Kochler, J. P. Bowen, R. E. Carter, M. M. Francl, J. L. Font, T. A. Ford, S. Rubenstein, P. Weiner, J. C. Hempel, L. Glasser, H. Wikstrom, P. G. Seybold, W. C. Harris, D. R. Kelsey, M. Wise.



Figure 2 Group photo taken at the Gordon Research Conference on Computational Chemistry, Donald B. Boyd (Lilly) and Peter A. Kollman (UCSF), Co-Chairmen, July 4–8, 1988, Plymouth State College, Plymouth, New Hampshire.

Row 1 (left to right): C. H. Reynolds, E. Martin, W. Swope, M. M. Franci, D. T. Nguyen, D. L. Camper, D. A. Pearlman, A. H. Katz, A. G. Anderson, J. Badger, M. Khalil, K. D. Dobbs, L. E. Chirlian.

Row 2 (left to right): W. Braun, N. Gō, J. W. Lauher, S. H. Bryant, J. Wendoloski, T. Lilje fors, P. A. Kollman, D. B. Boyd, Y. Oka, I. D. Kuntz, M. C. Zerner, A. T. Brunger, T. A. Halgren, S. Wodak, J. K. Burdett.

Row 3 (left to right): R. S. Bohacek, P. M. W. Gill, M. Head-Gordon, J. A. Pople, H. Sellers, T. Schlick, S. Vajda, J. K. Labanowski, N. L. Allinger, J. M. Blaney, S. Dixon, R. P. Sheridan, A. Tomonaga, R. S. Pearlman, M. R. Reddy, T. R. Stouch, R. Breckenridge, S. Grigoras, K. E. Gilbert, C. M. Cook, D. F. DeTar, J. P. Brown, M. Froimowitz.

Row 4 (left to right): R. W. Pastor, P. G. Seybold, K. Watanabe, P. Weiner, F. Manaut, M. L. McKee, K. Jayasuriya, N. C. Cohen, G. Klebe, C. A. Arrington, R. D. Cramer III, L. Kuyper, N. C. Perry, P. R. Menard, D. A. Smith, J. M. Leonard, A. J. Hoffman, J. D. Madura, M. E. Snow, K. Müller, L. Reid.

Row 5 (left to right): J. W. Frazer, C. A. Venanzi, M. Murcko, S. Profeta Jr., E. P. Jaeger, D. A. Case, G. Barnickel, J. L. Font, D. E. Bashford, A. Treasurywala, M. Waldman.

Row 6 (left to right): R. M. Venable, T. J. Venanzi, J. Cioslowski, K. Kuczera, R. J. Woods, B. K. Lee, S. R. Wilson, W. P. Anderson, J. R. Damewood Jr., L. P. Davis, J. J. P. Stewart, D. W. Deerfield II, V. Buss.

Row 7 (left to right): D. A. Kleier, T. J. O'Donnell, D. A. Bassolino, J. Cicariello, L. Glasser, J. Silvestre, M. S. Gordon, P. D. J. Grootenhuis, M. K. Holloway, P. A. Cruickshank, R. D. Sindelar, D. P. Gieschen, R. L. Hilderbrandt, S. K. Burt, R. E. Bruccoleri, L. Traynor, I. V. Pettersson, R. L. DesJarlais, G. Seibel, M. T. Marron.

Row 8 (left to right): M. M. Marsh, G. Chang, F. S. Jørgensen, J. R. Blinn, A. Jensen, C. Hutchins, R. E. Carter, S. G. Wierschke, J. Boatz, A. J. Wilkinson, W. F. van Gunsteren, N. G. Rondan, K. N. Houk, F. K. Brown, M. Saunders, K. B. Lipkowitz, M. E. Brewster, W. J. Welsh, C. J. Manly, H. R. Almond, F. H. Clarke, J. T. Blair.



Figure 3 Group photo taken at the Gordon Research Conference on Computational Chemistry, William L. Jorgensen (Yale), Chair, and John M. McKelvey (Kodak), Vice-Chair, June 18–22, 1990, Plymouth State College, Plymouth, New Hampshire.

Row 1 (left to right): A. Anderson, J. Brady, R. Venable, D. L. Severance, P. A. Kollman, K. B. Lipkowitz, N. G. J. Richards, J. M. Leonard, S. Singh, S. Vajda, G. Lamm.

Row 2 (left to right): W. J. Hehre, M. H. Whangbo, P. Bartlett, J. Wendoloski, O. Telemann, H. A. Scheraga, K. N. Houk, W. L. Jorgensen, J. M. McKelvey, P. Gund, G. Marshall, J. A. McCammon, K. Schulten, P. Wolynes, P. Bash.

Row 3 (left to right): R. Bacquet, J. Andose, R. Reddy, G. Rao, R. D. Cramer III, L. C. Allen, M. C. Zerner, H.-J. Böhm, M. Murcko, D. B. Boyd, D. Pearlman, K. Gilbert, N. G. Mirkin, V. Roberts, C. Schiffer, M. Saunders, K. B. Wiberg, K. Kim, A. Ames, P. Swaminathan, T. J. O'Donnell, K. R. Stewart.

Row 4 (left to right): M. M. Francl, P. Weiner, L. E. Chirlan, K. Miller, P. Payne, D. Janezic, P. Cruickshank, F. K. Brown, W. Schubert, A. R. Leach, D. F. DeTar, R. S. Bohacek, C. McMartin, T. R. Stouch.

Row 5 (left to right): A. Shusterman, E. Eckle, C. M. Cook, D. Schnur, V. N. Viswanadhan, J. S. Mason, A. Brunetiere, J. Anderson, D. Ricketts, R. L. DesJarlais, S. N. Rao, K. Kuczera, R. Nilakantan, P. W. Kenny, J. Blair.

Row 6 (left to right): M. Shibata, S.-Y. Liu, D. Kofke, M. Froimowitz, J. Ugolini, O. Guner, P. G. Seybold, J. Jasinski, S. Ha, J. Labanowski, C. K. Foley.

Row 7 (left to right): T. J. Zielinski, E. Oleksiowicz, W. J. Welsh, E. Mehler, A. Mark, J. P. Bowen.

Row 8 (left to right): R. C. Fort, H. R. Almond, J. Kaminski, T. Woolf, G. Chang, D. R. Henry, J. Dunbar, K. J. Miller, B. V. Cheney, I. V. Pettersson, T. Liljefors.

Row 9 (left to right): S. R. Wilson, T. Lee, J. Wade, E. P. Jaeger, C. J. Manly, R. E. Bruccoleri, G. D. Purvis, S. Evans, D. M. Gange, J. D. Madura, C. E. Peishoff, J. Gao, S. McDonald, W. C. Guida, J. W. Ponder, S. Garcia.

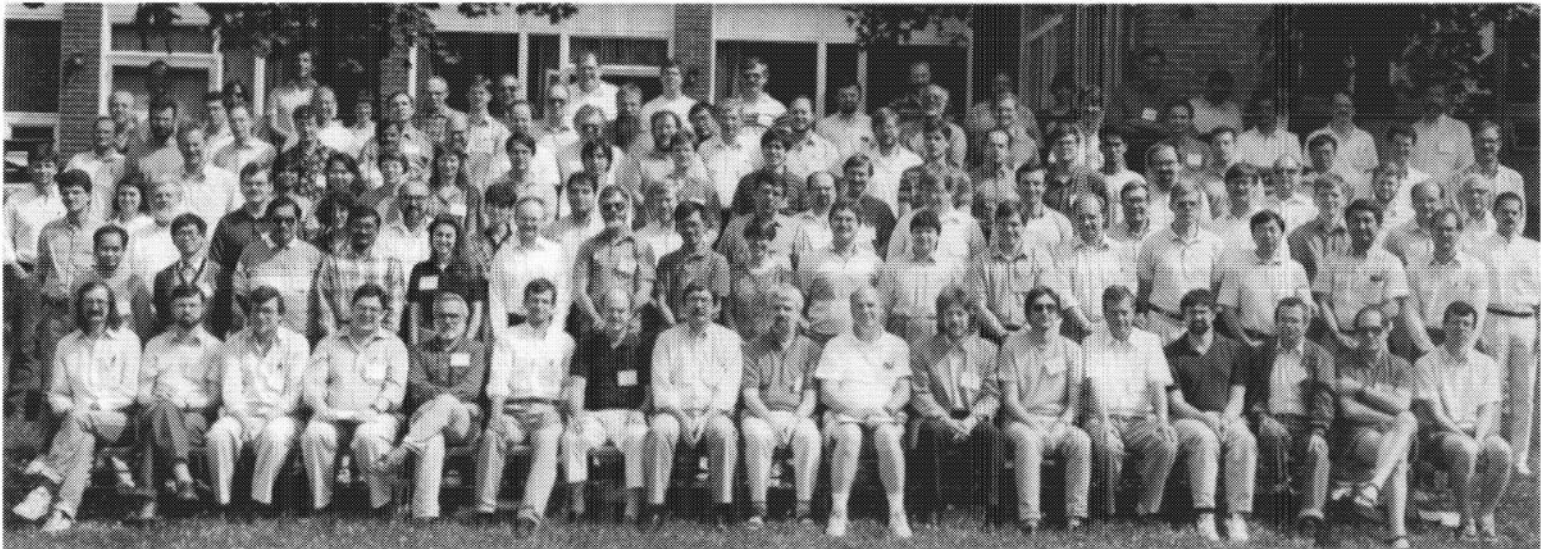


Figure 4 Group photo taken at the Gordon Research Conference on Computational Chemistry, John M. McKelvey (Kodak), Chair, and Kendall N. Houk (UCLA), Vice-Chair, June 29–July 3, 1992, New Hampton School, New Hampton, New Hampshire.

Row 1 (left to right): R. Elber, A. Becke, D. Salahub, S. Topiol, K. B. Lipkowitz, A. Brunger, K. N. Houk, J. M. McKelvey, W. Thiel, M. Teter, M. F. Guest, N. G. J. Richards, J. Weber, R. A. Friesner, A. Warshel, B. Honig, M. Field.

Row 2 (left to right): Y.-T. Wong, C. Wong, J. Seminario, S. Vijayakumar, R. Susnow, D. B. Boyd, K. E. Gilbert, N. G. Rondan, M. M. Franci, M. Murcko, J. Cicariello, K. Haug, P. Cieplak, G. Klebe, S. Miyamoto, Y. Ishikawa, B. Masek.

Row 3 (left to right): L. Carlacci, V. Smith, G. Purvis, S. Hammes-Schiffer, J. Font, M. Kontoyianni, A. Papazyan, R. L. Hilderbrandt, S. Grigoras, N. Weinberg, T. A. Halgren, D. A. Pearlman, W. Anderson, C. J. Manly, D. Hartsough, K. Koehler, I. Kolossvary.

Row 4 (left to right): J. D. Evanseck, D. Joseph-McCarthy, P. Grootenhuis, S. Das, Y.-P. Liu, J. Ugolini, K. K. Osapay, D. Gange, D. Agrafiotis, R. J. Woods, S. Smithline, K. Black, T. Simonson, B. R. Brooks, G. Barnickel, R. Felton, C. J. Cramer, D. F. DeTar.

Row 5 (left to right): P. Das, P. A. Kollman, R. D. Cramer III, S. Schroder, B. G. Rao, A. Anderson, J. Blair, J. Medrano, J. M. Leonard, J. J. P. Stewart, D. A. Smith, D. Dixon, G. Verkhivker, Y. Takaoka, J. Straub, J. Gao, J. D. Madura, P. Kowalczyk.

Row 6 (left to right): T. Ziegler, G. King, P. W. Kenny, J. Labanowski, P. King, P. Cruickshank, M. Hodoscek, Y. Lee, R. E. Carter, F. K. Brown, W. Guida, S. R. Wilson, V. C. Epa, B. Smith, J. Tesch.

Row 7 (left to right): P. Weiner, E. Zoebisch, E. Martin, A. M. Schmiedekamp, H. R. Almond, J. Kaminski, J. T. Golab, C. Foley, J. C. Culberson, A. Buda, F. Blaney, K. Moschner, M. Foucrault, T. Brinck, K. Kuczera, C. Lim.



Figure 5 Group photo taken at the Gordon Research Conference on Computational Chemistry, Kendall N. Houk (UCLA), Chair, and Thomas A. Halgren (Merck), Vice-Chair, July 4–8, 1994, New Hampton School, New Hampton, New Hampshire.

Row 1 (left to right): A. K. Rappé, K. Muller, M. Pettitt, D. G. Truhler, J. M. Blaney, W. T. Borden, E. A. Carter, K. N. Houk, T. A. Halgren, D. B. Boyd, K. B. Lipkowitz, B. O. Roos, P. Pulay, M. A. Murcko, J. Skolnick, A. G. St. Amant.

Row 2 (left to right): N. G. Mirkin, M. L. Lamb, I. Kolossvary, M. M. Mader, D. Kominos, D. I. Sverdlik, D. Joseph-McCarthy, A. L. Wressell, D. Sitkoff, M. M. Francz, A. M. Schmiedekamp, H. Nakanishi, K. Black, K. E. Gilbert, E. G. Zoebisch, C. M. Cook.

Row 3 (left to right): A. G. Anderson, K. K. Osopay, P. Hecht, S. W. Topiol, R. J. Czerminski, Y. Won, D. C. Wiser, G. E. Marlow, R. L. Hilderbrandt, D. A. Smith, A. Tropsha, A. Nayeem, R. J. Woods, T. G. Lenz, Y. S. Lee, D. A. Pearlman, R. E. Venegas, J. L. Banks, O. Zheng.

Row 4 (left to right): T. J. You, T. R. Stouch, T. E. Cheatham III, D. W. Deerfield, W. P. Anderson, J. Tirado-Rives, F. K. Brown, L. X. Dang, B. Simkin, M. McGregor, C. A. Venanzi, R. P. Dunlap, T. Zhang, D. M. Gange, X. Wang.

Row 5 (left to right): K. Kuczera, G. L. Seibel, P. A. Kollman, J. M. Leonard, P.-O. Norrby, T. Liljefors, I. V. Pettersson, B. P. Grasso, M. Schaefer, R. Le Goas, J. D. Madura, T. J. Mitchell, D. C. Chatfield, A. Caflisch, J. S. Evans, T. M. Glennon.

Row 6 (left to right): F. A. Momany, J. M. McKelvey, O. G. Wiest, D. F. DeTar, P. Svensson, A. Nicholls, A. R. Leach, B. V. Cheney, R. A. Wheeler, M. J. Mitchell, J. M. Blaney, J. H. Schnitker, S. D. Pickett, J. Shen, R. W. DeSimone, C. J. Manly.

Row 7 (left to right): D. Lu, P. A. Cruickshank, J. Gao, K. Dobbs, G. Kohler, H. R. Almond, T. A. Darden, D. M. York, J. Simpson, A. Kolinski, G. M. Verkhivker, A. E. Roitberg, J. Zhuo, B. J. Smith.

Row 8 (left to right): J. W. Essex, Y. Li, P. W. Kenny, W. C. Guida, A. J. Holder, C. K. Foley, P. D. Soper, C. J. Cramer, R. A. Kendall, L. G. Pederson, T. J. Venanzi, R. V. Stanton, C. R. Landis, D. L. Severance.



Figure 6 Group photo taken at the Gordon Research Conference on Computational Chemistry, Thomas A. Halgren (Merck), Chair, and Jeffry D. Madura (University of South Alabama), Vice-Chair, June 30–July 5, 1996, New Hampton School, New Hampton, New Hampshire.

Row 1 (left to right): D. Janezic, R. A. Friesner, T. R. Stouch, D. A. Pearlman, T. A. Darden, J. Aqvist, R. Levy, B. J. Berne, T. A. Halgren, J. D. Madura, C. J. Cramer, B. R. Brooks, D. M. York, T. Woolf, B. L. Bush, J. Tomasi, A. Lemon.

Row 2 (left to right): E. M. Duffy, I. Kolossvary, R. Susnow, M. Davis, M. A. Murcko, E. Alexov, K. E. Gilbert, D. B. Boyd, M. M. Frandl, Z. Weng, A. Pathiaseril, D. E. Bashford, N. Vaidehi, P. Subramanian, J. Banks.

Row 3 (left to right): B. D. Marten, H. J. Kim, M. Hodosek, B. Fuchs, T. Liljefors, A. J. Mulholland, P. Lyne, S. Vajda, D. Joseph-McCarthy, F. K. Brown, M. McCarrick, J. Miller, W. C. Swope.

Row 4 (left to right): T. Simonson, D. F. DeTar, M. C. Zerner, P. E. Smith, T. J. Marrone, M. L. Lamb, W. L. Jorgensen, N. G. Mirkin, I. T. Oliveira, X. J. Hou, D. Qiu, V. N. Viswanadhan, P. V. Kumar, T. E. Cheatham, F. P. Hollinger.

Row 5 (left to right): C. Ehrhardt, E. Alexov, I. V. Pettersson, S. Schroder, R. A. Wheeler, B. V. Cheney, P. Svensson, A. M. Schmiedekamp, P. W. Payne, R. J. Czerminski, M. Freindoff, T. Furlani, J. D. Evanseck, K. Kuczera, J. S. Bader, D. T. Mainz, W. P. Van Horn, A. K. Felts, X. Feng, F. Zhou.

Row 6 (left to right): R. J. Woods, D. L. Severance, A. M. Mathiowetz, W. Damm, B. Luty, W. van Gunsteren, L. Perera, M. Lindvall, T. Ewing, R. M. A. Knegtel, J. M. Briggs, G. S. Jas, T. J. Mitchell, P. W. Kenny, A. Nicholls, M. K. Gilson, J. S. Evans, C. Salter.

Row 7 (left to right): A. Wallqvist, D. Chatfield, J. M. McKelvey, S. Bogusz, J. Apostolakis, P.-O. Norrby, A. Papazyan, S. Grigoras, D. J. Willock, D. Horvath, S. Dixon, H. R. Almond, N. Ota, A. Good, J. W. Essex, C. J. Manly, B. G. Johnson, G. Fitzgerald, T. Mietzner.

Row 8 (left to right): T. Wang, D. A. Case, F. A. Momany, Y. Won, C. S. Ewig, J. W. Ponder, D. W. Deerfield, L. G. Pedersen, M. M. Kubo, F. Figueirido, A. E. Garcia, D. A. Gschwend, J. P. Bond, P. A. Kollman, G. A. Peterson, N. Gresh, M. Miller, A. Holmen.

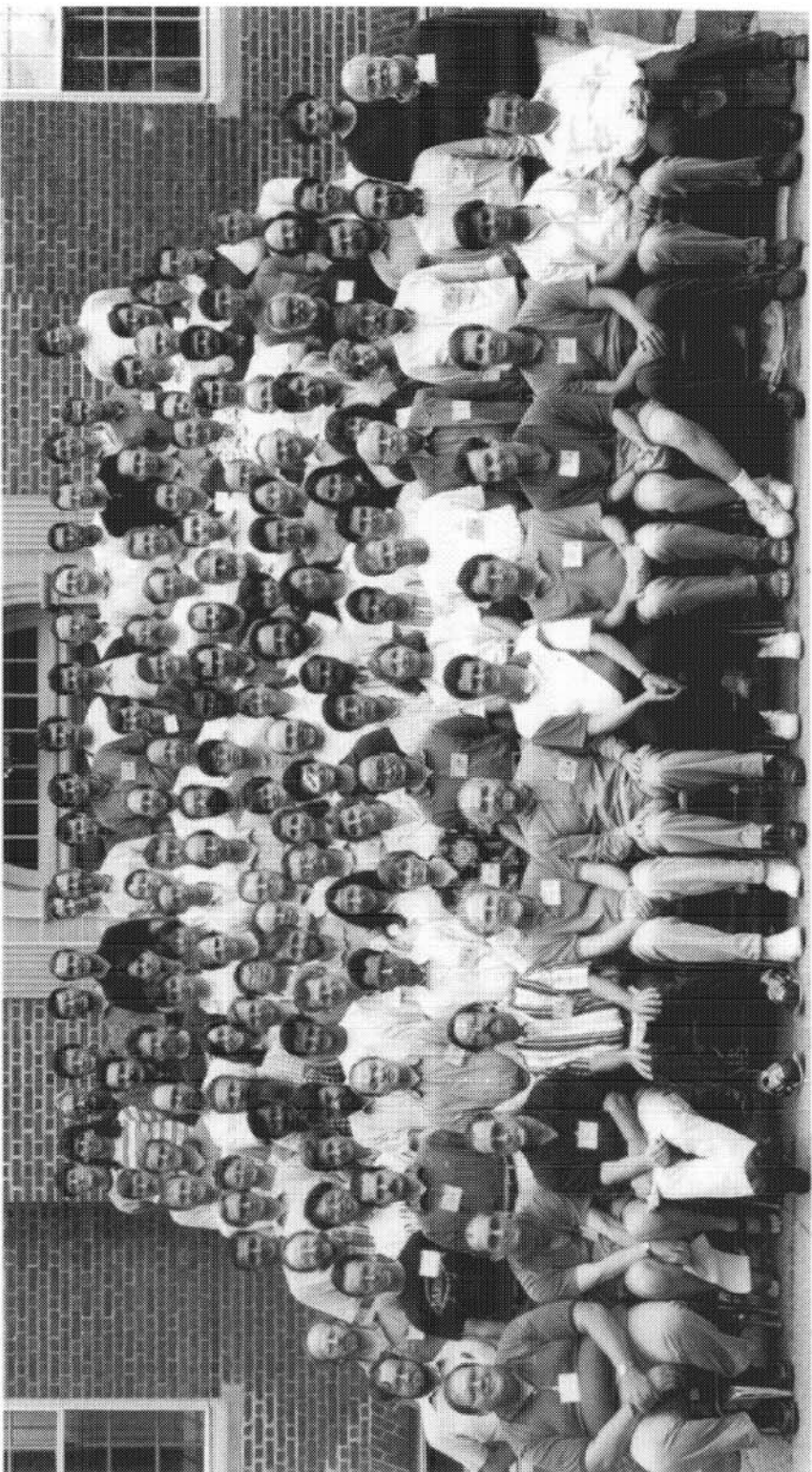


Figure 7 Group photo taken at the Gordon Research Conference on Computational Chemistry, Jeffry D. Madura (Duquesne University), Chair, and Terry R. Stouch (Bristol-Myers Squibb), Vice-Chair, June 28–July 3, 1998, Tilton School, Tilton, New Hampshire.

Row 1 (left to right): J. T. Golab, J. C. Smith, B. H. Honig, M. Pettitt, J. A. McCammon, T. R. Stouch, J. D. Madura, A. MacKerell, D. A. Pearlman, S. J. Plimpton, B. Laird, A. Warshel.

Row 2 (left to right): F. S. Sussman, D. E. Bashford, I. Kolossvary, W. Wenzel, P. Ferrara, M. S. Head, W. Yang, C. E. Peishoff, D. Spellmeyer, D. F. DeTar, J. M. McKelvey, M. Zerner, D. L. Beveridge.

Row 3 (left to right): T. A. Darden, S. Wang, G. M. Keseru, B. Wroblowski, D. Janezic, N. G. Mirkin, Y. Duan, A. Pathiaseril, D. Joseph-McCarthy, C. B. Post, E. Michonova-Alexova, A. Haymet, J. S. Evans.

Row 4 (left to right): M. E. Davis, M. C. Menziani, M. Scarsi, R. J. Czerminski, K. Kuczera, M. A. Young, B. G. Rao, A. Toy-Palmer, E. M. Duffy, J. D. Evanseck, K. R. Liedl.

Row 5 (left to right): A. Caflisch, D. Das, C. L. Simmerling, E. L. Mehler, M. O. Fenley, J. Banks, J. Tirado-Rives, S. Topiol, D. B. Boyd, K. B. Lipkowitz, T. Woolf.

Row 6 (left to right): T. Liljefors, M. Hodoscek, Y. Zhang, J. L. Nauss, A. M. Schmiedekamp, S. K. Gregurick, M. Kontoyianni, Z. Guo, W. F. Schmidt.

Row 7 (left to right): I. V. Pettersson, C. A. Wells, M. S. Stave, J. E. Carpenter, R. Luo, S. Moro, K. E. Gilbert, T. Fox, A. E. Roitberg, J. W. Pitera, L. Hemmingsen.

Row 8 (left to right): P.-O. Norrby, P. F. Stouten, P. D. Lyne, W. Weber, M. Vasquez, L. Perera, C. Williams, M. Baginski, G. D. Parks, S. Ravichandran.

Row 9 (left to right): D. B. Lawson, R. Lavery, T. Iwama, N. Gresh, P. W. Kenny, R. J. Woods, R. B. Shirts, D. C. Chatfield, B. Space, O. P. Mark, C. Alhambra.

Row 10 (left to right): D. B. Kitchen, D. Horvath, E. Gallicchio, J. Barriocanal, J. M. Briggs, R. A. Wheeler, J. M. Leonard, P. E. Smith, R. H. Winger, R. H. Smith, M. Kroeger Smith.

Row 11 (left to right): D. Philipp, E. Alexov, W. van Gunsteren, W. C. Swope, V. Z. Spassov, P. Beroza, K. J. McConnell, W. Damm, S. W. Rick, C. J. Manly.

Row 12 (left to right): W. P. van Hoorn, J. Hermans, H. Resat, C. Jenson, S. D. Bond, V. P. Sokhan, C. S. Ewig, R. V. Pappu, J. W. Ponder, B. R. Brooks.

are generally proximal horizontally, vertically, or diagonally. In several of the photographs, some the faces in the back rows are unfortunately lost in the tree shadows. A small number of attendees at the conferences did not participate in the group photographic sessions.

In any event, we present these photographs so that you can reminisce and look back at a part of your history as computational chemists.

ACKNOWLEDGMENTS

We appreciate the interest the community of computational chemists has shown in the conferences. Without their participation, lectures, poster papers, and discussions, the conferences would not have been successful. We thank the former director of the GRCs, Dr. Alexander M. Cruickshank, for guidance, and the present director, Dr. Carlyle B. Storm, for his interest in this review. The GRC office, now in West Kingston, Rhode Island, can be reached at grc@grcmail.grc.uri.edu.

APPENDIX 1: 1986 Program¹¹

* Program *

GORDON RESEARCH CONFERENCE ON COMPUTATIONAL CHEMISTRY

Donald B. Boyd and Kenny Lipkowitz, Co-Chairmen
Colby-Sawyer College (North), New London, New Hampshire
August 18–22, 1986

Monday Morning, August 18, 9:00 a.m.–noon

Donald B. Boyd (Eli Lilly and Company)
“Introductory Remarks: Scope of Computational Chemistry.”

William N. Lipscomb Jr. (Harvard University)
Session Chairman and Discussion Leader

Kendall N. Houk (University of California, Los Angeles)
“Ab Initio Transition Structures and Force Field Models for Organic Reactions.”

William L. Jorgensen (Purdue University)
“Theoretical Investigations of Organic Reactions in Solution.”

William A. Goddard III (California Institute of Technology)
“Use of Theory to Extract Mechanisms of Catalytic Reactions.”

Monday Evening Poster Session, 7:30–9:30 p.m.

Kenny Lipkowitz (Indiana University–Purdue University at Indianapolis)
Session Chairman

Robert R. Holmes (University of Massachusetts at Amherst) and Joan A. Deiters (Vassar College)

“Pathways for Nucleophilic Substitution at Silicon. A Molecular Orbital Approach.”

D. Eric Walters (Nutrasweet Company)

“Modeling and Analysis of Sterically Controlled Reactions.”

George D. Purvis (University of Florida)

“Application of Isopotential Electrostatic Potentials.”

Delos F. DeTar (Florida State University)

“New Applications of Formal Steric Enthalpy.”

William J. Welsh (University of Cincinnati) and Vivian Cody (Medical Foundation of Buffalo)

“Structural, Conformational, and Electronic Properties of Antifolate Inhibitors of Dihydrofolate Reductase.”

Gernot Frenking (SRI International, Menlo Park)

“Structure–Activity Relationships on 4-Substituted Phenyl Piperidines.”

Adel M. Naylor (California Institute of Technology)

“Molecular Modeling on Mutants of Dihydrofolate Reductase (DHFR).”

Chung F. Wong (University of Houston) and J. A. McCammon

“Enzymes and Inhibitors: Computer-Aided Design.”

Michelle M. Franc (Haverford College)

“Correction of Electrostatic Potentials for Polarization: Application to Nucleophilic Attack in Aspartyl Proteases.”

Michael McKee (Auburn University)

“Theoretical Study of the Intramolecular Proton Transfer in Lithium–Enolate Amine Complexes.”

Steve Scheiner (Southern Illinois University at Carbondale)

“Theoretical Studies of Proton Transfers.”

Suse Broyde (New York University) and Brian E. Hingerty (Oak Ridge National Laboratory)

“Energy Refined Polymer Models of DNA Modified by Polycyclic Aromatic Carcinogens.”

James R. Damewood Jr. (University of Delaware)

“Computational Studies of Molecular Recognition.”

Frank K. Brown (University of California, San Francisco), U. Chandra Singh, George L. Seibel, and Peter A. Kollman

“An Investigation of the Trypsin Reaction Mechanism and the Prediction of Stereoselectivity of Cycloadditions with QUEST, a Tandem QM-MM Method.”

David A. Case (University of California, Davis)

“Finding Stationary Points on Potential Energy Surfaces: Conformational Analyses of Heterocyclic Rings and Polypeptides.”

Stelian Grigoras (Dow Corning Corporation)

“New Si Parameters for Molecular Mechanics Obtained from Ab Initio Computations.”

Norman L. Allinger and Phillip Bowen (The University of Georgia)

“Molecular Mechanics Parameterization of Organic Phosphites.”

M. A. Bright, T. T. Fujimoto, B. A. Hohne, Charles A. Reynolds (Rohm and Haas Company), and Thomas Pierce (Rohm and Haas Company)

“Computational Chemistry on an Apollo Workstation Network.”

Richard W. Harper (Eli Lilly and Company), Nancy G. Bollinger, and David K. Herron

“Conformational Analysis of Leukotriene D4. A Methodological Study.”

John D. Goddard (University of Guelph)

“Applications of Ab Initio Quantum Chemistry to Some Organic and Inorganic Sulfur Compounds.”

Martha M. Teeter (Boston University) and M. Karplus

“The Form of the Hydrogen Bond Potential: Empirical Analysis of the Angular Dependence of the Hydrogen Bond for the High Resolution Structure of Crambin.”

Larry D. Strawser (U.S. Air Force Academy), Donn M. Storch (U.S. Air Force Academy), and J. J. P. Stewart

“Computational Studies of Enzyme Catalysis.”

Robert B. Nachbar (Merck and Company)

“MM2 Force Field Parameters for Sulfones, Sulfonamides, and Sulfonates.”

Yvonne C. Martin (Abbott Laboratories), Elizabeth B. Danaher, and David Weininger (Pomona College)

“AIMM: 3D Models from 2D MACCS Connection Tables— Use of the GENIE Target Language to Specify Rules for Structure Building.”

Paul Weiner, Rutgers (The State University of New Jersey)
“Uses of AI in Drug Design.”

Kevin E. Gilbert (Indiana University)
“Computational Chemistry and Microcomputers.”

Tuesday Morning, August 19, 9:00 a.m.–noon

J. Andrew McCammon (University of Houston)
Session Chairman and Discussion Leader

Peter Kollman (University of California at San Francisco)
“Combined Use of Computer Graphics, Molecular Mechanics,
Molecular Dynamics, and Quantum Mechanics in Studies of Complex
Molecules.”

Leland C. Allen (Princeton University)
“Transition States in NADH Hydride Transfer.”

Jay W. Ponder (Yale University)
“Computational Approaches to Protein Tertiary Structure.”

Tuesday Evening, 7:30–9:30 p.m.

Eiji Ōsawa (Hokkaido University)
Session Chairman and Discussion Leader

Norman L. Allinger (The University of Georgia)
“Recent Work in Molecular Mechanics.”

David N. J. White (The University, Glasgow)
“Molecular Modelling and Molecular Mechanics Calculations with
Personal Parallel Processors.”

Wednesday Morning, August 20, 9:00 a.m.–noon

Sidney W. Topiol (Berlex Laboratories)
Session Chairman and Discussion Leader

James J. P. Stewart (U.S. Air Force Academy)
“Molecular Orbital Calculations of Polymers.”

Daniel A. Kleier (Shell Development Company)
“Computer-Assisted Design of Agricultural Chemicals.”

John M. McKelvey (Eastman Kodak Research Laboratories)
“Studies of Excited State Valence Electronic Structures of Dyes.”

Wednesday Evening Poster Session, 7:30–9:30 p.m.

Kenny Lipkowitz (Indiana University–Purdue University at Indianapolis)
Session Chairman

Eiji Ōsawa (Hokkaido University), Dora J. Barbiric, and Jerzy M. Rudzinski
“Further Improvements on the Molecular Mechanics Calculation
of Vicinal Coupling Constants in Flexible Chain Molecules.”

T. A. Ford (University of the Witwatersrand) and G. A. Yeo
“Theoretical Predictions of the Infrared Spectra of Hydrogen-Bonded
and Charge Transfer Complexes: Ammonia and Boron Trifluoride
Dimers.”

Gunter Trummlitz (Dr. Karl Thomae GmbH)
“An Approach for the Calculation of Amine Out-of-Plane
Angles in Large Drug Molecules Using a Modified Version of MMPI.”

Dieter Cremer (Universität Köln) and Elfi Kraka (Argonne National
Laboratory)
“Barrier to Inversion at a Divalent Oxygen Atom.”

Hakan Wikstrom (The University of Georgia) and Tommy Liljefors
(Chemistry Center, Lund)
“Conformational Analysis (MMP2) of S(–)-3-PPP and Its Fit to Both
Pre- and Postsynaptic Dopamine Receptors as Agonist and Antagonist,
Respectively.”

Terry P. Lybrand (University of Houston) and J. A. McCammon
“Application of Statistical Mechanical Perturbation Theory to Compute
Relative Free Energies of Ligand–Receptor Interactions.”

R. Voets (Limburgs Universitair Centrum) and J.-P. François
“Theoretical Study of the Acid–Base Behavior of Substituted Pyridines
in the Gas Phase by Means of Semi-empirical M.O. Calculations
(MINDO/3 and MNDO).”

Walter Thiel (Universität Wuppertal)
“Correlation Effects on Semiempirical Transition Structures for
Thermal Organic Reactions.”

Ingrid Pettersson (School of Pharmacy, Copenhagen), Tommy Liljefors
(Chemistry Center, Lund), and Robert E. Carter (Chemistry Center, Lund)
“Benzene–Benzene Interactions: Molecular Mechanics Calculations.”

J. M. A. Baas, J. A. Geurtzen, B. van de Graaf (Delft University of
Technology), and M. A. Hoefnagel
“Implementation of Polarization in Molecular Mechanics.”

George P. Ford (Southern Methodist University), Christopher T. Smith,
Jennifer L. Robison, and Peter R. Andrews (Victorian College of Pharmacy,
Australia)

“Design of Transition State Analogs for Dihydroorotate. Semiempirical AM1 Molecular Orbital Calculations.”

Shashidhar N. Rao (University of California, San Francisco) and Peter A. Kollman

“Bis Intercalation by 9-Aminoacridine in the Deoxyoligomer d(GCGCGC).d(CGCGC).”

Tamara Gund (New Jersey Institute of Technology), H. Hermsmeier, R. F. Liang, J. Yadav, C. E. Spivak (National Institute of Drug Abuse), and J. A. Waters (National Institute of Arthritis, Diabetes, Digestive, and Kidney Diseases)

“Conformational and Electrostatic Approaches for Design of Receptor Agonists and Antagonists.”

Donald P. Gieschen (Chemical Abstracts Service)
“Overview of the CAS Reaction Search Service.”

Tsuneo Hirano (University of Tokyo), Akio Morita, and Hiroshi Watanabe
“Momentum Correction: A Long-Forgotten But Necessary Correction to Fill the Gap Between Theoretical and Experimental Conformational Energies.”

Robert Glen (Wellcome Research Laboratories)
“Molecular Modelling at Wellcome.”

Timothy K. Dickens (Glaxo Group Research Limited), C. K. Prout (Crystallography Laboratory, Oxford), and M. Saunders
“Rapid Interactive Graphical Display of Molecular Orbitals.”

G. Ranghino, Camillo Tosi (Istituto Guido Donegani, Novara), V. Malatesta, and N. Sacchi

“Redox Properties of Antitumor Anthracyclines as Predicted from Ab Initio Calculations and Electrochemical Experiments.”

V. N. Balaji (Allergan Pharmaceuticals), S. Profeta Jr., and S. W. Dietrich
“Molecular Modeling Studies and Conformational Energy Calculations on Dithiopeptides: Mean Geometry of the Thiopeptide Unit and Conformational Flexibility of Peptide–Thiopeptides and Dithiopeptides.”

N. C. Perry, Patricia R. Laurence (Chemical Design Limited), and E. K. Davies

“Some Graphical QM Studies on Hydrogen-Bonding in Histamine H₂ Antagonists.”

Amatz Y. Meyer (Hebrew University of Jerusalem)
“Geometrical Attributes of Molecules—Mensuration and Exploitation.”

A. R. Srinivasan (Rutgers, The State University of New Jersey) and W. K. Olson

"Nucleic Acid Model Building: Multiple Conformations of *E. coli trp* Operator DNA."

N. C. J. Stutchbury (Imperial Chemical Industries PLC)

"Use of Computer Graphics in the Display of Low Energy Conformations of Flexible Molecules."

Ch. van der Brempt, D. P. Vercauteran (Université Notre Dame de la Paix, Namur), G. Evrard, and F. Durant

"Use of X-Ray Diffraction, Molecular Modeling, Molecular and Quantum Mechanics in Comparative Study of MAO-A Enzyme Inhibitors."

Joseph W. Lauher (State University of New York, Stony Brook)

"Molecular Mechanics Simulations of Ligand Structures in Transition Metal Carbonyl Clusters. ROTOCHEM— A Molecular Graphics Program."

Lisa Chirlian (Princeton University)

"Calculation of Net Atomic Charges from Ab Initio Molecular Electrostatic Potentials."

Thursday Morning, August 21, 9:00 a.m.–noon

Martin Gall (The Upjohn Company)

Session Chairman and Discussion Leader

Clifford E. Dykstra (University of Illinois, Urbana–Champaign)

"Hydrogen Bonding Interactions. Computational Studies from the Most Detailed Level Up."

David G. Watson (Crystallographic Data Centre, Cambridge)

"A Revision of Sutton's Tables of Interatomic Distances: The Cambridge Structural Database."

A. Peter Johnson (Leeds University)

"Expert Systems and Smart Databases as Aids to Organic Synthesis Planning."

Thursday Dinner: New England Banquet

Thursday Evening, 7:30–9:30 p.m.

Tommy Liljefors (University of Lund)

Session Chairman and Discussion Leader

Robert Langridge (University of California at San Francisco)

“Molecular Graphics: Computer-Assisted Insight and Reasoning in Three Dimensions.”

Michael Connolly (Biohedron, Del Mar, California)

“Molecular Graphics, Volume and Shape.”

Friday Morning, August 22, 9:00 a.m.–noon

Erich Wimmer (Cray Research)

Session Chairman and Discussion Leader

Neil S. Ostlund (University of Waterloo)

“Parallel Architectures and Algorithms for Computational Chemistry.”

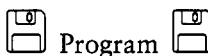
Bernard R. Brooks (National Institutes of Health)

“GEMM (Generate, Emulate, and Manipulate Macromolecules) on the Star Technologies ST-100: Interactive Energy Determination and Molecular Simulations—Methods and Applications.”

Hiroshi Kashiwagi (Institute of Molecular Structure, Okazaki)

“New Supercomputer System, Quantum Chemistry Database, and Some Calculations on Metal Complexes.”

APPENDIX 2: 1988 Program¹¹



GORDON RESEARCH CONFERENCE on Computational Chemistry

Donald B. Boyd and Peter Kollman, Co-Chairmen
Boyd Hall, Plymouth State College, Plymouth, New Hampshire
July 4–8, 1988

July 4, 1988, Monday Morning, 9:00 a.m.–12:20 p.m.

Donald B. Boyd (Eli Lilly and Company) and Peter Kollman (University of California, San Francisco)

“Introductory Remarks.”

John J. Wendeloski (DuPont)

Session Chairman and Discussion Leader

“Macromolecular Simulations.”

Axel T. Brunger (Yale University)

“Computational Tools for Structural Biology.”

Terry R. Stouch (Naval Research Laboratory)

“Molecular Dynamics Simulations of Simple Lipid Systems.”

Wilfred F. van Gunsteren (University of Groningen)

“On Comparing Computer Simulations of Macromolecules with Experimental Data.”

Monday Evening Poster Session, 7:30 p.m.–9:30 p.m.

Jeffry D. Madura (University of Houston), B. Montgomery Pettitt, and J. Andrew McCammon

“Determination of Transition State Geometries and Relative Free Energies of Activation in Condensed Phase.”

James R. Damewood Jr. (University of Delaware) and Wolfgang C. F. Muehlbauer

“Calculation of Intermolecular Potential Energy Surfaces Using Modified Molecular Mechanics Techniques.”

Lee F. Kuyper (Burroughs Wellcome Company), Kenneth M. Merz Jr. (University of California, San Francisco), and Peter A. Kollman

“Relative Solvation Free Energies of Benzene, Anisole, and 1,2,3-Tdimethoxybenzene: Theoretical and Experimental Analysis.”

Salvatore Profeta Jr. (Glaxo Inc., Research Triangle Park) and V. N. Balaji (Allergan)

“Conformational Energy Mapping Using MM2: Utility and Validity of Variable Energy Convergence Criteria with Applications to 2-D Energy Maps for Peptides and Drug Molecules.”

Jerry A. Boatz (North Dakota State University) and Mark S. Gordon
“Decomposition of Normal Coordinate Vibrational Frequencies.”

Mark S. Gordon (North Dakota State University), Kiet Nguyen, Larry P. Davis (Air Force Office of Scientific Research), Larry W. Burggraf, and Krishnan Raghavachari (AT&T Bell Laboratories)

“Theoretical Analysis of the Reaction $\text{Si}^+ + \text{SiH}_3\text{CH}_3$.”

Kim K. Baldridge (North Dakota State University) and Mark S. Gordon
“Illustration of Electronic Structure–Dynamics Interface.”

Krzysztof Kuczera (Harvard University), John Kuriyan, and Martin Karplus
“Molecular Dynamics of Myoglobin.”

J. Phillip Bowen (University of North Carolina at Chapel Hill), Vikram Reddy (Center for Disease Control), Donald G. Patterson, Jr., and Norman L. Allinger (University of Georgia)

“Molecular Mechanics Treatment of Halogenated Dibenzo-*p*-dioxins and Dibenzofurans: MM2 Parameters for Aromatic Halides, Divinyl Ethers, and Related Compounds.”

Kerwin D. Dobbs (University of Texas at Austin), James E. Boggs, and Alan H. Cowley

“New, Unsaturated Three- and Four-Membered Rings: Formal Addition of CH₂, SiH₂, GeH₂, or SnH₂ to Phospha-alkyne Triple Bonds.”

Donald B. Boyd (Eli Lilly and Company), David W. Smith, James J. P. Stewart (U.S. Air Force Academy), and Erich Wimmer (Cray Research)

“Importance of Criteria for Self-Consistent Field Convergence and Geometry Optimization in AM1, MNDO, and MINDO/3 Molecular Orbital Calculations.”

William J. Welsh (University of Missouri, St. Louis), Eric Towler, and Mary Dudley

“Computational Chemistry Studies of Antifolate Drugs for Treatment of *Pneumocystis carinii* Pneumonia (PCP) in AIDS Patients: Trimetrexate and Analogues.”

John T. Blair (Rutgers University), Karsten Krogh-Jespersen, and Ronald M. Levy

“Solute–Solvent Interactions in Ground and Excited Electronic States.”

George Chang (Columbia University), Wayne C. Guida (Ciba-Geigy), and W. C. Still (Columbia University)

“Examination of Monte Carlo Approaches for Analysis of Conformational Space.”

Donald Bashford (Harvard University), C. Chothia (MRC Laboratory of Molecular Biology, Cambridge), and A. M. Lesk

“The Use of Sequence Templates to Investigate the Determinants of Protein Folds.”

Kyoko Watanabe (University of Pennsylvania) and Michael L. Klein

“Molecular Dynamics Study of a Sodium Octanoate Micelle in Aqueous Solution.”

Robert E. Brucolieri (Massachusetts General Hospital), Jiri Novotny, and Edgar Haber

“Prediction of Polypeptide Segments Using Conformational Search.”

Michael McKee (Auburn University)

“Ab Initio Calculations on the Boron Hydrides Through B₉H₁₅.”

Michelle M. Franci (Bryn Mawr College) and Yuh-Min Chook

“*cis*–*trans* Isomerization of Alkenyl Aluminum Complexes.”

Janet Cicariello (Rutgers University) and Wilma K. Olson

"Theoretical Analysis of the Long-Range Electrostatic Potential of Supercoiled DNA."

Mark A. Murcko (Merck Sharp and Dohme, West Point)

"Using Ab Initio Calculations to Develop Molecular Mechanics Parameters for Use in Biological Simulations."

Mark Froimowitz (McLean Hospital) and Ahammadunny P. A.

"Conformational Free Energies of Cyclic Enkephalin Analogs."

Donna A. Bassolino (Rutgers University), Douglas B. Kitchen, Dorothea Kominos, Arthur Pardi, and Ronald M. Levy

"New Methods for the Refinement of Protein Structures

Generated from Solution NMR Data: Application to Rabbit Neutrophil Polypeptide (NP-5)."

Byungkook Lee (National Institutes of Health)

"Thermodynamics of Solvent Reorganization Upon Dissolution of Hydrocarbon Solutes in Aqueous and Hydrocarbon Solvents."

Daniel A. Kleier (DuPont)

"The Role of Electronic Structure Calculations in Optimizing the Activity of a New Class of Photosystem I Herbicides."

Peter D. J. Grootenhuis (Organon) and Peter A. Kollman (University of California, San Francisco)

"Free Energy Calculations on Molecular Host-Guest Complexes."

Marcus E. Brewster (Pharmatec), James J. Kaminski (University of Florida, College of Pharmacy), and Nicholas Bodor

"Hydride Transfer Between 1-Methyl-1,4-dihydronicotinamide and the 1-Methylnicotinamide Cation, a Theoretical Study."

T. J. O'Donnell (National Center for Supercomputing Applications) and John S. Garavelli (University of Illinois at Chicago)

"A Proposal for a Standard Format for Molecular Description Files."

James J. P. Stewart (U.S. Air Force Academy)

"Re-Optimization of Parameters for MNDO."

John McKelvey (Eastman Kodak, Rochester)

"Quick-Pi: A Generalized Omega Method."

July 5, 1988, Tuesday Morning, 9:00 a.m.-12:05 p.m.

Norman L. Allinger (University of Georgia)

Session Chairman and Discussion Leader

"Molecular Mechanics."

Tommy Liljefors (University of Lund)

“Molecular Mechanics in Structure–Activity Studies.”

W. Clark Still (Columbia University)

“Modeling of Molecular Complexes.”

Thomas A. Halgren (Merck Sharp and Dohme, Rahway)

“On the Representation of Angle Bending Potentials in Empirical Force Fields.”

Tuesday Evening, 7:30 p.m.–9:20 p.m.

Yoshikazu Oka (Takeda Chemical Industries)

Session Chairman and Discussion Leader

“Molecular Modeling in the Chemical and Pharmaceutical Industries of Japan.”

Klaus Müller (Hoffmann-LaRoche, Basel)

“Combined Use of Computer Modeling and Structural Databases in Chemical Research.”

Robert S. Pearlman (University of Texas, College of Pharmacy)

“Rapid Generation of High Quality Approximate 3D Molecular Structures.”

July 6, 1988, Wednesday Morning, 9:00 a.m.–12:05 p.m.

William L. Jorgensen (Purdue University)

Session Chairman and Discussion Leader

“Macromolecular Simulations.”

Nobuhiro Gō (Kyoto University)

“Simulation of Conformational Dynamics of Proteins: Harmonic and Anharmonic Aspects.”

Shoshana J. Wodak (Université Libre de Bruxelles)

“Contributions from Electronic Polarizability to Electrostatic Interactions in Proteins.”

Stephen H. Bryant (Brookhaven National Laboratory)

“Energy Functions from the Database of Known Protein Structures?”

Wednesday Evening Poster Session, 7:30 p.m.–9:30 p.m.

Volker Buss (Universität Duisburg) and Peter Faupel

“Evidence for, and Proposed Structure of, a New Folded Conformation of Methotrexate.”

Keerthi Jayasuriya (Picatinny Arsenal) and Sury Iyer

“A Computational Analysis of Ortho-lithiation Reaction Mechanism.”

Gerhard Barnickel (E. Merck, Darmstadt)

“Conversion Tools for Connection Between Different Force-Field Programs Using CPECM.”

Francesc Manaut (Institut Municipal d’Investigacio Medica, Barcelona), J. Jose, and F. Sanz

“Automatic Search of Maximum Similarity Between Molecular Electrostatic Potential Distributions.”

Nick C. Perry (Chemical Design Ltd., Oxford)

“A Multivariate QSAR Study on Histamine H₂ Antagonist Activity Using Structural Parameters Determined by Molecular Modelling.”

Scott G. Wierschke (Wright-Patterson Air Force Base)

“A Computational Study of the Tensile and Compressive Properties of Ordered Polymers Via the Austin Model 1 (AM1) Semiempirical Molecular Orbital Method.”

Jorge A. Medrano (Buenos Aires University), Roberto C. Bochicchio, and Hector F. Reale

“On the Extension of the Quantum Theory of Valence and Bonding to Periodic Systems.”

Ingrid Pettersson (Royal Danish School of Pharmacy), Tommy Liljefors (University of Lund), and Klaus Bøgesø (Lundbeck A/S, Denmark)

“Conformational Analysis of Some D-1 Dopamine Receptor Agonists and Antagonists.”

Flemming Steen Jørgensen (Royal Danish School of Pharmacy)

“Muscarinic Agonists—Towards a Common Pharmacophore Model for Enantiomers with Very Different Biological Potency.”

Carol A. Venanzi (New Jersey Institute of Technology) and Krishnan Namboodiri (Naval Research Laboratory)

“Structure–Function Relationships in Artificial Enzymes.”

Thomas J. Venanzi (College of New Rochelle) and Carol A. Venanzi (New Jersey Institute of Technology)

“Electrostatic Potential Patterns of Amiloride Analogs.”

M. Katharine Holloway (Merck Sharp and Dohme, West Point), Kenneth M. Merz (University of California, San Francisco), and Charles H. Reynolds (Rohm and Haas)

“A Theoretical Study of the Azophenine Potential Surface.”

Sandor Vajda (Mount Sinai School of Medicine), Istvan P. Sugar, and C. DeLisi

“Combinatorial Optimization Methods for Predicting the Backbone Structure in Polypeptides.”

Robin J. Breckenridge (Sandoz, Basel) and Hans-Peter Weber

“Tertiary Conformation of Marine Snail α -Conotoxin: Strategy for Conformational Searching Using Molecular Dynamics.”

Stephen R. Wilson (New York University), Jules W. Moskowitz, Kevin E. Schmidt, and Weili Cui

“Applications of Simulated Annealing to the Conformational Analysis of Flexible Molecules.”

Renée L. DesJarlais (University of California, San Francisco), Brian Shoichet, Dale Bodian, George L. Seibel, and Irwin D. Kuntz Jr.

“A Second-Generation Computer-Assisted Inhibitor Design Method.”

Martin Head-Gordon (Carnegie-Mellon University) and John A. Pople

“A New Method for Two-Electron Integral Evaluation.”

Kevin E. Gilbert (Indiana University, Bloomington), J. J. Gajewski, and T. W. Kreek

“Molecular Mechanics and Transition Metal Complexes.”

Alan H. Katz (Wyeth-Ayerst)

“An On-Line System to Guide the Chemist in Using Computational Chemistry Software.”

DeLos F. DeTar (Florida State University)

“Toward Standards for Force Field Representation.”

Paul Weiner (Alliant), Roberto Gomberts, and Nick Camp

“Parallel Processing in Computational Chemistry.”

Regine Snay Bohacek (Ciba-Geigy) and Robert Jernigan (National Institutes of Health)

“Configurational Statistics of Methyl Vinyl Ether–Maleic Anhydride Copolymer.”

Frank H. Clarke (Ciba-Geigy)

“Partition Coefficients of Ions: Determination of Distribution Profiles.”

M. Rami Reddy (University of North Carolina at Chapel Hill) and Max Berkowitz

“Hydration Forces Between Parallel DNA Double Helices: Computer Simulations.”

T. A. Halgren (Merck Sharp and Dohme, Rahway) and B. L. Bush

“The Use of Enzyme Site Maps in Designing Enzyme Inhibitors.”

Richard D. Cramer III (Tripos Associates), David E. Patterson, and Jeffrey D. Bunce

“Comparative Molecular Field Analysis (CoMFA).”

July 7, 1988, Thursday Morning, 9:00 a.m.–12:05 p.m.

Werner Braun (Eidgenössische Technische Hochschule, Zürich)

Session Chairman and Discussion Leader

“Distance Geometry.”

Irwin D. Kuntz Jr. (University of California, San Francisco)

“Use of Distance Geometry for Structural Analysis.”

Jeffrey M. Blaney (DuPont)

“Distance Geometry Approach to Ligand–Macromolecule Docking.”

J. Scott Dixon (Smith Kline and French)

“Ligand Design Methodology.”

Thursday Dinner: New England Buffet

Thursday Evening, 7:30 p.m.–9:20 p.m.

Kendall N. Houk (National Science Foundation)

Session Chairman and Discussion Leader

“Transition Structures of Pericyclic Reactions.”

Michael J. S. Dewar (University of Texas)

“Use of Quantum Mechanical Models for Studies of Reaction Mechanisms.”

John A. Pople (Carnegie-Mellon University)

“General Theory of Molecular Energies.”

July 8, 1988, Friday Morning, 8:50 a.m.–11:45 a.m.

Stelian Grigoras (Dow Corning)

Session Chairman and Discussion Leader

“Polymer Conformation in Liquid and Solid State.”

Michael C. Zerner (University of Florida)

“Quantum Chemical Studies on the Structure and Spectroscopy of Large Transition Metal Systems.”

Joseph W. Lauher (State University of New York, Stony Brook)

“Molecular Modeling in Organometallic Chemistry.”

Jeremy K. Burdett (University of Chicago)

“Theoretical Studies of Solids.”

REFERENCES

1. One reason the talks at GRCs are substantial is that the speakers know they will be extensively questioned during the discussion period following each talk. In contrast, the talks at large national society meetings too often are “hollow,” i.e., they consist of an introduction and some results and conclusions, but disclose little about how the work was done. Such talks circumvent the old rule of publication: there should be sufficient disclosure that other scientists could reproduce and confirm the work. In any case, the audiences at GRCs have a better chance of hearing the full story on a piece of work.
2. The meeting rooms at the conference sites are not like the vast, noisy, flat-floored hotel ballrooms typically used at large national and international meetings.
3. D. B. Boyd, *Chair's Notebook and Guidelines*, October 1995. (This massive assemblage of documentation was collected as an aid to T. A. Halgren and future chairmen of the Gordon Research Conference on Computational Chemistry. The documentation included prior conference programs, registration lists, evaluation forms, correspondence, and GRC guidelines for chairpersons. The notebook was intended to be passed from chair to chair upon completion of service.) Since January 1998, information about the conferences has been available on the World Wide Web at <http://chem.iupui.edu/rcc/grccc.html>.
4. J. D. Bolcer and R. B. Hermann, in *Reviews in Computational Chemistry*, K. B. Lipkowitz and D. B. Boyd, Eds., VCH Publishers, New York, 1994, Vol. 5, pp. 1–63. The Development of Computational Chemistry in the United States.
5. D. B. Boyd, Abstracts of the 183rd National Meeting of the American Chemical Society, Las Vegas, Nevada, March 28–April 2, 1982. Computational Chemistry in the Design of Biologically Active Molecules at Lilly.
6. K. B. Lipkowitz and D. B. Boyd, Eds., *Reviews in Computational Chemistry*, Wiley-VCH, New York, 1998, Vol. 12, pp. v–xiii. Preface.
7. These other meetings did not aim at the same broad scope and purpose as envisioned for our GRC on Computational Chemistry.
8. K. B. Lipkowitz and D. B. Boyd, Eds., *Reviews in Computational Chemistry*, VCH Publishers, New York, 1990, Vol. 1, pp. vii–xii. Preface.
9. The GRC office, based on its many years of running hundreds of conferences, has found that a small number of long talks with ample discussion is much preferred by participants to having a larger number of short talks. Dedicated poster sessions are also preferred.
10. Like much of the rest of the American workforce, computational chemists are increasingly experiencing multiple job changes during their professional careers.
11. The program listed here is a facsimile of the original one prepared for the conference. The program does not have last minute additions, withdrawals, or substitutions. For the poster presentations, affiliations and first names are listed for the presenter(s); such information for coauthors are listed if it was supplied with the original poster abstract.

APPENDIX

Published Force Field Parameters for Molecular Mechanics, Molecular Dynamics, and Monte Carlo Simulations

Mehran Jalaie and Kenny B. Lipkowitz

Department of Chemistry, Indiana University-Purdue University at Indianapolis, 402 North Blackford Street, Indianapolis, Indiana 46202-3274

INTRODUCTION

A large number of empirical force fields (EFFs) have been developed for use in molecular mechanics calculations as well as for simulations by molecular dynamics and Monte Carlo methods. Each force field has a more or less unique set of parameters for use with those potential energy functions. The potential energy functions together with the parameters determine how well the conformational energies and geometrical changes can be modeled by calculation. Whereas for a given EFF the potential functions remain unchanged from molecule to molecule, the selection of parameters do not. Their selection depends on the atom types and topology of the molecule being studied. The number of atom types and possible combinations is vast, so only a small fraction of possible combinations has been parameterized. Because of this, a commonly asked question among molecular modelers is “Do you have parameters for . . . ?”

Reviews in Computational Chemistry, Volume 14
Kenny B. Lipkowitz and Donald B. Boyd, Editors
Wiley-VCH, John Wiley and Sons, Inc., New York, © 2000

Many molecular modeling programs contain parameters published in the literature. The user of these programs is advised to go back to the original papers to see precisely what molecules were used in the parameterization data set. This point is crucial. The quality of your computed result depends, in part, on the quality of the parameters used. It is common to find EFF parameters developed for a very narrow range of structural types, whereas the modeling program may allow unrestricted application of the parameters to all types of molecule containing that functional group. It is easy to transgress the boundary between legitimate and illegitimate transferability of parameters because of this.

In the literature, one finds a bimodal distribution of parameter quality. On the one hand is the force field developer who makes monumental efforts to minimize the error between computed and experimental molecular properties. Parameterizations often involve fits to physical data such as molecular structure (bond lengths and bond angles), vibrational data, and heats of formation. Sometimes fittings also include molecular dipole moments, heats of sublimation, or rotational barriers from nuclear magnetic resonance or other spectroscopic measurements. Well-tested, high quality parameters are the result. Some of the better force fields were compared by Pettersson and Liljefors in Volume 9 of this series.¹

On the other end of the spectrum is the occasional molecular mechanics user who needs to compute a molecular structure quickly. If the requisite parameters are missing, it is common to approximate or guess a set by extrapolation or by assuming analogy to existing parameters. In contrast to the type of EFF developer described in the previous paragraph, the ad hoc user may work with a small set of experimental data for a few molecules, or perhaps only one, pulled from the Cambridge Structural Database or other source, thus allowing the parameterization to be less general than desired by most users. Many of the ad hoc parameterizations are fitted only to molecular structure. Use of these parameters for computing, say, vibrational frequencies may produce misleading results.

Some authors who published parameters also report caveats and potential hazards regarding their use. As a user, you should be aware of these issues. But because many molecular mechanics and molecular simulation programs do not describe where their parameters come from, this may not be possible.

We have been trying to keep track of published parameters for EFFs. To help you track down needed parameters, we list in this appendix the references we found. We include many of the commonly used force fields. They are arranged alphabetically. For each force field, we list the functional groups or atoms that have been parameterized. The notation is explained in the original papers, but some of the acronyms we use include FF (empirical force fields), OOP (out-of-plane bending), LP (lone pair), and vdW (van der Waals); the symbol “...” indicates nonbonded interactions. For each entry, there is one or more associated citations. Those citations are gathered after the table in alphabetical order by first author of the citation.

This appendix is an updated, expanded version of one published in Volume 6 of this book series.² We have deleted from that earlier appendix entries related to force fields that are no longer widely used; for example, MMI or those that have been abandoned by their original authors in favor of improved force fields. We have added entries for new force fields that are being marketed and/or appear to be in use by more than a single research group. Note that some entries are listed under a single name like AMBER. This is technically incorrect because the suite of modeling programs is called AMBER, but the functional form of the force field (and the associated parameter set) has changed over time and therefore should be called something else like the “Weiner force field” or the “Cornell force field,” depending on which is being used. But, with our apologies to the Kollman group and others whom we may unintentionally offend, we retain the name AMBER for the sake of simplicity, and let the reader determine which version of a force field was used.

Keeping track of force fields from the literature is problematic. Consider, for example, the Discover force fields: CVFF, CFFxx, and PCFF. Hagler, a main developer of these force fields, worked with Lifson, as did Rasmussen, Warshel, Karplus, and others who propagated their own programs. As Hagler pursued independent development of Lifson’s program, he developed a force field for organics called CVFF for use in the Discover molecular dynamics program. In the 1980s, BIOSYM, the company then marketing Discover, saw the need for more accurate and transferable parameters based on a combination of ab initio quantum data and experimental data. Fruits of this vision began to appear in the BIOSYM programs with the CFF91 force field, which has almost completely different functional forms from CVFF. Over time there were CFF93 and CFF95 updates and an offshoot called PCFF (which is not listed here separately). Some of the programs and parameter sets associated with academic CHARMM and commercial CHARMM are also a bit confusing, especially when there seem to be so many parameter sets being used by so many different groups. Again, rather than distinguish among force fields developed by Karplus, B. R. Brooks, Polygen (now part of Molecular Simulations Inc.), and others, we simply group the published parameters under the single moniker CHARMM.

This listing is by no means complete. Intentionally omitted from this compilation are the many papers from groups who presented quantum mechanically derived atomic charges for a molecule under study and called that a force field parameterization in the experimental section of their paper. Missing too are many publications in the literature from journals we do not read. We apologize for such omissions but confess that we cannot keep track of everything published. Nonetheless, this list will be of value to many readers of this book series. If you are aware of published parameters that are not included in the table, please forward them to the senior author. Likewise, if you find an error or an inappropriate entry, forward that information too, to ensure that the error is rectified.

SOURCES OF FORCE FIELD PARAMETERS

AMBER

Alcohol, amine, ether, sulfide, thiol
(Lennard-Jones parameters)

Kubo 1997

Alkanes

Derreumaux 1993a,c

Alkanes under high pressure (united-atom)

Koike 1998

All-atom FF for proteins/nucleic acids
Weiner 1986

All-atom FF for proteins, nucleic acids, organics using RESP charges
Cornell 1995

Aromatic methoxy group (for use in calixarenes)

Botta 1997

Ar—O—R arylalkyl ethers
Spellmeyer 1990

Ascorbic acid

Ventura 1995

Au . . . S and related parameters for cyclodextrin derivatives on Au(111)

Quian 1997

Benzene, methane, water nonbonded parameters

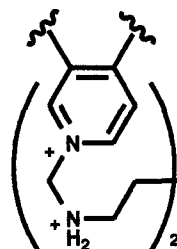
Chipot 1996a

[1,4]-Benzodiazepines
Moyna 1997

Biphenyls

Lombardy 1996

Bis-intercalators



de Pascual-Teresa 1996

Calixarenes

Grootenhuis 1990

Calixarenes

van Hoorn 1997

Camptothecin derivatives

Fan 1998

Carboranyl nucleotides (carboranes)

Fulcrand-El Kattan 1994
C• (carbon radical in glycine)
Barone 1997

C . . . O nonbonded parameters
Marrone 1995

CH₃CH₃ (ethane)

Pearlman 1994

CH₃CO₂⁻, CH₃CH₂NH₃⁺, H₂O
(POL3)

Meng 1994

Chloroform

Eksterowicz 1997

Chloroform (flexible potential)
Wang 1998

—C≡N

Hill 1991a

CO—CO—N

Pranata 1991

CONH (peptide)

Nuss 1979

CONH (amide), Lennard-Jones parameters
Cieplak 1991

$\text{CONH}-\text{C}_{\text{sp}^3}-\text{NHCO}$,
 $\text{NHCO}-\text{C}_{\text{sp}^3}-\text{CONH}$,
 retro-amide residues

Alemán 1995

$\text{Cu}-\text{N}$ (His), $\text{Cu}-\text{S}$ (Cys, Met)
 Moore 1991

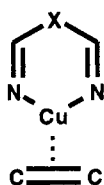
Crown ether, nitriles, nitro group
 Grootenhuis 1989b

Crown ether . . . Na^+
 Hase 1989

Crown ether, $\text{UO}_2^{2+}/\text{NO}_3^-$ complex
 Guilbaud 1993

Cryptophane ($\text{CA}-\text{OS}-\text{CT}$,
 $\text{O}-\text{C}-\text{OH}$, etc.)
 Kirchhoff 1996

$\text{Cu}^+ \cdots$ olefin and other complexes



Hæffner 1997
 $\text{CT}, \text{C}, \text{HC}, \text{HA}$ (sp^3 and sp^2 carbons;
 aliphatic and aromatic
 hydrogen) nonbonded
 parameters

Cornell 1993

$\text{C}, \text{CT}, \text{HC}$ vdW parameters for
 camphor . . . cytochrome
 Harris 1995

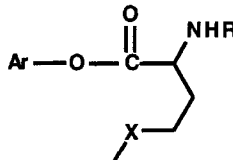
$\text{C}-\text{CA}-\text{CT}, \text{C}-\text{CA}-\text{OS},$
 $\text{CA}-\text{CT}-\text{NT}, \text{N3}-\text{CT}-\text{OS},$
 $\text{NT}-\text{CT}-\text{OH}$
 (naphthyridinomycin)

Hill 1991b

$\text{C}-\text{N}-\text{CT}-\text{C}, \text{N}-\text{CT}-\text{C}-\text{N},$
 $\text{CT}-\text{CT}-\text{N}-\text{C}$, and
 $\text{CT}-\text{CT}-\text{C}-\text{N}$ for additive,
 nonadditive, and polarizable
 force fields

Cornell 1997

$\text{C}-\text{OE}, \text{CT}-\text{OE}, \text{O}-\text{C}-\text{OE}$, etc.
 for $\text{R} = \text{CHO}, \text{COCH}_3$;
 $\text{X} = \text{CH}_2, \text{S}$



Fox 1997

Dehydroamino acid, peptide
 Alagona 1991

Dimethyl sulfoxide (DMSO)
 (polarizable potential)
 Kurinkova 1998

Dimethyl sulfoxide (DMSO)
 Fox 1998

1,3-Dioxanes
 Howard 1995

DNA (O^6 -alkylguanine)
 Sayle 1997

Fe-S clusters, bending constants for
 $\text{S}^*-\text{Fe}-\text{S}, \text{S}^*-\text{Fe}-\text{S}^*, \text{Fe}-$
 $\text{S}^*-\text{Fe}, \text{C}-\text{S}-\text{Fe}$, LP-S-Fe,
 LP-S-C (S = cysteine sulfur,
 S^* = inorganic sulfur)

Banci 1992

Ferryl heme unit, valproic acid
 Collins 1991

$\text{Fe}^{3+} \cdots \text{N}, \text{O}$ (transferrin)
 Lin 1994

$\text{Fe}^{3+} \cdots \text{O}$
 Fidelis 1990

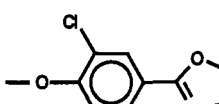
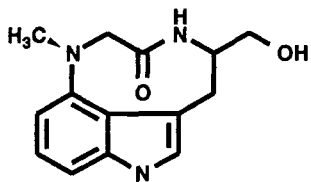
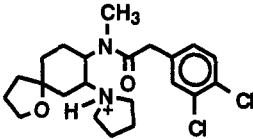
$\text{Gd}^+ \cdots \text{N}$
 Fosseim 1991

Glycine (intramolecular proton
 transfer in water)

Okuyama-Yoshida 1998

Guanosine triphosphate and imido/
 methylene analogs

Cannon 1994

H-bond	Methane, ethane, methanol, benzene, acetate, methylammonium, H ₂ O (SPC/E), H ₂ O (POL3) nonbonded parameters
Vedani, 1985, Damewood 1990, Ferguson 1991	
Heme group (porphyrin)	Meng 1996b
Jewsbury 1994	Mg ²⁺ , Ca ²⁺ , Sr ²⁺ , Lennard-Jones parameters
Heterocycles	Bartolotti 1991
	NAD ⁺ (nicotinamide moiety) de Kok 1998
	NH ₃ , NH ₂ CH ₃ , N(CH ₃) ₃ H ₂ O (POL3) nonbonded parameters
	Meng 1996a
	N—C—N, N—CT—N, N—CT—CA, CHCl ₃
Wade 1992	Fox 1996
Hydrazines (diacyl)	Na ⁺ , K ⁺ , Li ⁺ , Rb ⁺ , and Cs ⁺ interacting with oxygen
Chakravorty 1998	Wipff 1982, Kollman 1985, Wipff 1985, Grootenhuis 1989a
Hydrogen parameters	Nucleic acids
Veenstra 1992	Weiner 1984
Hydroxylamine glycoside linkage (DISCOVER)	O—C—O bending for sugars
Walker 1994	Sakurai 1997
Indolactam	O—C—S, C—O—C—S, O—C— S—C, O—C—C—S, S vdwW parameter (for use in thio-substituted nucleosides)
	Veal 1995
Kawai 1992	1-Octanol, SPC water
Li ⁺ , Na ⁺ , K ⁺ , Rb ⁺ , Cs ⁺ nonbonded parameters	DeBolt 1995
Ross 1994	Oligosaccharides
LP (lone pairs for Cornell FF)	Homans 1990
Dixon 1997	Oligosaccharides, glycoproteins (Glycam-93)
Metallocene catalysts	Woods 1995
RN(CH ₂) ₃ NRM(CH ₂) ₂ CH ₃ ⁺ , M = Hf, Ti, Zr (modified AMBER)	Opioid agonists
Deng 1998	
Metalloproteins (Zn · · · N, Zn · · · O)	Subramanian 1998
Hoops 1991	

Organic solvents

Fox 1998

Phosphorus compounds

Aagaard 1991

Polyamide nucleic acids (PNA)

Shields 1998

Poly(benzylglutamate),
dimethylformamide

Helfrich 1994

Proteins

Weiner 1984

Pt . . . DNA (Pt . . . guanine)

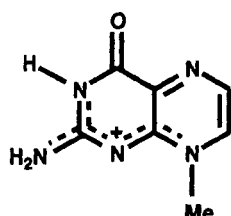
Yao 1994

Pt . . . ligand . . . nucleobase

Yuriev 1998

Pterin cation, TIP3, and SPC water

vdW parameters

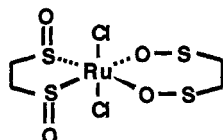


Cummins 1994

Pyrophosphate group, NADPH,
phenyl triazine

Leach 1995

Ruthenium bis-chelate disulfoxide
complexes (Hyperchem)



Geremia 1998

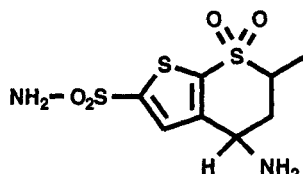
Saccharides (mono and 1 → 4 linked
polysaccharides)

Glennon 1994

Styrene and β-methyl analogs

Fruetel 1992

Sulfonamide-thiophene (carbonic
anhydrase II inhibitors)



Rossi 1995

Sulfate group

Kogelberg 1994

Sulfates, sulfamates

Huige 1995

Thymidine *cis-syn* dimer;
pyrimidine-pyrimidone
photoadduct

Spector 1997

Toluene, benzene, TIP3P water
nonbonded parameters

Chipot 1996b

Transition state for asymmetric
Michael addition

Brunet 1994

UO_2^{2+} , Sr^{2+} nonbonded parameters

Guilbaud 1996

Zirconocene dichlorides

Höweler 1994

$\text{Zn}-\text{C}$, $\text{C}-\text{N}$ for free/bound CN to
 $\text{Zn}, \text{N}-\text{C}-\text{Zn}-\text{N}$, others

Peng 1993

$\text{Zn}-\text{O}-\text{C}$ bending
(carboxypeptidase)

Banci 1994

$\text{Zn}-\text{O}$; $\text{Zn}-\text{S}$ (modified version of
AMBER)

McMartin 1997

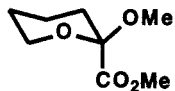
Zn^{2+} (4- and 5-coordinate) $\text{Zn}-\text{N}$,
 $\text{Zn}-\text{O}$, $\text{Zn}-\text{S}$, others for
alcohol dehydrogenase

Ryde 1995

AMBER* (MacroModel)

α -Amido esters
McDonald 1996b

Anomeric torsion



Bernardi 1995
Aryl diazo group



Keating 1997
Calixarene . . . M⁺, M = Na, K, Rb
(polyether . . . metal)
Groenen 1992
Co . . . N (cobaloxime)
Cini 1998
Fe—S, S—Fe—N, etc. for
ferryloxyheme group
Keserii 1997
M⁺ . . . O vdW radii, M = Li, Na
Inman 1989
N⁺—C—C—F torsional parameters
Larkin 1993
Phosphonamidates
Guida 1992
Proline
McDonald 1996a
Pyranoses
Parish 1998
Pyranoses (united-atom)
Senderowitz 1996
Pyranose oligomers (all-atom)
Senderowitz 1997
Zn²⁺ (attached to imidazoles, sulfur,
carbohydrate)
Guida 1992

BIOGRAF

Porphyrins, M . . . N equilibrium and
nonbonding lengths for M =
Ni²⁺, Co^{2+/3+}, UO₂²⁺, Sr²⁺ and
nonbonded for Cu²⁺, Zn²⁺, Fe³⁺
Shelnutt 1991, Sparks 1993

BOYD, R. H.

Alkanes
S. Chang 1970
Amino acid
Espinosa-Müller 1982
C=C, C=C—C=C
Anet 1978, Lenz 1989
Co³⁺ . . . N
Buckingham 1970, 1974,
Yoshikawa 1976, Pavelcik
1978
Cr—Cr coordination complexes
Boeyens 1998a
Cyclobutane
Wiberg 1980
H(D) . . . H(D)
S.-F. Lee 1981
Mo—Mo coordination complexes
Boeyens 1995, 1998b
N, O, P, S, halogen
Espinosa-Müller 1982, 1984
Ni²⁺ . . . N
McDougall 1978, Hancock 1988
R—I
Carballeira 1990
Si, Ge, Sn
Ouellette 1972a,b

Heterocycles and related fragments

CFF CVFF Hagler

Alkali metal/halide anion nonbonded parameters (Li^+ , Na^+ , K^+ , Rb^+ , Cs^+ , F^- , Cl^- , Br^- , I^-)

Peng 1997

Alkanes (CFF93)

Hwang 1994

Alkanes (QMFF)

Maple 1994a,b

$\text{Al}-\text{O}$, $\text{O}-\text{Al}-\text{O}$, $\text{O}-\text{Si}-\text{O}-\text{Al}$, etc. for aluminosilicates

Hill 1995

Amides, lactams, peptides (QMFF)

Maple 1998

Amine–ketone transannular bond ($\text{N}\rightarrow\text{C}=\text{O}$) for CFF91

Griffith 1997

Aromatic polyesters

Sun 1994a

$\text{C}-\text{C}-\text{C}-\text{O}$ (CFF93)

Liang 1995

C, CT, HC vdW parameters for camphor . . . cytochrome

Harris 1995

C, H, O vdW parameters for poly(ethylene oxide)

Fuson 1997

Carbonate ($-\text{OCOO}-$)

Sun 1994b

CHCl_3 and CH_3OH

Gratias 1998

Clay minerals (CFF91) general parameter set

Teppen 1997

Clay (hectorite), $\text{Eu}(\text{NO}_3)_3$, tributyl phosphate

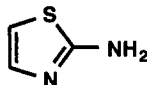
Hartzell 1998

Cyclopropane

Martin 1998

Heme group

Laberge 1996



Gaedt 1998

Rh–phosphine ligands (CFF91)

Gleich 1998

$\text{Si}-\text{O}$, $\text{Si}-\text{O}-\text{Si}$, $\text{O}-\text{Si}-\text{O}-\text{Si}$, etc. for silica

Hill 1994

Urea, melamine

Meier 1995

CFF Rasmussen

Alcohols, carbohydrates

Fabricius 1997

Aldehydes, ketones

Jónsdóttir 1995

Alkanes

Engelsen 1994

Alkanes, ethers, ketones, aldehydes

Rasmussen 1997

Anomeric carbons, aliphatic/alicyclic ethers

Fabricius 1995

$\text{C}=\text{S}$

Fausto 1989

Carbonate ($-\text{OCOO}-$)

Sun 1994b

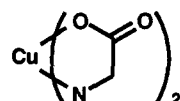
$\text{Co}^{3+} \cdots \text{N}$

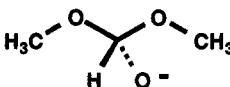
Niketic 1978

$\text{Co}^{3+}\text{Cl}_2\text{L}$, L = cyclam and tetraaza macrocycles (CFF modified with OOP bending term)

Creaser 1994

Cu^{2+} —bis-aminoacids



Sabolovic 1995	Veal 1993
Fe ²⁺ . . . N	C—S—O—C, C—S—N—C (sulfonamide, sulfonate)
Angelucci 1993	Bindal 1990
Glucopyranoses	1,4-Dihydropyridine
Melberg 1979	Young 1993
Imines (PEFIM)	Carbohydrate (glucopyranose)
Huige 1993	Ha 1988
Many others	Carbohydrates (extended atom)
Rasmussen 1985	Grootenhuis 1993
RNC and oligomers	Carbohydrates (CHEAT95)
Huige 1993	Kouwijzer 1995
RSH, RSR	Carbohydrates (glycol, glycerol, dimethoxymethanol, etc.)
Fausto 1987	Reiling 1996
Saccharides (PEF91L)	Carborane
Engelsen 1993	Holbrey 1993
<hr/>	
CHARMm/CHARMM	
Acetamide (<i>N</i> -methyl)	Dimethylorthooacetate
Baudry 1994	
Alkanes	Hæffner 1998
Kaminski 1994, Zhang 1996	Dipalmitoylphosphatidylcholine
Alkane Lennard-Jones parameters	Smondyrev 1999
Yin 1998	Ester
Alkenes	Nakagawa 1993
Feller 1997	Ester, acetyl (torsions) for bactereopheophytins
Amide	Foloppe 1995
Nakagawa 1993	Eu ³⁺ . . . amide-based macrocycle complex
Au—S, Au—S—C, Au—benzenethiolade	Frey 1994
Jung 1999	Fe . . . O (water), Na ⁺ , Cl ⁻ Lennard- Jones parameters
Calixarenes	Yelle 1995
Fischer 1995, van Hoorn 1997	Fe—S, S—Fe—S, etc. for oxidized and reduced rubredoxin
Calixarenes (derivatized)	Shenoy 1993
van Hoorn 1998	Ferrocene and other linear metallocenes
Calixarene . . . Eu ³⁺ van Veggel 1995	Doman 1992
Calixarene . . . M ⁺ , M = Na, K, Rb (polyether . . . metal, MacroModel)	Heme (myoglobin) Loncharich 1990
Groenen 1992	
C—O—C—O, C—C—C—O, C—O—C—C	

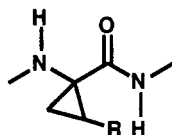
K^+ . . . amino acid side chains,
peptide backbone (modified
CHARMm)

Donini 1998

Lactose

Oh 1995

2,3-Methanoamino acids



Burgess 1995

Methyl torsional parameters
Chatfield 1998

Molybdenum, polyoxometalate
cages (molybdodiphosphato)
Lowe 1995

N-Methylacetamide, water
Baudry 1994

NAD^+ , NADH, ATP
Pavelites 1997

Nonbonded parameters for alanine
dipeptide in TIP3 water
Smith 1993

NO_3^- (nitrate), polyammonium
macrocycles [$24]N_6O_2$ and
[$18]N_4O_2$

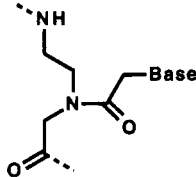
Papoyan 1996

Nucleic acids (united-atom)
MacKerell 1995

Ornithine, DMSO
Mihailescu 1999

Peptides, proteins
Momany 1993

Peptide nucleic acids (PNA)



Sen 1998

Phosphazenes (cyclic)

Amato 1995

$P=N$, $P-N$, $P-Cl$,
poly[bis(chloro)phosphazene]
Grassi 1994, Amato 1996

Phosphazene polymers
Caminiti 1997

Phospholipids (phosphatidylcholine)
Schlenkrich 1996

Pigment macrocycles for
bacteriochlorophylls (bond
lengths, angles)

Foloppe 1995

Proteins

Brooks 1983

Proteins (all-atom)
MacKerell 1998

Retinal

Humphrey 1995

$S-Fe-S$
Shenoy 1993

Sulfates, sulfamates
Huige 1995

Zn^{2+} . . . water, Zn^{2+} . . . protein
(bond/ionic models)

Stote 1995

DISCOVER

Dehydroalanine (parameters
developed but not published)

Palmer 1992

Ferryl intermediate, iron-oxo
complex for cytochrome P450

Filipovic 1992, Paulsen 1992

$Fe-S$ (axial cysteine in heme)
Paulsen 1991

Hydroxylamine glycoside linkage
Walker 1994

Lecithin lipids
Stouch 1991

Polybenzoxazine
Kim 1998

Silica, zeolites

Hill 1994

Silicates (Si, O, C, H nonbonded
parameters)

Bull 1993

Sulfonamide

Pisabarro 1994

 M^+SCN^-
Brink 1991**DREIDING**Alkane thiols/aromatic thiols on
Au(111) surface

Li 1998

Carbonate

Fan 1994

Generic

Mayo 1990

 Li^+ vdW parameters

Castonguay 1992b

Nickel porphyrins

Jentzen 1995

 Ni^{2+} porphyrins (OOP force
constants)

Song 1996

Pt . . . P

Castonguay 1991

Zirconium(tetrahedral),
cyclopentadienyl centroid, η^3 - π -
allyl centroid, olefin centroid

Castonguay 1992a

GROMOSAliphatic CH, CH_2 , CH_3 , CH_4 ,
united-atom
(reparameterization)

Daura 1998

 CH_2 Lennard-Jones radii for
dimyristoyl-phosphatidylcholine
Gabdoulline 1996 CH_2 , CH_3 Lennard-Jones parameters
(united-atom)

Berger 1997

 CH_2 , CH united-atom vdW radii for
DNA

Baleja 1990

 $CH_3 \cdots O$, $CH_2 \cdots O$

Marrink 1994, Tieleman 1996

 $CH_3-C\equiv C-CO_2H$ parameter set,
 CCl_4 Lennard-Jones parameters
Gavezzotti 1997Chlorobenzoic acid
van Helden 1992

Cyclodextrins

Koehler 1987, Luzhkov 1998

Dimethyl sulfoxide (bulk liquid)
Liu 1995General fitting
Breuer 1989Lennard-Jones parameters for
 $CH_3 \cdots O$ and $Ln^{3+} \cdots OH_2$
Kowall 1995 NH_3 , H_2O , O_2
Marrink 1996Oligosaccharides (exo-anomeric
effect)
Ott 1996**ECEPP**

Torsion term added with parameters

Kang 1996

EPEN/2Alkali metals, H_2O

Brink 1990

O—C—C—O, C—C—C—O
twofold dihedral values;
O—C—O bending constant
(all-atom and united-atom)
Klewinghaus 1997

Phenol and substituted phenols (*p*-Cl,
p-CN, *p*-OMe)
Mark 1994

Phosphate ions
van der Spoel 1996

Phosphonic acids (aminoalkyl)
Breuer 1989

Tryptophan, Ac-Trp, H₂O, CHCl₃
nonbonded parameters
Daura 1996

Water (protonizable water model for
QDGROMOS)
Billeter 1998

MM2

Alcohols, ethers

Allinger 1980a

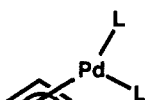
Alkylsilane, Si

Profeta 1986a, Abraham 1988,
Grigoras 1988, Unwalla 1988

Alkyne

Rogers 1979

η^3 -Allyl palladium, L = Cl, amine
(for MM2-91)

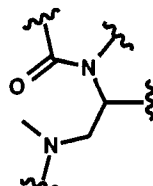


Norrby 1993

Amide

Pettersson 1992

Amide, amine: C_{sp²}—C_{sp³}—
carbonyl—N_{amide}, N_{amine}—
C_{sp³}—C_{sp³}—N_{amine}, torsional
parameters (provisional set for
MM2-87)



Froimowitz 1992

Amides (conjugated)

Berg 1996

Amides (MM2-85/BIGSTRN)
Susnow 1991

Ar—B

Okada 1992

Aromatic–aromatic

Loncharich 1988, Rudolf 1988,
Tsuzuki 1988, 1990b, Jaime
1989, Pettersson 1990

ArSiMe₃, ArGeMe₃
Weissensteiner 1986

Ar—SO₃H

Mattern 1991

ArX (X = halogen)

Bowen 1988

Benzene ring (mechanical treatment)

Carter 1976, Allinger 1983a,
Beckhaus 1983, Andersson

1984, Kao 1987, Liljefors

1987, Pettersson 1987,

Fukazawa 1988, Tsuzuki

1990a, Broeker 1991b, Brandt
1992

Bicyclopropyl

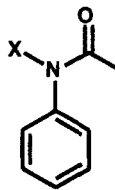
Ōsawa 1983

β -Carotene

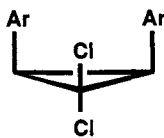
Hu 1997

C⁺

Müller 1984–1986

C• (radical)	C—O—C—C≡C
Imam 1985	Cano 1987, Jiménez-Barbero 1988
C• (radical transition state)	CO—CO
	Isaksson 1981, 1983
DeRiggi 1993	CONH (amide, peptide)
C=C	Karlsson 1977, Maryanoff 1986, Wolfe 1988a,b, Lii 1989, Schnur 1989
Broeker 1991b, Pettersson 1991	COO ⁻
C=C—Ar	Colucci 1986
Tsuzuki 1989	CO—O—CO
C=C/C=O	Ivanov 1984, F. K. Brown 1985, Polonski 1988
Corey 1984, Fukazawa 1986	COOR
C=C=C, C≡C (bent)	A. B. Brown 1989
Allinger 1987	C—OSO ₃ ⁻ , C—NHSO ₃ ⁻ , Na ⁺ , K ⁺ for sulfated carbohydrates
C=C—C=N	Ragazzi 1997
Klein 1987	C=S
C=C—CO ₂ R, O—C—CO ₂ R	Fausto 1989
Corey 1984, Bernardi 1987, Hanson 1988, Tucker 1990	C _{sp²} (tryptcene)
C=C—F	Yamamoto 1985a
Meyer 1980b	C _{sp²} —C _{sp²}
C=C—Me	Rudolf 1988, Tsuzuki 1989, 1990b
Liljefors 1985	C _{sp²} —C _{sp²} —N _{amide} —X torsional parameters
C=C=O (ketene)	
Biali 1989, Stewart 1992	Curran 1993
C=C—O—B (boron enolate)	C _{sp³} —C _{sp²} —C _{sp²} —S _{sp²}
Goodman 1987	Bøgesø 1991
C=C—O—C=C	Cyclobutane
Bowen 1988	Allinger 1980a
C=C—X	Cyclopropane
Sardinia 1986, Yates 1992	Ōsawa 1983, Bernlöhr 1984, Ivanov 1985, Dodziuk 1986, Aped 1992
C=N	
Klein 1987, Kao 1988a, Kontoyianni 1992a	
C≡N	
Castells 1988, Goldstein 1989	
C=O (ketone, aldehyde)	
Jaime 1984, Bowen 1987a,c, Goldsmith 1987, Allinger 1991a	
C=O ⁺ (oxocarbenium), O ⁺	
Broeker 1991b, Woods 1992	

Cyclopropane (1,1-dichloro)



Hossain 1994

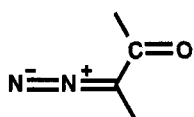
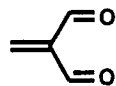
D (deuterium)

Allinger 1983b

Diarylphosphines, Ar—P—Ar
(MM2-87/BIGSTRN3)

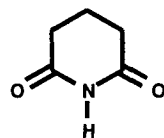
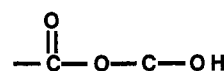
Weissensteiner 1992

Diazoketone

Goodman 1994
Enals (MMP2-87)Tuppurainen 1993
Enamines
Allinger 1994b
Epoxides (α -alkoxy and siloxy)
Dósen-Micovic 1993
Epoxides (MM2-91)
Sundin 1993
Epoxy-hexopyranosides
Fan 1995
General parameters
Allinger 1994c
General parameters
Martech, Inc. 1991
Germlycyclopropanes

Takeuchi 1993

Glutarimide ring

Laughton 1990
Graphite
Sprague 1980
Halides
Meyer 1980a, Bowen 1988, Gueu
1988
H-bondTaylor 1981, Kroon-Batenburg
1983, Abe 1984, Allinger
1988, Aped 1989, 1992,
Damewood 1990, Müller
1991H-bond (directional)
Senderowitz 1993a H_3PO_3
Santos 1991
Hydride (H^-) (MM2-88)
Dósen-Micovic 1993Hydroxy- γ -butyrolactones
(MM2-91, provisional set),
torsional parameters forJaime 1993
Imines

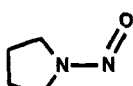
Bowen 1993, Huige 1993

Iodoketone
Lumbroso 1987Lactams (MM2-87) torsional
parameters
Matallana 1994 β -Lactam, penicillin
Wolfe 1988c,d, Durkin 1989Lactone
Watson 1986, Yoshida 1988

Mannich salts

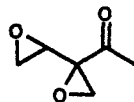


- McGaughey 1995
 N (amine)
 Froimowitz 1984a,b, Profeta 1985,
 Schmitz 1990
 N^+
 Colluci 1986, Dharanipragada
 1988
 $\text{N}_{\text{sp}^2}-\text{C}_{\text{sp}^3}-\text{C}_{\text{sp}^3}-\text{N}_{\text{sp}^2}$
 Pettersson 1992
 $\text{N}-\text{C}-\text{N}$ (anomeric effect,
 MM2-AE)
 Nørskov-Lauritsen 1984, Aped
 1987, 1989, 1992, Müller
 1991, Senderowitz 1992
 $\text{N}-\text{C}-\text{O}$ (anomeric effect)
 Fernandez 1991, Senderowitz
 1993a
 $\text{NH}_2^+ \text{COO}^-$
 Colucci 1986, Ascenso 1990
 $\text{N}=\text{N}$ (diazine, azoalkane)
 Crans 1980, Kao 1988b
 $\text{N}=\text{N}^+ (\rightarrow \text{O}^-)$
 Byström 1983
 $\text{N}-\text{N}=\text{O}$
 Lunazzi 1982
 Nitramines
 Delpeyroux 1994
 Nitrogen-containing compounds
 Leonard 1990
 $\text{N-Nitrosopyrrolidines}$

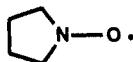


Polonski 1993

Nitroxides, periplanone B



- Sakakibara 1994
 Nitroxide radical (MM2+)
 Barone 1998
 Nitroxyl radical (MM2-87)



- Vila 1993
 NO_2
 Damewood 1988, Allinger 1990a
 $=\text{N}-\text{OH}$ (hydroxylamine),
 $=\text{N}-\text{OR}$ (oxime)
 Schnur 1988
 $\text{N}_{\text{sp}^3}-\text{C}_{\text{sp}^2}-\text{C}_{\text{sp}^2}-\text{S}$ torsional
 parameters (MM2-87)
 Froimowitz 1993
 O (ether, alcohol)
 Burkert 1979, Allinger 1980b,
 1990b, Meyer 1983b, Cano
 1986, Jiménez-Barbero 1988,
 Tsuzuki 1991, Vázquez 1991
 $\text{O}-\text{Ar}, \text{O}-\text{C}=\text{C}$
 Dodziuk 1982, H. M. Chang 1985,
 Decoret 1985, Moreland
 1985, Viswanadhan 1986,
 Dharanipragada 1988, A. B.
 Brown 1989, Tai 1989
 $\text{O}-\text{B}-\text{O}$ (borate)
 van Duin 1989, Goodman 1987
 $\text{O}-\text{C}-\text{C}-\text{C}$ (exo-deoxoanomeric
 effect)
 Houk 1993
 $\text{O}-\text{C}-\text{F}, \text{N}-\text{C}-\text{F}$ (anomeric
 effect)
 Senderowitz 1993b

O—C—O (anomeric effect, carbohydrate)	R—X (X = halogens)
Jeffrey 1980, Nørskov-Lauritsen 1984	Meyer 1977, 1978, 1981, 1982, 1983a
O—H stretch	S
Orozco 1993	Allinger 1991b
O—sulfate ester, C—O—SO ₃ ⁻	S—Ar
Whitfield 1993	Welsh 1990
Oxirane, thiirane	S—C _{sp} ²
	Kao 1985
	S—O
	Tai 1981
	S—S, S—S—S
	F. S. Jørgensen 1979
	SONH ₂
	Nicholas 1991
	Si—C=C (vinyl silane)
	Cho 1994
Oxiranes	Si—C—C=C
Tkachev 1994	Profeta 1986a,b
Oxymethylarennes	Si—C—C—Si
Norrby 1995	Unwalla 1988
P ^{III}	Si—C—Cl
Allinger 1978, Li 1985, Rithner 1985, Bowen 1987c	Cho 1990a
P ^V (pentacoordinated; phosphine oxide)	Si—Cl
Deiters 1977, Robinet 1989, 1991, Ugliengo 1989, Gasmi 1991	Cho 1989, 1990a,b, Forsyth 1990
Phosphazenes (cyclic)	Si—O (siloxane)
Amato 1995	Abraham 1988, Grigoras 1988, Frierson 1989
Phospholipids (general parameters)	Si—S
Jin 1994	Anderson 1990a,b
Phosphorus-containing compounds	Si—Si
Leonard 1990	Unwalla 1988, Profeta 1989
Polyene	Silacyclopentane
Jensen 1987, Kao 1987, Liljefors 1987	
Polysilane Si _n	
Hummel 1977, Höning 1982, Damewood 1985, Frierson 1988	
Porphyrin	Kelly 1988
Kaplan 1991	Sulfated polysaccharides
R—O—O—R (peroxide, dioxetane)	Ferro 1997
Carballeira 1988, 1989, Richardson 1989, Drew 1990	Sulfenates (Ar—S—O—R)
	Pasto 1994

Thiirane and dithiacyclobutane



Nicolaou 1990

Thymidine derivatives

Yates 1992

Thymidine-3',5'-bis(phosphate)

Deiters 1982, 1984

Urea

Kontoyianni 1992b

Urea and derivatives

Strassner 1996

Vinyl epoxides



Shimazaki 1993

Vinyl ethers



Tobiason 1993

 $X-C-C-C=O$ ($X = \text{halo, O, S}$)

Bowen 1987a

 $X-C-COCl$ ($X = \text{halo}$)

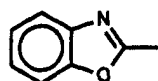
Borkar 1988

Heteroaromatics (MM2)

Aniline derivatives

Allinger 1994b

Benzisoxazole



Ohashi 1990

Indoles, piperidines, piperazines,
others

Andersen 1994

Isoxazole (N, O)

Krogsgaard-Larsen 1985, Schnur
1991

N-containing

Falk 1981, 1983, Nilsson 1986,
Kao 1988a, Tai 1988, Charles
1992

N,O-containing (thymidine)

Bandoli 1987, Yates 1992

N,S-containing

Berg 1987, Rochester 1987, 1989,
Garduño-Juárez 1989

N,S,O-containing

Toma 1990

Nitroimidazole

Rameau 1996

O,S-containing

Tai 1989

Oxymethylarennes

Norrby 1995

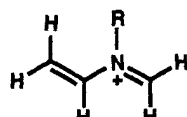
Phosphazenes (cyclic)

Amato 1995

Porphyrin

Kaplan 1991

Pyridinium,

N-vinylmethylenammonium

McGaughey 1996

Metals and Complexes (MM2)

Au/Ag surface . . . SH, SMe

Sellers 1993

 Ag^+ , Cu^+ cryptates of hexamino
cryptand

Sato 1996

 $\text{Ca}^{2+} \cdots \text{O}$

Deiters 1982

 Cd^{2+} , $\text{Zn}^{2+} \cdots \text{N, O}$

Adam 1990

Co . . . bleomycin

Charles 1992

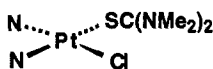
 $\text{Co}^{2+} \cdots$ corrinoids (hexacoordinate)

Marques 1995c

Co ³⁺ cobaloximes and reevaluation of cobalt corrin (MM2+)	Ferrocene Menger 1988, Thiem 1988
Marques 1998	Ferrocene, bridged Rudzinski 1992
Co ^{3+ . . . N, C, O in} cyanocobalamin, methylcobalt corrinoids (MM2+)	Gd . . . η[C ₆ H ₃ (t-Bu) ₃] ₂ Ren 1991
Brown 1998	Ge, Pb Hutchings 1979, Blount 1980, Hounshell 1980, Allinger 1989b
Co ^{2+ . . . N, S}	K . . . O (aliphatic crown ether) Hay 1993
Harding 1990, Lin 1991	Li (enolate) Spears 1987
Co ^{3+ . . . N}	Ln vdW radii Ren 1991
Hambley 1980, Endicott 1989, Yoshikawa 1990, Lessard 1992, Tueting 1994	Ln (Yb, Eu) Brechnell 1985
Cr . . . As	Ln ³⁺ (aqua complexes) Hay 1991
T. L. Brown 1992	Ni Drew 1986
Cr . . . P	Ni(0) π-allyl
Caffery 1991, T. L. Brown 1992, K. J. Lee 1992	
Cr(CO) ₅ L; L = amines (MMP2, BIOGRAF)	
Choi 1993b	
Cr(CO) ₅ L; L = alcohol, ether, thioether (MMP2 BIOGRAF)	
Choi 1994	
Cr(CO) ₅ . . . L, L = η ² ligand; RhCp(CO) . . . L, L = η ² ligand (dummy atoms used)	
White 1995	
Cu ²⁺ (N—Cu—N, N—Cu—O, S—Cu—N, etc.)	Gugelchuk 1994
Adam 1993	Ni ^{2+ . . . N} Yoshikawa 1990, Adam 1991
Cu ^{2+ . . . P, N, S}	Ni ^{2+ . . . porphyrin} Kaplan 1991, Munro 1992
Drew 1987, Canales 1991	Ni ^{2+ . . . N (tetrapyrrole; high and low spin)} Zimmer 1990
Fe . . . O	Os (osmaoxetane) Norrbj 1994
Bouraoui 1990a,b	Pd . . . N Yates 1994
Fe ^{3+ . . . N} (porphyrinates; low spin)	Pd . . . X (X = N, S, allyl) Norrbj 1993
Safo 1994	
Fe ^{2+ . . . N} (low spin) octahedral poly(pyrazolyl)borate (CAChe)	
Sohrin 1995	
Fe ³⁺ -porphyrin (low-spin) bisimidazole, bispyridine complexes	
Munro 1995	



Pt²⁺ complexes to N, Cl, S (MM2+)

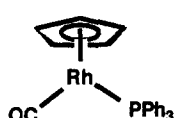


Bierbach 1998

Rh³⁺ · · · N (CAChe)

McClure 1992

Rhodium–cyclopentadienyl



Choi 1993a

Se, Te

Allinger 1989a

Sn

Allinger 1989c, Horner 1991

Sr

Bell 1991

Transition metal · · · CO

Lauher 1986

Zeolite

Mabilia 1987, No 1988

Zn—S, O⁻, N

Yates 1993

Miscellaneous (MM2)

Bond Moments

Damewood 1988, Huizoon 1989,
Ivanov 1991

Charges

Meyer 1982, 1985, Dósen-Micovic
1983, 1985, Hammerström
1988

Surfaces

Transition metal carbonyl cluster
Sironi 1992

Transition States

Acid-catalyzed lactonization
Dorigo 1987

C · · · C=C (radical addition)

Spellmeyer 1987, Broeker 1991a

C—H · · · OH (H abstraction by
•OH)

Green 1986, Dorigo 1988

C—H · · · X (abstraction by
Ar—I—Ci)

White 1990

C—Li · · · C=C (Li addition to
alkene)

Bailey 1991

C≡N—O⁻ (cycloaddition of nitrile
oxide)

Houk 1986, Annunziata 1987,
Hassner 1988

=C—O—B · · · O (aldol reaction of
boron enolate)

Bernardi 1990a, 1992, Goodman
1990, Gennari 1992

Diels–Alder

Raimondi 1992

Diels–Alder (heteroatomic 4+2)

Tietze 1994

Epoxide · · · H⁻

Dósen-Micovic 1993

General method (CAChe)

S. Y. Liu 1984

Hydride transfer (intramolecular)
Eurenius 1994

Michael addition

Rudolf 1988

Norrish type II H abstraction
Sauers 1989

Nucleophilic 1,2-addition to enone
and ketone

Wu 1991

Nucleophilic 1,4-addition to
α,β-unsaturated carbonyl

Bernardi 1990b

Radical–olefin addition
Bertrand 1995

S_N2

Berg 1983

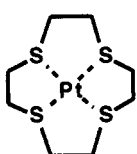
Modified MM2

Allinger 1993a

Carbohydrate

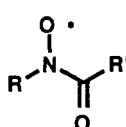
Kozar 1990, Murata 1993

β -Carotene	Silatrane
Hu 1997	
Co—N, Co—C (cobalt corrinoids)	
Marques 1995b,c	
C—OSO ₃ , C—NHSO ₃ [−] , Na ⁺ , K ⁺	
(sulfated carbohydrates)	
Ragazzi 1997	Tasaka 1996
Fe ²⁺ —N (low spin) octahedral	Solvent (implicit solvation model)
poly(pyrazoly)borate (CAChe)	Cossé-Bari 1994
Sohrin 1995	Sulfated polysaccharides
Fe ²⁺ . . . porphyrin (high and low spin), Fe ³⁺ . . . porphyrin (high and low spin), penta- and hexacoordinate	Ferro 1997
Marques 1995a	Vanadium peroxides ($L_nV(O_2)_m$; $m = 0–4$)
Fe ³⁺ . . . porphyrin (low spin) bisimidazole, bispyridine complexes	Cundari 1997
Munro 1995	MM2CARB
HIV-1 protease inhibitors and general parameters for MM2X	Tvaroska 1987
Holloway 1995	MM2ERW
Induced dipole terms	α -Hydroxyenone, torsional parameters, and OH bond moment
Torrens 1992	Stammen 1992
Ln ³⁺ aqua complexes	MM2'
Hay 1991	Jaime 1983
M . . . (pyo) ₂ [18]diene N ₆ complexes M = Zn ²⁺ , Cd ²⁺ , Hg ²⁺ , Pb ²⁺	Bipyridine
Bryant 1995	Ishida 1993
Organometallics, including atoms up to 12-coordinate (WMM2)	Radical–olefin addition transition state
Lopis 1997	Bertrand 1995
Pt . . . S coordination complexes	MM2* (MacroModel)



Watzky 1993

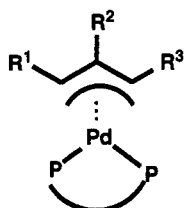
Acylaminoxyl radical



Komaromi 1997
 Allyl- and crotylborane aldol transition state
 Vulpetti 1993b

Allyl- and crotylboronate aldol transition state
Gennari 1994

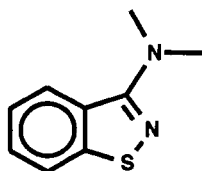
Allylpalladium complexes



Pregosin 1994

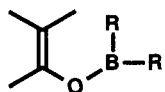
Azine ($C=N-N=C$), diazine ($C=C-N=N$), diimine ($N=C-C=N$)
Schmitz 1994

Benzisothiazole



Norman 1996

Boron enolate



Vulpetti 1993a

Boronate, boronate–carbonyl complexes (alkyl, aryl)
James 1996

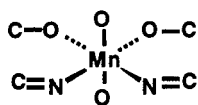
α , β -Cyclopropyl ketones
Mash 1996

Cyclopropylvinylketone
Mash 1997

Ferrocenyl acrylate ester
Sherrod 1989

Mn, di- μ -oxomanganese dimer
Manchanda 1994

Salen-type Mn complexes



Beagley 1996

Sulfonamides

Belvisi 1994

Sulfonamido peptides

Gennari 1996

Transition state for hydride addition to ketone
Ando 1998

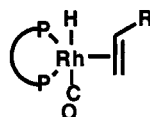
Transition state for nitrone–alkene cycloaddition
Annunziata 1998

Transition state for radical cyclization with alkene



Belvisi 1993

Transition state for rhodium alkyl formation



Casey 1995

MM3

Acyl halides: formyl, acetyl, propionyl, butyryl, and others
Shim 1998

Alkyl chlorides (mono-, di-, polyhalogen)
Kulkarni 1998

Alkyl iodides

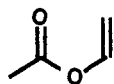
Zhou 1994

Alkyl peroxides (ROOR and ROOH) C—C—C—X (X = C, Si, F, Cl, Br, I)
K. Chen 1993 torsional parameters

Alkyl radicals Cho 1997
R. Liu 1994

Alkynes, nitriles Stewart 1992
Goldstein 1996

Allylacetate (and related) C—H length and stretching
frequencies accounting for electronegativity, carbonyl, and Bohlmann effect



Carrigan 1997
Allylvinylamine torsional parameters Thondorf 1997
Matsumoto 1994

Amides Strobl 1997
Sandrone 1999

Amide . . . metal complexes Allinger 1992a
Hay 1998a

Amino acid zwitterions Kirschner 1998
Liang 1997a

Ammonium, alkylammonium Alligner 1992a
Conjugated ketones, aldehydes

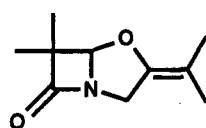
Aniline torsional potential C_{sp²}—O—C, C=C—O—C
(Ar—NH₂) (1,4-dioxane)

Rettig 1993
Choo 1993

Anilines Cho 1996b
Alligner 1994b

Azoxy compounds Shim 1997
Fan 1995

β -Lactams Hay 1997
Cyclohexanones with α - and



Fernández 1994
Bond moment, N(+)—H Cristina 1997
Lii 1998

Bond moments and charge flux for hydrocarbons Moberg 1996
Lii 1992

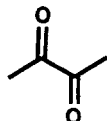
Furan, vinyl ether

Allinger 1993b

General parameters

Allinger 1994c

Glyoxals, 1,2- and 1,4-diketones



Allinger 1994a

 $\text{H}-\text{C}-\text{C}-\text{O}$ (methyl ester)

Salvatella 1998

Hydrazines

Ma 1996

Hydrocarbons

Allinger 1989d

Hydrogen bond (directional)

Lii 1998

Hydroxylamine, methoxylamine

Liang 1994

 $\text{Li}^+, \text{Na}^+, \text{K}^+, \text{Cs}^+, \text{Rb}^+, \text{Ca}^{2+}, \text{Ba}^{2+}$,
 Sr^{2+} nonbonded parameters

Hay 1996

 $\text{N}-\text{C}-\text{C}-\text{S}$, $\text{C}-\text{C}-\text{C}-\text{S}$,
 $\text{C}-\text{C}-\text{S}-\text{C}$, $\text{C}-\text{C}-\text{C}-\text{N}$
torsional parameters for thianes,
piperidines, and 1,4-thiazines

Gallego 1993

Mannich salts



McGaughey 1995

Metallocarboranes ($\text{C}_2\text{B}_4\text{H}_6\text{M}$, $\text{M} = \text{Mg, Si, Ge, Sn}$

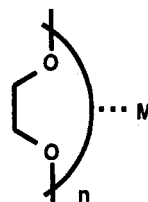
Timofeeva 1994a,b

 $\text{M}_3\text{L}_3(\text{CO})_3$ $\text{M} = \text{Co, Rh, Ir}$; $\text{L} = \eta^5\text{-Cp}$ and others; $\text{Co}_3\text{Cp}_3(\text{arene})_3$, metal clusters
(modified MM3)

Mercandelli 1996

Multidentate conjugated ether–metal
complexes (alkali/alkaline earth
cations)

Hay 1998b

Multidentate ether–metal complexes,
 $\text{M} = \text{Li}^+, \text{Na}^+, \text{K}^+, \text{Rb}^+, \text{Cs}^+$, and
 $\text{Mg}^{2+}, \text{Sr}^{2+}, \text{Ca}^{2+}, \text{Ba}^{2+}$ 

Hay 1994

 N -Vinylacetamide, N -allylpyridone,
and other N -vinylamides

Carrigan 1997

Nitro compounds (aliphatic and
aromatic)

Allinger 1990b

Nitrogen-containing aromatic
heterocycles

Tai 1993

 $\text{O}-\text{C}-\text{C}-\text{O}$, $\text{O}-\text{C}-\text{C}-\text{N}$,
 $\text{N}-\text{H}$

Grindley 1994

 $\text{O}-\text{C}-\text{C}-\text{O}$ (MM3-GE, gauche
effect)

Senderowitz 1994

 $\text{O}-\text{C}-\text{C}-\text{O}$

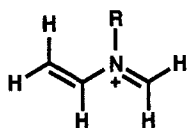
Rockwell 1996

 $\text{O}-\text{C}-\text{O}-\text{H}$ torsion for glucose
Barrows 1998

Phosphines (alkyl)

Fox 1992, Liang 1996

Pyridinium, *N*-vinyl-methyleneammonium



McGaughey 1996

Silanes

Chen 1997

Si—C—C—Si, C—C—Si—C, etc.

Núñez 1997

—SO_2^- , $\text{CH}_2=\text{CHSO}_2^-$, Ph_2SO_2^-

Allinger 1993a

Sulfate (O-sulfated monosaccharides)

Lamba 1994

Sulfonamides

Liang 1997b

Sulfones

Allinger 1993a

Sulfoxides

Allinger 1996a

Thiophene (benzo[*b*]thiophene), ammonium, other functionality of raloxifene

Boyd 1996

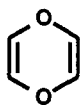
Thiophenes (hydroxylated oligomers)

Barbarella 1996

Thiophenes, thiazoles, thiadiazoles, etc.

Yang 1996

Vinyl ether



Choo 1993

MM3* (MacroModel)

Ethane, general automated parameterization procedure

Norrby 1998

Pyridine

Owens 1993

Ru—P, Ru—H, Ru . . . Ar in hydroruthenium complexes with chelating phosphenes

Trabesinger 1997

Ru²⁺-polypyridyl complexes

Brandt 1998

MM4

Alkenes

Nevins 1996a

Alkenes (hyperconjugated)

Allinger 1996c

Alkyl chlorides (mono-, di-, polyhalogen)

Kulkarni 1998

Conjugated hydrocarbons

Nevins 1996b

Hydrocarbons (saturated)

Allinger 1996b

Sulfides, mercaptans (thiols)

Allinger 1997

MMFF

Extended parameterization, Zn²⁺, Ca²⁺, Cu^{1+/2+}, Fe^{2+/3+}, F[−], Cl[−], Br[−], OH[−], H₃O⁺, other functionalities

Halgren 1996e

General nonbonded and electrostatic parameters

Halgren 1996a

General parameterization

Halgren 1996c

Geometries (torsional parameters)

Halgren 1996b

Parameters for organic and
bioorganic molecules

Halgren 1992

Vibrational frequencies (stretch and
bend parameters)

Halgren 1996d

MMX

Dicyanoanthracene

Acquavella 1994

M \cdots (pyo) $_2$ [18]diene N₆ complexes
M = Zn²⁺, Cd²⁺, Hg²⁺, Pb²⁺

Bryant 1995

Nitroimidazole

Rameau 1996

Oxiranes

Tkachev 1994

P—O (oxaphosphatanes)

Marí 1990

Se—C, Se—C—C, O—C—C—Se,
others

Markovic 1995

Transition metal complexes

Gajewski 1998

MOBY

Cu²⁺ \cdots N, Cu²⁺ \cdots O (square-
planar complexes)

Wiesemann 1994

Zirconocene dichlorides

Höweler 1994

MOMEC

C—Si, C—Si—C, Si—C—N, Si
vdW, Co³⁺ \cdots N for Morse
function

Comba 1997d

Cr³⁺, Fe³⁺, Co³⁺, Ni²⁺, Cu²⁺, Zn²⁺,
Rh³⁺ \cdots S, O, N

Bernhardt 1992

Co²⁺ \cdots N

Bond 1985

Co²⁺ \cdots S, Co³⁺ \cdots S
Hambley 1986Cu²⁺ \cdots N, Cu²⁺ \cdots O_{pentacoord.}
Cu²⁺ \cdots O_{hexacoord.}

Comba 1995

Cu²⁺ \cdots N₆ octahedral complexes
Bernhardt 1995Cu²⁺ \cdots cyclooctapeptides
Comba 1998bCu¹⁺ \cdots N parameter set (tetraamine
complexes)

Comba 1997c

Cu \cdots N_{sp²}, Cu \cdots N_{sp³},
Cu \cdots N_{amide}

Comba 1994

Lanthanoid metal complexes (aqua
and phosphato); La, Ce, Pr, Nd,
Pm, Sm, Eu, Gd, Tb, Dy, Ho, Y,
Er, Tm, Yb, Lu

Comba 1998a

Ligands (organic backbones) free and
coordinated to M = Ca²⁺, Cu²⁺,
Ni²⁺, Zn²⁺, Cr³⁺, Fe³⁺ (low
spin), others

Bol 1998

Metal diamine chelate rings

Hambley 1987

M—O—O—M, M = Co³⁺, Cu²⁺,
 μ -peroxodimethyl complexes
with pyridine, amine ligands

Comba 1997b

$\text{Ni}^{2+} \cdots$ hexaamines, $\text{Ni}^{2+} \cdots \text{N}$	Guanidinium acetate, methylammonium acetate (all-atom)
Bernhardt 1993	Saigal 1997
Pt \cdots N	Heterocycles: diazoles, furan, oxazoles, pyrrole (all-atom)
Hambley 1988	FKBP12 inhibitors
Tetrathiamacroyclic ligands with OH groups	
Comba 1997a	

OPLS

Acetals

W. L. Jorgensen 1994

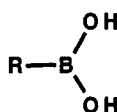
Ascorbic acid

Ventura 1995

Alkanes

Kaminski 1994

Alkyl boronic acids



X. Chen 1994

Benzene

W. L. Jorgensen 1990

t-Butyl alcohol

Yonker 1997

Calixarene \cdots bis(phenylurea)

McDonald 1998a

Carbohydrates (all-atom)

Damm 1997

CHFClBr

Costante-Crassous 1997

Cyclic peptides, crambin

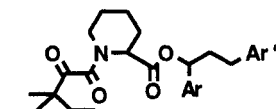
W. L. Jorgensen 1988

1,2-Dimethoxyethane torsional parameterse (AMBER*, OPLS*)

Williams 1996

Dimethylphosphate

Kamitakahara 1995



$\text{SO}_4^{2-} \cdots$ water nonbonded

parameters

W. R. Cannon 1994

Succinic acid, succinate ion

Price 1998

Sulfonamide, quinoline ring (all-atom)

Jones-Hertzog 1997

Urea, acetamide

Duffy 1993

QCFF

Alkanes, alkenes

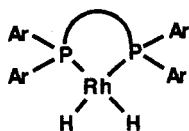
Kar 1994a,b

SHAPES

Rh \cdots P, O (complex)

Allured 1991

Rhodium (6-coordinate dihydride complexes)



Giovannetti 1993

Zirconocene dichloride

Höwler 1994

SPASIBA

Alkanes

Derreumaux 1993a,c

Alkenes

Chhiba 1994

Esters

Chhiba 1997

Ethers (aliphatic)

Tristram 1996

Proteins

Derreumaux 1995

TRIPOS

$\text{Co}^{2+} \cdots \text{N}, \text{N—Co—N}$, etc. (cobalt phthalocyanine)

Heuts 1995

Crown ether $\cdots \text{M}$, $\text{M} = \text{Rb}^+, \text{Cs}^+$; M—O—C parameters

Hancock 1994

$\text{Ga}^{3+}, \text{In}^{3+}$ complexes with M—N , M—O , M—S bonds

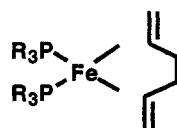
Li 1996

$\text{Gd}^{3+} \cdots \text{N}$, $\text{Gd}^{3+} \cdots \text{O}$ gadolinium polyamino carboxylate complexes

Reichert 1996

General purpose
Clark 1989

Iron complexes



Angermund 1998

Metal $\cdots \text{N}$

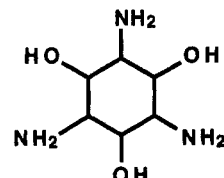
Hancock 1989

Metalloporphyrins

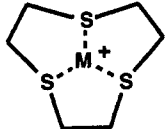
Hancock 1989

Mg, Ca, Sr, Ba, Cd; coordination complexes to tac1 ligand:

Siloxane



Hegetschweiler 1993

Malatesta 1993	
Technetium(V) complexes with Tc—S, Tc—N, Tc=O	VALBOND
Hancock 1996	Hypervalent, p-block atom parameters
	Cleveland 1996
UFF	Metal hydrides and alkyls
[9]aneS ₃	Landis 1995, 1998a,b
	Nonhypervalent, p-block atom parameters
Beech 1994	Root 1993
General parameters for all organic and inorganic molecules	
Rappé 1992	YETI
Nitroxide radical	General parameters
Barone 1998	Vedani 1988
	General parameter set for Co ²⁺ , Zn ²⁺ , metalloproteins
	Vedani 1990
	H-bond
	Vedani 1985
	Metalloproteins
	Vedani 1996

CITED LITERATURE

- O. Aagaard, R. A. J. Janssen, B. F. M. de Waal, and H. Buck, *Heteroat. Chem.* **2**, 32 (1991).
 K. Abe, M. Hirota, G. Yamamoto, and M. Oki, *Chem. Lett.*, 665 (1984).
 R. J. Abraham and G. H. Grant, *J. Comput. Chem.*, **9**, 709 (1988).
 M. F. Acquavella, M. E. Evans, S. W. Farraher, C. J. Névoret, and C. J. Abelt, *J. Org. Chem.*, **59**, 2894 (1994).
 K. R. Adam, B. J. McCool, A. J. Leong, L. F. Lindoy, C. W. G. Ansell, P. J. Baillie, K. P. Dancey, L. A. Drummond, K. Henrick, M. McPartlin, D. K. Uppal, and P. A. Tasker, *J. Chem. Soc., Dalton Trans.*, 3435 (1990).
 K. R. Adam, M. Antolovich, L. G. Brigden, and L. F. Lindoy, *J. Am. Chem. Soc.*, **113**, 3346 (1991).
 K. R. Adam, M. Antolovich, D. S. Baldwin, P. A. Duckworth, A. J. Leong, L. F. Lindoy, M. McPartlin, and P. A. Tasker, *J. Chem. Soc., Dalton Trans.*, 1013 (1993).

- G. Alagona, C. Ghio, and L. Pratesi, *J. Comput. Chem.*, **12**, 934 (1991).
C. Alemán and J. Puiggali, *J. Org. Chem.*, **60**, 910 (1995).
N. L. Allinger and H. von Voitenberg, *Tetrahedron*, **34**, 627 (1978).
N. L. Allinger, Y. Yuh, and J. T. Sprague, *J. Comput. Chem.*, **1**, 30 (1980a).
N. L. Allinger, S. H.-M. Chang, D. H. Glaser, and H. Höning, *Isr. J. Chem.*, **20**, 51 (1980b).
N. L. Allinger, *QCPE Bull.*, **3**, 32 (1983a).
N. L. Allinger and H. L. Flanagan, *J. Comput. Chem.*, **4**, 399 (1983b).
N. L. Allinger and A. Pathiaseril, *J. Comput. Chem.*, **8**, 1225 (1987).
N. L. Allinger, R. A. Kok, and M. R. Imam, *J. Comput. Chem.*, **9**, 591 (1988).
N. L. Allinger, J. A. Allinger, and L. Q. Yan, *J. Mol. Struct. (THEOCHEM)*, **201**, 363 (1989a).
N. L. Allinger, M. I. Quinn, K. Chen, B. Thompson, and M. R. Frierson, *J. Mol. Struct.*, **194**, 1 (1989b).
N. L. Allinger, J. A. Allinger, and L. Q. Yan, *J. Mol. Struct.*, **201**, 363 (1989c).
N. L. Allinger, Y. H. Yuh, and J.-H. Lii, *J. Am. Chem. Soc.*, **111**, 8551, 8566, 8576 (1989d).
N. L. Allinger, M. Rahman, and J.-H. Lii, *J. Am. Chem. Soc.*, **112**, 8293 (1990a).
N. L. Allinger, J. Kuang, and H. D. Thomas, *J. Mol. Struct. (THEOCHEM)*, **209**, 125 (1990b).
N. L. Allinger, K. Chen, M. Rahman, and A. Pathiaseril, *J. Am. Chem. Soc.*, **113**, 4505 (1991a).
N. L. Allinger, M. Quinn, M. Rahman, and K. Chen, *J. Phys. Org. Chem.*, **4**, 647 (1991b).
N. L. Allinger, S. Rodriguez, and K. Chen, *J. Mol. Struct. (THEOCHEM)*, **260**, 161 (1992a).
N. L. Allinger, Z. S. Zhu, and K. Chen, *J. Am. Chem. Soc.*, **114**, 6120 (1992b).
N. L. Allinger, and Y. Fan, *J. Comput. Chem.*, **14**, 655 (1993a).
N. L. Allinger and L. Yan, *J. Am. Chem. Soc.*, **115**, 11918 (1993b).
N. L. Allinger and Y. Fan, *J. Comput. Chem.*, **15**, 251 (1994a).
N. L. Allinger, L. Yan, and K. Chen, *J. Comput. Chem.*, **15**, 1321 (1994b).
N. L. Allinger, X. Zhou, and J. Bergsma, *J. Mol. Struct. (THEOCHEM)*, **312**, 69 (1994c).
N. L. Allinger, K. Chen, and J.-H. Lii, *J. Comput. Chem.*, **17**, 642 (1996a).
N. L. Allinger, K. Chen, J. A. Katzenellenbogen, S. R. Wilson, and G. M. Anstead, *J. Comput. Chem.*, **17**, 747 (1996b).
N. L. Allinger, Y. Fan, and T. Varnali, *J. Phys. Org. Chem.*, **9**, 159 (1996c).
N. L. Allinger and Y. Fan, *J. Comput. Chem.*, **18**, 1827 (1997).
V. S. Allured, C. M. Kelly, and C. R. Landis, *J. Am. Chem. Soc.*, **113**, 1 (1991).
M. E. Amato, K. B. Lipkowitz, G. M. Lombardo, and G. C. Pappalardo, *J. Mol. Struct.*, **372**, 69 (1995).
M. E. Amato, A. Grassi, K. B. Lipkowitz, G. Lombardo, G. C. Pappalardo, and C. Sadun, *J. Inorg. Organomet. Polym.*, **6**, 237 (1996).
K. Andersen, T. Liljefors, K. Gundertoft, J. Perregaard, and K. Bøgesø, *J. Med. Chem.*, **37**, 950 (1994).
K. Andersen, T. Liljefors, J. Hyttel, and J. Perregaard, *J. Med. Chem.*, **39**, 3723 (1996).
D. G. Anderson, V. A. Campbell, G. A. Forsyth, and D. W. H. Rankin, *J. Chem. Soc., Dalton Trans.*, 2125 (1990a).
D. G. Anderson, G. A. Forsyth, and D. W. H. Rankin, *J. Mol. Struct.*, **221**, 45 (1990b).
S. Anderson, R. E. Carter, and T. Drakenberg, *Acta Chem. Scand.*, **B38**, 479 (1984).
K. Ando, K. R. Condroski, K. N. Houk, Y.-D. Wu, S. K. Ly, and L. E. Overman, *J. Org. Chem.*, **63**, 3196 (1998).
F. A. L. Anet and I. Yavari, *Tetrahedron*, **34**, 2879 (1978).
L. Angelucci, L. De Gioia, and P. Fantucci, *Gazz. Chim. Ital.*, **123**, 111 (1993).
K. Angermund, S. Geier, P. W. Jolly, M. Kessler, C. Krüger, and F. Lutz, *Organometallics*, **17**, 2399 (1998).
R. Annunziata, M. Cinquini, F. Cozzi, C. Gennari, and L. Raimondi, *J. Org. Chem.*, **52**, 4674 (1987).
R. Annunziata, M. Benaglia, M. Cinquini, F. Cozzi, and L. Raimondi, *Eur. J. Org. Chem.*, 1823 (1998).
P. Aped, Y. Apeloig, A. Ellencweig, B. Fuchs, I. Goldberg, M. Karni, and E. Tartkovsky, *J. Am. Chem. Soc.*, **109**, 1486 (1987).
P. Aped, L. Schleifer, B. Fuchs, and S. Wolfe, *J. Comput. Chem.*, **10**, 265 (1989).
P. Aped and N. L. Allinger, *J. Am. Chem. Soc.*, **114**, 1 (1992).
J. R. Ascenso, M. A. Santos, J. J. R. Frausto de Silva, M. C. T. A. Vaz, and M. G. B. Drew, *J. Chem. Soc., Perkin Trans. 2*, 2211 (1990).

- W. F. Bailey, A. D. Khanolkar, K. Gavaskar, T. V. Ovaska, K. Rossi, Y. Thiel, and K. B. Wiberg, *J. Am. Chem. Soc.*, **113**, 5720 (1991).
- J. D. Baleja, M. W. Germann, J. H. van de Sande, and B. D. Sykes, *J. Mol. Biol.*, **215**, 411 (1990).
- L. Banci, I. Bertini, P. Carloni, C. Luchinat, and P. L. Orioli, *J. Am. Chem. Soc.*, **114**, 10683 (1992).
- L. Banci, I. Bertini, and G. La Penna, *Proteins: Struct. Funct., Genet.*, **18**, 186 (1994).
- G. Bandoli, M. Nicolini, H. Lumbroso, A. Grassi, and G. C. Pappalardo, *J. Mol. Struct.*, **160**, 297 (1987).
- G. Barbarella, M. Zambianchi, A. Bongini, and L. Antolini, *J. Org. Chem.*, **61**, 4708 (1996).
- V. Barone, G. Capecchi, Y. Brunel, M.-L. D. Andriés, and R. Subra, *J. Comput. Chem.*, **18**, 1720 (1997).
- V. Barone, A. Bencini, M. Cossi, A. Di Matteo, M. Mattesini, and F. Totti, *J. Am. Chem. Soc.*, **120**, 7069 (1998).
- S. E. Barrows, J. W. Storer, C. J. Cramer, A. D. French, and D. G. Truhlar, *J. Comput. Chem.*, **19**, 1111 (1998).
- L. J. Bartolotti, L. G. Pedersen, and P. S. Charifson, *J. Comput. Chem.*, **12**, 1125 (1991).
- J. Baudry and J. C. Smith, *J. Mol. Struct. (THEOCHEM)*, **308**, 103 (1994).
- B. Beagley, N. C. Edge, N. Jaiboon, J. J. James, C. A. McAuliffe, M. S. Thorp, M. Watkinson, A. Whiting, and D. C. Wright, *Tetrahedron*, **52**, 10193 (1996).
- H.-D. Beckhaus, *Chem. Ber.*, **116**, 86 (1983).
- J. Beech, P. J. Cragg, and M. G. B. Drew, *J. Chem. Soc., Dalton Trans.*, 719 (1994).
- T. W. Bell, F. Guzzo, and M. G. B. Drew, *J. Am. Chem. Soc.*, **113**, 3115 (1991).
- L. Belvisi, C. Gennari, G. Poli, C. Scolastico, and B. Salom, *Tetrahedron: Asymmetry*, **4**, 273 (1993).
- L. Belvisi, O. Carugo, and G. Poli, *J. Mol. Struct.*, **318**, 189 (1994).
- U. Berg and R. Gallo, *Acta Chem. Scand.*, **B37**, 661 (1983).
- U. Berg and I. Petterson, *J. Org. Chem.*, **52**, 5177 (1987).
- U. Berg and N. Bladh, *J. Comput. Chem.*, **17**, 396 (1996).
- O. Berger, O. Edholm, and F. Jähnig, *Biophys. J.*, **72**, 2002 (1997).
- A. Bernardi, M. G. Beretta, V. Malatesta, and C. Tosi, *Chem. Phys. Lett.*, **133**, 496 (1987).
- A. Bernardi, A. M. Capelli, C. Gennari, J. M. Goodman, and I. Paterson, *J. Org. Chem.*, **55**, 3576 (1990a).
- A. Bernardi, A. M. Capelli, C. Gennari, and C. Scolastico, *Tetrahedron: Asymmetry*, **1**, 21 (1990b).
- A. Bernardi, A. M. Capelli, A. Comotti, C. Gennari, M. Gardner, J. M. Goodman, and I. Paterson, *Tetrahedron*, **47**, 3471 (1991).
- A. Bernardi, A. Cassinari, A. Comotti, M. Gardner, G. Gennari, J. M. Goodman, and I. Paterson, *Tetrahedron*, **48**, 4183 (1992).
- A. Bernardi and L. Raimondi, *J. Org. Chem.*, **60**, 3370 (1995).
- P. V. Bernhardt and P. Comba, *Inorg. Chem.*, **31**, 2638 (1992).
- P. V. Bernhardt and P. Comba, *Inorg. Chem.*, **32**, 2798 (1993).
- P. V. Bernhardt, R. Bramley, L. M. Engelhardt, J. M. Harrowfield, D. C. R. Hockless, B. R. Korybut-Daszkiewicz, E. R. Krausz, T. Morgan, A. M. Sargeson, B. W. Skelton, and A. H. White, *Inorg. Chem.*, **34**, 3589 (1995).
- W. Bernlöhr, H.-D. Beckhaus, H.-G. von Schnering, and C. Rüchardt, *Chem. Ber.*, **117**, 1013 (1984).
- M. P. Bertrand, I. DeRiggi, C. Lesueur, S. Gastaldi, R. Nouguier, C. Jaime, and A. Virgili, *J. Org. Chem.*, **60**, 6040 (1995).
- S. E. Biali, M. Gozin, and Z. Rappoport, *J. Phys. Org. Chem.*, **2**, 271 (1989).
- U. Bierbach, T. W. Hambley, and N. Farrell, *Inorg. Chem.*, **37**, 708 (1998).
- S. R. Billetter and W. F. van Gunsteren, *J. Phys. Chem. B*, **102**, 4669 (1998).
- R. D. Bindal, J. T. Golab, and J. A. Katzenellenbogen, *J. Am. Chem. Soc.*, **112**, 7861 (1990).
- J. F. Blount, F. Cozzi, J. R. Damewood Jr., L. D. Iroff, U. Sjöstrand, and K. Mislow, *J. Am. Chem. Soc.*, **102**, 99 (1980).
- J. C. A. Boeyens and F. M. M. O'Neill, *Inorg. Chem.*, **34**, 1988 (1995).
- J. C. A. Boeyens and F. M. M. O'Neill, *Inorg. Chem.*, **37**, 5346 (1998a).
- J. C. A. Boeyens and F. M. M. O'Neill, *Inorg. Chem.*, **37**, 5352 (1998b).
- K. Bøgesø, T. Liljefors, J. Arnt, J. Hyttel, and H. Pedersen, *J. Med. Chem.*, **34**, 2023 (1991).

- J. E. Bol, C. Buning, P. Comba, J. Reedijk, and M. Ströhle, *J. Comput. Chem.*, **19**, 512 (1998).
- A. M. Bond, T. W. Hambley, and M. R. Snow, *Inorg. Chem.*, **24**, 1920 (1985).
- N. L. Borkar, C. A. Kingsbury, and E. P. Rack, *J. Mol. Struct.*, **178**, 287 (1988).
- B. Botta, G. D. Monache, M. C. DeRosa, C. Seri, E. Benetti, R. Iacovino, M. Botta, F. Corelli, V. Massignani, A. Tafi, E. Gacs-Baitz, A. Santini, and D. Misiti, *J. Org. Chem.*, **62**, 1788 (1997).
- A. Bouraoui, M. Fathallah, B. Blaive, R. Gallo, and F. M'Henni, *J. Chem. Soc., Perkin Trans. 2*, 1211 (1990a).
- A. Bouraoui, M. Fathallah, F. M'Henni, B. Blaive, and R. Gallo, [in *Modeling of Molecular Structures and Properties*, Proceedings of International Meeting, Nancy, France, September 11–15, 1989, J.-L. Rivail, Ed.,] *Stud. Phys. Theor. Chem.*, **71**, 381 (1990b).
- J. P. Bowen and N. L. Allinger, *J. Org. Chem.*, **52**, 1830 (1987a).
- J. P. Bowen and N. L. Allinger, *J. Org. Chem.*, **52**, 2937 (1987b).
- J. P. Bowen, A. Pathiaseril, S. Profeta Jr., and N. L. Allinger, *J. Org. Chem.*, **52**, 5162 (1987c).
- J. P. Bowen, V. V. Reddy, D. G. Patterson Jr., and N. L. Allinger, *J. Org. Chem.*, **53**, 5471 (1988).
- J. P. Bowen, M. Kontoyianni, E. L. Stewart, and A. J. Hoffman, *QCPE Bull.*, **13**, 71 (1993).
- D. B. Boyd and R. D. Coner, *J. Mol. Struct. (THEOCHEM)*, **368**, 7 (1996).
- E. V. Brandt, J. P. Steynberg, and D. Fereira, in *Plant Polyphenols*, R. W. Hemingway and P. E. Lakes, Eds., Plenum Press, New York, pp. 487–493, 1992.
- P. Brandt, T. Norrby, B. Åkermark, and P.-O. Norrby, *Inorg. Chem.*, **37**, 4120 (1998).
- D. J. Brechnell, D. J. Raber, and D. M. Ferguson, *J. Mol. Struct. (THEOCHEM)*, **124**, 343 (1985).
- M. Breuer and G. Häggele, *Comput. Chem.*, **13**, 123 (1989).
- G. Brink and L. Glasser, *J. Phys. Chem.*, **94**, 981 (1990).
- G. Brink and L. Glasser, *J. Mol. Struct.*, **224**, 277 (1991).
- J. L. Broeker, R. W. Hoffmann, and K. N. Houk, *J. Am. Chem. Soc.*, **113**, 5006 (1991a).
- J. L. Broeker and K. N. Houk, *J. Org. Chem.*, **56**, 3651 (1991b).
- B. R. Brooks, R. E. Bruccoleri, B. D. Olafson, D. J. States, S. Swaminathan, and M. Karplus, *J. Comput. Chem.*, **4**, 187 (1983).
- A. B. Brown and H. W. Whitlock Jr., *J. Am. Chem. Soc.*, **111**, 3640 (1989).
- F. K. Brown and K. N. Houk, *J. Am. Chem. Soc.*, **107**, 1971 (1985).
- K. L. Brown, X. Zou, and H. M. Marques, *J. Mol. Struct. (THEOCHEM)*, **453**, 209 (1998).
- T. L. Brown, *Inorg. Chem.*, **31**, 1286 (1992).
- E. Brunet, A. M. Poveda, D. Rabasco, E. Oreja, L. M. Font, M. S. Batra, and J. C. Rodríguez-Ubis, *Tetrahedron: Asymmetry*, **5**, 935 (1994).
- L. H. Bryant Jr., A. Lachgar, and S. Jackels, *Inorg. Chem.*, **34**, 4230 (1995).
- D. A. Buckingham and A. M. Sargeson, *Top. Stereochem.*, **6**, 219 (1970).
- D. A. Buckingham, P. J. Cresswell, R. J. Dellaca, M. Dwyer, G. J. Gainsford, L. G. Marzilli, I. E. Maxwell, W. T. Robinson, A. M. Sargeson, and K. R. Turnbull, *J. Am. Chem. Soc.*, **96**, 1713 (1974).
- L. M. Bull, N. J. Henson, A. K. Cheetham, J. M. Newsam, and S. J. Heyes, *J. Phys. Chem.*, **97**, 11776 (1993).
- K. Burgess, K.-K. Ho, and B. Pal, *J. Am. Chem. Soc.*, **117**, 3808 (1995).
- U. Burkert, *Tetrahedron*, **35**, 209 (1945) (1979).
- K. Byström, *J. Comput. Chem.*, **4**, 308 (1983).
- M. L. Caffery and T. L. Brown, *Inorg. Chem.*, **30**, 3907 (1991).
- R. Caminiti, M. Gleria, K. B. Lipkowitz, G. M. Lombardo, and G. C. Pappalardo, *J. Am. Chem. Soc.*, **119**, 2196 (1997).
- C. R. Canales and M. Zimmer, *J. Mol. Struct.*, **245**, 341 (1991).
- J. F. Cannon, *J. Comput. Chem.*, **14**, 995 (1993).
- W. R. Cannon, B. M. Pettitt, and J. A. McCammon, *J. Phys. Chem.*, **98**, 6225 (1994).
- F. H. Cano, C. Foces-Foces, J. Jiménez-Barbero, A. Alemany, M. Bernabe, and M. Martin-Lomas, *Tetrahedron*, **42**, 2539 (1986).
- F. H. Cano, C. Foces-Foces, J. Jiménez-Barbero, A. Alemany, M. Bernabe, and M. Martin-Lomas, *J. Chem. Soc., Perkin Trans. 2*, 791 (1987).
- L. Carballera, R. A. Mosquera, and M. A. Ríos, *J. Comput. Chem.*, **9**, 851 (1988).
- L. Carballera, R. A. Mosquera, and M. A. Ríos, *J. Comput. Chem.*, **10**, 911 (1989).
- L. Carballera, A. J. Pereiras, and M. A. Ríos, *J. Comput. Chem.*, **11**, 734 (1990).

- S. W. Carrigan, J.-H. Lii, and J. P. Bowen, *J. Comput.-Aided Mol. Des.*, **11**, 61 (1997).
R. E. Carter and T. Liljefors, *Tetrahedron*, **32**, 2915 (1976).
C. P. Casey and L. M. Petrovich, *J. Am. Chem. Soc.*, **117**, 6007 (1995).
J. Castells, C. Jaime, F. Lopez-Calaborda, N. Santalo, and D. Velasco, *J. Org. Chem.*, **53**, 5363 (1988).
L. A. Castonguay, A. K. Rappé, and C. J. Casewit, *J. Am. Chem. Soc.*, **113**, 7177 (1991).
L. A. Castonguay and A. K. Rappé, *J. Am. Chem. Soc.*, **114**, 5832 (1992a).
L. A. Castonguay, J. W. Guiles, A. K. Rappé, and A. I. Meyers, *J. Org. Chem.*, **57**, 3819 (1992b).
S. J. Chakravorty, R. E. Hormann, and C. H. Reynolds, Abstracts of the 216th American Chemical Society National Meeting, Boston, MA, August 23–27, (1998, COMP 114).
H. M. Chang, B. B. Mase, and D. A. Dougherty, *J. Am. Chem. Soc.*, **107**, 1124 (1985).
S. Chang, D. McNally, S. Shary-Tehrany, M. J. Hickey, and R. H. Boyd, *J. Am. Chem. Soc.*, **92**, 3109 (1970).
R. Charles, M. Ganly-Cunningham, R. Warren, and M. Zimmer, *J. Mol. Struct.*, **265**, 385 (1992).
D. C. Chatfield, A. Szabo, and B. R. Brooks, *J. Am. Chem. Soc.*, **120**, 5301 (1998).
K. Chen and N. L. Allinger, *J. Comput. Chem.*, **14**, 755 (1993).
K. Chen and N. L. Allinger, *J. Phys. Org. Chem.*, **10**, 697 (1997).
X. Chen, L. Bartolotti, K. Ishaq, and A. Tropsha, *J. Comput. Chem.*, **15**, 333 (1994).
M. Chhiba and G. Vergoten, *J. Mol. Struct.*, **326**, 35 (1994).
M. Chhiba, F. Tristram, and G. Vergoten, *J. Mol. Struct.*, **405**, 113 (1997).
C. Chipot, P. A. Kollman, and D. A. Pearlman, *J. Comput. Chem.*, **17**, 1112 (1996a).
C. Chipot, R. Jaffe, B. Maigret, D. A. Pearlman, and P. A. Kollman, *J. Am. Chem. Soc.*, **118**, 11217 (1996b).
S. G. Cho, R. J. Unwalla, F. K. Cartledge, and S. Profeta Jr., *J. Comput. Chem.*, **10**, 832 (1989).
S. G. Cho, R. J. Unwalla, F. K. Cartledge, and S. Profeta Jr., *J. Mol. Struct. (THEOCHEM)*, **204**, 79 (1990a).
S. G. Cho, F. K. Cartledge, R. J. Unwalla, and S. Profeta Jr., *Tetrahedron*, **46**, 8005 (1990b).
S. G. Cho and O. K. Rim, *Bull. Korean Chem. Soc.*, **15**, 509 (1994).
S. G. Cho, *J. Organomet. Chem.*, **510**, 25 (1996a).
S. G. Cho, *J. Mol. Struct. (THEOCHEM)*, **364**, 59 (1996b).
S. G. Cho and G. Park, *Bull. Korean Chem. Soc.*, **18**, 143 (1997).
M.-G. Choi and T. L. Brown, *Inorg. Chem.*, **32**, 5603 (1993a).
M.-G. Choi and T. L. Brown, *Inorg. Chem.*, **32**, 1548 (1993b).
M.-G. Choi, D. White, and T. L. Brown, *Inorg. Chem.*, **33**, 5591 (1994).
J. Choo, J. Laane, R. Majors, and J. R. Villarreal, *J. Am. Chem. Soc.*, **115**, 8396 (1993).
P. Cieplak and P. A. Kollman, *J. Comput. Chem.*, **12**, 1232 (1991).
R. Cini, S. J. Moore, and L. G. Marzilli, *Inorg. Chem.*, **37**, 6890 (1998).
M. Clark, R. D. Cramer III, and N. Van Opdenbosch, *J. Comput. Chem.*, **10**, 982 (1989).
T. Cleveland and C. R. Landis, *J. Am. Chem. Soc.*, **118**, 6020 (1996).
J. R. Collins, D. L. Camper, and G. H. Loew, *J. Am. Chem. Soc.*, **113**, 2736 (1991).
W. J. Colucci, R. D. Gandom, and E. Mooberry, *J. Am. Chem. Soc.*, **108**, 7141 (1986).
P. Comba and M. Zimmer, *Inorg. Chem.*, **33**, 5368 (1994).
P. Comba, T. W. Hambley, M. A. Hitchman, and H. Stratermeier, *Inorg. Chem.*, **34**, 3903 (1995).
P. Comba, A. Fath, A. Kühner, and B. Nuber, *J. Chem. Soc., Dalton Trans.*, 1889 (1997a).
P. Comba, P. Hilfenhaus, and K. Karlin, *Inorg. Chem.*, **36**, 2309 (1997b).
P. Comba and H. Jakob, *Helv. Chim. Acta*, **80**, 1983 (1997c).
P. Comba and A. F. Sickmüller, *Inorg. Chem.*, **36**, 4500 (1997d).
P. Comba, K. Gloe, K. Inoue, T. Krüger, H. Stephan, and K. Yoshizuka, *Inorg. Chem.*, **37**, 3310 (1998a).
P. Comba, R. Cusack, D. P. Fairlie, L. R. Gahan, G. R. Hanson, U. Kazmaier, and A. Ramlow, *Inorg. Chem.*, **37**, 6721 (1998b).
E. J. Corey and J. W. Ponder, *Tetrahedron Lett.*, **25**, 4325 (1984).
W. D. Cornell, P. Cieplak, C. I. Bayly, and P. A. Kollman, *J. Am. Chem. Soc.*, **115**, 9620 (1993).
W. D. Cornell, P. Cieplak, C. I. Bayly, I. R. Gould, K. M. Merz Jr., D. M. Ferguson, D. C. Spellmeyer, T. Fox, J. W. Caldwell, and P. A. Kollman, *J. Am. Chem. Soc.*, **117**, 5179 (1995).
W. D. Cornell, J. W. Caldwell, and P. A. Kollman, *J. Chim. Phys.*, **94**, 1417 (1997).
E. Cortez, R. Verastegui, J. Villarreal, and J. Laane, *J. Am. Chem. Soc.*, **115**, 12132 (1993).
A. Cossé-Barbi, C. R. Acad. Sci. Paris, **318**, Ser. II, 461 (1994).

- J. Costante-Crassous, T. J. Marrone, J. M. Briggs, J. A. McCammon, and A. Collet, *J. Am. Chem. Soc.*, **119**, 3818 (1997).
- D. C. Crans and J. P. Snyder, *Chem. Ber.*, **113**, 1201 (1980).
- I. I. Creaser, T. Komorita, A. M. Sargeson, A. C. Willis, and K. Yamanari, *Aust. J. Chem.*, **47**, 529 (1994).
- M. Cristina, A. Costa, and Y. Takahata, *J. Comput. Chem.*, **18**, 712 (1997).
- P. L. Cummins and J. E. Gready, *J. Comput. Chem.*, **15**, 704 (1994).
- T. R. Cundari, L. L. Sisterhen, and C. Stylianopoulos, *Inorg. Chem.*, **36**, 4029 (1997).
- J. Cuntze, L. Owens, V. Alcázar, P. Seiler, and F. Diederich, *Helv. Chim. Acta*, **78**, 367 (1995).
- D. P. Curran and N. C. DeMello, *J. Chem. Soc., Chem. Commun.*, 1314 (1993).
- J. R. Damewood Jr. and R. West, *Macromolecules*, **18**, 159 (1985).
- J. R. Damewood Jr., W. P. Anderson, and J. J. Urban, *J. Comput. Chem.*, **9**, 111 (1988).
- J. R. Damewood Jr., R. A. Kumpf, C. F. Mühlbauer, J. J. Urban, and J. E. J. Eksterowicz, *J. Phys. Chem.*, **94**, 6619 (1990).
- W. Damm, A. Frontera, J. Tirado-Rives, and W. L. Jorgensen, *J. Comput. Chem.*, **18**, 1955 (1997).
- X. Daura, P. H. Hünenberger, A. E. Mark, E. Querol, F. X. Avilés, and W. F. van Gunsteren, *J. Am. Chem. Soc.*, **118**, 6285 (1996).
- X. Daura, A. E. Mark, and W. F. van Gunsteren, *J. Comput. Chem.*, **19**, 535 (1998).
- S. E. DeBolt and P. A. Kollman, *J. Am. Chem. Soc.*, **117**, 5316 (1995).
- C. Decoret, B. Tinland, and G. Bertholon, *J. Mol. Struct. (THEOCHEM)*, **124**, 269 (1985).
- J. A. Deiters, J. C. Gallucci, T. E. Clark, and R. R. Holmes, *J. Am. Chem. Soc.*, **99**, 5461 (1977).
- J. A. Deiters, J. C. Gallucci, and R. R. Holmes, *J. Am. Chem. Soc.*, **104**, 5457 (1982).
- J. A. Deiters and R. R. Holmes, *J. Am. Chem. Soc.*, **106**, 3307 (1984).
- P. M. T. de Kok, N. A. Neijer, H. M. Buck, L. A. Æ. Sluyterman, and E. M. Meijer, *Recl. Trav. Chim. Pays-Bas*, **107**, 355 (1988).
- D. Delpeyroux, B. Blaive, R. Gallo, H. Grindorge, and P. Lescop, *Propellants, Explosives, Pyrotechnics*, **19**, 70 (1994).
- L. Deng, T. Ziegler, T. K. Woo, P. Margl, and L. Fan, *Organometallics*, **17**, 3240 (1998).
- B. de Pascual-Teresa, J. Gallego, A. R. Ortiz, and F. Gago, *J. Med. Chem.*, **39**, 4810 (1996).
- I. De Riggi, R. Nouguier, J. M. Surzur, C. Lesueur, M. Bertrand, C. Jaime, and A. Virgili, *Bull. Soc. Chim.*, **130**, 229 (1993).
- P. Derreumaux, M. Dauchez, and G. Vergoten, *J. Mol. Struct.*, **295**, 203 (1993a).
- P. Derreumaux, P. Lagant, and G. Vergoten, *J. Mol. Struct.*, **295**, 223 (1993b).
- P. Derreumaux and G. Vergoten, *J. Mol. Struct.*, **295**, 233 (1993c).
- P. Derreumaux and G. Vergoten, *J. Chem. Phys.*, **102**, 8586 (1995).
- R. Dharanipragada, S. B. Ferguson, and F. Diederich, *J. Am. Chem. Soc.*, **110**, 1679 (1988).
- R. W. Dixon and P. A. Kollman, *J. Comput. Chem.*, **18**, 1632 (1997).
- H. Dodziuk, H. von Voitenberg, and N. L. Allinger, *Tetrahedron*, **38**, 2811 (1982).
- H. Dodziuk, *Bull. Polish Acad. Sci.*, **34**, 34, 49 (1986).
- T. N. Doman, C. R. Landis, and B. Bosnich, *J. Am. Chem. Soc.*, **114**, 7264 (1992).
- O. Donini and D. F. Weaver, *J. Comput. Chem.*, **19**, 1515 (1998).
- A. E. Dorigo and K. N. Houk, *J. Am. Chem. Soc.*, **109**, 3698 (1987).
- A. E. Dorigo and K. N. Houk, *J. Org. Chem.*, **53**, 1650 (1988).
- L. Dósen-Micovic, D. Jeremic, and N. L. Allinger, *J. Am. Chem. Soc.*, **105**, 1716, 1723 (1983).
- L. Dósen-Micovic, D. Jeremic, and N. L. Allinger, *J. Am. Chem. Soc.*, **107**, 3741 (1985).
- L. Dósen-Micovic and B. Solaja, *J. Chem. Soc., Perkin Trans. 2*, 585 (1993).
- M. G. B. Drew, D. A. Rice, S. B. Silong, and P. C. Yates, *J. Chem. Soc., Dalton Trans.*, 1081 (1986).
- M. G. B. Drew and P. C. Yates, *J. Chem. Soc., Dalton Trans.*, 2563 (1987).
- M. G. B. Drew, W. W. A. Hopkins, and P. C. H. Mitchell, *J. Chem. Soc., Faraday Trans.*, **86**, 47 (1990).
- M. G. B. Drew, N. J. Jutson, P. C. H. Mitchell, R. J. Potter, and D. Thompsett, *J. Chem. Soc., Faraday Trans.*, **89**, 3963 (1993).
- E. M. Duffy, D. L. Severance, and W. L. Jorgensen, *Isr. J. Chem.*, **33**, 323 (1993).
- K. A. Durkin, M. J. Sherrod, and D. Liotta, *J. Org. Chem.*, **54**, 5839 (1989).
- J. E. Eksterowicz, J. L. Miller, and P. A. Kollman, *J. Phys. Chem. B*, **101**, 10971 (1997).

- J. F. Endicott, K. Kumar, C. L. Schwarz, M. W. Perkovic, and W.-K. Li, *J. Am. Chem. Soc.*, **111**, 7411 (1989).
- S. B. Engelsen and K. Rasmussen, *Int. J. Biol. Macromol.*, **15**, 56 (1993).
- S. B. Engelsen, J. Fabricius, and K. Rasmussen, *Acta Chem. Scand.*, **48**, 553 (1994).
- A. W. Espinosa-Müller and A. N. Bravo, *J. Mol. Struct. (THEOCHEM)*, **90**, 187 (1982).
- A. W. Espinosa-Müller and A. N. Bravo, *J. Mol. Struct. (THEOCHEM)*, **110**, 349 (1994).
- K. P. Eurenius and K. N. Houk, *J. Am. Chem. Soc.*, **116**, 9943 (1994).
- T. J. A. Ewing and T. P. Lybrand, *J. Phys. Chem.*, **98**, 1748 (1994).
- J. Fabricius, S. B. Engelsen, and K. Rasmussen, *New J. Chem.*, **19**, 1123 (1995).
- J. Fabricius, S. B. Engelsen, and K. Rasmussen, *J. Carbohydr. Chem.*, **16**, 751 (1997).
- H. Falk, G. Hollbacher, O. Höfer, and N. Müller, *Monatsh. Chem.*, **112**, 391 (1981).
- H. Falk and N. Müller, *Tetrahedron*, **39**, 1875 (1983).
- C. F. Fan, T. Cagin, Z. M. Chen, and K. A. Smith, *Macromolecules*, **27**, 2383 (1994).
- Y. Fan and N. L. Allinger, *J. Comput. Chem.*, **15**, 1446 (1995).
- Y. Fan, J. N. Weinstein, K. W. Kohn, L. M. Shi, and Y. Pommier, *J. Med. Chem.*, **41**, 2216 (1998).
- R. Fausto, J. C. C. Teixeira-Dias, and P. R. Carey, *J. Mol. Struct.*, **159**, 137 (1987).
- R. Fausto, J. C. C. Teixeira-Dias, and P. R. Carey, *J. Mol. Struct.*, **212**, 61 (1989).
- S. E. Feller, D. Yin, R. W. Pastor, and A. D. MacKerell Jr., *Bioophys. J.*, **73**, 2269 (1997).
- D. M. Ferguson and P. A. Kollman, *J. Comput. Chem.*, **12**, 620 (1991).
- B. Fernández, M. A. Ríos, and L. Carballeira, *J. Comput. Chem.*, **12**, 78 (1991).
- B. Fernández and M. A. Ríos, *J. Comput. Chem.*, **15**, 455 (1994).
- D. R. Ferro, J. Gajdos, M. Ragazzi, F. Ungarelli, and S. Piani, *Carbohydr. Res.*, **277**, 25 (1995).
- D. R. Ferro, P. Pumilia, and M. Ragazzi, *J. Comput. Chem.*, **18**, 351 (1997).
- K. Fidelis, M. B. Hossain, M. A. F. Jalal, and D. van der Helm, *Acta Crystallogr.*, **C46**, 1612 (1990).
- D. Filipovic, M. D. Paulsen, P. J. Loida, S. G. Sligar, and R. L. Ornstein, *Biochem. Biophys. Res. Commun.*, **189**, 488 (1992).
- S. Fischer, P. D. J. Grootenhuis, L. C. Groenen, W. P. van Hoorn, F. C. J. M. van Veggel, D. N. Reinhoudt, and M. Karplus, *J. Am. Chem. Soc.*, **117**, 1611 (1995).
- N. Foloppe, M. Ferrand, J. Breton, and J. C. Smith, *Proteins: Struct., Funct., Genet.*, **22**, 226 (1995).
- G. A. Forsyth and D. W. H. Rankin, *J. Mol. Struct.*, **222**, 467 (1990).
- R. Fossheim, H. Dugstadt, and S. V. Dahl, *J. Med. Chem.*, **34**, 819 (1991).
- P. C. Fox, J. P. Bowen, and N. L. Allinger, *J. Am. Chem. Soc.*, **114**, 8536 (1992).
- T. Fox, B. E. Thomas IV, M. McCarrick, and P. A. Kollman, *J. Phys. Chem.*, **100**, 10779 (1996).
- T. Fox, T. S. Scanlan, and P. A. Kollman, *J. Am. Chem. Soc.*, **119**, 11571 (1997).
- T. Fox and P. A. Kollman, *J. Phys. Chem. B*, **102**, 8070 (1998).
- S. T. Frey, A. Chang, J. F. Carvalho, A. Varadarajan, L. M. Schultze, K. L. Pounds, and W. DeW. Horrocks Jr., *Inorg. Chem.*, **33**, 2882 (1994).
- M. R. Frierson, M. R. Imam, V. B. Zalkow, and N. L. Allinger, *J. Org. Chem.*, **53**, 5248 (1988).
- M. R. Frierson and N. L. Allinger, *J. Phys. Org. Chem.*, **2**, 573 (1989).
- M. Froimowitz and P. A. Kollman, *J. Comput. Chem.*, **5**, 507 (1984a), and *QCPE Bull.*, **3**, 36 (1983).
- M. Froimowitz, P. Salva, G. J. Hite, G. Gianutso, P. Suzdak, and R. Heyman, *J. Comput. Chem.*, **5**, 291 (1984b).
- M. Froimowitz, C. M. DiMeglio, and A. Makriyannis, *J. Med. Chem.*, **35**, 3085 (1992).
- M. Froimowitz and V. Cody, *J. Med. Chem.*, **36**, 2219 (1993).
- J. A. Fruetel, J. R. Collins, D. L. Camper, G. H. Loew, and P. R. Ortiz de Montellano, *J. Am. Chem. Soc.*, **114**, 6987 (1992).
- Y. Fukazawa, S. Usui, and Y. Uchio, *Tetrahedron Lett.*, **27**, 1825 (1986).
- Y. Fukazawa, Y. Takeda, S. Usui, and M. Kodama, *J. Am. Chem. Soc.*, **110**, 7842, 7847 (1988).
- G. Fulcrand-El Kattan, Z. J. Lesinkowski, S. Yao, F. Tanious, W. D. Wilson, and R. F. Schinazi, *J. Am. Chem. Soc.*, **116**, 7494 (1994).
- M. M. Fuson and M. D. Ediger, *Macromolecules*, **30**, 5704 (1997).
- R. R. Gabdoulline, G. Vanderkooi, and C. Zheng, *J. Phys. Chem.*, **100**, 15942 (1996).
- K. Gaedt and H.-D. Höltje, *J. Comput. Chem.*, **19**, 935 (1998).
- J. J. Gajewski, K. E. Gilbert, and T. W. Kreek, *J. Comput. Chem.*, **19**, 1167 (1998).
- M. T. Gallego, E. Brunet, J. L. G. Ruano, and E. L. Eliel, *J. Org. Chem.*, **58**, 3905 (1993).

- R. Garduño-Járez and E. Ocampo-Garcia, *Comput. Chem.*, **13**, 117 (1989).
 V. Gasmi, G. Robinet, M. Barthelat, and J. Devillers, *Struct. Chem.*, **2**, 621 (1991).
 A. Gavezzotti, G. Filippini, J. Kroon, B. P. van Eijck, and P. Klewinghaus, *Chem. Eur. J.*, **3**, 893 (1997).
 C. Gennari, C. T. Hewkin, F. Molinari, A. Bernardi, A. Comotti, J. M. Goodman, and I. Paterson, *J. Org. Chem.*, **57**, 5173 (1992).
 C. Gennari, E. Fioravanzo, A. Bernardi, and A. Vulpetti, *Tetrahedron*, **50**, 8815 (1994).
 C. Gennari, B. Salom, D. Potena, C. Longari, E. Fioravanzo, O. Carugo, and N. Sardone, *Chem. Eur. J.*, **2**, 644 (1996).
 S. Geremia, L. Vicentini, and M. Calligaris, *Inorg. Chem.*, **37**, 4094 (1998).
 J. S. Giovannetti, C. M. Kelly, and C. R. Landis, *J. Am. Chem. Soc.*, **115**, 4040 (1993).
 D. Gleich, R. Schmid, and W. A. Herrmann, *Organometallics*, **17**, 4828 (1998).
 T. M. Glennon, Y.-J. Zheng, S. M. LeGrand, B. A. Shutzberg, and K. M. Merz Jr., *J. Comput. Chem.*, **15**, 1019 (1994).
 D. J. Goldsmith, J. P. Bowen, E. Qamhiyeh, and W. C. Still, *J. Org. Chem.*, **52**, 951 (1987).
 E. Goldstein and N. L. Allinger, *J. Mol. Struct. (THEOCHEM)*, **188**, 149 (1989).
 E. Goldstein, B. Ma, J.-H. Lii, and N. L. Allinger, *J. Phys. Org. Chem.*, **9**, 191 (1996).
 J. M. Goodman, I. Paterson, and S. D. Kahn, *Tetrahedron Lett.*, **28**, 5290 (1987).
 J. M. Goodman, S. D. Kahn, and I. Paterson, *J. Org. Chem.*, **55**, 3295 (1990).
 J. M. Goodman, J. J. James, and A. Whiting, *J. Chem. Soc., Perkin Trans. 2*, 109 (1994).
 A. Grassi, G. M. Lombardo, and G. C. Pappalardo, *J. Mol. Struct. (THEOCHEM)*, **311**, 101 (1994).
 R. Gratias and H. Kessler, *J. Phys. Chem. B*, **102**, 2027 (1998).
 M. M. Green, B. A. Boyle, M. Vairamani, T. Mukhopadhyay, W. H. Saunders Jr., J. P. Bowen, and N. L. Allinger, *J. Am. Chem. Soc.*, **108**, 2381 (1986).
 R. Griffith, J. B. Bremner, and S. J. Titmuss, *J. Comput. Chem.*, **18**, 1211 (1997).
 S. Grigoras and T. H. Lane, *J. Comput. Chem.*, **9**, 25 (1988).
 T. B. Grindley, A. Cude, J. Kralovic, and R. Thangarasa, in *Levoglucosanome and Levoglucosans, Chemistry and Applications*, Z. J. Witczak, Ed., ATL Press, Shrewsbury, MA, 1994.
 L. C. Groenen, J. A. J. Brunink, W. I. I. Bakker, S. Harkema, S. S. Wijmenga, and D. N. Reinhoudt, *J. Chem. Soc., Perkin Trans. 2*, 1899 (1992).
 P. D. J. Grootenhuis and P. A. Kollman, *J. Am. Chem. Soc.*, **111**, 2152 (1989a).
 P. D. J. Grootenhuis and P. A. Kollman, *J. Am. Chem. Soc.*, **111**, 4046 (1989b).
 P. D. J. Grootenhuis, P. A. Kollman, L. C. Groenen, D. N. Reinhoudt, G. J. van Hummel, F. Ugozzoli, and G. D. Andreetti, *J. Am. Chem. Soc.*, **112**, 4165 (1990).
 P. D. J. Grootenhuis and C. A. G. Haasnoot, *Mol. Simul.*, **10**, 75 (1993).
 P. Gueu, A. Proutiere, V. Quiroa, and H. Bodot, *J. Chim. Phys.*, **85**, 361 (1988).
 M. M. Gugelchuk and K. N. Houk, *J. Am. Chem. Soc.*, **116**, 330 (1994).
 W. C. Guida, R. S. Bohacek, and M. D. Erion, *J. Comput. Chem.*, **13**, 214 (1992).
 P. Guilbaud and G. Wipff, *J. Phys. Chem.*, **97**, 5685 (1993).
 P. Guilbaud and G. Wipff, *New J. Chem.*, **20**, 631 (1996).
 S. N. Ha, A. Giammona, M. Field, and J. W. Brady, *Carbohydr. Res.*, **180**, 207 (1988).
 F. Häffner, T. Brinck, M. Haeberlein, and C. Moberg, *J. Mol. Struct. (THEOCHEM)*, **397**, 39 (1997).
 F. Häffner, T. Norin, and K. Hult, *Biophys. J.*, **74**, 1251 (1998).
 T. A. Halgren, *J. Am. Chem. Soc.*, **114**, 7827 (1992).
 T. A. Halgren, *J. Comput. Chem.*, **17**, 490 (1996a).
 T. A. Halgren, *J. Comput. Chem.*, **17**, 520 (1996b).
 T. A. Halgren, *J. Comput. Chem.*, **17**, 553 (1996c).
 T. A. Halgren, *J. Comput. Chem.*, **17**, 587 (1996d).
 T. A. Halgren, *J. Comput. Chem.*, **17**, 616 (1996e).
 T. W. Hambley, C. J. Hawkins, J. A. Palmer, and M. R. Snow, *Aust. J. Chem.*, **34**, 45 (1980).
 T. W. Hambley and M. R. Snow, *Inorg. Chem.*, **25**, 1378 (1986).
 T. W. Hambley, *J. Comput. Chem.*, **8**, 651 (1987).
 T. W. Hambley, *Inorg. Chem.*, **27**, 1073 (1988).
 L. G. Hammerström, T. Liljefors, and J. Gasteiger, *J. Comput. Chem.*, **9**, 424 (1988).
 R. D. Hancock, S. M. Dobson, A. Evers, P. W. Wade, M. P. Ngwenya, J. C. A. Boeyens, and K. P. Wainwright, *J. Am. Chem. Soc.*, **110**, 2788 (1988).
 R. D. Hancock, J. S. Weaving, and H. M. Marques, *J. Chem. Soc., Chem. Commun.*, 1176 (1989).

- R. D. Hancock, *J. Inclusion Phenom. Mol. Recognit.*, **17**, 63 (1994).
R. D. Hancock, D. E. Reichert, and M. J. Welch, *Inorg. Chem.*, **35**, 2165 (1996).
B. A. Hanson and J. D. White, *J. Am. Chem. Soc.*, **110**, 6314 (1988).
C. Harding, D. McDowell, J. Nelson, S. Raghunathan, C. Stevenson, M. G. B. Drew, and P. C. Yates, *J. Chem. Soc., Dalton Trans.*, 2521 (1990).
D. Harris and G. Loew, *J. Am. Chem. Soc.*, **117**, 2739 (1995).
C. J. Hartzell, R. T. Cygan, and K. L. Nagy, *J. Phys. Chem. A*, **102**, 6722 (1998).
W. L. Hase, M.-C. Richou, and S. L. Mondro, *J. Phys. Chem.*, **93**, 539 (1989).
A. Hassner, A. S. Amarasekara, A. Padwa, and W. H. Bullock, *Tetrahedron Lett.*, **29**, 715 (1988).
B. P. Hay, *Inorg. Chem.*, **30**, 1991 (1991).
B. P. Hay, J. R. Rustad, and C. J. Hostettler, *J. Am. Chem. Soc.*, **115**, 11158 (1993).
B. P. Hay and J. R. Rustad, *J. Am. Chem. Soc.*, **116**, 6316 (1994).
B. P. Hay, D. Zhang, and J. R. Rustad, *Inorg. Chem.*, **35**, 2650 (1996).
B. P. Hay, L. Yang, D. Zhang, J. R. Rustad, and E. Wasserman, *J. Mol. Struct. (THEOCHEM)*, **417**, 19 (1997).
B. P. Hay, O. Clement, G. Sandrone, and D. A. Dixon, *Inorg. Chem.*, **37**, 5887 (1998a).
B. P. Hay, L. Yang, J.-H. Lii, and N. L. Allinger, *J. Mol. Struct. (THEOCHEM)*, **428**, 203 (1998b).
F. Heffner, T. Brinck, M. Haeberlein, and C. Moberg, *J. Mol. Struct. (THEOCHEM)*, **397**, 39 (1997).
K. Hegetschweiler, R. D. Hancock, M. Ghisletta, T. Kradolfer, V. Gramlich, and W. H. Schmalle, *Inorg. Chem.*, **32**, 5273 (1993).
J. Helfrich, R. Hentschke, and U. M. Apel, *Macromolecules*, **27**, 472 (1994).
J. P. A. Heuts, E. T. W. M. Schipper, P. Piet, and A. L. German, *J. Mol. Struct. (THEOCHEM)*, **333**, 39 (1995).
G. C. Hill and W. A. Remers, *J. Med. Chem.*, **34**, 1990 (1991a).
G. C. Hill, T. P. Wunz, N. E. MacKenzie, P. R. Gooley, and W. A. Remers, *J. Med. Chem.*, **34**, 2079 (1991b).
J.-R. Hill and J. Sauer, *J. Phys. Chem.*, **98**, 1238 (1994).
J.-R. Hill and J. Sauer, *J. Phys. Chem.*, **99**, 9536 (1995).
J. D. Holbrey, P. B. Iveson, J. C. Lockhart, N. P. Tomkinson, F. Teixidor, A. Romerosa, C. Vinas, and J. Rius, *J. Chem. Soc., Dalton Trans.*, 1451 (1993).
M. K. Holloway, J. M. Wai, T. A. Halgren, P. M. D. Fitzgerald, J. P. Vacca, B. D. Dorsey, R. B. Levin, W. J. Thompson, L. J. Chen, S. J. deSolms, N. Gaffin, A. K. Ghosh, E. A. Giuliani, S. L. Graham, J. P. Guare, R. W. Hungate, T. A. Lyle, W. M. Sanders, T. J. Tucker, M. Wiggin, C. M. Wiscount, O. W. Woltersdorf, S. D. Young, P. L. Darke, and J. A. Zugay, *J. Med. Chem.*, **38**, 305 (1995).
S. W. Homans, *Biochemistry*, **29**, 9110 (1990).
H. Höning and K. Hassler, *Monatsh. Chem.*, **113**, 129, 285 (1982).
S. C. Hoops, K. W. Anderson, and K. M. Merz Jr., *J. Am. Chem. Soc.*, **113**, 8262 (1991).
J. H. Horner and M. Newcomb, *Organometallics*, **10**, 1732 (1991).
M. B. Hossain, D. van der Helm, F. J. Schmitz, E. O. Pordesimo, R. A. Magarian, K. L. Meyer, L. B. Overacre, and B. W. Day, *J. Med. Chem.*, **37**, 1670 (1994).
K. N. Houk, H.-Y. Duh, Y.-D. Wu, and S. R. Moses, *J. Am. Chem. Soc.*, **108**, 2754 (1986).
K. N. Houk, J. E. Eksterowicz, Y.-D. Wu, C. D. Fuglesang, and D. B. Mitchell, *J. Am. Chem. Soc.*, **115**, 4170 (1993).
W. D. Hounshell, F. A. L. Anet, F. Cozzi, J. R. Damewood Jr., C. A. Johnson, U. Sjöstrand, and K. Mislow, *J. Am. Chem. Soc.*, **102**, 5941 (1980).
A. E. Howard, P. Cieplak, and P. A. Kollman, *J. Comput. Chem.*, **16**, 243 (1995).
U. Höweler, R. Mohr, M. Knickmeister, and G. Erker, *Organometallics*, **13**, 2380 (1994).
Y. Hu, H. Hashimoto, G. Mooine, U. Hengartner, and Y. Koyama, *J. Chem. Soc., Perkin Trans. 2*, 2699 (1997).
C. J. M. Huige, A. M. F. Hezemans, R. J. M. Nolte, and W. Drenth, *Recl. Trav. Chim. Pays-Bas*, **112**, 33 (1993).
C. J. M. Huige and C. Altona, *J. Comput. Chem.*, **16**, 56 (1995).
C. Huizoon, *J. Chem. Soc., Faraday Trans.*, **85**, 727 (1989).
J. P. Hummel, J. Stackhouse, and K. Mislow, *Tetrahedron*, **33**, 1925 (1977).
W. Humphrey, D. Xu, M. Sheves, and K. Schulten, *J. Phys. Chem.*, **99**, 14549 (1995).
M. G. Hutchings and I. Watt, *J. Organomet. Chem.*, **177**, 329 (1979).
M. J. Hwang, T. P. Stockfisch, and A. T. Hagler, *J. Am. Chem. Soc.*, **116**, 2515 (1994).

- M. R. Imam and N. L. Allinger, *J. Mol. Struct.*, **126**, 345 (1985).
W. Inman, P. Crews, and R. McDowell, *J. Org. Chem.*, **54**, 2523 (1989).
P. Iratcabal, D. Liotard, M.-F. Grenier-Loustalot, and A. Lichanot, *J. Mol. Struct. (THEOCHEM)*, **124**, 51 (1985).
R. Isaksson and T. Liljefors, *J. Chem. Soc., Perkin Trans. 2*, 1344 (1981).
R. Isaksson and T. Liljefors, *J. Chem. Soc., Perkin Trans. 2*, 1351 (1983).
H. Ishida, T. Hamada, Y. Fujishita, Y. Saito, and K. Ohkubo, *Bull. Chem. Soc. Jpn.*, **66**, 714 (1993).
P. M. Ivanov and I. G. Pojarlieff, *J. Chem. Soc., Perkin Trans. 2*, 245 (1984).
P. M. Ivanov, *J. Chem. Res.*, (S) 86, (M) 1173 (1985).
P. M. Ivanov, T. G. Momchilova, and I. G. Pojarlieff, *J. Comput. Chem.*, **12**, 427 (1991).
C. Jaime and E. Ōsawa, *Tetrahedron*, **39**, 2769 (1983).
C. Jaime, A. J. Buda, and E. Ōsawa, *Tetrahedron Lett.*, **25**, 3883 (1984).
C. Jaime and J. Font, *J. Mol. Struct.*, **195**, 103 (1989).
C. Jaime, C. Segura, I. Dinares, and J. Font, *J. Org. Chem.*, **58**, 154 (1993).
J. J. James and A. Whiting, *J. Chem. Soc., Perkin Trans. 2*, 1861 (1996).
G. A. Jeffrey and R. Taylor, *J. Comput. Chem.*, **1**, 99 (1980).
F. Jensen and C. S. Foote, *J. Am. Chem. Soc.*, **109**, 6376 (1987).
W. Jentzen, M. C. Simpson, J. D. Hobbs, X. Song, T. Ema, N. Y. Nelson, C. J. Medforth, K. M. Smith, M. Veyrat, M. Mazzanti, R. Ramasseul, J.-C. Marchon, T. Takeuchi, W. A. Goddard III, and J. A. Shelnutt, *J. Am. Chem. Soc.*, **117**, 11085 (1995).
P. Jewsbury and T. Kitagawa, *Biophys. J.*, **67**, 2236 (1994).
J. Jiménez-Barbero, M. Bernabé, and M. Martin-Lomas, *Tetrahedron*, **44**, 1441 (1988).
A. Y. Jin, L. A. Benesch, and D. F. Weaver, *Can. J. Chem.*, **72**, 1596 (1994).
D. K. Jones-Hertzog and W. L. Jorgensen, *J. Med. Chem.*, **40**, 1539 (1997).
S. O. Jónsdóttir and K. Rasmussen, *New J. Chem.*, **19**, 1113 (1995).
F. S. Jørgensen and J. P. Snyder, *Tetrahedron*, **35**, 1399 (1979).
W. L. Jorgensen and J. Tirado-Rives, *J. Am. Chem. Soc.*, **110**, 1657 (1988).
W. L. Jorgensen, and D. L. Severance, *J. Am. Chem. Soc.*, **112**, 4768 (1990).
W. L. Jorgensen, P. L. Morales de Tirado, and D. L. Severance, *J. Am. Chem. Soc.*, **116**, 2199 (1994).
W. J. Jorgensen, D. S. Maxwell, and J. Tirado-Rives, *J. Am. Chem. Soc.*, **118**, 11225 (1996).
W. L. Jorgensen and N. A. McDonald, *J. Mol. Struct. (THEOCHEM)*, **424**, 145 (1998).
H. H. Jung, Y. D. Won, S. Shin, and K. Kim, *Langmuir*, **15**, 1147 (1999).
G. Kaminski, E. M. Duffy, T. Matsui, and W. L. Jorgensen, *J. Phys. Chem.*, **98**, 13077 (1994).
G. A. Kaminski and W. L. Jorgensen, *J. Phys. Chem. B*, **102**, 1787 (1998).
A. Kamitakahara, C.-H. Hsu, and J. Pranta, *J. Mol. Struct. (THEOCHEM)*, **334**, 29 (1995).
Y. K. Kang, K. T. No, and H. A. Scheraga, *J. Phys. Chem.*, **100**, 15588 (1996).
J. Kao, C. Eyermann, E. Southwick, and D. Leister, *J. Am. Chem. Soc.*, **107**, 5323 (1985).
J. Kao, *J. Am. Chem. Soc.*, **109**, 3817 (1987).
J. Kao, *J. Comput. Chem.*, **9**, 905 (1988a).
J. Kao and D. Leister, *J. Am. Chem. Soc.*, **110**, 7286 (1988b).
W. A. Kaplan, K. S. Suslick, and R. A. Scott, *J. Am. Chem. Soc.*, **113**, 9824 (1991).
M. Kar, T. G. Lenz, and J. D. Vaughn, *J. Phys. Chem.*, **98**, 2489 (1994a).
M. Kar, T. G. Lenz, and J. D. Vaughn, *J. Comput. Chem.*, **15**, 1254 (1994b).
S. Karlsson, T. Liljefors, and J. Sandström, *Acta Chem. Scand.*, **B31**, 399 (1977).
T. Kawai, T. Ichinose, Y. Endo, K. Shudo, and A. Itai, *J. Med. Chem.*, **35**, 2248 (1992).
A. E. Keating, S. H. Shin, K. N. Houk, and M. A. Garcia-Garibay, *J. Am. Chem. Soc.*, **119**, 1474 (1997).
M. B. Kelly and J. Laane, *J. Phys. Chem.*, **92**, 4056 (1988).
G. M. Keserii, I. Kolossvary, and B. Bertók, *J. Am. Chem. Soc.*, **119**, 5126 (1997).
W.-K. Kim and W. L. Mattice, *Macromolecules*, **31**, 9337 (1998).
P. D. Kirchhoff, M. A. Bass, B. A. Hanks, J. M. Briggs, A. Collet, and J. A. McCammon, *J. Am. Chem. Soc.*, **118**, 3237 (1996).
K. N. Kirschner, A. H. Lewin, and J. P. Bowen, Abstracts of the 216th American Chemical Society National Meeting, Boston, MA, August 23–27, (1998, COMP 115).
M. Klein, U. Wingen, and V. Buss, *J. Am. Chem. Soc.*, **109**, 6486 (1987).
P. Klewinghaus, B. P. van Eijck, M. L. C. E. Kouwijzer, and J. Kroon, *J. Mol. Struct. (THEOCHEM)*, **395–396**, 289 (1997).
J. E. H. Koehler, W. Sanger, and W. F. van Gunsteren, *Eur. Biophys. J.*, **15**, 197 (1987).

- H. Kogelberg and T. J. Rutherford, *Glycobiology*, **4**, 49 (1994).
A. Koike and M. Yoneya, *J. Phys. Chem. B*, **102**, 3669 (1998).
P. A. Kollman, G. Wipff, and U. C. Singh, *J. Am. Chem. Soc.*, **107**, 2212 (1985).
I. Komaromi and J. M. J. Tronchet, *J. Mol. Struct. (THEOCHEM)*, **395–396**, 15 (1997).
M. Kontoyianni, A. J. Hoffman, and J. P. Bowen, *J. Comput. Chem.*, **13**, 57 (1992a).
M. Kontoyianni and J. P. Bowen, *J. Comput. Chem.*, **13**, 657 (1992b).
M. L. C. E. Kouwijzer and P. D. J. Grootenhuis, *J. Phys. Chem.*, **99**, 13426 (1995).
T. Kowall, F. Foglia, L. Helm, and A. E. Merbach, *J. Am. Chem. Soc.*, **117**, 3790 (1995).
T. Kozar, F. Peterak, Z. Galova, and I. Tvaroska, *Carbohydr. Res.*, **204**, 27 (1990).
J. Kozelka, R. Savinelli, G. Berhier, J.-P. Flament, and R. Lavery, *J. Comput. Chem.*, **14**, 45 (1993).
P. Krogsaard-Larsen, L. Brehm, J. S. Johansen, P. Vinzento, J. Lauritsen, and D. R. Curtis, *J. Med. Chem.*, **28**, 673 (1985).
L. M. J. Kroon-Batenburg, and J. A. Kanters, *J. Mol. Struct. (THEOCHEM)*, **105**, 417 (1983).
M. M. Kubo, E. Gallicchio, and R. M. Levy, *J. Phys. Chem. B*, **101**, 10527 (1997).
S. C. Kulkarni and N. L. Allinger, Abstracts of the 216th American Chemical Society National Meeting, Boston, MA, August 23–27, (1998, COMP 122).
M. G. Kurnikova, N. Balabai, D. H. Waldeck, and R. D. Coalson, *J. Am. Chem. Soc.*, **120**, 6121 (1998).
M. Laberge, J. M. Vanderkooi, and K. A. Sharp, *J. Phys. Chem.*, **100**, 10793 (1996).
M. L. Lamb and W. L. Jorgensen, *J. Med. Chem.*, **41**, 3928 (1998).
D. Lamba, S. Glover, W. Mackie, A. Rashid, B. Sheldrick, and S. Pérez, *Glycobiology*, **4**, 151 (1994).
C. R. Landis, T. Cleveland, and T. K. Firman, *J. Am. Chem. Soc.*, **117**, 1859 (1995).
C. R. Landis, T. K. Firman, D. M. Root, and T. Cleveland, *J. Am. Chem. Soc.*, **120**, 1842 (1998a).
C. R. Landis, T. Cleveland, and T. K. Firman, *J. Am. Chem. Soc.*, **120**, 2641 (1998b).
D. C. Lankin, N. S. Chandrakumar, S. N. Rao, D. P. Spangler, and J. P. Snyder, *J. Am. Chem. Soc.*, **115**, 3356 (1993).
C. A. Laughton, R. McKenna, S. Neidle, M. Jarman, R. McCague, and M. G. Rowlands, *J. Med. Chem.*, **33**, 2673 (1990).
J. W. Lauher, *J. Am. Chem. Soc.*, **108**, 1521 (1986).
A. R. Leach and T. E. Klein, *J. Comput. Chem.*, **16**, 1378 (1995).
K. J. Lee and T. L. Brown, *Inorg. Chem.*, **31**, 289 (1992).
S.-F. Lee, G. Barth, and C. Djerassi, *J. Am. Chem. Soc.*, **103**, 295 (1981).
T. G. Lenz and J. D. Vaughan, *J. Phys. Chem.*, **93**, 1588 (1989).
J. M. Leonard and W. P. Ashman, *J. Comput. Chem.*, **11**, 952 (1990).
R. Lessard, M. J. Heeg, T. Buranda, M. W. Perkovic, C. L. Schwarz, Y. Rudong, and J. F. Endicott, *Inorg. Chem.*, **31**, 3091 (1992).
S. Li and D. B. Chesnut, *Magn. Reson. Chem.*, **23**, 625 (1985).
T.-W. Li, I. Chao, and Y.-T. Tao, *J. Phys. Chem. B*, **102**, 2935 (1998).
Y. Li, A. E. Martell, R. D. Hancock, J. H. Reibenspies, C. J. Anderson, and M. J. Welch, *Inorg. Chem.*, **35**, 404 (1996).
C. Liang, L. Yan, J.-R. Hill, C. S. Ewig, T. R. Stouch, and A. T. Hagler, *J. Comput. Chem.*, **16**, 883 (1995).
G. Liang, J. P. Bowen, and J. A. Bentley, *J. Comput. Chem.*, **15**, 866 (1994).
G. Liang, P. C. Fox, and J. P. Bowen, *J. Comput. Chem.*, **17**, 940 (1996).
G. Liang, X. Chen, J. A. Dustman, A. H. Lewin, and J. P. Bowen, *J. Comput. Chem.*, **18**, 1371 (1997a).
G. Liang, J. P. Bays, and J. P. Bowen, *J. Mol. Struct. (THEOCHEM)*, **401**, 165 (1997b).
J.-H. Lii, S. Gallion, C. Bender, H. Wikstrom, N. L. Allinger, K. M. Flurchick, and M. M. Teeter, *J. Comput. Chem.*, **10**, 503 (1989).
J.-H. Lii and N. L. Allinger, *J. Comput. Chem.*, **13**, 1138 (1992).
J.-H. Lii and N. L. Allinger, *J. Comput. Chem.*, **19**, 1001 (1998).
T. Liljefors and N. L. Allinger, *J. Comput. Chem.*, **6**, 478 (1985).
T. Liljefors, J. C. Tai, S. Li, and N. L. Allinger, *J. Comput. Chem.*, **8**, 1051 (1987).
W.-K. Lin, N. W. Alcock, and D. H. Busch, *J. Am. Chem. Soc.*, **113**, 7603 (1991).
W.-K. Lin, W. J. Welsh, and W. R. Harris, *Inorg. Chem.*, **33**, 884 (1994).
H. Liu, F. Müller-Plathe, and W. F. van Gunsteren, *J. Am. Chem. Soc.*, **117**, 4363 (1995).
R. Liu and N. L. Allinger, *J. Comput. Chem.*, **15**, 283 (1994).

- S.-Y. Liu and G. D. Purvis III, unpublished report from CAChe, Oxford Molecular, Beaverton, OR, 1984.
- R. L. Lombardy, F. A. Tanius, K. Ramachandran, R. R. Tidwell, and W. D. Wilson, *J. Med. Chem.*, **39**, 1452 (1996).
- R. J. Loncharich, E. Seward, S. B. Ferguson, F. K. Brown, F. Diederich, and K. N. Houk, *J. Org. Chem.*, **53**, 3479 (1988).
- R. J. Loncharich and B. R. Brooks, *J. Mol. Biol.*, **215**, 439 (1990).
- A. S. Lopis, L. Glasser, and F. Marsicano, *QCPE Bull.*, **17** (2), 16 (1997). QCPE Program No. 673.
- M. P. Lowe, J. C. Lockhart, G. A. Forsyth, W. Clegg, and K. A. Fraser, *J. Chem. Soc., Dalton Trans.*, 145 (1995).
- H. Lumbruso, C. Liegeois, S. Guerrero, P. R. Olivato, and Y. Hase, *J. Mol. Struct.*, **162**, 141 (1987).
- L. Lunazzi, M. Guerra, D. Macciantelli, and G. Cerioni, *J. Chem. Soc., Perkin Trans. 2*, 1527 (1982).
- V. Luzhkov and J. Åqvist, *J. Am. Chem. Soc.*, **120**, 6131 (1998).
- B. Ma, J.-H. Lii, K. Chen, and N. L. Allinger, *J. Phys. Chem.*, **100**, 11297 (1996).
- M. Mabilia, R. A. Pearlstein, and A. J. Hopfinger, *J. Am. Chem. Soc.*, **109**, 7960 (1987).
- A. D. MacKerell Jr., J. Wiórkiewicz-Kucera, and M. Karplus, *J. Am. Chem. Soc.*, **117**, 11946 (1995).
- A. D. MacKerell Jr., D. Bashford, M. Bellott, R. L. Dunbrack Jr., J. D. Evanseck, M. J. Field, S. Fischer, J. Gao, H. Guo, S. Ha, D. Joseph-McCarthy, L. Kuchnir, K. Kuczera, F. T. K. Lau, C. Mattos, S. Michnick, T. Ngo, D. T. Nguyen, B. Prodhom, W. E. Reiher III, B. Roux, M. Schlenkrich, J. C. Smith, R. Stote, J. Straub, M. Watanabe, J. Wiórkiewicz-Kucera, D. Yin, and M. Karplus, *J. Phys. Chem. B*, **102**, 3586 (1998).
- V. Malatesta, C. Neff, G. Ranghino, L. Montanari, and P. Fantucci, *Macromolecules*, **26**, 4287 (1993).
- R. Manchanda, M. Zimmer, G. Brudvig, and R. H. Crabtree, *J. Mol. Struct.*, **323**, 257 (1994).
- J. R. Maple, M.-J. Hwang, T. P. Stockfisch, and A. T. Hagler, *Isr. J. Chem.*, **34**, 195 (1994a).
- J. R. Maple, M.-J. Hwang, T. P. Stockfisch, U. Dinur, M. Waldman, C. S. Ewig, and A. T. Hagler, *J. Comput. Chem.*, **15**, 162 (1994b).
- F. Marí, P. M. Lahti, and W. E. McEwen, *Heterroat. Chem.*, **1**, 255 (1990).
- A. E. Mark, S. P. van Helden, P. E. Smith, L. H. M. Janssen, and W. F. van Gunsteren, *J. Am. Chem. Soc.*, **116**, 6293 (1994).
- Z. Markovic, L. Dösen-Micovic, I. Juranic, and S. Konstantinovic, *Indian J. Chem.*, **34B**, 695 (1995).
- H. M. Marques and K. L. Brown, *Inorg. Chem.*, **34**, 3733 (1995a).
- H. M. Marques and K. L. Brown, *J. Mol. Struct. (THEOCHEM)*, **340**, 97 (1995b).
- H. M. Marques, O. Q. Munro, N. E. Grimmer, D. C. Levendis, F. Marsicano, G. Patrick, and T. Markoulides, *J. Chem. Soc., Faraday Trans.*, **91**, 1741 (1995c).
- H. M. Marques, C. Warden, M. Monye, M. S. Shongwe, and K. L. Brown, *Inorg. Chem.*, **37**, 2578 (1998).
- S.-J. Marrink and H. J. C. Berendsen, *J. Phys. Chem.*, **98**, 4155 (1994).
- S.-J. Marrink and H. J. C. Berendsen, *J. Phys. Chem.*, **100**, 16729 (1996).
- T. J. Marrone and K. M. Merz Jr., *J. Am. Chem. Soc.*, **117**, 779 (1995).
- F. J. Marsh, P. Weiner, J. E. Douglas, P. A. Kollman, G. L. Kenyon, and J. A. Gerlt, *J. Am. Chem. Soc.*, **102**, 1660 (1980).
- Martech, Inc., General Manager Marketing and Administration, 541 Tokyo Club Bldg., Kasumigaseki 3-2-6 Chiyoda-ku, Tokyo 100, Japan, 1991.
- S. F. Martin, G. O. Dorsey, T. Gane, M. C. Hillier, H. Kessler, M. Baur, B. Mathä, J. W. Erickson, T. N. Bhat, S. Munshi, S. V. Gulnik, and I. A. Topol, *J. Med. Chem.*, **41**, 1581 (1998).
- B. E. Maryanoff, D. F. McComsey, H. R. Almond Jr., M. S. Mutter, G. W. Bemis, R. R. Whittle, and R. A. Olofson, *J. Org. Chem.*, **51**, 1341 (1986).
- E. A. Mash, T. M. Gregg, M. T. Stahl, and W. P. Walters, *J. Org. Chem.*, **61**, 2738 (1996).
- E. A. Mash, T. M. Gregg, and M. T. Stahl, *J. Org. Chem.*, **62**, 3715 (1997).
- A. Matallana, A. W. Kruger, and C. A. Kingsbury, *J. Org. Chem.*, **59**, 3020 (1994).
- T. Matsumoto, N. Matsunaga, A. Kanai, T. Aoyama, T. Shioriri, and E. Ōsawa, *Tetrahedron*, **50**, 9781 (1994).
- D. L. Mattern and X. Chen, *J. Org. Chem.*, **56**, 5903 (1991).

- S. L. Mayo, B. D. Olafson, and W. A. Goddard III, *J. Phys. Chem.*, **94**, 8897 (1990).
 L. J. McClure and P. C. Ford, *J. Phys. Chem.*, **96**, 6640 (1992).
 D. Q. McDonald and W. C. Still, *J. Org. Chem.*, **61**, 1385 (1996a).
 D. Q. McDonald and W. C. Still, *J. Am. Chem. Soc.*, **118**, 2073 (1996b).
 N. A. McDonald, E. M. Duffy, and W. L. Jorgensen, *J. Am. Chem. Soc.*, **120**, 5104 (1998a).
 N. A. McDonald and W. L. Jorgensen, *J. Phys. Chem. B*, **102**, 8049 (1998b).
 G. J. McDougall, R. D. Hancock, and J. C. A. Boeyens, *J. Chem. Soc., Dalton Trans.*, 1438 (1978).
 G. B. McGaughey, E. L. Stewart, and J. P. Bowen, *J. Comput. Chem.*, **16**, 1250 (1995).
 G. B. McGaughey, E. L. Stewart, and J. P. Bowen, *J. Comput. Chem.*, **17**, 1395 (1996).
 C. McMartin and R. S. Bohacek, *J. Comput.-Aided Mol. Des.*, **11**, 333 (1997).
 R. J. Meier, J. R. Maple, M. J. Hwang, and A. T. Hagler, *J. Phys. Chem.*, **99**, 5445 (1995).
 S. Melberg and K. Rasmussen, *Carbohydr. Res.*, **69**, 27 (1979).
 E. C. Meng, P. Cieplak, J. W. Caldwell, and P. A. Kollman, *J. Am. Chem. Soc.*, **116**, 12061 (1994).
 E. C. Meng, J. W. Caldwell, and P. A. Kollman, *J. Phys. Chem.*, **100**, 2367 (1996a).
 E. C. Meng and P. A. Kollman, *J. Phys. Chem.*, **100**, 11460 (1996b).
 F. M. Menger and M. J. Sherrod, *J. Am. Chem. Soc.*, **110**, 8606 (1988).
 P. Mercandelli and A. Sironi, *J. Am. Chem. Soc.*, **118**, 11548 (1996).
 A. Y. Meyer, *J. Mol. Struct.*, **40**, 127 (1977).
 A. Y. Meyer, *J. Mol. Struct.*, **49**, 383 (1978).
 A. Y. Meyer, N. L. Allinger, and Y. Yuh, *Isr. J. Chem.*, **20**, 57 (1980a).
 A. Y. Meyer, *J. Comput. Chem.*, **1**, 111 (1980b).
 A. Y. Meyer and N. Ohmichi, *J. Mol. Struct.*, **73**, 145 (1981).
 A. Y. Meyer, *J. Chem. Soc., Perkin Trans. 2*, 1199 (1982).
 A. Y. Meyer, *J. Mol. Struct.*, **105**, 143 (1983a).
 A. Y. Meyer, *J. Mol. Struct. (THEOCHEM)*, **94**, 95 (1983b).
 A. Y. Meyer and F. R. F. Forrest, *J. Comput. Chem.*, **6**, 1 (1985).
 D. Mihailescu and J. C. Smith, *J. Phys. Chem. B*, **103**, 1586 (1999).
 C. Moberg, H. Adolfsson, K. Wärnmark, P.-O. Norrby, K.-M. Marstokk, and H. Möllental, *Chem. Eur. J.*, **2**, 516 (1996).
 F. A. Momany, R. Ronc, H. Kunz, R. F. Frey, S. Q. Newton, and L. Schäfer, *J. Mol. Struct. (THEOCHEM)*, **289**, 1 (1993).
 J. H. Moore, C. A. Lepre, G. P. Gippert, W. J. Chazin, D. A. Case, and P. E. Wright, *J. Mol. Biol.*, **221**, 533 (1991).
 D. W. Moreland and W. G. Dauben, *J. Am. Chem. Soc.*, **107**, 2264 (1985).
 G. Moyna, G. Hernandez, H. J. Williams, R. J. Nachman, and A. I. Scott, *J. Chem. Inf. Comput. Sci.*, **37**, 951 (1997).
 P. Müller and J. Mareda, *Tetrahedron Lett.*, **25**, 1703 (1984a).
 P. Müller, J. Blanc, and J. Mareda, *Chimica*, **38**, 389 (1984b).
 P. Müller and J. Mareda, *Helv. Chim. Acta*, **68**, 119 (1985a).
 P. Müller, J. Blanc, and J. Mareda, *Chimica*, **39**, 234 (1985b).
 P. Müller, J. Blanc, and J. Mareda, *Helv. Chim. Acta*, **69**, 635 (1986).
 R. Müller, W. von Philipsborn, L. Schleifer, P. Aped, and B. Fuchs, *Tetrahedron*, **47**, 1013 (1991).
 O. Q. Munro, J. C. Bradley, R. D. Hancock, H. M. Marques, F. Morsicano, and P. W. Wade, *J. Am. Chem. Soc.*, **114**, 7218 (1992).
 O. Q. Munro, H. M. Marques, P. G. Debrunner, K. Mohanrao, and W. R. Scheidt, *J. Am. Chem. Soc.*, **117**, 935 (1995).
 M. Murata, N. Yoshie, M. Sakurai, and Y. Inoue, *Bull. Chem. Soc. Jpn.*, **66**, 957 (1993).
 S. Nakagawa, H.-A. Yu, M. Karplus, and H. Umeyama, *Proteins: Struct., Funct., Genet.*, **16**, 172 (1993).
 N. Nevins, K. Chen, and N. L. Allinger, *J. Comput. Chem.*, **17**, 669 (1996a).
 N. Nevins, J.-H. Lii, and N. L. Allinger, *J. Comput. Chem.*, **17**, 695 (1996b).
 J. B. Nicholas, R. Vance, E. Martin, J. B. Burke, and A. J. Hopfinger, *J. Phys. Chem.*, **95**, 9803 (1991).
 K. C. Nicolaou, S. A. DeFrees, C.-K. Hwang, N. Stylianides, P. J. Carroll, and J. P. Snyder, *J. Am. Chem. Soc.*, **112**, 3029 (1990).
 S. R. Niketic and K. Rasmussen, *Acta Chem. Scand.*, **A32**, 391 (1978).
 I. Nilsson, U. Berg, and J. Sandström, *Acta Chem. Scand.*, **B40**, 625 (1986).

- K. Y. No, B. H. Seo, J. M. Park, and M. S. Jhon, *J. Phys. Chem.*, **92**, 6783 (1988).
- K. T. No, O. Y. Kwon, S. Y. Kim, K. H. Cho, C. N. Yoon, Y. K. Kang, K. D. Gibson, M. S. Jhon, and H. A. Scheraga, *J. Phys. Chem.*, **99**, 13019 (1995).
- M. H. Norman, D. J. Minick, and G. C. Rigdon, *J. Med. Chem.*, **39**, 149 (1996).
- L. Nørskov-Lauritsen and N. L. Allinger, *J. Comput. Chem.*, **5**, 326 (1984).
- P.-O. Norrby, B. Åkermark, F. Häffner, S. Hansson, and M. Blomberg, *J. Am. Chem. Soc.*, **115**, 4859 (1993).
- P.-O. Norrby, H. C. Kolb, and K. B. Sharpless, *J. Am. Chem. Soc.*, **116**, 8470 (1994).
- P.-O. Norrby, K. Wärnmark, B. Åkermark, and C. Moberg, *J. Comput. Chem.*, **16**, 620 (1995).
- P.-O. Norrby and T. Liljefors, *J. Comput. Chem.*, **19**, 1146 (1998).
- R. Núñez, R. J. Unwalla, F. K. Cartledge, S. G. Cho, B. H. Riches, M. P. Glenn, N. L. Hungerford, L. K. Lambert, D. J. Brecknell, and W. Kitching, *J. Chem. Soc., Perkin Trans. 2*, 1365 (1997).
- M. E. Nuss, F. J. Marsh, and P. A. Kollman, *J. Am. Chem. Soc.*, **101**, 825 (1979).
- J. Oh, Y. Kim, and Y. Won, *Bull. Korean Chem. Soc.*, **16**, 1153 (1995).
- M. Ohashi, K. Kasatani, H. Shinohara, and H. Sato, *J. Am. Chem. Soc.*, **112**, 5824 (1990).
- C. Okada, H. Inokawa, T. Sugawa, and M. Oda, *J. Chem. Soc., Chem. Commun.*, 448 (1992).
- N. Okuyama-Yoshida, M. Nagaoka, and T. Yamabe, *J. Phys. Chem. A*, **102**, 285 (1998).
- M. Orozco and F. J. Luque, *J. Comput. Chem.*, **14**, 881 (1993).
- E. Ōsawa, G. Szalontai, and A. Tsurumoto, *J. Chem. Soc., Perkin Trans. 2*, 1209 (1983).
- K.-H. Ott and B. Meyer, *J. Comput. Chem.*, **17**, 1068 (1996).
- R. J. Ouelette, *J. Am. Chem. Soc.*, **94**, 7674 (1972a).
- R. J. Ouelette, D. Baron, J. Stolfo, A. Rosenblum, and P. Weber, *Tetrahedron*, **28**, 2163 (1972b).
- L. Owens, C. Thilgen, F. Diederich, and C. B. Knobler, *Helv. Chim. Acta*, **76**, 2757 (1993).
- D. E. Palmer, C. Partaroni, K. Nunami, R. K. Chadha, M. Goodman, T. Wakamiya, K. Fukase, S. Horimoto, M. Kitazawa, H. Fujita, A. Kuba, and T. Shiba, *J. Am. Chem. Soc.*, **114**, 5634 (1992).
- G. Papoyan, K.-j. Gu, J. Wiórkiewicz-Kuczera, K. Kuczera, and K. Bowman-James, *J. Am. Chem. Soc.*, **118**, 1354 (1996).
- C. Parish, H. Senderowitz, and W. C. Still, Abstracts of the 216th American Chemical Society National Meeting, Boston, MA, August 23–27, (1998, COMP 158).
- D. J. Pasto and F. Cottard, *J. Am. Chem. Soc.*, **116**, 8973 (1994).
- M. D. Paulsen and R. L. Ornstein, *Proteins: Struct., Funct., Genet.*, **11**, 184 (1991).
- M. D. Paulsen and R. L. Ornstein, *J. Comput.-Aided Mol. Des.*, **6**, 449 (1992).
- F. Pavelcik and J. Majer, *Collect. Czech. Chem. Commun.*, **43**, 239, 1450 (1978).
- J. J. Pavelites, J. Gao, P. A. Bash, and A. D. MacKerell Jr., *J. Comput. Chem.*, **18**, 221 (1997).
- D. A. Pearlman, *J. Phys. Chem.*, **98**, 1487 (1994).
- Z. Peng, K. M. Merz Jr., and L. Banci, *Proteins: Struct., Funct., Genet.*, **17**, 203 (1993).
- Z. Peng, C. S. Ewig, M.-J. Hwang, M. Waldman, and A. T. Hagler, *J. Phys. Chem. A*, **101**, 7243 (1997).
- I. Pettersson and T. Liljefors, *J. Comput. Chem.*, **8**, 1139 (1987).
- I. Pettersson, T. Liljefors, and K. Bøgesø, *J. Med. Chem.*, **33**, 2197 (1990).
- I. Pettersson and K. Gundertofte, *J. Comput. Chem.*, **12**, 839 (1991).
- I. Pettersson and T. Liljefors, *J. Med. Chem.*, **35**, 2355 (1992).
- M. T. Pisabarro, A. R. Ortiz, A. Palomer, F. Gabré, L. García, R. C. Wade, F. Gago, D. Mauleón, and G. Carganico, *J. Med. Chem.*, **37**, 337 (1994).
- B. L. Podlogar and D. J. Raber, *J. Org. Chem.*, **54**, 5032 (1989).
- T. Polonski, *J. Chem. Soc., Perkin Trans. 1*, 629 (1988).
- T. Polonski, M. J. Milewska, and A. Katrusiak, *J. Am. Chem. Soc.*, **115**, 11410 (1993).
- J. Pranata and W. L. Jorgensen, *J. Am. Chem. Soc.*, **113**, 9483 (1991).
- P. S. Pregosin, H. Ruegger, R. Salzmann, A. Albinati, F. Lianza, and R. W. Kunz, *Organometallics*, **13**, 83 (1994).
- D. J. Price, J. D. Roberts, and W. L. Jorgensen, *J. Am. Chem. Soc.*, **120**, 9072 (1998).
- S. Profeta Jr. and N. L. Allinger, *J. Am. Chem. Soc.*, **107**, 1907 (1985).
- S. Profeta Jr., R. J. Unwalla, B. T. Nguyen, and F. K. Cartledge, *J. Comput. Chem.*, **7**, 528 (1986a).
- S. Profeta Jr., R. J. Unwalla, and F. K. Cartledge, *J. Org. Chem.*, **51**, 1884 (1986b).
- S. Profeta Jr., R. J. Unwalla, and F. K. Cartledge, *J. Comput. Chem.*, **10**, 99 (1989).
- J. Qian, R. Hentschke, and W. Knoll, *Langmuir*, **13**, 7092 (1997).

- M. Ragazzi and D. R. Ferro, *J. Mol. Struct. (THEOCHEM)*, **395–396**, 107 (1997).
- L. Raimondi, F. K. Brown, J. Gonzalez, and K. N. Houk, *J. Am. Chem. Soc.*, **114**, 4796 (1992).
- J.-P. Rameau, J. Devillers, J.-P. Declercq, G. Chauviere, and J. Perie, *Struct. Chem.*, **7**, 187 (1996).
- A. K. Rappé, C. J. Casewit, K. S. Colwell, W. A. Goddard III, and W. M. Skiff, *J. Am. Chem. Soc.*, **114**, 10024 (1992).
- K. Rasmussen, *Potential Energy Functions in Conformational Analysis*, Springer-Verlag, Berlin, 1985.
- K. Rasmussen, *J. Mol. Struct. (THEOCHEM)*, **395–396**, 91 (1997).
- D. E. Reichert, R. D. Hancock, and M. J. Welch, *Inorg. Chem.*, **35**, 7013 (1996).
- S. Reiling, M. Schlenkrich, and J. Brickmann, *J. Comput. Chem.*, **17**, 450 (1996).
- J. Ren and H.-D. Amberger, *J. Mol. Struct. (THEOCHEM)*, **236**, 231 (1991).
- W. Rettig, D. Braun, P. Suppan, E. Vauthey, K. Rotkiewicz, R. Luboradzki, and K. Suwinska, *J. Phys. Chem.*, **97**, 13500 (1993).
- W. H. Richardson, *J. Org. Chem.*, **54**, 4677 (1989).
- C. D. Rithner and C. H. Bushweller, *J. Am. Chem. Soc.*, **107**, 7823 (1985).
- G. Robinet, M. Barthelat, V. Gasmi, and J. Devillers, *J. Chem. Soc., Chem. Commun.*, 1103 (1989).
- G. Robinet, M. Barthelat, J. Devillers, V. Gasmi, D. Houalla, and R. Wolf, *Struct. Chem.*, **2**, 11 (1991).
- J. Rochester, U. Berg, M. Pierrot, and J. Sandström, *J. Am. Chem. Soc.*, **109**, 492 (1987).
- J. Rochester and J. Sandström, *Tetrahedron*, **45**, 5081 (1989).
- G. D. Rockwell and T. B. Grindley, *Aust. J. Chem.*, **49**, 379 (1996).
- D. W. Rogers, O. A. Dagdagian, and N. L. Allinger, *J. Am. Chem. Soc.*, **101**, 671 (1979).
- D. M. Root, C. R. Landis, and T. Cleveland, *J. Am. Chem. Soc.*, **115**, 4201 (1993).
- W. S. Ross and C. C. Hardin, *J. Am. Chem. Soc.*, **116**, 6070 (1994).
- K. A. Rossi, K. M. Merz Jr., G. M. Smith, and J. J. Baldwin, *J. Med. Chem.*, **38**, 2061 (1995).
- K. Rudolf, J. M. Hawkins, R. J. Loncharich, and K. N. Houk, *J. Org. Chem.*, **53**, 3879 (1988).
- J. M. Rudzinski and E. Ōsawa, *J. Phys. Org. Chem.*, **5**, 382 (1992).
- U. Ryde, *Proteins: Struct., Funct., Genet.*, **21**, 40 (1995).
- J. Sabolovics and K. Rasmussen, *Inorg. Chem.*, **34**, 1221 (1995).
- M. K. Safo, F. A. Walker, A. M. Raitsimring, W. P. Walters, D. P. Dolata, P. G. Debrunner, and W. R. Scheidt, *J. Am. Chem. Soc.*, **116**, 7760 (1994).
- S. Saigal and J. Pranata, *Bioorg. Chem.*, **25**, 11 (1997).
- K. Sakakibara, H. Kawamura, T. Nagata, J. Ren, M. Hirota, K. Shimazaki, and T. Chuman, *Bull. Chem. Soc. Jpn.*, **67**, 2768 (1994).
- M. Sakurai, M. Murata, Y. Inoue, A. Hino, and S. Kobayashi, *Bull. Chem. Soc. Jpn.*, **70**, 847 (1997).
- L. Salvatella, A. Mokrane, A. Cartier, and M. F. Ruiz-López, *J. Org. Chem.*, **63**, 4664 (1998).
- G. Sandrone, D. A. Dixon, and B. P. Hay, *J. Phys. Chem. A*, **103**, 693 (1999).
- M. A. Santos and M. G. B. Drew, *J. Chem. Soc., Faraday Trans.*, **87**, 1321 (1991).
- F. J. Sardinia, E. Quiñóa, L. Castedo, R. Riguera, R. A. Mosquera, and S. Vázquez, *J. Org. Chem.*, **51**, 4970 (1986).
- T. Sato, A. Suzuki, K. Sakai, and T. Tsutomura, *Bull. Chem. Soc. Jpn.*, **69**, 379 (1996).
- R. R. Sauers and K. Krogh-Jespersen, *Tetrahedron Lett.*, **30**, 527 (1989).
- T. X. T. Sayle and J. M. Goodfellow, *J. Chem. Soc., Faraday Trans.*, **93**, 2341 (1997).
- M. Schlenkrich, J. Brickmann, A. D. MacKerell Jr., and M. Karplus, in *Biological Membranes*, K. Merz Jr. and B. Roux, Eds., Birkhäuser, Boston, 1996, Ch. 2, pp. 31–81.
- B. K. Schmitz and W. B. Euler, *J. Comput. Chem.*, **15**, 1163 (1994).
- L. R. Schmitz and N. L. Allinger, *J. Am. Chem. Soc.*, **112**, 8307 (1990).
- D. M. Schnur and D. R. Dalton, *J. Org. Chem.*, **53**, 3313 (1988).
- D. M. Schnur, Y. H. Yuh, and D. R. Dalton, *J. Org. Chem.*, **54**, 3779 (1989).
- D. M. Schnur, M. V. Grieshaber, and J. P. Bowen, *J. Comput. Chem.*, **12**, 844 (1991).
- H. Sellers, A. Ulman, Y. Shnidman, and J. E. Eilers, *J. Am. Chem. Soc.*, **115**, 9389 (1993).
- S. Sen and L. Nilsson, *J. Am. Chem. Soc.*, **120**, 619 (1998).
- H. Senderowitz, P. Aped, and B. Fuchs, *Tetrahedron*, **48**, 1131 (1992).
- H. Senderowitz, P. Aped, and B. Fuchs, *J. Comput. Chem.*, **14**, 944 (1993a).
- H. Senderowitz, P. Aped, and B. Fuchs, *Tetrahedron*, **49**, 3879 (1993b).
- H. Senderowitz, L. Golender, and B. Fuchs, *Tetrahedron*, **50**, 9707 (1994).

- H. Senderowitz, C. Parish, and W. C. Still, *J. Am. Chem. Soc.*, **118**, 2078 (1996); see erratum, *ibid.*, 8985.
- H. Senderowitz and W. C. Still, *J. Org. Chem.*, **62**, 1427 (1997).
- J. A. Shelnutt, C. J. Medforth, M. D. Berber, K. M. Barkigia, and K. M. Smith, *J. Am. Chem. Soc.*, **113**, 4077 (1991).
- V. S. Shenoy and T. Ichiyi, *Proteins: Struct., Funct., Genet.*, **17**, 152 (1993).
- M. J. Sherrod, *Carbohydr. Res.*, **192**, 17 (1989).
- G. C. Shields, C. A. Laughton, and M. Orozco, *J. Am. Chem. Soc.*, **120**, 5895 (1998).
- J. Y. Shim, N. L. Allinger, and J. P. Bowen, *J. Phys. Org. Chem.*, **10**, 3 (1997).
- J. Y. Shim and J. P. Bowen, *J. Comput. Chem.*, **19**, 1370 (1998).
- K. Shimaaki, M. Mori, K. Okada, T. Chuman, S. Kuwahara, T. Kitahara, K. Mori, H. Goto, E. Ōsawa, K. Sakakibara, and M. Hirota, *J. Chem. Soc., Perkin Trans. 2*, 1167 (1993).
- B. D. Silverman, *Cancer Biochem. Biophys.*, **6**, 131 (1983).
- A. Sironi, *Inorg. Chem.*, **31**, 2467 (1992).
- P. E. Smith, B. M. Pettitt, and M. Karplus, *J. Phys. Chem.*, **97**, 6907 (1993).
- A. M. Smolyrev and M. L. Berkowitz, *J. Comput. Chem.*, **20**, 531 (1999).
- J.-C. Soetens, C. Millot, and B. Maigret, *J. Phys. Chem. A*, **102**, 1055 (1998).
- Y. Sohrin, H. Kokusen, and M. Matsui, *Inorg. Chem.*, **34**, 3928 (1995).
- X.-Z. Song, W. Jentzen, S.-L. Jai, L. Jaquinod, D. J. Nurco, C. J. Medforth, K. M. Smith, and J. A. Shelnutt, *J. Am. Chem. Soc.*, **118**, 12975 (1996).
- J. Sorensen and J. P. Bowen, Abstracts of the 216th American Chemical Society National Meeting, Boston, MA, August 23–37, (1998, COMP 116).
- L. D. Sparks, C. J. Medforth, M.-S. Park, J. R. Chamberlain, M. R. Ondrias, M. O. Senge, K. M. Smith, and J. A. Shelnutt, *J. Am. Chem. Soc.*, **115**, 581 (1993).
- G. W. Spears, C. E. Caufield, and W. C. Still, *J. Org. Chem.*, **52**, 1226 (1987).
- T. I. Spector, T. E. Cheatham III, and P. A. Kollman, *J. Am. Chem. Soc.*, **119**, 7095 (1997).
- D. C. Spellmeyer, P. D. Grootenhuis, M. D. Miller, L. F. Kuyper, and P. A. Kollman, *J. Phys. Chem.*, **94**, 4483 (1990).
- D. C. Spellmeyer and K. N. Houk, *J. Am. Chem. Soc.*, **52**, 959 (1987).
- J. T. Sprague and N. L. Allinger, *J. Comput. Chem.*, **1**, 257 (1980).
- B. Stammen, U. Bedage, R. Kindermann, M. Kaiser, B. Günter, W. S. Sheldrick, P. Welzel, and W. R. Roth, *J. Org. Chem.*, **57**, 6566 (1992).
- E. L. Stewart and J. P. Bowen, *J. Comput. Chem.*, **13**, 1125 (1992).
- R. H. Stote and M. Karplus, *Proteins: Struct., Funct., Genet.*, **23**, 12 (1995).
- T. R. Stouch, K. B. Ward, A. Altieri, and A. T. Hagler, *J. Comput. Chem.*, **12**, 1033 (1991).
- T. Strassner, *J. Mol. Model.*, **2**, 217 (1996).
- E. Strobl, J. Weiser, and L. Fitjer, *Tetrahedron*, **53**, 2767 (1997).
- G. Subramanian, M. G. Paterlini, D. L. Larson, P. Portoghesi, and D. M. Ferguson, *J. Med. Chem.*, **41**, 4777 (1998).
- H. Sun, *J. Comput. Chem.*, **15**, 752 (1994a).
- H. Sun, S. J. Mumby, J. R. Maple, and A. T. Hagler, *J. Am. Chem. Soc.*, **116**, 2978 (1994b).
- Y. Sun and P. A. Kollman, *J. Comput. Chem.*, **16**, 1164 (1995).
- A. Sundin, H. Anke, K.-E. Bergquist, A. Mayer, W. S. Sheldrick, M. Stadler, and O. Sternert, *Tetrahedron*, **49**, 7519 (1993).
- R. Susnow, R. B. Nachbar Jr., C. Schutt, and H. Rabitz, *J. Phys. Chem.*, **95**, 10662 (1991).
- J. C. Tai, *J. Comput. Chem.*, **2**, 161 (1981).
- J. C. Tai and N. L. Allinger, *J. Am. Chem. Soc.*, **110**, 2050 (1988).
- J. C. Tai, J.-H. Li, and N. L. Allinger, *J. Comput. Chem.*, **10**, 635 (1989).
- J. C. Tai, L. Yang, and N. L. Allinger, *J. Am. Chem. Soc.*, **115**, 11906 (1993).
- Y. Takeuchi, I. Zicmane, G. Manuel, and R. Boukherroub, *Bull. Chem. Soc. Jpn.*, **66**, 1732 (1993).
- M. Tasaka, M. Hirotsu, M. Kojima, S. Utsuno, and Y. Yoshikawa, *Inorg. Chem.*, **35**, 6981 (1996).
- R. Taylor, *J. Mol. Struct.*, **71**, 311 (1981).
- B. J. Teppen, K. Rasmussen, P. M. Bertsch, D. M. Miller, and L. Schäfer, *J. Phys. Chem. B*, **101**, 1579 (1997).
- H.-J. Thiem, M. Brandl, and R. Breslow, *J. Am. Chem. Soc.*, **110**, 8612 (1988).
- H. D. Thomas, K. Chen, and N. L. Allinger, *J. Am. Chem. Soc.*, **116**, 5887 (1994).

- I. Thondorf and J. Brenn, *J. Mol. Struct. (THEOCHEM)*, **398–399**, 307 (1997).
D. P. Tielman and H. J. C. Berendsen, *J. Chem. Phys.*, **105**, 4871 (1996).
L. F. Tietze, H. Geissler, J. Fennen, T. Brumby, S. Brand, and G. Schulz, *J. Org. Chem.*, **59**, 182 (1994).
T. V. Timofeeva, N. L. Allinger, M. Buehl, and U. Mazurek, *Izv. Akad. Nauk, Ser. Khim.*, **11**, 1906 (1994a).
T. V. Timofeeva, N. L. Allinger, M. Buehl, and U. Mazurek, *Russ. Chem. Bull.*, **43**, 1795 (1994b).
T. V. Timofeeva, U. Mazurek, and N. L. Allinger, *J. Mol. Struct. (THEOCHEM)*, **363**, 35 (1996).
A. V. Tkachev, A. Y. Denisov, Y. V. Gatilov, I. Y. Bagryanskaya, S. A. Shevtsov, and T. V. Rybalova, *Tetrahedron*, **50**, 11459 (1994).
F. L. Tobiason, F. R. Fronczwk, and J. P. Steynberg, *Tetrahedron*, **49**, 5927 (1993).
L. Toma, C. Cignarella, D. Barlocco, and F. Ronchetti, *J. Med. Chem.*, **33**, 1591 (1990).
F. Torrens, M. Ruiz-López, C. Cativiela, J. I. Garcia, and J. A. Moyoral, *Tetrahedron*, **48**, 5209 (1992).
G. Trabesinger, A. Albinati, N. Feiken, R. W. Kunz, P. S. Pregosin, and M. Tschoerner, *J. Am. Chem. Soc.*, **119**, 6315 (1997).
F. Tristram, V. Durier, and G. Vergoten, *J. Mol. Struct.*, **377**, 47 (1996).
S. Tsuzuki, K. Tanabe, Y. Nagawa, H. Nakanishi, and E. Ōsawa, *J. Mol. Struct.*, **178**, 277 (1988).
S. Tsuzuki, K. Tanabe, Y. Nagawa, and H. Nakanishi, *J. Mol. Struct.*, **212**, 45 (1989).
S. Tsuzuki, K. Tanabe, Y. Nagawa, and H. Nakanishi, *J. Mol. Struct.*, **216**, 279 (1990a).
S. Tsuzuki and K. Tanabe, *J. Chem. Soc., Perkin Trans. 2*, 1687 (1990b).
S. Tsuzuki and K. Tanabe, *J. Chem. Soc., Perkin Trans. 2*, 181 (1991).
J. A. Tucker, K. N. Houk, and B. M. Trost, *J. Am. Chem. Soc.*, **112**, 5465 (1990).
J. L. Tueting, K. L. Spence, and M. Zimmer, *J. Chem. Soc., Dalton Trans.*, 551 (1994).
K. Tuppurainen and R. Laatikainen, *J. Mol. Struct. (THEOCHEM)*, **281**, 1520 (1993).
I. Tvaroska and L. Vadavik, *Carbohydr. Res.*, **160**, 137 (1987).
P. Ugliengo, J. Ahmed, D. Viterbo, and M. Ceruti, *Gazz. Chim. Ital.*, **119**, 493 (1989).
R. J. Unwalla, S. Profeta, Jr., and F. K. Cartledge, *J. Org. Chem.*, **53**, 5658 (1988).
F. van der Spoel, K. A. Feenstra, M. A. Hemminga, and H. J. C. Berendsen, *Biophys. J.*, **71**, 2920 (1996).
M. van Duin, J. M. A. Baas, and B. van de Graaf, *Delft Progr. Prep.*, **13**, 375 (1989).
S. P. van Helden, B. P. van Eijck, and L. H. M. Janssen, *J. Biomol. Struct. Dyn.*, **9**, 1269 (1992).
W. P. van Hoorn, Ph.D. thesis, University of Twente, The Netherlands, 1997.
W. P. van Hoorn, F. C. J. M. van Veggel, and D. N. Reinhoudt, *J. Phys. Chem. A*, **102**, 6676 (1998).
F. C. J. M. van Veggel, and D. N. Reinhoudt, *Rec. Trav. Chim. Pays-Bas*, **114**, 387 (1995).
S. A. Vázquez, M. A. Ríos, and L. Carballera, *J. Comput. Chem.*, **12**, 872 (1991).
J. M. Veal, X. Gao, and F. K. Brown, *J. Am. Chem. Soc.*, **115**, 7139 (1993).
J. M. Veal and F. K. Brown, *J. Am. Chem. Soc.*, **117**, 1873 (1995).
A. Vedani and J. D. Dunitz, *J. Am. Chem. Soc.*, **107**, 7653 (1985).
A. Vedani, M. Dobler, and J. Dunitz, *J. Comput. Chem.*, **7**, 701 (1986).
A. Vedani, *J. Comput. Chem.*, **9**, 269 (1988).
A. Vedani and D. W. Huhta, *J. Am. Chem. Soc.*, **112**, 4759 (1990).
D. L. Veenstra, D. M. Ferguson, and P. A. Kollman, *J. Comput. Chem.*, **13**, 971 (1992).
M. M. Ventura, *An. Acad. Bras. Ci.*, **67**, 157 (1995).
F. Vila, P. Tordo, D. Siri, and G. Pépe, *Free Radical Res. Commun.*, **19**, Suppl. S17 (1993).
V. N. Viswanadhan and W. Mattice, *J. Comput. Chem.*, **7**, 711 (1986).
A. Vulpetti, A. Bernardi, C. Gennari, J. M. Goodman, and I. Paterson, *Tetrahedron*, **49**, 685 (1993a).
A. Vulpetti, M. Gardner, C. Gennari, A. Bernardi, J. M. Goodman, and I. Paterson, *J. Org. Chem.*, **58**, 1711 (1993b).
R. C. Wade and J. A. McCammon, *J. Mol. Biol.*, **225**, 679 (1992).
S. Walker, D. Gange, V. Gupta, and D. Kahne, *J. Am. Chem. Soc.*, **116**, 3197 (1994).
J. Wang and P. A. Kollman, *J. Am. Chem. Soc.*, **120**, 11106 (1998).
W. H. Watson and R. O. Kashyap, *J. Org. Chem.*, **51**, 2521 (1986).
M. A. Watzky, D. Waknine, M. J. Heeg, J. F. Endicott, and L. A. Ochrymowycz, *Inorg. Chem.*, **32**, 4882 (1993).

- S. J. Weiner, P. A. Kollman, D. A. Case, U. C. Singh, C. Ghio, G. Alagona, S. Profeta Jr., and P. Weiner, *J. Am. Chem. Soc.*, **106**, 765 (1984).
- S. J. Weiner, P. A. Kollman, D. T. Nguyen, and D. A. Case, *J. Comput. Chem.*, **7**, 230 (1986).
- W. Weissensteiner, I. I. Schuster, J. F. Blount, and K. Mislow, *J. Am. Chem. Soc.*, **108**, 6664 (1986).
- W. Weissensteiner, *Monatsch. Chem.*, **123**, 1135 (1992).
- W. Welsh and V. Cody, *J. Comput. Chem.*, **11**, 531 (1990).
- D. P. White and T. L. Brown, *Inorg. Chem.*, **34**, 2718 (1995).
- P. White and R. Breslow, *J. Am. Chem. Soc.*, **112**, 6842 (1990).
- D. M. Whitfield and T.-H. Tang, *J. Am. Chem. Soc.*, **115**, 9648 (1993).
- K. Wiberg, L. K. Olli, N. Golembeski, and R. D. Adams, *J. Am. Chem. Soc.*, **102**, 7467 (1980).
- F. Wiesemann, S. Teipel, B. Krebbs, and U. Höweler, *Inorg. Chem.*, **33**, 1891 (1994).
- D. J. Williams and K. B. Hall, *J. Phys. Chem.*, **100**, 8224 (1996).
- G. Wipff, P. Weiner, and P. A. Kollman, *J. Am. Chem. Soc.*, **104**, 3249 (1982).
- G. Wipff and P. A. Kollman, *Nouv. J. Chim.*, **9**, 457 (1985).
- S. Wolfe, D. F. Weaver, and K. Yang, *Can. J. Chem.*, **66**, 2687 (1988a).
- S. Wolfe, S. Bruder, D. F. Weaver, and K. Yang, *Can. J. Chem.*, **66**, 2703 (1988b).
- S. Wolfe, M. Khalil, and D. F. Weaver, *Can. J. Chem.*, **66**, 2715 (1988c).
- S. Wolfe, K. Yang, and M. Khalil, *Can. J. Chem.*, **66**, 2733 (1988d).
- R. J. Woods, C. W. Andrews, and J. P. Bowen, *J. Am. Chem. Soc.*, **114**, 850 (1992).
- R. J. Woods, R. A. Dwek, C. J. Edge, and B. Fraser-Reid, *J. Phys. Chem.*, **99**, 3832 (1995).
- Y.-D. Wu, K. N. Houk, J. Florez, and B. M. Trost, *J. Org. Chem.*, **56**, 3656 (1991).
- G. Xiao, D. van der Helm, R. C. Hider, and B. L. Rai, *J. Phys. Chem.*, **100**, 2345 (1996).
- G. Yamamoto and M. Oki, *Bull. Chem. Soc. Jpn.*, **58**, 1690 (1985a).
- G. Yamamoto and M. Oki, *Bull. Chem. Soc. Jpn.*, **58**, 1953 (1985b).
- G. Yamamoto and M. Oki, *Bull. Chem. Soc. Jpn.*, **63**, 3550 (1990).
- L. Yang and N. L. Allinger, *J. Mol. Struct. (THEOCHEM)*, **370**, 71 (1996).
- S. Yao, J. P. Plastaras, and L. G. Marzilli, *Inorg. Chem.*, **33**, 6061 (1994).
- P. C. Yates and S. T. Patel, *J. Mol. Struct. (THEOCHEM)*, **276**, 249 (1992).
- P. C. Yates, *J. Mol. Struct. (THEOCHEM)*, **281**, 275 (1993).
- P. C. Yates, *J. Mol. Struct. (THEOCHEM)*, **303**, 55 (1994).
- R. B. Yelle, N.-S. Park, and T. Ichiye, *Proteins: Struct., Funct., Genet.*, **22**, 154 (1995).
- D. Yin and A. D. MacKerell Jr., *J. Comput. Chem.*, **19**, 334 (1998).
- C. R. Yonker, S. L. Wallen, B. J. Palmer, and B. C. Garrett, *J. Phys. Chem. A*, **101**, 9564, (1997).
- M. Yoshida, Y. Hidaka, Y. Nawata, J. M. Rudzinski, E. Ōsawa, and K. Kanematsu, *J. Am. Chem. Soc.*, **110**, 1232 (1988).
- Y. Yoshikawa, *Bull. Chem. Soc. Jpn.*, **49**, 156 (1976).
- Y. Yoshikawa, *J. Comput. Chem.*, **11**, 326 (1990).
- L. Young and C. B. Post, *J. Am. Chem. Soc.*, **115**, 1964 (1993).
- E. Yuriev and J. D. Orbell, *Inorg. Chem.*, **37**, 6269 (1998).
- Y. Zhang, R. M. Venable, and R. W. Pastor, *J. Phys. Chem. B*, **100**, 2652 (1996).
- X. Zhou and N. L. Allinger, *J. Phys. Org. Chem.*, **7**, 420 (1994).
- M. Zimmer and R. H. Crabtree, *J. Am. Chem. Soc.*, **112**, 1062 (1990).

REFERENCES

- I. Pettersson and T. Liljefors, in *Reviews in Computational Chemistry*, K. B. Lipkowitz and D. B. Boyd, Eds., VCH Publishers, New York, 1996, Vol. 9, pp. 167–189. Molecular Mechanics Calculated Conformational Energies of Organic Molecules: A Comparison of Force Fields.
- E. Ōsawa and K. B. Lipkowitz, in *Reviews in Computational Chemistry*, K. B. Lipkowitz and D. B. Boyd, Eds., VCH Publishers, New York, 1995, Vol. 6, pp. 355–381. Published Force Field Parameters.

Author Index

- Aagaard, O., 469
Aakeroy, C. B., 283
Abe, K., 469
Abelt, C. J., 469
Abraham, F. F., 396
Abraham, R. J., 469
Acquavella, M. F., 469
Adam, K. R., 469
Adamowicz, L., 127, 135
Adams, J. B., 217
Adams, R. D., 486
Adolfsson, H., 481
Ahlrichs, R., 132
Ahlstrom, P., 287
Ahmed, J., 485
Åkermark, B., 472, 482
Alagona, G., 282, 470, 486
Alberti, A., 220
Alberts, I. L., 134, 286
Albinati, A., 482, 485
Alcázar, V., 474
Alcock, N. W., 479
Alder, B., 392
Alderton, M., 285, 286
Alemán, D., 470
Alemany, A., 472
Ali, S., 284
Al-Laham, M. A., 29
Allan, D. C., 221
Allen, F. H., 283
Allen, M. P., 215, 395
Allen, W. D., 131, 132, 134
Allinger, J. A., 470
Allinger, N. L., 29, 222, 281, 470, 472, 473,
474, 475, 476, 477, 478, 479, 480, 481,
482, 483, 484, 485, 486
Allouche, A., 220
Allured, V. S., 470
Almlöf, J., 132, 136
Almond, H. R., Jr., 480
Altieri, A., 484
Altona, C., 477
Amarasekara, A. S., 477
Amato, M. E., 470
Amberger, H.-D., 483
Amos, R. D., 131, 132, 133, 134, 283, 286
Andersen, H. C., 220, 392
Andersen, K., 470
Anderson, C. J., 479
Anderson, D. G., 470
Anderson, K. W., 477
Anderson, M. W., 222
Anderson, S., 470
Anderson, W. P., 474
Ando, K., 470
Andreotti, G. D., 476
Andres, J. L., 29
Andrews, C. W., 486
Andrews, J. S., 131, 286
Andrey, L., 394
Andriés, M.-L. D., 471
Anet, F. A. L., 470, 477
Angelucci, L., 470
Angermund, K., 470
Angyan, J. G., 285, 286
Anke, H., 484
Annunziata, R., 470
Ansell, C. W. G., 469
Anstead, G. M., 470
Antolini, L., 471
Antolovich, M., 469
Aoki, K., 135
Aono, S., 134
Aoyama, T., 480
Aped, P., 470, 481, 483
Apel, U. M., 477
Apeloig, Y., 470
Åqvist, J., 480

- Areshkin, D. A., 396
Arfken, G., 394
Arias, T. A., 221
Arnold, V. I., 393
Arnt, J., 471
Arponen, J. S., 129
Ascenso, J. R., 470
Ashman, W. P., 479
Ashurst, W. T., 392, 396
Astorino, E., 222
Astrand, P. O., 287
Auerbach, S. M., 217
Auerbach, S. P., 394
Augspurger, J. D., 285
Avilés, F. X., 474
Axilrod, P. M., 281
Ayala, P. Y., 29
- Baas, J. M. A., 219, 220, 289, 485
Bachrach, S. M., 29
Bader, R. F. W., 30, 288
Badger, R. M., 220
Baekelandt, B. G., 218
Baerlocher, C., 214
Bagchi, K., 394, 395
Bagryanskaya, I. Y., 485
Bailey, W. F., 471
Baillie, P. J., 469
Baker, J., 29
Baker, M. D., 222
Bakker, W. I. I., 476
Balabai, N., 479
Balasubramanian, S., 394, 395
Balbes, L. M., 281
Baldridge, K. K., 30
Baldwin, D. S., 469
Baldwin, J. J., 483
Baleja, J. D., 471
Balkova, A., 133
Bally, T., 134
Banci, L., 471, 482
Bandoli, G., 471
Banerjee, A., 135
Barbarella, G., 471
Barber, D. J., 395
Barkigia, K. M., 484
Barlocco, D., 485
Barnes, L. A., 134
Baron, D., 482
Barone, V., 471
Barrat, J. L., 395
Barrie, P. J., 222
Barrows, S. E., 471
- Barth, G., 479
Barthelat, M., 476, 483
Bartlett, R. J., 125, 126, 127, 128, 129, 130,
 131, 132, 133, 134, 135, 217, 282
Bartolotti, L. J., 218, 471, 473
Bärtsch, M., 219
Bash, P. A., 482
Bashford, D., 480
Bass, M. A., 478
Bates, S. P., 214
Batra, M. S., 472
Baudry, J., 471
Baur, H., 394
Baur, M., 480
Bayly, C. I., 31, 282, 473
Bays, J. P., 479
Beachy, M. D., 284
Beagley, B., 471
Beazley, D. M., 396
Beckhaus, H.-D., 471
Bedage, U., 484
Beech, J., 471
Belak, J., 396
Bell, A. T., 214, 216
Bell, T. W., 471
Bellemans, A., 394
Bellott, M., 480
Bellussi, G., 222
Belvisi, L., 471
Bernis, G. W., 480
Benaglia, M., 470
Benard, M., 285
Bencini, A., 471
Bender, C., 479
Benesh, L. A., 478
Benetti, E., 472
Bentley, J. A., 479
Bérard, D. R., 392
Berber, M. D., 484
Berendsen, H. J. C., 220, 221, 480, 485
Berens, H. C., 220
Berens, P. H., 221
Beretta, M. G., 471
Berg, U., 471, 481, 483
Berger, O., 471
Bergquist, K.-E., 484
Bergsma, J., 470
Berheir, G., 479
Berkowitz, M. L., 484
Bernabé, M., 472, 478
Bernardi, A., 471, 476, 485
Berne, B. J., 221, 393, 395
Bernhardt, P. V., 471

- Berning, A., 132
Bernlöhr, W., 471
Bernstein, F. C., 283
Bertaut, F., 220
Bertini, I., 471
Bertholon, G., 474
Bertók, B., 478
Bertrand, M., 474
Bertrand, M. P., 471
Bertsch, P. M., 484
Besler, B. H., 30
Beu, T. A., 287
Beveridge, D. L., 217
Bhat, T. N., 480
Bhupathiraju, R., 394
Biali, S. E., 471
Bierbach, U., 471
Billeter, S. R., 471
Bindal, R. D., 471
Binkley, J. S., 29, 30, 125
Bishop, R. F., 129
Biskupic, S., 132
Bissonnette, C., 285
Bladh, N., 471
Blaisdell, J., 287
Blaive, B., 472, 474
Blake, G. A., 284
Blanc, J., 481
Blaszkowski, S. R., 217, 223
Blöchl, P. E., 217, 223
Blomberg, M., 482
Blount, J. F., 471, 486
Blumenfeld, A. L., 216
Boatz, J. A., 30
Boccuti, M. R., 221
Bocquet, L., 395
Bodot, H., 476
Boeyens, J. C. A., 471, 476, 481
Bøgesø, K., 470, 471, 482
Bohacek, R. S., 476, 481
Bohm, H. J., 284
Bol, J. E., 472
Bolcer, J. D., 439
Bond, A. M., 472
Bongini, A., 471
Bopp, P., 222
Borden, W. T., 134
Bordiga, S., 218, 222
Borkar, N. L., 472
Born, M., 220
Bornhauser, P., 219, 221
Boscherini, F., 222
Bosnich, B., 474
Botta, B., 472
Botta, M., 472
Bougeard, D., 215, 219, 221
Boukherroub, R., 484
Bouraoui, A., 472
Boutin, A., 216
Bowen, J. P., 29, 281, 472, 473, 475, 476,
 478, 479, 481, 483, 484, 486
Bowman-James, K., 482
Boyd, D. B., 29, 30, 128, 134, 215, 217, 218,
 219, 220, 281, 282, 285, 286, 287, 392,
 395, 396, 397, 439, 472, 486
Boyd, R. H., 473
Boyle, B. A., 476
Bradley, J. C., 481
Brady, J. W., 476
Bramley, R., 471
Brand, H. V., 217
Brand, S., 485
Brandl, M., 484
Brändle, M., 216
Brandt, E. V., 472
Brandt, P., 472
Brant, L. H., 472
Braun, D., 483
Bravo, A. N., 475
Brecknell, D. J., 472, 482
Brehm, L., 479
Brémard, C., 219
Bremner, J. B., 476
Breneman, C. M., 30
Brenn, J., 485
Brenner, D. W., 397
Breslow, R., 484, 486
Breton, J., 475
Breuer, M., 472
Brice, M. D., 283
Brickmann, J., 217, 222, 483
Brigden, L. G., 469
Briggs, J. M., 474, 478
Brinck, T., 476, 477
Brink, D. M., 281
Brink, G., 472
Brobjer, J. T., 284
Brodbeck, D., 396
Brode, S., 284
Broeker, J. L., 472
Brooks, B. R., 132, 282, 472, 473, 480
Brown, A. B., 472
Brown, D., 392
Brown, F. K., 472, 480, 483, 485
Brown, K. L., 472, 480
Brown, T. L., 472, 473, 479, 486

- Brucolieri, R. E., 282, 472
Bruder, S., 486
Brudvig, G., 480
Brueckner, K. A., 133
Brumbaugh, D. V., 283
Brumby, T., 485
Brunel, Y., 471
Brunet, E., 472, 475
Brunink, J. A. J., 476
Bruno, I. J., 283
Bryant, L. H., Jr., 472
Buck, H. M., 469, 474
Buck, U., 287
Buckingham, A. D., 281, 283, 472
Buda, A. J., 478
Buehl, M., 485
Buffa, F., 222
Bull, L. M., 472
Bullock, W. H., 477
Bumgarner, R. E., 284
Buning, C., 472
Buranda, T., 479
Burgess, K.-K., 472
Burke, J. B., 481
Burkert, U., 472
Burton, N. A., 134, 223
Busca, G. J., 222
Busch, D. H., 479
Bushweller, C. H., 483
Buss, V., 478
Buzzoni, R., 218
Byrd, E. F. C., 134
Byström, K., 472
- Caffery, M. L., 472
Cagin, T., 475
Caldwell, J. W., 282, 473, 481
Califano, S., 219
Calligaris, M., 476
Calzaferri, G., 219, 221
Caminiti, R., 472
Campbell, S., 397
Campbell, V. A., 470
Camper, D. L., 473, 475
Canales, C. R., 472
Cannon, J. F., 472
Cannon, W. R., 472
Cano, F. H., 472
Capecchi, G., 471
Capelli, A. M., 471
Car, R., 221, 393
Carballeira, L., 472, 475, 485
Carey, C., 30
- Carey, P. R., 475
Carganico, G., 482
Carloni, P., 471
Carrazza, J., 215
Carrigan, S. W., 473
Carroll, M. T., 288
Carroll, P. J., 481
Carruthers, J. R., 223
Cársky, P., 131, 132
Carter, R. E., 470, 473
Cartier, A., 483
Cartledge, F. K., 473, 482, 485
Carugo, O., 471, 476
Carvalho, J. F., 475
Case, D. A., 282, 481, 486
Casewit, C. J., 473, 483
Casey, C. P., 473
Cassinari, A., 471
Castedo, L., 483
Castells, J., 473
Castonguay, L. A., 473
Cativielo, C., 485
Catlow, C. R. A., 214, 215, 216, 217, 218,
 219, 223, 287
Caufield, C. E., 484
Cerioni, G., 480
Cernusak, I., 131
Ceruti, M., 485
Chadha, R. K., 482
Chakraborty, A. K., 216
Chakravorty, S. J., 473
Challacombe, M., 29
Chamberlain, J. R., 484
Chambers, C. C., 29
Chandler, D., 392, 394
Chandra, A. K., 215, 216
Chandrakumar, N. S., 479
Chang, A., 475
Chang, H. M., 473
Chang, S., 473
Chang, S. H.-M., 470
Chao, I., 479
Charifson, P. S., 471
Charles, R., 473
Chasman, D., 284
Chatfield, D. C., 473
Chatterjee, A., 215
Chaudhuri, R., 130
Chauqui, C. E., 285
Chauviere, G., 483
Chazin, W. J., 481
Cheatham, T. E., III, 484
Cheeseman, J. R., 29

- Cheetham, A. K., 215, 216, 472
 Chen, K., 470, 473, 480, 481, 484
 Chen, L. J., 477
 Chen, W., 29
 Chen, X., 473, 479, 480
 Chen, Z. M., 475
 Chesnut, D. B., 479
 Chhiba, M., 473
 Chiles, R. A., 133
 Chipot, C., 286, 473
 Chirlian, L. E., 30, 218, 286
 Cho, K. H., 482
 Cho, S. G., 473, 482
 Choi, M.-G., 473
 Choo, J., 473
 Christiansen, O., 128, 130, 133, 135
 Chuman, T., 483, 484
 Chynoweth, S., 394
 Ciccotti, G., 220, 394, 396
 Cieplak, P., 30, 31, 282, 473, 477, 481
 Cignarella, C., 485
 Cini, R., 473
 Cinquini, M., 470
 Cioslowski, J., 29, 288
 Cizek, J., 125, 130, 134
 Clark, M., 473
 Clark, R. J., 221
 Clark, T. E., 474
 Clarke, J. H. R., 392
 Clary, D. C., 287
 Claverie, P., 285, 287
 Clegg, W., 480
 Clement, O., 477
 Cleveland, T., 473, 479, 483
 Coalson, R. D., 479
 Cochran, H. D., 394, 395
 Cody, V., 475, 486
 Cole, J. C., 283
 Cole, S. J., 126
 Collet, A., 474, 478
 Collins, J. R., 473, 475
 Colucci, W. J., 473
 Coluccia, S., 222
 Colwell, K. S., 483
 Colwell, S. M., 286
 Comba, P., 471, 472, 473
 Combariza, J. E., 217, 281
 Comotti, A., 471, 476
 Condroski, K. R., 470
 Coner, R. D., 472
 Cook, R., 396
 Coombes, D. S., 287
 Cooper, D. L., 132, 285
 Copenhagen, A. S., 286
 Corbin, D. R., 223
 Corelli, F., 472
 Corey, E. J., 473
 Cornell, W. D., 31, 282, 473
 Cortez, E., 473
 Cossé-Barbi, A., 473
 Cossi, M., 471
 Costa, A., 474
 Costa, M., 287
 Costante-Crassous, J., 474
 Cottard, F., 482
 Cox, D. E., 222
 Cox, P. A., 215, 216
 Cox, S. R., 30, 282, 286
 Cozzi, F., 470, 471, 477
 Crabtree, R. H., 480, 486
 Cragg, P. J., 471
 Cramer, C. J., 29, 471
 Cramer, R. D., III, 473
 Crans, D. C., 474
 Crawford, T. D., 126, 130, 131, 132, 133,
 135, 217
 Creaser, I. I., 474
 Creighton, J. A., 215, 219
 Cresswell, P. J., 472
 Crews, P., 478
 Cristina, M., 474
 Crowell, K. G., 285
 Cude, A., 476
 Cui, S. T., 395
 Cummings, P. T., 394, 395
 Cummins, P. L., 474
 Cundari, T. R., 474
 Cuntze, J., 474
 Curran, D. P., 474
 Curtis, D. R., 479
 Cusak, R., 473
 Cygan, R. T., 477
 Dagdagán, O. A., 483
 Dahl, S. V., 475
 Daivis, P. J., 395
 Dalton, D. R., 483
 Damewood, J. R., Jr., 471, 474, 477
 Damm, W., 474
 Dancey, K. P., 469
 Darke, P. L., 477
 Dasgupta, S., 284
 Daubert, W. G., 481
 Dauchez, M., 474
 Daudel, R., 130
 Daura, X., 282, 474

- Davidson, E. R., 130, 131, 134, 217, 282
Davies, J. E., 283
Davydov, A. S., 281
Day, B. W., 477
de Boer, K., 219
De Gennes, P. G., 395
De Gioia, L., 470
de Kok, P. M. I., 474
de Man, A. J. M., 215, 218, 221
De Merás, A. S., 128, 133
de Pascual-Teresa, B., 474
De Riggis, I., 474
de Vos Burchart, E., 215, 219, 220, 222
de Waal, B. F. M., 469
DeBolt, W. E., 474
Debrunner, P. G., 481, 483
Deckman, H. W., 219
Declercq, J.-P., 483
Decoret, C., 474
Deegan, M. J. O., 126, 132
Deem, M. W., 215
DeFrees, D. J., 29, 30
DeFrees, S. A., 481
Deguchi, K., 134
Deiters, J. A., 474
DeKock, R. L., 134
Del Barco, B., 221
DeLeeuw, B. J., 131
Dellaca, R. J., 472
Delpeyroux, D., 474
DeMello, N. C., 474
Demontis, P., 214, 215, 218, 220, 222
Deng, L., 474
Denisov, A. Y., 485
Deo, G., 222
DeRiggis, I., 471
DeRosa, M. C., 472
Derouane, E. G., 217
Derreumaux, P., 474
Desiraju, G. R., 283, 284
deSolms, S. J., 477
Devillers, J., 476, 483
Dham, A. K., 282
Dharanipragada, R., 474
Di Matteo, A., 471
Diederich, F., 474, 480, 482
Diercksen, G. H. F., 133
DiMeglio, C. M., 475
Dinares, I., 478
Ding, D., 216
Dinur, U., 219, 282, 480
Dirac, P. A. M., *vi*
Dixon, D. A., 477, 483
Dixon, M., 393
Dixon, R. W., 286, 474
Djerassi, C., 479
Dobbyn, A. J., 132
Dobler, M., 485
Dobson, S. M., 476
Dodziuk, H., 474
Dolata, D. P., 483
Doman, T. N., 474
Donini, O., 474
Dorigo, A. E., 474
Dorsey, B. D., 477
Dorsey, G. O., 480
Dósen-Micovic, L., 474, 480
Dougherty, D. A., 473
Douglas, J. E., 480
Dowd, K., 132
Drakenberg, T., 470
Drenth, W., 477
Drew, M. G. B., 470, 474, 477, 483
Drummond, L. A., 469
Dubrovin, B. A., 393
Duckworth, P. A., 469
Dudek, M. J., 288
Duffy, E. M., 474, 478, 481
Dugstadt, H., 475
Duh, H.-Y., 477
Dunbrack, R. L., Jr., 480
Dunitz, J. D., 283, 485
Dunning, T. H., 136
Durier, V., 485
Durkin, K. A., 474
Dustman, J. A., 479
Dutta, P. K., 221
Dwek, R. A., 486
Dwyer, M., 472
Dyall, K. G., 133
Dybowski, C., 223
Dykstra, C. E., 129, 133, 285, 286
East, A. L. L., 132
Eckert, F., 132
Edberg, R., 394
Edge, C. J., 486
Edge, N. C., 471
Edholm, O., 471
Ediger, M. D., 475
Edwards, S. F., 392
Egert, E., 288
Eichler, U., 216
Eilers, J. E., 483
Eisenstein, M., 288
Eksterowicz, J. E., 474, 477

- Elbert, S. T., 30
Eliel, E. L., 475
Ellencweig, A., 470
Ema, T., 478
Emrich, K., 128
Endicott, J. F., 475, 479, 485
Endo, Y., 478
Engelhardt, L. M., 471
Engelsen, S. B., 475
Erickson, J. W., 480
Erion, M. D., 476
Erker, G., 477
Ermoshin, V. A., 219
Erpenbeck, J. J., 395
Ertl, G., 214
Espinosa-Müller, A. W., 475
Essex, J. W., 288, 289
Etchepare, J., 219
Euler, W. B., 483
Eurenius, K. P., 475
Evans, D. J., 220, 392, 394, 395, 396
Evans, M. E., 469
Evanseck, J. D., 480
Evers, A., 476
Ewald, P. P., 220
Ewig, C. S., 479, 480, 482
Ewing, T. J. A., 475
Eyermann, C., 478
Fabricius, J., 475
Faerman, C. H., 284, 288
Fairlie, D. P., 473
Fajula, F., 216
Falk, H., 475
Famini, G. R., 30
Fan, C. F., 475
Fan, J., 218
Fan, L., 474
Fan, Y., 470, 475
Fantucci, P., 470, 480
Farragher, N. P., 218
Farraher, S. W., 469
Farrell, N., 471
Fath, A., 473
Fathallah, M., 472
Fausto, R., 475
Faux, D. A., 222
Feenstra, K. A., 485
Feller, D., 217, 282
Feller, S. E., 475
Fellmann, J. D., 217
Fennen, J., 485
Fereira, D., 472
Ferenczy, G. G., 286, 289
Ferguson, D. M., 282, 472, 473, 475, 484, 485
Ferguson, S. B., 474, 480
Fermann, J. T., 132, 135
Fernández, B., 475
Ferrand, M., 475
Ferro, D. R., 475, 483
Fichthorn, K. A., 217
Fidelis, K., 475
Field, M. J., 476, 480
Filipovic, D., 475
Filippini, G., 282, 476
Fineberg, J., 396
Fioravanzo, E., 476
Firman, T. K., 479
Fischer, R., 220
Fischer, S., 475, 480
Fitjer, L., 484
Fitzgerald, G. B., 127, 132
Fitzgerald, P. M. D., 477
Flament, J.-P., 479
Flanagan, H. L., 470
Flanagan, K., 284
Flanigen, E. M., 215, 221
Flannery, B. P., 31, 220
Florez, J., 486
Fluder, E. M., 30
Flurhick, K. M., 218, 479
Foces-Foces, C., 472
Foglia, F., 479
Fois, E. S., 216, 218, 220
Foloppe, N., 475
Fomenko, A. T., 393
Font, J., 478
Font, L. M., 472
Foote, C. S., 478
Ford, P. C., 481
Foresman, J. B., 29
Forester, T. R., 222, 288
Forrest, F. R. F., 481
Fürstet, H., 222
Forsyth, G. A., 470, 475, 480
Fossheim, R., 475
Fowler, P. W., 283, 284
Fox, D. J., 29, 132
Fox, P. C., 475, 479
Fox, T., 282, 473, 475
Fraissard, J., 218
Franci, M. M., 30, 31, 218, 286
Fraschini, E., 286
Fraser, G. T., 283
Fraser, K. A., 480

- Fraser-Reid, B., 486
Frash, M. V., 216, 217
Frausto de Silva, J. J. R., 470
Freed, K. F., 130
Freeman, C. M., 216, 217
Freeman, D. L., 129
French, A. D., 471
Frenkel, D., 215, 221
Frey, R. F., 481
Frey, S. T., 475
Friedman, A., 394
Frieken, N., 485
Frierson, M. R., 470, 475
Friesner, R. A., 284
Fripiat, J. J., 216
Frisch, M. J., 29, 30, 131, 133
Froimowitz, M., 475
Froncwk, F. R., 485
Frontera, A., 474
Fruetel, J. A., 475
Fuchs, A. H., 216
Fuchs, B., 470, 481, 483
Fuglesang, C. D., 477
Fujishita, Y., 478
Fujita, H., 482
Fukase, K., 482
Fukazawa, Y., 475
Fulcrand-El Kattan, G., 475
Fuson, M. M., 475
Fyfe, C. A., 222
- Gabdualline, R. R., 475
Gabré, F., 482
Gacs-Baitz, E., 472
Gaedt, K., 475
Gaffin, N., 477
Gago, F., 474, 482
Gahan, L. R., 473
Gainsford, G. J., 472
Gajdos, J., 475
Gajewski, J. J., 475
Gale, J. D., 215, 217, 223
Gallego, J., 474
Gallego, M. T., 475
Gallicchio, E., 479
Gallion, S., 479
Gallo, R., 471, 472, 474
Gallo, J. J., 283
Gallucci, J. C., 474
Galova, Z., 479
Gamba, A., 216, 218, 220
Gandeour, R. D., 473
Gane, T., 480
- Gange, D., 30, 485
Ganly-Cunningham, M., 473
Gao, J., 30, 215, 480, 482
Gao, X., 485
Garcia, J. I., 485
García, L., 482
Garcia-Garibay, M. A., 478
Gardner, M., 471, 485
Garduño-Juárez, R., 476
Garmer, D. R., 287
Garrett, B. C., 486
Garrone, E., 223
Gasmi, V., 476, 483
Gass, D., 392
Gastaldi, S., 471
Gasteiger, J., 476
Gatilov, Y. V., 485
Gatti, C., 288
Gauss, J., 125, 126, 127, 128, 131, 132, 134
Gavaskar, K., 471
Gavezzotti, A., 282, 476
Gaw, J. F., 132
Geidel, E., 222
Geier, S., 470
Geissler, H., 485
Gennari, C., 470, 471, 476, 485
Genoni, F., 222
Geremia, S., 476
Gerlich, G., 393
Gerlt, J. A., 480
German, A. L., 477
Germann, M. W., 471
Ghio, C., 282, 470, 486
Ghisletta, M., 477
Ghose, K. B., 135
Ghosh, A. K., 477
Ghosh, S., 128
Ghosh, S. K., 218, 288
Giammona, A., 476
Gianutsos, G., 475
Gibson, K. D., 482
Gies, H., 222
Gilbert, K. E., 475
Gill, P. M. W., 29
Gillan, M., 393
Giovannetti, J. S., 476
Gippert, G. P., 481
Glaser, D. H., 470
Glasser, L., 472, 480
Gleich, D., 476
Glenn, M. P., 482
Glennon, T. M., 476
Gleria, M., 472

- Gloe, K., 473
Glover, S., 479
Godber, J., 222
Goddard, J. D., 134
Goddard, W. A., III, 218, 219, 220, 284, 288,
 478, 481, 483
Golab, J. T., 471
Goldberg, I., 470
Goldsmith, D. J., 476
Goldstein, E., 476
Goldstein, H., 393
Golembeski, N., 486
Golender, L., 483
Golub, G. H., 31
Gomperts, R., 29
Gonzales, N., 216
Gonzalez, C., 29
Gonzalez, J., 483
Goodfellow, J. M., 284, 483
Goodman, J. M., 471, 476
Goodman, M., 482, 485
Gooley, P. R., 477
Gordon, M. S., 30
Gordon, R. G., 221
Gorman, A. M., 216
Goscinski, O., 134
Goto, H., 484
Gould, I. R., 282, 473
Goursot, A., 216
Gozin, M., 471
Graham, S. L., 477
Graindorge, H., 474
Gramlich, V., 477
Grant, G. H., 469
Grassi, A., 470, 471, 476
Gratias, R., 476
Gray, C. G., 285
Gray, G. W., 281
Gready, J. E., 474
Greatbanks, S. P., 223
Grebowicz, J., 394
Green, M., 394
Green, M. M., 476
Green, P. G., 284
Gregg, T. M., 480
Gregory, J. K., 287
Grenier-Loustalot, M.-F., 478
Gresh, N., 287
Grest, G. S., 395, 396
Grieshaber, M. V., 483
Griffith, R., 476
Grigoras, S., 476
Grillo, M. E., 215
Grimmer, N. E., 480
Grindley, T. B., 476, 483
Groenen, L. C., 475, 476
Grootenhuis, P. D. J., 475, 476, 479, 484
Gross, S. P., 396
Gu, K.-J., 482
Guare, J. P., 477
Gubbins, K. E., 285
Guerra, M., 480
Guerrero, S., 480
Guest, M. F., 396
Gueu, P., 476
Gugelchuk, M. M., 476
Guida, W. C., 476
Guilbaud, P., 476
Guiles, J. W., 473
Guiliani, E. A., 477
Guillen, M., ν
Gulnik, S. V., 480
Gundertofte, K., 470, 482
Günter, B., 484
Guo, H., 480
Gupta, S. A., 395
Gupta, V., 485
Gussoni, M., 221
Gwaltney, S. R., 128
Ha, S. N., 476, 480
Haase, F., 132, 223
Haasnoot, C. A. G., 476
Hadzi, D., 282
Haeberlein, M., 476, 477
Haeffner, F., 476, 482
Hägele, G. 472
Hagler, A. T., 219, 282, 477, 479, 480, 481,
 482, 484
Hagstrom, R., 220
Halgren, T. A., 284, 476, 477
Halkier, A., 128
Hall, K. B., 486
Hamada, T., 478
Hambley, T. W., 471, 472, 473, 476
Hamilton, T. P., 132
Hammerström, L. G., 476
Hampel, C., 126, 132, 135
Hancock, R. D., 476, 477, 479, 481, 483
Handy, N. C., 131, 132, 133, 134, 135, 283,
 286
Hanks, B. A., 478
Hanley, H. J. M., 395
Hanson, B. A., 477
Hanson, G. R., 473
Hanson, R. J., 31

- Hansson, S., 482
Hardin, C. C., 483
Harding, C., 477
Hariharan, P. C., 287
Haring, M., 132
Harkema, S., 476
Harp, G. D., 393
Harris, D., 477
Harris, F. E., 129
Harris, W. R., 479
Harrison, R., 127
Harrison, R. J., 396
Harrowfield, J. M., 471
Hartzell, C. J., 477
Hase, W. L., 477
Hase, Y., 480
Häser, M., 132
Hashimoto, H., 477
Hass, K. C., 217
Hassler, K., 477
Hassner, A., 477
Hattig, C., 285, 286
Hawkins, C. J., 476
Hawkins, G. D., 29
Hawkins, J. M., 483
Hay, B. P., 477, 483
Hay, P. J., 217
Hayes, I. C., 283
Haynam, C. A., 283
Head-Gordon, M., 29, 126, 128, 130, 132, 133, 134
Heeg, M. J., 479, 485
Heffner, F., 477
Hegetschweiler, K., 477
Helfrich, J., 477
Helgaker, T., 127, 128, 130, 132, 133, 136
Helm, L., 479
Hemingway, R. W., 472
Hemmings, M. A., 485
Hengartner, U., 477
Henrick, K., 469
Henson, N. J., 472
Hentschke, R., 477, 482
Herden, H., 223
Hermann, R. B., 439
Hernandez, G., 481
Herrero, C. P., 216
Herrmann, W. R., 476
Hess, B. A., 132, 285, 286
Hess, S., 396
Hesse, U., 284
Hester, R., 221
Heuts, J. P. A., 477
Hewkin, C. T., 476
Heyes, D. M., 396
Heyes, S. J., 472
Heyman, R., 475
Hezemans, A. M. F., 477
Hickey, M. J., 473
Hickman, R., 392
Hidaka, Y., 486
Hider, R. C., 486
Hilfenhaus, P., 473
Hill, G. C., 477
Hill, J.-R., 219, 477, 479
Hillier, I. W., 223
Hillier, M. C., 480
Hino, A., 483
Hinsen, K., 31
Hirao, K., 130
Hirota, M., 469, 483, 484
Hirotsu, M., 484
Hirshfeld, F. L., 285
Hitchman, M. A., 473
Hite, G. J., 475
Ho, K.-K., 472
Hobbs, J. D., 478
Hockless, D. C. R., 471
Hodges, M. P., 287
Höfer, O., 475
Hoffman, A. J., 472, 479
Hoffmann, M. R., 126, 129
Hoffmann, R. W., 472
Hofmann, D. W. M., 283
Hoheisel, C., 394
Hohenberg, P., 218
Holbrey, J. D., 477
Hölderich, W., 219, 222
Holian, B. L., 393, 394, 396
Hollbacher, G., 475
Holloway, M. K., 477
Holmes, R. R., 474
Höltje, H.-D., 475
Homans, S. W., 477
Hönig, H., 470, 477
Hoops, S. C., 477
Hoover, W. G., 220, 392, 393, 396
Hopfinger, A. J., 219, 480, 481
Hopkins, W. W. A., 474
Horimoto, S., 482
Hormann, R. E., 473
Horner, D. A., 134
Horner, J. H., 477
Horrocks, W. DeW., Jr., 475
Horsley, J. A., 217
Hossain, M. B., 475, 477

- Hostetler, C. J., 477
Houalla, D., 483
Houk, K. N., 470, 472, 474, 475, 476, 477,
 478, 480, 483, 484, 485, 486
Hounshell, W. D., 477
Houpt, D. J., 282
Howard, A. E., 477
Howard, J. A. K., 283
Höweler, U., 477, 486
Hoy, V. J., 283
Hrusák, J., 134
Hsu, C.-H., 478
Hsu, L.-Y., 282
Hu, Y., 477
Huang, K., 220, 393
Hubac, I., 126, 131
Huhta, D. W., 485
Huige, C. M. J., 477
Huiszoon, C., 285, 477
Huler, E., 282
Hult, K., 476
Hummel, J. P., 477
Humphrey, W., 477
Hünenberger, P. H., 474
Hungate, R. W., 477
Hungerford, N. L., 482
Hunter, C. A., 283
Hurley, A. C., 125
Hurst, G. J. B., 283
Hutchings, G. J., 216
Hutchings, M. G., 477
Hutter, J., 223
Huybrechts, D. R. C., 221, 222
Hwang, C.-K., 481
Hwang, M.-J., 477, 480, 481, 482
Hyttel, J., 470, 471

Iacobino, R., 472
Ichinose, T., 478
Ichiye, T., 484, 486
Imam, M. R., 470, 475, 478
Imhof, R., 219
Inman, W., 478
Inokawa, H., 482
Inoue, K., 473
Inoue, Y., 481, 483
Inui, T., 216
Iratcabal, P., 478
Irisawa, J., 217
Iroff, L. D., 471
Isaksson, R., 478
Ishaq, K., 473
Ishida, H., 478

Ishida, M., 217
Ishikawa, N., 128
Israelachvili, J., 396
Itai, A., 478
Iton, L. E., 219
Ivanov, P. M., 478
Iveson, P. B., 477
Iwata, S., 134
Iyer, K. A., 221

Jackels, S., 472
Jackson, R. A., 214, 219
Jacobs, P. A., 221, 222
Jacucci, G., 396
Jaffe, R., 473
Jähnig, F., 471
Jai, S.-L., 484
Jaiboon, N., 471
Jaime, C., 471, 473, 474, 478
Jakob, H., 473
Jalal, M. A. F., 475
James, J. J., 471, 476, 478
Jänenchen, J., 223
Jansen, A. P. J., 219
Jansen, G., 285
Jansen, J. C., 215, 216, 222
Janssen, C. L., 125, 126, 132
Janssen, L. H. M., 480, 485
Janssen, R. A. J., 469
Janssens, G. O. A., 218
Jaquinod, L., 484
Jarman, M., 479
Jayatilaka, D., 131, 133, 286
Jeffrey, G. A., 478
Jensen, F., 478
Jensen, H. J. A., 127, 130, 132
Jentys, A., 215
Jentzen, W., 478, 484
Jeremic, D., 474
Jewsbury, P., 478
Jeziorski, B., 283
Jhon, M. S., 482
Jiménez-Barbero, J., 472, 478
Jin, A. Y., 478
Jin, Q., 216
Joannopoulos, J. D., 221
Johansen, J. S., 479
Johnson, C. A., 477
Johnson B. G., 29
Johnson, O., 283
Jolly, P. W., 470
Jones-Hertzog, D. K., 478
Jónsdóttir, S. Ó., 478

- Jorgensen, F. S., 478
Jørgensen, P., 127, 128, 129, 130, 132, 133,
 134, 135
Jorgensen, W. L., 30, 474, 478, 479, 481, 482
Joseph-McCarthy, D., 480
Josephs, R., 220
Jousse, F., 217
Jung, H. H., 478
Juranic, I., 480
Jutson, N. J., 474
- Kahn, S. D., 476
Kahne, D., 485
Kaiser, M., 484
Kaku, M., 394
Kaldor, U., 129, 130
Kalia, R. K., 396
Kaminski, G., 478
Kamitakahara, A., 478
Kanai, A., 480
Kanematsu, K., 486
Kang, Y. K., 478, 482
Kanters, J. A., 479
Kanzansky, V. B., 217
Kao, J., 478
Kaplan, W. A., 478
Kar, M., 478
Karaborni, S., 394
Karasawa, N., 220
Karge, H. G., 219, 222
Karlin, K., 473
Karlsson, S., 478
Karlstrom, G., 287
Karni, M., 470
Karplus, M., 282, 472, 475, 480, 481, 483,
 484
Kasatani, K., 482
Kashyap, R. O., 485
Katrusiak, A., 482
Katzenellenbogen, J. A., 470, 471
Kaufman, J. J., 287
Kawai, T., 478
Kawamura, H., 483
Kazmaier, U., 473
Keating, A. E., 478
Keith, T. A., 29, 30
Kellö, V., 131
Kelly, C. M., 470, 476
Kelly, M. B., 478
Kendall, R. A., 396
Kennard, O., 283
Kenyon, G. L., 480
Keserii, G. M., 478
- Kessler, H., 476, 480
Kessler, M., 470
Kestner, N. R., 217, 281
Khalil, M., 486
Khanolkar, A. D., 471
Khatami, H., 221
Kim, K., 478
Kim, S. Y., 482
Kim, W.-K., 478
Kim, Y., 482
Kindermann, R., 484
Kindler, J., 222
King, R. A., 135
Kingsbury, C. A., 472, 480
Kirchhoff, P. D., 478
Kirschner, K. N., 478
Kirtman, B., 285
Kitagawa, T., 478
Kitahara, T., 484
Kitaigorodsky, A. I., 282
Kitaura, K., 281
Kitazawa, M., 482
Kitching, W., 482
Klebe, G., 284
Klein, M., 478
Klein, M. L., 393, 394, 395, 397
Klein, T. E., 479
Klemperer, W., 283
Klewinghaus, P., 476, 478
Klinowski, J., 222, 223
Klomp, U. C., 394
Klopper, W., 136
Knickmeister, M., 477
Knobler, C. B., 482
Knoll, W., 482
Knowles, P. J., 286
Knözinger, H., 214
Kobayashi, R., 133, 134, 286
Kobayashi, S., 483
Koch, H., 127, 128, 130, 133, 134, 134, 135,
 136
Koch, U., 288, 289
Kodama, M., 475
Koegler, J. H., 222
Koehler, J. E. H., 478
Koetzle, T. F., 283
Koga, N., 286
Kogan, M. K., 395
Kogelberg, H., 479
Kohn, K. W., 475
Kohn, W., 218
Koike, A., 479
Kojima, M., 484

- Kok, R. A., 470
Kokotailo, G. T., 222
Kokusen, H., 484
Kolb, H. C., 482
Kollman, P. A., 30, 31, 282, 286, 473, 474,
 475, 476, 477, 479, 480, 481, 482, 484,
 485, 486
Kollwitz, M., 132
Kolossvary, I., 478
Komaromi, I., 479
Komornicki, A., 131
Komorita, T., 474
Konstantinovic, S., 480
Kontoyianni, M., 472, 479
Kooiman, P. J., 216
Korybut-Daszkiewicz, B. R., 471
Koseki, S., 30
Kouwijzer, M. L. C. E., 478, 479
Kowall, T., 479
Koyama, Y., 477
Kozar, T., 479
Kozelka, J., 479
Kozlov, V. A., 134
Kozlowski, P. M., 131
Kradolfer, T., 477
Kralovic, J., 476
Kramer, G. J., 218
Krause, K., 222
Krausz, E. R., 471
Krebbs, B., 486
Kreek, T. W., 475
Krishnan, R., 30, 125, 131
Krogh-Jespersen, K., 483
Krogsgaard-Larsen, P., 479
Kroon, J., 476, 478
Kroon-Batenburg, L. M. J., 479
Kruger, A. W., 480
Krüger, C., 470
Krüger, T., 473
Krylov, A. I., 134
Kuang, J., 470
Kuba, A., 482
Kubelková, L., 223
Kubo, M., 216
Kubo, M. M., 479
Kubo, R., 393
Kucharski, S. A., 125, 126, 129, 132
Kuchnir, L., 480
Kuczera, K., 480, 482
Kudryashova, M. V., 215
Kühner, A., 473
Kulkarni, S. C., 479
Kumar, A., 281
Kumar, K., 475
Kume, M., 217
Kumpf, R. A., 474
Kunz, H., 481
Kunz, R. W., 482, 485
Kurnikova, M. G., 479
Kutteh, R., 220, 392
Kutzelnigg, W., 129
Kuwahara, S., 484
Kuyper, L. F., 484
Kvasnicka, V., 132
Kwon, O. Y., 482
La Penna, G., 471
Laane, J., 473, 478
Laatikainen, R., 485
Laberge, M., 479
Lacheck, H., 288
Lachet, V., 216
Lachgar, A., 472
Ladd, A., 392
Lagant, P., 474
Lago, E. C., 287
Lahti, P. M., 480
Laidig, K. E., 285, 286
Laidig, W. D., 127, 132, 135
Laks, P. E., 472
Lam, B., 30
Lamb, M. L., 479
Lamba, D., 479
Lambert, L. K., 482
Lamberti, C., 222
Landis, C. R., 470, 473, 474, 476, 479,
 483
Lane, T. H., 476
Langhoff, S. R., 129, 130
Lankin, D. C., 479
Larouche, A., 288
Larson, D. L., 484
Laskowski, R. A., 283
Lau, F. T. K., 480
Lauderdale, W. J., 127, 131, 132
Laughton, C. A., 479, 484
Lauher, J. W., 479
Lauritsen, J., 479
Lavery, R., 479
Lawson, C. L., 31
Le Maire, M., 219
Le Sueur, C. R., 285
Leach, A. R., 479
Lecomte, C., 285, 288
Lee, A. M., 135
Lee, K. J., 479

- Lee, M.-H., 223
Lee, S.-F., 479
Lee, T. J., 125, 126, 127, 128, 129, 131, 132,
 133, 134
Lee, Y. S., 125
Lees, A. W., 392
Legon, A. C., 283, 284
LeGrand, S. M., 476
Leininger, T., 132
Leister, D., 478
Lengauer, T., 283
Lenz, T. G., 478, 479
Leofanti, G., 221, 222
Leonard, J. M., 479
Leong, A. J., 469
Leopold, K. R., 283
Lepre, C. A., 481
Lercher, J. A., 222
Leroy, R. J., 285
Lescop, P., 474
Lesinkowski, Z. J., 475
Leslie, M., 218, 287
Lessard, R., 479
Lesueur, C., 471, 474
Leusen, F. J. J., 287
Levendis, D. C., 480
Levin, R. B., 477
Levitz, P., 216
Levy, D. H., 283
Levy, R. M., 479
Lewchenko, V., 287
Lewin, A. H., 478, 479
Lewis, D. W., 216
Li, B., 216
Li, H. X., 221
Li, S., 479
Li, T.-W., 479
Li, W., 396
Li, W.-K., 475
Li, X., 127, 132
Li, Y., 479
Liang, C., 479
Liang, G., 479
Lianza, F., 482
Lichanot, A., 478
Liegeois, C., 480
Liem, S. Y., 392
Lifson, S., 282
Lii, J.-H., 222, 470, 473, 476, 477, 479, 480,
 481, 484
Liljefors, T., 29, 281, 470, 471, 473, 476,
 478, 479, 482, 486
Lin, W.-K., 479
Lindh, R., 132, 134
Lindoy, L. F., 469
Ling, M. S. H., 281
Liotard, D., 478
Liotta, D., 474
Lipkowitz, K. B., 29, 30, 128, 134, 215, 217,
 218, 219, 220, 281, 282, 285, 286, 287,
 392, 395, 396, 397, 439, 470, 472, 486
Littlefield, R. J., 396
Liu, H., 479
Liu, R., 479
Liu, S.-Y., 480
Lloyd, A. W., 132
Lo Celso, F., 284
Lockhart, J. C., 477, 480
Loew, G. H., 473, 475, 477
Loewenstein, W., 216
Loida, P. J., 475
Lombardo, G., 470
Lombardo, G. M., 472, 476
Lombardy, R. L., 480
Lomdahl, P. S., 396
Lommers, J. P. M., 283, 284, 288
Loncharich, R. J., 480, 483
Longari, C., 476
Loose, W., 396
Lopez-Calahorra, F., 473
Lopis, A. S., 480
Loudon, R., 395
Louwen, J. N., 218
Lovas, F. J., 284
Löwdin, P.-O., 133, 134
Lowe, M. P., 480
Lowrey, A. H., 287
Loyens, L. D. J. C., 216
Luboradski, R., 483
Lucas, J., 284
Lucas, K., 394
Luchinat, C., 471
Luckhurst, G. R., 281
Luengo, G., 397
Luo, H., 394
Lumbroso, H., 471, 480
Lunazzi, L., 480
Luque, F. J., 482
Lurinc, V., 132
Lustig, S. R., 396
Lutz, F., 470
Luz, Z., 222
Luzhkov, V., 480
Ly, S. K., 470
Lybrand, T. P., 281, 392, 475
Lyle, T. A., 477

- Ma, B., 476, 480
Mabilia, M., 480
Macchiantelli, D., 480
Macdougall, P. J., 288
MacKenzie, N. E., 477
MacKerell, A. D., Jr., 475, 480, 482, 483, 486
Mackie, W., 479
Macrae, C. F., 283
Madden, P. A., 221
Magarian, R. A., 477
Maginn, E. J., 214, 216, 217
Maigret, B., 473, 484
Maitland, G. C., 281
Majer, J., 482
Majors, R., 473
Makarova, M. A., 216
Makriyannis, A., 475
Malatesta, V., 471, 480
Malik, D. J., 285
Manchanda, R., 480
Manuel, G., 484
Maple, J. R., 480, 481, 484
Marchese, L., 222
Marchon, J.-C., 478
Marder, M., 396
Mareda, J., 481
Mareschal, M., 394
Margl, P., 217, 474
Mari, F., 480
Mark, A. E., 282, 474, 480
Markoulides, T., 480
Markovic, Z., 480
Marques, H. M., 472, 476, 480, 481
Marrink, S.-J., 480
Marrone, T. J., 474, 480
Marsh, F. J., 480, 482
Marsicano, F., 480
Marstokk, K.-M., 481
Martell, A. E., 479
Martin, E., 481
Martin, J. M. L., 133, 136
Martin, R. L., 29
Martin, S. F., 480
Martin-Lomas, M., 472, 478
Martyna, G. J., 221, 393, 395
Marx, D., 393
Maryanoff, B. E., 480
Marzilli, L. G., 472, 473, 486
Mascarella, S. W., 281
Mase, B. B., 473
Mash, E. A., 480
Masignani, V., 472
Maslen, P. E., 286
Matalana, A., 480
Mathä, B., 480
Matsuba, K., 216
Matsui, M., 484
Matsui, T., 478
Matsumoto, T., 480
Matsunaga, N., 480
Mattern, D. L., 480
Matthesini, M., 471
Mattice, W. L., 478, 485
Mattos, C., 480
Mauleón, D., 482
Mayer, A., 484
Mayo, S. L., 219, 481
Maxwell, D. S., 478
Maxwell, I. E., 472
Mazurek, U., 485
Mazzanti, M., 478
McAuliffe, C. A., 471
McCague, R., 479
McCammon, J. A., 472, 474, 478, 485
McCarrick, M., 475
McClure, L. J., 481
McComsey, D. F., 480
McCool, B. J., 469
McCormick, W. D., 396
McDonald, D. Q., 481
McDonald, I. K., 284, 288
McDonald, I. R., 396
McDonald, N. A., 478, 481
McDougall, G. J., 481
McDowell, D., 477
McDowell, R., 478
McEwen, W. E., 480
McGaughey, G. B., 481
McKenna, R., 479
McMartin, C., 481
McNalley, D., 473
McPartlin, M., 469
McQuarrie, D. A., 220, 393
McRae, W. B., 129
McWeeny, R., 217
Meath, W. J., 281, 282, 285
Medforth, C. J., 478, 484
Medrud, R. C., 222
Meier, R. J., 481
Meier, W. M., 214
Meijer, E. M., 474
Meissner, L., 128
Melberg, S., 481
Mellot, C. F., 216
Meng, E. C., 481
Menger, F. M., 481

- Merbach, A. E., 479
Mercandelli, P., 481
Merian, M., 219
Merz, K. M., Jr., 30, 282, 473, 476, 477, 480,
 482, 483
Merzbacher, E., 129
Messow, U., 223
Metropolis, N., 221
Meyer, A. Y., 481
Meyer, B., 482
Meyer, E. F., 283
Meyer, E. S., 220
Meyer, K. L., 477
Meyer, W., 132
Meyers, A. I., 473
Mezey, P. G., 30, 288
M'Henni, F., 472
Michnick, S., 480
Michopoulos, Y., 394
Mihailescu, D., 481
Milewska, M. J., 482
Millen, D. J., 283
Miller, D. M., 484
Miller, J. L., 474
Miller, M. D., 484
Millini, R., 215
Millot, C., 286, 287, 484
Minick, D. J., 482
Mirth, G., 222
Misiti, D., 472
Mislow, K., 471, 477, 486
Mitchell, D. B., 477
Mitchell, E. M., 283
Mitchell, G. F., 283
Mitchell, J. B. O., 283, 284, 285, 288
Mitchell, P. C. H., 474
Mitchell, P. J., 396
Miyamoto, A., 216, 217
Moberg, C., 476, 477, 481, 482
Moeller, M., 394
Moffat, S. H., 30
Mohanrao, K., 481
Mohr, R., 477
Mok, D. K. W., 283
Mokrane, A., 483
Molinari, F., 476
Møllendahl, H., 481
Møller, C., 131
Momany, F. A., 30, 481
Momchilova, T. G., 478
Monache, G. D., 472
Mondro, S. L., 477
Monkhorst, H. J., 125, 129, 133
Montanari, L., 480
Montgomery, J. A., 29
Monye, M., 480
Mooberry, E., 473
Mooine, G., 477
Moore, J. H., 481
Moore, S. J., 473
Morales de Tirado, P. L., 478
Moran, B., 392
Moreland, D. W., 481
Morgan, T., 471
Mori, K., 484
Mori, M., 484
Morokuma, K., 281
Morris, G. P., 392, 394, 395,
 396
Morsicano, F., 481
Mortier, W. J., 218, 288
Mosell, T., 217
Moses, S. R., 477
Mosquera, R. A., 472, 483
Mosynski, R., 283
Mountain, R. D., 287, 395
Moyna, G., 481
Moyoral, J. A., 485
Mühlbauer, C. F., 474
Mukherjee, D., 128, 130
Mukherjee, P. K., 128
Mukhopadhyay, D., 130
Mukhopadhyay, S., 130
Mukhopadhyay, T., 476
Mulder, F., 285
Müller, N., 475
Müller, P., 481
Müller, R., 481
Müller-Plathe, F., 479
Mulliken, R. S., 29, 218, 286
Mumby, S. J., 484
Mundy, C. J., 393, 394, 395
Munshi, S., 480
Munro, O. Q., 480, 481
Mura, M. E., 132
Murad, S., 220
Murata, M., 481, 483
Murphy, R. B., 284
Murray, C., 131
Murray, C. W., 286
Murray, J. S., 30
Murrell, J. N., 284
Mutter, M. S., 480
Nachbar, R. B., Jr., 484
Nachman, R. J., 481

- Nagaoka, M., 482
Nagata, T., 483
Nagawa, Y., 485
Nagi, G. K., 287
Nagy, K. L., 477
Nakagawa, S., 481
Nakagawa, Y., 222
Nakamura, H., 217
Nakanishi, H., 485
Nakano, T., 217
Nakatsui, H., 130
Nanayakkara, A., 29, 288
Nandi, C. L., 283, 284
Naray-Szabo, G., 286
Nawata, Y., 486
Nedomová, K., 223
Neff, C., 480
Neidle, S., 479
Neijer, N. A., 474
Nelson, J., 477
Nelson, N. Y., 478
Neogrády, P., 126
Nesbet, R. K., 133
Nevins, N., 481
Névoret, C. J., 469
Newcomb, M., 477
Newsam, J. M., 215, 219, 472
Newton, S. Q., 481
Ngo, T., 480
Nguyen, D. T., 480, 482, 486
Ngwenya, M. P., 476
Nicholas, J. B., 214, 219, 481
Nicklass, A., 132
Nicolaou, K. C., 481
Nicolini, M., 471
Niketic, S. R., 481
Nilsson, I., 481
Nilsson, L., 483
Nishikawa, K., 134
Njo, S. L., 216, 218, 222
No, K. T., 478, 482
Nobeli, I., 281, 284
Noga, J., 126, 129, 131, 132, 136
Nolte, R. J. M., 477
Nooijen, M., 127, 128, 129, 130
Norin, T., 476
Norman, M. H., 482
Norrby, P.-O., 472, 481, 482
Norrby, T., 472
Nørskov-Lauritsen, L., 482
Nortier, P., 217
Nosé, S., 221, 393, 396
Notari, B., 222
Nouguier, R., 471, 474
Nováková, J., 223
Novick, S. E., 283
Novikov, S. P., 393
Nuber, B., 473
Nunami, K., 482
Núñez, R., 482
Nurco, D. J., 484
Nuss, M. E., 482
Nusterer, E., 217, 223
Nyburg, S. C., 284
Ocampo-Garcia, E., 476
Ochrymowycz, L. A., 485
Oda, M., 482
Oh, J., 482
Ohashi, M., 482
Ohkubo, K., 478
Ohmichi, N., 481
Ohsuna, T., 222
Okada, C., 482
Okada, K., 484
Oki, M., 469, 486
Okuyama-Toshida, N., 482
Olafson, B. D., 219, 282, 472, 481
Oliphant, N., 135
Olivato, P. R., 480
Olli, L. K., 486
Olofson, R. A., 480
Olsen, J., 128
Olson, D. H., 214
Omelchenko, A., 396
Ondrias, M. R., 484
O'Neill, F. M. M., 471
Orbell, J. D., 486
Oreja, E., 472
Orioli, P. L., 471
Ornstein, R. L., 475, 482
Orozco, M., 482, 484
Ortiz, A. R., 474, 482
Ortiz, J. V., 29
Ortiz de Montellano, P. R., 475
Ósawa, E., 281, 478, 480, 482, 483, 484,
 485, 486
Ostlund, N. S., 129
Ott, K.-H., 482
Ouellette, R. J., 482
Oumi, Y., 216
Ovaska, T. V., 471
Overacre, L. B., 477
Overman, L. E., 470
Owens, L., 474, 482
Ozin, G. A., 222

- Padilla, P., 395
Padwa, A., 477
Pai, S.-I., 392
Pal, B., 472
Paldus, J., 125, 127, 129, 130, 132, 133, 134
Palmer, B. J., 486
Palmer, D. E., 482
Palmer, J. A., 476
Palmieri, P., 132
Palomer, A., 482
Paolini, G. V., 394
Papoyan, G., 482
Pappalardo, G. C., 470, 471, 472, 476
Parish, C., 482, 484
Park, G., 473
Park, J. M., 482
Park, M. S., 484
Park, N.-S., 486
Parker, S. C., 214
Parr, R. G., 217
Parrinello, M., 221, 393
Parthasarathy, R., 284
Pasto, D. J., 482
Pastor, R. W., 475, 486
Pasztor, C., 222
Patel, S. T., 486
Paterlini, M. G., 484
Paterson, I., 471, 476, 485
Pathiaseril, A., 470, 472
Pattaroni, C., 482
Patterson, D. G., Jr., 472
Patrick, G., 480
Paulsen, M. D., 475, 482
Pauncz, R., 132
Pavelcik, F., 482
Pavelites, J. J., 482
Payne, M. C., 217, 221, 223
Pearlman, D. A., 473, 482
Pearlstein, R. A., 480
Pedersen, H., 471
Pedersen, L. G., 471
Peebles, S. A., 284
Pell, W., 30
Pelmentschikov, A. G., 223
Peng, C. Y., 29
Peng, Z., 482
Penrose, R., 31
Pêpe, G., 485
Perego, G., 215, 222
Pérez, S., 479
Peri, J. B., 222
Perie, J., 483
Perkovic, M. W., 475, 479
Perregaard, J., 470
Perrin, M. A., 217
Persson, B. J., 136
Pertsin, A. J., 282
Peterak, F., 479
Peterson, K. A., 132
Pettersson, G. A., 29
Petrakis, L., 218
Petrini, G., 221, 222
Petrovich, L. M., 473
Pettersson, I., 29, 281, 471, 482, 486
Pettitt, B. M., 472, 484
Pfeifer, H., 219, 222
Piani, S., 475
Pichon-Pesme, V., 285, 288
Piecuch, P., 135
Pierleoni, C., 394
Pierrot, M., 483
Piet, P., 477
Pilar, F. L., 131
Pisabarro, M. T., 482
Pitzer, K. S., 281
Pitzer, R. M., 132
Plastaras, J. P., 486
Plesset, M. S., 131
Podlogar, B. L., 482
Pojarlieff, I. G., 478
Poli, G., 471
Politzer, P., 30, 281
Polonski, T., 482
Pommier, Y., 475
Ponder, J. W., 288, 473
Popelier, P. L. A., 30, 286, 287, 289
Pople, J. A., 29, 30, 125, 126, 129, 131, 132, 133, 217
Pordesimo, E. O., 477
Portoghesi, P., 484
Post, C. B., 486
Postma, J. P. M., 221
Potena, D., 476
Potter, R. J., 474
Pounds, K. L., 475
Pourcin, J., 220
Pranata, J., 482, 483
Pranta, J., 478
Pratesi, L., 470
Pregosin, P. S., 482, 485
Press, W. H., 31, 220
Previde Massara, E., 215
Price, D. J., 482
Price, S. L., 281, 283, 284, 285, 286, 287, 288
Prodhom, B., 480

- Profeta, S., Jr., 282, 472, 473, 482, 485, 486
Proutiere, A., 476
Proveda, A. M., 472
Puiggali, J., 470
Pulay, P., 132, 135
Pullman, A., 287
Pullman, B., 130, 133
Pumilia, P., 475
Pupyshev, V. I., 134
Purvis, G. D., III, 125, 131, 480

Qamhiyeh, E., 476
Qian, J., 482
Quartieri, S., 218, 220
Querol, E., 474
Quinn, M. I., 470
Quiñóá, E., 483
Quiroa, V., 476
Quitzsch, K., 223

Rabasco, D., 472
Raber, D. J., 472, 482
Rabitz, H., 484
Rablen, P. R., 286
Rack, E. P., 472
Rafey, R. A., 396
Ragazzi, M., 475, 483
Raghavachari, K., 29, 126, 132, 133
Raghunathan, S., 477
Rahman, A., 221, 393
Rahman, M., 470
Rai, B. L., 486
Raimondi, L., 470, 471, 483
Raitsimring, A. M., 483
Ramachandran, K., 480
Ramasseul, R., 478
Ramlow, A., 473
Ramprasad, R., 217
Ranghino, G., 480
Rankin, D. W. H., 470, 475
Rao, K. M., 221
Rao, S. N., 479
Rappé, A. K., 218, 288, 473, 483
Rappoport, Z., 471
Rashid, A., 479
Rasmussen, K., 475, 478, 481, 483, 484
Rastogi, S. R., 396
Rauhut, G., 132
Reddy, V. V., 472
Redondo, A., 217
Reedijk, J., 472
Reibenspies, J. H., 479
Reichert, D. E., 477, 483

Reiher, W. E., III, 480
Reiling, S., 483
Reinhoudt, D. N., 475, 476, 485
Remers, W. A., 477
Remington, R. B., 132, 134
Remler, D. K., 221
Ren, J., 483
Rendell, A. P., 127, 131, 133
Replogle, E. S., 29, 132
Rettig, W., 483
Reynolds, C. A., 288, 289
Reynolds, C. H., 473
Ricchiardi, G., 215
Rice, D. A., 474
Rice, J. E., 125, 127, 132, 286
Richards, N. G. J., 286
Richards, W. G., 288, 289
Richardson, W. H., 483
Riches, B. H., 482
Richou, M.-C., 477
Rico, R. J., 130
Rigby, A. M., 216, 217
Rigby, M., 281
Rigdon, G. C., 482
Rigos, A. A., 396
Riguera, R., 483
Rigutto, M. S., 222
Rim, O. K., 473
Rios, M. A., 472, 475, 485
Ritchie, J. P., 285, 286
Rithner, C. D., 483
Rittby, C. M. L., 130
Rittby, M., 126
Rius, J., 477
Rivail, J.-L., 472
Robb, M. A., 29
Robbins, M. O., 395, 396
Roberts, J. D., 482
Robinet, G., 476, 483
Robinson, W. T., 472
Rochester, J., 483
Rockwell, G. D., 483
Rodger, P. M., 288
Rodgers, J. R., 283
Rodham, D. A., 284
Rodriguez, S., 470
Rodríguez-Ubis, J. C., 472
Roethlisberger, U., 397
Rogers, D. W., 483
Romerosa, A., 477
Ronchetti, F., 485
Rone, R., 481
Roos, B. O., 129

- Root, D. M., 479, 483
Rosenblum, A., 482
Rosenbluth, A. W., 221
Rosenbluth, M. N., 221
Ross, W. S., 483
Rossi, K., 471
Rossi, K. A., 483
Roszak, S., 287
Roth, R., 484
Rotkiewicz, K., 483
Roux, B., 31, 480, 483
Rowland, R. S., 283, 284
Rowlands, M. G., 479
Ruano, J. L. G., 475
Rüchardt, C., 471
Rudge, W. E., 396
Rudolf, K., 483
Rudong, Y., 479
Rudzinski, J. M., 483, 486
Ruegger, H., 482
Ruiz-López, M. F., 483, 485
Runnebaum, R. C., 217
Rustad, J. R., 477
Rutherford, T. J., 479
Rybalova, T. V., 485
Ryckaert, J. P., 220, 394
Ryde, U., 31, 286, 483
- Sabolovic, J., 483
Sadun, C., 470
Sæbø, S., 135
Safo, M. K., 483
Saigal, S., 483
St-Amant, A., 218
Saito, Y., 478
Sakai, K., 483
Sakakibara, K., 483, 484
Sakuma, H., 222
Sakurai, M., 481, 483
Salom, B., 471, 476
Salter, E. A., 127
Saltzmann, R., 482
Salva, P., 475
Salvatella, L., 483
Sanders, M. L., 218
Sanders, W. M., 477
Sanderson, R. T., 218
Sandrone, G., 477, 483
Sandström, J., 478, 481, 483
Sanger, W., 478
Santalo, N., 473
Santini, A., 472
Santos, M. A., 470, 483
- Sanz, J., 286
Sardinia, F. J., 483
Sardone, N., 476
Sargeson, A. M., 471, 472, 474
Satchler, G. R., 281
Sato, H., 482
Sato, T., 483
Sauer, J., 215, 216, 219, 223, 477
Sauers, R. R., 483
Saunders, V. R., 223
Saunders, W. H., Jr., 476
Savinelli, R., 479
Sawaryn, A., 285, 286
Saxe, P., 132
Sayle, T. X. T., 483
Scanlan, T. S., 475
Schaad, L. J., 132
Schaefer, H. F. III, 125, 126, 127, 129, 131, 132, 133, 134, 135, 217
Schäfer, L., 481, 484
Scheidt, W. R., 481, 483
Scheiner, A. C., 125, 127, 132
Scheiner, S., 282
Scheraga, H. A., 478, 482
Schinazi, R. F., 475
Schipper, E. T. W. M., 477
Schlegel, H. B., 29, 30, 125
Schleifer, L., 470, 481
Schlenkrich, M., 222, 480, 483
Schlick, T., 215
Schmalle, W. H., 477
Schmid, R., 476
Schmidt, M. W., 30
Schmitz, B. K., 483
Schmitz, F. J., 477
Schmitz, L. R., 483
Schneider, W. F., 217
Schnur, D. M., 483
Schoonheydt, R. A., 218
Schrumpf, G., 217, 222
Schröder, K.-P., 219
Schulten, K., 477
Schultze, L. M., 475
Schulz, G., 485
Schuster, I. I., 486
Schutt, C., 484
Schutz, B., 397
Schütz, M., 132
Schwarz, C. L., 475, 479
Schwarz, K., 217, 223
Scolastico, C., 471
Scott, A. I., 481
Scott, R. A., 478

- Scrocco, E., 30
Scuseria, G. E., 125, 126, 127, 129, 132, 133,
 134
Seeger, R., 30
Segura, C., 478
Seidl, E. T., 132
Seiler, P., 474
Seiti, K., 215
Sekino, H., 125, 128
Sellers, H., 483
Sen, S., 483
Senge, M. O., 484
Senderowitz, H., 482, 483, 484
Seo, B. H., 482
Seri, C., 472
Severance, D. L., 474, 478
Seward, E., 480
Shah, R., 223
Sham, L. J., 218
Shankar, S., 218, 288
Sharp, K. A., 479
Sharpless, K. B., 482
Shary-Tehrany, S., 473
Shavitt, I., 129, 131
Sheldrick, B., 479
Sheldrick, W. S., 484
Shelley, J. C., 392
Shelnutt, J. A., 478, 484
Shenoy, V. S., 484
Sheves, M., 477
Shenderova, O. A., 397
Sherrill, C. D., 129, 132, 134, 135
Sherrod, M. J., 474, 481, 484
Sherwood, P., 223
Shevtsov, S. A., 485
Shi, L. M., 475
Shiba, T., 482
Shields, G. C., 484
Shim, J. Y., 484
Shimaaki, K., 484
Shimanouchi, T., 283
Shimazaki, K., 483
Shin, S., 478
Shinohara, H., 482
Shioriri, T., 480
Shnidman, Y., 483
Shongwe, M. S., 480
Shubuya, K., 135
Shudo, K., 478
Shutzberg, B. A., 476
Sickmüller, A. F., 473
Siebers, J. G., 287
Siepmann, J. I., 221, 394, 395
Sigfridsson, E., 31, 286
Silong, S. B., 474
Silver, D. M., 130
Silverman, B. D., 484
Simandiras, E. D., 286
Simons, J., 127, 129, 135
Simpson, M. C., 478
Sinanoglu, O., 128
Singer, S. J., 221
Singh, J., 283, 284
Singh, U. C., 282, 479, 486
Siri, D., 485
Sironi, A., 481, 484
Sisterhen, L. L., 474
Sjöstrand, U., 471, 477
Skelton, B. W., 471
Skiff, W. M., 483
Sligar, S. G., 475
Sluyterman, L. A. Å., 474
Smetankine, L., 219
Smirnov, K. S., 215, 219, 220, 221, 222
Smit, B., 215, 216, 394
Smith, D. W., 129
Smith, E. B., 281
Smith, G. M., 483
Smith, J. C., 471, 475, 480, 481
Smith, J. M., 283
Smith, K. A., 475
Smith, K. M., 478, 484
Smith, P. E., 480, 484
Smith, V. H., Jr., 30
Smith, W., 222, 288
Smondyrev, A. M., 484
Snarey, M., 283
Snow, M. R., 472, 476
Snyder, J. P., 474, 478, 479, 481
Soetens, J.-C., 287, 484
Sohrin, Y., 484
Sokalski, W. A., 285, 286, 287
Soloja, B., 474
Song, X.-Z., 478, 484
Sorensen, J., 484
Southwick, E., 478
Spackman, M. A., 286
Spangler, D. P., 479
Sparks, L. D., 484
Spears, G. W., 484
Spector, T. I., 484
Spellmeyer, D. C., 282, 473, 484
Spence, K. L., 485
Sprague, J. T., 470, 484
Sprik, M., 397
Srđanov, V., 397

- Stackhouse, J., 477
Stadler, M., 484
Stahl, M. T., 480
Stammen, B., 484
Stanton, J. F., 125, 126, 127, 128, 129, 130,
 131, 132, 133, 134, 135, 217, 282
States, D. J., 282, 472
Stefanov, B. B., 29
Steiner, T., 284
Stephan, H., 473
Stephan, K., 394
Sterner, O., 484
Stevens, A. P., 215, 216
Stevens, E. D., 284
Stevens, M. J., 396
Stevenson, C., 477
Stewart, E. L., 472, 481, 484
Stewart, J. J. P., 29, 218
Steynberg, J. P., 472, 485
Stich, I., 217
Still, W. C., 476, 481, 482, 484
Stockfisch, T. P., 477, 480
Stolarszyk, L. Z., 133
Stolfo, J., 482
Stoll, H., 132
Stone, A. J., 132, 281, 282, 283, 284, 285,
 286, 287, 288, 289
Storer, J. W., 471
Stote, R. H., 480, 484
Stouch, T. R., 30, 31, 288, 479, 484
Straatsma, T. P., 220, 392
Strassner, T., 484
Stratemeier, H., 473
Straty, G. C., 395
Straub, J., 480
Strobl, E., 484
Strobl, H., 222
Ströhle, M., 472
Stutchbury, N. C. J., 285
Stylianides, N., 481
Stylianopoulos, C., 474
Su, M. D., 286
Su, Z., 29
Subra, R., 471
Subramanian, G., 484
Suenram, R. D., 284
Suffritti, G. B., 214, 215, 218, 220, 222
Sugawa, T., 482
Sugawara, M., 135
Sun, H., 484
Sun, P., 216
Sundin, A., 484
Suppan, P., 483
Surzur, J. M., 474
Suslick, K. S., 478
Susnow, R., 484
Sutcliffe, B. T., 217
Suwinska, K., 483
Suzdak, P., 475
Suzuki, A., 483
Suzuki, M., 394
Suzuki, S., 284
Swaminathan, S., 282, 472
Swinney, H. L., 396
Swope, W. C., 220
Sykes, B. D., 471
Szabo, A., 129, 473
Szalay, P. G., 127, 128, 129, 135
Szalewicz, K., 283
Szalontai, G., 482
Szymanski, H. A., 221
Tafi, A., 472
Tai, J. C., 479, 484
Takahashi, Y., 217
Takahata, Y., 474
Takeda, Y., 475
Takeuchi, T., 478
Takeuchi, Y., 484
Tanabe, K., 485
Tang, T.-H., 486
Tanious, F. A., 475, 480
Tao, Y.-T., 479
Taramaso, M., 222
Tartkovsky, E., 470
Tasaka, M., 484
Tasker, P. A., 469
Tasumi, M., 283
Tavitian, B., 216
Taylor, P. R., 129, 131, 132, 136
Taylor, R., 283, 284, 478, 484
Teeter, M. M., 479
Teipel, S., 486
Teixeira-Dias, J. C. C., 475
Teixidor, F., 477
Teller, A. H., 221
Teller, E., 221, 281
Teppen, B. J., 484
Teraishi, K., 217
Terakura, K., 217
Terasaki, O., 222
Terauchi, C., 135
Teter, M. P., 221
Teukolsky, S. A., 31, 220

- Thangarasa, R., 476
Theodorou, D. N., 214, 216
Thiel, Y., 471
Thiem, H.-J., 484
Thilgen, C., 482
Thomas, B. E., IV, 475
Thomas, H. D., 470, 484
Thomas, J. M., 216
Thomas, J. R., 131
Thompson, D., 474
Thompson, B., 470
Thompson, C. J., 393
Thompson, P. A., 395
Thompson, W. J., 477
Thondorf, I., 485
Thornley, A. E., 284
Thornton, J. M., 283, 284
Thorp, M. S., 471
Thorsteinsson, T., 132
Tidwell, R. R., 480
Tieleman, D. P., 485
Tietze, L. F., 485
Tildesley, D. J., 215, 288, 393
Timofeeva, T. V., 485
Tinland, B., 474
Tirado-Rives, J., 474, 478
Titmuss, S. J., 476
Tkachev, A. V., 485
Tobias, D. J., 393
Tobiason, F. L., 485
Toma, L., 485
Tomasi, J., 30
Tomkinson, N. P., 477
Tong, C. S., 282, 285
Tong, W., 135
Topol, I. A., 480
Tordo, P., 485
Torrens, F., 485
Tosi, C., 471
Tosi, M. P., 220
Totti, F., 471
Toufar, H., 218
Tough, R. J. A., 281
Toxvaerd, S., 395
Trabesinger, G., 485
Travis, K. P., 395
Treichel, J. A., 284
Tristram, F., 473, 485
Tronchet, J. M. J., 479
Tropsha, A., 473
Trost, B. M., 485, 486
Trotter, H. F., 394
Trouw, F. R., 219
Trucks, G. W., 29, 126, 127, 129, 133
Truhlar, D. G., 29, 281, 471
Tsaio, C., 223
Tschaufeser, P., 214
Tschoerner, M., 485
Tsubomura, T., 483
Tsuchiya, S., 135
Tsuiji, K., 135
Tsurumoto, A., 482
Tsuzuki, S., 485
Tucker, J. A., 485
Tucker, T. J., 477
Tuckerman, M. E., 221, 393, 394, 395
Tueting, J. L., 485
Tuppurainen, K., 485
Turek, A. M., 222
Turnbull, K. R., 472
Tvaroska, I., 479, 485
Uchio, Y., 475
Ugliengo, P., 223, 485
Ugozzoli, F., 476
Ulman, A., 483
Umeyama, H., 481
Umranaia, Y., 284
Ungarelli, F., 475
Unwalla, R. J., 473, 482, 485
Uppal, D. K., 469
Urban, J. J., 30, 474
Urban, M., 126, 131, 132
Usui, S., 475
Utsuno, S., 484
Vacca, J. P., 477
Vacek, G., 131, 132
Vadavik, L., 485
Vairamani, M., 476
van Beest, B. W. H., 218
van Bekkum, H., 215, 216, 219, 222
van de Graaf, B., 215, 216, 218, 219, 220,
 222, 289, 485
van de Sande, J. H., 471
van der Helm, D., 475, 477, 486
van der Linden, B., 222
van der Spoel, F., 485
van der Waal, J. C., 216
van Duijveneldt, F. B., 281, 282
van Duijveneldt-van de Rijdt, J. G. C. M.,
 281, 282
van Duin, A. C. T., 219, 289
van Duin, M., 485

- van Eijck, B. P., 476, 478, 485
van Gunsteren, W. F., 220, 221, 282, 471,
 474, 478, 479, 480
van Helden, S. P., 480, 485
van Hoorn, W. P., 475, 485
van Hummel, G. J., 476
van Koningsveld, H., 216, 222
van Lenthe, J. H., 281
van Loan, C. F., 31
Van Opdenbosch, N., 473
van Santen, R. A., 214, 217, 218, 219, 221,
 223
van Veggel, F. C. J. M., 475, 485
van Wolput, J. H. M. C., 223
Vance, R., 481
Vanderkooi, G., 475
Vanderkooi, J. M., 479
Varadarajan, A., 475
Varnali, T., 470
Vashishta, P., 396
Vásquez, S., 483
Vásquez, S. A., 485
Vassen, I., 221
Vaughn, J. D., 478, 479
Vauthey, E., 483
Vaz, M. C. T. A., 470
Veal, J. M., 485
Vedani, A., 485
Veenstra, D. L., 485
Vega, A. J., 222
Velasco, D., 473
Venable, R. M., 486
Ventura, M. M., 485
Verastegui, R., 473
Verbist, G. L. M. M., 216
Verdonk, M. L., 283
Vergoten, G., 473, 474, 485
Verheij, V. A., 219
Versichel, W., 283
Verwer, P., 287
Vetterling, W. T., 31, 220
Veyrat, M., 478
Vicentini, L., 476
Vigne-Maeder, F., 285
Vila, F., 485
Villarreal, J. R., 473
Vinas, C., 477
Vinter, J. G., 286
Vinzento, P., 479
Virgili, A., 471, 474
Viswanadhan, V. N., 485
Vitale, G., 216
Viterbo, D., 485
Vlaic, G. J., 222
Vogt, E. T. C., 218, 219
von Philipsborn, W., 481
von Schnering, H.-G., 471
von Voitenberg, H., 470, 474
Vulpetti, A., 476, 485
Wachs, I. E., 222
Wade, P. W., 476, 481
Wade, R. C., 482, 485
Wagner, N. J., 396
Wai, M., 477
Wainwright, K. P., 476
Wainwright, T., 392
Wakamiya, T., 482
Wakeham, W. A., 281
Waknine, D., 485
Waldeck, D. H., 479
Waldman, M., 480, 482
Waldram, J. R., 392
Wales, D. J., 286
Walker, F. A., 483
Walker, P. D., 288
Walker, S., 485
Wallen, S. L., 486
Wallqvist, A., 287, 395
Walshaw, J., 284
Walters, W. P., 480, 483
Wang, J., 216, 485
Ward, K. B., 484
Warden, C., 480
Wärnmark, K., 481, 482
Warren, R., 473
Wasserman, E., 477
Watanabe, D., 222
Watanabe, M., 480
Watkinson, M., 471
Watowich, S. J., 220
Watson, D. G., 283
Watson, W. H., 485
Watt, I., 477
Watts, J. D., 125, 126, 127, 128, 129, 131,
 132, 134, 135
Watzky, M. A., 485
Waugh, J. S., 221
Weaver, D. F., 474, 478, 486
Weaving, J. S., 476
Weber, H., 394
Weber, P., 482
Weeks, J. D., 392
Weinberg, W. H., 217
Weiner, P., 282, 480, 486
Weiner, S. J., 282, 486

- Weinstein, J. N., 475
Weiser, J., 484
Weissensteiner, W., 486
Weitkamp, J., 214, 219, 222
Welch, M. J., 477, 479, 483
Welsh, W. J., 479, 486
Welzel, P., 484
Werner, H.-J., 126, 132, 135
West, R., 474
Wheatley, R. J., 281, 284, 285, 287
Whitaker, S., 393
White, A. H., 471
White, D. P., 473, 486
White, J. D., 477
White, P., 486
White, S. R., 221
Whiteside, R. A., 30
Whitfield, D. M., 486
Whiting, A., 471, 476, 478
Whitlock, H. W., Jr., 472
Whittle, R. R., 480
Wiberg, K., 486
Wiberg, K. B., 30, 286, 288, 471
Wibley, K. S., 287
Wick, G. C., 130
Wiesemann, F., 486
Wiggins, M., 477
Wijmenga, S. S., 476
Wilemski, G., 396
Willey, R. J., 222
Williams, D. E., 30, 31, 282, 286, 288
Williams, D. J., 486
Williams, G. J. B., 283
Williams, H. J., 481
Willis, A. C., 474
Willock, D. J., 216, 287
Wilson, K. R., 220, 221
Wilson, S., 131, 132, 133
Wilson, S. R., 470
Wilson, W. D., 475, 480
Wingen, U., 478
Winn, P. J., 289
Wiórkiewicz-Kucera, J., 480, 482
Wipff, G., 476, 479, 486
Wiscount, C. M., 477
Witczak, Z. J., 476
Wolf, R., 483
Wolfe, S., 470, 486
Wolfram, S., 133
Woltersdorf, O. W., 477
Wolynes, P. G., 395
Won, Y., 482
Won, Y. D., 478
Wong, M. W., 29
Woo, T. K., 474
Woods, R. J., 30, 486
Wright, D. C., 471
Wright, P. E., 481
Wu, Y.-D., 470, 477, 486
Wudl, F., 397
Wunderlich, B., 394
Wunz, T. P., 477
Xiao, G., 486
Xie, Y., 132, 134
Xu, D., 477
Xue, W., 396
Yamabe, T., 482
Yamada, T., 396
Yamaguchi, Y., 131, 132, 134
Yamamoto, G., 469, 486
Yamanari, K., 474
Yan, L. Q., 470, 479
Yang, K., 486
Yang, L., 477, 484, 486
Yang, W., 217
Yao, S., 475, 486
Yarkony, D. R., 129
Yashonath, S., 288
Yates, P. C., 474, 477, 486
Yavari, I., 470
Yelle, R. B., 486
Yeoh, S. L., 284
Yin, D., 475, 480, 486
Yoneya, M., 479
Yonker, C. R., 486
Yoon, C. N., 482
Yoshida, H., 394
Yoshida, M., 486
Yoshie, N., 481
Yoshikawa, Y., 484, 486
Yoshizuka, K., 473
Young, L., 486
Young, S. D., 477
Yu, J., 396
Yu, H.-A., 481
Yuh, Y., 470
Yuh, Y. H., 222, 483
Yuriev, E., 486
Zakrzewski, V. G., 29
Zalkow, V. B., 475
Zambianchi, M., 471
Zecchina, A., 221, 222
Zerner, M. C., 218

- Zhang, D., 477
Zhang, Y., 486
Zheng, C., 475
Zheng, Y.-J., 476
Zhou, S. J., 396
Zhou, X., 470, 486
- Zhu, Z. S., 470
Zicmane, I., 484
Ziegler, T., 474
Zimmer, M., 472, 473, 480, 485, 486
Zou, X., 472
Zugay, J. A., 477

Subject Index

Computer programs are denoted in boldface; databases and journals are in italics.

- Ab initio calculations, 226
Ab initio charge distributions, 269
Ab initio molecular dynamics, 296
Absorption line shape, 181
Accuracy of distributed multipole electrostatic energies, 261
ACES II, 110, 111
Acetamide, 4, 22, 24, 274
N-Acetyl-*N'*-methylamide, 279
N-Acetyl-*N'*-methylamine diglycine, 277
N-Acetylalanine-*N'*-methylamide, 261
Acetylene, 256, 264
N-Acetyl-L-alanylamide, 8
N-Acetyl-L-serinylamide, 8
Acidity, 144
Acrolein, 279
Active site, 183
Additive approximation, 234
Adsorption, 147, 186, 211
Adsorption sites, 140, 141, 147
Alanine, 122
Alanine dipeptide, 22, 24
Alanyl dipeptide, 13
Alkanes, 256, 363
Aluminophosphates, 157, 161
Aluminosilicates, 137, 157, 161, 162, 163
AMBER force field, 245, 443, 444
AMBER* (MacroModel) force field, 448
American Theory Conferences, 401
Amino acids, 8
Ammonia, 253, 262
Analytic derivatives, 34, 115
Angular momentum theory, 231
Anisotropic atom-atom potentials, 227, 234, 256, 264, 268, 270, 271, 272, 280
Anisotropic multipole moments, 269
Annihilation operators, 39, 48, 55, 60, 78
[10]Annulene, 123
Anticommutation relation, 40, 48, 55, 76
Antisymmetrization, 35, 37, 247
Argon, 226, 228, 238, 318
Aromatic compounds, 259
Aromatic heterocycles, 252
Aromatic pi-pi interactions, 251
Atlas of Protein Side-Chain Interactions, 250
Atlas of Zeolite Structure Types, 138, 165, 175
Atom electronegativity, 153
Atom hardness, 153
Atom-atom potential method, 244
Atom-centered point charges, 2, 3, 4
Atomic charge distribution, 273
Atomic charges, 1, 2, 154, 163, 182, 210, 275
Atomic point charge model, 263
Atoms-in-Molecules partitioning scheme, 258
Augmented triples correction, 106
Autocorrelation functions, 376
Automobile exhaust, 150
Axilrod-Teller term, 239, 242
Axis system, 228
Azabenzenes molecules, 274
Bader partitioning, 275
Bader population analyses, 3
Baker-Campbell-Hausdorff theorem, 340
Barostat, 305, 318, 323
Basis functions, 263
Basis set selection, 15
Basis set superposition errors (BSSE), 152, 208, 240, 246, 247
Basis sets, 114, 152
 3-21G, 26
 3-21G*, 5, 23, 162
 6-31G*, 277

- Basis sets (*continued*)
 6–31G**, 11, 248, 261
 double-zeta, 162
Bending potential, 159
Benzene, 148, 149, 251, 253, 271, 274
Beta-turns, 277
Biased thermostating, 378
BIGSTRN force field, 453
BIGSTRN3 force field, 455
BIOGRAF force field, 448
Biomolecular simulations, 245
Biorthonormality, 53
BIOSYM Technologies, Inc., 443
Biradicals, 124
Boltzmann H-theorem, 309
Boltzmann-weighted charges, 279
Bond breaking, 123
Bond moments, 460
Bond polarizabilities, 182
Bond polarizability tensor, 183
Born–Oppenheimer approximation, 151, 189
Boundary conditions, 355, 365
Box dynamics method, 358
Boyd, R. H., force field, 448
Bra-state excitation operators, 52
Brenner potential, 387
Brillouin zone, 183
Brillouin’s theorem, 51, 64, 68, 96, 106
Brønsted acid site, 149
Brønsted acidity, 144
Brueckner condition, 119
Brueckner coupled cluster doubles (B-CCD), 120
Brueckner determinant, 121
Brueckner methods, 34
Brueckner orbitals, 113, 119
Bulk behavior, 294
Bulk fluids, 365, 368
Bulk homogeneous conditions, 387
Bulk properties, 293, 355
Bulk transport coefficient, 369
Buried atoms, 20
Butane, 139, 271, 363
Butanol, 28
tert-Butoxide, 22, 24, 26
- C₆₀, 389
CADPAC, 258, 272
Calculus, *v.*
Cambridge Structural Database, 250, 442
CAMM electrostatic models, 268
Canadian Symposia on Theoretical Chemistry,
 401
- Canonical distribution function, 383
Canonical (NVT) ensemble, 180, 302, 310,
 316, 344
Carbohydrates, 273
Carbonyl bond, 4
Car–Parrinello molecular dynamics, 187, 210,
 211, 214
Cartesian coordinates, 165
Catalysts, 137
Catalytic activity, 200
Catechol, 139
Cation mobility, 196
CCSD amplitude equations, 70, 88
CCSD energy equation, 67, 82
Center of mass (CoM), 176
Central cell, 166
Central force field, 156
Central multipole expansion, 257
CFF and CVFF force field, 449
CFF Rasmussen force field, 448
CFF91, 443
CFF93, 443
CFF95, 443
Chabazite, 209, 212
Characteristic relaxation time, 373
Charge density, 277
Charge density difference maps, 258
Charge distribution, 1, 2, 3, 4, 7, 8, 11, 13,
 22, 154, 155, 163, 182, 227, 233, 237,
 259, 269, 273, 274, 280, 460
Charge equilibration method (QE), 155
Charge sensitivity, 12
Charge sensitivity analysis (CSA), 155, 164
Charge transfer, 228, 240, 246, 247, 249,
 252, 266
Charge variability, 14
Charge-compensating cations, 148, 195
CHARMm force field, 443, 450
CHARMM force field, 245, 443, 450
CHEAT95, 450
CHELP, 6, 7, 8, 9, 22, 23, 25, 27
CHELP-BOW, 27, 29
CHELPG, 7, 11, 27
CHELP-SVD, 7, 25
Chemical bonds, 37
Chemical design, 251
Chemical intuition, 2, 14, 158, 273
Chemical potential, 152, 302
Chlorine molecule, 226, 252, 265
Class III charges, 8, 13, 22
Classical mechanics, 140
Classical propagator, 299
Classical properties, 299

- Closed-shell atoms, 226
 Cluster amplitudes, 45, 47, 53, 55, 70, 107, 111
 Cluster approach, 150, 165
 Cluster function, 35, 36, 38
 Cluster operator diagrams, 82
 Cluster operator expansion, 53
 Cluster operators, 41, 47, 49, 52, 63, 78, 84, 99, 100, 116, 119
 Clusters, 144, 203, 208
 Colloids, 379
 Combining rules, 244, 269
 Commutation relations, 41
 Competition effects, 253
 Complementary error function, 168
 Composite set of charges, 13
 Computational chemistry, 401, 404
 Computational problems, 116
 Computer code, 343, 346, 349, 351, 353, 354, 356
 Computer implementation of coupled cluster theory, 107
Computers and Chemistry, 403
 Configuration interaction (CI), 35, 42, 152
 Configuration interaction with singles and doubles (CISD), 43, 44
 Configurational space, 142, 147
 Configuration-biased Monte Carlo, 186, 363
 Configurations, 303
 Confined fluids, 364, 365, 368, 371, 389
 Conformation, 176, 275, 276
 Conformational energies, 441
 Conformational instability, 8
 Conformation-dependent charge distributions, 13, 276, 278
 Conformation-dependent potential, 276
 Conjugate gradient method, 171
 Connected cluster, 67, 92
 Conservation of energy, 179, 367
 Conservation of total momenta, 377
 Consistent implementation of the electronegativity equalization method (CIEEM), 163, 173
 Constant energy hypersurface, 298, 303
 Constrained internal coordinates, 189
 Constrained minimization, 172
 Constrained reaction coordinate dynamics, 149
 Constraint matrix, 27
 Continuity, 307, 391
 Contraction theorem, 59
 Contractions between operator pairs, 57
 Coordinate systems, 228
 Coordinates, 297
 Core orbitals, 37
 Correlated wavefunctions, 115
 Correlation operators, 63
 Couette flow, 331, 336, 337, 344, 349, 357, 358, 379
 Coulombic energy, 153, 364
 Coulombic interaction, 236, 255
 Coulombic potentials, 158
 Counterpoise procedure, 246
 Coupled-cluster amplitude equation, 96
 Coupled-cluster analytic second derivative, 112
 Coupled-cluster (CC) methods, 33, 35, 45
 Coupled-cluster diagrams, 77, 78
 Coupled-cluster doubles (CCD), 33
 Coupled-cluster energy, 49, 95, 97
 Coupled-cluster Hamiltonian, 53, 63, 100
 Coupled-cluster singles and doubles (CCSD), 34, 44
 Coupled-cluster theory, 98, 115, 152
 Coupled-cluster wavefunction, 70
 Crack branching, 387
 Crack propagation, 384
 Crack simulation, 385
 Creation operator strings, 78
 Creation operators, 39, 48, 55, 60
 Creation-annihilation operator pairs, 40
 Crystal engineering, 250
 Crystal field, 157
 Crystal structure modeling, 245
 Crystal structures, 245, 250, 251, 269
 Crystallographic data, 245
 Crystals, 240
 Cu-exchanged zeolites, 150
 Cumulative atomic multipole moments (CAMM), 258, 272
 Cutoff distance, 359
 Cutoff radius, 167, 168, 169, 177
 Cutoff region, 169
 CVFF force field, 443
 Cyclophane host, 271
 L-Cysteine, 22, 24
 Damping, 240, 266
 Database searches, 251
 Davidson correction, 97
 Decane, 335, 363
 De-excitation operators, 50, 52
 Degrees of freedom, 176
 Densities of alkanes, 245
 Density functional theory (DFT), 152, 209, 210

- Density matrix element, 4
Design of new materials, 225
Detergents, 138
Diagrammatic techniques, 55, 77, 82, 88, 110, 119
Diatomics, 256, 260
trans-Diazabutene, 273
Di(cyclohexylmethyl)dimethylammonium ion, 146
N,N-Diethyl-3,5-diethylpiperidinium ions, 197
Diffusion coefficients, 148, 149, 183, 292
Diffusion constant, 364
Diffusion of adsorbates, 140, 143
Diffusion in zeolites, 148
Diffusion process, 183, 296
N,N-Dimethylacetamide, 279
Dimethylamide, 273
Dimethylphosphate, 22, 24, 25
Dipole, 237
Dipole moment, 2, 7, 15, 116, 161, 181, 261
Dipole tensor autocorrelation function, 181
Dipole-dipole polarizability, 238
Dirac's dictum, *vi*
Dirac's notation, 62, 86
Direct product decomposition (DPD), 112
Disconnected wavefunction contributions, 43
Discover force field, 443, 450
Disilicic acid, 161
Dispersion, 167, 242, 244, 263, 266
Dispersion damping, 256
Dispersion energy, 238, 239, 246
Dissipative flux, 329, 334, 368
Distributed dispersion, 256
Distributed multipole analysis (DMA), 249, 258, 260, 276, 277
Distributed multipoles, 251, 255, 256
Distributed polarizabilities, 256, 263
Distributed sites, 259
Distribution function, 143, 300
Divergence theorem, 300, 391
Division of Computers in Chemistry of the American Chemical Society (COMP), 403
DL_POLY, 271
DMAREL, 271
Docking, 145, 175
DOLL's algorithm, 293
Dopamine, 13
Doubly excited states, 123
DREIDING force field, 452
Drift velocity, 368
Drug design, 250
Dynamic friction coefficient, 313
Dynamical operators, 78
ECEPP force field, 452
Effective viscosity, 362
Einstein relationship, 183
Elastic moduli, 161
Elastic scattering amplitudes, 180
Electric field, 292, 323
Electron correlation, 35, 37, 152, 263
Electron density, 152
Electron density distribution, 2
Electron fluctuations, 246
Electronegativity, 154, 173
Electronegativity equalization method (EEM), 153, 154, 163
Electron-electron interaction energy, 153
Electronic Hamiltonian, 38, 47, 53, 55, 71, 78, 88, 99, 100, 117
Electrons, 2
Electrostatic damping, 266
Electrostatic energy, 236, 249, 262
Electrostatic interactions, 154, 167, 169, 226, 255, 269, 277, 319
Electrostatic parameters, 273
Electrostatic potential derived charges, 155
Electrostatic potentials, 1, 210, 275
Embedding, 165
Empirical fitting, 244
Empirical force fields (EFF), 269, 292, 441
Empirical parameterization, 244
Energy, 266
Energy minimization, 141, 142, 147, 166, 171, 212, 405
Energy of interaction, 236
Ensemble, 300
Enthalpies of vaporization, 245
Entropy, 292, 308
EOMEA-CC method, 54
EOMIP-CC method, 54
EPEN/2 force field, 452
Equation of constraint, 173
Equation-of-motion coupled cluster (EOM-CC), 54, 107, 123
Equations of motion, 174, 175, 179, 293
Equilibration, 177
Equilibrium distribution function, 308
Equilibrium ensemble, 302
Equilibrium fluctuations, 379
Equilibrium geometry, 172, 266
Equilibrium molecular dynamics, 292, 346, 380
Equilibrium state, 308, 367
Equilibrium statistical mechanics, 296
Equilibrium time correlation function, 303, 331

- Equipartition principle, 177
 Ergodic trajectory, 303, 312, 315
 Ergodicity principle, 174
 Error in charges, 15
 Ethane, 148
 Ethanol, 279
 Euler angles, 176, 228, 230
 Evans-Morriss PUT equation, 374
 Ewald summation, 167, 271, 319, 360, 364
 Exact wavefunction, 43, 46
 Exchange energy, 247
 Exchange-correlation energy, 153
 Exchange-repulsion energy, 266, 273, 240
 Excimer, 239
 Excitation operators, 42, 81
 Excited determinants, 71
 Excited states, 34, 53, 54, 123, 187
 Excluded determinant, 46
 Expectation value coupled cluster (XCC)
 method, 50
 Exponential ansatz, 38, 46
 Exponentiated cluster operators, 42, 46
 Exposed atoms, 10
 Extended coupled cluster method (ECCM), 50
 Extended Lagrangian, 177, 188
 External field, 292, 305, 323, 325, 355, 358,
 368, 380
 External heat reservoir, 177
 Extra-framework cations, 157, 195
- Factorization, 109
 FAU zeolite, 138
 Faujasite, 149, 194
 Fermi resonance, 207
 Fermi vacuum, 60
 Fermions, 35
 Feynman diagrams, 33, 54
 Field-driven dynamics, 365
 Fine chemical processes, 143
 Finite difference, 175, 179
 Fixed charge approximation, 163, 182
 Fixed electrostatic model, 279
 Flexible molecules, 225, 279
 Flexible zeolite lattice, 148, 178
 Fluctuation dissipation relations, 331
 Fluctuation potential, 99
 Fluorine molecule, 265
 Fluid catalyst cracking, 139
 Fluid density, 295
 Fluid flow, 364
 Fluid-fluid interactions, 369
 Fluids, 292
 Fluid-wall interactions, 369, 370
- Fock matrix element, 71
 Fock operator, 64, 117
 Fock-space multireference coupled cluster theory (FS-MRCC), 54
 Force constants, 160, 161, 243, 272
 Force field parameters, 161, 441
 Force fields, 13, 139, 140, 142, 156, 157,
 166, 174, 187, 189, 225, 241, 252, 278,
 340, 405
 Formamide, 11, 12, 22, 27, 230, 272, 274,
 278
FORTRAN, 356
 Four-body term, 234
 Fractional coordinates, 165
 Fracture, 387
 Framework structure, 142
 Framework topologies, 137, 165
 Free energy of hydration, 275
 Friction, 389
 Friction coefficient, 365, 366, 369, 370, 386
 Frictional force, 369, 372
 Fructopyranose, 8
 Full coupled cluster, 43
 Full configuration interaction, 43
 Full-matrix second-derivative minimizer, 171
 Functional group interactions, 250
 Functional group replacement, 252
 Furan, 252
- GAMESS**, 9
 Gas flows, 365
 Gauche effect, 464
Gaussian, 2, 9
 Gaussian isokinetic thermostats, 373
 Gaussian multipoles, 256, 262
 Gaussian-type basis functions, 124
 Generalized equations of motion, 323
 Generalized Liouville equation, 390
 Generalized valence force field (GVFF), 158
 Generalized Wick's theorem, 59
 Generic repulsion-dispersion parameters, 273
 Geometric mean combining rule, 244
 Geometry-dependent charges, 162, 163, 173
 Geometric derivation, 391
 Gibb's ensemble Monte Carlo, 363
 Gibb's entropy, 308
 Global molecular electronegativity, 154
 Global properties, 15
 Global thermostat, 373
 Glucose, 26
 Glycerylphosphorylcholine (GPC), 13, 14, 16,
 22, 24
 Golub's algorithm, 21

- Gordon Research Conference on Computational Chemistry, 399, 406
Gordon Research Conference on Quantitative Structure-Activity Relationships in Biology, 403
Gordon Research Conferences (GRCs), 399
Grand-canonical Monte Carlo method, 186
Grand-canonical (μ VT) ensemble, 302
Green-Kubo relations, 329, 331, 335, 361, 379
Grid sampling, 11
GROMOS, 245, 452
GSLOD equations, 336, 338
- Hamiltonian diagrams, 84
Hamiltonian dynamics, 297, 344
Hamiltonian systems, 313
Hamiltonians, 38, 47, 48, 51, 53, 55, 61, 71, 78, 79, 80, 88, 99, 100, 103, 117, 151, 179, 246, 328
Hamilton's equations of motion, 297, 340
Hard-sphere repulsion, 249
Harmonic approximation, 158
Harmonic frequencies, 266
Harmonic oscillator, 298, 299, 315, 316, 317, 370
Harmonic spring, 156
Harmonic vibrational frequencies, 116
Hartree-Fock energy, 62
Hartree-Fock (HF) theory, 151
Hartree-Fock self-consistent field (SCF) procedure, 35
Hausdorff expansion, 34, 47, 48, 63, 74, 87, 100
Heat bath, 294, 305
Heat capacity, 296, 311, 312
Heat gradient, 292
Heat transfer, 295
Heats of sublimation, 245
Helium, 226
Hellmann-Feynman theorem, 189
Hermitian operators, 50
Herringbone crystal structure, 252
Hessian matrix, 162, 172
Heteroaromatics, 458
High accuracy methods, 124
High strength materials, 384
High temperature molecular dynamics, 145
Hirshfeld partitioning, 258
Histidine, 262
Hole lines, 78, 83
Hole states, 60, 78
Homogeneous flows, 362
- Homogeneous methods, 293
Homo-parameters, 244
Hopping processes, 148
Host-guest interactions, 145, 186
Hybrid models, 141, 164
Hybridization state, 273
Hydrated molecules, 279
Hydration effects, 268
Hydrazine clusters, 268
Hydrodynamic boundary conditions, 364, 365
Hydrodynamics, 365, 369
Hydrogen bonding, 248, 249, 250, 252, 253, 254
Hydrogen cyanide, 249
Hydrogen fluoride, 44, 226, 249, 255
Hydrogen fluoride dimer, 259, 264, 268
Hydrogen molecule, 44
Hydrogen peroxide radical cation, 121
Hydrogen sulfide, 256, 265
Hydrogen-bonding potentials, 252
Hydroquinone, 139
- Imaginary frequency, 172, 239
Importance sampling, 185
Imprinting, 145
IMPT charge transfer, 256
Incoherent scattering function, 181
Independent-particle approximation, 36
Induction, 263, 266
Induction energy, 237, 247
Industrial lubricant design, 364
Inelastic neutron scattering experiments, 181
Infrared intensities, 116, 182
Infrared spectra, 159, 181, 190, 198
Inhomogeneous differential equation, 348
Inhomogeneous environment, 387
Inhomogeneous methods, 293
Initial conditions, 184
Instantaneous dipolar fluctuations, 238
Instantaneous secondary flows, 374
Interatomic potentials, 140, 385
Intermolecular forces, 226, 242, 262, 268, 280
Intermolecular pair potential, 227, 235, 241, 243, 256
Intermolecular perturbation theory (IMPT), 247, 249, 251, 252, 266
Intermolecular potentials, 225, 241, 272, 280
Intermolecular synthons, 250
Internal coordinates, 159, 160, 166, 172, 176
Internal fractures, 385
Internal hydrogen bonds, 277
Internal pressure, 350

- Internal pressure tensor, 321
 International Zeolite Association (IZA), 138
 Intrafragment excitations, 43
 Intramolecular hydrogen bond, 279
 Intrinsic errors, 273
 Ionic solids, 156
 Irreducible representations, 111
 Irving-Kirkwood procedure, 338
 Isobaric-isenthalpic ensemble, 177
 Isobaric-isothermic (NPT) ensemble, 177, 302, 317, 349, 351
 Isomorphic substitution, 138, 177, 200
 Isomorphous framework substitution, 143
 Isomorphous substitution, 143
ISOSTAR library, 250, 252
 Isotropic atom-atom model, 233, 252
 Isotropic atom-atom potentials, 227, 268, 270, 280
 Isotropic cell fluctuations, 350
 Jacobian, 301, 307, 389
Journal of Computational Chemistry, 403
Journal of Molecular Graphics, 403
Journal of Molecular Structure, 403
 Kohn-Sham orbitals, 153
 Kronecker delta functions, 40, 48, 55, 57, 62
 Laboratory velocity, 334
 Lactose, 27
 Lagrange multipliers, 7, 27
 Lagrangian, 188
 Large molecules, 122
 Lattice, 165, 202, 204, 205
 Lattice dynamics, 171
 Lattice energy, 234, 264, 269, 271
 Lattice vibrations, 166
 Lees-Edwards boundary condition, 360
 Leibniz rule, 392
 Leibniz, G. W., ν
 Lennard-Jones potential, 158, 167, 241, 319, 376, 385
 Levi-Civita tensor, 391
 Lie derivative, 391
 Ligand binding, 252
 Linear combination of atomic orbitals molecular orbital (LCAO-MO), 3, 35, 152
 Linear combination of excited determinants, 99
 Linear combination of Slater determinants, 37
 Linear least squares (LLS), 16, 17, 22, 23
 Linear molecules, 231
 Linear response coupled cluster (LR-CC), 54
 Linear response theory, 323, 324, 361, 368
 Linear velocity profile, 333
 Link atom, 164
 Liouville equation, 301, 307, 325, 390
 Liouville operator, 300, 339
 Liouville's theorem, 302
 Liquid flow, 364
 Local correlation, 123
 Local density approximation (LDA), 153
 Local energy minimum, 142, 147
 Local streaming velocity, 373
 Localization schemes, 264
 Long chain molecules, 186
 Longitudinal polarizability, 183
 Long-range energy terms, 239
 Long-range interactions, 166
 Long-time-scale studies, 385
 Lookup tables, 170
 LTA zeolite, 138
 Lubricants, 292, 294, 361, 363, 388
 Macroscopic observables, 296
 Madelung sum, 167
 Magic angle spinning (MAS) NMR, 209
 Magnetic interactions, 239
 Many-body effects, 235, 268
 Many-body perturbation theory (MBPT), 34, 35, 55, 77, 85, 98
 Many-electron wavefunction, 151
 Martyna-Tuckerman-Klein (MTK) thermostat, 317
 Material failure, 384
 Matrix-based storage, 110
 Maxwellian velocity distribution, 334
 Mechanical piston, 305
 Metals, 458
 Methane, 148, 228, 265
 Methanol, 9, 10, 11, 208, 211, 212, 231, 248, 251, 268, 273
 Methanol-to-gasoline (MTG) process, 149, 206
 Methoxonium ion, 149, 207
 Methyl cyanide, 262, 273
 Methylacetate, 27
 N-Methylacetamide, 13, 272, 274, 279
 N-Methylformamide, 274
 Metric determinant, 307
 Metropolis Monte Carlo method, 142, 185
 MFI zeolite, 138, 199, 200, 201, 203
 MFL zeolite, 199, 201, 202
 Mica, 389
 Microcanonical (NVE) ensemble, 176, 302
 Microcanonical partition function, 303

- Micropores, 137, 145
Microscopic motion, 296
Microstates, 367
Migration path, 148
Millot-Stone potential, 267
Minimal image convention, 168
Minimization, 171
Minimum imaging, 355, 356, 360
MMI force field, 443
MM2 force field, 453, 458
MM2' force field, 461
MM2+ force field, 456, 459
MM2* (MacroModel) force field, 461
MM2AE force field, 456
MM2CARB force field, 461
MM2ERW force field, 461
MM2X force field, 461
MM3 force field, 463
MM3* (MacroModel) force field, 465
MM3-GE force field, 464
MM4 force field, 465
MMFF force field, 465
MMP2 force field, 459
MMX force field, 465
MOBY force field, 465
Modeling schemes, 150
Molecular crystal structures, 280
Molecular dynamics (MD), 139, 141, 168,
 174, 268, 271, 291, 296, 363, 441
Molecular electrostatic potential (MEP), 1, 3,
 15, 22
Molecular geometries, 116
Molecular graphics, 139
Molecular mechanics, 402, 441
Molecular mechanics force fields, 2, 157, 263
Molecular modeling, 140
Molecular orbital theory, 2, 35
Molecular properties, 33, 103
Molecular reactivity, 2
Molecular sieve, 137, 157
Molecular Simulations Inc. (MSI), 443
Molecular structure, 1
Molecular surface, 7
Molecule centered expansions, 232
Møller—Plesset (MP) perturbation theory,
 100, 106, 152, 162
MOLPRO, 110, 111
MOMEC force field, 466
Momenta, 297
Momentum transfer, 365
MOMO, 271
Monopole charges, 4
Monopole potentials, 3
Monosaccharides, 8
Monte Carlo (MC) methods, 147, 174, 185
Monte Carlo simulations, 141, 268, 271, 441
MOR zeolite, 138
Mori-Zwanzig formalism, 369
Morse potential, 158, 252, 386
Mulliken population analysis, 2, 3, 11, 154,
 258, 275
Multiconfigurational SCF (MCSCF), 123
Multiple minima, 172
Multipolar interactions, 167
Multipolar moments, 257
Multipole expansion, 237
Multireference coupled cluster (MRCC), 123
Myoglobin, 27
Navier-Stokes equation, 364
NaY zeolite, 198
Nearest-neighbor atoms, 274
NEMO method, 268
Neopentane, 22, 24, 26
Nested commutators, 47, 63
Net atomic charges, 11
Newton, I., *v*
Newton's equations of motion, 175, 179
Nitrate radical, 121, 122
Nitrobenzene, 257
Nitrogen dimer, 264
Nitrogen molecule, 228, 255, 256, 265
NO, 150
NO₂, 121, 122
Nonadditivity, 234, 244
Nonbonded atoms, 158
Nonbonded interactions, 166
Nonbonded parameters, 245, 273
Nonbonded potential, 225
Noncentral forces, 270
Nonequilibrium ensemble, 330
Nonequilibrium field, 379
Nonequilibrium molecular dynamics
 (NEMD), 291, 292, 324
Nonequilibrium properties, 363
Nonequilibrium response, 379
Nonequilibrium statistical mechanics, 308,
 329
Nonequilibrium steady states, 293
Nonergodicity, 315
Non-Hamiltonian dynamics, 293, 304, 305,
 325
Non-Hamiltonian equations of motion, 297,
 305
Non-Hamiltonian systems, 313
Normal mode analysis (NMA), 159, 172, 190

- Normal modes, 191
 Normal ordering, 55, 60
 Normal-ordered dynamical operators, 77
 Normal-ordered electron Hamiltonian, 61, 62,
 78
 Normal-ordered operators, 82
 Normal-ordered second-quantized operators,
 55
 Nosé thermostat, 310
 Nosé-Hoover chain (NHC), 315, 370
 Nosé-Hoover equations of motion, 313, 370
 Nosé-Hoover thermostat, 315, 333, 338, 344,
 370, 372, 373, 375, 382
 No-slip, 364
 NPT ensemble, 302, 317, 322, 349, 357
 Nuclear magnetic resonance (NMR), 207, 210
 Nucleic acid bases, 262
 Nucleic acids, 273
 Numerically integrating SLLOD equations,
 339
 NVT dynamics, 344
 NVT ensemble, 310, 330
- O₃, 106
 O₄⁺ ion, 121
 Observable, 155, 185
 Occupation-number formalism, 34
 Occupied orbitals, 36, 40, 48
 Octopole, 237
 One-electron wavefunctions, 35, 152,
 187
 One-particle excitation operators, 46
 Onsager regression hypothesis, 331
 Open-shell methods, 34
 Open-shell molecules, 116
 Open-shell perturbation theory, 107
 Operator, 151, 340
 Operator identities, 326
 Operator products, 77
 Operator strings, 58
 OPLS force field, 467
 Optimized potential for liquid simulation
 (OPLS), 13
 Orbital exponent, 155
 Organic molecules, 225, 241, 243, 245, 249,
 256, 269, 272, 280
 ORIENT, 259, 268, 271
 ORIENT3, 271
 Orientational dependence, 228, 249
 Orthonormality, 53
 Oscillator strength, 239
 Overlap model, 256
 Oxygen molecule, 120, 239
- Packing motifs, 251
 Pair distribution function, 180
 Pairwise additive approximation, 234
 Pairwise additivity, 158
 Parallel computing, 385
 Parameters for potential functions, 161
 Particle lines, 78, 83
 Particle states, 60, 78
 Particle-hole formalism, 60, 77
 Partition function, 311, 312, 313, 318
 Path integral molecular dynamics, 316
 Pauli exclusion principle, 240
 PCFF force field, 443
PDQC (Potential Derived Quantities Charge),
 9, 11
 Peculiar frame, 334
 Peculiar momentum, 334, 357, 368, 374
 PEF91L force field, 449
 PEFIM force field, 449
 Penetration energy, 262, 266
 Penetration model, 256
 Peptide charge distribution, 277
 Peptide conformations, 252
 Peptides, 273
 Periodic boundary conditions (PBC), 166,
 183, 318, 337, 355, 378
 Periodicity, 151, 154, 165
 Permutation operators, 76, 95, 104
 Perturbation operator, 99
 Perturbation theory, 235, 242, 247, 256
 Petrochemical industry, 137, 149
 Petrochemistry, 139, 143
 Phase space, 174, 180, 184, 297, 298, 305,
 306, 307, 346
 Phase space compressibility, 301, 314, 319,
 324
 Phase space distribution function, 301, 367
 Phase space probability density, 301
 Phase transition, 142, 177
 Phenol, 22, 24, 26, 139
 Phenyl rings, 251
 Phenylalanine dipeptide, 253
 Physical data, 442
 Physical observables, 49
 Planar Couette flow, 337, 344, 349, 358, 360,
 372, 379
 Planar Couette geometry, 365
 Plane waves basis, 209
 Poincaré section, 316
 Point charge approximation, 2, 155, 277
 Point distribution schemes, 8
 Point group symmetry, 111
 Poisson bracket, 298

- Polar fluids, 364
Polarizability, 161, 182, 264
Polarizability tensor autocorrelation function, 181
Polarization, 157, 244
Polarization energy, 237
Polygen, 443
Polymer, 388
Polymer flows, 365
Polymorphism, 142, 269
Polypeptide charge distribution, 275
Polypeptides, 272
Population analysis, 2
Pore-opening vibrations, 193
Post-Hartree-Fock models, 152, 246
Potential derived atomic charges, 275
Potential derived charges (PDC), 210
Potential energy function, 229
Potential energy surfaces, 123, 155, 161, 171, 172, 246, 255
Potential functions, 174
Potential model, 156, 163
Power series expansion, 50
Power spectra, 181, 192, 197
Pressure, 302
Pressure tensor, 296, 334, 368
Principal components analysis (PCA), 15
Profile-biased thermostat (PBT), 373
Profile-unbiased thermostat (PUT), 372, 373
Propagator, 326, 327, 352
Propane, 148
Protein backbone atoms, 253, 277
Protein binding energies, 252
Protein Data Bank (PDB), 250
Protein structure predictions, 251
Protein structures, 251
Protein-ligand binding, 268
Proteins, 271, 316
Proton affinities, 145
Proton-catalyzed reactions, 149
Proton-exchange, 212
PSI, 110, 111
Pyrazine, 257
Pyridazine, 248, 274
Pyridine, 231, 252, 273, 274
Pyrimidine, 262, 274
- q-annihilation operators, 60, 78
QCFF force field, 468
q-creation operators, 60, 78
QDGROMOS force field, 453
QMFF force field, 449
- q-particle construction operators, 60
Quadrupole, 237
Quadrupolar polarizability, 238
Quantum chemistry, 33
Quantum mechanical models, 151
Quantum mechanical observable, 1, 3
Quantum mechanical region, 164
Quantum mechanics, 49, 139, 140
Quartz, 161, 167
Quasiparticle construction operators, 60
Quasi-restricted Hartree-Fock (QRHF) orbitals, 113
Quaternions, 176
- Radical cation, 116
Raman spectra, 159, 181, 190
Random point distribution, 8
Rank, 19
Rank deficiency, 17, 22, 27
Rank estimates, 24
Rank-deficient problem, 22
Rate constants, 149
RATTLE method, 176
Rayleigh-Schrödinger perturbation theory, 99, 235
Reactions, 296
Reactive bond order potential, 387
Reactive center, 164
Reciprocal space sum, 360
Redistribution of energy, 178
Reduced normal-ordered strings, 59
Redundant internal coordinates, 160
Reentrant solid phase, 378
Reference determinant, 95
Reference state, 60
Reference wavefunction, 78, 84
Repulsion-dispersion parameters, 273
Resistance to shear, 362
Resonance interactions, 239
RESP method, 24, 27
Response operators, 54
Reversible integration, 339
Reversible profile-unbiased thermostat (RPUT), 376
Rheological properties, 388
Riemannian manifold, 390
Rigid framework approach, 166
Rigid ion potential model, 156
Rigid molecule approximation, 176
Rigid zeolite framework approximation, 176
Rotation-vibration microwave spectrum, 241
Rules for diagrammatic representation, 83

- Saddle point, 172
 Sampling of microstates, 141
 Sanibel Symposia, 401
 Scattering calculations, 232
 Schrödinger equation, 33, 45, 47, 95, 141, 151, 246
 Scoring functions, 250
 Second quantization, 33, 34, 39, 55
 Second virial coefficients, 242, 266
 Secondary flows, 373
 Second-quantized equations, 75
 Second-quantized operator strings, 119
 Second-quantized operators, 40, 48, 55, 58, 60, 71
 Self-consistent field (SCF), 152
 Self-diffusion coefficient, 331
 Semicanonical molecular orbital basis, 117
 Semiempirical models, 153
 SHAKE method, 176, 189
 Shape selectivity, 148
 SHAPES force field, 468
 Shear, 364, 368, 378
 Shear field, 333
 Shear flow, 323, 361
 Shear induced collisions, 362
 Shear induced microstructure, 377
 Shear motion, 294
 Shear rates, 296, 324, 377
 Shear thinning, 362
 Shear viscosity, 292, 324, 331, 335, 369
 Shell model, 156, 161, 162
 Shielded Coulomb potential, 169
 Shift operator, 342
 Shifted-force Coulomb potential, 169
 Shifted-force method, 168
 Shifted-force potential, 177
 Short-range terms, 264
 SIBFA (sum of interaction between fragments ab-initio-computed) approach, 268, 272
 Sign sequence, 88
 Silica faujasite, 179, 182, 184, 192, 193, 195
 Silica polymorphs, 161
 Silicate structures, 159
 Silicates, 157, 161, 162
 Siliceous zeolites, 158
 Similarity-transformed equation of motion coupled cluster (STEOM-CC), 54
 Similarity-transformed Hamiltonian, 67
 Similarity-transformed normal-ordered Hamiltonian, 63
 Simulated annealing, 142, 147
 Simulation noise, 380
 Simulations, 225
 Single-determinant reference, 120
 Single-determinant wavefunction, 36, 78
 Single-orbital cluster operators, 40
 Singular value decomposition (SVD), 18, 28
 Size consistency, 42, 44, 95
 Size extensivity, 34, 45, 95
 Size extensivity error, 97
 Slater determinant, 35, 39, 151
 Slater orbitals, 155
 Slater-Kirkwood approximation, 239
 Slater's rules, 70, 95
 Slip, 364
 SLLOD algorithm, 293, 362
 SLLOD dynamics, 296, 339, 364, 365, 382
 SLLOD equations of motion, 316, 330, 331, 335, 336, 344, 366, 379
 Small-field methods, 379
 Small-field nonequilibrium simulations, 380
 Sodalite, 191, 209, 212
 Sodalite cage, 161
 Sorption of molecules, 177
 Spartan, 2
 SPASIBA force field, 468
 Spatial inhomogeneities, 293
 Spatial symmetry, 111
 SPC/E water, 332, 364
 Spherical cutoff, 360
 Spherical harmonic function, 231
 Spherical molecules, 228, 242
 Spherical tensor distributed multipoles, 272
 Spherical tensor theory, 227
 Spin contamination, 116
 Spin factorization, 112
 Spin-adapted open-shell coupled cluster wavefunctions, 117
 Spin-orbital Fock operators, 62
 Spin-restricted Hartree-Fock orbitals, 113
 Spin-restricted open-shell B-CC theory (RB-CC), 121
 Spin-restricted open-shell Hartree-Fock (ROHF), 116
 Spin-restricted open-shell Hartree-Fock (ROHF) orbitals, 113
 Spin-restricted open-shell Hartree-Fock (ROHF) reference functions, 99
 Spin-restricted reference determinants, 116
 Spin-restricted reference wavefunction, 107
 Spin-restricted triple-excitation corrections, 117
 Spin-unrestricted Hartree-Fock (UHF) orbitals, 113

- Squalane, 363
Stacked geometries, 254
Static equilibrium properties, 304
Statistical ensembles, 297
Statistical mechanics, 185
Steady state, 292, 293
Steam, 266
Steric energy, 157, 163
Strain, 324
Strain rate tensor, 358
Streaming velocities, 377
Stress autocorrelation function, 363
Stress tensor, 324
Stress-stress autocorrelation function, 332
String phase orientations, 378
String phases, 372, 377
Structural properties, 296
Structural transformations, 296
Structure directing agents, 145
Subtraction method, 379, 380
Supermolecule calculations, 246, 247
Supermolecules, 247
Supramolecular complexes, 254
Surface area, 23
Surface force apparatus (SFA), 389
Surfaces, 294, 460
Symmetric spin orbital basis, 118
Symmetry orbital (SO), 114
Symmetry-adapted cluster configuration interaction (SAC-CI), 54
Symmetry-adapted perturbation theories, 247
Symmetry-breaking orbital instabilities, 120
Symposium on Molecular Mechanics, 402
Synthetic fuels, 143
Systematic potential approach, 255, 266
(T) correction, 34, 103, 117
Taper functions, 169, 170, 177
Taylor series expansion, 153, 156, 163, 171, 182, 342
Teflon, 388
Temperature, 178, 296, 302
Templates in zeolites, 145
Tensor properties, 231
Test particle model, 256, 265
Tetrabutylammonium (TBA) ions, 197, 200, 201, 202
Tetracosane, 363
Tetrahydrofuran, 252
Tetrapropylammonium (TPA) ions, 197, 200
Tetrazine, 244, 274
Thermal bath, 177
Thermal fluctuations, 373
Thermal velocity, 334
Thermodynamic quantities, 296
Thermostats, 295, 305, 318, 323, 334
Three-body term, 234, 242
Three-orbital cluster functions, 38
Through-space polarization, 276
Time correlation functions, 183, 296, 304, 329
Time dependence, 340, 389
Time scale, 181, 293, 313, 318, 319, 377
Time-dependent boundary conditions, 337
Time-dependent external field, 308
Time-dependent Liouvillian, 325
Time-dependent phase space compressibility, 308
Time-independent boundary conditions, 367
Time-reversal symmetry, 340
Time-step procedure, 348
Toluene, 389
Topologically partitioned dispersion energies, 256
Topologically partitioned electric properties, 256
Topologically partitioned polarizabilities, 256
Torques, 270
Trajectory, 174, 298, 312
Trajectory average, 304
Transferability, 227, 275, 277
Transferability of potentials, 272
Transient time correlation functions (TTCF), 380, 381
Transition state theory, 148
Transition states, 460
Transport coefficients, 183, 304, 324, 329, 331, 365, 368
Transport properties, 141, 361
Triaccontane, 363
Trial configurations, 185
Triazine, 274
Triply excited determinants, 123
TRIPoS force field, 468
Trotter factorizations, 340, 345, 352, 376
Truncated Hausdorff expansion, 49
T-sites, 203, 205
Two-electron cluster function, 39
Two-electron integral, 85
Two-particle operators, 46
Two-phase coexistence, 377
UFF force field, 469
UNI force field, 245
Uniform shear viscosity, 365

- University of Rhode Island, 400
 Unlinked diagrams, 98
 Unstable system, 175
 Uracil, 230, 246, 262
 Urey-Bradley potential, 158
- Vacuum state, 56, 58
 VALBOND force field, 469
 Valence electrons, 153, 187, 233
 Valence orbitals, 37
 van der Waals clusters, 271
 van der Waals complexes, 226, 240, 242, 249, 252, 253, 262, 263, 280
 van der Waals surface, 9, 23, 277
 Vapor pressures, 245
 Variable charges, 20
 Variation in atomic charge with conformation, 13, 275
 Variational approaches, 34
 Variational principle, 152
 Velocity, 334, 373
 Velocity autocorrelation function, 181
 Velocity distribution functions, 322
 Velocity gradient, 293
 Velocity Verlet algorithm, 343
 Velocity Verlet operator, 351
 Velocity-velocity autocorrelation function, 332
 Verlet algorithm, 175
 Verlet integrator, 344
 Vibrational frequencies, 172, 181, 209
 Vibrational modes, 271
 Vibrational spectra, 158, 162, 191, 304
 Vibrational spectroscopy, 143, 181
 Virial coefficients, 241
 Virtual orbitals, 36, 40, 48
 Viscosity, 296, 361, 363
 Viscous damping, 386
 Viscous heating, 294, 379
 Volume, 302
 Volume distribution functions, 322
- Wall atoms, 295
 Water, 226, 228, 230, 253, 256, 262, 274
 Water dimer, 246, 266, 267
 Water potential, 266
 Water-accessible surface, 277
 Wavefunction separability, 42
 Wavefunctions, 1
 Weeks-Chandler-Andersen fluid, 377
 Weeks-Chandler-Andersen (WCA) potential, 295
 Well-conditioned data set, 19
 Wick's theorem, 55, 56, 59, 64, 72, 75, 87, 88, 95, 100, 119
 Wigner 3- j symbol, 231
 Wigner rotation matrices, 231, 246
 Wobbly charges, 8
- Xenon, 148
 X-ray charge densities, 275
 X-ray diffraction, 142, 180
- YETI force field, 468
- Z-averaged perturbation theory (ZAPT), 118
 Zeolite A, 191, 196
 Zeolite acidity, 144
 Zeolite aperture dimensions, 142
 Zeolite aperture dynamics, 159, 193
 Zeolite beta, 146
 Zeolite channels, 175
 Zeolite framework flexibility, 141
 Zeolite framework local modes 190
 Zeolite frameworks, 138, 156, 171, 189
 Zeolite modeling, 137
 Zeolite reactivity, 206
 Zeolite structures, 142
 Zeolite vibrational spectra, 159
 Zeolite window diameters, 183
 Zeolite-catalyzed chemical reactions, 140, 149
 Zeolite-template interactions, 197
 Zeolites, 137, 161, 186